

# پلتفرم اختصاصی مهندسی کنترل



<https://controlengineers.ir>



<https://t.me/controlengineers>



<https://www.instagram.com/controlengineers.ir>

# Linear and Nonlinear Multivariable Feedback Control

controlengineers.ir

# Linear and Nonlinear Multivariable Feedback Control: A Classical Approach

Oleg N. Gasparyan

*State Engineering University of Armenia*

controlengineers.ir



John Wiley & Sons, Ltd

Copyright © 2008 John Wiley & Sons Ltd, Baffins Lane, Chichester  
West Sussex, PO19 1UD, England

National 01243 779777  
International (+44) 1243 779777

Email (for orders and customer service enquiries): cs-books@wiley.co.uk

Visit our Home Page on [www.wileyeurope.com](http://www.wileyeurope.com) or [www.wiley.com](http://www.wiley.com)

All Rights Reserved. No part of this publication may be reproduced, stored in a retrieval system or transmitted in any form or by any means, electronic, mechanical, photocopying, recording, scanning or otherwise, except under the terms of the Copyright, Designs and Patents Act 1988 or under the terms of a licence issued by the Copyright Licensing Agency Ltd, 90 Tottenham Court Road, London W1T 4LP, UK, without the permission in writing of the Publisher. Requests to the Publisher should be addressed to the Permissions Department, John Wiley & Sons Ltd, The Atrium, Southern Gate, Chichester, West Sussex PO19 8SQ, England, or emailed to [permreq@wiley.co.uk](mailto:permreq@wiley.co.uk), or faxed to (+44) 1243 770571.

This publication is designed to provide accurate and authoritative information in regard to the subject matter covered. It is sold on the understanding that the Publisher is not engaged in rendering professional services. If professional advice or other expert assistance is required, the services of a competent professional should be sought.

#### ***Other Wiley Editorial Offices***

John Wiley & Sons Inc., 111 River Street, Hoboken, NJ 07030, USA

Jossey-Bass, 989 Market Street, San Francisco, CA 94103-1741, USA

Wiley-VCH Verlag GmbH, Boschstr. 12, D-69469 Weinheim, Germany

John Wiley & Sons Australia Ltd, 33 Park Road, Milton, Queensland 4064, Australia

John Wiley & Sons (Asia) Pte Ltd, 2 Clementi Loop #02-01, Jin Xing Distripark, Singapore 129809

John Wiley & Sons Canada Ltd, 6045 Freemont BLVD, Mississauga, Ontario, Canada M9W 1L1

Wiley also publishes its books in a variety of electronic formats. Some content that appears in print may not be available in electronic books.

#### ***Library of Congress Cataloging-in-Publication Data***

Gasparyan, Oleg.

Linear and nonlinear multivariable feedback control : a classical approach / Oleg Gasparyan.  
p. cm.

Includes bibliographical references and index.

ISBN 978-0-470-06104-6 (cloth)

1. Control theory. 2. Feedback control systems. 3. Functions of complex variables. I. Title.  
QA402.3.G37 2008  
629.8'36—dc22

2007044550

#### ***British Library Cataloguing in Publication Data***

A catalogue record for this book is available from the British Library

ISBN 978-0-470-06104-6

Typeset in 10/12pt Times by Aptara Inc., New Delhi, India

Printed and bound in Great Britain by Antony Rowe Ltd, Chippenham, Wiltshire

This book is printed on acid-free paper responsibly manufactured from sustainable forestry in which at least two trees are planted for each one used for paper production.

To my beloved family: Lilit, Yulia, and Nikolay

controlengineers.ir

# Contents

<b>Preface</b>	<b>xi</b>
<b>Part I Linear Multivariable Control Systems</b>	
<b>1 Canonical representations and stability analysis of linear MIMO systems</b>	<b>3</b>
1.1 Introduction	3
1.2 General linear square MIMO systems	3
1.2.1 Transfer matrices of general MIMO systems	3
1.2.2 MIMO system zeros and poles	5
1.2.3 Spectral representation of transfer matrices: characteristic transfer functions and canonical basis	10
1.2.4 Stability analysis of general MIMO systems	19
1.2.5 Singular value decomposition of transfer matrices	31
1.3 Uniform MIMO systems	40
1.3.1 Characteristic transfer functions and canonical representations of uniform MIMO systems	41
1.3.2 Stability analysis of uniform MIMO systems	43
1.4 Normal MIMO systems	51
1.4.1 Canonical representations of normal MIMO systems	51
1.4.2 Circulant MIMO systems	53
1.4.3 Anticirculant MIMO systems	62
1.4.4 Characteristic transfer functions of complex circulant and anticirculant systems	70
1.5 Multivariable root loci	74
1.5.1 Root loci of general MIMO systems	76
1.5.2 Root loci of uniform systems	89
1.5.3 Root loci of circulant and anticirculant systems	93
<b>2 Performance and design of linear MIMO systems</b>	<b>100</b>
2.1 Introduction	100
2.2 Generalized frequency response characteristics and accuracy of linear MIMO systems under sinusoidal inputs	101
2.2.1 Frequency characteristics of general MIMO systems	101
2.2.2 Frequency characteristics and oscillation index of normal MIMO systems	117
2.2.3 Frequency characteristics and oscillation index of uniform MIMO systems	121

2.3	Dynamical accuracy of MIMO systems under slowly changing deterministic signals	124
2.3.1	Matrices of error coefficients of general MIMO systems	124
2.3.2	Dynamical accuracy of circulant, anticirculant and uniform MIMO systems	129
2.3.3	Accuracy of MIMO systems with rigid cross-connections	132
2.4	Statistical accuracy of linear MIMO systems	135
2.4.1	Accuracy of general MIMO systems under stationary stochastic signals	135
2.4.2	Statistical accuracy of normal MIMO systems	139
2.4.3	Statistical accuracy of uniform MIMO systems	141
2.4.4	Formulae for mean square outputs of characteristic systems	145
2.5	Design of linear MIMO systems	151
<b>Part II Nonlinear Multivariable Control Systems</b>		<b>171</b>
<b>3</b>	<b>Study of one-frequency self-oscillation in nonlinear harmonically linearized MIMO systems</b>	<b>173</b>
3.1	Introduction	173
3.2	Mathematical foundations of the harmonic linearization method for one-frequency periodical processes in nonlinear MIMO systems	181
3.3	One-frequency limit cycles in general MIMO systems	184
3.3.1	Necessary conditions for the existence and investigation of the limit cycle in harmonically linearized MIMO systems	184
3.3.2	Stability of the limit cycle in MIMO systems	194
3.4	Limit cycles in uniform MIMO systems	199
3.4.1	Necessary conditions for the existence and investigation of limit cycles in uniform MIMO systems	199
3.4.2	Analysis of the stability of limit cycles in uniform systems	205
3.5	Limit cycles in circulant and anticirculant MIMO systems	214
3.5.1	Necessary conditions for the existence and investigation of limit cycles in circulant and anticirculant systems	214
3.5.2	Limit cycles in uniform circulant and anticirculant systems	229
<b>4</b>	<b>Forced oscillation and generalized frequency response characteristics of nonlinear MIMO systems</b>	<b>236</b>
4.1	Introduction	236
4.2	Nonlinear general MIMO systems	244
4.2.1	One-frequency forced oscillation and capturing in general MIMO systems	244
4.2.2	Generalized frequency response characteristics and oscillation index of stable nonlinear MIMO systems	251
4.2.3	Generalized frequency response characteristics of limit cycling MIMO systems	260
4.3	Nonlinear uniform MIMO systems	265
4.3.1	One-frequency forced oscillation and capturing in uniform systems	265
4.3.2	Generalized frequency response characteristics of stable nonlinear uniform systems	268

4.3.3 Generalized frequency response characteristics of limit cycling uniform systems	271
4.4 Forced oscillations and frequency response characteristics along the canonical basis axes of nonlinear circulant and anticirculant systems	274
4.5 Design of nonlinear MIMO systems	278
<b>5 Absolute stability of nonlinear MIMO systems</b>	<b>284</b>
5.1 Introduction	284
5.2 Absolute stability of general and uniform MIMO systems	287
5.2.1 Multidimensional Popov's criterion	287
5.2.2 Application of the Bode diagrams and Nichols plots	293
5.2.3 Degree of stability of nonlinear MIMO systems	296
5.3 Absolute stability of normal MIMO systems	299
5.3.1 Generalized Aizerman's hypothesis	301
5.4 Off-axis circle and parabolic criteria of the absolute stability of MIMO systems	304
5.4.1 Off-axis circle criterion	305
5.4.2 Logarithmic form of the off-axis criterion of absolute stability	309
5.4.3 Parabolic criterion of absolute stability	313
5.5 Multidimensional circle criteria of absolute stability	314
5.5.1 General and normal MIMO systems	316
5.5.2 Inverse form of the circle criterion for uniform systems	319
5.6 Multidimensional circle criteria of the absolute stability of forced motions	321
<b>Bibliography</b>	<b>327</b>
<b>Index</b>	<b>335</b>

# Preface

This textbook provides a unified control theory of linear and nonlinear multivariable feedback systems, also called multi-input multi-output (MIMO) systems, as a straightforward extension of the classical control theory. The central idea of the book is to show how the *classical* (frequency- and root-domain) engineering methods look in the multidimensional case, and how a practising engineer or researcher can apply them to the analysis and design of linear and nonlinear MIMO systems.

At present, there is a great number of fundamental textbooks on classical feedback control as applied to single-input single-output (SISO) systems, such as the books by Dorf and Bishop (1992), K. Ogata (1970), Franklin, Powell and Emami-Naeini (1991), Atherton (1975) and E. Popov (1973), the last two being devoted to nonlinear SISO systems, and many others. A general quality of all these books is a united conceptual approach to introducing the classical control theory, as well as clearly indicated branches of that theory; in fact, a lecturer can successfully use any of these books in teaching his course on related subjects. On the other hand, there are many remarkable textbooks and monographs on multivariable feedback control, but the situation here is not so plain. Historically, at the outset, the development of multivariable control theory was conducted in different ways and manners, varying from massive efforts to extend directly the basic classical methods and techniques, to no less massive attempts to reformulate radically and even ‘abolish’ the classical heritage of control theory. Besides, the initial stages of formation of multivariable control essentially coincided with the advent of state-space methods and approaches, and with rapid development of optimal control theory, equally dealing with SISO and MIMO systems. At last, at around that time, there the robust control theory also applicable to both SISO and MIMO systems emerged. As a result, the notion of ‘modern’ multivariable control is so manifold and embraces so many directions and aspects of feedback control that it is difficult to list them all without running the risk of missing something significant. Nevertheless, it is obvious that optimal, adaptive and robust methods (and their variations) are predominant in the scientific and technical literature, and advances in these methods considerably exceed the achievements of the ‘classical’ branch in multivariable control. At the same time, it should be acknowledged that modern MIMO control theory just ‘jumped over’ many important problems of the classical theory and now there is an evident gap between the topics presented in most textbooks on SISO control and those in many books on multivariable control (Skogestad and Postlethwaite 2005; Safonov 1980; Maciejowski 1989, etc.).

The goal of this book is to bridge that gap and to provide a holistic multivariable control theory as a direct and natural extension of the classical control theory, for both linear and

nonlinear MIMO systems. The need for such a book is particularly evident now that modern computer aids and specialized programming languages (first of all, MATLAB<sup>®1</sup>) allow control specialists to restore and successfully use in practice many powerful classical approaches which in fact have been disregarded recently as useless and non-effective, especially for multivariable control. That is why the author hopes that a text in which many key problems of multivariable control are introduced and explained in common terms and notions of the classical control would be helpful for practitioners and researchers engaged in control engineering, as well as for lecturers on both classical and modern control.

The textbook can be used for an advanced undergraduate (fourth-year) course or for an introductory graduate course in multivariable feedback control. The necessary prerequisites for understanding the book contents are a typical introductory course in classical control and some elementary knowledge of the theory of matrices and linear spaces. The presented material has partially been used in an undergraduate multivariable control course given by the author in the Cybernetics Department at State Engineering University of Armenia (SEUA) since 2002.

The restrictions on the book's length forced the author to exclude some material that had been regarded as very useful and appropriate for the textbook. The matter concerns problems, exercises, appendices on the theory of matrices and functional analysis, etc. All these materials are available over the internet from the author's home page ([www.seua.am/ogasp](http://www.seua.am/ogasp)).

All worked examples in the book were solved with the help of graphical user interface (GUI) *ControlSysCAD*, working in the MATLAB environment, which was developed by the author. A very simplified version of that GUI destined for solving simple exercises on two-dimensional linear MIMO systems of different structural classes is also available over the internet from the author's home page.

The author will be grateful for any comments, remarks, discovered errors, etc. concerning the book. Please send them to the author's email address ([ogasparyan@seua.am](mailto:ogasparyan@seua.am)).

The companion website for the book is <http://www.wiley.com/go/gasparyan>

<sup>1</sup> MATLAB<sup>®</sup> is a registered trademark of The MathWorks, Inc.

# Part I

## Linear Multivariable Control Systems

controlengineers.ir

# 1

## Canonical representations and stability analysis of linear MIMO systems

### 1.1 INTRODUCTION

In the first section of this chapter, we consider in general the key ideas and concepts concerning canonical representations of linear multi-input multi-output (MIMO) control systems (also called *multivariable* control systems) with the help of the *characteristic transfer functions* (or *characteristic gain functions*) method (MacFarlane and Belletrutti 1970; MacFarlane *et al.* 1977; MacFarlane and Postlethwaite 1977; Postlethwaite and MacFarlane 1979). We shall see how, using simple mathematical tools of the theory of matrices and linear algebraic operators, one can associate a set of  $N$  so-called *one-dimensional characteristic systems* acting in the complex space of input and output vector-valued signals along  $N$  linearly independent directions (axes of the *canonical basis*) with an  $N$ -dimensional (i.e. having  $N$  inputs and  $N$  outputs) MIMO system. This enables us to reduce the stability analysis of an interconnected MIMO system to the stability analysis of  $N$  *independent* characteristic systems, and to formulate the generalized Nyquist criterion. We also consider some notions concerning the *singular value decomposition* (SVD) used in the next chapter for the performance analysis of MIMO systems. In the subsequent sections, we focus on the structural and geometrical features of important classes of MIMO systems – *uniform* and *normal* systems – and derive canonical representations for their transfer function matrices. In the last section, we discuss multivariable root loci. That topic, being immediately related to the stability analysis, is also very significant for the MIMO system design.

### 1.2 GENERAL LINEAR SQUARE MIMO SYSTEMS

#### 1.2.1 Transfer matrices of general MIMO systems

Consider an  $N$ -dimensional controllable and observable *square* (that is having the same number of inputs and outputs) MIMO system, as shown in Figure 1.1. Here,  $\varphi(s)$ ,  $f(s)$  and  $\varepsilon(s)$

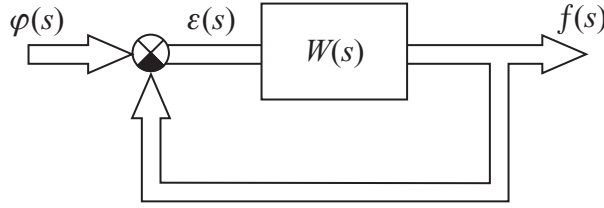


Figure 1.1 Block diagram of a general-type linear MIMO feedback system.

stand for the Laplace transforms of the  $N$ -dimensional input, output and error vector signals  $\varphi(t)$ ,  $f(t)$  and  $\varepsilon(t)$ , respectively (we shall regard them as elements of some  $N$ -dimensional complex space  $\mathbb{C}^N$ );  $W(s) = \{w_{kr}(s)\}$  denotes the square transfer function matrix of the open-loop system of order  $N \times N$  (for simplicity, we shall call this matrix the *open-loop transfer matrix*) with entries  $w_{kr}(s)$  ( $k, r = 1, 2, \dots, N$ ), which are scalar proper rational functions in complex variable  $s$ . The elements  $w_{kk}(s)$  on the principal diagonal of  $W(s)$  are the transfer functions of the *separate* channels, and the nondiagonal elements  $w_{kr}(s)$  ( $k \neq r$ ) are the transfer functions of *cross-connections* from the  $r$ th channel to the  $k$ th.

Henceforth, we shall not impose any restrictions on the number  $N$  of separate channels, i.e. on the dimension of the MIMO system, and on the *structure* (type) of the matrix  $W(s)$ . At the same time, so as not to encumber the presentation and to concentrate on the primary ideas, later on, we shall assume that the scalar transfer functions  $w_{kr}(s)$  do not have multiple poles (we mean each individual transfer function). Also, we shall refer to the general-type MIMO system of Figure 1.1 as simply the *general* MIMO system (so as not to introduce any ambiguity concerning the *type* of system, which is conventionally defined in the classical control theory as the number of pure integrators in the open-loop system transfer function).

The output  $f(s)$  and error  $\varepsilon(s)$  vectors, where

$$\varepsilon(s) = \varphi(s) - f(s), \quad (1.1)$$

are related to the input vector  $\varphi(s)$  by the following operator equations:

$$f(s) = \Phi(s)\varphi(s), \quad \varepsilon(s) = \Phi_\varepsilon(s)\varphi(s), \quad (1.2)$$

where

$$\Phi(s) = [I + W(s)]^{-1} W(s) = W(s) [I + W(s)]^{-1} \text{ and} \quad (1.3)$$

$$\Phi_\varepsilon(s) = [I + W(s)]^{-1} \quad (1.4)$$

are the transfer function matrices of the closed-loop MIMO system (further, for short, referred to as the *closed-loop transfer matrices*) with respect to output and error signals, and  $I$  is the unit matrix. The transfer matrices  $\Phi_\varepsilon(s)$  and  $\Phi(s)$  are usually called the *sensitivity function matrix* and *complementary sensitivity function matrix*.<sup>1</sup>

By straightforward calculation, it is easy to check that  $\Phi_\varepsilon(s)$  and  $\Phi(s)$  satisfy the relationship:

$$\Phi(s) + \Phi_\varepsilon(s) = I. \quad (1.5)$$

<sup>1</sup> The terms *sensitivity function* and *complementary sensitivity function* were introduced by Bode (1945).

From here, we come to the important conclusion that it is impossible to bring to zero the system error if the input signal is a sum (mixture) of a reference signal and disturbances, where the latter may be, for example, the measurement or other noises. Indeed, if the system ideally tracks the input reference signal, that is if the matrix  $\Phi_e(s)$  identically equals the zero matrix, then, due to the superposition principle (Ogata 1970; Kuo 1995), that system also ideally reproduces at the output the input noise [since, if  $\Phi_e(s) = 0$ , then the matrix  $\Phi(s)$  in Equation (1.5) is equal to the unit matrix  $I$ ]. A certain trade-off may only be achieved provided the input reference signal and the measurement noise have nonoverlapping (at least, partially) frequency ranges.<sup>2</sup>

## 1.2.2 MIMO system zeros and poles

### 1.2.2.1 Open-loop MIMO systems

A single-input single-output (SISO) feedback control system with the open-loop transfer function  $W(s)$  is depicted in Figure 1.2. That system may be regarded, if  $N = 1$ , as a specific case of

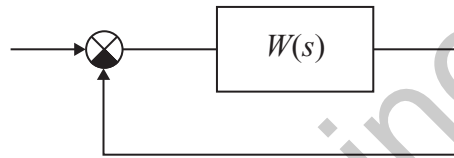


**Figure 1.2** Block diagram of a SISO control system ( $N = 1$ ).

the MIMO system of Figure 1.1. The transfer function  $W(s)$  is a rational function in complex variable  $s$  and can be expressed as a quotient of two polynomials  $M(s)$  and  $D(s)$  with real coefficients:

$$W(s) = \frac{M(s)}{D(s)}, \quad (1.6)$$

where the order  $m$  of  $M(s)$  is equal to or less than the order  $n$  of  $D(s)$ , that is we consider only physically feasible systems.

From the classical control theory, we know that the *poles*  $p_i$  of  $W(s)$  are the roots of the denominator polynomial  $D(s)$ , and *zeros*  $z_i$  are the roots of the numerator polynomial  $M(s)$  (Ogata 1970; Kuo 1995). In the case of usual SISO systems with *real* parameters, complex poles and zeros always occur in complex conjugate pairs. Obviously, at the zeros  $z_i$ , the transfer function  $W(s)$  vanishes and, at the poles  $p_i$ , it tends to infinity (or  $1/W(s)$  vanishes).

In the multivariable case, the situation is not so simple, and this refers to the MIMO system zeros in particular. This indeed explains the large number of papers in which there are given different definitions and explanations of the MIMO system zeros: from the state-space positions, by means of polynomial matrices and the Smith-McMillan form, etc. (Sain and Schrader 1990; Wonham 1979; Rosenbrock 1970, 1973; Postlethwaite and MacFarlane 1979; Vardulakis 1991).

First, let us consider the *open-loop* MIMO system *poles*. We call any complex number  $p_i$  the *pole* of the open-loop transfer matrix  $W(s)$  if  $p_i$  is the pole of at least one of the entries

<sup>2</sup> The MIMO system accuracy is discussed in Chapter 2.

## 6 Canonical Representations and Stability Analysis of Linear MIMO Systems

$w_{kr}(s)$  of the matrix  $W(s)$ . In fact, if at least one of the entries  $w_{kr}(s)$  of  $W(s)$  tends to infinity as  $s \rightarrow p_i$ , then  $W(s)$  tends (strictly speaking, by norm) to infinity. Therefore,  $p_i$  may be regarded as the pole of  $W(s)$ . As a result, we count the set of the poles of all  $w_{kr}(s)$  as the poles of  $W(s)$ . Such a *prima facie* formal definition of the MIMO system pole seems evident but it leads, as we shall see later, to rather interesting results.

Let the transfer matrix  $W(s)$  be expanded, taking into account the above assumption that  $w_{kr}(s)$  have no multiple roots, into partial fractions as:

$$W(s) = \sum_{i=1}^n \frac{K_i}{s - p_i} + D, \quad (1.7)$$

where  $n$  is the total number of simple poles of  $W(s)$ ;

$$K_i = \lim_{s \rightarrow p_i} (s - p_i)W(s) \quad (1.8)$$

are the *residue matrices* of  $W(s)$  at the finite poles  $p_i$ ; and the constant matrix  $D$  is

$$D = \lim_{s \rightarrow \infty} W(s). \quad (1.9)$$

Note that the matrix  $D$  differs from the zero matrix if any of  $w_{kr}(s)$  have the same degree of the numerator and denominator polynomials.

The *rank*  $r_i$  of the  $i$ th pole  $p_i$  is defined as the rank of the residue matrix  $K_i$ , and it is called the *geometric multiplicity* of that pole. Among all poles of the open-loop MIMO system, of special interest are those of rank  $N$ , which are also the poles of *all* the nonzero elements  $w_{kr}(s)$ . In what follows, we shall call such poles the *absolute* poles of the open-loop MIMO system. It is easy to see that if a complex number  $p_i$  is an absolute pole of the transfer matrix  $W(s)$ , then the latter can be represented as

$$W(s) = \frac{1}{s - p_i} W_1(s), \quad (1.10)$$

where the matrix  $W_1(p_i)$  is nonsingular [that matrix cannot have entries with poles at the same point  $p_i$  owing to the assumption that  $w_{kr}(s)$  have no multiple poles].

In a certain sense, it is more complicated to introduce the notion of *zero* of the transfer matrix  $W(s)$ , as an arbitrary complex number  $s$  that brings any of the transfer functions  $w_{kr}(s)$  to vanishing, cannot always be regarded as the zero of  $W(s)$ . We introduce the following two definitions:

1. A complex number  $z_i$  is said to be an *absolute* zero of the transfer matrix  $W(s)$  if it reduces the latter to the zero matrix.
2. A complex number  $z_i$  is said to be a *local* zero of rank  $k$  of  $W(s)$ , if substituting it into  $W(s)$  makes the latter singular and of rank  $N - k$ . The local zero of rank  $N$  is, evidently, the absolute zero of  $W(s)$ .<sup>3</sup>

<sup>3</sup> The notion of MIMO system zero as a complex number  $z$  that reduces at  $s = z$ , the *local rank* of the matrix  $W(s)$ , is given, for example, in MacFarlane (1975).

Let us discuss these statements. It is clear that if a number  $z_i$  is an absolute zero of  $W(s)$ , then we can express that matrix as

$$W(s) = (s - z_i)W_1(s), \quad (1.11)$$

where  $W_1(z_i)$  differs from the zero matrix and has rank  $N$ . In other words, the absolute zero must also be the *common zero* of all the nonzero elements  $w_{kr}(s)$  of  $W(s)$ .

We are not quite ready yet for detailed discussion of the notion of the open-loop MIMO system local zero, but, as a simple example, consider the following situation. Let  $z_i$  be the common zero of all elements  $w_{kr}(s)$  of the  $k$ th row or the  $r$ th column of  $W(s)$ , i.e.  $w_{kr}(z_i) = 0$  when  $k = \text{const}$ ,  $r = 1, 2, \dots, N$ , or when  $r = \text{const}$ ,  $k = 1, 2, \dots, N$ . Then, obviously, if the rank of  $W(s)$  is  $N$  for almost all values of  $s$  [i.e. the *normal* rank of  $W(s)$  is  $N$ ], then the matrix  $W(z_i)$  will have at least rank  $N - 1$ , since, for  $s = z_i$ , the elements of the  $k$ th row or the  $r$ th column of  $W(z_i)$  are zero. Structurally, the equality to zero of all elements of the  $k$ th row of  $W(s)$  means that for  $s = z_i$ , both the direct transfer function  $w_{kk}(s)$  of the  $k$ th channel and the transfer functions of all cross-connections leading to the  $k$ th channel from all the remaining channels become zeros. Analogously, the equality to zero of all elements of the  $r$ th column of  $W(s)$  means that for  $s = z_i$ , both the direct transfer function  $w_{rr}(s)$  of the  $r$ th channel and the transfer functions of all cross-connections leading from the  $r$ th channel to all the remaining channels become zeros. This situation may readily be expanded to the case of local zero of rank  $k$ . Thus, if, for  $s = z_i$ , the elements of any  $k$  rows or any  $k$  columns of  $W(s)$  become zeros, then  $z_i$  is the local zero of rank  $k$ . At this point, however, a natural question arises of whether local zeros of the matrix  $W(s)$  exist which reduce its normal rank but do not have the above simple explanation and, if such zeros, then what is their number?

A sufficiently definite answer to that question is obtained in the following subsections, and here we shall try to establish a link between the introduced notions of the open-loop MIMO system poles and zeros, and the determinant of  $W(s)$ . It is easy to see that both the absolute and local zeros of  $W(s)$  make  $\det W(s)$  vanishing, since the determinants of the zero matrices as well as of the singular matrices identically equal zero. Besides, from the standard rules of calculating the determinants of matrices (Gantmacher 1964; Bellman 1970), we have that if some elements of  $W(s)$  tend to infinity, then the determinant  $\det W(s)$  also tends to infinity. In other words, the poles of  $W(s)$  are the poles of  $\det W(s)$ . Based on this, we can represent  $\det W(s)$  as a quotient of two polynomials in  $s$ :

$$\det W(s) = \frac{Z(s)}{P(s)} \quad (1.12)$$

and call the *zeros* of  $W(s)$  the roots of the equation

$$Z(s) = 0 \quad (1.13)$$

and the *poles* of  $W(s)$  the roots of the equation

$$P(s) = 0. \quad (1.14)$$

Let us denote the degrees of polynomials  $Z(s)$  and  $P(s)$  as  $m$  and  $n$ , respectively, where, in practice,  $m \leq n$ . We shall call  $Z(s)$  the *zeros polynomial* and  $P(s)$  the *poles polynomial*, or the *characteristic polynomial*, of the open-loop MIMO system.

Strictly speaking, the given heuristic definition of the zeros and poles of  $W(s)$  as the roots of Equations (1.13) and (1.14), which are obtained from Equation (1.12), is only valid if the polynomials  $Z(s)$  and  $P(s)$  do not have coincident roots.<sup>4</sup> The rigorous determination of the zeros and poles polynomials  $Z(s)$  and  $P(s)$  can be accomplished via the Smith-McMillan canonical form (Kailath 1980).<sup>5</sup> Besides, there exists another important detail concerning the definition of the MIMO system poles with the help of Equation (1.14), which deserves special attention and will be discussed in Remark 1.6.

Based on the introduced notions of the open-loop MIMO system absolute poles and zeros, we can generally write down for the matrix  $W(s)$  the following expression:

$$W(s) = \frac{\alpha(s)}{\beta(s)} W_1(s). \quad (1.15)$$

where  $\alpha(s)$  and  $\beta(s)$  represent scalar polynomials of order  $m_0$  and  $n_0$ , whose roots are absolute zeros and poles of  $W(s)$ . Here, the matrix  $W_1(s)$  in Equation (1.15) must have rank  $N$  at the absolute zeros  $z_i$  and poles  $p_i$ . Substituting Equation (1.15) into Equation (1.12) and taking into account the rule of multiplying the determinant by a scalar number yields

$$\det W(s) = \frac{[\alpha(s)]^N}{[\beta(s)]^N} \det W_1(s) = \frac{[\alpha(s)]^N Z_1(s)}{[\beta(s)]^N P_1(s)}, \quad (1.16)$$

from which it follows that *all absolute zeros and poles of the open-loop MIMO system have the algebraic multiplicity  $N$*  (this is another, equivalent, definition of absolute zeros and poles). Returning to the definition of the open-loop MIMO system poles and summarizing, we can finally formulate the following:

– *the absolute pole of  $W(s)$  is the pole whose algebraic multiplicity, considering the latter as that of the root of Equation (1.14), and geometric multiplicity, as the rank of the residue matrix in Equation (1.7), coincide and are equal to the number of channels  $N$ .*

This notion, as well as the notion of absolute zero, will be very useful when studying properties of multivariable root loci and MIMO systems performance (see Section 1.6 and Chapter 2).

### 1.2.2.2 Closed-loop MIMO systems

Let us first consider, as in the previous part, the SISO system of Figure 1.2. The closed-loop transfer functions of that system with respect to output and error signals are:

$$\Phi(s) = \frac{W(s)}{1 + W(s)} = \frac{M(s)}{D(s) + M(s)} \quad (1.17)$$

$$\Phi_\varepsilon(s) = \frac{1}{1 + W(s)} = \frac{D(s)}{D(s) + M(s)}. \quad (1.18)$$

<sup>4</sup> If polynomials  $P(s)$  and  $Z(s)$  do have common roots (i.e. coincident *zeros* and *poles*), and they are cancelled in Equation (1.12), then there always exists a danger that the mentioned zeros and poles correspond to *different directions* of the MIMO system (see Subsection 1.2.3).

<sup>5</sup> The Smith-McMillan canonical form is discussed in Remark 1.6.

From here, we can see that the zeros of the open-loop and closed-loop systems [the zeros of the transfer functions  $W(s)$  and  $\Phi(s)$ ] coincide, and the zeros of the transfer function with respect to error (the sensitivity function)  $\Phi_\varepsilon(s)$  coincide with the poles of the open-loop system. The last fact is very significant when analyzing the accuracy of control systems subjected to slowly changing deterministic signals (see Chapter 2).

The expression  $1 + W(s)$  is usually called the *return difference* of the SISO system<sup>6</sup> and the closed-loop poles are zeros of the equation

$$1 + W(s) = \frac{D(s) + M(s)}{D(s)} = 0, \quad (1.19)$$

i.e. are the roots of the equation

$$D(s) + M(s) = 0. \quad (1.20)$$

Now let us proceed to MIMO systems. From the closed-loop transfer matrix with respect to output (complimentary sensitivity function)  $\Phi(s)$  [Equation (1.3)]:

$$\Phi(s) = [I + W(s)]^{-1} W(s) = W(s) [I + W(s)]^{-1}, \quad (1.21)$$

we can immediately notice that if a complex number  $z_i$  is an *absolute zero* of the open-loop MIMO system, i.e. at  $s = z_i$ , the matrix  $W(s)$  vanishes, then it is also the absolute zero of the closed-loop MIMO system. Further, based on the well known *Silvester's law of degeneracy*,<sup>7</sup> we have that the local zeros of  $W(s)$  (which drop the rank of the latter) are also the local zeros of  $\Phi(s)$ . Hence, quite similarly to the SISO case, the zeros of the open-loop and closed-loop transfer matrices  $W(s)$  and  $\Phi(s)$  coincide.

The corresponding result for the closed-loop transfer matrix with respect to the error signal (sensitivity function)  $\Phi_\varepsilon(s)$  [Equation (1.4)]:

$$\Phi_\varepsilon(s) = [I + W(s)]^{-1} \quad (1.22)$$

may be obtained quite easily if we remember that the inverse matrix in the right-hand part of that expression is found as follows:

$$[I + W(s)]^{-1} = \frac{1}{\det[I + W(s)]} \text{Adj}([I + W(s)]), \quad (1.23)$$

where  $\text{Adj}(\cdot)$  denotes the *adjoint* matrix formed from the initial matrix by replacing all its elements by their cofactors and by subsequent transposing. By analogy with the SISO case, in the MIMO case, the matrix  $I + W(s)$  is called the *return difference* matrix, and its determinant is equal to

$$\det[I + W(s)] = \det[I + W(\infty)] \frac{P_{cl}(s)}{P(s)}, \quad (1.24)$$

<sup>6</sup> The origin of the term *return difference*, introduced by Bode, is due to the fact that if we break the closed-loop system with unit negative feedback at an arbitrary point and inject at that point some signal  $y(s)$ , then the difference between that signal and the signal  $-W(s)y(s)$  returning through the feedback loop to the break point is equal to  $[1 + W(s)]y(s)$ .

<sup>7</sup> That law states that the degeneracy of the product of two matrices is at least as great as the degeneracy of either matrix and, at most, as great as the sum of degeneracies of the matrices (Derusso *et al.* 1965).

where  $P(s)$  and  $P_{cl}(s)$  are the *characteristic polynomials* of the open-loop and closed-loop MIMO system, respectively (Postlethwaite and MacFarlane 1979). The constant matrix  $W(\infty)$  in Equation (1.24) coincides with  $D$  [Equations (1.7) and (1.9)], and differs from the zero matrix under indicated conditions there.<sup>8</sup> Substituting Equation (1.24) into Equation (1.23) and then into Equation (1.4), we obtain for  $\Phi_\varepsilon(s)$

$$\Phi_\varepsilon(s) = \frac{P(s)}{\det[I + W(\infty)]P_{cl}(s)} \text{Adj}([I + W(s)]). \quad (1.25)$$

From Equation (1.25) it ensues that the open-loop MIMO system poles, i.e. the roots of the characteristic polynomial  $P(s)$ , are, as in the SISO case, the zeros of the closed-loop transfer matrix  $\Phi_\varepsilon(s)$ , where the absolute poles of  $W(s)$  become the absolute zeros of  $\Phi_\varepsilon(s)$ .<sup>9</sup>

Thus, we have ascertained that zeros of open-loop and closed-loop MIMO systems are related just as zeros of open-loop and closed-loop SISO systems. We can state once more that SISO systems are a special case of MIMO systems, when  $N = 1$ .

### 1.2.3 Spectral representation of transfer matrices: characteristic transfer functions and canonical basis

The significant notions of poles and zeros of linear square MIMO systems discussed in the preceding sections form the necessary basis on which the frequency-domain multivariable control theory is built. At the same time, we have not yet succeeded in understanding the geometrical and structural properties of multivariable control systems and in establishing links between frequency-domain representations of SISO and MIMO systems. Now, we proceed to solving that task. Note also that, speaking about structural properties of MIMO systems, we shall mean both the ‘internal’ features ensuing from the geometrical properties of linear algebraic operators acting in finite-dimensional Hilbert spaces and the ‘external’ features depending, first of all, on the technical characteristics of MIMO systems (though, ultimately, all these features and characteristics are inseparably linked).

#### 1.2.3.1 Open-loop MIMO systems

Equations (1.1)–(1.4) describe the behaviour of the closed-loop MIMO system of Figure 1.1 with respect to a *natural* coordinate system (natural basis) formed by a set of  $N$  *orthonormal* unit vectors  $e_i$  ( $i = 1, 2, \dots, N$ ), where the  $k$ th component of  $e_k$  is unity and all other components are zero. The  $\varphi_i(s)$ ,  $f_i(s)$  and  $\varepsilon_i(s)$  coordinates of the vectors  $\varphi(s)$ ,  $f(s)$  and  $\varepsilon(s)$  with respect to that basis are just the Laplace transforms of the actual input, output and error signals, respectively, in the  $i$ th separate channel of the system. Formally, the transfer matrices  $W(s)$ ,  $\Phi(s)$  and  $\Phi_\varepsilon(s)$  may be regarded as some linear operators mapping an  $N$ -dimensional complex space  $\mathbb{C}^N$  of the input vectors  $\varphi(s)$  into the corresponding spaces of the output or error vectors  $f(s)$  or

<sup>8</sup> Later on, we shall omit the case of the *singular* matrix  $[I + W(\infty)]$ , which has no practical significance.

<sup>9</sup> Strictly speaking, inherent only in the MIMO systems, situations in which some poles of the open-loop system do not change after closing the feedback loop and coincide with the corresponding poles of the closed-loop system are not included here. In such cases, the coincident roots of  $P_{cl}(s)$  and  $P(s)$  in Equation (1.25) must be cancelled, and they should not be regarded as zeros of the transfer function matrix  $\Phi_\varepsilon(s)$ . That issue will be considered in more detail when studying the properties of multivariable root loci in Section 1.5 and Remark 1.6.

$\varepsilon(s)$ . This suggests using the mathematical tools of the theory of linear algebraic operators and functional analysis for the study of linear MIMO systems (Strang 1976; Vulich 1967; Danford and Schwarts 1962). It is known that internal, structural properties of linear algebraic operators exhibit much more saliently, not in the natural, but in some other, specially chosen coordinate systems (Porter 1966; Derusso *et al.* 1965; Gantmacher 1964). In particular, that refers to the so-called *canonical* basis formed by the *normalized* (i.e. having unit length) *characteristic vectors* of the matrix operator, with respect to which the latter has diagonal form with the *characteristic values* (*eigenvalues*) on the principal diagonal. Since the  $w_{kr}(s)$  elements of the open-loop transfer matrix  $W(s)$  are scalar proper rational functions in complex variable  $s$ , the eigenvalues  $q_i(s)$  of  $W(s)$ , i.e. the roots of the equation

$$\det[qI - W(s)] = 0 \tag{1.26}$$

are also functions of variable  $s$ . These complex functions  $q_i(s)$  are called *characteristic transfer functions* (CTF) of the open-loop MIMO system (MacFarlane and Belletrutti 1970; Postlethwaite and MacFarlane 1979).<sup>10</sup>

If we assume, for the sake of simplicity, that all CTFs  $q_i(s)$  ( $i = 1, 2, \dots, N$ ) are *distinct*,<sup>11</sup> then the corresponding normalized eigenvectors  $c_i(s)$  ( $|c_i(s)| = 1$ ) of  $W(s)$  are *linearly independent*, and constitute the basis of the  $N$ -dimensional complex space  $\mathbb{C}^N$  (recall that  $\varphi(s)$ ,  $f(s)$  and  $\varepsilon(s)$  belong to that space). We call that basis the *canonical basis* of the open-loop MIMO system.

Having formed from  $c_i(s)$ , the *modal matrix*  $C(s) = [c_1(s) \ c_2(s) \ \dots \ c_N(s)]$  [the latter is nonsingular owing to the assumption of linear independency of  $c_i(s)$ ], we can represent the matrix  $W(s)$  by the *similarity transformation* in the following form:

$$W(s) = C(s) \text{diag}\{q_i(s)\}C^{-1}(s), \tag{1.27}$$

where  $\text{diag}\{q_i(s)\}$  denotes the diagonal matrix with the elements  $q_i(s)$  on the principal diagonal.

Before proceeding, let us consider briefly some mathematical notions and pre-requisites which are inherent in complex Hilbert spaces and which are necessary for the further exposition. The first of these notions is the *scalar* (or *inner*) product, which is written for two arbitrary  $N$ -dimensional column vectors  $x$  and  $y$  with components  $x_i$  and  $y_i$  as  $\langle x, y \rangle$ , and is defined as

$$\langle x, y \rangle = \tilde{x}^T y = y^T \tilde{x} = \sum_{i=1}^N \tilde{x}_i y_i, \tag{1.28}$$

where  $^T$  is the symbol of transposition, and the wavy line above denotes the complex conjugation (Derusso *et al.* 1965). Based on Equation (1.28), we can represent the Euclidean norm (length) of the vector  $x$  as

$$|x| = \sqrt{\langle x, x \rangle} \tag{1.29}$$

<sup>10</sup> We give here rather a simplified interpretation of characteristic transfer functions, which is quite enough for engineering applications. In essence, the reader may assume that  $q_i(s)$  are found for fixed values  $s = \text{const}$ , for which  $W(s)$  reduces to a usual numerical matrix with complex elements (see also Remark 1.2).

<sup>11</sup> When accomplishing an engineering design, this may always be achieved by arbitrary small perturbations of the MIMO system parameters within the accuracy of their specifications.

and, for *real* vectors  $x$  and  $y$ , we can define the angle  $\theta$  between them by the equation

$$\langle x, y \rangle = |x| |y| \cos \theta. \tag{1.30}$$

In particular, two vectors  $x$  and  $y$  are said to be *orthogonal* if  $\langle x, y \rangle = 0$  and *collinear* if  $\langle x, y \rangle = \pm |x| |y|$ . Note that the complex conjugation of components of  $x$  in Equation (1.28) is needed to provide the coincidence of the usual norm and the norm specified by scalar product for complex-valued vectors [Equation (1.29)]. In the mathematical and technical literature, one can encounter a definition of scalar product in which the complex conjugate components of the second, instead of the first, vector in Equation (1.28) are taken. This should not introduce ambiguity, as, in principle, it is an equivalent definition of the scalar product. For our aims, it is more convenient to introduce the scalar product in the form of Equation (1.28), and the reader should remember this in what follows. Now, as the product  $\langle x, y \rangle$  in complex space  $\mathbb{C}^N$  is not always real-valued, in general, we are not able to introduce the notion of an angle between two vectors  $x$  and  $y$ . Nevertheless, the conditions  $\langle x, y \rangle = 0$  and  $\langle x, y \rangle = \pm |x| |y|$  determine, as before, orthogonality and collinearity of any two vectors, and these two notions turn out to be as useful as in the real space.

Along with the notion of a basis in  $\mathbb{C}^N$  (as such a basis may serve any set of  $N$  linearly independent vectors in  $\mathbb{C}^N$ ), we also need the notion of a *dual* (or *reciprocal*) basis, which is defined as follows. Let the set of  $N$  normalized vectors  $c_i$  constitute a basis of  $\mathbb{C}^N$ , i.e. any vector  $y$  in  $\mathbb{C}^N$  may be represented as a linear combination of the form

$$y = \sum_{i=1}^N \alpha_i c_i, \tag{1.31}$$

where the  $\alpha_i$  scalars are the coordinates of  $y$  in the basis  $\{c_1, c_2, \dots, c_N\}$ . Let us define a set  $\{c_1^+, c_2^+, \dots, c_N^+\}$  of  $N$  vectors such that

$$\langle c_i, c_j^+ \rangle = \delta_{ij} \quad (i, j = 1, 2, \dots, N), \tag{1.32}$$

where  $\delta_{ij}$  is the symbol of Kronecker ( $\delta_{ij} = 1$  for  $i = j$ , and  $\delta_{ij} = 0$  for  $i \neq j$ ) (Derusso *et al.* 1965). It is easy to show that the vectors  $c_1^+, c_2^+, \dots, c_N^+$  in Equation (1.32) are linearly independent and also constitute a basis in  $\mathbb{C}^N$ . That basis is said to be dual to the basis  $\{c_1, c_2, \dots, c_N\}$ . From the way of finding the dual basis [Equation (1.32)], where the axis  $c_i^+$  dual to  $c_i$  must be orthogonal to all other axes  $c_k$  ( $k \neq i$ ), it follows that orthonormal bases always coincide with their dual bases. The major benefit of the dual basis is that the  $\alpha_i$  coordinates of  $y$  in the basis  $\{c_1, c_2, \dots, c_N\}$  in Equation (1.31) are expressed as<sup>12</sup>

$$\alpha_i = \langle c_i^+, y \rangle \tag{1.33}$$

and this feature of the dual basis proves to be extremely useful when studying geometrical properties of linear MIMO systems. Note that if we denote by  $C$  the matrix composed of the normalized vectors  $\{c_1, c_2, \dots, c_N\}$ , the rows of the inverse matrix  $C^{-1}$  are complex conjugate to the reciprocal basis axes (given the initial basis, this is, in fact, a way to calculate numerically the dual basis) (Derusso *et al.* 1965; Gasparyan 1976).

<sup>12</sup> We suggest that the reader checks this as an exercise.

The last notion, needed in the future, is based on the so-called *dyadic* designations (Porter 1966). To proceed, we have to impart some additional shading to what we mean by the symbols  $\langle$  and  $\rangle$  in Equation (1.28). In the following, we shall formally attribute the symbol  $\rangle$  to a *column* vector, i.e. the designation  $y \rangle$  we shall consider identical to the designation  $y$ . Similarly, the symbol  $\langle$  will be attributed to a complex conjugate *row* vector, i.e. the designation  $\langle x$  will be regarded as equivalent to  $\tilde{x}^T$ . Then, preserving the usual definition of scalar product [Equation (1.28)], we can impart a certain sense to the expression  $y \rangle \langle x$ . Now, in accordance with the conventional rules, multiplying the column vector  $y \rangle$  by the complex conjugate row vector  $\langle x$  yields a square matrix  $S$ :

$$S = y \rangle \langle x. \tag{1.34}$$

Multiplying that matrix by an arbitrary vector  $z$  (or by  $z \rangle$ , which is the same) yields

$$v = Sz = (y \rangle \langle x)z \rangle = y \rangle \underbrace{\langle x, z \rangle}_{\alpha} = \alpha y. \tag{1.35}$$

From Equation (1.35), it is clear that the range of values of  $S$  is one-dimensional, and is a linear subspace of  $\mathbb{C}^N$  generated (spanned) by the vector  $y$ . In other words, the  $S$  matrix transforms any vector  $z$  in  $\mathbb{C}^N$  to a vector which is always directed along  $y$ . Also, those vectors  $z$  that are perpendicular to  $x$  are transformed to a zero vector (because, in that case, the scalar  $\alpha = \langle x, z \rangle$  equals zero). The matrix  $S$  represented in Equation (1.34) is said to be a *dyad of rank one*.

Given a normalized basis  $\{c_1, c_2, \dots, c_N\}$  of  $\mathbb{C}^N$  and a set  $\{\gamma_1, \gamma_2, \dots, \gamma_N\}$  of  $N$  linearly independent (but not necessarily normalized) vectors, the matrix  $S$  represented as

$$S = \sum_{i=1}^N c_i \rangle \langle \gamma_i, \tag{1.36}$$

i.e. as a sum of  $N$  dyads of rank one, is said to be a *dyad of rank  $N$* . Its range of values is, obviously, the whole space  $\mathbb{C}^N$ . Among all possible dyads composed via the basis  $\{c_1, c_2, \dots, c_N\}$  [Equation (1.36)], the most significant is the dyad for which the vectors  $\gamma_1, \gamma_2, \dots, \gamma_N$  coincide with the dual basis  $c_1^+, c_2^+, \dots, c_N^+$ . It is easy to show, in that case, that the *identity operator*  $I$  in  $\mathbb{C}^N$  may be represented through the dyads  $c_i \rangle \langle c_i^+$  of rank one as a sum:

$$I = \sum_{i=1}^N c_i \rangle \langle c_i^+. \tag{1.37}$$

Further, which is far more important, if a square matrix  $A$  is a matrix of *simple structure*, i.e. possesses the full set of  $N$  linearly independent eigenvectors  $c_i$ , then it can be represented not only by the similarity transformation, but also in the form of a *spectral decomposition*, as a sum of  $N$  dyads:

$$A = \sum_{i=1}^N c_i \rangle \lambda_i \langle c_i^+, \tag{1.38}$$

where  $\lambda_i$  are the eigenvalues of the matrix  $A$ .

Now, we have proceeded enough in the understanding of the geometrical structure of linear operators in finite-dimensional Hilbert spaces and can use the corresponding apparatus for investigating properties of the open-loop MIMO system. Based on Equation (1.38) and remembering that all CTFs  $q_i(s)$  are assumed distinct,<sup>13</sup> we can write down the open-loop transfer matrix  $W(s)$  of the MIMO system in the form of the spectral decomposition:

$$W(s) = \sum_{i=1}^N c_i(s) > q_i(s) < c_i^+(s). \quad (1.39)$$

The spectral representation in Equation (1.39) permits a visual geometric interpretation of the internal structure of the open-loop and, as will be seen later, closed-loop MIMO systems. The CTFs  $q_i(s)$  may be regarded as transfer functions of some abstract, fictitious one-dimensional ‘characteristic’ systems, in which each characteristic system ‘acts’ in  $\mathbb{C}^N$  along one axis  $c_i(s)$  of the open-loop MIMO system canonical basis. For any  $s$ , the vector  $f(s)$  is represented, based on Equation (1.39) and Figure 1.1, as

$$f(s) = W(s)\varepsilon(s) = \left[ \sum_{i=1}^N c_i(s) > q_i(s) < c_i^+(s) \right] \varepsilon(s) = \sum_{i=1}^N [q_i(s)\beta_i(s)]c_i(s), \quad (1.40)$$

where

$$\beta_i(s) = \langle c_i^+(s), \varepsilon(s) \rangle, \quad i = 1, 2, \dots, N \quad (1.41)$$

are the projections of  $\varepsilon(s)$  on  $c_i(s)$ , i.e. as a linear combination of ‘responses’ of the open-loop MIMO system along the canonical basis axes.

On the other hand, having Equation (1.37) for the identity operator  $I$  in  $\mathbb{C}^N$ , we are able to write down the expansion of the output vector  $f(s)$  along the canonical axes in the form

$$f(s) = If(s) = \left[ \sum_{i=1}^N c_i > < c_i^+ \right] f(s) = \sum_{i=1}^N \alpha_i(s)c_i(s), \quad (1.42)$$

where

$$\alpha_i(s) = \langle c_i^+(s), f(s) \rangle, \quad i = 1, 2, \dots, N \quad (1.43)$$

are the coordinates of  $f(s)$  along the axes  $c_i(s)$ . Comparing Equations (1.40)–(1.43) yields

$$\alpha_i(s) = q_i(s)\beta_i(s), \quad i = 1, 2, \dots, N, \quad (1.44)$$

from which we come to the conclusion that the projection  $\alpha_i(s)$  of the output vector  $f(s)$  on any canonical basis axis  $c_i(s)$  is equal to the corresponding projection  $\beta_i(s)$  of the error vector  $\varepsilon(s)$  multiplied by the CTF  $q_i(s)$  of the one-dimensional characteristic system acting along that very axis  $c_i(s)$ . If the error vector  $\varepsilon(s)$  is directed along one, say the  $k$ th, canonical basis axis,

<sup>13</sup> The matrices of the *simple structure* can always be brought to diagonal form via the similarity transformation. The assumption of distinct CTFs guarantees this possibility, but is not necessary. For example, *normal* matrices with multiple eigenvalues can always be brought to diagonal form. More strictly, a square matrix can be brought to diagonal form in a certain basis if the *algebraic* and *geometric* multiplicities of all eigenvalues coincide.

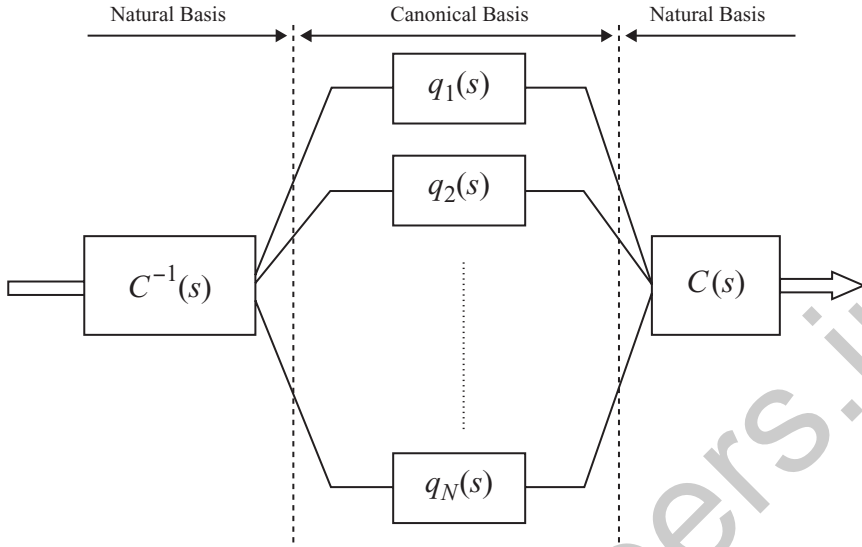


**Figure 1.3** Representation of the open-loop MIMO system via the similarity transformation.

i.e. if  $\varepsilon(s) = \beta_k(s)c_k(s)$ , then, based on the properties of the dual basis [Equation (1.32)], all  $\beta_i(s)$  ( $i \neq k$ ) in Equation (1.41) are identically equal to zero and the output vector

$$f(s) = q_k(s)\beta_k(s)c_k(s) \quad (1.45)$$

is also directed along the same axis  $c_k(s)$ . In other words, the axes of the open-loop MIMO system canonical basis determine those  $N$  directions in complex space  $\mathbb{C}^N$  along which the system acts as a certain fictitious one-dimensional system, and only ‘stretches’ or ‘squeezes’ the input signals.<sup>14</sup> The block diagrams in Figures 1.3 and 1.4, which represent in graphical form Equations (1.27) and (1.39)–(1.44), schematically illustrate all these statements.

It must be noted that both forms of the canonical representation of transfer matrices – by means of similarity transformation [Equation (1.27)] and dyadic notation [Equation (1.39)] – are equivalent, and the reader should always remember this. The first representation seems to be useful and convenient due to its compactness for some general derivations and proofs, and the second one, possibly, gives the reader a better intuitive or physical feeling for the geometrical structure and behaviour of the MIMO system.

We already have enough knowledge to gain a deeper insight into the notions of poles and zeros of MIMO control systems. Based on Equation (1.27), the determinant of the open-loop transfer matrix  $W(s)$  is equal to

$$\begin{aligned} \det W(s) &= \frac{Z(s)}{P(s)} = \det [C(s)\text{diag}\{q_i(s)\}C^{-1}(s)] \\ &= \underbrace{\det C(s) \det C^{-1}(s)}_I \det[\text{diag}\{q_i(s)\}] = \prod_{i=1}^N q_i(s), \end{aligned} \quad (1.46)$$

<sup>14</sup> It is worth noting here that we have not yet spoken about such important geometrical properties of the canonical basis as *orthogonality* or *skewness* of axes; as we shall see in the next chapters, it is difficult to overestimate, from the MIMO system performance viewpoint, the significance of these features.

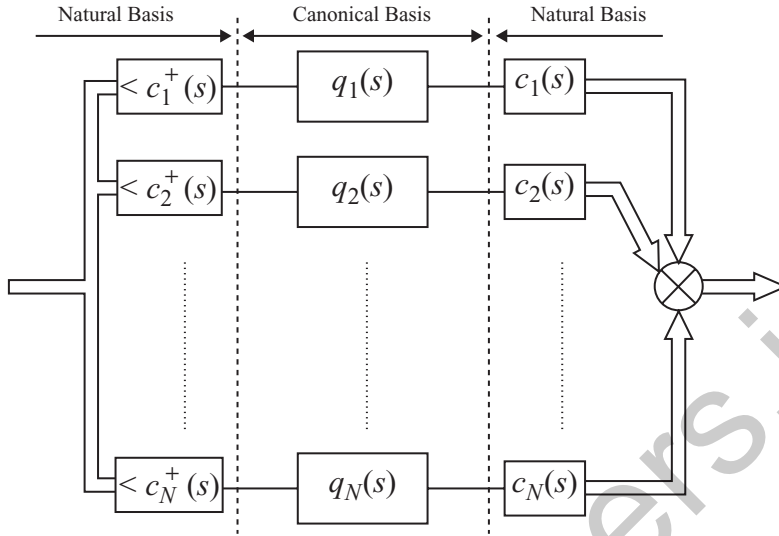


**Figure 1.4** Spectral representation of the open-loop MIMO system by means of dyads.

where it is taken into account that the product of determinants of a matrix and its inverse is equal to unity, and the determinant of a diagonal matrix is equal to the product of diagonal elements.

Thus, we have obtained that poles and zeros of the open-loop MIMO system coincide with poles and zeros of all open-loop characteristic systems associated with the MIMO system. Moreover, starting from Equation (1.15) and recalling that if a matrix is multiplied by a scalar, then all eigenvalues of that matrix are multiplied by the same scalar, we come to the important conclusion that the *absolute zeros and poles of the open-loop MIMO system are common poles and zeros of all CTFs  $q_i(s)$* . Further, if a complex number  $z$  is a local zero of rank  $k$  ( $1 \leq k \leq N$ ), then that number must be the zero of any  $k$  CTFs  $q_i(s)$ . It is easy to ascertain that at the local zero of rank  $k$ , the rank of  $W(s)$  is equal to  $N - k$ , since the rank of each dyad in spectral representation [Equation (1.39)] is unity and each dyad projects complex space  $\mathbb{C}^N$  onto one of the canonical basis axes. Therefore, if  $k$  terms in Equation (1.39) are zero, then the remaining  $N - k$  terms define  $N - k$  basis axes, and the matrix  $W(s)|_{s=z}$  itself is of rank  $N - k$ . Eventually, we realize that evaluating zeros and poles of the open-loop MIMO system with the help of Equations (1.12)–(1.14), i.e. based on the computation of the determinant  $\det W(s)$ , may bring about the incorrect cancellation of poles and zeros of characteristic systems which, in fact, act along *different* axes of the canonical basis.

In conclusion, note that, for many classes of MIMO systems widespread in practice, the CTFs  $q_i(s)$  can be expressed as a quotient of two polynomials  $M_i(s)$  and  $D_i(s)$ , i.e. in the form

$$q_i(s) = \frac{M_i(s)}{D_i(s)}, \quad i = 1, 2, \dots, N, \quad (1.47)$$

where  $M_i(s)$  and  $D_i(s)$  are defined analytically for any number  $N$  of separate channels. This fact plays an extremely important role, as it allows us to rigorously select zeros and poles [the roots of the equations  $M_i(s) = 0$  and  $D_i(s) = 0$ ] of each *separate* one-dimensional characteristic

system. We accentuate here that Equation (1.46) indicates only that the roots of zeros and poles polynomials  $Z(s)$  and  $P(s)$  taken together are equal to zeros and poles of the CTFs  $q_i(s)$ . Generally, we do not have any specific information (except for the conclusion concerning absolute zeros and poles) about the distribution of the MIMO system poles and zeros among individual characteristic systems. As for the above-mentioned prevailing classes of MIMO systems, and to those classes belong the so-called uniform, circulant, anticirculant and some other systems, we can immediately write down for their zeros and poles polynomials

$$Z(s) = \prod_{i=1}^N M_i(s) = 0, \quad P(s) = \prod_{i=1}^N D_i(s) = 0, \quad (1.48)$$

which, as will be seen in the following, considerably simplifies the analysis of such systems.

Although representation of the CTFs  $q_i(s)$  as a quotient of two polynomials [Equation (1.47)] in the general case is, unfortunately, impossible, sometimes, we shall formally suppose that the CTFs  $q_i(s)$  are of the form in Equation (1.47). It will allow us, without encumbering the presentation, to make a number of statements indicating a close relationship between the stability and performance of SISO and MIMO systems.

### 1.2.3.2 Closed-loop MIMO systems

In this section, we bring to a logical completion the task of describing linear MIMO control systems by means of the CTFs. Substituting the representation of the open-loop transfer matrix  $W(s)$  via the similarity transformation [Equation (1.27)] into the complementary sensitivity function matrix  $\Phi(s)$  [Equation (1.3)] and the sensitivity function matrix  $\Phi_\varepsilon(s)$  [Equation (1.4)], after a number of simple transformations, yields

$$\Phi(s) = C(s) \text{diag} \left\{ \frac{q_i(s)}{1 + q_i(s)} \right\} C^{-1}(s), \quad \Phi_\varepsilon(s) = C(s) \text{diag} \left\{ \frac{1}{1 + q_i(s)} \right\} C^{-1}(s). \quad (1.49)$$

Analogously, substituting the spectral decomposition in Equation (1.39) into Equations (1.3) and (1.4) gives

$$\Phi(s) = \sum_{i=1}^N c_i(s) > \frac{q_i(s)}{1 + q_i(s)} < c_i^+(s), \quad \Phi_\varepsilon(s) = \sum_{i=1}^N c_i(s) > \frac{1}{1 + q_i(s)} < c_i^+(s). \quad (1.50)$$

The examination of these expressions enables us to draw the important conclusion that the modal matrix  $C(s)$  and, consequently, the canonical basis of the closed-loop MIMO system coincide with the modal matrix and canonical basis of the open-loop system. In other words, introducing the unit negative feedback does not change the canonical basis of the system. Moreover, if  $q_i(s) (i = 1, 2, \dots, N)$  are the CTFs of the open-loop MIMO system, then the corresponding CTFs of the closed-loop MIMO system with respect to the output and error

$$\Phi_i(s) = \frac{q_i(s)}{1 + q_i(s)}, \quad \Phi_{\varepsilon i}(s) = \frac{1}{1 + q_i(s)}, \quad i = 1, 2, \dots, N \quad (1.51)$$

are related to  $q_i(s)$  by the very same relationships as the usual transfer functions of open- and closed-loop SISO feedback systems.

As for the geometrical interpretation of the closed-loop MIMO system internal structure, it is entirely inherited, based on Equations (1.50) and (1.39), from the open-loop system. In particular, the output  $f(s)$  and error  $\varepsilon(s)$  vectors of the closed-loop system can be represented as linear combinations of the system ‘responses’ along the canonical basis axes:

$$f(s) = \sum_{i=1}^N [\Phi_i(s) \langle c_i^+(s), \varphi(s) \rangle] c_i(s), \quad \varepsilon(s) = \sum_{i=1}^N [\Phi_{\varepsilon i}(s) \langle c_i^+(s), \varphi(s) \rangle] c_i(s) \tag{1.52}$$

where the CTFs  $\Phi_i(s)$  and  $\Phi_{\varepsilon i}(s)$  are defined by Equation (1.51). Analogously, if the input vector  $\varphi(s)$  is directed along one of the canonical basis axes, only the corresponding closed-loop characteristic system will take part in the MIMO system response, and the output and error vectors will be directed along the same axis. All this is illustrated schematically in Figures 1.5 and 1.6, and the reader can compare these diagrams with those of the open-loop MIMO system in Figures 1.3 and 1.4.

Before proceeding to the stability analysis of the general MIMO system of Figure 1.1, let us summarize some results. We have ascertained, based on the theory of linear algebraic operators, that a set of  $N$  one-dimensional so-called characteristic systems may be associated with an  $N$ -dimensional linear MIMO system.

Each of the characteristic systems acts in  $\mathbb{C}^N$  along one specified direction – the canonical basis axis – and, in  $\mathbb{C}^N$ , in all, there are, assuming no multiple CTFs, just  $N$  such linearly independent directions. If we formally accept that the CTFs  $q_i(s)$  may be represented as a quotient of two polynomials in the form of Equation (1.47), and this is always possible for a great number of practical multivariable systems, then, instead of Equation (1.49), we can write:

$$\Phi(s) = C(s) \text{diag} \left\{ \frac{M_i(s)}{D_i(s) + M_i(s)} \right\} C^{-1}(s), \quad \Phi_{\varepsilon}(s) = C(s) \text{diag} \left\{ \frac{D_i(s)}{D_i(s) + M_i(s)} \right\} C^{-1}(s), \tag{1.53}$$

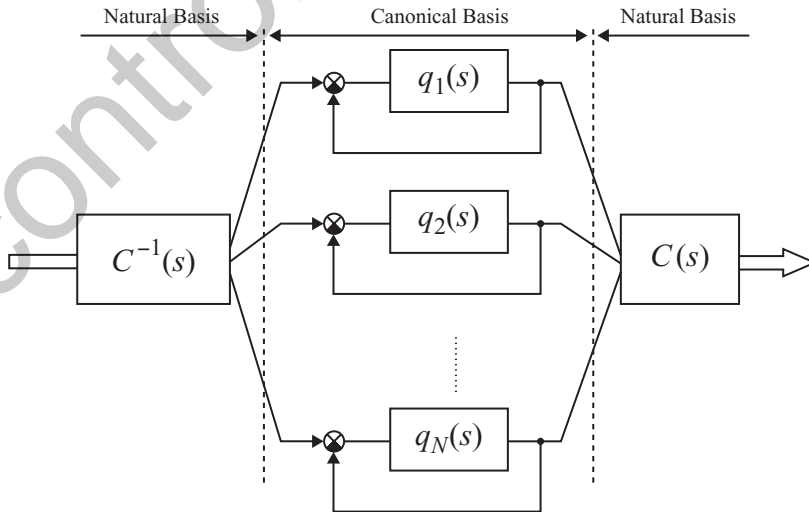


**Figure 1.5** Representation of the closed-loop MIMO system via the similarity transformation.

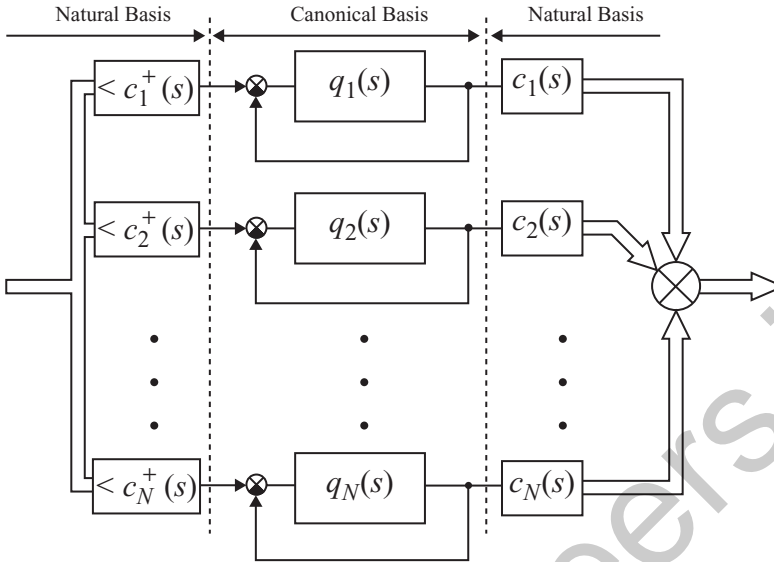


Figure 1.6 Spectral representation of the closed-loop MIMO system by means of dyads.

from which it immediately ensues that the zeros of the complementary sensitivity function matrix  $\Phi(s)$  coincide with *zeros* of the open-loop characteristic systems, i.e. with the roots of the equations  $M_i(s) = 0$ , and the zeros of the sensitivity function matrix  $\Phi_e(s)$  coincide with *poles* of the open-loop characteristic systems, i.e. with the roots of the equations  $D_i(s) = 0$ , where, in both cases,  $i = 1, 2, \dots, N$ . All this indicates a deep internal relationship between dynamical and other properties of a real MIMO system and the corresponding properties of  $N$  fictitious isolated SISO characteristic systems associated with the given MIMO system. We thereby have a necessary basis for extending the fundamental principles of the classical control theory to the multivariable case, and the rest of the textbook is devoted to that task. As we shall see later, many results of the classical theory concerning linear and nonlinear SISO feedback systems may indeed directly be generalized to the MIMO case (i.e. to  $N$ -channel MIMO systems) in such a manner that if we assume  $N = 1$ , then the ‘multidimensional’ methods simply coincide with their conventional ‘one-dimensional’ counterparts. At the same time, in the multivariable case, the *structural features* of MIMO systems are of considerable interest and, in a number of cases, the mentioned features allow a reduction in the analysis and design of a MIMO system to the analysis and design of a single SISO characteristic system, regardless of the actual number  $N$  of separate channels.

### 1.2.4 Stability analysis of general MIMO systems

Earlier, considering the properties of the MIMO system zeros and poles, we used Equation (1.24), which is basic for analyzing the stability of the closed-loop MIMO system. Let us write that equation once again:

$$\det[I + W(s)] = \det[I + W(\infty)] \frac{P_{cl}(s)}{P(s)}, \quad (1.54)$$

where  $P(s)$  and  $P_{cl}(s)$  are the characteristic polynomials of the open-loop and closed-loop MIMO system. As follows from Equation (1.54), the poles of the closed-loop MIMO system, i.e. the roots of the characteristic polynomial  $P_{cl}(s)$ , coincide with zeros of the determinant of the return difference matrix  $I + W(s)$ . Therefore, for the stability of the linear MIMO system in Figure 1.1, which, recall, is assumed controllable and observable, it is necessary and sufficient that the roots of the equation

$$\det[I + W(s)] = 0 \tag{1.55}$$

lie in the open left half-plane of the complex plane (Postlethwaite and MacFarlane 1979). Further, for simplicity, we shall call Equation (1.55) the characteristic equation of the closed-loop MIMO system. Using the canonical representation of the transfer matrix  $W(s)$  via similarity transformation [Equation (1.27)], Equation (1.55) may be reduced to the following form:

$$\det[C(s) \text{diag}\{1 + q_i(s)\} C^{-1}(s)] = 0, \tag{1.56}$$

which immediately yields

$$\det[I + W(s)] = \underbrace{\det C(s) \det C^{-1}(s)}_I \det[\text{diag}\{1 + q_i(s)\}] = \prod_{i=1}^N [1 + q_i(s)] = 0. \tag{1.57}$$

Assuming that the CTFs  $q_i(s)$  may be represented as a quotient of two polynomials  $M_i(s)$  and  $D_i(s)$  [Equation (1.47)], instead of Equation (1.57), we can also write

$$\det[I + W(s)] = \prod_{i=1}^N [1 + q_i(s)] = \frac{\prod_{i=1}^N [D_i(s) + M_i(s)]}{\prod_{i=1}^N D_i(s)} = 0. \tag{1.58}$$

Equations (1.57) and (1.58) show that the characteristic equation of the  $N$ -dimensional closed-loop MIMO system splits into  $N$  corresponding equations of the one-dimensional characteristic systems

$$1 + q_i(s) = 0, \quad \text{or} \quad D_i(s) + M_i(s) = 0, \quad i = 1, 2, \dots, N. \tag{1.59}$$

This means that the complex plane of the closed-loop MIMO system roots can be regarded as superpositions of  $N$  complex planes of the closed-loop characteristic systems roots.<sup>15</sup> Hence, for the stability of a linear MIMO system, it is necessary and sufficient that all closed-loop characteristic systems be stable. Even if only one of the characteristic systems is on the stability boundary or is unstable, the corresponding equation in Equation (1.59) will have roots on the imaginary axis or in the right half-plane, and then, owing to Equations (1.57) and (1.58), just the same roots will have the closed-loop MIMO system. And, vice versa, in the case of an unstable closed-loop MIMO system, there always exists such an unstable characteristic system

<sup>15</sup> More rigorously, in general, these roots lie on  $N$  different sheets of the Riemann surface (Postlethwaite and MacFarlane 1979).

whose right half-plane roots coincide with the corresponding roots of Equation (1.55). So, we can state that the described approach enables replacing the stability analysis of an  $N$ -channel linear MIMO system by the stability analysis of  $N$  SISO characteristic systems, or, in other words, it reduces an  $N$ -dimensional task to  $N$  one-dimensional tasks.

At this point, before proceeding with our study of the linear MIMO system stability issues and running, to a certain extent, ahead, note a specific and very significant feature of characteristic systems, which has no analogues in the classical control theory. As the CTFs  $q_i(s)$  are transfer functions of abstract SISO systems with, in general, complex parameters, the location of zeros and poles of each single open- and closed-loop characteristic system is not necessarily symmetric with respect to the real axis of the complex plane, which takes place in the case of usual SISO systems. At the same time, the entire set of the open- and closed-loop MIMO system zeros and poles must be symmetric with respect to the real axis, as all coefficients of the entries of  $W(s)$ ,  $\Phi(s)$  and  $\Phi_\varepsilon(s)$  are real-valued numbers. This means that for any characteristic system with a nonsymmetrical zeros and poles distribution, there always exists a 'complex conjugate' characteristic system whose distribution of zeros and poles can be obtained from the previous by mirror mapping with respect to the real axis.

**Example 1.1** When introducing any theory, the well chosen examples are very important, and it is difficult to overestimate the significance of such examples. According to a prominent mathematician, (note, the mathematician!) I. M. Gelfand, 'the theories come and go, but the examples stay'. We shall try to explain various theoretical concepts with the help of different examples, but some of the central examples in the textbook will be the indirect guidance (tracking) systems of orbital astronomic telescopes. This is not only because the author worked for many years in the area of development and manufacture of such systems. First of all, this is because the diversity and 'flexibility' of structures and schemes of indirect guidance systems allow us to visually and readily illustrate, by means of a few examples taken from the practice systems, the very miscellaneous topics in the theory of linear and nonlinear MIMO control systems. The kinematic scheme of an indirect guidance system of the telescope (i.e. of the system in which guiding is accomplished with the help of two reference stars<sup>16</sup>) is depicted in Figure 1.7. In such systems, the sensitivity axes of the measuring devices (in this case, the stellar sensors) do not coincide with the telescope tracking axes (the axes of the gimbal mount). As a result, in the system, there appear rigid cross-connections among the separate channels (sometimes called *kinematical*), which depend on angles between the explored and reference stars and on some construction factors. These cross-connections are constant for the given mutual location of stars and they change only on passing to another explored star, for which a new pair of suitable reference stars is usually chosen.

The expanded block diagram of that system, for the case of tracking with respect to the telescope's two transverse axes, is given in Figure 1.8.<sup>17</sup> The matrix  $R$  of the rigid cross-connections in Figure 1.8 has the form

$$R = \begin{pmatrix} \cos \alpha_1 & \sin \alpha_1 \\ -\sin \alpha_2 & \cos \alpha_2 \end{pmatrix}, \quad (1.60)$$

<sup>16</sup> The *reference stars* are stars which are noticeably brighter than the surrounding stars and therefore may be used for tracking purposes.

<sup>17</sup> If, for solving scientific (in particular, astronomical) tasks, the tracking around the telescope optical axis is also needed, in the system, the third channel also exists, generally cross-connected with the two previous channels (Gasparyan 1986).

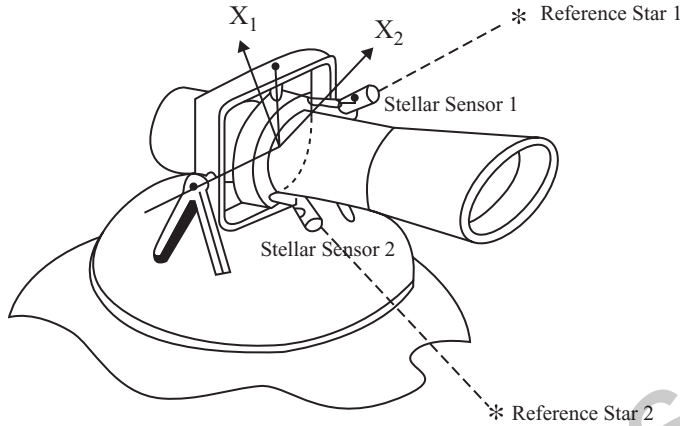


Figure 1.7 Kinematic scheme of the indirect guidance system of the space telescope.

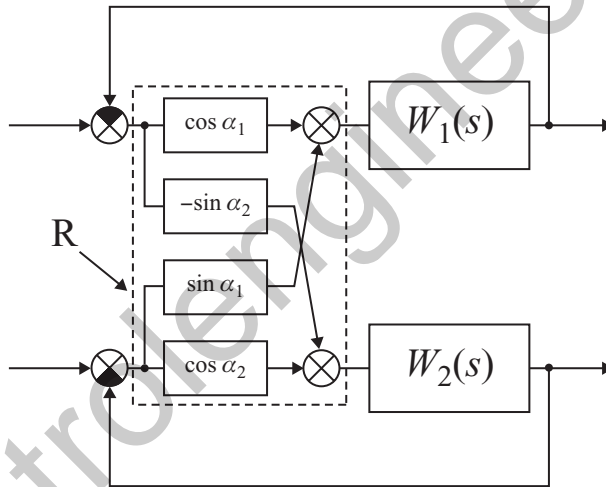
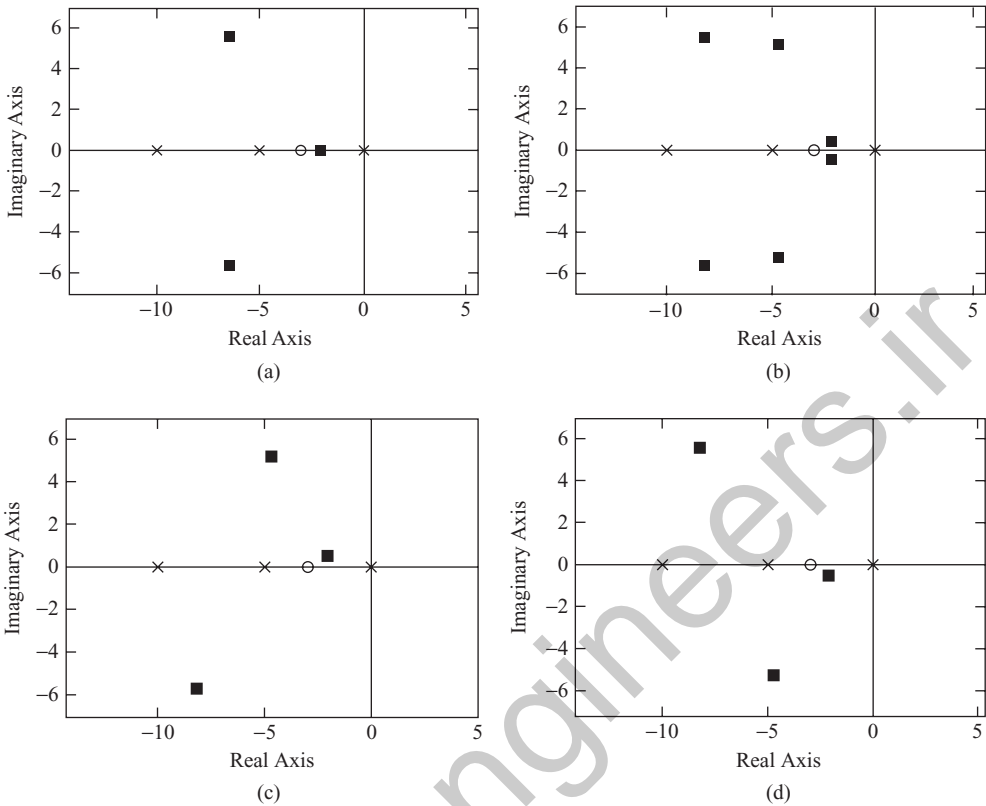


Figure 1.8 Expanded block diagram of the indirect guidance system of Figure 1.7.

where constant angles  $\alpha_1$  and  $\alpha_2$  depend on the above-mentioned factors;  $W_1(s)$  and  $W_2(s)$  are the transfer functions of separate channels of the system.

Note that for  $\alpha_1 = 0$ ,  $\alpha_2 = 0$ , which geometrically corresponds to using the explored star as a reference one, the matrix  $R$  [Equation (1.60)] becomes the unit matrix  $I$ , and the MIMO system of Figure 1.8 splits into two *independent* channels. The above statements about the distribution of the MIMO system zeros and poles are illustrated by the examples of a common SISO system and the two-dimensional system of Figure 1.8 in Figure 1.9. In Figure 1.9, the crosses and circles denote poles and zeros of the open-loop systems, and black squares denote poles of the closed-loop systems. The transfer function of the open-loop SISO system is taken as

$$W(s) = \frac{50(s + 3)}{s(s + 5)(s + 10)}. \quad (1.61)$$



**Figure 1.9** Typical distribution of zeros and poles of SISO and MIMO control systems. (a) One-dimensional system ( $N = 1$ ); (b) two-dimensional system ( $N = 2$ ); (c)  $N = 2$ , the first characteristic system; (d)  $N = 2$ , the second characteristic system.

As for the two-dimensional system, we assume that it has identical transfer functions in the separate channels, which are the same as the transfer function in Equation (1.61), i.e.  $W_1(s) = W_2(s) = W(s)$ , and rigid cross-connections described by a numerical matrix  $R$  [Equation (1.60)] (such MIMO systems, called *uniform*, are considered at length in the next section), where  $\alpha_1 = 30^\circ$ ,  $\alpha_2 = 20^\circ$ . The matrix  $R$  [Equation (1.60)] for these values of angles  $\alpha_1$  and  $\alpha_2$  is equal to

$$R = \begin{pmatrix} 0.866 & 0.50 \\ -0.342 & 0.94 \end{pmatrix}. \quad (1.62)$$

Note that in this example, the poles and zeros of the open-loop characteristic systems are located symmetrically with respect to the real axes and coincide with the poles and zeros of the transfer function  $W(s)$  [Equation (1.61)]. Nevertheless, the roots of each closed-loop characteristic system are nonsymmetrical.

In principle, for the stability analysis of characteristic systems, any of the well known stability criteria used for common SISO systems can be applied, after some modifications

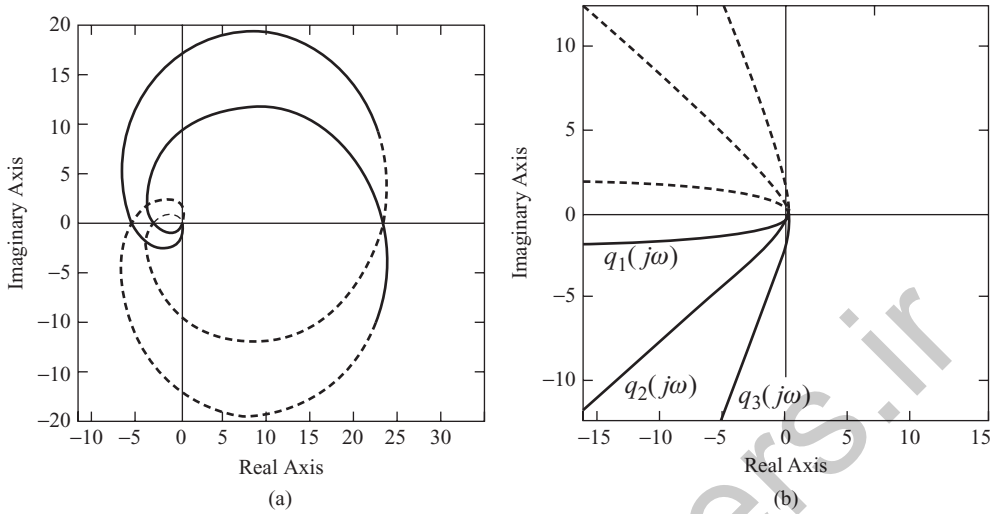


**Figure 1.10** Characteristic gain loci of stable MIMO systems; (a) stable two-dimensional system; (b) stable three-dimensional system. (a)  $N = 2, k = 2$ ; (b)  $N = 3, k = 0$ .

(Ogata 1970; Kuo 1995). However, for practical applications, the most convenient is possibly the Nyquist criterion, of which various generalizations to the multivariable case are given, for example, in (Postlethwaite and MacFarlane 1979; Desoer and Wang 1980; Stevens 1981). For the objectives of this book, we shall formulate that criterion, sacrificing to a certain extent the mathematical rigour, in the following way. Define as the Nyquist plots (or the *characteristic gain loci*) of the open-loop CTFs  $q_i(s)$  ( $i = 1, 2, \dots, N$ ) the curves in the complex plane which correspond to the CTFs  $q_i(j\omega)$  as angular frequency  $\omega$  changes from  $-\infty$  to  $+\infty$ .<sup>18</sup> Then, if the open-loop MIMO characteristic equation has  $k$  poles in the right half-plane, for the stability of the closed-loop system, it is necessary and sufficient that the total sum of anticlockwise encirclements of the critical point  $(-1, j0)$  by the characteristic gain loci  $q_i(j\omega)$  be equal to  $k$ .

If the open-loop MIMO system is stable, none of the  $q_i(j\omega)$  loci must encircle the point  $(-1, j0)$ . Note that in the formulation of the generalized Nyquist criterion, we speak about the *total sum* of encirclements of  $(-1, j0)$ , and no restrictions or conditions are imposed on the number of encirclements of that point by each isolated  $q_i(j\omega)$  locus. The characteristic gain loci of a stable two-dimensional system, which is unstable in the open-loop state and has, in that state, two right half-plane poles, are shown in Figure 1.10(a). The gain loci of a stable three-dimensional system, in the case of stable  $W(s)$ , are depicted in Figure 1.10(b). The solid lines in these plots correspond to the  $q_i(j\omega)$  loci for positive frequencies  $\omega \geq 0$  and the dotted lines to negative frequencies  $\omega < 0$ .

One of the primary advantages of the above-stated Nyquist criterion is that it allows, just as in the SISO case, judging about stability of the closed-loop MIMO system by frequency characteristics, namely the characteristic gain loci  $q_i(j\omega)$  of the open-loop MIMO system.

<sup>18</sup> Strictly speaking, the so-called *Nyquist contour*, which we have simplistically replaced by the imaginary axis, must pass around from the right, moving along the semicircle of an infinitesimal radius, all poles and zeros of the open-loop MIMO system, as well as the *branch points*, located on the imaginary axis (Postlethwaite and MacFarlane 1979).

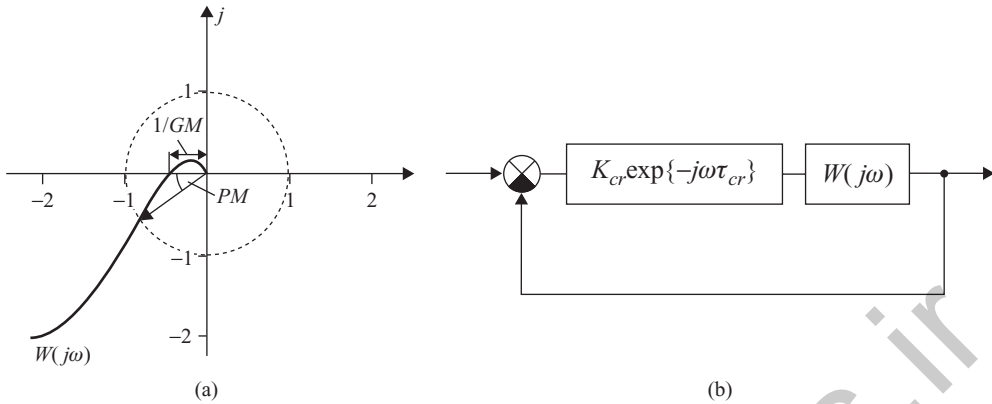


Figure 1.11 Gain and phase margins of SISO systems.

Besides, on substituting  $s = j\omega$ , the matrix  $W(s)$  becomes a usual numerical matrix  $W(j\omega)$  with complex entries, and finding the eigenvalues  $q_i(j\omega)$  of the latter for the fixed values  $\omega = \omega_k$  does not now present any difficulty. In particular, the modern application programs and packages (for example, those in MATLAB) enable the user to calculate the eigenvalues of complex-valued square matrices of practically any size, and, consequently, to create tools for the computer-aided stability analysis of linear MIMO systems with practically any number  $N$  of separate channels.

Note that on substituting  $s = -j\omega$ , the matrix  $W(-j\omega)$  is complex conjugate to the matrix  $W(+j\omega)$ . Therefore, the eigenvalues  $q_i(-j\omega)$  of  $W(-j\omega)$  are complex conjugate to those of  $W(+j\omega)$ . This implies that the branches of loci  $q_i(j\omega)$  ( $i = 1, 2, \dots, N$ ) for negative frequencies  $\omega < 0$  are the mirror mapping with respect to the real axis of a set of the  $q_i(j\omega)$  loci branches for positive frequencies  $\omega > 0$  (generally, each of these loci may not possess the indicated symmetry). That is why, in the analysis of the MIMO system stability, it is enough to consider only positive frequencies  $\omega \geq 0$ . Accordingly, the formulation of the Nyquist criterion is changed to a certain extent, and now it states that *if the open-loop MIMO system is unstable, then the closed-loop system will be stable, provided the total sum of anticlockwise encirclements of the critical point  $(-1, j0)$  by all  $q_i(j\omega)$  loci is equal to  $k/2$ , where  $k$  is the number of unstable poles of  $W(s)$ .*

The discussion of the issues related to the MIMO system stability analysis by means of the generalized Nyquist criterion would be incomplete if we did not dwell on such classical notions as *gain and phase margins*, which originated in the control theory on the basis of Nyquist plots (Ogata 1970; Kuo 1995).<sup>19</sup> For common SISO systems, these notions are clarified in Figure 1.11.

The *phase margin* (PM) is defined as the angle between the real negative axis and the line to the point at which  $W(j\omega)$  intersects the circle of unit radius.<sup>20</sup> The *gain margin* (GM)

<sup>19</sup> Further, for brevity, we shall confine our presentation to systems with ‘usual’  $W(j\omega)$  loci. Therefore, we shall not consider the *conditionally stable* systems, which have the ‘beak-shaped’ Nyquist plots, and the systems *unstable* in the open-loop state. The conditionally stable systems become unstable *on both increasing and decreasing* the open-loop gain  $K$ . For systems unstable in the open-loop state, the zero value  $K = 0$  always belongs to the unstable region, and the stable closed-loop system may become unstable *on decreasing* the gain  $K$ .

<sup>20</sup> At that point,  $|W(j\omega_c)| = 1$ , and the corresponding frequency  $\omega = \omega_c$  is called *crossover frequency*.

is defined as the reciprocal to the magnitude  $|W(j\omega)|$  at the point of intersection of  $W(j\omega)$  with the real negative axis [at that point,  $\arg\{W(j\omega)\} = -180^\circ$ ], and is usually expressed in decibels. For stable systems, both stability margins are reckoned positive. In fact, the phase margin indicates which additional negative phase shift should be introduced in the open-loop system at the crossover frequency  $\omega_c$  to bring the closed-loop system to the stability boundary. Analogously, the gain margin is equal to the additional gain, which should be introduced in the open-loop system to bring the closed-loop system to the stability boundary.

Recall that the ideal time delay element

$$W_{TD} = \exp\{-j\omega\tau\}, \tag{1.63}$$

has unitary magnitude at all frequencies, and introduces a negative linear phase shift  $-\omega\tau$ . That allows us to define the *critical delay* as  $\tau_{cr} = PM/\omega_c$ <sup>21</sup> and to explain visually the notions of gain and phase margins with the help of the block diagram in Figure 1.11(b), in which the entered conventional element  $K_{cr} \exp\{-j\omega\tau_{cr}\}$  illustrates the discussed notions.

Taking into account the significance of these notions in the classical control theory, it would be natural to introduce analogous notions for MIMO systems. A great number of papers in the scientific and technical literature are devoted to that issue, among which the works of Safonov (1980, 1981), in which gain and phase margins of MIMO systems are introduced from the position of the robustness theory, should be especially noted. As for us, we shall pursue here, for us, the simpler and more natural way, based on the observation that the utilization of the generalized Nyquist criterion to a MIMO system is equivalent, roughly speaking, to the utilization of the classical Nyquist criterion to each of characteristic systems associated with the MIMO system. As the gain and phase margins of *each* characteristic gain locus  $q_i(j\omega)$  may readily be evaluated [just as shown in Figure 1.11(a)], then we can, in such a way, associate two sets of  $N$  gain margins  $\{GM_i\}$  and  $N$  phase margins  $\{PM_i\}$  with an  $N$ -dimensional MIMO system. Now, it seems quite logical to count as MIMO system stability margins the *least*s of values  $GM_i$  and  $PM_i$  ( $i = 1, 2, \dots, N$ ), i.e. to define the gain  $GM$  and phase  $GM$  margins of a MIMO system as:

$$GM = \min\{GM_i\}, \quad PM = \min\{PM_i\}. \tag{1.64}$$

Here, however, the specific features of MIMO systems should be taken into account. First, we should realize that the quantities  $GM$  and  $PM$  determined by Equation (1.64) may, in general, correspond to *different* characteristic systems, which is evident from Figure 1.12.

Further, and far more importantly, on trying to build a matrix analogue to the block diagram in Figure 1.11, we *have no right* to introduce in the MIMO system a *diagonal* conventional element  $\text{diag}\{K_{icr} \exp\{-j\omega\tau_{icr}\}\}$  with different critical gains  $K_{icr}$  and time delays  $\tau_{icr}$ , and must introduce a *scalar* matrix  $K_{cr} \exp\{-j\omega\tau_{cr}\}I$ , i.e. introduce the *same* elements  $K_{cr} \exp\{-j\omega\tau_{cr}\}$  in all channels (Figure 1.13). This is because introducing a diagonal matrix  $\text{diag}\{K_{icr} \exp\{-j\omega\tau_{icr}\}\}$  violates the canonical representation of  $W(s)$ , since the multiplication of a diagonal matrix by a square matrix changes both the eigenvalues and the eigenvectors of the latter. As for the multiplication of  $W(j\omega)$  by a scalar matrix  $K_{cr} \exp\{-j\omega\tau_{cr}\}I$ , which corresponds to the multiplication of  $W(j\omega)$  by a *scalar*  $K_{cr} \exp\{-j\omega\tau_{cr}\}$ , the canonical basis

<sup>21</sup> That quantity is sometimes called *delay margin* (Bosgra *et al.* 2004).

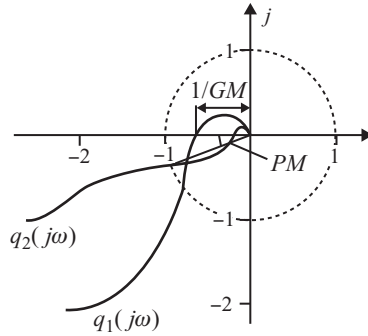


Figure 1.12 MIMO system stability margins ( $N = 2$ ).

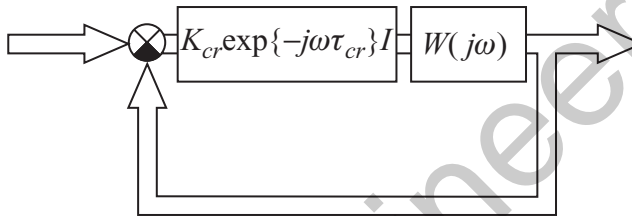


Figure 1.13 Definition of the MIMO system stability margins.

of the MIMO system does not change, and all CTFs  $q_i(j\omega)$  multiply by the same scalar.<sup>22</sup> Only in such a case will the changes in the coefficient  $K_{cr}$  bring about the proportional changes of magnitudes of *all* characteristic gain loci  $q_i(j\omega)$ , and changes in the time delay  $\tau_{cr}$  bring about the rotation about the origin of the complex plane of *all*  $q_i(j\omega)$  by the same angle. This preserves the geometrical and physical sense of the above notions of the MIMO system gain and phase margins as the least gain and phase margins of characteristic systems.

Hence, when using the quantities  $GM$  and  $PM$  [Equation (1.64)] as measures of the stability margins, we should always remember which sense is given to these values; namely, they define the gain and phase margins of the MIMO system only for *simultaneous and identical* changes of gains and time delays in all channels. Note, finally, the evident fact that the MIMO system stability analysis on the base of the generalized Nyquist criterion may be accomplished, as in the SISO case, with the help of the logarithmic characteristics (the Bode diagrams) and the Nichols plots.

**Remark 1.1** Of course, the introduced notions of the MIMO system stability margins may seem somewhat narrow from the point of view of their practical application for the MIMO system analysis and design. Indeed, this does in fact happen in some situations, as we shall see in the example given below. In these situations, we have to deal with the MIMO systems that are in a certain sense not *robust*, i.e. in which even slight perturbations of the system parameters may bring about significant changes in the dynamics, and even instability of the

<sup>22</sup> This ensues from the well known in the theory of matrices rule of multiplication of a square matrix by a scalar (Gantmacher 1964).

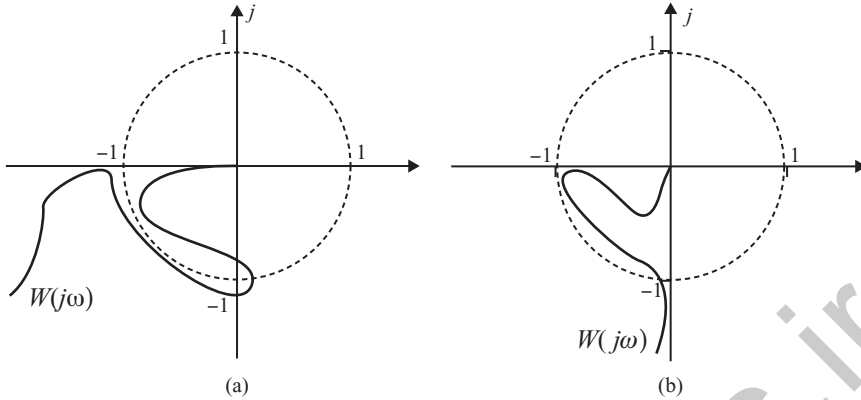


Figure 1.14 Nyquist plots of ‘non-robust’ SISO systems.

system. Recall, however, that the notions of gain and phase margins are subjected to some ‘criticism’ (mainly by the specialists on the robustness theory), even in the case of SISO systems. In Figure 1.14, the Nyquist plots of the SISO systems are shown, which, having excellent gain and phase margins, are not robust nonetheless, because their plots are too close to the critical point  $(-1, j0)$  (Bosgra *et al.* 2004). On the other hand, for common control systems – and such systems are by far more numerous than the systems with the exotic characteristics of Figure 1.14 (it would probably be very difficult, if possible at all, to achieve such characteristics for real systems) – the gain and phase margins have been, and are now, quite good, convenient and intuitively comprehensible notions, generally recognized by practicing engineers. In this connection, the introduction of the analogous, that is having the same clear and visual physical interpretation, characteristics for MIMO systems may be considered as a quite grounded and necessary step, though those characteristics should be treated with certain caution.

**Example 1.2** Below, we consider the stability analysis of a general two-axis guidance system of the telescope, for two different variants of the separate channel transfer functions and rigid cross-connections described by the matrix in Equation (1.60). In the first variant, we have a simple system with the following transfer functions:

$$W_1(s) = \frac{1}{s}, \quad W_2(s) = \frac{0.5}{s + 0.2} \quad (1.65)$$

The Nyquist plots of the CTFs  $q_1(j\omega)$  and  $q_2(j\omega)$  of the guidance system with transfer functions as in Equation (1.65), for two different combinations of angles  $\alpha_1$  and  $\alpha_2$ :  $\alpha_1 = 30^\circ$ ,  $\alpha_2 = 20^\circ$  and  $\alpha_1 = 30^\circ$ ,  $\alpha_2 = -20^\circ$ , are shown in Figure 1.15. The inspection of these plots shows that the system is stable for both combinations of  $\alpha_1$  and  $\alpha_2$ , and the Nyquist plots of  $q_1(j\omega)$  and  $q_2(j\omega)$  are quite close to the corresponding plots of the isolated separate channels [Equation (1.65)].

Consider now the same system with more complicated transfer functions of separate channels:

$$W_1(s) = \frac{50(s + 3)}{s(s + 5)(s + 10)}, \quad W_2(s) = \frac{100}{s(s + 2)(s + 4)(s + 8)}. \quad (1.66)$$

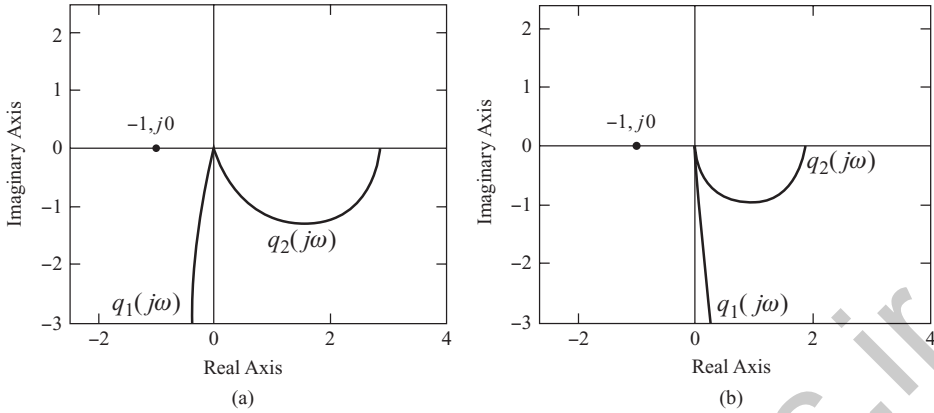


**Figure 1.15** Stability analysis of the general two-dimensional guidance system with transfer functions [Equation (1.65)] for different angles  $\alpha_1$  and  $\alpha_2$  (the Nyquist plots). (a)  $\alpha_1 = 30^\circ$ ,  $\alpha_2 = 20^\circ$ ; (b)  $\alpha_1 = 30^\circ$ ,  $\alpha_2 = -20^\circ$ .

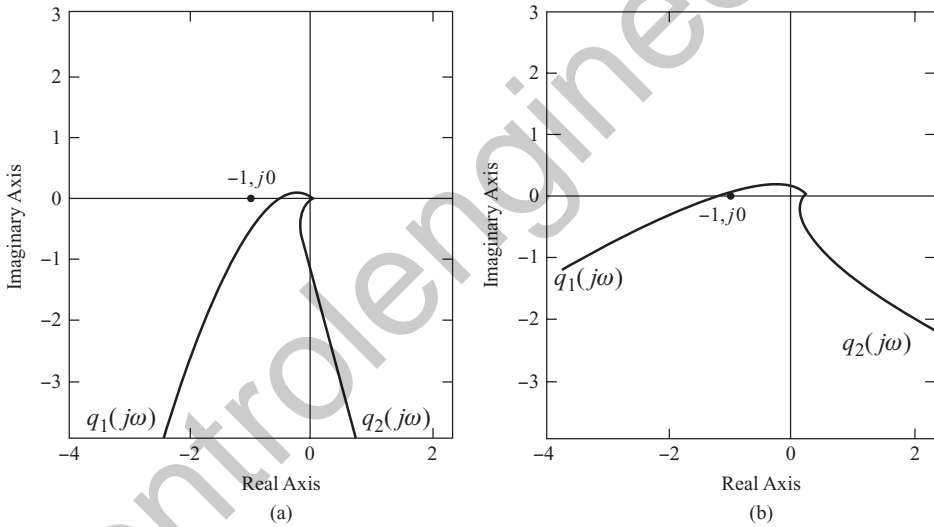


**Figure 1.16** Stability analysis in the case of transfer functions [Equation (1.66)]. (a)  $\alpha_1 = 30^\circ$ ,  $\alpha_2 = 20^\circ$ ; (b)  $\alpha_1 = 60^\circ$ ,  $\alpha_2 = 70^\circ$ .

The characteristic gain loci of that system for different angles  $\alpha_1$  and  $\alpha_2$  are shown in Figure 1.16. The plots in Figure 1.16 show that cross-connections may considerably affect the stability of the guidance system, and even bring about instability (the case of  $\alpha_1 = 60^\circ$ ,  $\alpha_2 = 70^\circ$ ).

**Example 1.3** As another example of the MIMO system stability analysis which illustrates the need to exercise caution when estimating the stability margins on the base of Equation (1.64), consider the celebrated example attributed usually to J. Doyle (Doyle and Stein 1981). As a result of that example, many authors have drawn conclusions about the certain inefficiency, not to say unreliability, of the approaches based on the characteristic gain loci method.

Given the open-loop system with the transfer function matrix

$$W(s) = \frac{1}{(s+1)(s+2)} \begin{pmatrix} -47s+2 & 56s \\ -42s & 50s+2 \end{pmatrix}. \quad (1.67)$$

In Doyle and Stein (1981), it is shown that this matrix can be represented in the form

$$W(s) = \begin{pmatrix} 7 & -8 \\ -6 & 7 \end{pmatrix} \begin{pmatrix} \frac{1}{s+1} & 0 \\ 0 & \frac{2}{s+2} \end{pmatrix} \begin{pmatrix} 7 & 8 \\ 6 & 7 \end{pmatrix}, \quad (1.68)$$

i.e. for this system, the CTFs  $q_1(s)$  and  $q_2(s)$  have, assuming the unit regulator  $K = I$ , the form of the first order transfer functions:

$$q_1(s) = \frac{1}{s+1}, \quad q_2(s) = \frac{2}{s+2}, \quad (1.69)$$

which indicate an infinite gain margin, and the phase margin of  $180^\circ$ . The loci  $q_1(j\omega)$  and  $q_2(j\omega)$  of the system corresponding to Equation (1.69) are shown in Figure 1.17(a) and justify that conclusion {though both these loci are identical in form, their frequency numberings along the loci differ due to the different time constants of  $q_1(s)$  and  $q_2(s)$  [Equation (1.69)]}.

However, as established in Doyle and Stein (1981), introducing in the system the diagonal static regulator of the form

$$K = \begin{pmatrix} 1.13 & 0 \\ 0 & 0.88 \end{pmatrix} \quad (1.70)$$

i.e. *simultaneously* increasing the gain of the first channel by 0.13 and decreasing that of the second channel by 0.12, makes the closed-loop system unstable! The given example is rather instructive and, from another point of view, it clearly discloses how unpredictable and unexpected changes in the MIMO system's characteristics may be, even in the case of slight perturbations of their parameters.

This, at first sight, irrefutable demonstration that the stability margins calculated through the CTFs may lead to an erroneous conclusion in fact demands more careful and deeper treatment. We have already stated before that gain and phase margins [Equation (1.64)] are valid only for *simultaneous and identical* changes in the separate channel gains. In this regard, the discussed MIMO system indeed remains stable for arbitrary large but the *same* gains in separate channels, since, in that case, the MIMO system modal decomposition is not violated and the canonical basis is unchanged. However, if we multiply together the matrices  $W(s)$  [Equation (1.67)] and  $K$  [Equation (1.70)], then the resulting canonical basis and the CTFs will be completely different.<sup>23</sup> The characteristic gain loci of the new perturbed system with regulator  $K$  [Equation (1.70)] are depicted in Figure 1.17(b), from which it is quite clear that the MIMO system is unstable and its new CTFs have nothing in common with those in Figure 1.17(a).

<sup>23</sup> We shall return to this example in Example 1.13 and Chapter 2, with more detailed explanation.

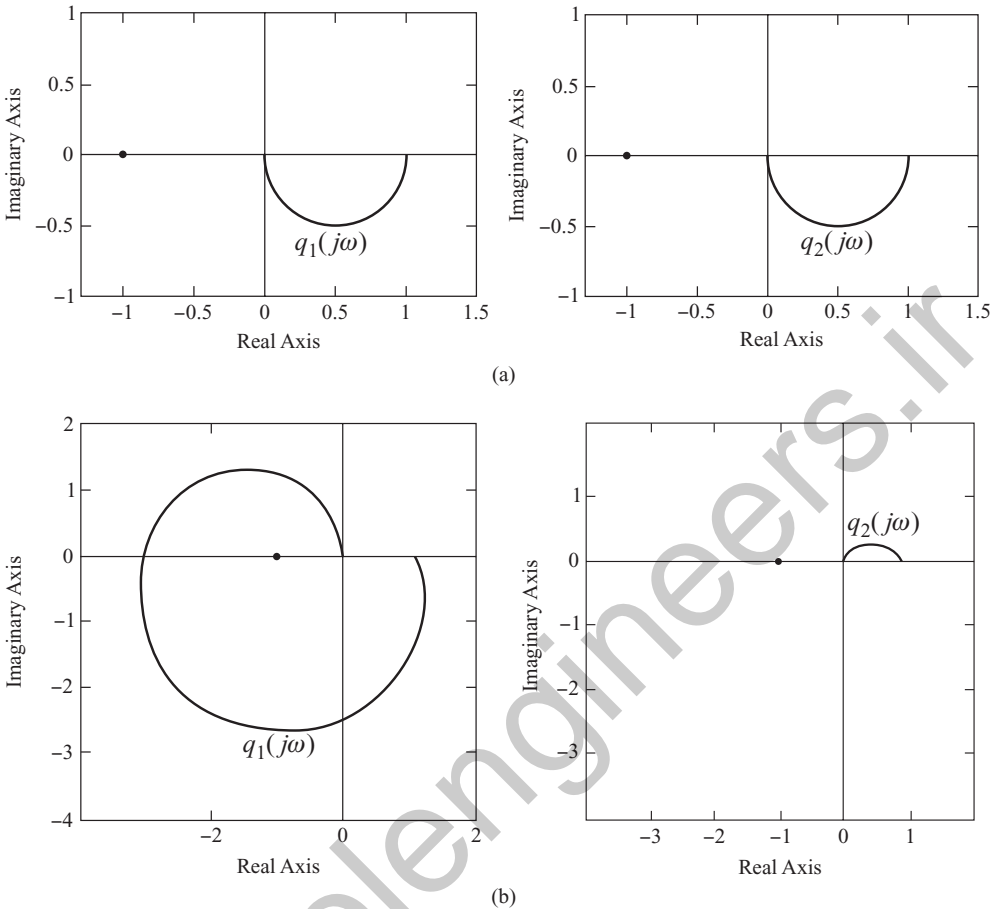


**Figure 1.17** Stability analysis of a two-dimensional system [Equation (1.67)]. (a) Characteristic gain loci in the case of the unit regulator  $K = I$ ; (b) characteristic gain loci of the system with the perturbed regulator  $K$  [Equation (1.70)].

### 1.2.5 Singular value decomposition of transfer matrices

As we already know, to any  $N$ -dimensional linear MIMO system of *simple structure* correspond  $N$  linearly independent ‘canonical’ directions (canonical basis axes) in complex space  $\mathbb{C}^N$ , along which the MIMO system acts as a certain SISO system. The canonical bases of the open- and closed-loop MIMO systems are the same. This feature is very remarkable, since it assures that all transfer matrices  $W(s)$ ,  $\Phi(s)$  and  $\Phi_\varepsilon(s)$  of the open- and closed-loop MIMO systems are brought to diagonal form by a similarity transformation via a *unique* transformation (modal) matrix. Moreover, all CTFs of the closed- and open-loop one-dimensional characteristic systems associated with the MIMO system are related in the canonical basis by the very same expressions as usual transfer functions of common SISO systems. Thus, the  $|q_i(s)|$ ,  $|q_i(s)|/|1 + q_i(s)|$  and  $1/|1 + q_i(s)|$  magnitudes of the corresponding CTFs give, for

any fixed value of complex variable  $s$ , the ‘gain magnitude’ of the MIMO system along the corresponding  $i$ th axis of the canonical basis.<sup>24</sup>

Together with the canonical basis axes, another set of directions in  $\mathbb{C}^N$  which are uniquely defined by the MIMO system transfer matrices may be associated with a linear MIMO system. These directions are no less (and many specialists on robust control quite soundly believe that more) important for the understanding of the internal structure and performance of multivariable systems than the directions of the canonical basis axes. The matter concerns the so-called *singular value decomposition* of the transfer function matrices.

Recall in brief that any square matrix  $A$  of order  $N \times N$  allows decomposing in the form<sup>25</sup>

$$A = U \text{diag}\{\sigma_i\} V^*, \quad (1.71)$$

where the asterisk  $*$  denotes the operation of complex conjugation and transposition (from here on, we call this operation the *conjugation* of a matrix);  $U$  and  $V$  are *unitary* matrices, for which the inverse matrices coincide with conjugated (i.e.  $U^{-1} = U^*$ ,  $V^{-1} = V^*$ );  $\text{diag}\{\sigma_i\}$  is the diagonal matrix of nonnegative real numbers,<sup>26</sup> arranged in descending order, i.e.  $\sigma_1 \geq \sigma_2 \geq \dots \geq \sigma_N$  (Marcus and Minc 1992; Voevodin and Kuznetsov 1984).

Decomposition [Equation (1.71)] is said to be a *singular value decomposition* and numbers  $\sigma_i$  are called the *singular values* of  $A$ . These numbers are equal to positive values of the square roots taken of the eigenvalues of the Hermitian matrix  $AA^*$  (or  $A^*A$ ).<sup>27</sup> The columns of the matrix  $U$  in Equation (1.71) constitute the orthonormal *left* (or *output*) *singular basis* of the matrix  $A$  in  $\mathbb{C}^N$  and are the eigenvectors of the matrix  $AA^*$ . The columns of the matrix  $V$  constitute, accordingly, the orthonormal *right* (or *input*) *singular basis* and are the eigenvectors of the matrix  $A^*A$ . Denoting the columns of  $U$  by  $u_i$  and the columns of  $V$  by  $v_i$ , Equation (1.71) can be written down as a sum of  $N$  dyads of rank one:

$$A = \sum_{i=1}^N u_i \sigma_i v_i^*. \quad (1.72)$$

From here, it is evident that  $A$  transforms the orthonormal right singular basis into a mutually orthogonal set of vectors directed along the axes of the left singular basis, and real numbers  $\sigma_i$  serve as ‘gains’ in the corresponding directions. This can also be written as follows:

$$A v_i = \sigma_i u_i, \quad i = 1, 2, \dots, N, \quad (1.73)$$

where it is more clearly accentuated that numbers  $\sigma_i$  relate *different* directions in  $\mathbb{C}^N$ .

The singular values of square matrices possess a number of features relating them to eigenvalues  $\lambda_i$  and determinants of matrices. Thus, in particular, a square matrix is nonsingular if

<sup>24</sup> For arbitrary values of variable  $s$  with a nonzero real part, the listed magnitudes have no definite sense, but, when considering the steady-state oscillations in stable MIMO systems, i.e. when we accept  $s = j\omega$ , they obtain a clear and simple physical interpretation and may be viewed as ‘gains’ for the given frequency  $\omega$ .

<sup>25</sup> The singular value decomposition is applicable to any *rectangular* matrix, but, here, for simplicity, we consider only the case of square matrices, which are interesting for us.

<sup>26</sup> For zero singular values, which are, in principle, possible, see Remark 1.7.

<sup>27</sup> A matrix  $A$  is said to be Hermitian if it coincides with its conjugate, i.e. if  $A = A^*$ . The eigenvalues of a Hermitian matrix are always real and, for a Hermitian matrix  $B$ , written in the form  $B = AA^*$ , they are always nonnegative (Marcus and Minc 1992).

and only if all its singular values are nonzero. This ensues from the following, well known in the theory of matrices rule:

$$|\det A| = \prod_{i=1}^N \sigma_i \tag{1.74}$$

from which, in addition, it follows (as  $\det A = \prod_{i=1}^N \lambda_i$ ) that the product of the eigenvalues magnitudes (or the magnitude of the eigenvalues product) is also equal to the product of the singular values. Among the singular values, of primary interest are the largest and smallest of them, where the largest number  $\sigma_{\max}$  is called the *spectral norm* of the matrix  $A$ , and is usually denoted by  $\|A\|$  (Gantmacher 1964).<sup>28</sup> This norm possesses the property that for any two vectors  $x$  and  $y$  in  $\mathbb{C}^N$ , where  $y = Ax$ , the following inequality holds:

$$|y| \leq \|A\| |x|, \tag{1.75}$$

where the (Euclidian) norms of vectors  $x$  and  $y$  are defined by Equation (1.29). According to the inequality in Equation (1.75), the spectral norm  $\|A\|$  may be interpreted as the maximum ‘gain’ of the matrix  $A$  with respect to the *magnitude* of the ‘input’ vectors  $x$  in  $\mathbb{C}^N$ . Analogously, the least singular value  $\sigma_{\min}$  guarantees that the following inequality holds:

$$|y| \geq \sigma_{\min} |x|, \tag{1.76}$$

i.e. it gives the lower boundary of the  $A$  matrix gain (by magnitudes) for any vectors  $x$ .

Recalling that, by the definition of eigenvalues  $\lambda_i$  and eigenvectors  $c_i$ , we have, for any  $i$  ( $i = 1, 2, \dots, N$ ), the equality  $y = Ac_i = \lambda_i c_i$ , it is easy to understand that the magnitudes of all eigenvalues of any square matrix are bounded from above and below by singular values  $\sigma_{\max}$  and  $\sigma_{\min}$ :

$$\sigma_{\min} \leq |\lambda_i| \leq \sigma_{\max}, \quad i = 1, 2, \dots, N. \tag{1.77}$$

All that has been stated about singular values and their relationship with eigenvalues may be summarized as follows. With any square matrix  $A$ , there are related two orthonormal coordinate systems (input and output singular bases) and one more, generally nonorthogonal, coordinate system formed by the eigenvectors of the matrix  $A$ . The two specific axes of singular bases give the directions of the largest and smallest of the  $A$  matrix ‘gains’, and these two directions are always mutually orthogonal, both in the ‘input’ and in the ‘output’. In the directions of the eigenvectors, the matrix  $A$  acts as scalar multipliers with intermediate, owing to Equation (1.77), ‘gains’.

Now, we can readily use the introduced notions to transfer matrices  $W(s)$ ,  $\Phi(s)$  and  $\Phi_\varepsilon(s)$  of the MIMO system. Here, we emphasize immediately that, in the general case, as opposed to the unique set of the canonical basis axes, all listed transfer matrices have their own pairs of input and output singular bases, i.e. two *distinct* orthonormal coordinate systems are associated with each matrix, as well as their own sets of singular values. Another essential feature of the singular value decomposition of transfer matrices is that nothing can generally be said, for

<sup>28</sup> We shall consider this matter in more detail in Chapter 2.

example, about the relationship between the corresponding characteristics of the open-loop and closed-loop MIMO system, and each transfer matrix must be considered individually and independently of other matrices. Taking this into account, we shall consider only the case of the transfer matrix  $\Phi(s)$  with respect to the MIMO system output. That matrix can be expressed by the singular value decomposition in the form

$$\Phi(s) = [I + W(s)]^{-1}W(s) = U_{\Phi}(s)\text{diag}\{\sigma_{\Phi_i}(s)\}V_{\Phi}(s) = \sum_{i=1}^N u_{\Phi_i}(s) > \sigma_{\Phi_i}(s) < v_{\Phi_i}(s), \quad (1.78)$$

where  $U_{\Phi}(s)$ ,  $V_{\Phi}(s)$  are the unitary matrices composed of the orthonormal vectors  $u_{\Phi_i}(s)$  and  $v_{\Phi_i}(s)$ ;  $\sigma_{\Phi_i}(s)$  are real positive singular values arranged in descending order, where the subscripts in Equation (1.78) explicitly indicate that all these characteristics belong *only* to the transfer matrix  $\Phi(s)$ .

The *output singular basis* of  $\Phi(s)$  consists of the orthonormal eigenvectors  $u_{\Phi_i}(s)$  of the Hermitian matrix  $\Phi(s)\Phi^*(s)$ , and the *input singular basis* consists of the eigenvectors  $v_{\Phi_i}(s)$  of  $\Phi^*(s)\Phi(s)$ . The singular values  $\sigma_{\Phi_i}(s)$  are square roots of the eigenvalues of  $\Phi(s)\Phi^*(s)$  [or  $\Phi^*(s)\Phi(s)$ ]. The largest singular value  $\sigma_{\Phi_{\max}}(s)$  is equal to the spectral norm  $\|\Phi(s)\|$  of the transfer matrix  $\Phi(s)$  and defines the maximum gain with respect to the input vectors magnitude, and the smallest singular value  $\sigma_{\Phi_{\min}}(s)$  yields the lower boundary of the gain. The axes of the largest and the smallest ‘gains’ are always mutually orthogonal, both in the input and in the output spaces. It is worth especially emphasizing that if the input vector  $\varphi(s)$  of the MIMO system is directed along any one axis of the input singular basis, then, in forming the output vector  $f(s)$ , which is also directed along the corresponding axis of the output singular basis, all  $N$  one-dimensional characteristic systems generally participate.

The singular value decomposition of transfer matrices does not allow judgment about the system stability (due to the reality of singular values), but it is very important when analysing the performance and especially the robustness of the system. We shall return to that point in Chapter 2. Note finally that, in Section 1.4, we shall consider the so-called *normal* MIMO systems, for which both input and output singular bases coincide with the canonical one. In conclusion, we make some general remarks, which are quite important for proper comprehension of the essence of the presented material, as well as for the sensible assessment of those assumptions and suppositions on which we rely.

**Remark 1.2** In most textbooks and monographs on multivariable control, the open-loop transfer matrix  $W(s)$  is usually represented as a series connection of the plant and the controller (also frequently called the regulator, compensator, etc.). Moreover, in the practical tasks, the matrix block diagram in Figure 1.1 may have much more complicated form and consist of different matrix elements connected in series, in parallel or forming inner feedback loops. In the mentioned cases, however, all such schemes can readily be brought, based upon the well known rules of transformation of matrix block diagrams (Morozovski 1970), to the form of Figure 1.1. We have intentionally chosen in this section such a structure, to emphasize the significant fact that the CTFs and canonical basis depend on the *resultant* transfer matrix  $W(s)$  of the open-loop MIMO system, and, in the general case, *nothing can be said about the relationship of the canonical representations of  $W(s)$  and those of the individual matrix elements constituting the system*. This circumstance seemingly explains the situation that in the scientific and technical literature, there are actually no efficient *engineering* techniques

presented for the MIMO systems design based on the CTFs method, and the latter is mainly viewed as a sophisticated method applicable only for the MIMO systems stability analysis.

As for the singular value decomposition, here, we generally cannot even speak about analytical relationships between the corresponding decompositions of the open-loop and closed-loop MIMO systems, which, in the context of the CTFs approach, are very simple and visual.

**Remark 1.3** We have considered the principal ideas of the CTFs method in a somewhat simplified fashion, sacrificing in many respects the mathematical rigour. As shown in Postlethwaite and MacFarlane (1979), the CTFs, being the roots of Equation (1.26), generally belong to the class of multi-valued *algebraic functions* and constitute one mathematical entity. The *branches* of the characteristic gain loci are situated on different sheets of a Riemann surface, and transition from one sheet to another is accomplished through the ‘cuts’ connecting the point in infinity with the *branch points* of the algebraic function, at which two or more CTFs are equal. The presence of these branch points explains many of the not quite usual features of, say, root loci of multivariable systems, i.e. the features that are difficult or even impossible to explain from the position of the classical control theory. At the same time, if, when solving practical engineering tasks, we neglect the behaviour of the CTFs in the neighborhood of branch points, then, for any fixed value  $s = const$  not coinciding with the branch points and poles of  $W(s)$ , the latter may be viewed as a usual numerical matrix with complex entries. Then, as was already noted in Section 1.2.3, the problem of finding the CTFs is simply reduced to computing the eigenvalues of the matrix  $W(s)$ .

It is also worth noting that in the case of two-dimensional systems which frequently occur in practice, the roots of Equation (1.26), i.e. the CTFs of the open-loop system, can be written in the analytical form

$$q_{1,2}(s) = \frac{tr\{W(s)\}}{2} \pm \sqrt{\frac{tr\{W(s)\}^2}{4} - \det W(s)}, \quad (1.79)$$

where  $tr\{W(s)\}$  denotes the *trace* (the sum of diagonal elements) of  $W(s)$ , from which it is clear that, in general, the CTFs of the linear MIMO system cannot always be represented as a quotient of two rational polynomials in  $s$ .<sup>29</sup> If all CTFs could be represented as proper rational functions in  $s$ , then many MIMO system analysis and design issues would be solved far more simply and effectively.

Incidentally, the above-mentioned branch points are determined by equating the *discriminant* (the radical expression) in Equation (1.79) to zero.

**Remark 1.4** The assumption of no repeated (multiple) CTFs of the matrix  $W(s)$  is not very restrictive. First, in the following text, we shall consider some MIMO systems which have multiple CTFs but, at the same time, are of simple structure and can be brought to diagonal form. Further, as is known from the theory of matrices (Gantmacher 1964), in the case of multiple eigenvalues, it is always possible to reduce a matrix in a specially chosen *Jordan basis* to a *Jordan canonical form*, which can be viewed as the best approach to diagonal form, and in which, with the multiple eigenvalues, are related *Jordan blocks*. In any Jordan block, whose order is determined by the algebraic multiplicity of the given repeated eigenvalue, the principal diagonal is formed of these identical eigenvalues. The first subdiagonal (immediately

<sup>29</sup> On replacing  $W(s)$  by  $W(s)W^*(s)$  in Equation (1.79), we obtain the analogous equation for calculating the singular values of matrix  $W(s)$ .

above and to the right of the principal diagonal) consists of ones and zeros, in the proportions determined by the algebraic and geometric multiplicities of eigenvalues.

Structurally, the Jordan blocks will determine, in the canonical representations of the MIMO system transfer matrices in Figures 1.3–1.6, the blocks with identical elements in the direct channels and *one-sided* unit connections from the lower channel to the upper one (if the numbering of channels is from the top down). It is interesting to note here that the presence of unit subdiagonals in the Jordan blocks does not alter the characteristic equation expressed via the CTFs  $q_i(s)$  [Equation (1.59)], i.e. does not affect the stability of the MIMO system.

Broadly speaking, the problem of multiple eigenvalues, as well as the adjacent problem of determining the corresponding Jordan blocks, belongs to complicated problems of the theory of matrices. However, for us, it represents more of a theoretical rather than a practical interest, since the presence of multiple eigenvalues is, for the most part, the exception but not the rule (at least for the general type of matrices). And, above all, in engineering practice, all linear models are mathematical idealizations of real objects, in which all the model parameters are specified with certain accuracy. Therefore, as was already noted in Section 1.2.3, we are always able to choose the parameters of any MIMO system model, within the given specification accuracy, in a way that excludes the presence of multiple roots. All this explains why the general MIMO systems with repeated CTFs are not considered in the following.

**Remark 1.5** It is not out of place to put, what is at first sight, a trivial question: what is a multivariable control system? Formally, any set of  $N$  independent SISO systems, regarded as an integrated unit, may serve as a paradigm of a MIMO system. However, such an approach intuitively gives rise to some doubts about its appropriateness; in fact, these independent SISO systems can readily be handled by means of conventional methods of the classical control theory. Note that if we classify MIMO systems by the type of their transfer matrices, then even the set of independent SISO systems may be divided into two classes – *scalar* MIMO systems, i.e. a set of  $N$  identical SISO systems, and *diagonal* MIMO systems, consisting of  $N$  different SISO subsystems. The next class of MIMO systems, from the point of view of complexity, includes *triangular* systems, i.e. MIMO systems with zero entries above or below the principal diagonal. Such systems do not differ much in complexity from the scalar or diagonal systems, since the triangularity of the transfer matrices implies the presence in the system of one-sided connections from the previous channels to the subsequent ones, or in the reverse order. Such one-sided connections, which are equivalent to the external disturbances, cannot affect the stability of the system. All listed systems have a common feature, namely all their CTFs coincide with the transfer functions of direct channels of the open-loop MIMO system [with the diagonal elements of  $W(s)$ ]. From here, we come to the following rule: *if the determinant of the open-loop transfer matrix  $W(s)$  coincides with the product of diagonal elements  $w_{ii}(s)$  of that matrix, i.e. if*

$$\det W(s) = \prod_{i=1}^N w_{ii}(s), \quad (1.80)$$

*then the cross-connections do not affect the stability of separate channels, and the stability of the MIMO system can be investigated exploiting conventional methods of the classical control theory.*

Of course, this rule is heuristic, but if it holds, then we can reduce the system, from the stability analysis viewpoint, to a set of  $N$  usual SISO systems, and thereby do not resort

to more complicated techniques of the multivariable control theory. Incidentally, in practice, when checking the condition in Equation (1.80), one can use a numerical matrix composed of the gains of nonzero entries in  $W(s)$ .

Proceeding in the same way, it would be possible to speak about *block-scalar*, *block-diagonal* and *block-triangular* MIMO systems, which are structurally divided into a number of blocks. To each of these blocks corresponds an individual set of cross-connected SISO systems. From the stability viewpoint, all diagonal blocks of such MIMO systems are independent, and the characteristic gain loci method may be applied to each of them. We will not, however, encumber the following presentation with such systems. The interested reader will be able to extend, without any difficulty, all of the above results to the case of block MIMO systems.

Note also that triangular systems represent a plain and simple example of MIMO systems, for which the introduction of feedback does not alter the location of some closed-loop poles, i.e. for which some of the open-loop system poles coincide with the closed-loop poles. This concerns the poles of the *nondiagonal* elements of a triangular MIMO system.

Further, we shall mainly suppose that the condition in Equation (1.80) does not hold, which is equivalent to irreducibility of the MIMO system characteristic equation (i.e. to impossibility of representing it as a product of two or more equations of a lesser degree).

**Remark 1.6** Recall in brief the main concepts concerning the representation of proper rational matrices via *the Smith-McMillan canonical form*. Note immediately that this canonical form is generally applicable to rectangular matrices, but we shall only consider the interesting case for us of square matrices having normal rank  $N$ . As is well known, any square proper rational transfer matrix  $W(s)$  of order  $N \times N$  can be represented in the following canonical form (Kailath 1980):

$$W(s) = H(s) \text{diag} \left\{ \frac{\varepsilon_i(s)}{\psi_i(s)} \right\} M(s), \quad (1.81)$$

where both square polynomial matrices  $H(s)$  and  $M(s)$  are *unimodular*, i.e. their determinants do not depend on complex variable  $s$  and are equal to constant, nonzero values. The polynomials  $\varepsilon_i(s)$  and  $\psi_i(s)$  in Equation (1.81) possess the property that each  $\varepsilon_i(s)$  divides all *subsequent*  $\varepsilon_{i+j}(s)$ , and each  $\psi_i(s)$  divides all *preceding*  $\psi_{i-j}(s)$ . Strictly speaking, the zeros and poles polynomials  $N(s)$  and  $P(s)$  of the open-loop MIMO system, which we heuristically defined in Section 1.2.2 via the determinant  $\det W(s)$  [Equation (1.11)], must in fact be expressed by polynomials  $\varepsilon_i(s)$  and  $\psi_i(s)$  in the form (Postlethwaite and MacFarlane 1979):

$$N(s) = \prod_{i=1}^N \varepsilon_i(s) = 0, \quad P(s) = \prod_{i=1}^N \psi_i(s) = 0, \quad (1.82)$$

The point is that when determining poles and zeros of the open-loop MIMO system by means of the determinant in Equation (1.11), mutual cancellation of poles and zeros, which actually correspond to *different* diagonal entries of the Smith-McMillan form [Equation (1.81)] (i.e. correspond to *different* directions) and therefore are not to be cancelled, is not excluded. Only in the case of no coincident roots of polynomials  $N(s)$  and  $P(s)$  in Equation (1.82) can we avoid such situations.

There exists, however, another significant feature inherent only in multivariable systems, which should be taken into account when dealing with them. Recall that the determinant of a

square matrix  $A$  of order  $N \times N$  represents an algebraic sum of  $N!$  terms, where each term is formed in such a way that it contains the product of  $N$  entries of  $A$ , taken one by one from each row and column (Marcus and Minc 1992). If there are any *zero* entries in  $A$ , then it may turn out that some *nonzero* entries of  $A$  will not be presented in the determinant  $\det A$ . To explain more clearly the possible consequence of such a situation, consider the following variants of the transfer matrix  $W(s)$ , for  $N = 3$ :

$$W(s) = \begin{pmatrix} w_{11}(s) & 0 & 0 \\ w_{21}(s) & w_{22}(s) & w_{23}(s) \\ w_{31}(s) & 0 & w_{33}(s) \end{pmatrix}, \quad W(s) = \begin{pmatrix} w_{11}(s) & w_{12}(s) & 0 \\ w_{21}(s) & w_{22}(s) & w_{23}(s) \\ 0 & 0 & w_{33}(s) \end{pmatrix}. \quad (1.83)$$

It is easy to see that all nondiagonal scalar transfer functions are not presented in the determinant of the first matrix  $W(s)$ , and the transfer function  $w_{23}(s)$  is not presented in the determinant of the second matrix. This implies that the corresponding poles of nonzero transfer functions will be *absent* in the poles polynomial  $P(s)$  determined by means of  $\det W(s)$  [in Equation (1.82), those poles are always present owing to the way of finding the polynomials  $\psi_i(s)$ ]. The simplest instance of such structures is the class of *triangular* MIMO systems discussed in the previous remark.

Hence, in the case of zero entries in the open-loop transfer matrix  $W(s)$ , it makes sense to check whether all transfer functions of cross-connections are present in the expression for the determinant  $\det W(s)$ , and, accordingly, in the poles polynomial  $P(s)$ . The importance of such a test lies in the fact that all poles of the ‘hidden’ transfer functions *do not change on closing the feedback loop*, i.e. they become the poles of the closed-loop system (we shall always suppose such poles are stable).

**Remark 1.7** Considering the *gain matrix* of the MIMO system, or, more correctly, the open-loop transfer matrix  $W(s)$  for  $s = 0$ , we should pay proper attention to another significant aspect. Below, to present more visually the essence of the matter, we discuss a simplified situation and assume that all zero poles of the open-loop MIMO system are *absolute* poles, i.e.  $W(s)$  can be represented as

$$W(s) = \frac{1}{s^r} W_1(s), \quad (1.84)$$

where the  $r$  integer defines the closed-loop system *type*.<sup>30</sup>

Recall that in Section 1.2.2, we set the requirement that the matrix  $W_1(s)$  be nonsingular at any absolute pole, i.e. be of rank  $N$ . Now, we approach this question from the position of the CTFs method, and impose some additional restrictions on the ‘gain matrix’  $W_1(0)$ . Since the CTFs [Equation (1.84)] of the open-loop system can be represented in the form

$$q_i(s) = \frac{1}{s^r} q_{1i}(s), \quad i = 1, 2, \dots, N, \quad (1.85)$$

it becomes clear that if the ‘gain’ of the  $i$ th CTF  $K_i = q_{1i}(0)$  is real and equal to zero, which corresponds to singularity of the matrix  $W_1(0)$ , this physically means *breaking the feedback*

<sup>30</sup> See Chapter 2, in which the issue of the MIMO system *type* is considered in more detail.

loop in the  $i$ th SISO characteristic system in Figures 1.5 and 1.6. Actually, this involves *loss of control* along the  $i$ th axis of the MIMO system canonical basis. Further, if  $K_i = q_{1i}(0)$  is real and negative, then this implies the *change from negative feedback to positive in the  $i$ th characteristic system*, which generally (but not necessarily) can also bring about nonoperability of the overall MIMO system. Therefore, the case of negative  $q_{1i}(0)$  requires especially careful consideration.

Since the matrix  $W_1(0)$  in Equation (1.84) is always real-valued, then, together with the real coefficients  $K_i = q_{1i}(0)$ , the CTFs  $q_i(s)$  may as well have (for  $s = 0$ ) complex conjugate pairs of coefficients  $K_i = \alpha_i + j\beta_i$ ,  $K_{i+1} = \alpha_i - j\beta_i$ , to which correspond two complex conjugate eigenvectors  $c_i(0)$ ,  $c_{i+1}(0) = \tilde{c}_i(0)$  [columns of the modal matrix  $C(0)$ ]. In such cases, to understand the physical nature of the complex conjugate coefficients  $K_i$  and  $K_{i+1}$ , it is worthwhile passing to the *real-valued canonical form* of the matrix  $W_1(0)$ . It can be shown (Sobolev 1973) that by replacing in  $C(0)$  the complex conjugate columns  $c_i(0)$  and  $c_{i+1}(0)$  by a pair of real ones, which are the real and complex parts of the replaced ones (this operation yields a new *real-valued* transformation matrix  $T$ ), the expression

$$W_1(0) = C(0) \text{diag}\{K_i\} C^{-1}(0) \tag{1.86}$$

can be reduced to a *real-valued* form

$$W_1(0) = T \Lambda T^{-1} \tag{1.87}$$

Here, the *block-diagonal* matrix  $\Lambda$  is composed as follows: all real coefficients  $K_i$  in the diagonal matrix  $\text{diag}\{K_i\}$  in Equation (1.86) become the corresponding diagonal entries of the matrix  $\Lambda$ , and the complex cells

$$\begin{pmatrix} \alpha_i + j\beta_i & 0 \\ 0 & \alpha_i - j\beta_i \end{pmatrix} \tag{1.88}$$

are replaced in  $\Lambda$  by real cells<sup>31</sup>

$$\begin{pmatrix} \alpha_i & -\beta_i \\ \beta_i & \alpha_i \end{pmatrix} \tag{1.89}$$

Now, it becomes evident that the complex conjugate ‘gains’  $K_i$  and  $K_{i+1}$  of the matrix  $W_1(0)$  physically correspond in the real-valued space to *two* interconnected characteristic systems with the same gains  $\alpha_i$  in the *direct channels* and *antisymmetrical* cross-connections with the coefficients  $\beta_i$ .

Summarizing, the following conclusion can be drawn: *to preserve the operability of the MIMO system, all real parts of the characteristic system ‘gains’  $K_i = q_{1i}(0)$  ( $i = 1, 2, \dots, N$ ) must be nonzero*. Otherwise, in some characteristic systems, breaking of the feedback loop occurs. If the real parts of some coefficients  $q_{1i}(0)$  are negative, which corresponds to replacing the negative feedback by positive, then it can impose essential restrictions on the stability and performance of the MIMO system.

<sup>31</sup> We assume here, for simplicity, that the complex conjugate eigenvalues in Equation (1.84) are arranged in pairs.

Note, finally, that since the product of singular values of any square matrix is equal to the product of the magnitudes of its eigenvalues (see Section 1.2.4), the equality to zero of any singular value of  $W(s)$  [or  $\Phi(s)$ ] also implies breaking the feedback loop in some characteristic system.

**Remark 1.8** Obviously, the theoretical statements of this section do not impose any restrictions or conditions on the number of separate channels of MIMO systems, and serve for making up an intuitive insight into such significant concepts as poles and zeros, as well as intrinsic geometrical and structural features of the systems in question. As a result, the necessary foundation is created, based on which we can proceed to the issues of the MIMO system performance analysis and design. Of course, everyone realizes that together with the increase in the MIMO system dimension and/or that in the order of scalar transfer functions forming the matrix  $W(s)$ , the computational difficulties increase. And, here, it turns out that within the frame of frequency-domain analysis and design methods for MIMO systems, the considered approach actually *does not impose any restrictions on the number of separate channels, and on the order of individual transfer functions*. Such well known issues in the modern control theory as model reduction or approximation [these issues constitute an integral part of the state-of-the-art design methods due to a number of factors (Skogestad and Postlethwaite 2005)] simply lose their significance, if not sense, when using the ideas and concepts of the CTFs method! Recall that, in Section 1.2.4, it was indicated that the practical analysis of the MIMO system stability based on the generalized Nyquist criterion in fact reduces to the computation of eigenvalues of complex numerical matrices of order  $N \times N$ , which result by substituting  $s = j\omega$  into  $W(s)$ . This is clear, since, for  $s = j\omega$ , all transfer functions  $w_{kr}(s)$  ( $k, r = 1, 2, \dots, N$ ) in  $W(s)$  become usual complex scalars, regardless of the orders of their numerator and denominator polynomials, from which  $W(j\omega)$  is composed. Concerning the computation of eigenvalues, for example, the MATLAB software readily performs it in a few seconds (or a few fractions of a second) for matrices whose order may be of several tens and even hundreds – this is quite adequate for the existing needs in MIMO systems practical design. In this respect, the CTFs method has an indisputable advantage over the methods that are more or less based on the MIMO systems representation in state space. Finally, another essential merit of the considered approach consists in its applicability to the MIMO systems with time delays, i.e. the elements  $w_{kr}(s)$  can contain transcendental transfer functions  $\exp\{-\tau_{kr}s\}$ . Of course, here, the MIMO system transfer matrices become ones with transcendental entries, and standard notions of poles and zeros lose their sense. However, the generalized Nyquist criterion and the geometrical features of the MIMO systems hold.

### 1.3 UNIFORM MIMO SYSTEMS

We proceed now to the study of some special *types* (or *classes*) of linear MIMO systems, which possess, owing to their specific structures, quite peculiar features and characteristics. In various technical applications, such as aerospace engineering, chemical industry and many others, the so-called *uniform* MIMO systems (Sobolev 1973; Gasparyan 1976, 1986) very often occur. The separate channels of uniform MIMO systems have identical transfer functions, and the cross-connections are rigid, i.e. are characterized by a real-valued numerical matrix, or are described, up to the values of gain, by a common (scalar) transfer function.

### 1.3.1 Characteristic transfer functions and canonical representations of uniform MIMO systems

The matrix block diagram of a linear uniform MIMO system is shown in Figure 1.18, where

$$w(s) = \frac{M(s)}{D(s)} \quad (1.90)$$

is the scalar transfer function of identical separate channels, which is a proper rational function in complex variable  $s$ , and  $R$  is a numerical matrix of order  $N \times N$  describing rigid cross-connections.

It is easy to notice that the transfer matrix  $W(s)$  of the open-loop uniform system in Figure 1.18

$$W(s) = w(s)R \quad (1.91)$$

coincides, up to complex scalar multiplier  $w(s)$ , with the numerical matrix of cross-connections  $R$ . This leads to interesting structural and dynamic properties of uniform MIMO systems and allows separating them into an individual class of multivariable control systems.

The comparison of Equation (1.91) with Equation (1.15) immediately shows that all poles and zeros of the transfer function  $w(s)$  [Equation (1.13)] are *absolute poles and zeros of the open-loop uniform system*, and, as a consequence, must be common poles and zeros of all open-loop CTFs  $q_i(s)$ . Consider the canonical representations of the uniform MIMO system transfer matrices. From the theory of matrices, we know that the multiplication of numerical matrices by a scalar multiplier does not change the eigenvectors, and results in the multiplication of all eigenvalues by the same multiplier (Gantmacher 1964). Hence, if we denote by  $\lambda_i (i = 1, 2, \dots, N)$  the eigenvalues of  $R$ , which, by analogy with the assumptions made when discussing general MIMO systems, we shall suppose *distinct*, and by  $C$ , the modal matrix composed of the linearly independent normalized eigenvectors  $c_i$  of  $R$ , then canonical representations [Equations (1.27) and (1.39)] of the open-loop uniform system have the following form:

$$W(s) = C \text{diag}\{\lambda_i w(s)\} C^{-1} \quad (1.92)$$

$$W(s) = \sum_{i=1}^N c_i > \lambda_i w(s) < c_i^+, \quad (1.93)$$

where  $c_i^+$  are dual to  $c_i$ . Note here that the eigenvalues  $\lambda_i$  of the real-valued matrix  $R$  can be real or complex numbers, and the complex eigenvalues must always occur in complex conjugate pairs (Gelfand 1966).

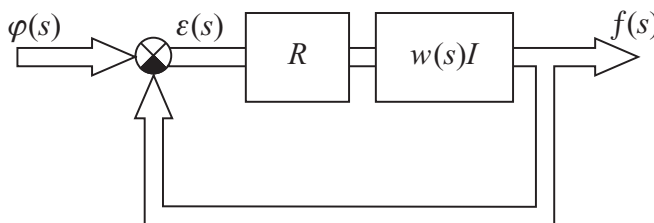
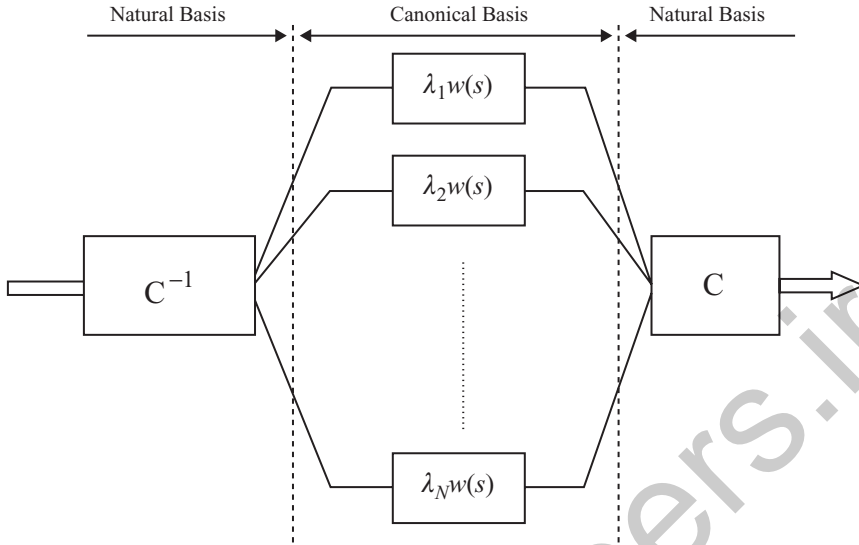


Figure 1.18 Matrix block diagram of a linear uniform MIMO system.



**Figure 1.19** Canonical representation of the open-loop uniform MIMO system via the similarity transformation.

Based upon Equations (1.92) and (1.93), the following evident conclusions can be drawn. First, the canonical basis of the linear uniform MIMO system is completely defined by the numerical matrix of cross-connections  $R$ , and does not depend on the transfer function  $w(s)$  of separate channels. As a consequence, that basis is *constant*, whereas in the general case, the canonical basis of the MIMO system is a function in complex variable  $s$ . Secondly, all CTFs

$$q_i(s) = \lambda_i w(s) = \lambda_i \frac{M(s)}{D(s)}, \quad i = 1, 2, \dots, N \quad (1.94)$$

coincide, up to constant ‘gains’  $\lambda_i$ , with transfer function  $w(s)$  (Figure 1.19), i.e. we verify the above conclusion that in the case of uniform systems, the poles and zeros of transfer function  $w(s)$  are common poles and zeros of all CTFs  $q_i(s)$ .

The listed properties, especially the latter, enable us to bring very closely the methods of investigating uniform systems to the corresponding classical methods for common SISO systems, and the reader will comprehend that in the following sections.

It is easy to see that having the singular value decomposition of the real matrix  $R$  in the form

$$R = U \text{diag}\{\sigma_{Ri}\} V^T, \quad (1.95)$$

where  $U$  and  $V$  are real *orthogonal* matrices (i.e.  $U^{-1} = U^T$  and  $V^{-1} = V^T$ ),<sup>32</sup> for the corresponding decomposition of the open-loop transfer matrix  $W(s)$  [Equation (1.91)], we have

$$W(s) = \exp\{\arg w(s)\} U \text{diag}\{\sigma_{Ri} |w(s)|\} V^T, \quad (1.96)$$

<sup>32</sup> Recall that, for real matrices, the operations of conjugation and transposition coincide.

where  $w(s) = |w(s)| \exp\{j \arg w(s)\}$ , and from which it is obvious that for any  $s = const$ , the singular values of  $W(s)$  are equal to the products of singular values  $\sigma_{Ri}$  of  $R$  and the magnitude of transfer function  $w(s)$ . The left and right singular bases of the matrix  $W(s)$  coincide, up to complex scalar multiplier  $\exp\{j \arg w(s)\}$ , with the singular bases of the matrix  $R$ .<sup>33</sup> Note also that the ratio of the largest singular value of  $W(s)$  to the smallest one does not depend on  $w(s)$  and is equal to the ratio of the corresponding singular values of  $R$ .

Taking into account Equations (1.92)–(1.94), we have, for the canonical representations of the closed-loop uniform system, transfer matrices with respect to output and error:

$$\Phi(s) = C \text{diag} \left\{ \frac{\lambda_i w(s)}{1 + \lambda_i w(s)} \right\} C^{-1} = \sum_{i=1}^N c_i > \frac{\lambda_i w(s)}{1 + \lambda_i w(s)} < c_i^+ \quad (1.97)$$

$$\Phi_\varepsilon(s) = C \text{diag} \left\{ \frac{1}{1 + \lambda_i w(s)} \right\} C^{-1} = \sum_{i=1}^N c_i > \frac{1}{1 + \lambda_i w(s)} < c_i^+ \quad (1.98)$$

All that has been stated in the previous section about the geometrical interpretation of the internal structure of general MIMO systems remains, naturally, valid, and also for uniform systems. Unfortunately, for the closed-loop uniform system transfer matrices  $\Phi(s)$  [Equation (1.97)] and  $\Phi_\varepsilon(s)$  [Equation (1.98)], there is no well defined relationship between the singular values and singular bases of these matrices, and the corresponding values and bases of the matrix  $R$ , as it is in the case of the open-loop transfer matrix  $W(s)$ . Moreover, the singular bases of the matrices  $\Phi(s)$  and  $\Phi_\varepsilon(s)$  depend generally on the transfer function  $w(s)$  of separate channels. However, from the point of view of practical computing, this fact is not very burdensome and just emphasizes the less intimate connections of the singular values, as compared with the CTFs, with the open-loop and closed-loop MIMO system transfer matrices.

### 1.3.2 Stability analysis of uniform MIMO systems

The stability of the linear closed-loop uniform system is determined by the distribution of roots of the characteristic equation

$$\det [I + w(s)R] = \prod_{i=1}^N [1 + \lambda_i w(s)] = 0, \quad (1.99)$$

which, apparently, is equivalent to a set of  $N$  equations

$$1 + \lambda_i w(s) = 0, \quad i = 1, 2, \dots, N \quad (1.100)$$

or, taking into account Equation (1.90), to a set of equations

$$D(s) + \lambda_i M(s) = 0, \quad i = 1, 2, \dots, N \quad (1.101)$$

coinciding with characteristic equations of the closed-loop one-dimensional characteristic systems (Sobolev 1973; Gasparyan 1976).

<sup>33</sup> That multiplier with the unity magnitude can be referred to either  $U$  or  $V$ .

The fact that the CTFs  $q_i(s)$  [Equation (1.94)] differ from the common transfer function  $w(s)$  of separate channels only by numerical coefficients  $\lambda_i$  considerably simplifies the stability analysis of uniform systems. Here, two formulations of the generalized Nyquist criterion are possible, leading to different graphical techniques and procedures (for simplicity, we shall call them the *direct* and *inverse*). The first of them (the ‘direct’ formulation) essentially coincides with that presented in Section 1.2.4. The only difference is that for the stability of the closed-loop uniform system, it is necessary that the sum of anticlockwise encirclements of the critical point  $(-1, j0)$  by *each* characteristic gain locus (the Nyquist plot)  $\lambda_i w(j\omega)$ , as the angular frequency  $\omega$  changes from  $-\infty$  to  $+\infty$ , be equal to  $k_0$ , where  $k_0$  is the number of the right half-plane poles of transfer function  $w(s)$ . If the characteristic gain loci  $\lambda_i w(j\omega)$  are plotted only for positive frequencies  $\omega \geq 0$ , then the mentioned sum must be  $k_0/2$ . According to this formulation,  $N$  Nyquist plots of  $\lambda_i w(j\omega)$  are plotted in the complex plane. Each of them is obtained from  $w(j\omega)$  by multiplying the magnitude of the latter by  $|\lambda_i|$ , and subsequently rotating about the origin by angle  $\arg \lambda_i$ . Next, the location of all Nyquist plots of  $\lambda_i w(j\omega)$  with respect to the point  $(-1, j0)$  is analysed.

In accordance with the second ‘inverse’ formulation, Equation (1.100) should be rewritten in the form

$$w(s) = -\frac{1}{\lambda_i}, \quad i = 1, 2, \dots, N. \tag{1.102}$$

In this case, in the complex plane, we have a *single* locus  $w(j\omega)$  (i.e. the Nyquist plot) of identical separate channels and  $N$  *critical points*  $-1/\lambda_i$ . For the stability of the closed-loop uniform system, it is necessary and sufficient that the Nyquist plot of  $w(j\omega)$  encircles *each* of  $N$  points  $-1/\lambda_i$  in an anticlockwise direction  $k_0$  times (Sobolev 1973). In the case of stable  $w(s)$ , i.e. for  $k_0 = 0$ , both variants of using the generalized Nyquist criterion are qualitatively illustrated in Figure 1.20 for  $N = 4$ , in which the characteristic gain loci are plotted for positive frequencies  $\omega \geq 0$ .

The simple form of CTFs of the open-loop uniform system makes it very convenient using the logarithmical form of the Nyquist criterion, since the Bode magnitude and phase plots of characteristic systems are obtained from the corresponding plots of transfer function  $w(s)$

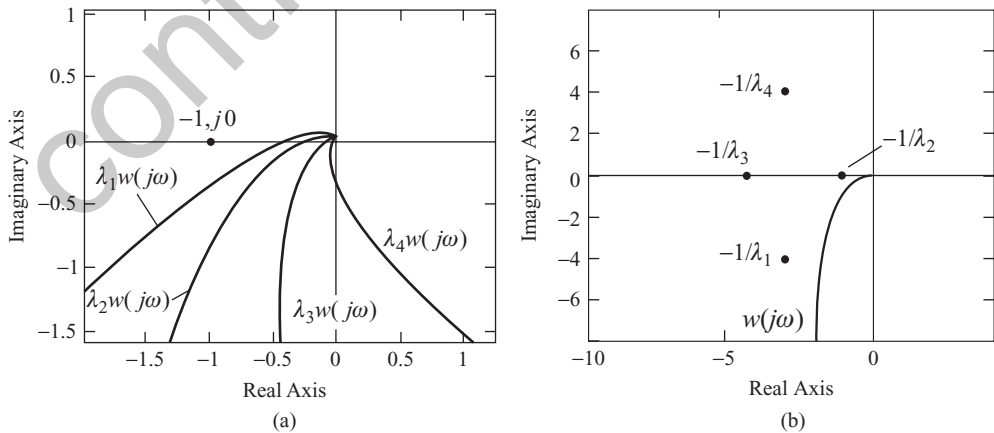


**Figure 1.20** Stability analysis of the uniform system with the help of the Nyquist criterion ( $N = 4$ ). (a) ‘direct’ form; (b) ‘inverse’ form.

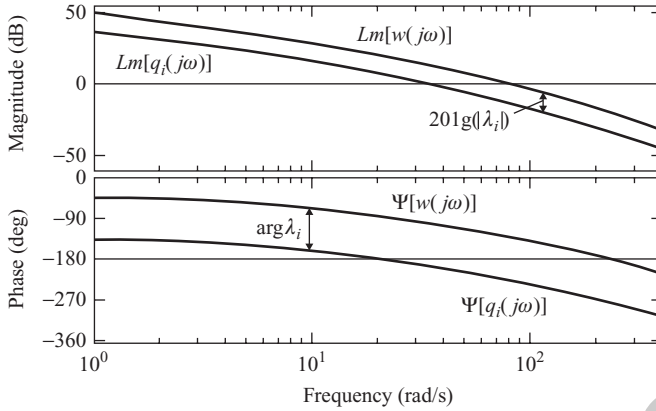


**Figure 1.21** Stability analysis of the uniform system by means of the Bode diagram.

by simple shifts along the ordinate axis. The Bode magnitude plot  $Lm[w(j\omega)]$  is shifted by magnitudes  $Lm[\lambda_i] = 20 \lg(|\lambda_i|)$ , and the Bode phase plot  $\Psi[w(j\omega)]$  is shifted by  $\arg \lambda_i$  ( $i = 1, 2, \dots, N$ ) (Figure 1.21).<sup>34</sup> With respect to the shifted plots, the Nyquist criterion has the standard form known from the classical control theory (Ogata 1970; Kuo 1995).

**Example 1.4** Consider the two-axis indirect guidance system described in Example 1.1. Let the transfer functions of both channels be identical, i.e.  $W_1(s) = W_2(s) = W_0(s)$ , and have the form

$$W_0(s) = \frac{15000000000(s + 3)}{s(s + 0.33)(s + 400)^2(s + 500)}. \quad (1.103)$$

With such transfer functions, the two-axis system in Figures 1.7 and 1.8 is uniform. Consider two cases, with different combinations of angles  $\alpha_1$  and  $\alpha_2$ :  $\alpha_1 = 40^\circ$ ,  $\alpha_2 = 35^\circ$  and  $\alpha_1 = 40^\circ$ ,  $\alpha_2 = -35^\circ$ , i.e. the magnitudes of  $\alpha_1$  and  $\alpha_2$  in the second case do not change, but the angle  $\alpha_2$  has a negative sign. The matrix of cross-connections [Equation (1.60)]:

$$R = \begin{pmatrix} \cos \alpha_1 & \sin \alpha_1 \\ -\sin \alpha_2 & \cos \alpha_2 \end{pmatrix} \quad (1.104)$$

for the given combinations of  $\alpha_1$  and  $\alpha_2$  is

$$R_+ = \begin{pmatrix} 0.766 & 0.643 \\ -0.574 & 0.819 \end{pmatrix}, \quad R_- = \begin{pmatrix} 0.766 & 0.643 \\ 0.574 & 0.819 \end{pmatrix}, \quad (1.105)$$

where the matrix  $R_+$  corresponds to the positive angle  $\alpha_2$ , and  $R_-$  to the negative one. The eigenvalues of  $R$  are defined by the following expression:

$$\lambda_{1,2} = \frac{\cos \alpha_1 + \cos \alpha_2}{2} \pm \sqrt{\frac{(\cos \alpha_1 + \cos \alpha_2)^2}{4} - \cos(\alpha_1 - \alpha_2)} \quad (1.106)$$

<sup>34</sup> Further, everywhere,  $Lm[\cdot]$  and  $\Psi[\cdot]$  denote the Bode magnitude and phase plots of the corresponding transfer functions.

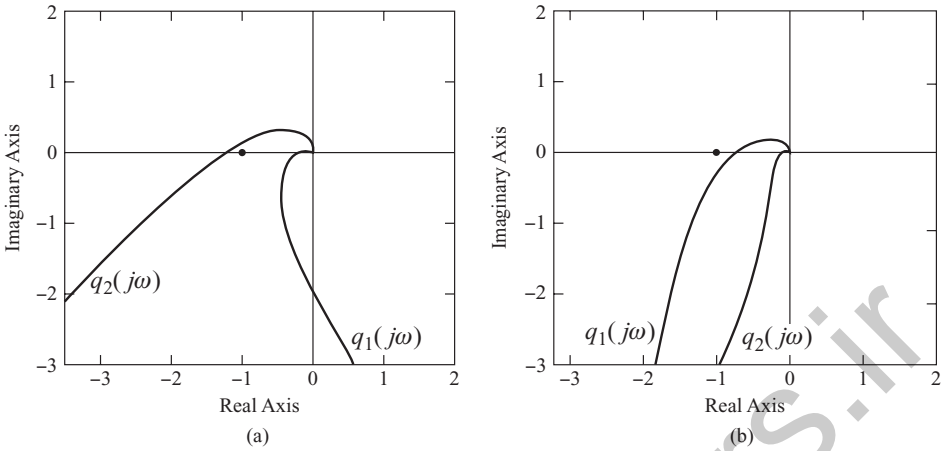


**Figure 1.22** Stability analysis of the uniform guidance system ('direct' form). (a)  $\alpha_1 = 40^\circ, \alpha_2 = 35^\circ$ ; (b)  $\alpha_1 = 40^\circ, \alpha_2 = -35^\circ$ .

and, correspondingly, are equal to

$$\lambda_1 = 0.7926 + j0.6066, \quad \lambda_2 = 0.7926 - j0.6066, \quad \text{for } R_+, \quad (1.107)$$

and

$$\lambda_1 = 1.4004, \quad \lambda_2 = 0.1848, \quad \text{for } R_-, \quad (1.108)$$

i.e. in the case of positive angle  $\alpha_2$ , the eigenvalues are complex conjugate and, in the second case, they are real. The Nyquist plots of the uniform guidance system with the given combinations of  $\alpha_1$  and  $\alpha_2$  are shown in Figures 1.22 and 1.23, where Figure 1.22 corresponds to the

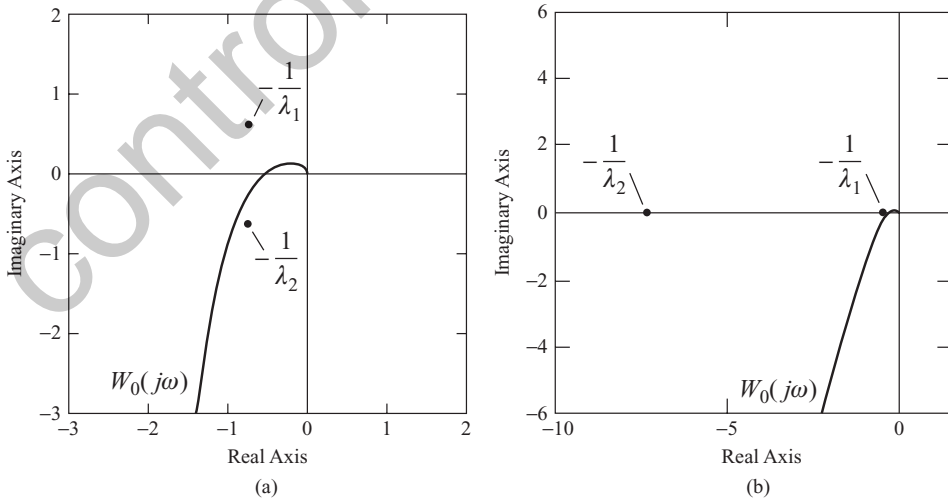


**Figure 1.23** Stability analysis of the uniform guidance system ('inverse' form). (a)  $\alpha_1 = 40^\circ, \alpha_2 = 35^\circ$ ; (b)  $\alpha_1 = 40^\circ, \alpha_2 = -35^\circ$ .

first ('direct') formulation of the Nyquist criterion and Figure 1.23 to the second ('inverse') formulation. These figures show that the stability of the guidance system depends considerably on the sign of  $\alpha_2$ . For the positive value of  $\alpha_2$  and complex conjugate eigenvalues [Equation (1.106)], the system is unstable and, for the negative  $\alpha_2$  and real eigenvalues, it is stable. That fact is not a mandatory rule but, in practice, the complex conjugate eigenvalues of the matrix  $R$  are usually more 'dangerous' from the stability viewpoint. In conclusion, we point out that the gain and phase margins of the uniform guidance system for  $\alpha_2 = -35^\circ$  are determined by the first characteristic system ( $\lambda_1 = 1.4004$ ) and are equal, respectively, to  $GM = 3.16$  dB and  $PM = 15.36^\circ$ .

**Example 1.5** The second example in this section can serve as a visual illustration that the CTFs method allows not only the obtaining of quantitative data and estimates, but also the drawing of qualitative conclusions about stability margins of MIMO systems. Consider the same uniform guidance system as in the previous example, assuming angles  $\alpha_1$  and  $\alpha_2$  are equal, i.e.  $\alpha_1 = \alpha_2 = \alpha$ , and find the value of angle  $\alpha$  for which the system reaches the stability boundary.

Geometrically, the equal values of angles  $\alpha_1$  and  $\alpha_2$  mean that the 'measurement' coordinate system  $OX_1X_2$ , composed of the sensitivity axes of the stellar sensors, is orthogonal, and is rotated by angle  $\alpha$  with respect to the telescope-fixed orthogonal coordinate system ('guidance' coordinate system)  $OY_1Y_2$  (Figure 1.24).

The matrix  $R$  [Equation (1.60)] in this case has the form

$$R = \begin{pmatrix} \cos \alpha & \sin \alpha \\ -\sin \alpha & \cos \alpha \end{pmatrix} \quad (1.109)$$

and is antisymmetrical (Gasparyan 1976) and, more significantly for us at this point, orthogonal, i.e.  $\det R = 1$  and  $R^{-1} = R^T$  (Bellman 1970). Eigenvalues [Equation (1.106)] of  $R$  have a simple form and are expressed as

$$\lambda_{1,2} = \cos \alpha \pm j \sin \alpha = \exp\{\pm j\alpha\} \quad (1.110)$$

i.e. they are located on the unit circle and form angles  $\pm\alpha$  with the positive direction of the real axis. For  $\alpha = 0^\circ$ , the coordinate systems  $OX_1X_2$  and  $OY_1Y_2$  in Figure 1.24 coincide, the matrix  $R$  [Equation (1.109)] becomes the unit matrix  $I$ , and both eigenvalues  $\lambda_{1,2}$  [Equation (1.110)] are equal to unity. Structurally, this means that the two-axis guidance system splits

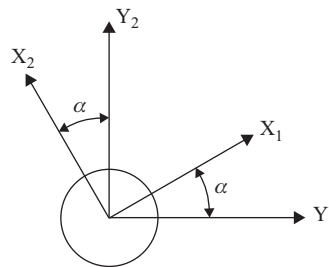


**Figure 1.24** Reciprocal location of the coordinate systems for  $\alpha_1 = \alpha_2 = \alpha$ .

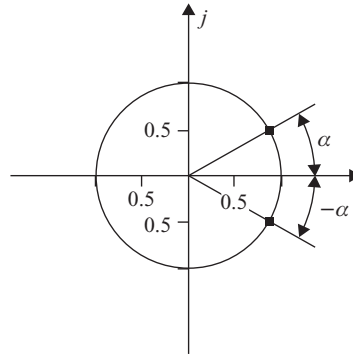


Figure 1.25 Eigenvalues location on the unit circle.

into two independent channels. For  $\alpha \neq 0$ , there appear cross-connections, and eigenvalues  $\lambda_{1,2}$  move from the point  $(+1, j0)$  in the opposite directions along the unit circle (Figure 1.25). The CTFs  $q_1(j\omega)$  and  $q_2(j\omega)$  of the open-loop system are

$$q_1(j\omega) = \exp\{j\alpha\}W_0(j\omega), \quad q_2(j\omega) = \exp\{-j\alpha\}W_0(j\omega), \quad (1.111)$$

i.e. the first characteristic gain locus  $q_1(j\omega)$  is obtained from the Nyquist plot of  $W_0(j\omega)$  by the anticlockwise rotation of  $W_0(j\omega)$  about the origin through the angle  $\alpha$ , and the second locus  $q_2(j\omega)$  is obtained by the clockwise rotation of  $W_0(j\omega)$  through the same angle. In the case of ‘inverse’ formulation of the Nyquist criterion, graphical plotting is carried out on the plane of the single Nyquist plot of  $W_0(j\omega)$ , where critical points  $-1/\lambda_{1,2}$  coincide with the point  $(-1, j0)$  for  $\alpha = 0^\circ$  and, for  $\alpha \neq 0$ , they move along the unit circle, forming with the negative real axis angles  $-\alpha$  and  $+\alpha$ . All this is illustrated in Figure 1.26, from which it is finally clear that the critical value of angle  $\alpha$ , for which the cross-connected guidance system reaches the

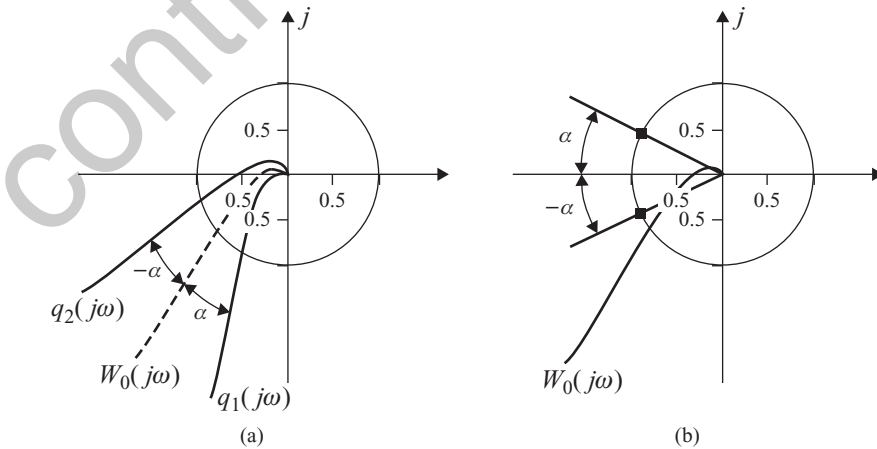
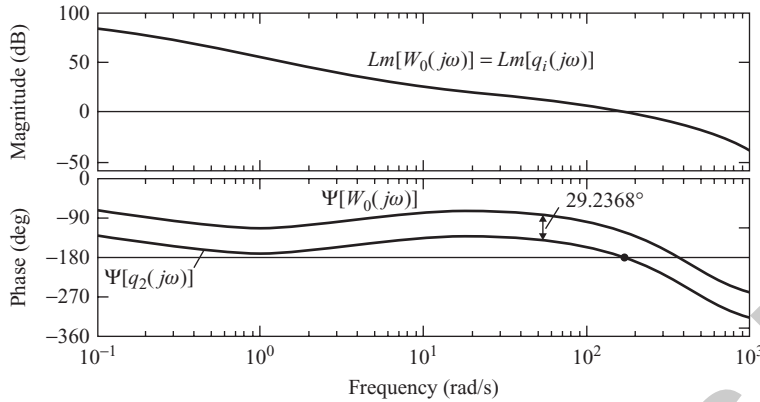


Figure 1.26 Stability analysis of the guidance system for  $\alpha_1 = \alpha_2$ . (a) ‘direct’ form; (b) ‘inverse’ form.



**Figure 1.27** Bode diagram of the guidance system for  $\alpha = 29.2368^\circ$ .

stability boundary, is equal to the *phase margin* of identical isolated separate channels of the system. This inference is general for two-dimensional uniform systems with the orthogonal matrix of cross-connections  $R$  [Equation (1.109)] and is valid for any transfer function  $W_0(s)$  of separate channels. For our system with transfer function  $W_0(j\omega)$  [Equation (1.103)], the phase margin of the separate channel is  $PM = 29.2368^\circ$ . Letting the angle  $\alpha$  be equal to that value, the guidance system is on the stability boundary. The Bode diagram given in Figure 1.27 verifies that conclusion. In this figure, the bold dot at the intersection of the line  $-180^\circ$  with the Bode phase plot of the second characteristic system is mapping of the point  $(-1, j0)$ . Note that the Bode magnitude plots of the CTFs  $q_1(j\omega)$  and  $q_2(j\omega)$  coincide with the corresponding plot of  $W_0(j\omega)$  (since  $|\lambda_1| = |\lambda_2| = 1$ ), and the Bode phase plots of  $q_1(j\omega)$  and  $q_2(j\omega)$  are obtained from the phase plot of  $W_0(j\omega)$  by the parallel shifts  $\pm\alpha$  along the ordinate axis.

Thus, in the considered example, we have obtained not only the *quantitative*, but also the *qualitative* information about the stability margins of the two-dimensional uniform system with an orthogonal matrix of cross-connections. This confirms the effectiveness of approaches based on the CTFs.

**Remark 1.9** As we know, in the case of general linear MIMO systems, the CTFs are *algebraic functions* and are situated on different sheets of a unique Riemann surface, and the transition from one branch of the characteristic gain loci to another is related to the so-called *branch points*.<sup>35</sup> A natural question arises of whether the specific structural features of uniform MIMO systems lead, from that point of view, to some peculiarities, if we take into account that the CTFs of these systems have quite a simple form [Equation (1.105)] and can readily be found analytically. To answer this question from the general position of the CTFs method, we substitute the transfer matrix of the open-loop uniform system [Equation (1.102)] into Equation (1.26), from which, after some elementary transformations, we obtain

$$\det[qI - C \text{diag}\{\lambda_i w(s)\} C^{-1}] = \det[C \text{diag}\{q - \lambda_i w(s)\} C^{-1}] = \prod_{i=1}^N [q - \lambda_i w(s)] = 0. \quad (1.112)$$

<sup>35</sup> See Remark 1.3.

This expression shows that Equation (1.26), the solution to which gives the CTFs of linear MIMO systems, in the case of uniform systems, splits into  $N$  first-order equations, linear with respect to  $q$ . Then, based on the general theory (Postlethwaite and MacFarlane 1979), we can state that in the case of uniform systems, we have  $N$  *isolated* algebraic functions, and each of them is situated on an individual *one-sheeted* Riemann surface. In other words, the CTFs of uniform systems, being proper rational functions in complex variable  $s$ , *do not have branch points* and thereby can be treated, not in the least disregarding the mathematical rigour, as a set of  $N$  independent SISO systems.

**Remark 1.10** The matrix block diagram of Figure 1.18 is, broadly speaking, typical for uniform MIMO systems. At the same time, in different technical applications, systems having far more complicated structures, with several contours of feedforward or/and feedback connections occur; these systems may formally be viewed as uniform, since all their separate channels are identical, and different blocks of cross-connections are described by some numerical matrices (Sobolev 1973). For example, one such structure is depicted in Figure 1.28, where  $R_1$  and  $R_2$  are numerical matrices, and  $w_1(s)$  and  $w_2(s)$  are scalar transfer functions. Unfortunately, not all such MIMO systems with identical channels and several matrices of rigid cross-connections can be referred to as uniform systems, and the point is that different numerical matrices of cross-connections are generally brought to diagonal form in different canonical bases. However, it is also possible to select among such MIMO systems those that satisfy the uniformity requirements and can be studied on the base of the techniques developed in this section. The fact is that, as is well known from the theory of matrices (Marcus and Minc 1992), different square matrices (in our case,  $R_1$  and  $R_2$ ) can be brought simultaneously to diagonal form in a certain basis if they are *commutative*, i.e.  $R_1 R_2 = R_2 R_1$ .

From here, we have the following main rule determining when a MIMO system belongs to the class of uniform systems:

*A MIMO system is uniform if all separate channels of the system are identical, i.e. all dynamical blocks constituting the system are described by some scalar transfer matrices, and all numerical matrices of cross-connections are commutative.*

The indicated condition of commutativity actually means that all matrix blocks of the uniform MIMO system can be interchanged, and that condition reinforces the analogy between methods of study of uniform systems and common SISO systems. Accordingly, if the mentioned condition is not satisfied, then the system must be regarded as a general MIMO system, and its study can be accomplished only by the corresponding methods and computational procedures.

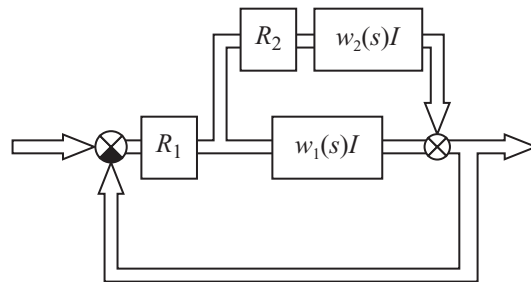


**Figure 1.28** Definition of the notion ‘uniform MIMO system’.

## 1.4 NORMAL MIMO SYSTEMS

So far, we have considered general and uniform MIMO systems, paying no special attention to geometrical features or peculiarities of their canonical bases. In this section, we discuss the so-called *normal* systems,<sup>36</sup> which constitute a significant class of multivariable control systems with individual attributes and characteristics inherent only to that class.

### 1.4.1 Canonical representations of normal MIMO systems

A linear MIMO system is said to be *normal* if the open-loop transfer matrix of the system is normal, i.e. commutes with its conjugate (complex conjugate and transposed) matrix:

$$W(s)W^*(s) = W^*(s)W(s) \quad (1.113)$$

It is easy to show that normality of  $W(s)$  implies normality of the closed-loop MIMO system transfer matrices  $\Phi(s)$  and  $\Phi_\varepsilon(s)$ , and, vice versa, normality of  $\Phi(s)$  or  $\Phi_\varepsilon(s)$  implies normality of  $W(s)$ . In other words, instead of Equation (1.113), we can write two equivalent conditions of the MIMO system normality:

$$\Phi(s)\Phi^*(s) = \Phi^*(s)\Phi(s) \quad (1.114)$$

and

$$\Phi_\varepsilon(s)\Phi_\varepsilon^*(s) = \Phi_\varepsilon^*(s)\Phi_\varepsilon(s). \quad (1.115)$$

The primary, principal property of normal MIMO systems consists in the orthogonality of their canonical bases composed of the normalized eigenvectors  $c_i(s)$  ( $|c_i(s)| = 1$ ) of  $W(s)$ . Owing to the conditions in Equation (1.32), the dual basis of a normal MIMO system is also orthogonal and identically coincides with the canonical basis (Derusso *et al.* 1965; Gasparyan 1976, 1986). As will be shown in the following chapters, all this predetermines a number of remarkable features of normal MIMO systems, essentially distinguishing them from all other types of MIMO systems.

Since the canonical basis of normal MIMO systems is orthonormal, the modal matrix  $C(s)$  belongs to the class of *unitary* matrices for which  $C^{-1}(s) = C^*(s)$ , i.e. the inverse matrix coincides with conjugate. From that, and taking into account the coincidence of the dual and canonical bases ( $c_i^+(s) = c_i(s)$ ), we obtain the following canonical representations of the transfer matrices of normal MIMO systems via the similarity transformation and dyadic designations:

$$W(s) = C(s)diag\{q_i(s)\}C^*(s) = \sum_{i=1}^N c_i(s) > q_i(s) < c_i(s) \quad (1.116)$$

$$\Phi(s) = C(s)diag\left\{\frac{q_i(s)}{1+q_i(s)}\right\}C^*(s) = \sum_{i=1}^N c_i(s) > \frac{q_i(s)}{1+q_i(s)} < c_i(s) \quad (1.117)$$

$$\Phi_\varepsilon(s) = C(s)diag\left\{\frac{1}{1+q_i(s)}\right\}C^*(s) = \sum_{i=1}^N c_i(s) > \frac{1}{1+q_i(s)} < c_i(s). \quad (1.118)$$

<sup>36</sup> The term *normal* MIMO system originates from the theory of matrices (Bellman 1970; Gantmacher 1964).

To normal systems belong circulant, anticirculant, simple symmetrical and antisymmetrical MIMO systems (Gasparyan 1976, 1981, 1986), including two-dimensional systems with symmetrical and antisymmetrical cross-connections (Barski 1966; Kazamarov *et al.* 1967; Krassovski 1957) frequently occurring in various technical applications.

Consider now the singular value decomposition of the normal MIMO system. In Section 1.2.5, it was indicated that with each transfer matrix of the open- or closed-loop MIMO system, there are two associated orthonormal bases called the *left* and *right* (or *input* and *output*) *singular bases* of the MIMO system, as well as a set of  $N$  real numbers called the *singular values*. Generally, each transfer matrix  $W(s)$ ,  $\Phi(s)$  or  $\Phi_\varepsilon(s)$  has its own set of singular bases and singular values, and there is no explicit relationship among the sets belonging to different matrices. As was pointed out in Section 1.2.5, the left singular basis of a square matrix  $A$  consists of eigenvectors of the Hermitian matrix  $AA^*$ , and the right singular basis consists of eigenvectors of the Hermitian matrix  $A^*A$ ; the singular values of  $A$  are equal to positive values of the square roots taken of the eigenvalues of  $AA^*$  (or  $A^*A$ ). Let us compose the corresponding Hermitian matrices for the transfer matrix  $W(s)$  of the open-loop normal MIMO system. Taking into account that for unitary matrices, the inverse matrix coincides with its conjugate yields

$$\begin{aligned}
 W(s)W^*(s) &= C(s)\text{diag}\{q_i(s)\} \underbrace{C^*(s)C(s)}_I \text{diag}\{\tilde{q}_i(s)\}C^*(s) \\
 &= C(s)\text{diag}\{|q_i(s)|^2\}C^*(s),
 \end{aligned} \tag{1.119}$$

from which we come to an extremely important conclusion that for the open-loop normal system, *the left and right singular bases coincide with each other and coincide with the canonical basis, and singular values are equal to the magnitudes of the CTFs  $q_i(s)$  of the open-loop characteristic systems*. Proceeding in the same manner, we find for the transfer matrices  $\Phi(s)$  and  $\Phi_\varepsilon(s)$  of the closed-loop normal system:

$$\Phi(s)\Phi^*(s) = C(s)\text{diag} \left\{ \left| \frac{q_i(s)}{1 + q_i(s)} \right|^2 \right\} C^*(s) \tag{1.120}$$

$$\Phi_\varepsilon(s)\Phi_\varepsilon^*(s) = C(s)\text{diag} \left\{ \frac{1}{|1 + q_i(s)|^2} \right\} C^*(s). \tag{1.121}$$

Hence, *all singular bases of the closed-loop normal MIMO system coincide with the canonical basis, and the singular values are equal to magnitudes of the corresponding transfer functions of the closed-loop SISO characteristic systems*. The spectral norms of the transfer matrices  $W(s)$ ,  $\Phi(s)$  and  $\Phi_\varepsilon(s)$  are equal to the *largest of the CTFs magnitudes*, i.e.

$$\|W(s)\| = \max_i(|q_i(s)|), \quad \|\Phi(s)\| = \max_i \left( \left| \frac{q_i(s)}{1 + q_i(s)} \right| \right), \quad \|\Phi_\varepsilon(s)\| = \max_i \left( \frac{1}{|1 + q_i(s)|} \right). \tag{1.122}$$

Thus, in the case of the normal MIMO system, all singular bases coincide with the canonical basis, and the singular values are directly expressed through the transfer functions of the corresponding characteristic systems, i.e. here, we have a unified and visual internal geometrical structure of the system.

We proceed now to the case of normal uniform systems. We show first that the normality condition of the uniform system is entirely determined by properties of the numerical matrix of cross-connections  $R$  (Figure 1.18) and does not depend on the transfer function  $w(s)$  of identical separate channels. Let the uniform system be normal. Then, from Equations (1.113) and (1.91), taking into account the equality  $w(s)w^*(s) = |w(s)|^2$  and knowing that for real matrices, the operations of conjugation and transposing are equivalent, instead of Equation (1.113), we have

$$|w(s)|^2 RR^T = |w(s)|^2 R^T R. \quad (1.123)$$

From here, canceling the common factor  $|w(s)|^2$  on both sides, we finally obtain the following condition of normality of the uniform system:

$$RR^T = R^T R, \quad (1.124)$$

which has the form of the condition of normality of the real matrix  $R$  (Gantmacher 1964), well known in the theory of matrices. We will not write out the expressions for transfer matrices of normal uniform systems – they evidently ensue from Equations (1.119)–(1.122), and the reader is able to do it without difficulty on his own.

To normal systems belong to the uniform systems with circulant and anticirculant, symmetrical and antisymmetrical, as well as with orthogonal matrices of cross-connections, that is the types of uniform systems described most in the scientific and technical literature (Gasparyan 1976, 1986). By antisymmetrical matrices, here, we mean, as it is accepted in the multivariable control theory (Chorol *et al.* 1976), such matrices  $R$  that can be represented in the form

$$R = rI + R_o, \quad (1.125)$$

where  $r$  is a scalar, and  $R_o$  is a usual skew-symmetrical matrix (Gantmacher 1964) satisfying the condition  $R_o = -R_o^T$ .<sup>37</sup>

In conclusion, note that in the case of normal MIMO systems, the Euclidian norms (‘lengths’) of the input, output and error vectors are, by pairs, the same in both the natural and canonical bases. This is explained by the fact that magnitudes of the vectors are invariant under the similarity transformations via the unitary modal matrix  $C(s)$  (or  $C$  for uniform systems) (Derusso *et al.* 1965).

## 1.4.2 Circulant MIMO systems

In the last part of this section, we consider two special subclasses of normal systems, namely the circulant and anticirculant MIMO systems. The chief distinctive feature of these systems is independence of their canonical bases from  $s$ . Generally, in contrast to normal uniform systems, these systems can have different *dynamical* cross-connections between the separate channels. Moreover, the class of normal uniform systems includes the corresponding subclasses

<sup>37</sup> To such uniform systems belong the two-axis guidance system with the orthogonal (and, at the same time, anti-symmetrical) matrix of cross-connections  $R$  [Equation (1.109)] discussed in Example 1.5.

of systems which, by the structure of the numerical matrix of cross-connections, also belong to circulant or anticirculant systems.

The distinctive feature of *circulant* MIMO systems is that their transfer matrices  $W(s)$ ,  $\Phi(s)$  and  $\Phi_g(s)$  are circulant. Recall that in a circulant matrix, each subsequent row is obtained from the preceding row by shifting all elements (except for the  $N$ th) by one position to the right; the  $N$ th element of the preceding row then becomes the first element of the following row (Davis 1979; Voevodin and Kuznetsov 1984). For the matrix  $W(s)$ , this looks like this:

$$W(s) = \begin{pmatrix} w_0(s) & w_1(s) & w_2(s) & \dots & w_{N-1}(s) \\ w_{N-1}(s) & w_0(s) & w_1(s) & \dots & w_{N-2}(s) \\ w_{N-2}(s) & w_{N-1}(s) & w_0(s) & \dots & w_{N-3}(s) \\ \dots & \dots & \dots & \dots & \dots \\ w_1(s) & w_2(s) & w_3(s) & \dots & w_0(s) \end{pmatrix} \quad (1.126)$$

Each diagonal of a circulant matrix consists of the same elements, and the diagonals located at the same distance from the lower left corner and from the principal diagonal consist of identical elements.<sup>38</sup> Physically, this means that in the circulant MIMO system, it is possible to single out some groups of subsystems with identical transfer functions of all cross-connections, i.e. having internal symmetry. The MIMO systems described by circulant matrices constitute a significant class of multivariable control systems especially widespread in process control. Industrial and other examples of circulant systems include cross-directional control of paper machines if the edge effects are neglected, multizone crystal growth furnaces, dyes for plastic films, burner furnaces, some gyroscopic platforms (Hovd and Skogestad 1992, 1994a; Chorol *et al.* 1976; Sobolev 1973) and many others.

It is easy to see that any circulant matrix is completely defined by the first (or any other) row. Using the designations  $w_0(s)$ ,  $w_i(s) (i = 1, 2, \dots, N - 1)$ <sup>39</sup> [Equation (1.126)] for the first row of the circulant matrix  $W(s)$ , the latter can be represented in the matrix polynomial form

$$W(s) = w_0(s)I + \sum_{k=1}^{N-1} w_k(s)U^k, \quad (1.127)$$

where  $I$  is the unit matrix and

$$U = \begin{pmatrix} 0 & 1 & 0 & \dots & 0 \\ 0 & 0 & 1 & \dots & 0 \\ \dots & \dots & \dots & \dots & \dots \\ 1 & 0 & 0 & \dots & 0 \end{pmatrix} \quad (1.128)$$

is the orthogonal *permutation matrix* (Marcus and Minc 1992).<sup>40</sup> Since the permutation matrix  $U$  plays a crucial role in the theory of circulant MIMO systems, let us consider it at more

<sup>38</sup> From the general positions of the theory of matrices, the circulant matrices belong to the so-called *Toeplitz* matrices (Voevodin and Kuznetsov 1984).

<sup>39</sup> These designations differ from those used before for describing general MIMO systems, but are more convenient in this case.

<sup>40</sup> In essence, the permutation matrix  $U$  can be regarded as the simplest circulant matrix.

length. Like all orthogonal matrices (Gantmacher 1964), the matrix  $U$  satisfies the following conditions:  $U^{-1} = U^T$ ,  $\det U = -1$  (the so-called *improper* orthogonality); all eigenvalues of  $U$  have unit magnitudes. If we multiply  $U$  by a vector  $x$ , then the first component  $x_1$  becomes the  $N$ th, the second component becomes the first, etc. On increasing the power of  $U$ , both nonzero diagonals shift to the place of the next diagonal on the right, and the powers of  $U$  satisfy the following conditions that can be readily checked by direct calculations:

$$U^k = (U^{N-k})^T = (U^{N-k})^{-1}, \quad U^N = I, \quad k = 1, 2, \dots, N - 1. \quad (1.129)$$

The eigenvalues  $\beta_i$  ( $i = 1, 2, \dots, N$ ) of the permutation matrix  $U$  are the roots of the characteristic equation

$$\det[\beta I - U] = \beta^N - 1 = 0 \quad (1.130)$$

and, for any  $N$ , are expressed in the analytical form

$$\beta_i = \exp \left\{ j \frac{2\pi(i-1)}{N} \right\}, \quad i = 1, 2, \dots, N. \quad (1.131)$$

Geometrically, the roots  $\beta_i$  are situated in the complex plane at the vertices of a regular  $N$ -sided polygon inscribed in the unit circle, and the first root  $\beta_1$  is always real and equal to unity (Figure 1.29). The normalized eigenvectors  $c_i$  of  $U$  have a very simple form (Bellman 1970):

$$c_i = \frac{1}{\sqrt{N}} [1 \ \beta_i \ \beta_i^2 \ \dots \ \beta_i^{N-1}]^T, \quad i = 1, 2, \dots, N. \quad (1.132)$$

Note that since the permutation matrix  $U$  belongs to normal matrices, the modal matrix  $C$  of  $U$  composed of  $c_i$  [Equation (1.132)] is unitary, i.e.  $C^{-1} = C^*$ . It is worth emphasizing that all components of the vectors  $c_i$  [Equation (1.132)] have the same magnitudes, equal to  $1/\sqrt{N}$ . This fact plays an important role in analyzing self-oscillations in nonlinear circulant systems (see Chapter 3).

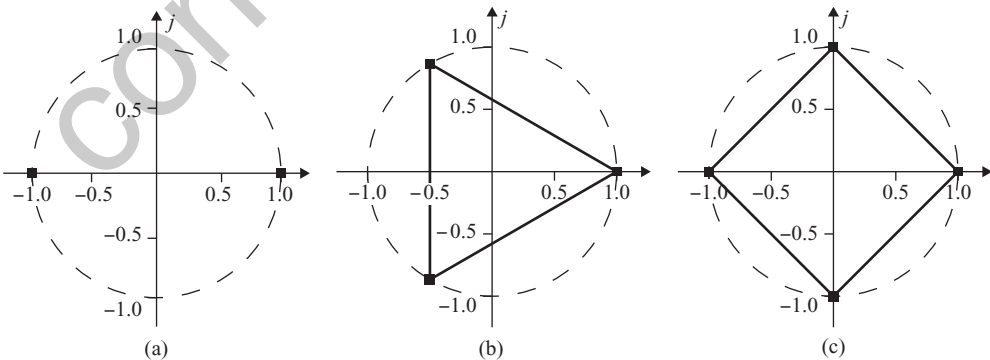


**Figure 1.29** The eigenvalues of the permutation matrix  $U$  [Equation (1.128)]. (a)  $N = 2$ ; (b)  $N = 3$ ; (c)  $N = 4$ .

In the theory of matrices, it is proved that if a square matrix  $A$  is represented as the matrix polynomial in some matrix  $B$ , then the eigenvalues of  $A$  are equal to the values of the corresponding scalar polynomials that are obtained from the matrix polynomial by replacing  $B$  with the eigenvalues of the latter. Also, the eigenvectors of the matrices  $A$  and  $B$ , corresponding to the associated eigenvalues, coincide (Marcus and Minc 1992). Applying this to the circulant matrix  $W(s)$  [Equation (1.127)] yields that the CTFs  $q_i(s)$  can be represented, for any number  $N$  of separate channels, in the analytical form

$$q_i(s) = w_0(s) + \sum_{k=1}^{N-1} w_k(s) \exp \left\{ j \frac{2\pi(i-1)}{N} k \right\}, \quad i = 1, 2, \dots, N. \quad (1.133)$$

Further, from the above statement concerning eigenvectors of matrix polynomials, it follows that the canonical basis of the circulant matrix  $W(s)$ , i.e. the canonical basis of the circulant system (and, naturally, the modal matrix  $C$ ), is inherited from the permutation matrix  $U$  [Equation (1.128)].

The possibility of representing the CTFs  $q_i(s)$  in analytical form for any  $N$  considerably simplifies the study of circulant systems. It is interesting and important to note that canonical bases of circulant systems do not depend on complex variable  $s$  and are the same for all circulant systems with the same number of channels  $N$ , independently of the specific form of the transfer functions  $w_0(s)$  and  $w_k(s) (k = 1, 2, \dots, N - 1)$ .

Consider briefly the uniform circulant MIMO systems. It is easy to understand that for a uniform system to be circulant, it is necessary and sufficient that the matrix of cross-connections  $R$  be circulant. Denoting by  $r_0$  and  $r_k (k = 1, 2, \dots, N - 1)$  the elements of the first row of  $R$ , we obtain for the matrix  $W(s)$  and the CTFs  $q_i(s)$  of the circulant uniform system the following expressions:

$$W(s) = w(s) \left[ r_0 I + \sum_{k=1}^{N-1} r_k U^k \right] \quad (1.134)$$

and

$$q_i(s) = \left[ r_0 + \sum_{k=1}^{N-1} r_k \exp \left\{ j \frac{2\pi(i-1)}{N} k \right\} \right] w(s), \quad i = 1, 2, \dots, N, \quad (1.135)$$

where  $w(s)$  is the scalar transfer function of identical separate channels. The canonical basis and modal matrix of the circulant uniform system are also inherited, evidently, from the permutation matrix  $U$ .

Circulant MIMO systems can be symmetrical and, for odd  $N$ , antisymmetrical. A circulant system is said to be *symmetrical* if the open-loop transfer matrix  $W(s)$  [together with  $\Phi(s)$  and  $\Phi_g(s)$ ] is symmetrical, i.e. if the condition  $W(s) = W^T(s)$  holds. In view of the structural cyclicity of circulant matrices, for a circulant system to be symmetrical, it is enough that the following equalities take place:

$$w_k(s) = w_{N-k}(s), \quad k = 1, 2, \dots, N - 1. \quad (1.136)$$

### 1.4.2.1 Simple symmetrical systems

Among symmetrical circulant systems, the so-called *simple symmetrical* MIMO systems demand special attention, for which the transfer functions of all cross-connections coincide (Sobolev 1973; Gasparyan 1981, 1986; Hovd and Skogestad 1992, 1994a), i.e.

$$w_k(s) = w_1(s), \quad k = 2, \dots, N - 1. \quad (1.137)$$

A significant feature of simple symmetrical MIMO systems is that they have only *two distinct CTFs*. Substituting Equation (1.137) into Equation (1.133) and carrying out some simple transformations yields

$$q_1(s) = w_0(s) + (N - 1)w_1(s) \quad (1.138)$$

and

$$q_2(s) = q_3(s) = \dots = q_N(s) = w_0(s) - w_1(s). \quad (1.139)$$

Hence, in the case of simple symmetrical MIMO systems, there exist, independently of the number of separate channels  $N$ , *only two* transfer functions of the characteristic systems *differing from each other*. In multivariable control theory, the first function  $q_1(s)$  [Equation (1.138)] is frequently called the transfer function of the *average motion*, and all the others [Equation (1.139)] are called the transfer functions of the *relative motions*. These terms have a simple explanation. Let the vectors  $y$  and  $x$  be related by a simple symmetrical matrix  $W(s)$ , i.e.

$$y = W(s)x \quad (1.140)$$

or, in the expanded form,

$$y_i = w_0(s)x_i + w_1(s) \sum_{\substack{k=1 \\ k \neq i}}^N x_k, \quad i = 1, 2, \dots, N. \quad (1.141)$$

Let us introduce the so-called *average* scalar coordinates

$$\bar{y} = \frac{1}{N} \sum_{k=1}^N y_k, \quad \bar{x} = \frac{1}{N} \sum_{k=1}^N x_k, \quad (1.142)$$

having an obvious physical sense. Then, summing  $N$  equations [Equation (1.141)] term by term and performing simple transformations, we obtain the relationship between the average coordinates  $\bar{y}$  and  $\bar{x}$  in the form

$$\bar{y} = [w_0(s) + (N - 1)w_1(s)] \bar{x}. \quad (1.143)$$

The comparison of this expression with Equation (1.138) completely explains the name for  $q_1(s)$ : *the transfer function of the average motion*.

Let us determine now the difference between any two (say, the  $r$ th and the  $k$ th) equations in Equation (1.141). We obtain

$$y_r - y_k = [w_0(s) - w_1(s)](x_r - x_k). \quad (1.144)$$

The comparison of this equation with Equation (1.139) shows that *the transfer functions of the relative motions* relate to each other the differences between the output and input variables of any two channels of the simple symmetrical system. Besides, if we introduce  $N - 1$  *relative* coordinates  $y'_k$  and  $x'_k$  for the components  $y_k$  and  $x_k$  ( $k = 2, \dots, N$ ), defining them as the deviation of each component  $y_k, x_k$  from the corresponding *average* values of  $\bar{y}$  and  $\bar{x}$ :  $y'_k = y_k - \bar{y}$ ,  $x'_k = x_k - \bar{x}$ , then it is easy to show that these variables are also related by the CTFs [Equation (1.139)]. In other words, the CTFs of relative motions can also be viewed as the functions relating the *deviations* from the corresponding *average motion* of the output and input variables of separate channels.

### 1.4.2.2 Antisymmetrical circulant systems

A circulant system with an *odd* number of separate channels  $N$  is called *antisymmetrical* if elements of the first row of the transfer matrix  $W(s)$  satisfy the conditions:

$$w_k(s) = -w_{N-k}(s), \quad k = 1, 2, \dots, N - 1 \quad (1.145)$$

and the matrix  $W(s)$  can be represented in the form

$$W(s) = w_0(s)I + \underbrace{\left\{ \sum_{k=1}^{(N-1)/2} w_k(s)[U^k - (U^k)^{-1}] \right\}}_A, \quad (1.146)$$

where the matrix  $A$  is skew-symmetrical, i.e.  $A = -A^T$ .

The CTFs  $q_i(s)$  of antisymmetrical circulant systems have the form

$$q_i(s) = w_0(s) + j2 \sum_{k=1}^{(N-1)/2} w_k(s) \sin\left(\frac{2\pi(i-1)k}{N}\right), \quad i = 1, 2, \dots, N \quad (1.147)$$

and it is worth mentioning that for any odd  $N$ , the first CTF  $q_1(s)$  always coincides with the transfer function of direct channels  $w_0(s)$ . At last, note that if all transfer functions of cross-connection are the same, i.e. together with the condition of 'correct signs' [Equation (1.145)], the condition in Equation (1.137) holds, then such systems are called *simple antisymmetrical* circulant systems. Simple antisymmetrical systems of odd order  $N$  are described by Equations (1.145) and (1.147), assuming that  $w_k(s) = w_1(s)$  for all  $k = 2, \dots, N - 1$ .

In conclusion, circulant systems of even order  $N$  can be antisymmetrical only if the transfer function  $w_{N/2}(s)$  is identically equal to zero, which is unacceptable in most practical tasks. In particular, the above expressions do not allow describing such important in practice systems as two-dimensional systems with identical channels and antisymmetrical

cross-connections. In the case of an even number of channels, to study the simple antisymmetrical systems, we must apply the theory of anticirculant MIMO systems discussed in the next section.

**Example 1.6** In Chorol *et al.* (1976), a three-axis stabilized platform in which the measurements of angular velocities are accomplished by single-channel two-dimensional gyroscopic devices with amplitude-phase modulation is considered. The open-loop transfer matrix of that system has the form

$$W(s) = w(s) \begin{pmatrix} w_0(s) & w_1(s) & -w_1(s) \\ -w_1(s) & w_0(s) & w_1(s) \\ w_1(s) & -w_1(s) & w_0(s) \end{pmatrix}, \quad (1.148)$$

where the scalar multiplier  $w(s)$  corresponds to the transfer functions of identical channels in the system power part. As evident from Equation (1.148), the control system belongs to simple antisymmetrical systems and can be handled by the above methods. Substituting the elements of  $W(s)$  [Equation (1.148)] into Equation (1.147) immediately yields

$$q_1(s) = w(s)w_0(s), \quad q_{2,3}(s) = w(s)[w_0(s) \pm j\sqrt{3}w_1(s)]. \quad (1.149)$$

This completely agrees with the results developed in Chorol *et al.* (1976) based on the *complex coordinates and complex transfer functions method*.

**Example 1.7** For the last two to three decades, the so-called *hexapods* have found wide application in various technical branches, such as active vibration isolation, control of the secondary mirror for large telescopes, laboratory testing devices, etc. (Geng and Haynes 1994; Pernechele *et al.* 1998; Joshi and Kim 2004, 2005). Physically, a hexapod consists of a movable payload platform connected to the fixed base by six variable-length struts. The length of each strut can be controlled independently by six linear actuators and sensors, to achieve independent translational and rotational motions along the  $X$ -,  $Y$ - and  $Z$ -axes. The simplified kinematic scheme of the hexapod is shown in Figure 1.30.

In general, hexapods provide six degrees of freedom to the platform. If each pair of struts works synchronously to increase or decrease their length, then the hexapod has three degrees of freedom. In view of the constructional symmetry of hexapods, the corresponding control systems are described by the matrices of order  $3 \times 3$  and  $6 \times 6$ , having the following form

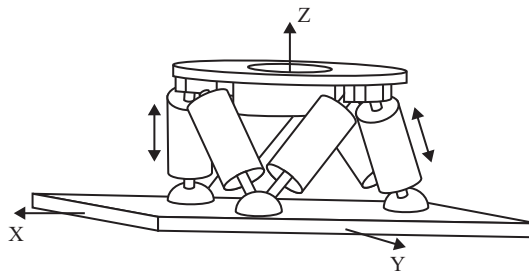


**Figure 1.30** The kinematics of a hexapod.

(Joshi and Kim 2004):

$$W_{H3}(s) = \begin{pmatrix} w_0(s) & w_1(s) & w_1(s) \\ w_1(s) & w_0(s) & w_1(s) \\ w_1(s) & w_1(s) & w_0(s) \end{pmatrix},$$

$$W_{H6}(s) = \begin{pmatrix} w_0(s) & w_1(s) & w_1(s) & w_1(s) & w_1(s) & w_1(s) \\ w_1(s) & w_0(s) & w_1(s) & w_1(s) & w_1(s) & w_1(s) \\ w_1(s) & w_1(s) & w_0(s) & w_1(s) & w_1(s) & w_1(s) \\ w_1(s) & w_1(s) & w_1(s) & w_0(s) & w_1(s) & w_1(s) \\ w_1(s) & w_1(s) & w_1(s) & w_1(s) & w_0(s) & w_1(s) \\ w_1(s) & w_1(s) & w_1(s) & w_1(s) & w_1(s) & w_0(s) \end{pmatrix}. \quad (1.150)$$

As we can see from Equation (1.150), the control systems for hexapods belong to simple symmetrical systems. Let the transfer functions  $w_0(s)$  and  $w_1(s)$  in Equation (1.150) be

$$w_0(s) = \frac{1}{s(0.2s + 1)}, \quad w_1(s) = \frac{0.4}{0.1s + 1}. \quad (1.151)$$

Then, the CTFs of average motion [Equation (1.138)] are

$$q_1^{H3}(s) = w_0(s) + 2w_1(s) = \frac{0.16s^2 + 0.9s + 1}{0.02s^3 + 0.3s^2 + s}$$

$$q_1^{H6}(s) = w_0(s) + 5w_1(s) = \frac{0.4s^2 + 2.1s + 1}{0.02s^3 + 0.3s^2 + s} \quad (1.152)$$

and all the CTFs of relative motion associated with both matrices  $W_{H3}(s)$  and  $W_{H6}(s)$  are identical and have the form [Equation (1.139)]

$$q_2(s) = w_0(s) - w_1(s) = \frac{-0.08s^2 - 0.3s + 1}{0.02s^3 + 0.3s^2 + s}. \quad (1.153)$$

The characteristic gain loci of the CTFs [Equations (1.152) and (1.153)] are shown in Figure 1.31, from which it is evident that the stability of both systems is determined by the CTFs of relative motion [Equation (1.153)] which do not depend on  $N$  and coincide for all  $2 \leq i \leq N$ . The identical gain and phase margins of the discussed systems are equal to  $GM = 6.76$  dB and  $PM = 53.92^\circ$ .

**Example 1.8** As an example of a uniform circulant system, consider a hypothetic 16-channel ( $N = 16$ ) system with the transfer function of separate channels given by Equation (1.103), in which we decrease the gain by a factor of 25, and with a circulant matrix of rigid cross-connections  $R$  having the form

$$R = I + 0.6U, \quad (1.154)$$

where  $I$  is the unit matrix and  $U$  is the permutation matrix [Equation (1.128)] (both matrices have order  $16 \times 16$ ). Physically, such cross-connections mean that in each channel of the system

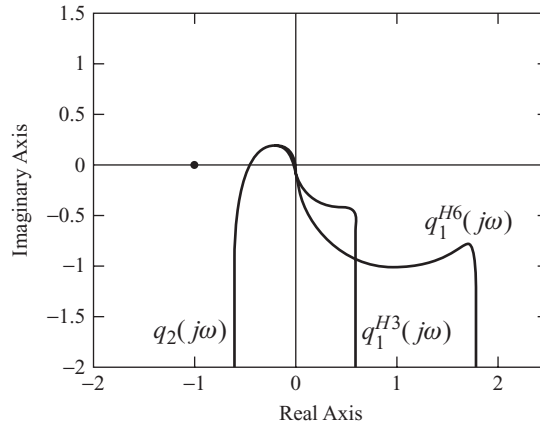


**Figure 1.31** Characteristic gain loci of the hexapods, for  $N = 3$  and  $N = 6$ .

enters the signal from the next channel multiplied by 0.6, and in the last channel enters the corresponding signal from the first channel. In other words, all channels of the given uniform circulant system are connected anticlockwise by a ‘ring scheme’ with the factor of 0.6. The characteristic gain loci of the system in the ‘direct’ and ‘inverse’ forms are given in Figure 1.32. These graphs show that the system is stable. Note that the indicated above decrease of the gain by a factor of 25 was caused by the desire to obtain a stable system, since, for the initial gain, the system would be unstable.

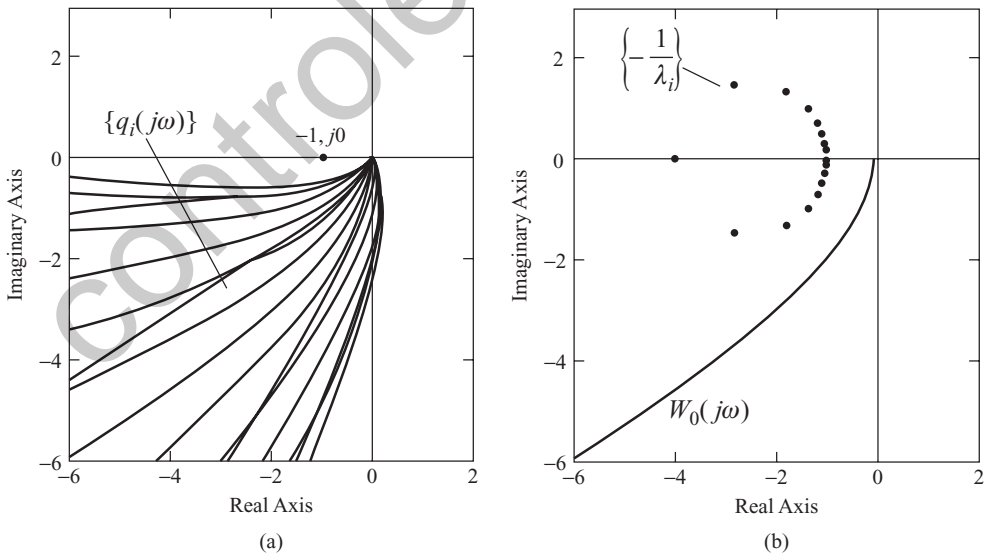


**Figure 1.32** Characteristic gain loci of the uniform circulant system ( $N = 16$ ). (a) ‘direct’ form; (b) ‘inverse’ form.

### 1.4.3 Anticirculant MIMO systems

Below, we discuss a specific subclass of normal MIMO systems referred to as *anticirculant*<sup>41</sup> systems, i.e. systems with anticirculant transfer matrices  $W(s)$ ,  $\Phi(s)$  and  $\Phi_e(s)$ . The major distinction of anticirculant matrices, as compared with common circulant matrices, is that the elements located on both sides of the principal diagonal have opposite signs. This means that each subsequent row of an anticirculant matrix is obtained from the preceding row by shifting all elements (except for the  $N$ th) by one position to the right; the  $N$ th element of the preceding row becomes the first element of the following, with an opposite sign. Thus, the transfer matrix  $W(s)$  of the open-loop anticirculant system can be written as

$$W(s) = \begin{pmatrix} w_0(s) & w_1(s) & w_2(s) & \dots & w_{N-1}(s) \\ -w_{N-1}(s) & w_0(s) & w_1(s) & \dots & w_{N-2}(s) \\ -w_{N-2}(s) & -w_{N-1}(s) & w_0(s) & \dots & w_{N-3}(s) \\ \dots & \dots & \dots & \dots & \dots \\ -w_1(s) & -w_2(s) & -w_3(s) & \dots & w_0(s) \end{pmatrix} \quad (1.155)$$

We know that the simplest of circulant matrices is the permutation matrix  $U$  [Equation (1.128)], and any circulant matrix can be represented as a matrix polynomial in  $U$ . In the case of anticirculant matrices, the *anticirculant permutation matrix* plays a similar role, which we denote by  $U_-$ :

$$U_- = \begin{pmatrix} 0 & 1 & 0 & \dots & 0 \\ 0 & 0 & 1 & \dots & 0 \\ \dots & \dots & \dots & \dots & \dots \\ -1 & 0 & 0 & \dots & 0 \end{pmatrix} \quad (1.156)$$

If we multiply  $U_-$  by a vector  $x$ , then the second component  $x_2$  becomes the first, the third becomes the second, etc.; the first component  $x_1$  becomes the  $N$ th, with the opposite sign. Like  $U$  [Equation (1.128)], the matrix  $U_-$  is orthogonal, i.e. satisfies the conditions  $U_-^{-1} = U_-^T$ ,  $\det U_- = 1$  (the *proper* orthogonality), and all eigenvalues of  $U_-$  have unit magnitudes. On increasing the power of  $U_-$ , both nonzero diagonals shift to the place of the next diagonal on the right; the powers of  $U_-$  satisfy the following conditions:

$$U_-^{N-k} = -(U_-^k)^T = -(U_-^k)^{-1}, \quad U_-^N = I, \quad k = 1, 2, \dots, N - 1. \quad (1.157)$$

The characteristic equation of  $U_-$  [Equation (1.156)] is

$$\det[\beta I - U_-] = \beta^N + 1 = 0. \quad (1.158)$$

The roots  $\beta_i$  of Equation (1.158) are

$$\beta_i = \exp \left\{ j \frac{[2(i - 1) + 1]\pi}{N} \right\}, \quad i = 1, 2, \dots, N \quad (1.159)$$

<sup>41</sup> Seemingly, the term *anticirculant matrix* was introduced in Gasparyan (1981).

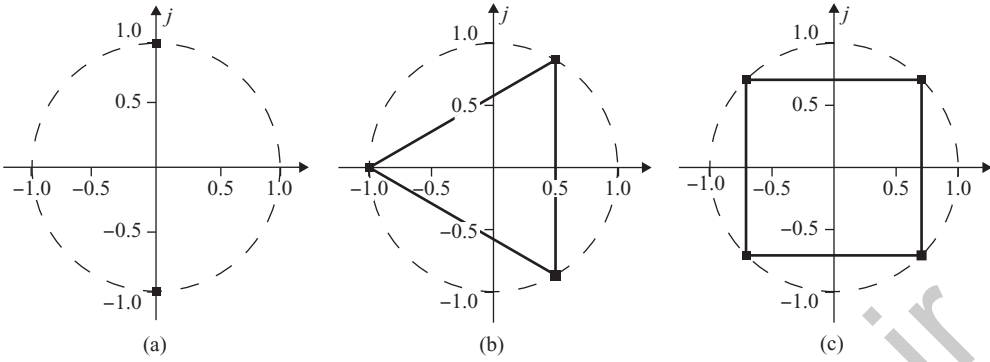


**Figure 1.33** The eigenvalues of the anticirculant permutation matrix  $U_-$ . (a)  $N = 2$ ; (b)  $N = 3$ ; (c)  $N = 4$ .

and, like the eigenvalues of the permutation matrix  $U$  [Equation (1.128)], are situated in the complex plane at the vertices of a regular  $N$ -sided polygon inscribed in the unit circle. For  $N = 2, 3, 4$ , this is illustrated in Figure 1.33 (it is interesting to compare this figure with Figure 1.29). Recall that the first eigenvalue  $\beta_1$  of  $U$  is always real and equal to unity. Unlike this, for *even*  $N$ , all eigenvalues of  $U_-$  [Equation (1.156)] are complex conjugate numbers.<sup>42</sup> The orthonormal eigenvectors  $c_i$  of  $U_-$  are expressed through the eigenvalues  $\beta_i$  [Equation (1.159)] by the same expressions [Equation (1.132)].

As follows from what has been stated, any anticirculant matrix in the form of Equation (1.155) can be represented as a matrix polynomial in  $U_-$  of degree  $(N - 1)$ :

$$W(s) = w_0(s)I + \sum_{k=1}^{N-1} w_k(s)U_-^k. \quad (1.160)$$

For anticirculant MIMO systems of even order  $N$ , which are of primary interest to us, it is usually more convenient to transform Equation (1.160) to another form:

$$W(s) = w_0(s)I + w_{N/2}(s)U_-^{N/2} + \sum_{k=1}^{(N/2)-1} [w_k(s)U_-^k - w_{N-k}(s)(U_-^k)^{-1}]. \quad (1.161)$$

Based on the properties of matrix polynomials given in Section 1.4.2, the CTFs  $q_i(s)$  of an anticirculant system can be represented for any  $N$  in the analytical form

$$q_i(s) = w_0(s) + \sum_{k=1}^{N-1} w_k(s) \exp \left\{ j \frac{[2(i-1) + 1]\pi k}{N} \right\}, \quad i = 1, 2, \dots, N. \quad (1.162)$$

The modal matrix  $C$  and the orthonormal canonical basis of that system do not depend on complex variable  $s$  and coincide with the modal matrix and canonical basis of the anticirculant permutation matrix  $U_-$ .

<sup>42</sup> In the case of odd  $N$  and  $i = (N + 1)/2$ , the eigenvalue  $\beta_i$  is always equal to minus one.

From the practical viewpoint, the most significant are anticirculant systems with an even number of channels  $N$ . The basic statement of this section, completely clarifying the necessity of introducing the concept of anticirculant MIMO systems, can be formulated as follows:

If the number of separate channels  $N$  is even and the conditions

$$w_k(s) = w_{N-k}(s), \quad k = 1, 2, \dots, N - 1 \quad (1.163)$$

hold, then the anticirculant MIMO system is antisymmetrical.

Substituting Equation (1.163) in Equations (1.161) and (1.162) yields, for even-order antisymmetrical MIMO systems:

$$W(s) = w_0(s)I + \left\{ w_{N/2}(s)U_-^{N/2} + \sum_{k=1}^{(N/2)-1} w_k(s)[U_-^k - (U_-^k)^{-1}] \right\} \quad (1.164)$$

and

$$q_i(s) = w_0(s) + j(-1)^{i+1}w_{N/2}(s) + 2j \sum_{k=1}^{(N/2)-1} w_k(s) \sin \left\{ \frac{[2(i-1)+1]\pi}{N} k \right\} \quad (1.165)$$

$i = 1, 2, \dots, N,$

where the braces in Equation (1.164) encompass a skew-symmetrical matrix.

Hence, anticirculant matrices enable us to describe analytically a certain class of antisymmetrical MIMO systems of even order, which was impossible by means of circulant matrices. First of all, this concerns the *simple antisymmetrical* MIMO systems (and, naturally, the simple antisymmetrical uniform systems) of even order, for which, in Equations (1.164) and (1.165),  $w_k(s) = w_1(s)$  ( $k = 2, \dots, N - 1$ ) should be assumed. In the specific, but very important, case of two-dimensional systems with antisymmetrical cross-connections, from Equation (1.165), the well known expression follows (Krassovski 1957):<sup>43</sup>

$$q_{1,2}(s) = w_0(s) \pm j w_1(s). \quad (1.166)$$

This indicates that two-dimensional antisymmetrical systems with constant parameters, studied at great length by the method of *complex coordinates* and *complex transfer functions*, constitute a specific case of even-order anticirculant MIMO systems. In Example 1.9, we shall return to that issue in more detail.

**Remark 1.11** As shown above, the CTFs  $q_i(s)$  of circulant and anticirculant systems can be written in analytical form for any number of separate channels  $N$ . From Equations (1.133) and (1.162), it is evident that these CTFs can be represented, after reducing to a common denominator, as a quotient of two rational polynomials in complex variable  $s$ . From Equations (1.133) and (1.162), it ensues that for all  $q_i(s)$  ( $i = 1, 2, \dots, N$ ), the denominator polynomials are the same, have real coefficients and are equal to the product of denominator polynomials of the elements of the first row of  $W(s)$ . In other words, all poles of the CTFs  $q_i(s)$  of circulant or anticirculant systems are the same, and are *absolute*. As for the numerator polynomials of the CTFs  $q_i(s)$ , they are generally different and have complex coefficients. The only exception from the last rule constitutes *simple symmetrical* MIMO systems for which the numerator

<sup>43</sup> Eigenvalues [Equation (1.110)] of the antisymmetrical matrix  $R$  [Equation (1.109)] of the uniform system in Example 1.5 can be directly obtained from this expression.

polynomials of  $q_i(s)$  have real coefficients and  $N - 1$  CTFs of *relative motions* [Equation (1.139)] coincide. A common feature of circulant and anticirculant systems is that their orthonormal canonical bases do not depend on  $s$  and on the specific form of the transfer functions  $w_0(s)$  and  $w_k(s)$  ( $k = 1, 2, \dots, N - 1$ ), and coincide, respectively, with the canonical bases of the permutation matrix  $U$  [Equation (1.128)] and the anticirculant permutation matrix  $U_-$  [Equation (1.156)].

**Remark 1.12** In a sense, circulant and anticirculant systems are rather similar in their structural properties to normal uniform systems with orthogonal canonical bases, but the significant feature of the former systems is the presence of *dynamical* cross-connections, which is excluded for uniform systems. At the same time, all that was stated in Remark 1.9 about the CTFs of uniform systems is completely valid, taking into account the preceding remark, for circulant and anticirculant systems, i.e. here, we also have  $N$  *isolated, one-sheeted algebraic functions not possessing any branch points*. The last fact allows handling the CTFs  $q_i(s)$  of the systems in question, preserving the mathematical rigour, as a set of  $N$ -independent SISO systems.

**Example 1.9** Below, we outline those significant practical tasks that have stimulated the formation and evolution of the *complex coordinates and complex transfer functions method*, and obtain the CTFs for an axially symmetrical spinning body.

As is well known, the angular motion of a rigid body about the principal axes of inertia is described by Euler's nonlinear dynamical equations (Goldstein 1959):

$$J_X \frac{d\omega_x}{dt} + (J_Z - J_Y) \omega_z \omega_y = M_x \quad (1.167)$$

$$J_Y \frac{d\omega_y}{dt} + (J_X - J_Z) \omega_x \omega_z = M_y \quad (1.168)$$

$$J_Z \frac{d\omega_z}{dt} + (J_X - J_Y) \omega_x \omega_y = M_z, \quad (1.169)$$

where  $J_X$ ,  $J_Y$  and  $J_Z$  denote the principal moments of inertia;  $\omega_x$ ,  $\omega_y$  and  $\omega_z$  the angular velocities; and  $M_x$ ,  $M_y$  and  $M_z$  the external torques. Generally, these torques represent the sum of control torques and disturbances, but, for simplicity, we shall assume them be control torques.

In many technical applications, such as satellite spin stabilization, some guidance systems of rockets and torpedoes, gyroscopic systems, etc. (Kazamarov *et al.* 1967), engineers have to deal with an *axially-symmetrical body* spinning about the symmetry axis with constant angular velocity (usually, that velocity is chosen high enough to impart the gyroscopic, i.e. stabilizing, effect to the body). Assuming for certainty the symmetry axis to be the  $Z$ -axis, i.e. assuming  $J_X = J_Y = J$ , and denoting by  $\Omega = \text{const}$  the constant angular velocity about that axis<sup>44</sup> yields, instead of Equation (1.168), a set of two equations about the transversal axes  $X$  and  $Y$ :

$$J \frac{d\omega_x}{dt} + a\omega_y = M_x \quad (1.170)$$

$$J \frac{d\omega_y}{dt} - a\omega_x = M_y, \quad (1.171)$$

<sup>44</sup> That velocity is imparted to the body at the beginning (at zero time), and, as a first approximation, can be accepted as constant if  $M_z = 0$ , i.e. in the case of neglecting the influence of various external disturbances and applying no control torques about the symmetry axis.

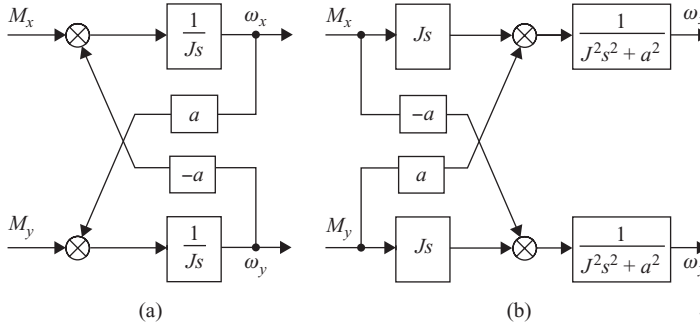


**Figure 1.34** Block diagrams of a spinning axially symmetrical body. (a) initial block diagram; (b) equivalent block diagram with direct cross-connections.

where

$$a = (J_Z - J)\Omega = \text{const.} \tag{1.172}$$

Hence, we obtain a set of two linear cross-connected differential equations with respect to the angular velocities  $\omega_x$  and  $\omega_y$ , with the constant antisymmetrical cross-connections  $a$  [Equation (1.172)]. If we pass to operator form, then the block diagram with *inverse* antisymmetrical connections shown in Figure 1.34(a) corresponds to these equations. An equivalent block diagram with *direct* cross-connections is given in Figure 1.34(b). This block diagram represents the following matrix operator equation, which is the result of transformation of initial Equations (1.170) and (1.171):

$$\begin{bmatrix} \omega_x \\ \omega_y \end{bmatrix} = \frac{1}{J^2s^2 + a^2} \begin{pmatrix} Js & a \\ -a & Js \end{pmatrix} \begin{bmatrix} M_x \\ M_y \end{bmatrix}. \tag{1.173}$$

The specific pattern of the cross-terms in Equations (1.170), (1.171) and (1.173) has led to an idea of using some duly chosen *complex-valued coordinates* instead of the system coordinates. If we introduce the complex angular velocities and control torques:

$$\bar{\omega} = \omega_x + j\omega_y, \quad \bar{M} = M_x + jM_y, \tag{1.174}$$

then, multiplying Equation (1.171) by the imaginary unit  $j$  and adding to Equation (1.170) yields

$$J \frac{d\bar{\omega}}{dt} + ja = \bar{M} \tag{1.175}$$

or, in the operator form,  $\bar{\omega} = W_c(s)\bar{M}$ , where the function

$$W_c(s) = \frac{1}{Js + ja} \tag{1.176}$$

is called the *complex transfer function* (Krassovski 1957).

Thus, the conversion to complex coordinates [Equation (1.174)] allows decreasing of twice the order of initial Equations (1.170) and (1.171), although the resulting equation has complex coefficients. At first, this approach was mainly used in the engineering mechanics and theory of gyroscopes, and, afterwards, it was adopted in the control theory.<sup>45</sup> It should be noted that owing to complex coefficients, the complex transfer functions generally lose the symmetry with respect to the ordinate axis in the plane of Bode diagrams, and distribution with respect to the real axis in the plane of Nyquist plots – with respect to the real axis, as well as the symmetry of poles and zeros.<sup>46</sup>

Apply now to Equation (1.173) the results of the present section, noticing that the system is antisymmetrical. Based upon Equation (1.166), we immediately obtain

$$q_{1,2}(s) = \frac{1}{J^2 s^2 + a^2} (Js \pm ja) = \frac{1}{Js \mp ja}, \quad (1.177)$$

i.e. one of the CTFs associated with the two-dimensional antisymmetrical system coincides with the complex transfer function  $W_c(s)$  [Equation (1.176)]. This once more verifies the conclusion that for systems with fixed parameters, the approach in terms of the CTFs embraces as a special case many results of the complex coordinates and transfer functions method.<sup>47</sup>

**Example 1.10** One of the classical instances of nonrobust MIMO systems is the two-dimensional system discussed by J. K. Doyle and others (Doyle 1984; Packard and Doyle 1993). The transfer matrix of that system has the form

$$W(s) = \frac{1}{s^2 + a^2} \underbrace{\begin{pmatrix} s - a^2 & a(s + 1) \\ -a(s + 1) & s - a^2 \end{pmatrix}}_{W_1(s)}, \quad a = 10 \quad (1.178)$$

and is antisymmetrical. Introducing into this system the unit negative feedback and static regulator  $K = \text{diag}\{K_i\} = I$ , we obtain a closed-loop system, both roots of which are equal to  $-1$ . In Doyle (1984) and Packard and Doyle (1993), it is indicated that breaking by turns one loop at a time, one can erroneously infer that the system has an infinite gain margin and a phase margin of  $90^\circ$ . However, simultaneously changing the unit gains in the separate channels to  $K_1 = 1.1$  and  $K_2 = 0.9$  makes the system unstable! Consider now the system in Equation (1.178) in terms of the CTFs. Note first that this system, being formally very similar to the control system for the spinning axially-symmetrical body of Example 1.9, possesses rather original features. Thus, despite the scalar multiplier  $1/(s^2 + a^2)$  in Equation (1.178), the poles  $p_{1,2} = \pm ja$  of the latter *are not the absolute poles of the open-loop system*. This can readily be checked by determining that the matrix  $W_1(s)$  in Equation (1.178) is singular for  $s_{1,2} = \pm ja$  [this is due to the fact that the values  $s_{1,2} = \pm ja$  are *zeros* of the matrix  $W_1(s)$  belonging to

<sup>45</sup> Seemingly, the first works in the feedback control theory on the complex coordinates and transfer functions method belong to Krassovski (1957).

<sup>46</sup> See also Section 1.1.4.

<sup>47</sup> The complex coordinates and transfer functions method allows the united handling of two- and three-dimensional antisymmetrical systems having single-channel alternating current sections with amplitude-phase modulation of signals (Kazamarov *et al.* 1967). Strictly speaking, such systems are described by differential equations with periodic coefficients.

different CTFs and each of these zeros compensates *one* of the poles  $p_{1,2} = \pm ja$ . Besides, at the zero frequency  $\omega = 0$ , the eigenvalues of the matrix  $W(s)$  are

$$q_{1,2}(j0) = -1 \pm j \frac{1}{a}, \tag{1.179}$$

which, in accordance with Remark 1.7, implies *positive* feedback. These features also appear in the frequency characteristics. It is easy to show that the CTFs  $q_{1,2}(s)$  of the system [Equation (1.178)] are

$$q_1(s) = \frac{1 + ja}{s - ja}, \quad q_2(s) = \tilde{q}_1(s) = \frac{1 - ja}{s + ja}. \tag{1.180}$$

The characteristic gain loci  $q_1(j\omega)$  and  $q_2(j\omega)$  shown in Figure 1.35(a) and (b), in which the dashed lines correspond to  $q_2(j\omega)$ , do not encircle the critical point  $(-1, j0)$ , i.e. the system is stable. The enlarged area around the origin is shown in Figure 1.35(b), in which the bold dots indicate the zero frequency  $\omega = 0$ .<sup>48</sup> These points are quite close to  $(-1, j0)$ , which suggests the need to study in detail their behaviour under small perturbations of gains of the static regulator  $K$ .

If we denote the perturbations of gains by  $\Delta K_1$  and  $\Delta K_2$ , then it can be shown that the starting points  $q_{1,2}(j0)$  of the characteristic gain loci are described by the expression

$$q_{1,2}(j0) = -\frac{2 + \Delta K_1 + \Delta K_2}{2} \pm \sqrt{\frac{(2 + \Delta K_1 + \Delta K_2)^2}{4} - \frac{(1 + \Delta K_1)(1 + \Delta K_2)(a^2 + 1)}{a^2}}. \tag{1.181}$$

For zero perturbations  $\Delta K_1 = \Delta K_2 = 0$ , Equation (1.181) coincides, naturally, with Equation (1.179). For nonzero but equal by magnitude and sign deviations  $\Delta K_1 = \Delta K_2 = \Delta K$ , we have, from Equation (1.181):

$$q_{1,2}(j0) = (1 + \Delta K) \left( -1 \pm j \frac{1}{a} \right) \tag{1.182}$$

i.e. the starting points  $q_{1,2}(j0)$  shift proportionally to perturbations  $\Delta K$ , approaching or moving away (depending on the sign of  $\Delta K$ ) from the origin. Since, for identical perturbations  $\Delta K$ , both loci  $q_1(j\omega)$  and  $q_2(j\omega)$  are multiplied by a real factor  $(1 + \Delta K)$ , it is easy to understand that the form of these loci does not change. This means that the system in Equation (1.178) cannot become unstable under arbitrary large but *identical*  $\Delta K_1$  and  $\Delta K_2$ . The picture changes drastically if the perturbations  $\Delta K_1$  and  $\Delta K_2$  have different signs. Assuming, for simplicity, that these perturbations are the same by magnitude, i.e. assuming in Equation (1.182) that  $\Delta K_1 = -\Delta K_2 = \Delta K$ , yields

$$q_{1,2}(j0) = -1 \pm j \frac{1}{a} \sqrt{(a^2 + 1)\Delta K^2 - 1}, \tag{1.183}$$

<sup>48</sup> The characteristic gain loci  $q_1(j\omega)$  and  $q_2(j\omega)$  considered in the range  $-\infty \leq \omega \leq +\infty$  are complex conjugate, i.e. symmetrical with respect to the real axis.

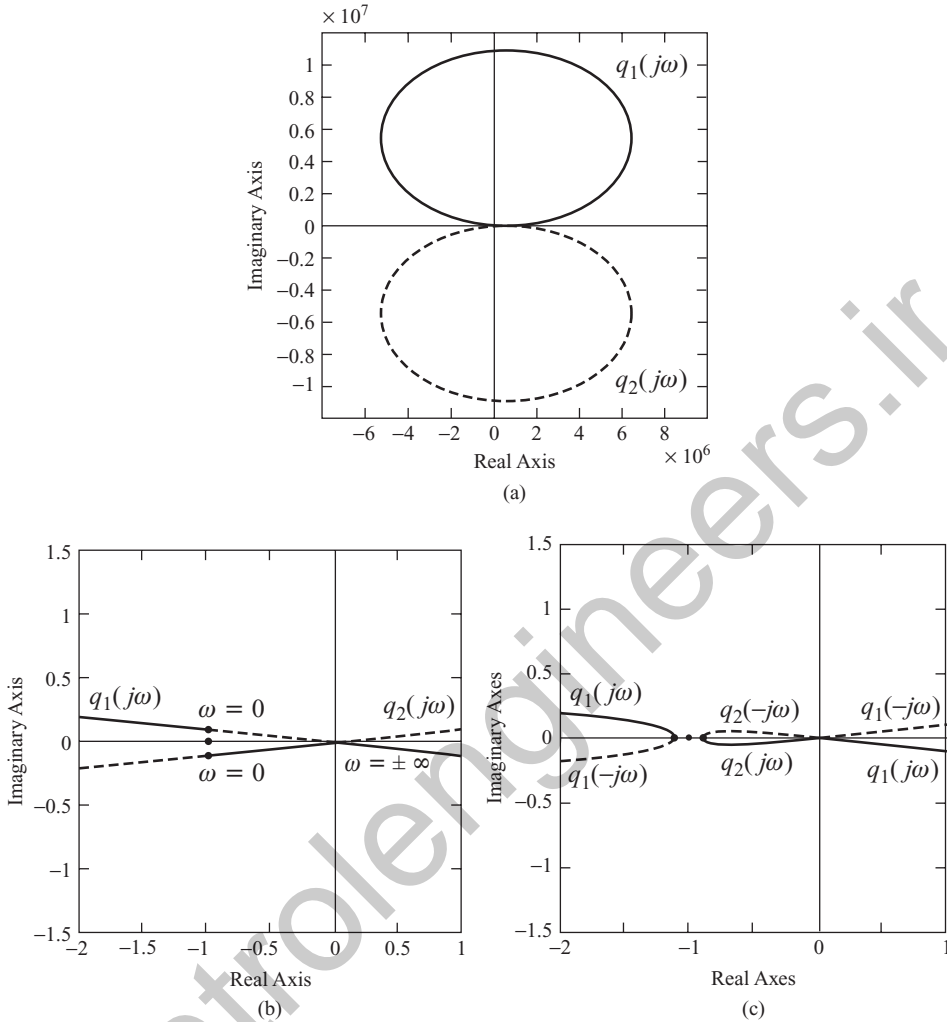


**Figure 1.35** Characteristic gain loci of antisymmetrical system [Equation (1.178)]. (a) general view; (b) area around the origin; (c) the CTFs  $q_1(j\omega)$  and  $q_2(j\omega)$  for  $\Delta K_1 = -\Delta K_2 = 0.15$ .

from which it is evident that for<sup>49</sup>

$$\Delta K = \frac{1}{\sqrt{a^2 + 1}} \approx 0.0995, \quad (1.184)$$

both starting points of the characteristic gain loci  $q_1(j\omega)$  and  $q_2(j\omega)$  coincide with the critical point  $(-1, j0)$ . If we continue increasing  $\Delta K$  by magnitude, the starting points move from the critical point along the real axis in opposite directions; as a result, one of the characteristic

<sup>49</sup> Equation (1.184) was obtained in (Skogestad and Postlethwaite 1995), based on the characteristic equation of the closed-loop system.

gain loci will necessarily encircle the point  $(-1, j0)$  and the system will become unstable. The gain loci  $q_1(j\omega)$  and  $q_2(j\omega)$  in the area around the origin for  $\Delta K_1 = -\Delta K_2 = 0.15$  are shown in Figure 1.35(c), confirming that the locus  $q_1(j\omega)$  encircles  $(-1, j0)$  [slightly larger perturbations are taken here to obtain more visual results, as, for  $\Delta K_1 = -\Delta K_2 = 0.1$ , the starting points of  $q_1(j\omega)$  and  $q_2(j\omega)$  actually merge with  $(-1, j0)$ ]. It is interesting to note that the shapes of the loci have essentially changed in the discussed case. Here, we have, for  $-\infty \leq \omega \leq +\infty$ , one ‘large’ closed contour corresponding to  $q_1(j\omega)$  and one ‘small’, corresponding to  $q_2(j\omega)$ , i.e. now, the loci are not complex conjugate. The point is that for different signs of  $\Delta K_1$  and  $\Delta K_2$ , the system loses the property of antisymmetry and belongs to the class of general MIMO systems.

### 1.4.4 Characteristic transfer functions of complex circulant and anticirculant systems

The fact that the canonical basis of any circulant or anticirculant transfer matrix  $W(s)$  does not depend on the specific form of its elements  $w_0(s), w_i(s) (i = 1, 2, \dots, N - 1)$  and coincides with the orthogonal basis composed of the normalized eigenvectors of the permutation matrix  $U$  [Equation (1.113)] or anticirculant permutation matrix  $U_-$  [Equation (1.137)] plays a crucial role in determining the CTFs of complex systems belonging to the discussed classes. In Section 1.2, it was noted<sup>50</sup> that if the block diagram of an open-loop general MIMO system consists of different matrix elements connected in series, in parallel or forming inner feedback loops, then, for determining the CTFs, it is necessary to find the *resultant* transfer matrix  $W(s)$ , based upon standard rules of matrix block diagram transformation (Morozovski 1970). In such cases, nothing can be said about the relationship of the CTFs  $q_i(s)$  of  $W(s)$  with the corresponding CTFs of the separate matrices constituting  $W(s)$ , since, in general, all these elements are brought to diagonal form in different canonical bases.<sup>51</sup>

The situation is quite different for MIMO systems with circulant or anticirculant transfer matrices. In the following, analyzing complex circulant and anticirculant systems, we assume that all matrix elements constituting the open-loop system are circulant or anticirculant, i.e. we exclude the situations in which the individual elements do not belong, but their sum, product or any other combination belong, to the mentioned classes. Besides, since the structures of the CTFs and eigenvectors (canonical basis axes) of circulant and anticirculant transfer matrices are actually identical, we discuss only circulant systems. Consider, first, the series connection of  $m$  matrix elements described by the circulant matrices  $W_k(s) (k = 1, 2, \dots, m)$  [Figure 1.36(a)].

In accordance with the general rules (Morozovski 1970), the transfer matrix  $W(s)$  of such a connection is equal to the product of transfer matrices of the individual elements arranged in the reversed order

$$W(s) = W_m(s)W_{m-1}(s) \dots W_2(s)W_1(s). \quad (1.185)$$

Since the product of any number of circulant matrices yields a matrix of the same type (Voevodin and Kuznetsov 1984), the matrix  $W(s)$  [Equation (1.185)] is circulant for any  $m$ .

<sup>50</sup> See Remark 1.2.

<sup>51</sup> All the indicated matrix blocks of a general MIMO system are brought to diagonal form in the same canonical basis if all the corresponding transfer matrices are commutative (see also Remark 1.10).

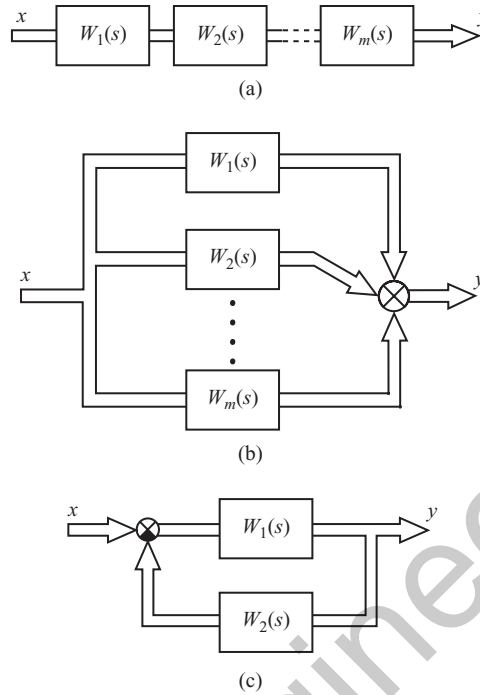


**Figure 1.36** Basic structural connections of circulant elements. (a) series connection; (b) parallel connection; (c) feedback connection.

Further, taking into account that each matrix  $W_k(s)$  in Equation (1.185) has the canonical representation of the form

$$W_k(s) = C \text{diag}\{q_i^k(s)\} C^*, \quad (1.186)$$

where  $C$  is the unitary matrix formed by the eigenvectors  $c_i$  of the permutation matrix  $U$  [Equation (1.113)], and the same representation has the resultant matrix  $W(s)$ , instead of Equation (1.185), we can write

$$W(s) = C \text{diag}\{q_i(s)\} C^* = C \text{diag}\left\{\prod_{k=1}^m q_i^k(s)\right\} C^*, \quad (1.187)$$

from which there immediately follow  $N$  equalities

$$q_i(s) = \prod_{k=1}^m q_i^k(s), \quad i = 1, 2, \dots, N. \quad (1.188)$$

Thus, the  $i$ th CTF  $q_i(s)$  of the series connection of  $m$  circulant elements is equal to the product of the corresponding  $i$ th CTFs of the individual elements. It should be emphasized that the order of connection does not play any role, i.e. these matrix elements can be interchanged just as in the case of usual scalar elements in SISO systems (Kuo 1995).

Let us find out now the properties of the parallel connection of  $m$  circulant elements [Figure 1.36(b)]. In this case, the resultant matrix  $W(s)$  is also circulant and equal to the sum of the individual matrices, i.e.

$$W(s) = \sum_{k=1}^m W_k(s). \tag{1.189}$$

From Equation (1.189), taking into account that  $W(s)$  is circulant, we obtain

$$W(s) = C \text{diag}\{q_i(s)\} C^* = C \text{diag} \left\{ \sum_{k=1}^m q_i^k(s) \right\} C^* \tag{1.190}$$

and

$$q_i(s) = \sum_{k=1}^m q_i^k(s), \quad i = 1, 2, \dots, N. \tag{1.191}$$

Hence, the  $i$ th CTF  $q_i(s)$  of the parallel connection of  $m$  circulant elements is equal to the sum of the corresponding  $i$ th CTFs of the individual elements.

Consider, finally, the feedback connection of two circulant elements [Figure 1.36(c)], assuming for certainty the negative feedback. The transfer matrix  $W(s)$  of such a connection, relating the input and output vectors  $x$  and  $y$ , is

$$W(s) = [I + W_1(s)W_2(s)]^{-1} W_1(s). \tag{1.192}$$

Substituting the canonical representations in Equation (1.186) into this expression yields

$$W(s) = C \text{diag}\{q_i(s)\} C^* = C \text{diag} \left\{ \frac{q_i^1(s)}{1 + q_i^1(s)q_i^2(s)} \right\} C^*. \tag{1.193}$$

From Equation (1.193), it is evident that the matrix  $W(s)$  is circulant (as it is brought to diagonal form in the canonical basis of the permutation matrix  $U$ ), and the CTFs of  $W(s)$

$$\{q_i(s)\} = \frac{q_i^1(s)}{1 + q_i^1(s)q_i^2(s)} \tag{1.194}$$

$i = 1, 2, \dots, N$

are expressed through the  $i$ th CTFs  $q_i^1(s)$  and  $q_i^2(s)$  of  $W_1(s)$  and  $W_2(s)$  by the same formulae as usual SISO transfer functions in the case of nonunit negative feedback.

Now, it is clear that any arbitrary complex connection pattern of circulant elements forming the open-loop MIMO system can be described by a certain resultant circulant matrix  $W(s)$ . For determining the CTFs  $q_i(s)$  of the latter, we have to replace the matrix block diagram of the open-loop circulant system with a scalar block diagram analogous by form, in which, instead of the matrix elements  $W_k(s)$ , the CTFs  $q_i^k(s)$  are shown.<sup>52</sup> The obtained block diagram can be

<sup>52</sup> Recall that these CTFs can be found in analytical form for any number  $N$  of separate channels.

handled in just the same way as a common diagram of a SISO system. It must be emphasized once more that it is possible because all circulant (and anticirculant) matrices are brought to diagonal form in the same canonical basis.

**Example 1.11** Consider the three-axis gyrostabilized platform described in Chorol *et al.* (1976), in which angular velocities are measured by special devices with amplitude-phase modulation of signals. The expanded block diagram of the system is depicted in Figure 1.37. If the reference voltage has a nonzero phase shift  $\gamma$ , then, among the system channels, there appear direct antisymmetrical connections. Besides, the noncoincidence of the resonance frequency in the measuring devices with the carrier frequency results in reverse antisymmetrical connections with coefficients  $K_r$ . The corresponding matrix block diagram of the gyrostabilized platform is shown in Figure 1.38 (Sobolev 1973), in which  $U$  denotes the permutation matrix of order  $3 \times 3$ . The inspection of that block diagram shows that the system belongs to uniform antisymmetrical systems. Therefore, based on the results of

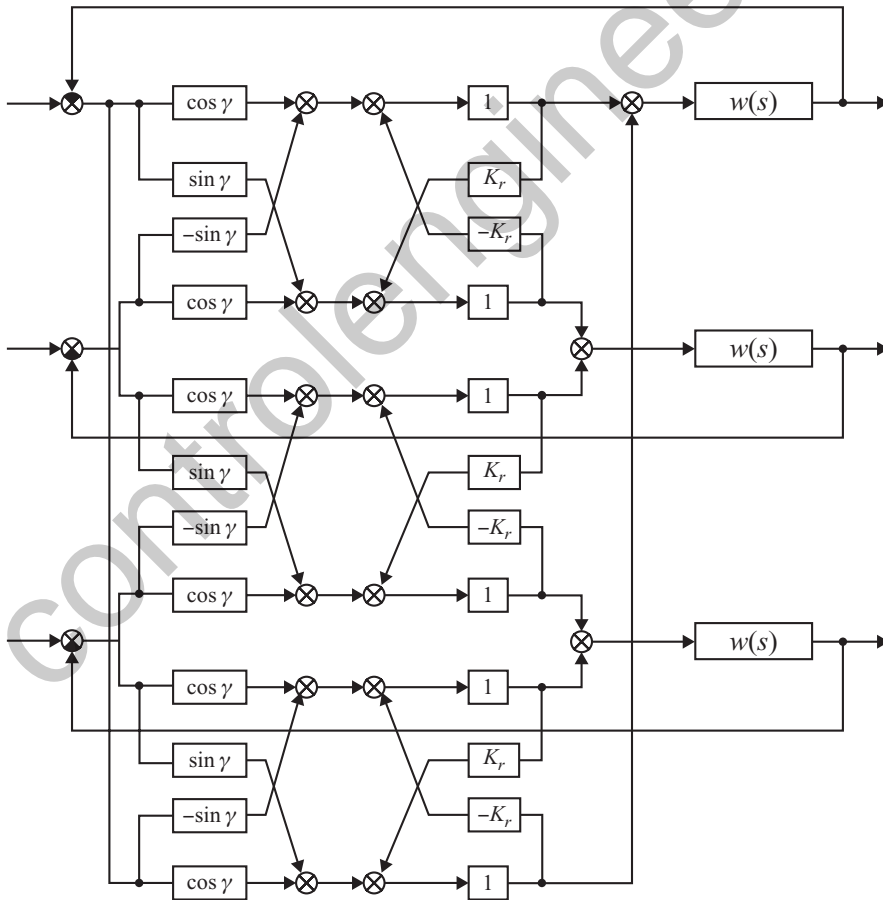


**Figure 1.37** Expanded block diagram of the three-axis gyrostabilized platform.

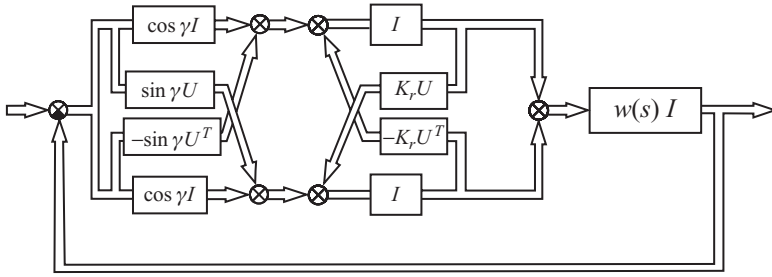


Figure 1.38 Matrix block diagram of the gyrostabilized platform.

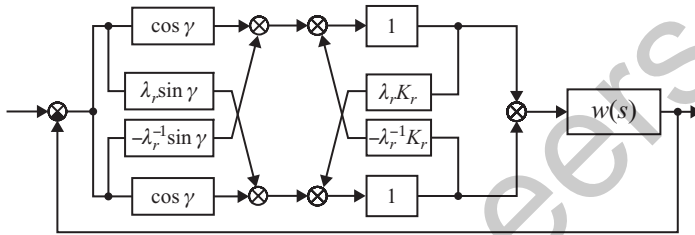


Figure 1.39 Block diagram of one-dimensional characteristic systems ( $i = 1, 2, 3$ ).

Section 1.3,<sup>53</sup> we can draw equivalent block diagrams of one-dimensional characteristic systems. For this purpose, we must replace all vector connections in Figure 1.38 with scalar ones. Then, we must replace the permutation and unit matrices  $U$  and  $I$  with, respectively, the eigenvalues  $\lambda_i$  and ones (Figure 1.39), where, based on Equation (1.131), the eigenvalues of  $U$  are

$$\lambda_1 = 1, \quad \lambda_{2,3} = \cos 120^\circ \pm j \sin 120^\circ = -0.5 \pm j0.866. \quad (1.195)$$

Note that in Figure 1.39, we take into account that the matrix  $U$  is orthogonal, i.e. its inverse matrix coincides with the transposed, and that the eigenvalues of any matrix of simple structure and of its inverse matrix are mutually inverse. As an exercise, the reader can check that the CTFs of the *open-loop* characteristic systems determined by the block diagram in Figure 1.39 have the following form:

$$q_1(s) = \frac{2(\cos \gamma - K_r \sin \gamma)}{1 + K_r^2} w(s),$$

$$q_{2,3}(s) = \frac{2[\cos \gamma - K_r \sin \gamma \pm j0.866(\sin \gamma + K_r \cos \gamma)]}{1 + K_r^2} w(s). \quad (1.196)$$

## 1.5 MULTIVARIABLE ROOT LOCI

The *root locus method* proposed by Evans in 1948 is, together with the frequency-domain approaches, one of the key and most effective methods of the linear SISO systems analysis

<sup>53</sup> See Remark 1.10.

and design (Evans 1948, 1950, 1954; Horowitz 1963; Krall 1970; Kuo 1995; Ogata 1970). Based upon a number of simple graphical rules and procedures, the root locus technique allows predicting, given the distribution of zeros and poles of an *open-loop* SISO system, the behaviour of the roots of the *closed-loop system*, as the total gain (or any other parameter) changes from zero to infinity. Simplicity and clearness of that method predetermined its exceptional popularity among practising engineers, which, in turn, stimulated the strong interest of scientists and researchers. Later, there appeared other variants of root locus techniques, such as the logarithmical root locus method (Kuzovkov 1959; Glaria *et al.* 1994), the analytical method of Bendrikov and Teodorichik (1964), Uderman's method (1963), the method of generalized root loci (Rimski 1969), etc.

With progress of the multivariable control theory, that topic became the object of researchers' close attention. Frequently, in this connection, systems with two inputs and outputs or some special classes of multivariable systems were considered. Thus, the properties of root loci of two- and three-dimensional systems with identical channels and rigid antisymmetrical cross-connections were discussed in Bendrikov and Ogorodnikova (1967, 1968) and Fortescue (1976). The problem of *general properties* of multivariable root loci (called also root trajectories) was studied at great length in Owens (1976), Shaked (1976), Kouvaritakis and Shaked (1976), Postlethwaite and MacFarlane (1979), Hung and MacFarlane (1981), etc.<sup>54</sup> Some specific features of multivariable root loci, having no analogues in the one-dimensional case, were discovered and theoretically justified in Kouvaritakis and Shaked (1976) and Kouvaritakis and Edmunds (1979) on the basis of state-space representation of MIMO systems. Thus, in these and some other works, it was established that the root loci of MIMO systems may intersect or superimpose; in certain situations, the roots of the MIMO system may move along some trajectory, and then change their movement to the opposite direction along the same trajectory, etc. It was also shown that in the case of 'infinite' zeros, i.e. if the total number of poles exceeds the number of 'finite' zeros (which is a usual situation), the MIMO system may have several *groups of asymptotes* (and not one group, as in the SISO case) constituting the so-called *Butterworth configuration* (or *pattern*).<sup>55</sup> Besides, generally, the centres (*pivots*) of these groups are not necessarily located on the real axis.

The task of constructing multivariable root loci in terms of the CTFs was discussed in the pioneering works of MacFarlane and Postlethwaite (1977, 1979). The theory of algebraic functions and concept of Riemann surfaces used by them proved to be very fruitful. In particular, this approach allowed establishing, with necessary mathematical rigour, the basic properties (as well as explaining some 'strange' features) of multivariable root loci, attributing these properties and features to the presence of *branch points* and to the location of root loci branches on *different sheets* of a unique Riemann surface.

Unfortunately, many theoretical results of the cited works considerably yield in simplicity to their classical counterparts. As a result, it is very difficult to apply them in practice. A paradoxical situation has arisen. Many modern mathematical and application program packages enable the user to find without difficulty the roots of closed-loop MIMO systems of, actually, any dimension, as well as to draw the root loci corresponding to changes of any parameter of

<sup>54</sup> Another essential and extensive branch of research concerns the asymptotic behavior of linear *optimal* systems roots, as a scalar weight coefficient in the quadratic cost index changes from 0 to  $\infty$  (Kwakernaak 1976; Shaked and Kouvaritakis 1977; Kouvaritakis 1978).

<sup>55</sup> An  $r$ -order Butterworth pattern consists of  $r$  straight, evenly spaced lines starting from a common centre (pivot), and forming with positive direction of the real axis angles, equal to  $(2k + 1)180^\circ / r$  ( $k = 0, 1, \dots, r - 1$ ) (Butterworth 1930).

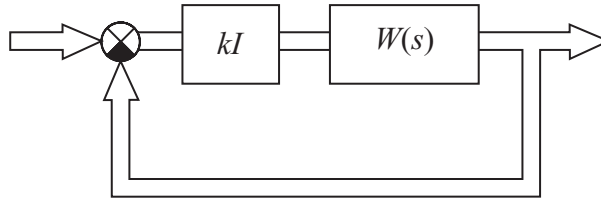


**Figure 1.40** Block diagram used for the study of multivariable root loci.

the system. On the other hand, the algorithmical procedures for finding the pivots of MIMO systems asymptotes described, for example, in Kouvaritakis and Shaked (1976) considerably exceed in complexity the mentioned straightforward procedures of finding the multivariable root loci. This should not be interpreted as a call to reject research in that direction; we should just clearly apprehend that theoretical results are needed, chiefly to *explain, understand and justify* the character and behaviour of multivariable root loci, and not for immediate utilization in numerical computations. It is worth noting that even in the case of SISO systems, an engineer is now free from the burden of calculating root loci ‘by hand’. This task may readily be solved using the application packages of many companies and firms. Thus, the function *rlocus* available in *The Control System Toolbox* in MATLAB is destined for constructing the root loci of SISO systems given the transfer function of the open-loop system. Similar functions exist and in many other packages.

Concluding our introduction, note that, below, we consider properties of multivariable root loci in the context of their relation to analogous properties of usual root loci known from the classical control theory (Evans 1954; Horowitz 1963). At that, we base on the MIMO system representation in terms of the CTFs. Therefore, many significant results demanding the state-space representation of MIMO systems or using the mathematical apparatus that is beyond the scope of this book are omitted or replaced by a heuristic interpretation from the standpoint of the CTFs method.

### 1.5.1 Root loci of general MIMO systems

The matrix block diagram of a general linear MIMO system used for the study of multivariable root loci is shown in Figure 1.40, in which  $W(s)$  is the transfer matrix of the open-loop system of order  $N \times N$ ,  $I$  is the unit matrix and  $k$  is a real scalar multiplier.

The problem is to construct the root loci of the MIMO system as the ‘gain’  $k$  changes from zero to infinity.<sup>56</sup> Recalling the common assumption of no repeated CTFs  $q_i(s)$ , the characteristic equation of the closed-loop MIMO system can be represented as

$$\det[I + kW(s)] = \prod_{i=1}^N [1 + kq_i(s)] = 0, \quad (1.197)$$

where it is taken into account that multiplication of a matrix by a scalar results in the multiplication of all the matrix eigenvalues by the same scalar. Evidently, Equation (1.197) is equivalent

<sup>56</sup> For brevity, we consider only the case of positive  $k$ . The case of negative  $k$  is left for the reader as an exercise.

to the following system of  $N$  equations:

$$1 + kq_i(s) = 0 \quad \text{or} \quad kq_i(s) = -1, \quad i = 1, 2, \dots, N, \quad (1.198)$$

from which it is clear that the roots of the closed-loop MIMO system must satisfy, for any  $k = \text{const}$  and some  $i$ , the following two conditions:

$$|kq_i(s)| = 1, \quad \arg q_i(s) = \pm(2r + 1)180^\circ, \quad r = 0, 1, 2, \dots \quad (1.199)$$

In other words, the roots of the closed-loop MIMO system are those values of complex variable  $s$  for which some CTFs  $q_i(s)$  become real negative numbers.

An apparent similarity of conditions in Equation (1.199) to the corresponding conditions for SISO systems (Evans 1954; Horowitz 1963) suggests that no essential problems should arise in extending to the multivariable case the standard ‘one-dimensional’ root locus techniques. Unfortunately, everything is far from being so simple. As was indicated in Section 1.2, in general, the CTFs of MIMO systems are algebraic functions located on different sheets of a Riemann surface and constituting a unique mathematical entity. Based upon Equation (1.46),

$$\det W(s) = \frac{Z(s)}{P(s)} = \prod_{i=1}^N q_i(s), \quad (1.200)$$

where  $Z(s)$  and  $P(s)$  are the zeros and poles polynomials of the open-loop MIMO system, we know that zeros and poles of the open-loop system coincide with all zeros and poles of *all* the CTFs  $q_i(s)$ .<sup>57</sup> However, in the general case, we do not know how the zeros and poles of the MIMO system are distributed among different characteristic systems, or, more strictly, how these zeros and poles participate, taking into account the branch points, in forming the branches of the root loci on different sheets of the Riemann surface. If we knew this information, then, really, it would not be difficult to find the multivariable root loci based upon Equations (1.197)–(1.199) and using common classical procedures. At the same time, based upon Equations (1.197)–(1.200), we can draw some conclusions and formulate a number of rules which, as was accentuated before, serve rather for the understanding of the properties of multivariable root loci already constructed, by means of the computer aids, than for using them for calculations ‘by hand’ (Gasparyan *et al.* 2006). We shall list these rules following the order existing in the classical control theory (Evans 1954).

**Rule 1:** *Number of root loci.* The number of root loci is equal to the total number  $n$  of poles of the open-loop MIMO system, i.e. to the degree  $n$  of the poles polynomial  $P(s)$ ; the multivariable root loci are the combination of the set of root loci of the SISO characteristic systems. This rule immediately follows from Equations (1.58) and (1.59), and does not require any special comments.

**Rule 2:** *Multivariable root loci are continuous curves.* The root loci are continuous because the roots of Equation (1.198) are continuous functions of  $k$ , i.e. the arbitrarily small changes of  $k$  result in the arbitrary small displacements of any roots of these equations.<sup>58</sup> *The derivatives*

<sup>57</sup> Further, we shall assume that the poles polynomial  $P(s)$  is *monic*, i.e. its higher degree coefficient is 1.

<sup>58</sup> See also Remark 1.6 concerning the roots of the closed-loop MIMO systems that do not change as the coefficient  $k$  changes.

of multivariable root loci are continuous everywhere except for the denumerable number of the points at which the CTFs  $q_i(s)$  become infinity, or their derivatives with respect to  $s$  are not determined, or  $dq_i(s)/ds = 0$ , or, finally,  $k = 0$ . This can be readily checked, differentiating Equation (1.198) with respect to  $k$ , which yields

$$\frac{ds}{dk} = -\frac{q_i(s)}{k(dq_i(s)/ds)}. \quad (1.201)$$

Note that, unlike the SISO case, in which the derivatives of root loci lose their continuity only at the poles of the open-loop system or at the points of the loci intersections, in the multivariable case, we have, in addition, the branch points, at which the branches of root loci pass from one sheet of the Riemann surface to another. At these points, the values of some (two or more) CTFs coincide. In the simplest case of two-dimensional systems, the branch points are those values of  $s$  for which the CTFs  $q_1(s)$  and  $q_2(s)$  are equal. From Equation (1.79), it is evident that these branch points are given by the expression

$$D(s) = \text{tr}\{W(s)\}^2 - 4 \det W(s) = 0, \quad (1.202)$$

where  $D(s)$  [the radicand in Equation (1.79)] is called the *discriminant* of the algebraic function. In the case of MIMO systems of an arbitrary dimension ( $N \geq 3$ ), the branch points are also determined by equating to zero the discriminant; however, in the general case, simple analytical expressions for  $D(s)$  do not exist (Bliss 1966; Postlethwaite and MacFarlane 1979).

**Rule 3:** *Starting and ending points of multivariable root loci.* The root loci commence at the poles of the CTFs  $q_i(s)$  (for  $k = 0$ ) and terminate at the zeros of  $q_i(s)$  (for  $k = \infty$ ). The condition  $k = 0$  physically means breaking the feedback loop of the MIMO system, i.e. the roots of the MIMO system must coincide with poles of the open-loop system and, owing to Equation (1.200), with the set of all poles of the CTFs  $q_i(s)$  ( $i = 1, 2, \dots, N$ ). If  $k$  tends to infinity, then, to preserve the equality  $kq_i(s) = -1$ , the CTFs  $q_i(s)$  must tend to zero, i.e. the complex variable  $s$  must tend to zeros of  $q_i(s)$ , or, taking into account Equation (1.200), to zeros of the open-loop transfer matrix  $W(s)$ . A significant feature of MIMO systems is that in the presence of *branch points*, to the zeros of the  $i$ th CTF  $q_i(s)$  generally can tend the root loci that begin at the poles of the CTF  $q_r(s)$  ( $r \neq i$ ) belonging to the adjacent sheets of the Riemann surface.

**Rule 4:** *Number of the branches tending to infinity.* If the  $i$ th CTF  $q_i(s)$  has  $np_i$  poles and  $nz_i$  zeros and *there are no branch points*, then, as  $k \rightarrow \infty$ , those of the  $np_i$  root locus branches of the given CTF which do not tend to  $nz_i$  finite zeros must tend to infinity, to preserve equality [Equation (1.198)]. This implies that for each  $q_i(s)$ , we have  $e_i = np_i - nz_i$  locus branches tending to infinity and, in all, there are  $e = n - m$  such branches, where  $n$  and  $m$  are the degrees of the poles and zeros polynomials  $P(s)$  and  $Z(s)$  in [Equation (1.200)].<sup>59</sup> In the presence of branch points, on the  $i$ th sheet of the Riemann surface can tend to infinity the locus branches that begin at the poles of the CTFs belonging to the adjacent sheets of the Riemann surface. In the latter case, the total number of the root loci approaching infinity, naturally, does not change.

<sup>59</sup> These root trajectories are frequently referred to as tending to *infinite zeros* of the MIMO system.

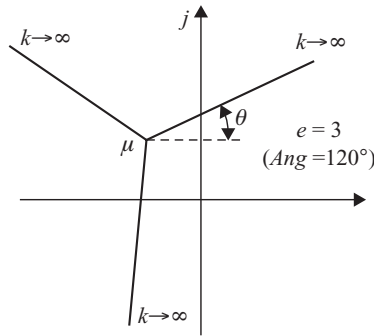


Figure 1.41 A third-order group of asymptotes.

**Rule 5:** *Angles and pivots of asymptotes of multivariable root loci.* Unfortunately, in contrast to SISO systems, in the case of MIMO systems, there are no simple formulae expressing the angles and pivots of the root loci asymptotes through the poles and zeros of the open-loop system. Therefore, we shall give here only some comments concerning the possible asymptotic behaviour of multivariable root loci, explaining, as far as possible, that behaviour in terms of the CTFs method. Since Rule 5 is a logical continuation of the preceding one, the presence of *branch points* is also of great importance here. If the  $i$ th CTFs  $q_i(s)$  is situated on a *one-sheeted* (isolated) Riemann surface, i.e. it has no branch points, then, in principle, to find the pivot and angles of the asymptotes of that CTF, one can use the expressions analogous to those well known in the classical control theory (Evans 1954; Horowitz 1963).<sup>60</sup> In the general case, i.e. in the presence of branch points, the pivots and angles of asymptotes of the multivariable root loci situated on the  $i$ th sheet of the Riemann surface and associated with the  $i$ th CTF  $q_i(s)$  depend also on the poles, zeros and ‘gains’ of the adjacent CTFs  $q_r(s)$  ( $r \neq i$ ). It is possible, however, to indicate some general patterns of relationship. In the MIMO system of order  $N$ , there may exist  $N$  groups of asymptotes constituting the Butterworth configuration, in which each group corresponds to *one* of the CTFs  $q_i(s)$  ( $i = 1, 2, \dots, N$ ) of the open-loop MIMO system. The pivots of these groups can be situated both on the real axis and at the arbitrary points of the complex plane, where all complex pivots must be complex conjugate in pairs. The latter property ensues from the fact that the multivariable root loci as a whole must be symmetrical with respect to the real axis.

A third-order group of asymptotes with a complex pivot at the point  $\mu$  is schematically depicted in Figure 1.41, in which the angles between the asymptotes are equal to  $120^\circ$ . The starting angle of the asymptotes  $\theta$  depends on the specific characteristics of the MIMO system. Another fundamental distinction of the multivariable root loci from the root loci of SISO systems should be pointed out. In the one-dimensional case, if  $e = 1$ , i.e. if the number of poles exceeds the number of zeros by one, then the corresponding asymptote always belongs to the real axis and the ‘redundant’ pole<sup>61</sup>  $p_r$  tends to infinity remaining on that axis. In the multivariable case, if any  $i$ th CTF  $q_i(s)$  has the difference  $e_i = np_i - nz_i = 1$ , then the corresponding pole  $p_r$  does not necessarily tend to infinity along the real axis, and its asymptote

<sup>60</sup> We shall discuss such situations in the next two parts of this section.

<sup>61</sup> This pole, naturally, can be only real.

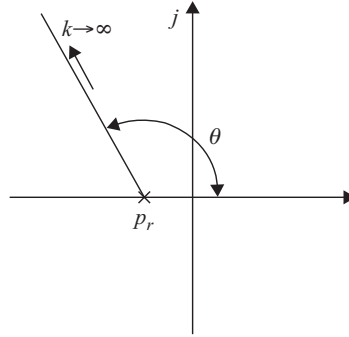


**Figure 1.42** A possible asymptote of a real pole of  $q_i(s)$  for  $e_i = 1$ .

may form with that axis a certain constant angle  $\theta$  (Figure 1.42). In such situations, however, there always exists a CTF  $q_r(s)$  ( $r \neq i$ ) with the identical pole  $p_r$ , but having a ‘complex conjugate’ asymptote situated in the lower half-plane.

**Rule 6:** *Sections of the real axis, belonging to multivariable root loci.* In the SISO case, the root trajectories coinciding with the finite or semi-infinite intervals of the real axis can be found very easily – those are the sections of the real axis located to the left of the *odd* number of the real-valued singular points<sup>62</sup> of the open-loop transfer function (Evans 1954; Horowitz 1963). To a certain extent, the sections of the multivariable root loci belonging to the real axis can also be found relatively easily, but the main obstacle here is that there is a possibility that at the same point of the real axis, there may exist *more than one branch* of the root loci. In other words, in the multivariable case, we have to determine not only the real sections of the root loci, but also their number in each section. As always, for the high-dimension MIMO systems, this procedure is rather difficult. However, for the case of two-dimensional systems, we can, following Yagle (1981), indicate some simple rules for finding the sought sections. For such systems, based upon Equation (1.198), we have that the real values of complex variable  $s$  may belong to the root loci if Equation (1.79), rewritten below,

$$q_{1,2}(s) = \frac{tr\{W(s)\}}{2} \pm \sqrt{\frac{tr\{W(s)\}^2}{4} - \det W(s)} \quad (1.203)$$

produces real and negative values for  $q_{1,2}(s)$ . As the open-loop transfer matrix  $W(s)$  [and, consequently, the trace  $tr\{W(s)\}$  and the determinant  $\det W(s)$ ] always becomes a real-valued numerical matrix for real values of  $s$ , then, from an inspection of Equation (1.203), it is easy to determine under which conditions the CTFs  $q_{1,2}(s)$  are real and negative. For this purpose, we need to consider the possible values of the discriminant  $D(s)$  [Equation (1.202)]. Thus, for the negative values  $\det W(s) < 0$ , only one of the CTFs  $q_{1,2}(s)$  [which corresponds to the minus sign before the radical in Equation (1.203)] will be negative and, for that real value of  $s$ , we have *one* branch of the root loci at the point  $s$ .

<sup>62</sup> Here, and from now on, *singular points* means the poles and zeros.

If  $\det W(s) > 0$ , then, at the point  $s$  of the real axis, we may have *either two or no branches*. For  $D(s) < 0$ ,  $q_{1,2}(s)$  [Equation (1.203)] are complex conjugate numbers and do not satisfy the conditions of forming the roots of the closed-loop MIMO system [Equation (1.198)], i.e. the real point  $s$  does not belong to the root loci. For  $D(s) > 0$ , we have to analyse two additional conditions:

- (a) if  $\text{tr}\{W(s)\} > 0$ , then *none of the branches* lies on the real axis at the point  $s$ , since both values  $q_{1,2}(s)$  [Equation (1.203)] will be positive;
- (b) if  $\text{tr}\{W(s)\} < 0$ , then we have *two branches* of the root loci, since both values  $q_{1,2}(s)$  will be negative.

Finally, the zero value of the discriminant  $D(s) = 0$  corresponds, as was stated above, to the *branch point*, at which the CTFs  $q_{1,2}(s)$  are equal, i.e.  $q_1(s) = q_2(s)$ , and we have the transition from one sheet of the Riemann surface to another. At that point, the *direction* of the root trajectories along the real axis may change to the opposite.

In principle, there are similar rules for determining the number of real-valued branches of the multivariable root loci for  $N > 2$ , under the additional restriction of no repeated real poles and zeros of the open-loop MIMO system (Yagle 1981). We shall not dwell on them, as, for an engineer, it is much simpler to construct directly the root loci of the investigated MIMO system, rather than utilize the mentioned rules for finding the number of the root loci branches at the various points of the real axis. In the next two sections, while discussing the root loci of uniform as well as circulant and anticirculant MIMO systems, we shall give some quite simple rules for determining the real branches of the root loci of the listed classes of MIMO systems, which actually do not yield in simplicity to those in the SISO case.

**Rule 7:** *Angles of departure and arrival of multivariable root loci.* Here, we once again encounter the situation already familiar to us from some of the preceding rules, namely that the results existing in the literature are not very convenient for practical application (Shaked 1976) and, with the programs for numerical computations of the multivariable root loci available, the formulae for these angles play no role, since the angles of departure and arrival can be found immediately on having constructed and plotted the trajectories. Historically, interest in the angles of departure and arrival was most likely due to the absence of computer aids,<sup>63</sup> when the developer had to calculate the root loci of SISO systems with the help of a calculator or a slide-rule, or by means of a special tool called the *Spirule* (very likely, many contemporary readers are not even familiar with the latter device or the slide-rule) (Evans 1954).

**Rule 8:** *Breakaway points of multivariable root loci.* In the classical control theory, the term *breakaway point* usually is used for the points at which two or more branches of the root loci intersect (Evans 1954; Horowitz 1963). In the multivariable case, a significant and vital peculiarity exists, which has already been mentioned above. Unlike the common SISO systems in which we always have at the breakaway points a symmetrical picture of the ‘approaching’ and ‘leaving’ root trajectories (Figure 1.43), in the case of MIMO systems, two different situations are possible. The first of them corresponds to the intersections of the root loci situated on *one sheet* of the Riemann surface, related to the  $i$ th CTF  $q_i(s)$ , and is completely analogous to that shown in Figure 1.43, i.e. all entering and leaving trajectories form a symmetrical picture. In

<sup>63</sup> It is not excluded, of course, that in some tasks, knowledge of the departure and arrival angles can bring about qualitative estimates about the investigated MIMO system, and therefore can present certain theoretical interest.

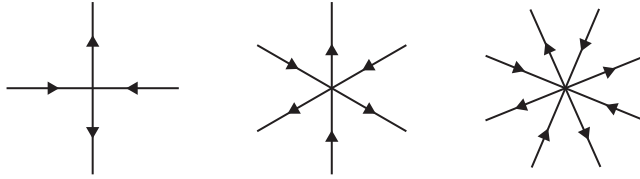


**Figure 1.43** The breakaway points of SISO systems. (a)  $l = 2$ ; (b)  $l = 3$ ; (c)  $l = 4$  ( $l$  is the number of trajectories).

the second situation, the picture is quite different; here, we have an apparent intersection of the root trajectories in which the latter in fact belong to the *different* CTFs and are situated on *different* sheets of the Riemann surface. In this case, the matter concerns not the *approaching* and *leaving* root trajectories, but an apparent *intersection* of two different independent trajectories, with arbitrary relative angles at the intersection point and with another character of the continuation of the trajectories (each of them preserves the previous direction of its motion after the intersection) (Figure 1.44).

The procedure of determining the breakaway points that are situated on the same, say the  $i$ th, sheet of the Riemann surface is practically analogous to that known from the classical control theory. Thus, if we have the intersection of two trajectories, then, at the point of intersection  $s = s_o$ , the  $i$ th equation in Equation (1.198) must have two equal roots  $s_o$ , i.e. it can be expressed in the form

$$1 + kq_i(s) = (s - s_o)^2 H(s) = 0. \tag{1.204}$$

Therefore, at the point  $s_o$ , not only the expression  $[1 + kq_i(s)]$  but also its derivative with respect to  $s$  must be equal to zero, i.e. at that point, the condition  $dq_i(s)/ds = 0$  must also be satisfied. Similarly, if trajectories of three roots of the  $i$ th characteristic system pass through the point  $s_o$ , then the point  $s = s_o$  satisfies the corresponding equation in Equation (1.198) and the first and the second derivatives of  $q_i(s)$  with respect to  $s$  at the point  $s_o$  are equal to zero. All this gives us analytical expressions for determining the breakaway points of the  $i$ th characteristic system if, of course, we have an analytical expression of the CTFs  $q_i(s)$  itself.

**Rule 9:** *Intersection of the root loci with the imaginary axis.* Just as in the SISO case (Evans 1954; Horowitz 1963), the intersections of multivariable root loci with the imaginary axis can

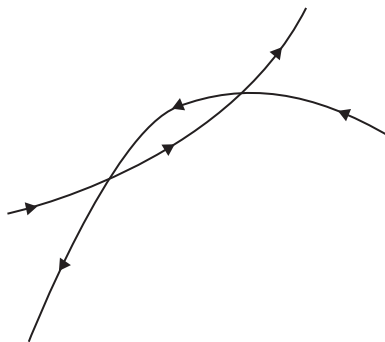


**Figure 1.44** Intersections of the root loci of the CTFs situated on different sheets of a Riemann surface.

be easily found with the help of frequency-domain techniques, such as Nyquist, Bode and Nichols plots. Indeed, if we have, for instance, the Nyquist plots of the open-loop CTFs  $q_i(j\omega)$  ( $i = 1, 2, \dots, N$ ), then the frequencies  $\omega$  at the points of intersections, if any, of these plots with the negative real axis<sup>64</sup> determine the ordinates of the points at which the corresponding branches of root loci intersect the imaginary axis. This follows from the fact that at the points of intersection of  $q_i(j\omega)$  with the negative real axis, we have the equality  $\arg q_i(j\omega) = \pm 180^\circ$ , i.e. the phase condition of forming the roots of the closed-loop MIMO system [the second condition in Equation (1.199)] is satisfied.

**Rule 10:** *Sum and product of the MIMO system roots.* In accordance with Viète's theorem (Derusso *et al.* 1965), the sum of the roots of a monic algebraic equation of order  $n$  is equal to the coefficient of the term of degree  $n - 1$  taken with the opposite sign, and the product of the roots is equal to the absolute term multiplied by  $(-1)^n$ . Based upon these properties, it is possible to obtain some useful relationships between the sum and product of the roots situated on the root loci of a MIMO system and the singular points of the transfer matrix  $W(s)$ . The characteristic equation of the MIMO system [Equation (1.197)] can be represented in the following expanded form:

$$\det[I + kW(s)] = 1 - k \text{tr}\{W(s)\} + \dots + (-1)^N k^N \det W(s) = 0, \quad (1.205)$$

where the terms expressed through the sums of the principle minors of different orders [from the second to the  $(N - 1)$ th] of  $W(s)$  are denoted by dots. After reducing to a common denominator, this equation can be rewritten, taking into account Equation (1.200), in the form

$$P(s) - kP_1(s) + \dots + (-1)^N k^N Z(s) = 0, \quad (1.206)$$

where  $P_1(s) = P(s)\text{tr}\{W(s)\}$ , i.e. in the form of an equation of degree  $n$  with respect to  $s$ , where  $n$  is the number of MIMO system poles. It is easy to understand that if the difference between the orders of the numerator and denominator polynomials of all diagonal elements of  $W(s)$  is greater than two, which is a very typical situation in practice, then the difference in the orders of the poles polynomial  $P(s)$  and the polynomial  $P_1(s)$  in Equation (1.206) will also be greater than two. Therefore, the coefficient of the term of degree  $n - 1$  in Equation (1.206) is equal to the corresponding coefficient of the polynomial  $P(s)$  and *does not depend* on the parameter  $k$ . This, in turn, implies that as  $k$  changes, the sum of the roots of the closed-loop MIMO system must remain constant and equal to the sum of the poles of the open-loop system. As a result, if some of the roots of the characteristic Equation (1.205) move in the complex plane to the left, then some other roots of that equation must move to the right. Besides, the product of the MIMO system poles, which is equal to the absolute term of Equation (1.206), is proportional to  $k^N$  and increases infinitely with adequate increasing of  $k$ . Consequently, those branches of multivariable root loci that do not terminate at the finite zeros must tend to infinity.

A straightforward extension of these statements to the case of individual characteristic systems, the combination of the root loci of which constitutes the overall root loci of the MIMO systems, is not so evident. If no branch points exist and the CTFs  $q_i(s)$  can be represented as a quotient of the two algebraic polynomials  $M_i(s)$  and  $D_i(s)$  (we know that this is possible for uniform, circulant and anticirculant systems), then, for those  $q_i(s)$  for which the difference

<sup>64</sup> The gain margins of the characteristic systems are determined at these points (see Section 1.1.4).

between the numbers of poles and zeros exceeds two, i.e.  $e_i = np_i - nz_i > 2$ , the sum of the roots along the root loci of the given CTF is constant and does not depend on  $k$ . The reason is that in the absence of branch points, the root loci of the corresponding CTFs lie on the *isolated one-sheeted surfaces*. Then, this rule is a direct consequence of the same Viète's theorem. If  $e_i > 2$ , then, instead of Equation (1.198), we can write

$$D_i(s) + kM_i(s) = s^{np_i} + d_1s^{np_i-1} + (d_2 + km_0)s^{np_i-2} + \dots + (d_{np_i} + km_{n_z}) = 0, \quad (1.207)$$

where the  $d_1$  coefficient, taken with the opposite sign, is equal to the sum of all roots of that equation, and is equal to the sum of all poles of the  $i$ th open-loop CTF. Since the coefficient of the term of degree  $np_i - 1$  in Equation (1.207) does not depend on  $k$ , then, if some roots on the  $i$ th sheet of the Riemann surface move to the right, the other roots must move to the left, and their sum should be constant and equal to the sum of the poles of  $q_i(s)$ . Besides, the product of the roots of Equation (1.207) increases with the increase in  $k$ , and, for  $d_{np_i} = 0$ , which is equivalent to the presence of zero poles in  $q_i(s)$ , this product is directly *proportional* to the value of  $k$ . These properties are complete analogues of the corresponding properties of the roots of common SISO systems (Evans 1954; Horowitz 1963).

In the presence of branch points, the picture becomes far more complicated. The chief problem is that in this case, some trajectories pass from one sheet of the Riemann surface to another. Therefore, as the coefficient  $k$  changes, there may be a change in *the number of roots* on a certain sheet of the Riemann surface, with a corresponding change in the number of roots on the adjacent sheet. This circumstance excludes generally the application to the individual CTFs of the above-stated simple rules concerning behaviour of the root loci of the MIMO systems taken as a whole.

In the classical control theory, one can find some other rules (Horowitz 1963), but we shall restrict our discussion to the listed ones, since they are quite sufficient for understanding the general features of multivariable root loci and their relationship with the root loci of common SISO systems.

**Remark 1.13** In Sections 1.2.2 and 1.2.3, the definition of the *absolute poles* and *zeros*, as poles and zeros that are *common* to all CTFs  $q_i(s)$  of the open-loop MIMO system was given. From the above exposition, it ensues that from any absolute pole originate, taking into account its multiplicity, exactly  $N$  branches of the root loci, and at any absolute zero terminate, taking into account its multiplicity, exactly  $N$  branches of the root loci of the MIMO system; such (generally, non-coincident) branches has each characteristic system. This can serve as another equivalent definition of the absolute poles and zeros of MIMO systems.

**Remark 1.14** In Remark 1.6, we indicated that in the presence of zero entries in the open-loop transfer matrix  $W(s)$ , the situations in which some transfer functions of the cross-connections do not appear in the determinant  $\det W(s)$  and their poles do not change on introducing the feedback and become the poles of the closed-loop MIMO system are possible. These poles represent the so-called *degenerate* branches of the multivariable root loci (Postlethwaite and MacFarlane 1979), consisting of a set of isolated points that preserve their positions as the coefficient  $k$  changes from zero to infinity.

Below, we give some specific examples which illustrate, on the one hand, the above-stated general rules of behaviour of multivariable root loci and which show, on the other hand, how

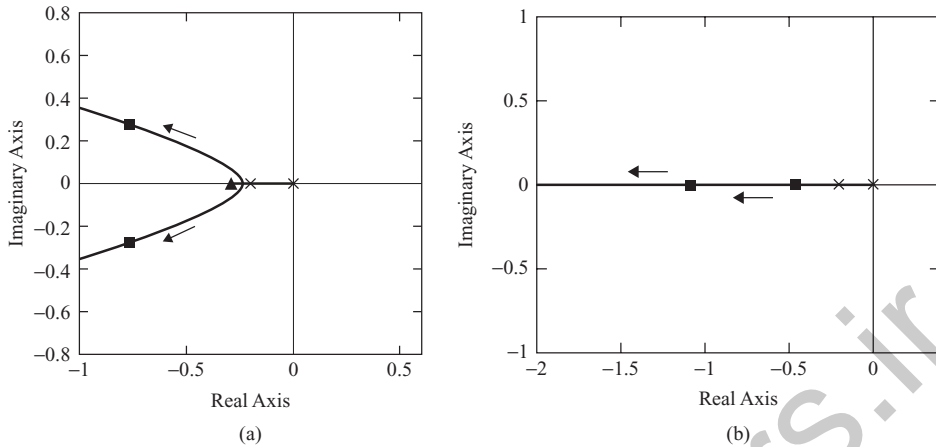


**Figure 1.45** Root loci of the two-axis guidance system with transfer functions [Equation (1.65)]. (a)  $\alpha_1 = 30^\circ, \alpha_2 = 20^\circ$ ; (b)  $\alpha_1 = 30^\circ, \alpha_2 = -20^\circ$ .

difficult may be in some cases to predict, based upon the given open-loop transfer matrix  $W(s)$ , even the general character of the roots' trajectories.

**Example 1.12** Consider the two-axis general guidance system of Example 1.2. The root loci of that system in the case of the transfer functions [Equation (1.65)] and for the same two combinations of angles  $\alpha_1$  and  $\alpha_2$ , as in Example 1.2:  $\alpha_1 = 30^\circ, \alpha_2 = 20^\circ$  and  $\alpha_1 = 30^\circ, \alpha_2 = -20^\circ$ , are shown in Figure 1.45. The crosses in Figure 1.45 denote the open-loop system poles ( $p_1 = 0, p_2 = -0.2$ ), the squares the closed-loop system roots (corresponding to  $k = 1$ ) and the triangles the branch points. The arrows show the directions of movements of the roots as the coefficient  $k$  increases. As can be seen from these figures, we have two completely different pictures of the root loci.

For  $\alpha_1 = 30^\circ, \alpha_2 = 20^\circ$ , when the eigenvalues of the cross-connections matrix  $R$  [Equation (1.60)] are complex conjugate numbers, there is one branch point on the real axis at  $-0.2575$ . For  $k = 0$ , the root trajectories begin at the indicated above poles of the open-loop system, which are situated on the *different* sheets of the Riemann surface. As  $k$  increases, both poles first shift along the real axis to the left. Then, when the left root reaches the branch point, it passes to the adjacent sheet and begins moving in the opposite direction, towards the second root. For  $k = 0.2039$ , both roots meet (notice, on the *second* sheet of the Riemann surface!) at the point  $-0.2362$ , then depart from the real axis in opposite directions, and begin moving to infinity along two asymptotes making angles  $\approx \pm 17.85^\circ$  with the negative real axis. For  $k = 1$ , the closed-loop system has two complex conjugate poles:  $-0.768 \pm j0.2755$ . Here, we have encountered the specific feature of multivariable root loci, when some branches, beginning their motion on one sheet of the Riemann surface, tend to infinity on the other sheet. This confirms once more the fact that the CTFs constitute a unique mathematical entity and should generally be considered a single whole.

For  $\alpha_1 = 30^\circ, \alpha_2 = -20^\circ$ , when the eigenvalues of  $R$  are real, the pattern of behaviour of the closed-loop system roots drastically differs from that considered above. Here, *there are no* branch points and the roots of each CTF move along the real axis, remaining on their own sheet of the Riemann surface. The configuration of root loci for each CTF in this case is quite

analogous to that of the root loci of the SISO systems, having one zero pole or one real negative pole. For  $k = 1$ , this system has two real negative roots at the points  $-1.0764$  and  $-0.4595$ .

Hence, depending on the specific forms of cross-connections and transfer functions of MIMO systems, the root trajectories may have quite different characters, and it is very difficult to predict the general behaviour of multivariable root loci. At the same time, if the root loci have already been constructed, then it can be verified that they indeed obey the above-listed rules.

Let us proceed now to a system with more complicated transfer functions  $W_1(s)$  and  $W_2(s)$  [Equation (1.66)]. The root loci of the systems for  $\alpha_1 = 0^\circ, \alpha_2 = 0^\circ$ , i.e. the root loci of the isolated separate channels of the system, are given in Figure 1.46(a) and (b), which show that as the coefficient  $k$  indefinitely increases, six branches of the root loci tend to infinity (two branches in the first channel and four in the second).

The root loci of the cross-connected system for  $\alpha_1 = 30^\circ, \alpha_2 = 20^\circ$ , that is for complex conjugate eigenvalues of the matrix  $R$ , are shown in Figure 1.46(c). The analysis of these root loci gives the following picture. Since  $N = 2$ , we have *two* sheets of the Riemann surface.

On one of them, which we shall call the first, there are situated *five* poles of the CTF  $q_1(s)$ : *two* zero poles  $p_{1,2}^1 = 0$  and three real poles:  $p_3^1 = -2, p_4^1 = -4, p_5^1 = -8$ . On the second

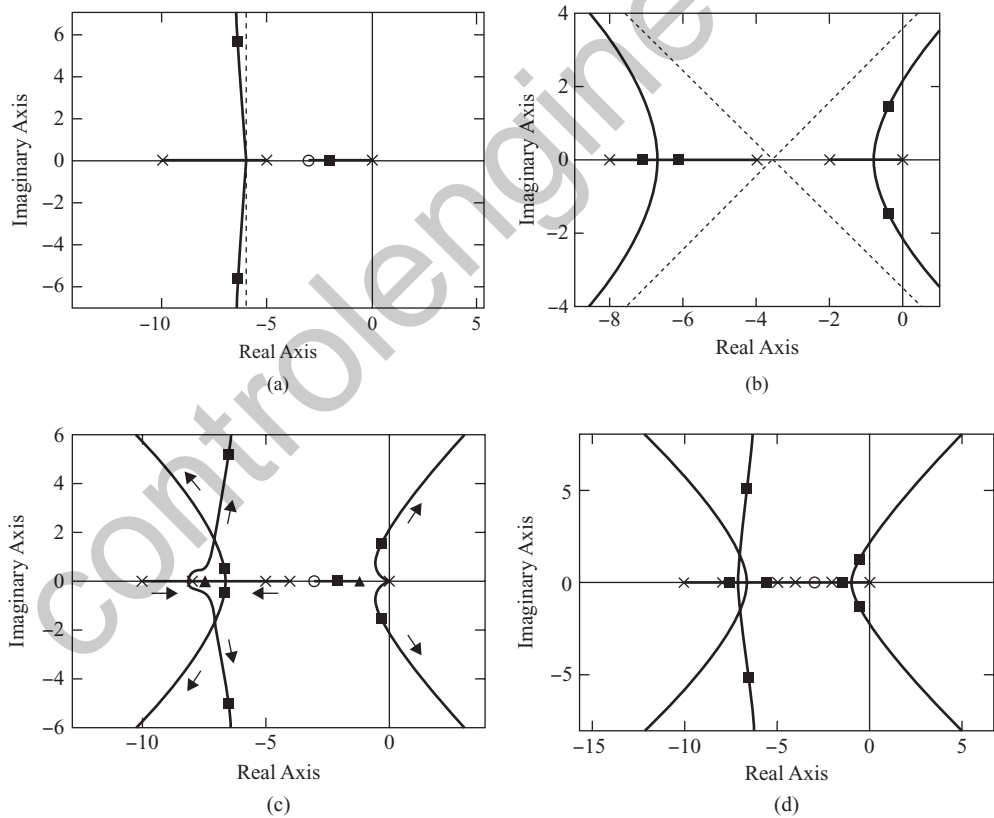


**Figure 1.46** The root loci of the two-dimensional system [Equation (1.66)] for different combinations of angles  $\alpha_1$  and  $\alpha_2$ . (a)  $\alpha_1 = 0^\circ, \alpha_2 = 0^\circ$  (the first channel); (b)  $\alpha_1 = 0^\circ, \alpha_2 = 0^\circ$  (the second channel); (c)  $\alpha_1 = 30^\circ, \alpha_2 = 20^\circ$ ; (d)  $\alpha_1 = 30^\circ, \alpha_2 = -20^\circ$ .

sheet, which corresponds to the CTF  $q_2(s)$ , there are *two* poles  $p_1^2 = -5$ ,  $p_2^2 = -10$  and *one* zero  $z_1^2 = -3$ . *Three* branch points exist in the complex plane, at  $s = -1.1545$ ,  $-7.66$  and  $-7.954$ , denoted in Figure 1.46(c) by the small triangles. As  $k$  increases from the zero value, the zero poles of the CTF  $q_1(s)$  form two complex conjugate branches of the root loci and move to the left; the root emerging from the pole  $p_3^1 = -2$  moves along the real axis to the right, towards the roots that emerged from the origin.

The poles at points  $-4$  and  $-5$  first move to the left, and the poles at  $-8$  and  $-10$  move to the right; thus, they are situated in pairs on the different sheets of the Riemann surface. For  $k = 0.1151$ , the root on the first sheet, moving to the right from the pole  $p_5^1 = -8$ , reaches the branch point at  $-7.954$ , and, passing to the second sheet of the Riemann surface, begins moving in the opposite direction, towards the root from the pole  $p_2^2 = -10$ . For  $k = 0.1975$ , both these real roots meet at the point  $-8.1622$  and then go into the complex plane, making angles  $\pm 90^\circ$  with the real axis; thus, they form two branches of the root trajectories on the second sheet of the Riemann surface which tend to infinity in parallel with the imaginary axis (the second-order Butterworth pattern). The root of the first CTF, which emerged from the pole  $p_3^1 = -2$ , reaches, for  $k = 0.307$ , the branch point at  $-1.1545$  and, passing to the second sheet of the Riemann surface, begins moving in the opposite direction, towards the zero  $z_1^2 = -3$ .<sup>65</sup> The two roots that emerged, on the first sheet, from the origin also change at that moment the moving direction to the opposite, towards the right half-plane. For  $k = 0.3271$ , the root of the second characteristic system, which emerged from the pole  $p_1^2 = -5$ , reaches the branch point at  $-7.66$  and, after passing to the first sheet, begins moving to the right, towards the root from  $-4$ . These two roots meet, for  $k = 0.9188$ , at the point  $-6.634$  and, breaking away from the real axis (and making with the latter the angles  $\pm 90^\circ$ ), move in the first sheet to the left, thereby forming with the two branches from the origin a fourth-order Butterworth pattern.

It is interesting to note that in this example, we have encountered both variants of root loci intersections; in Figure 1.46(c), we can see the root loci intersections on the same sheet (the intersections on the real axis), as well as intersections of the branches situated on the *different* sheets of the Riemann surface (the intersection of the two complex-valued branches). Note also that the closed-loop system roots corresponding to  $k = 1$  and marked in Figure 1.46(c) by the squares indicate the system stability. This agrees with the results obtained in Example 1.2 by means of the generalized Nyquist criterion.

The root loci of the system for  $\alpha_1 = 30^\circ$ ,  $\alpha_2 = -20^\circ$ , when the eigenvalues of the cross-connection matrix  $R$  are real numbers, have quite another nature. These root loci are shown in Figure 1.46(d) and, roughly speaking, can be viewed as the superposition of the root loci of the isolated separate channels in Figure 1.46(a) and (b). In this case, there are no branch points and therefore all trajectories remain within their own sheets of the Riemann surface. However, the distribution of the poles of the CTFs  $q_1(s)$  and  $q_2(s)$  does not coincide with that of the poles of transfer functions  $W_1(s)$  and  $W_2(s)$  [Equation (1.66)]. The inspection of the root trajectories in Figure 1.46(d) shows that  $q_1(s)$  and  $q_2(s)$  can be represented, up to the values of the real 'gains'  $K_1$  and  $K_2$ , as

$$q_1(s) = \frac{K_1(s + 2)}{s(s + 5)(s + 8)}, \quad q_2(s) = \frac{K_2}{s(s + 2)(s + 4)(s + 10)}. \quad (1.208)$$

<sup>65</sup> Note that in the case of rigid (static) cross-connections and a diagonal transfer matrix of the separate channels, the zeros and poles of the open-loop MIMO system coincide with the zeros and poles of the separate channels.

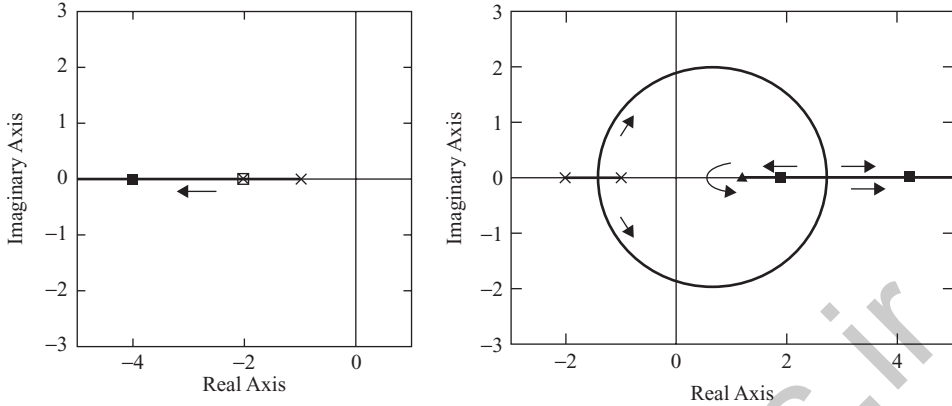


**Figure 1.47** Root loci of the two-dimensional system of Example 1.3. (a) initial system; (b) varied system.

Comparison of Equation (1.208) with Equation (1.66) shows that the distribution of poles and zeros of  $q_1(s)$  and  $q_2(s)$  differs from that of  $W_1(s)$  and  $W_2(s)$  only by the fact that the poles  $-10$  and  $-8$  have interchanged. Correspondingly, the pairs of the poles that form the complex conjugate branches of the root loci in Figure 1.46(d) have changed.

**Example 1.13** In Example 1.3, we discussed a peculiar two-dimensional system [Equation (1.67)], which, having, at first sight, an infinite gain margin, becomes unstable under the *simultaneous* additive increase of the first channel gain by 0.13 and decrease of the second channel gain by 0.12. A question arises of how these changes affect the root loci of the system. The root trajectories of the initial system are shown in Figure 1.47(a) and those of the varied system with the diagonal regulator [Equation (1.70)] in Figure 1.47(b). The comparison of these graphs confirms once more that the simultaneous change in the gains of separate channels, but with opposite signs, results in drastic changes in the internal structure of the system. The root loci of the initial system represent the combination of the root loci of two usual first-order systems with the poles at  $-1$  and  $-2$ , i.e. here, we have two real branches along which the closed-loop system roots tend to  $-\infty$ , remaining on their sheets of the Riemann surface.<sup>66</sup> However, under the indicated variations of the gains, the picture completely changes. For  $k = 0$ , both poles of the MIMO system belong to *one* CTF and are situated on one sheet of the Riemann surface, at the points  $-1$  and  $-2$ . As  $k$  increases, the closed-loop system roots, emerging from these poles, move towards each other and (for  $k = 0.0144$ ) meet at the breakaway point  $s = -1.4346$ , where they depart from the real axis. Then, the complex conjugate poles move along a circle to the right half-plane and meet (for  $k = 0.9284$ ) on the real axis at the point  $s = 2.7288$ . It should be accentuated that all these trajectories belong to one sheet of the Riemann surface. After meeting on the real axes, the roots begin moving along that axis in opposite directions, where the left root moves towards the branch point at  $s = 1.2916$ . For  $k = 1.7191$ , the left root reaches the branch point, then passes to the *second* sheet of the Riemann surface and, changing to the opposite moving direction, begins moving (like the root

<sup>66</sup> In Figure 1.47(a), the root of the *closed-loop* first characteristic system coincides at point  $-2$  with the pole of the *open-loop* second characteristic system.

remaining on the first sheet) in the positive direction of the real axis. All this is shown in Figure 1.47(b) by arrows. Note that the moving direction of both poles along the real axis to  $+\infty$  happens because the product of the roots must increase together with the increase in  $k$  (Rule 10).

**Remark 1.15** In Example 1.13, we encountered an interesting situation in which, in the presence of branch points, some CTFs may have no poles or zeros on their sheets of the Riemann surface, but those sheets contain branches of multivariable root loci, starting from a certain value of  $k$ .

In the classical control theory, there is one more rarely used rule called the *shift of the root loci starting points* (Horowitz 1963). According to that rule, if we have found the roots of a closed-loop SISO system which correspond to some value  $k = k_0$ , then these roots may serve as the *poles* of a certain new *open-loop* system, whose zeros coincide with the zeros of the initial system. If the root loci of the new system are constructed as the *new gain*  $k' = k - k_0$  changes from zero to infinity, then these loci will be the continuation of the root loci of the initial system, as  $k$  changes from 0 to  $k_0$ . Or, similarly, the new root loci are part of the root loci of the initial system as  $k$  changes from zero to infinity. In other words, the poles of the initial system can always be replaced by a set of other poles that are situated at the corresponding points of the root loci.

As applied to our situation, we can regard the root of the MIMO system which has appeared, for some  $k = k_0$ , through a branch point on the  $i$ th sheet of the Riemann surface as a *fictitious pole* of a new CTF. Then, we can consider this sheet independently of all other sheets, assuming that the new gain  $k' = k - k_0$  changes from zero to infinity. Such an approach may be useful for understanding, to a certain extent, the properties of multivariable root loci within each sheet of the Riemann surface.

**Remark 1.16** The examination of the above examples allows us to draw another heuristic conclusion about the branch points of multivariable root loci. With respect to the branches of root loci, which begin on the given sheet of the Riemann surface, the branch points may be regarded as some *fictitious zeros* to which the roots of the closed-loop characteristic systems approach, obeying the general properties and features of the root loci. However, unlike the *actual* finite or infinite zeros belonging to the same sheet, the roots of the closed-loop system are ‘compensated’ (or ‘merged’) by the branch points for *finite* values of the gain  $k$ . The reader can ascertain this conclusion by inspection of the root loci in Figures 1.46 and 1.47. In particular, the behaviour of the root trajectories of the varied two-dimensional system in Figure 1.47(b) immediately becomes apparent.

Hence, combining the last two remarks, we can say that from the ‘entrance’ side, each branch point may be viewed as a *fictitious zero* to which one of the root trajectories of a certain characteristic system approaches, obeying the customary rules. From the ‘exit’ side, each branch point may be viewed as a *fictitious pole* from which one of the root trajectories of some other characteristic system originates. It is of importance here that the ‘compensation’ of a pole on one sheet of the Riemann surface is accompanied by the ‘origination’ of a new pole on another sheet, and all this occurs for some *finite* value of the parameter  $k$ .

## 1.5.2 Root loci of uniform systems

In Section 1.3, we pointed out that the structural features of uniform systems, i.e. MIMO systems with identical channels and rigid cross-connections, enable us to bring very closely

the methods of their investigation to the corresponding methods for usual SISO systems. Largely, this concerns also the problem of constructing root loci of uniform systems. In fact, that problem is reduced to the task of constructing  $N$  separate root loci of SISO characteristic systems, and the rules of constructing these loci appear as a slight modification of the standard rules known from the classical control theory (Evans 1954; Horowitz 1963).

As we know,<sup>67</sup> the CTFs  $q_i(s) = \lambda_i w(s)$  of uniform systems coincide, up to the constant ‘gains’  $\lambda_i$ , with the transfer function of the separate channels  $w(s) = M(s)/D(s)$ , where  $\lambda_i$  are the eigenvalues of the cross-connections matrix  $R$ , and these eigenvalues can be either real or in complex conjugate pairs. We also know that all poles and zeros of  $w(s)$  are absolute zeros and poles of the open-loop uniform system and, as a result, are common to all  $q_i(s)$ . Besides, the CTFs  $q_i(s)$  do not have branch points and are situated on  $N$  isolated one-sheeted Riemann surfaces. The latter means that the root loci of each characteristic system can be constructed independently of the root loci of other characteristic systems, i.e. the task of finding the root loci of uniform systems indeed reduces, as was mentioned above, to  $N$  independent one-dimensional tasks (Gasparyan and Vardanyan 2007).

Let us rewrite Equation (1.173), taking into account the above comments, in the form

$$1 + k\lambda_i w(s) = D(s) + k\lambda_i M(s) = 0 \quad \text{or} \quad k\lambda_i w(s) = k\lambda_i \frac{M(s)}{D(s)} = -1, \quad i = 1, 2, \dots, N. \quad (1.209)$$

The last of these equations may also be written down in the equivalent form

$$kw(s) = -\frac{1}{\lambda_i} = -\frac{1}{|\lambda_i|} \exp\{-j \arg \lambda_i\}, \quad (1.210)$$

from which we have somewhat different conditions of the formation of root trajectories in comparison with Equation (1.174):

$$|kw(s)| = \frac{1}{|\lambda_i|}, \quad \arg w(s) = \pm(2r + 1)180^\circ - \arg \lambda_i, \quad r = 0, 1, 2, \dots \quad (1.211)$$

From Equations (1.209)–(1.211), the following additional rules describing the properties of the root loci of uniform systems immediately ensue.<sup>68</sup>

**Rule 1:** *Number of branches of the root loci.* The number of root trajectories of an  $N$ -dimensional uniform system is equal to  $Nnp_s$ , where  $np_s$  is the number of the absolute poles, i.e. the number of the poles of  $w(s)$ .

**Rule 2:** *Starting and ending points of the root loci.* For  $k = 0$ , the root trajectories begin at the roots of the equation  $D(s) = 0$ , i.e. at the absolute poles, and terminate, for  $k = \infty$ , at the roots of the equation  $M(s) = 0$ , i.e. at the absolute zeros of the uniform system. From each absolute pole originate exactly  $N$  trajectories and, at any absolute zero, terminate exactly  $N$  trajectories. In other words, the root loci of each of  $N$  characteristic systems begin at the poles of the transfer function  $w(s)$  and terminate at its zeros.

<sup>67</sup> See Equation (1.94).

<sup>68</sup> For simplicity, we shall list these rules starting from number 1. The reader should remember that they are additional to the general rules established in the previous section.

**Rule 3:** *Number of the root trajectories tending to infinity.* The number of root trajectories of each characteristic system tending to infinity as  $k$  increases indefinitely is equal to  $e_s = np_s - nz_s$ , where  $nz_s$  is the number of zeros of  $w(s)$  (the number of absolute zeros of the uniform system). Respectively, the number of root trajectories of the uniform system tending to infinity is equal to  $Ne_s$ .

**Rule 4:** *Angles of the asymptotes of the root loci.*<sup>69</sup> It can be shown that the set of  $e_s$  approaching infinity root trajectories of the  $i$ th characteristic system tend indefinitely to the Butterworth pattern of order  $e_s$ , whose evenly spaced lines (the root trajectory asymptotes) make with the positive direction of the real axis angles

$$\gamma_r = \frac{(2r + 1)180^\circ + \arg \lambda_i}{e_s}, \quad r = 0, 1, \dots, e_s - 1. \quad (1.212)$$

As is evident from Equation (1.212), the angles of root trajectory asymptotes of the characteristic systems with real-valued  $\lambda_i$ , i.e. with  $\arg \lambda_i = 0$ , are equal to the angles of asymptotes of a common SISO system with an open-loop transfer function  $w(s)$ . Further, each Butterworth pattern corresponding to a complex-valued  $\lambda_i$  is nonsymmetrical with respect to the real axis. However, taking into account that all complex eigenvalues  $\lambda_i$  must occur in complex conjugate pairs, for each such pattern, there exists a ‘complex conjugate’ pattern, which is obtained from the first one by mirror mapping around the real axis.

**Rule 5:** *Pivots of the asymptotes.* It can also be shown that the pivots (centres) of the asymptotes of all characteristic systems are situated at the same point on the real axis and coincide with the common centre of asymptotes  $A_c$  of isolated separate channels of the uniform system:

$$A_c = \frac{\sum_{r=1}^{np_s} p_r - \sum_{r=1}^{nz_s} z_r}{np_s - nz_s}, \quad (1.213)$$

where  $p_r$  and  $z_r$  denote the poles and zeros of the transfer function  $w(s)$ .

**Rule 6:** *Coincident symmetrical root trajectories.* The root trajectories of the characteristic systems corresponding to *all* real eigenvalues  $\lambda_i$  of  $R$  are symmetrical with respect to the real axis, coincide with each other and coincide with the root trajectories of isolated separate channels of the uniform system. This property becomes apparent if we consider the phase (the second) condition in Equation (1.211), which, for real  $\lambda_i$ , i.e. for  $\arg \lambda_i = 0$ , just transforms into the analogous condition for common SISO systems with an open-loop transfer function  $w(s)$ . The location of the roots of the corresponding characteristic systems on these trajectories is different and depends on the magnitudes  $|\lambda_i|$ .

**Rule 7:** *Complex conjugate and coincident nonsymmetrical root loci.* The root loci of the characteristic systems with complex conjugate eigenvalues  $\lambda_i$  are nonsymmetrical with respect to the real axis. All of these root loci can be obtained from each other by mirror

<sup>69</sup> The proof of Rules 4 and 5 is left to the reader as an exercise.

mapping around the real axis. All the root trajectories of a uniform system corresponding to  $\lambda_i$  with the same argument  $\arg \lambda_i$  but, possibly, with different magnitudes  $|\lambda_i|$  coincide. This rule is a logical continuation of the preceding ones and follows from Equation (1.212).

**Rule 8:** *Sections of the real axis belonging to root loci.* A uniform system can have root trajectories coinciding with finite or semi-infinite sections of the real axis only in the presence of real eigenvalues  $\lambda_i$ . In this case, such sections are those located to the left of the *odd* singular points<sup>70</sup> of  $w(s)$ . This rule also ensues from the previous rules. Concerning the characteristic systems with complex  $\lambda_i$ , such systems *cannot* have the root trajectories on the real axis. This is evident from the conditions in Equation (1.210), which cannot be satisfied for complex  $\lambda_i$  and real  $s$ , when the transfer function  $w(s)$  becomes real-valued.

**Rule 9:** *Value of  $k$ .* The value of the parameter  $k$  corresponding to any point  $s_0$  on the root trajectories of the  $i$ th characteristic system can be found from Equation (1.211) and is equal to  $k = 1/|\lambda_i w(s_0)|$ .<sup>71</sup>

Hence, we have formulated a number of additional rules describing the properties of root loci of uniform systems, which enable the engineer or researcher to construct those loci without any difficulty. The reader might have realized that these rules are quite similar to the standard rules of constructing root loci for usual SISO systems. Unlike general MIMO systems, in the case of uniform systems, the root loci represent the combination of  $N$  root loci corresponding to  $N$  isolated, i.e. having no branch points, characteristic systems. This statement, as well as the fact that the CTFs  $q_i(s) = \lambda_i w(s)$  of the discussed systems can be expressed analytically for any number of channels  $N$ ,<sup>72</sup> implies that the problem of construction of root loci for uniform MIMO systems is practically solved.

**Example 1.14** Consider the two-axis uniform guidance system of Example 1.4 with the gain of the transfer function decreased by a factor of 10 [Equation (1.103)]. This decrease in the gain is not essential at all, but it provides system stability for both combinations of angles  $\alpha_1$  and  $\alpha_2$ . The root loci of the system are shown in Figure 1.48, where the dashed lines represent the asymptotes. The overall view of the root loci for  $\alpha_1 = 40^\circ$  and  $\alpha_2 = 35^\circ$ , which corresponds to complex conjugate eigenvalues  $\lambda_1$  and  $\lambda_2$  of the cross-connections matrix  $R$  (see Example 1.4), is given in Figure 1.48(a). The root trajectories of both characteristic systems, for the above values of  $\alpha_1$  and  $\alpha_2$ , are shown in Figure 1.48(b) and (c). As is evident from Figure 1.48(a)–(c), for complex conjugate eigenvalues of  $R$ , the root loci of the guidance system do not have sections situated on the real axis, and the root loci and asymptotes of the characteristic systems are nonsymmetrical with respect to the real axis and can be obtained from each other by complex conjugation.

For  $\alpha_1 = 40^\circ$  and  $\alpha_2 = -35^\circ$ , when the eigenvalues  $\lambda_1$  and  $\lambda_2$  are real, the root loci of the two-dimensional guidance system coincide with the root loci of the isolated separate channels, but we have here two identical, superimposed patterns of the root trajectories belonging to two different characteristic systems [Figure 1.48(d)].

<sup>70</sup> That is, if the total number of poles and zeros of  $w(s)$  to the left of the section is *odd*.

<sup>71</sup> This rule may be rather useful for the development of interactive program packages intended for computer-aided investigation of linear uniform systems.

<sup>72</sup> Recall that modern application packages enable the user to calculate the eigenvalues of numerical matrices of, in fact, any order.

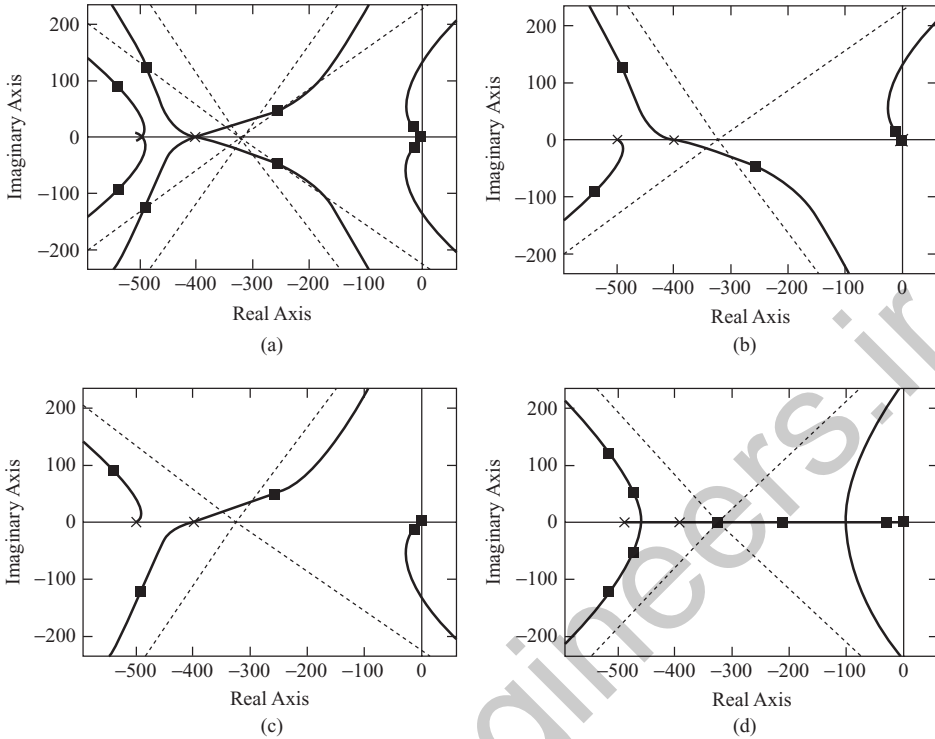


**Figure 1.48** The root loci of the two-axis uniform guidance system of Example 1.4. (a)  $\alpha_1 = 40^\circ$ ,  $\alpha_2 = 35^\circ$  (overall view); (b)  $\alpha_1 = 40^\circ$ ,  $\alpha_2 = 35^\circ$  (the first characteristic system); (c)  $\alpha_1 = 40^\circ$ ,  $\alpha_2 = 35^\circ$  (the second characteristic system); (d)  $\alpha_1 = 40^\circ$ ,  $\alpha_2 = -35^\circ$  (overall view).

### 1.5.3 Root loci of circulant and anticirculant systems

Internal structural characteristics and properties of circulant and anticirculant systems are so much alike that we shall discuss only the root loci of circulant systems below, noting, at the same time, some specific features inherent in anticirculant systems. The salient feature of circulant systems is that root loci of their characteristic systems are situated, similarly to uniform systems, on *isolated one-sheeted* Riemann surfaces, i.e. here, also, the problem of constructing root loci splits, without any assumptions or simplifications, into  $N$  independent one-dimensional tasks. Further, we know that the CTFs  $q_i(s)$  of circulant systems can be represented analytically for any number  $N$  of separate channels as proper rational functions in complex variable  $s$ . The poles of all CTFs are *absolute* and equal to all poles of the first (or any other) row elements of the open-loop transfer matrix  $W(s)$ . As a result, their distribution is symmetrical with respect to the real axis.<sup>73</sup> Concerning the zeros of the CTFs, and these

<sup>73</sup> We do not consider here the situations in which zeros of some other circulant transfer matrix can cancel some absolute poles of a circulant system (see also Example 1.10, in which zeros of the CTFs cancel poles of the common scalar multiplier, and the poles of the resulting CTFs are complex conjugate to each other). For simplicity, we shall also assume that the circulant transfer matrix  $W(s)$  does not have any scalar multipliers (i.e. multipliers in the form of scalar transfer functions), which originate *absolute poles and zeros* of circulant systems, *common* to all  $q_i(s)$ .

zeros give the zeros of a circulant system, in the general case, they are roots of the polynomials with complex-valued coefficients; therefore, their distribution for each characteristic system is nonsymmetrical. At the same time, to any such nonsymmetrical location of zeros corresponds a ‘complex conjugate’ location of zeros of some other characteristic system, resulting in the symmetrical picture for *all* zeros of the circulant system. Finally, it is worth noting that the *number* of zeros of all CTFs of the circulant system is the *same*, which ensues from the form of the CTFs  $q_i(s)$  [Equation (1.133)]. All this suggests that the properties of circulant systems’ root loci must be quite close to the corresponding properties of uniform systems. This is indeed the case, but, here, there are some essential distinctions due to the presence of *dynamical* cross-connections, or, in other words, due to the presence of  $N$  generally different transfer functions in any row of the open-loop matrix  $W(s)$ , whereas, in the case of uniform systems, we have *only one* transfer function  $w(s)$ .

If we denote by  $D(s)$  the *identical* denominator polynomials of all CTFs  $q_i(s)$  of circulant systems and by  $M_i(s)$  the numerator polynomials, i.e. if we represent the CTFs in the form  $q_i(s) = M_i(s)/D(s)$ , then Equations (1.198) and (1.199) can be rewritten as

$$1 + kq_i(s) = D(s) + kM_i(s) = 0 \quad \text{or} \quad kq_i(s) = k \frac{M_i(s)}{D(s)} = -1. \quad i = 1, 2, \dots, N \quad (1.214)$$

These conditions enable us to formulate some rules for constructing the root loci in a form that allows for the specific structural features of circulant systems. We shall list these rules, beginning, as in the previous section, from number 1.

**Rule 1:** *Number of branches of the root loci.* The number of root trajectories of an  $N$ -dimensional circulant system is equal to  $Nnp_0$ , where  $np_0$  is the number of absolute poles, i.e. the number of all poles of the elements of the first row of  $W(s)$ .

**Rule 2:** *Starting and ending points of the root loci.* For  $k = 0$ , the root trajectories of each (say, the  $i$ th) characteristic system begin at the same roots of the equation  $D(s) = 0$ , i.e. at the absolute poles, and terminate, for  $k = \infty$ , at the roots of the equation  $M_i(s) = 0$ . If we denote by  $nz_0$  the *same* order of all polynomials  $M_i(s)$  ( $i = 1, 2, \dots, N$ ), then this implies that  $nz_0$  root trajectories of each characteristic system approach, as  $k \rightarrow \infty$ ,  $nz_0$  finite zeros of the corresponding CTF  $q_i(s)$ .

**Rule 3:** *Number of root trajectories tending to infinity.* The number of root trajectories of each characteristic system tending to infinity (as  $k$  increases indefinitely) is the same and equal to  $e_0 = np_0 - nz_0$ . Respectively, the total number of root trajectories of a circulant system tending to infinity is equal to  $Ne_0$ .

**Rule 4:** *Angles of root loci asymptotes.* Let us represent  $q_i(s)$  in the factored form:

$$q_i(s) = \frac{M_i(s)}{D(s)} = \frac{K_c^i \prod_{j=1}^{nz_0} (s - z_j^i)}{\prod_{j=1}^{np_0} (s - p_j)}, \quad i = 1, 2, \dots, N, \quad (1.215)$$

where  $p_j$  are the poles (they are the same for all  $i$ ),  $z_j^i$  the zeros and  $K_c^i$  the ‘gains’ (generally complex-valued) of the characteristic systems. It can be shown<sup>74</sup> that the set of  $e_0$  approaching infinity root trajectories of the  $i$ th characteristic system tend indefinitely to the Butterworth pattern of order  $e_0$ , whose evenly spaced lines (the root trajectory asymptotes) make, with the positive direction of the real axis, angles equal to

$$\gamma_r = \frac{(2r + 1)180^\circ + \arg K_c^i}{e_0}, \quad r = 0, 1, \dots, e_0 - 1. \quad (1.216)$$

Comparison of Equation (1.216) with Equation (1.212) shows that the coefficients  $K_c^i$  play here the same role as the eigenvalues  $\lambda_i$  in the case of uniform systems, with all the geometrical features indicated in Rule 4 of the previous section.

**Rule 5:** *Pivots of the asymptotes.* The pivot of the Butterworth pattern for the  $i$ th characteristic system is located on the complex plane at the point

$$A_{ci} = \frac{\sum_{r=1}^{np_0} p_r - \sum_{r=1}^{nz_0} z_r^i}{np_0 - nz_0}, \quad i = 1, 2, \dots, N \quad (1.217)$$

where the designations are the same as in Equation (1.215).

Here, we have encountered an essential difference between the pivots of circulant and uniform systems. In the case of uniform systems, the pivots of asymptotes for all characteristic systems are at the same point on the real axis. For circulant systems, these pivots may be, in the general case, *complex-valued*. This is because the complex zeros  $z_j^i$  in Equation (1.217), being generally the roots of the polynomials with complex coefficients, are not complex conjugate. However, as the reader has most likely guessed, a complex conjugate pivot of some other characteristic system with the complex conjugate numerator polynomial of the CTF always corresponds to each complex pivot  $A_{ci}$ . For the circulant systems of *odd* order  $N$ , the number of such complex-valued pivots is equal to  $N - 1$  and, for *even* order  $N$ , their number is  $N - 2$ .

It should be pointed out that all pivots of anticirculant systems of *even* order are complex. This can be easily verified by examination of Figure 1.33, in which the eigenvalues of the anticirculant permutation matrix  $U_-$  [Equation (1.156)] for different values of  $N$  are shown. For anticirculant systems of *odd* order  $N$ , one pivot on the real axis generated by the eigenvalue  $\beta_{(N+1)/2} = -1$  always exists. Finally, all pivots of *simple symmetrical MIMO systems* lie on the real axis, since all the coefficients of their CTFs [Equations (1.138) and (1.139)] are real numbers.

**Rule 6:** *Symmetrical root trajectories.* Let us consider the eigenvalue distribution of the permutation matrix  $U$  [Equation (1.128)] (Figure 1.29). We know that, independently of order  $N$ , the first eigenvalue  $\beta_1$  of  $U$  is always equal to unity. Further, for even  $N$ , the  $(1 + N/2)$ -th eigenvalue  $\beta_{1+(N/2)}$  is always equal to minus one. Therefore, all CTFs  $q_i(s)$  generated by these eigenvalues will have, owing to Equation (1.133), polynomials with real coefficients, not only in the denominator, but also in the numerator. Correspondingly, the root loci of these characteristic systems possess all the well known properties of the SISO systems’ root loci.

<sup>74</sup> We address the proof of Rules 4 and 5 to the reader as an exercise.

This concerns the symmetry of root trajectories with respect to the real axis, sections of the root loci belonging to that axis, breakaway points, etc.

It is easy to understand that *simple symmetrical MIMO systems*, having for any  $N$  only two distinct characteristic systems with real coefficients [Equations (1.138) and (1.139)], also have the root loci completely analogous (considering each characteristic system separately) to root loci of usual SISO systems. It is also easy to understand that anticirculant systems of *even* order have only complex-valued CTFs, and therefore cannot have sections of the root loci on the real axis. As for *odd*  $N$  (the case of no actual interest in practice), only *one* characteristic system with real parameters exists.

The above simple rules reflect the specific character of the internal structure of circulant and anticirculant systems. The new and very significant point here is that the pivots of the root loci asymptotes are situated not only on the real axis, but can also be complex conjugate. At the same time, taking into account that for the pivots and angles of asymptotes, we have simple expressions [Equations (1.216) and (1.217)], as well as the fact that the CTFs  $q_i(s)$  can be expressed in analytical form for any number of channels  $N$ , the construction of root loci for circulant and anticirculant systems can be carried out without any difficulty.

**Example 1.15** As an example of MIMO systems having complex pivots of the root loci asymptotes, consider a two-dimensional antisymmetrical system described by a transfer matrix

$$W(s) = \frac{50}{(s+2)(s+3)(s+4)} \begin{pmatrix} 1 & \frac{4}{(s+8)} \\ -\frac{4}{(s+8)} & 1 \end{pmatrix}. \quad (1.218)$$

The CTFs  $q_{1,2}(s)$  of that system are

$$q_{1,2}(s) = \frac{50(s+8 \pm j4)}{(s+2)(s+3)(s+4)(s+8)} \quad (1.219)$$

and have two complex-conjugate zeros at  $z_1 = -8 - j4$  and  $z_2 = -8 + j4$ . The root loci of the system are shown in Figure 1.49(a), from which it can be seen that the pivots are located at the complex conjugate points  $A_{c1} = -3 + j1.333$  and  $A_{c2} = -3 - j1.333$  (these pivots are marked in Figure 1.49 by small black circles). The nonsymmetrical root loci of each characteristic system are presented in Figure 1.49(b) and (c).

**Example 1.16** In the last example of this section, we return to a nonrobust antisymmetrical system taken from Doyle (1984) and Packard and Doyle (1993) and discussed in Example 1.10. This system is of interest to us, not only as an *anticirculant* system, but also as a system which becomes, under slight perturbations of the parameters, a *general* MIMO system with rather remarkable features. In the case of an ideal unit regulator  $K = \text{diag}\{K_i\} = I$ , the characteristic equations of one-dimensional systems [Equation (1.180)] have, taking into account the ‘root loci coefficient’  $k$ , the form

$$\begin{aligned} s - ja + k(1 + ja) &= 0, \\ s + ja + k(1 - ja) &= 0. \end{aligned} \quad (1.220)$$

It is easy to see that as  $k$  changes from zero to infinity, the trajectories of the roots of Equation (1.220) are straight lines, beginning at the poles  $p_{1,2} = \pm ja$  of the open-loop system and

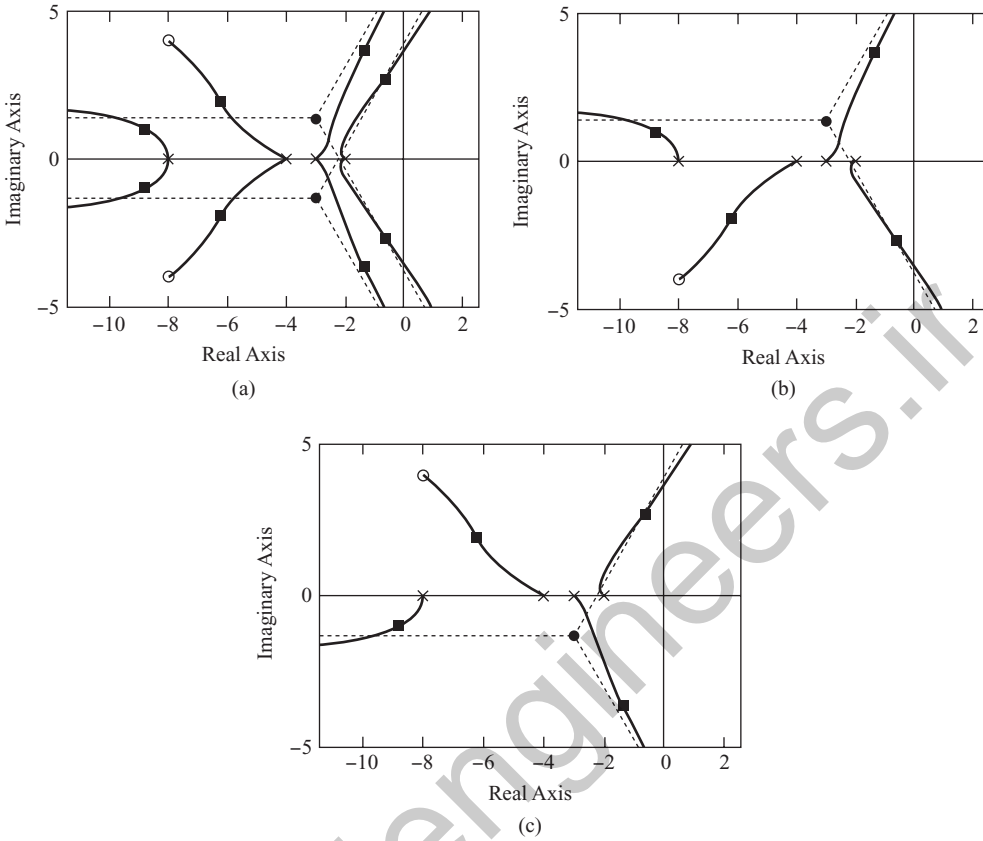


**Figure 1.49** The root loci of antisymmetrical system [Equation (1.218)]. (a) the overall view of the root loci; (b) the first characteristic system; (c) the second characteristic system.

intersecting, for  $k = 1$ , at the point  $(-1, j0)$ , at which both poles of the closed-loop system are located [Figure 1.50(a)]. Note also that each trajectory in Figure 1.50(a) is situated on an isolated one-sheeted Riemann surface. Assume, now, that the coefficients of the static regulator  $K$  have been changed to new values  $K_1 = 1.1$  and  $K_2 = 0.9$ . As was indicated in Example 1.10, with these values of  $K_1$  and  $K_2$ , the two-dimensional antisymmetrical system becomes an unstable *general MIMO* system. This fact is completely confirmed by the root loci of the varied system presented in Figure 1.50(b). As is evident from that figure, the root trajectories have drastically changed. Now, because the system is not circulant, its root loci are situated on a *two-sheeted* Riemann surface and have *two* branch points. For  $k = 0$ , both poles of the open-loop system are situated on *one* (say, the first) sheet, i.e. they belong to the first characteristic system. As  $k$  increases, the roots of the first characteristic system move in that sheet to the real axis and, for  $k = 0.9087$ , meet at the breakaway point  $-0.9087$  on that axis. As  $k$  increases further, both these roots depart from the breakaway point in opposite directions and move along the real axis towards the branch points (towards the *fictitious zeros* of the first characteristic system) at  $s_1 = -2.005$  and  $s_2 = +0.005$  (notice that the second branch point is located in the right

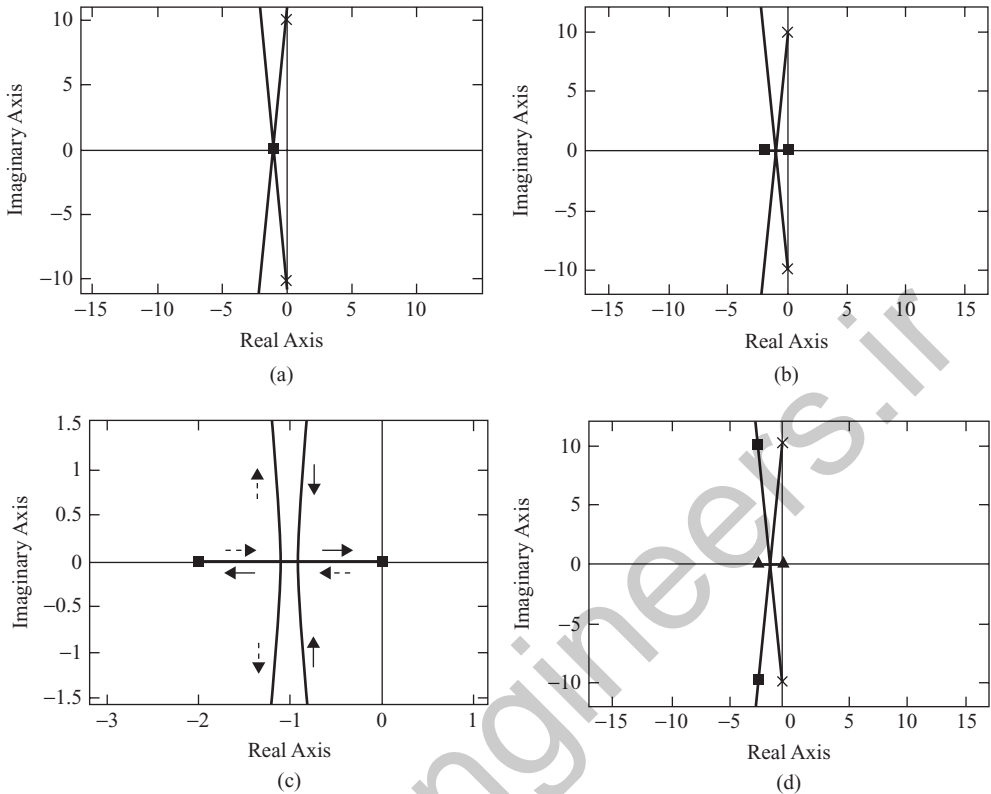


**Figure 1.50** The root loci of the non-robust antisymmetrical system from Doyle (1984). (a) the root trajectories of the ideal system (for  $K = I$ ); (b) the root trajectories of the varied system; (c) the root trajectories of the varied system (the enlarged view); (d) the location of the roots of the varied system (for  $k = 2$ ).

half-plane). For  $k = 1$ , both roots simultaneously (!) reach the branch points<sup>75</sup> and, as  $k$  increases further, they pass to the *second* sheet of the Riemann surface. Thus, we have obtained that for the nominal values  $K_1 = 1.1$  and  $K_2 = 0.9$  of the varied regulator (for  $k = 1$ ), the roots of the closed-loop system are equal to  $s_1 = -2.005$  and  $s_2 = +0.005$ , i.e. one of the roots is in the right half-plane and the system is *unstable*. However, as  $k$  increases further, the roots of the system begin moving on the second sheet from the branch points (from the *fictitious* poles) along the real axis towards each other, i.e. the ‘unstable’ right root begins moving in the opposite direction towards the left half-plane, reaching the imaginary axis for  $k = 1.0099$ . Further, for  $k = 1.1117$ , both roots meet on the second sheet of the Riemann surface at the breakaway point  $-1.1117$ <sup>76</sup> and depart from the real axis into the complex plane along the asymptotes that make, with the positive direction of the real axis, angles approximately equal to  $\pm 95.7^\circ$ . All of this is illustrated in Figure 1.50(c) by arrows, where the solid arrows correspond to the motion in the first sheet and the dashed arrows to that in the second sheet. For more clarity, the

<sup>75</sup> The right root reaches the imaginary axes for  $k = 0.995$ .

<sup>76</sup> The equality of the values of  $k$  at both breakaway points to the absolute values of these points abscissas  $-0.9087$  and  $-1.1117$  is not a misprint – it is obtained by calculations.

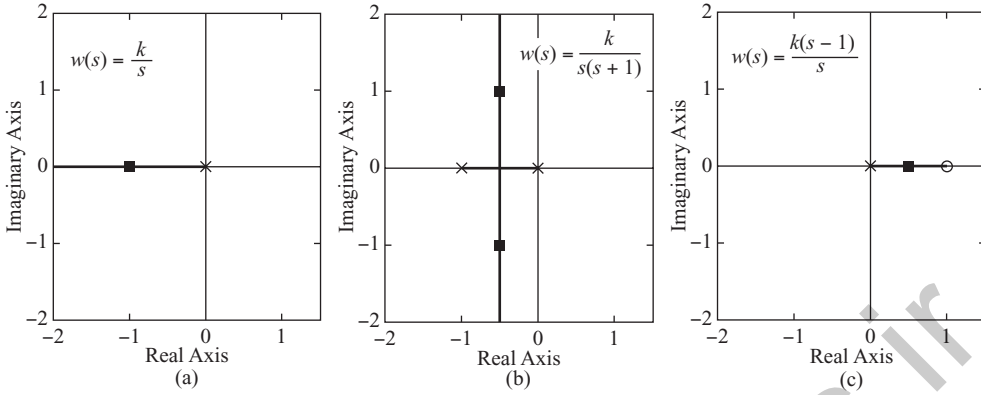


**Figure 1.51** The root loci of the SISO systems of Remark 1.17.

roots of the varied system for  $k = 2$ , which are equal to  $-2 \pm j9.7959$ , are shown in Figure 1.50(d). Hence, under the varied parameters of the regulator, the discussed system is unstable over a very small range of changes of  $k$ , from 0.995 to 1.0099, and this conclusion is obtained by an inspection of the root loci in Figure 1.50.

**Remark 1.17** In the scientific and technical literature, much attention is devoted to the limitations on the stability and performance of MIMO systems imposed by the *zeros situated in the right half-plane* (Skogestad and Postlethwaite 2005; Havre and Skogestad 1998). Having the multivariable root loci plotted, these limitations can be understood and assessed adequately, which allows (if needed) one to undertake the corresponding *justified* steps for diminishing the influence of the right half-plane zeros (frequently called the RHP-zeros). In principle, that problem is also inherent in the SISO case. As elementary examples, the root loci of two simple SISO systems having one pole at the origin in the open-loop state are shown in Figure 1.51(a) and (b). As is evident from these root loci, the closed-loop systems are stable for any arbitrary large values of the gain  $k$ . However, introducing a RHP-zero into these systems drastically changes the situation, and the systems become *unstable under any arbitrary small* values of  $k$  [in Figure 1.51(c), this is illustrated for the system in Figure 1.51(a)]. Similar examples can readily be given for the multivariable case. That can be done especially easily for uniform systems with real eigenvalues of the cross-connections matrix, for which the root loci of characteristic systems will qualitatively have, the transfer functions of the separate channels being chosen correspondingly, just the same form as in Figure 1.51. Rather, the problem here is that for general MIMO systems, as well as for circulant and anticirculant systems, it is very difficult, based on the open-loop transfer matrix  $W(s)$ , to judge the possible location (and even just the presence) of the zeros<sup>77</sup> in the right half-plane. As the location of these RHP-zeros may be quite unexpected, it may take a great deal of effort for the researcher or engineer to eliminate or diminish the inevitably negative influence of such zeros. To a certain extent, this issue is somewhat simpler for circulant and anticirculant systems, in which the system zeros coincide with the zeros of the CTFs, which can always be expressed analytically. Finally, it should be noted that for general MIMO systems, the *branch points located in the right half-plane* (see Figure 1.47) also impose similar limitations on the stability.

<sup>77</sup> For uniform systems, these zeros always coincide with the zeros of the identical separate channels.

# 2

## Performance and design of linear MIMO systems

### 2.1 INTRODUCTION

In the first part of this chapter, we shall consider in detail the analysis of steady-state dynamical processes, especially concentrating our attention on the investigation of MIMO systems *accuracy* under sinusoidal, slowly changing deterministic and stationary random input signals.

Throughout the whole chapter, we shall follow the idea that the accuracy and other performance characteristics of linear MIMO systems of any order  $N$  can be evaluated with the help of some *scalar* values calculated by readily ‘recognizable’ techniques, where the latter are straightforward extensions to the multivariable case of conventional techniques for SISO control systems. To the mentioned scalar values belong:

- magnitude of the vector of error complex amplitudes, under sinusoidal inputs;
- magnitude of the steady-state error vector, under slowly changing deterministic inputs;
- mean square value of the error vector magnitude, under stationary stochastic inputs.

Proceeding in such a way, we shall not stick rigidly to the standard framework of the CTFs method, resorting, when needed, to more wide resources of the functional analysis. Most frequently in these cases, the notion of a transfer matrix norm induced by the Euclidean norm (length) of the vector will be used, as it has already become conventional in modern control theory. At the same time, the relationship between the performance of a linear MIMO system on the whole and that of the SISO characteristic systems will be emphasized everywhere. As the reader will see, that relationship is especially clear and visual in the case of normal MIMO systems, i.e. systems with orthogonal canonical bases. For that very class of MIMO systems, the CTFs method allows easily building a bridge between the methods of investigation of SISO and MIMO control systems, thereby obtaining exhausting information about the accuracy and performance of MIMO systems based only upon the performance of characteristic systems; the problem here can completely be solved in terms of the CTFs.

In the last section, we shall present a design technique which is conceptually based on the methods of the stability and performance analysis of linear MIMO systems developed in the first two chapters. In essence, that technique allows reducing the design of a MIMO system with any number of channels to a *one-dimensional* task, in which the design principles and approaches of the classical control theory are used to the utmost.

## 2.2 GENERALIZED FREQUENCY RESPONSE CHARACTERISTICS AND ACCURACY OF LINEAR MIMO SYSTEMS UNDER SINUSOIDAL INPUTS

### 2.2.1 Frequency characteristics of general MIMO systems

Voluminous scientific and technical literature is devoted to the frequency-domain methods of study and design of linear MIMO systems. This is due not only to the fact that these methods are extremely widespread and popular in practical control engineering, but also to the fact that many modern methods of robust control theory are based on the frequency-domain concepts (Skogestad and Postlethwaite 2005; Morari and Zafiriou 1989; Doyle *et al.* 1992; Doyle 1984; Doyle and Stein 1981). Below, we introduce a notion of generalized frequency characteristics of linear MIMO systems, whose roots are in the classical control. In many respects, we just impart a slightly different, natural engineering tint to that, which has largely contributed to the origin of a branch in modern control theory conventionally referred to as  $H_\infty$ -control,  $H_\infty$ -optimization, etc. (Francis 1987; Maciejowski 1989; Bosgra *et al.* 2004). Our main goal here is to extend the well known notions of the *classical* control theory to the multivariable case.

In Section 1.2.4, we introduced the notions of gain and phase margins of a linear MIMO system as the *leasts* of the corresponding stability margins of  $N$  characteristic systems associated with the given MIMO system. Proceeding in the same fashion, i.e. choosing the ‘worst’, in a certain sense, of the SISO characteristic systems, we can carry over to the multidimensional case most of the frequency-domain performance indices adopted in the classical control theory (Kuo 1995; Ogata 1970). It is interesting that such a rather formal approach, in many cases, has a deeper implication than appears at first sight. In particular, this concerns the *resonant peak of the closed-loop SISO system*, which is a very convenient and widely used in the SISO systems study and design index. In what follows, we shall refer to that index as the *oscillation index*.<sup>1</sup> The oscillation index is equal to the maximum magnitude value of the closed-loop frequency transfer function, over the whole range of positive frequencies  $\omega \geq 0$  (Bessekierski and Popov 2002). Note that in Gerasimov (1962) and Tichonov (1969), based upon the *complex coordinates and transfer functions method* (Krasovskii 1957), the notion of the oscillation index for two-dimensional uniform antisymmetrical systems is introduced. In the present section, the classical notion of the oscillation index is generalized to the case of linear MIMO systems of an arbitrary dimension  $N$  without any restrictions on the form of the open-loop transfer matrix  $W(s)$ . It should be noted that the oscillation index of a MIMO system can be determined, like the SISO case (Fedorov 1959), with respect to both the *output* and the *error* signals. Below,

<sup>1</sup> The term *oscillation index* was widely used in the control literature in the former USSR, and it is quite convenient to emphasize that we are dealing with the closed-loop system *stability margins* as opposed to considering the resonant properties of the system as characterizing the *accuracy* with respect to input signals or disturbances.

we shall mainly discuss the last variant, since it provides information about both the stability margins and the accuracy of the MIMO system under sinusoidal input signals.

Let the inputs of an  $N$ -dimensional linear general MIMO system of Figure 1.1 be the sinusoidal functions  $\varphi_i(t) = \varphi_{Ai} \cos(\omega t + \psi_i)$  ( $i = 1, 2, \dots, N$ ) with the same frequency  $\omega$ , where  $\varphi_{Ai}$  and  $\psi_i$  are the amplitudes and phase shifts, respectively, in the  $i$ th channel. Then, the error vector  $\varepsilon(t)$  will have, in the *steady state*, the sinusoidal components  $\varepsilon_i(t) = \varepsilon_{Ai} \cos(\omega t + \gamma_i)$  of the same frequency  $\omega$ , but generally with different amplitudes  $\varepsilon_{Ai}$  and phase shifts  $\gamma_i$ . Denoting by  $\varepsilon_o$  and  $\varphi_o$  the vectors composed of the *complex amplitudes*  $\varepsilon_{Ai} \exp\{j\gamma_i\}$  and  $\varphi_{Ai} \exp\{j\psi_i\}$ , based on Equations (1.2) and (1.4), we obtain

$$\varepsilon_o = \Phi_\varepsilon(j\omega)\varphi_o = [I + W(j\omega)]^{-1} \varphi_o. \quad (2.1)$$

Further, for brevity, we shall just call the vectors of complex amplitudes  $\varepsilon_o$  and  $\varphi_o$  the error and input vectors of the MIMO system, and the *frequency transfer matrix*  $\Phi_\varepsilon(j\omega)$  the transfer matrix. Using the canonical representation of the MIMO system by means of the dyads [Equation (1.47)], instead of Equation (2.1), we can write

$$\varepsilon_o = \sum_{i=1}^N c_i(j\omega) \left[ \frac{\langle c_i^+(j\omega), \varphi_o \rangle}{1 + q_i(j\omega)} \right]. \quad (2.2)$$

An inspection of Equations (2.1) and (2.2) allows drawing the following conclusions. In the case of sinusoidal inputs, *one* strictly determined direction of the error vector  $\varepsilon_o$ , which does not depend on the ‘length’ (Euclidian norm) of the vector  $\varphi_o$  corresponds to any *direction* of the input vector  $\varphi_o$  in the complex space  $\mathbb{C}^N$ , since the MIMO system is linear. The vector  $\varepsilon_o$  can be represented as a linear combination of the MIMO system ‘responses’ along the canonical basis axes, where, for the given frequency  $\omega$ , that basis is *constant* and is entirely determined by the open-loop transfer matrix  $W(j\omega)$ . In the general case, for an arbitrary direction of the input vector  $\varphi_o$ , all  $N$  characteristic systems can participate in forming the error vector  $\varepsilon_o$ .

Given the unit vector  $\ell$  ( $|\ell| = 1$ ) in  $\mathbb{C}^N$ , we define the *generalized frequency characteristic of the MIMO system in the direction  $\ell$*  as a real function  $A_\ell(\omega)$ , equal for any frequency  $\omega$  to the ratio of magnitudes of the vectors  $\varepsilon_o$  and  $\varphi_o = \ell$ , i.e.

$$A_\ell(\omega) = \frac{|\varepsilon_o|}{|\varphi_o|} = |\Phi_\varepsilon(j\omega)\ell|. \quad (2.3)$$

Changing the frequency  $\omega$  from zero to infinity, it is easy to construct, with the help of Equation (2.3), the generalized frequency characteristic for any direction  $\ell$ . Evidently, this function characterizes the *accuracy* of the MIMO system in the given ‘direction’. The unique generalized frequency characteristic corresponds to any direction  $\ell$  in  $\mathbb{C}^N$  and, for different  $\ell$ , one can build infinitely many such characteristics. It is easy to understand that the tip of the vector  $\ell$  for various directions of the latter forms a unit sphere in  $\mathbb{C}^N$  with the centre at the origin. Therefore, let us call the *majorant* of the generalized frequency characteristics a function  $A_{\text{sup}}(\omega)$  equal, for any frequency  $\omega$ , to the *least upper bound* of the error vector magnitude  $|\varepsilon_o|$  on the unit sphere  $U_\varphi = \{\varphi_o : |\varphi_o| = 1\}$  in  $\mathbb{C}^N$ :

$$A_{\text{sup}}(\omega) = \sup_{|\varphi_o|=1} |\varepsilon_o| = \sup_{|\varphi_o|=1} |\Phi_\varepsilon(j\omega)\varphi_o|. \quad (2.4)$$

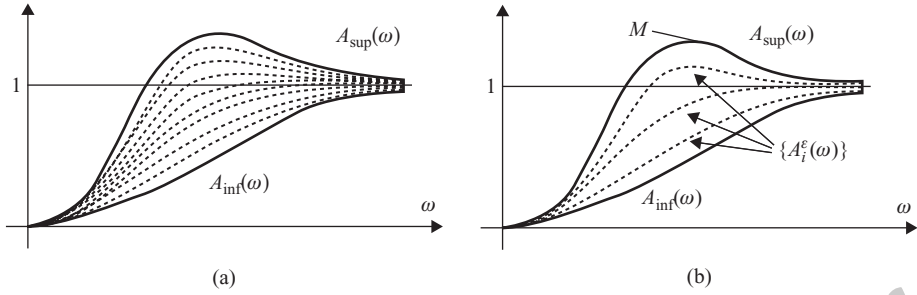


**Figure 2.1** Generalized frequency characteristics of the MIMO system. (a) In arbitrary directions; (b) in the directions of the canonical axes  $c_i(j\omega)$ .

It is necessary to note that, according to that definition, the majorant  $A_{sup}(\omega)$  is equal to the *spectral norm* of the matrix operator  $\Phi_\varepsilon(j\omega)$  induced by Euclidian norm of the vector  $\varphi_o$ , i.e.  $A_{sup}(\omega) = \|\Phi_\varepsilon(j\omega)\|$  (Porter 1966).

Similarly, we define the *minorant*  $A_{inf}(\omega)$  of the generalized frequency characteristics as a function equal for any  $\omega$  to the *greatest lower bound* of the magnitude  $|\varepsilon_o|$  on the unit sphere  $U_\varphi$ :

$$A_{inf}(\omega) = \inf_{|\varphi_o|=1} |\varepsilon_o| = \inf_{|\varphi_o|=1} |\Phi_\varepsilon(j\omega)\varphi_o|. \quad (2.5)$$

In essence, the majorant  $A_{sup}(\omega)$  and minorant  $A_{inf}(\omega)$  represent two *boundary curves*, encompassing from above and from below all generalized frequency characteristics for any directions of the input vector  $\varphi_o$ , and characterizing the maximum and minimum possible errors of the MIMO system under sinusoidal inputs [Figure 2.1(a)].

Recall now, that, in Section 1.2.5, we discussed the singular value decomposition of the transfer matrices, which supplements the considered picture by a necessary geometrical content and indicates the way of the numerical computation of the majorant  $A_{sup}(\omega)$  and minorant  $A_{inf}(\omega)$ . Similarly to Equation (1.71), for the transfer matrix  $\Phi_\varepsilon(j\omega)$ , we can write:

$$\Phi_\varepsilon(j\omega) = U_\Phi^\varepsilon(j\omega) \text{diag}\{\sigma_{\Phi_i}^\varepsilon(\omega)\} V_\Phi^\varepsilon(j\omega) = \sum_{i=1}^N u_{\Phi_i}^\varepsilon(j\omega) \sigma_{\Phi_i}^\varepsilon(\omega) v_{\Phi_i}^\varepsilon(j\omega), \quad (2.6)$$

where  $U_\Phi^\varepsilon(s)$  and  $V_\Phi^\varepsilon(s)$  are the unitary matrices composed of the orthonormal eigenvectors  $u_{\Phi_i}^\varepsilon(j\omega)$  and  $v_{\Phi_i}^\varepsilon(j\omega)$  of the Hermitian matrices  $\Phi_\varepsilon(j\omega)\Phi_\varepsilon^*(j\omega)$  and  $\Phi_\varepsilon^*(j\omega)\Phi_\varepsilon(j\omega)$ , and  $\sigma_{\Phi_i}^\varepsilon(\omega)$  are the (common) nonnegative eigenvalues of these matrices.

Having the *input* singular basis, composed of the vectors  $v_{\Phi_i}^\varepsilon(j\omega)$  ( $i = 1, 2, \dots, N$ ), the unit sphere  $U_\varphi$  of the input sinusoidal signals can be defined as

$$U_\varphi = \left\{ \varphi_o : \varphi_o = \sum_{i=1}^N \alpha_i(\omega) v_{\Phi_i}^\varepsilon(j\omega), \quad \sum_{i=1}^N |\alpha_i(\omega)|^2 = 1 \right\}. \quad (2.7)$$

Then, using the singular value decomposition of the matrix  $\Phi_\varepsilon(j\omega)$  in the dyadic form [Equation (2.6)], we find that the surface  $D_\varepsilon$ , which is the mapping of the unit sphere  $U_\varphi$  by the operator  $\Phi_\varepsilon(j\omega)$ , i.e.

$$D_\varepsilon = \{ \varepsilon_o : \varepsilon_o = \Phi_\varepsilon(j\omega)\varphi_o, \quad |\varphi_o| = 1 \}, \quad (2.8)$$

is given by the expression

$$D_\varepsilon = \left\{ \varepsilon_o : \varepsilon_o = \sum_{i=1}^N [\alpha_i(\omega) \sigma_{\Phi_i}^\varepsilon(\omega)] u_{\Phi_i}^\varepsilon(j\omega), \quad \sum_{i=1}^N |\alpha_i(\omega)|^2 = 1 \right\}. \quad (2.9)$$

Geometrically, the surface  $D_\varepsilon$  [Equation (2.9)] represents an ellipsoid in  $\mathbb{C}^N$  with principal axes directed along the axes  $u_{\Phi_i}^\varepsilon(j\omega)$  of the *output* singular basis and semi-axes equal to the singular values  $\sigma_{\Phi_i}^\varepsilon(\omega)$  of the transfer matrix  $\Phi_\varepsilon(j\omega)$ . Then, the majorant  $A_{\text{sup}}(\omega)$  and minorant  $A_{\text{inf}}(\omega)$  are equal for the given frequency  $\omega$  to the largest (major) and smallest of the ellipsoid [Equation (2.9)] semi-axes, or, in other words, to the largest  $\sigma_{\text{max}}^\varepsilon(\omega)$  and smallest  $\sigma_{\text{min}}^\varepsilon(\omega)$  of the singular values  $\sigma_{\Phi_i}^\varepsilon(\omega)$ . If the input unit vector  $\varphi_o = \ell$  is directed along the  $i$ th axis  $c_i(j\omega)$  of the canonical basis, then, from Equation (2.2), it follows that, in the MIMO system, only the  $i$ th characteristic system reacts, and the error vector  $\varepsilon_o$  is also directed along the same axis  $c_i(j\omega)$ . Based upon that, we introduce the notion of the *generalized frequency characteristics along  $N$  axes of the MIMO system canonical basis*. These characteristics are defined as follows:

$$A_i^\varepsilon(\omega) = \frac{|\varepsilon_o|}{|\varphi_o|} = \frac{1}{|1 + q_i(j\omega)|}, \quad i = 1, 2, \dots, N, \quad (2.10)$$

where  $\varphi_o = c_i(j\omega)$ , and coincide with the magnitudes of the closed-loop frequency transfer functions of the characteristic systems [see Equation (1.48)].

Since the canonical basis axes  $c_i(j\omega)$  of the general MIMO systems depend on the frequency  $\omega$ , each of the characteristics  $A_i^\varepsilon(\omega)$  corresponds not to one direction of the input vector  $\varphi_o$ , but to a conical surface in  $\mathbb{C}^N$  which is formed by the vector  $\varphi_o = c_i(j\omega)$  as  $\omega$  changes from zero to infinity. Evidently, all  $A_i^\varepsilon(\omega)$  [Equation (2.10)], like the generalized characteristics for arbitrary directions in  $\mathbb{C}^N$  discussed earlier, are bounded from above and below by the majorant  $A_{\text{sup}}(\omega)$  and minorant  $A_{\text{inf}}(\omega)^2$  [Figure 2.1(b)]. That very boundedness of the functions  $A_i^\varepsilon(\omega)$  by the majorant  $A_{\text{sup}}(\omega)$  from above allows, based on the form of the latter, assessing not only the accuracy, but also and stability margins of the MIMO system. Indeed, in Section 1.2.4, it was shown that if a MIMO system is on the stability boundary, i.e. has a root  $p = j\omega_1$  on the imaginary axis, then one of the characteristic systems is also on the stability boundary and has exactly the same root  $p = j\omega_1$ . So, the corresponding characteristic  $A_i^\varepsilon(\omega)$  and, together with it, the majorant  $A_{\text{sup}}(\omega)$  tend to infinity as the frequency  $\omega$  approaches  $\omega_1$  (Figure 2.2). If the pure imaginary root of the MIMO systems shifts to the left, then the resonant peak of  $A_{\text{sup}}(\omega)$  becomes finite. Hence, the value of the resonant peak of the majorant  $A_{\text{sup}}(\omega)$  can serve as a measure of the MIMO system stability margin, which leads to the following definition:

*The least upper bound of the error vector magnitude  $|\varepsilon_o|$  on the unit sphere  $U_\varphi$  in the complex space of input sinusoidal signals for  $0 \leq \omega \leq \infty$  is called the oscillation index  $M$  of the linear MIMO system.*

In the mathematical form, this can be expressed as

$$M = \sup_{0 \leq \omega \leq \infty} [\sup_{|\varphi_o|=1} |\Phi_\varepsilon(j\omega)\varphi_o|] = \sup_{0 \leq \omega \leq \infty} \|\Phi_\varepsilon(j\omega)\|. \quad (2.11)$$

<sup>2</sup> See also Equation (1.77).

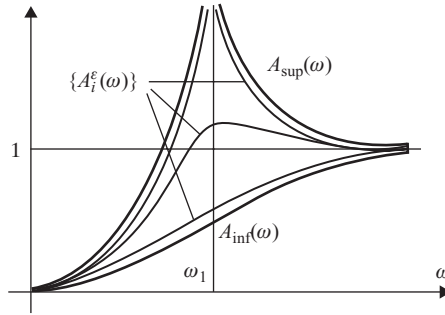


Figure 2.2 Stability boundary of a MIMO system.

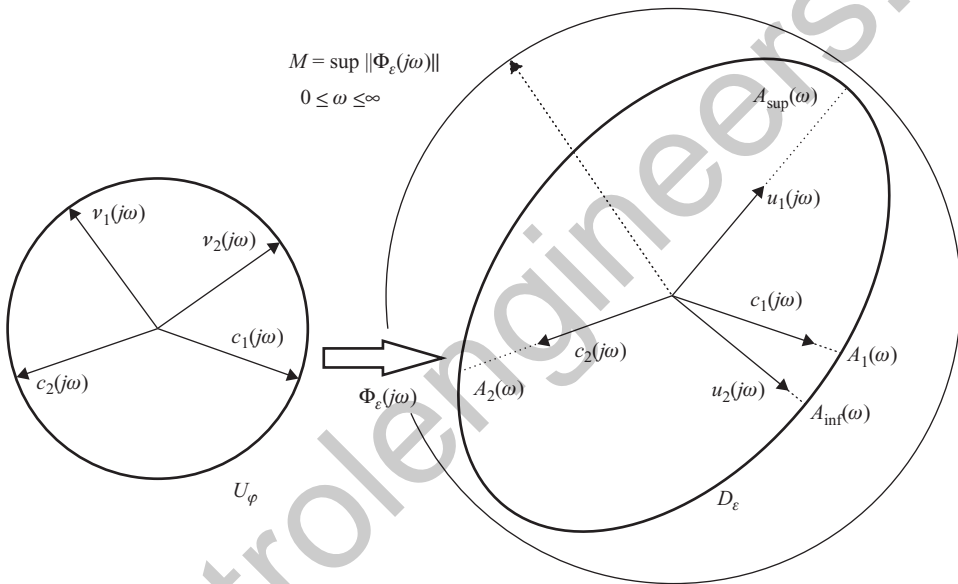


Figure 2.3 Mapping of the unit sphere  $U_\varphi$  into the ellipsoid  $D_\varepsilon$ .

In other words, the oscillation index  $M$  of a MIMO system is equal to the resonant peak of the majorant  $A_{\text{sup}}(\omega)$  and is defined as the maximum value of the norm  $\|\Phi_\varepsilon(j\omega)\|$  as  $\omega$  changes from zero to infinity<sup>3</sup> [Figure 2.1(b)].

All of the above allows the following simple geometrical interpretation, depicted schematically for  $N = 2$  and for some frequency  $\omega = \text{const}$  in Figure 2.3.<sup>4</sup> The oscillation index  $M$  is equal to the radius of the smallest sphere that contains all surfaces  $D_\varepsilon$  [Equation (2.9)], for all  $\omega \geq 0$ .

In practice, when designing MIMO systems, the value of  $M$  should be chosen within the range  $1.3 \leq M \leq 2.5 \div 3$ , generally accepted in the SISO case, although, sometimes, larger

<sup>3</sup> Further, the resonant frequency of  $A_{\text{sup}}(\omega)$  is denoted by  $\omega_M$ .

<sup>4</sup> In Figure 2.3, so as not to encumber the picture, the indices  $\Phi$  and  $\varepsilon$  of some axes and directions are omitted. In principle, this picture is valid not only for the transfer matrix  $\Phi_\varepsilon(j\omega)$ , but also for the matrices  $W(j\omega)$  and  $\Phi(j\omega)$ .

values of  $M$  can be allowed. We emphasize once more that the oscillation index evaluated by Equation (2.11) provides information not only about the stability margins, but also about the accuracy of a MIMO system under sinusoidal inputs, and all this information is contained, for any number of channels  $N$ , in a single number  $M$  having comparatively narrow limits of changes.<sup>5</sup>

The question of defining the oscillation index of a MIMO system as a measure of stability margins can be considered and, from a slightly different standpoint, more closely linked with the ideas of the CTFs method. The simple method discussed below is based on the evident statement that any other possible measure of the stability margins of the characteristic systems associated with the given MIMO system, besides the gain and phase margins introduced in Section 1.2.4, may serve as an unambiguous measure of the MIMO system stability margins. In particular, like the classical control theory (Bessekerski and Popov 2002), it is very convenient to assess the remoteness of the closed-loop characteristic systems from the oscillatory stability boundary with the help of the common notion of the SISO system oscillation index. Therefore, we introduce another definition:

*The least upper bound of the error vector magnitude  $|\varepsilon_o|$ , for the unit input vector  $\varphi_o$  ( $|\varphi_o| = 1$ ) directed along the  $i$ th axis  $c_i(j\omega)$  of the canonical basis, as the frequency  $\omega$  changes from zero to infinity, is called the oscillation index  $M_i$  of the  $i$ th characteristic system.*

Comparing this definition with that for the generalized frequency characteristics along  $N$  canonical basis axes, it is easy to understand that  $M_i$  is equal to the value of the resonant peak of the  $i$ th closed-loop characteristic system, i.e.

$$M_i = \sup_{0 \leq \omega \leq \infty} |\Phi_{\varepsilon_i}(j\omega)| = \sup_{0 \leq \omega \leq \infty} \frac{1}{|1 + q_i(j\omega)|}, \quad i = 1, 2, \dots, N. \quad (2.12)$$

The value of  $M_i$  [Equation (2.12)] can be directly found through the gain loci  $q_i(j\omega)$  of the open-loop characteristic system, without plotting the generalized characteristic  $A_i^\varepsilon(\omega)$  [Equation (2.10)] over the whole range of frequencies  $\omega$ . To this end, it is necessary to draw on the Nyquist plot of  $q_i(j\omega)$  the lines of constant values  $M_i = const$ . Writing  $M_i = 1/|1 + q_i(j\omega)|$ , and following the standard prescriptions given, for example, in Bessekerski and Popov (2002), one can readily obtain the equation

$$[1 + \operatorname{Re}\{q_i(j\omega)\}]^2 + [\operatorname{Im}\{q_i(j\omega)\}]^2 = \frac{1}{M_i^2}, \quad (2.13)$$

which describes on the complex plane of  $q_i(j\omega)$  a circle with the centre at  $(-1, j0)$  and the radius  $1/M_i$  (Figure 2.4). For different  $M_i = const$ , we have a family of concentric circles (frequently called *constant- $M$  loci* or *constant- $M$  circles*; we shall call them  *$M$ -circles*) which degenerate, as  $M_i \rightarrow \infty$ , into the point  $(-1, j0)$ , and spread out over the whole complex plane, as  $M_i \rightarrow 0$ . The actual value of the oscillation index  $M_i$  is reciprocal to the radius of the circle that is tangent to the  $q_i(j\omega)$  plot {apparently, the point at which the circle [Equation (2.13)] is tangent to  $q_i(j\omega)$  gives the resonant frequency  $\omega_{M_i}$  of the  $A_i^\varepsilon(\omega)$  [Equation (2.10)]}. Note also that the points of intersections of different  $M$ -circles [Equation (2.13)] (i.e. corresponding to different  $M_i = const$ ) with the  $q_i(j\omega)$  plot allows finding the entire generalized frequency characteristic  $A_i^\varepsilon(\omega)$  along the  $i$ th canonical basis axis. By plotting on the complex plane the whole family  $\{q_i(j\omega)\}$  of the open-loop MIMO system characteristic gain loci, one can find

<sup>5</sup> The relation of the resonant peak  $M$  with the robustness of the MIMO systems is discussed in Remark 2.1.

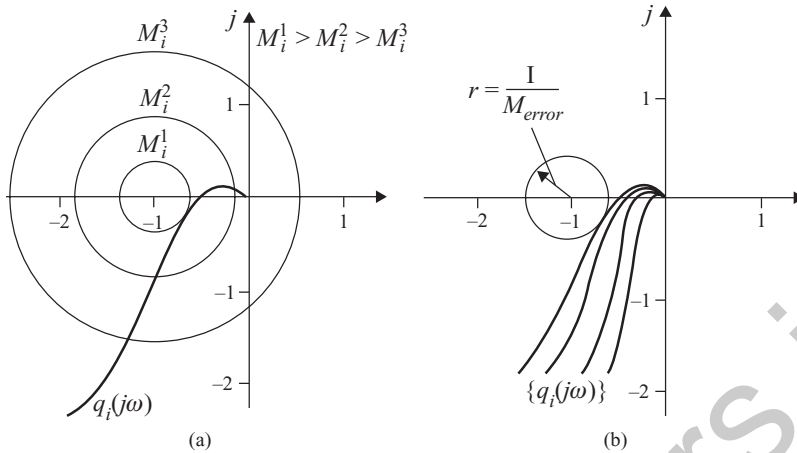


Figure 2.4 Determination of the oscillation index  $M_i$  of the characteristic systems.

all  $M_i$  ( $i = 1, 2, \dots, N$ ). The largest of them:

$$M_{i \max} = \max_i(M_i) \quad (2.14)$$

characterizes, obviously, the inclination of the closed-loop MIMO system to oscillations and therefore can serve as a measure of its stability margin. Practically, in this case, the task of finding  $M_{i \max}$  is equivalent to finding the radius of the ‘smallest’ circle tangent to the envelope of the family of the characteristic gain loci  $\{q_i(j\omega)\}$  [Figure 2.4(b)]. It is easy to note that for  $N = 1$ , the value of  $M_i$  computed in such a fashion is equal to the conventional oscillation index  $M$  of a SISO system (Fedorov 1959). Note also that the value  $M_i$  [Equation (2.12)] can be found, like the classical control theory (Bessekerski and Popov 2002), by mapping the circle [Equation (2.13)] on the Bode diagrams (so-called  $\mu$ -curves). In that case, we shall have, for each  $i$  ( $i = 1, 2, \dots, N$ ), one  $\mu$ -curve on the Bode phase plot of  $q_i(j\omega)$ , i.e. to a single  $M$ -circle on the complex plane of the family  $\{q_i(j\omega)\}$  will correspond  $N$  closed curves (frequently, they are called the *forbidden regions*) on the Bode diagrams. For any frequency  $\omega$ , these curves are determined through the magnitudes  $|q_i(j\omega)|$  via the expressions

$$\mu_i = -180^\circ + \arccos \left( \frac{1 + |q_i(j\omega)|^2 - 1/M_i^2}{2|q_i(j\omega)|} \right), \quad i = 1, 2, \dots, N \quad (2.15)$$

and are plotted for the magnitudes  $|q_i(j\omega)|$  within the limits

$$\frac{M_i - 1}{M_i} \leq |q_i(j\omega)| \leq \frac{M_i + 1}{M_i}. \quad (2.16)$$

The specified value of  $M_{i \max}$  will be provided if none of the Bode phase plots of  $q_i(j\omega)$  enters into its forbidden region, defined by Equation (2.15). Note finally that the  $M$ -circles [Equation (2.13)] can be readily transferred to the plane of the Nichols plots.<sup>6</sup>

<sup>6</sup> As an exercise, we suggest that the reader find Equation (2.15), as well as the equations for the forbidden regions  $M_i = \text{const}$  on the Nichols plots.

Thus, we have considered two alternative approaches to determining the oscillation index of general linear MIMO systems. The first of them may be regarded as a rigorous extension to the multidimensional case of the classical notion of the oscillation index, computed through the transfer function with respect to the error signal (the sensitivity transfer function). The second approach is entirely based on the geometrical concepts of the CTFs method, and leads to a more simple and convenient graphical technique for finding the oscillation index; in this case, it can be directly done by the characteristic gain loci  $q_i(j\omega)$  of the *open-loop* MIMO system. A natural and essential question arises here of whether the indices  $M_{i \max}$  and  $M$  [Equation (2.11)] can be related to each other. To answer this question, let us express the spectral norm  $\|\Phi_\varepsilon(j\omega)\|$  in Equation (2.11), taking into account the canonical representation of the matrix  $\Phi_\varepsilon(s)$  [Equation (1.46)] and the well known property of the norm of the product of two square matrices:  $\|AB\| \leq \|A\|\|B\|$  (Gantmacher 1964), in the form

$$\|\Phi_\varepsilon(j\omega)\| = \left\| C(j\omega) \text{diag} \left\{ \frac{1}{1+q_i(j\omega)} \right\} C^{-1}(j\omega) \right\| \leq v[C(j\omega)] \left\| \text{diag} \left\{ \frac{1}{1+q_i(j\omega)} \right\} \right\|. \quad (2.17)$$

The number

$$v[C(j\omega)] = \|C(j\omega)\| \|C^{-1}(j\omega)\| \quad (2.18)$$

in Equation (2.17), which is called the *condition number* (Vojevodin and Kuznetsov 1984) of the modal matrix  $C(j\omega)$ , plays a crucial role in the investigation of the accuracy and robustness of MIMO systems. This number characterizes the *degree of non-orthogonality* (or the *degree of skewness*) of the canonical basis axes in the sense that for an orthonormal basis, it is equal to unity and, on degenerating of  $C(j\omega)$  [i.e. when the number of linearly independent axes  $c_i(j\omega)$  becomes less than the number of channels  $N$ ], tends to infinity. As for the spectral norm of the diagonal matrix of the CTFs  $\Phi_{\varepsilon_i}(j\omega) = 1/[1+q_i(j\omega)]$  in Equation (2.17), for any frequency  $\omega$ , that norm is equal to

$$\left\| \text{diag} \left\{ \frac{1}{1+q_i(j\omega)} \right\} \right\| = \max_i \left( \frac{1}{|1+q_i(j\omega)|} \right) = \max_i (A_i^\varepsilon(\omega)), \quad (2.19)$$

where  $A_i^\varepsilon(\omega)$  are given by Equation (2.10), i.e. is equal to the largest of the values of the generalized frequency characteristics along the canonical basis axes of the MIMO system.

If assume now that the frequency  $\omega$  corresponding to the maximum  $M_{i \max}$  of the resonant peaks of the functions  $A_i^\varepsilon(\omega)$  [Equation (2.10)] coincides with the resonant frequency  $\omega_M$  of the majorant  $A_{\text{sup}}(\omega)$ ,<sup>7</sup> then, from Equations (2.11), (2.12) and (2.17)–(2.19), we get the following upper estimate for the oscillation index  $M$  [Equation (2.11)]:

$$M \leq v[C(j\omega_M)] M_{i \max} \quad (2.20)$$

expressed through the maximum  $M_{i \max}$  of the oscillation indices [Equation (2.14)] of characteristic systems and the condition number  $v[C(j\omega_M)]$ . This means that the accuracy of the

<sup>7</sup> That assumption appears quite natural and usually holds for real systems. However, taking into account that different MIMO systems may have the same CTFs but different canonical bases, the situations in which the condition number  $v[C(j\omega)]$  in Equation (2.17) has a ‘resonant peak’ at some other frequency  $\omega$  are theoretically not excluded. In such cases, the resonant peak of the majorant  $A_{\text{sup}}(\omega)$  might be determined by  $v[C(j\omega)]$  and not by the CTFs, and the assumption is not valid.

MIMO system with sinusoidal input signals *deteriorates, as the degree of non-orthonormality of the canonical basis increases*. In this sense, the normal MIMO systems that have orthogonal canonical bases {and the unity condition number [Equation (2.17)]<sup>8</sup>} are, all other things being equal, the most accurate. As we shall see later, that conclusion bears a general character and also holds true for the cases of slowly changing deterministic and random input signals.

Since  $M_{i \max}$  limits  $M$  from *below*, then, taking into account Equation (2.20), we can finally write down the inequality

$$M_{i \max} \leq M \leq \nu[C(j\omega_M)]M_{i \max}, \quad (2.21)$$

which characterizes the boundary values of the oscillation index  $M$ .

The practical significance of Equations (2.20) and (2.21) is that the value of  $M$  can actually be estimated by the characteristic gain loci of the *open-loop* MIMO system. This creates natural premises for developing the MIMO system design techniques, similar to conventional design techniques for SISO systems based on the notion of oscillation index. Note also that the estimates in Equations (2.20) and (2.21), in principle, are valid and, for the majorant of the generalized frequency characteristics, i.e. in these expressions, for any  $\omega$ , we can substitute  $A_{\text{sup}}(\omega)$  for  $M$ ,  $\omega$  for  $\omega_M$ , and  $\max_i([A_1^{\varepsilon}(\omega), A_2^{\varepsilon}(\omega), \dots, A_N^{\varepsilon}(\omega)])$  for  $M_{i \max}$ .

**Remark 2.1** Above, we have defined the oscillation index  $M$  through the transfer matrix  $\Phi_{\varepsilon}(j\omega)$  with respect to the error signals. However, in many cases, such as when investigating the robustness of MIMO systems, one may need to find  $M$  via the transfer matrix  $\Phi(j\omega)$  with respect to the output signals. That problem is solved quite analogously, although there are some distinctions that should be borne in mind. The curves depicted in Figure 2.1 are typical for the *type-1* MIMO systems,<sup>9</sup> for which all magnitudes of CTFs  $q_i(j\omega)$  tend to infinity as  $\omega \rightarrow 0$ , and to zero as  $\omega \rightarrow \infty$ . For such MIMO systems, the majorant  $A_{\text{sup}}(\omega)$  and minorant  $A_{\text{inf}}(\omega)$  are close to zero at low frequencies, and tend to unity at high frequencies. If the oscillation index is determined with respect to the output signals of the *type-1* MIMO systems, then we have, in a certain sense, an inverse picture: at low frequencies, the majorant and minorant of the generalized frequency characteristic begin from unity, and tend to zero as  $\omega \rightarrow \infty$  [Figure 2.5(a)]. In both cases, we have resonant peaks of the majorants  $A_{\text{sup}}(\omega)$ , and the values of these peaks and of the corresponding frequencies generally *do not coincide*. However, the general point here is that as the MIMO system approaches the stability boundary, the oscillation indices with respect to the output and error tend to infinity.

The oscillation indices  $M_i$  of the characteristic systems are defined by the expressions

$$M_i = \sup_{0 \leq \omega \leq \infty} |\Phi_i(j\omega)| = \sup_{0 \leq \omega \leq \infty} \left| \frac{q_i(j\omega)}{1 + q_i(j\omega)} \right|, \quad i = 1, 2, \dots, N \quad (2.22)$$

and the lines of equal values  $M_i = \text{const}$  ( $M$ -circles) on the complex plane of  $q_i(j\omega)$  have the form<sup>10</sup>

$$\left[ \text{Re}\{q_i(j\omega)\} + \frac{M_i^2}{M_i^2 - 1} \right]^2 + [\text{Im}\{q_i(j\omega)\}]^2 = \frac{M_i^2}{(M_i^2 - 1)^2} \quad (2.23)$$

<sup>8</sup> As we shall see in Section 2.1.2, for normal systems, Equation (2.20) becomes strict and reduces to an equality.

<sup>9</sup> More strictly, for MIMO systems whose *type* exceeds zero. The issue of determining the *type* of MIMO systems is discussed in Section 2.2.

<sup>10</sup> One more exercise for the reader.

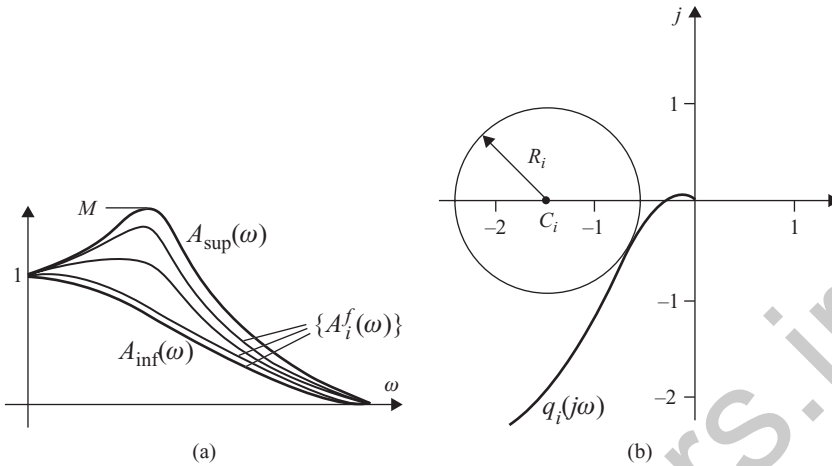


Figure 2.5 Definition of the oscillation index with respect to the output signals.

and describe a circle with the centre at  $C_i$  and radius  $R_i$  [Figure 2.5(b)]:

$$C_i = \frac{M_i^2}{M_i^2 - 1}, \quad R_i = \frac{M_i}{M_i^2 - 1}. \tag{2.24}$$

Correspondingly, the forbidden regions for the Bode phase plots of  $\arg q_i(j\omega)$  are constructed by the expressions

$$\mu_i = -180^\circ + \arccos \left( \frac{C_i + |q_i(j\omega)|^2}{2|q_i(j\omega)|C_i} \right), \quad i = 1, 2, \dots, N \tag{2.25}$$

for the magnitude  $|q_i(j\omega)|$  over the interval

$$\frac{M_i}{M_i + 1} \leq |q_i(j\omega)| \leq \frac{M_i}{M_i - 1}. \tag{2.26}$$

**Remark 2.2** The discussed notions of the MIMO system oscillation indices have a very simple physical interpretation related to the system response to sinusoidal inputs. In essence, they define the MIMO system ‘gains’, with respect to *magnitudes of the vectors of complex amplitudes* of input oscillations, and substantially depend on the *directions* of these oscillations. On the other hand, they represent quite simple estimates for the MIMO system *stability margins* and, as such, can be used in the design. For  $N = 1$ , all the introduced notions turn into the notions of the oscillation indices with respect to output or error signals well known from the classical control theory.

It should be noted that the term  $\|H\|_\infty$ , long established in control theory, defined as the least upper bound of the maximum singular value (denoted by a line from above  $\bar{\sigma}$ ) of the closed-loop MIMO system transfer matrix over the whole range of frequencies  $\omega$ :

$$\|H\|_\infty = \sup_{\omega} \bar{\sigma}(\Phi(j\omega)) \tag{2.27}$$

determines, as a matter of fact, the oscillation index of the MIMO system evaluated via the corresponding transfer matrix. Rather, this term has a somewhat more mathematical than engineering flavour. It combines the designation of the *Hardy space*, i.e. the space of stable and strictly proper transfer functions (Skogestad and Postlethwaite 2005), and index  $\infty$ , which corresponds to the limit  $p \rightarrow \infty$  in the norm

$$\|x(j\omega)\|_p = \left( \int_{-\infty}^{\infty} |x(j\omega)|^p d\omega \right)^{1/p}, \tag{2.28}$$

where we have

$$\|x(j\omega)\|_{\infty} = \sup_{\omega} |x(j\omega)|, \tag{2.29}$$

i.e. the norm  $\|x(j\omega)\|_{\infty}$  is equal to the resonant peak of the curve  $|x(j\omega)|$ .

The reader should remember this and not get confused when he or she encounters the symbols like  $\|H\|_{\infty}$ , since they have simple physical meaning closely related to the common frequency-domain notions of the classical control theory.

**Remark 2.3** The material of this section is immediately linked to the problems of MIMO systems' robustness. In the modern control theory, so much attention and effort is devoted to these problems that, although the goal of the textbook is to extend the main results of the *classical* control theory to the multidimensional case, we cannot disregard that fact.

The interest in robust control theory emerged in the mid-1970s and was inspired by a number of reasons. First, the engineers and researchers began putting questions as to what extent all those assumptions and/or simplifications that were usually made when considering the idealized models of control systems are crucial and how these assumptions could affect how the systems work in reality. Further, in many cases, the plants, in principle, might have *uncertain* parameters (i.e. parameters for which only the bounds of their possible values are known) and the parameters that could essentially change during the operation of the systems. All this brought control specialists to the problems of the study and design of control systems in the case of various uncertainties (Safonov 1980; Doyle and Stein 1981), which, in turn, promoted the formation of a significant branch in control theory, afterwards called the *robust theory*.

Let us briefly formulate one of the central tasks of the robust theory.<sup>11</sup> Assume that the transfer matrix  $W(s)$  of the MIMO systems in Figure 1.1 is uncertain. In the robust theory, there two main types of uncertainties in the system description are specified – *structured* and *unstructured*. Structured uncertainty usually means the parametric variations of the plant model due to inaccurate knowledge of gains, poles or zeros, etc. Unstructured uncertainties usually represent unmodelled dynamics in the transfer matrix  $W(s)$  (see any textbook on robust control). In the common formulation of the robust control, it is assumed that the investigated MIMO system can be represented in the form of a certain connection of the initial system and a system *in which all uncertainties are concentrated*. The simplest form of such a connection, sometimes called the *basic perturbation model*, is shown in Figure 2.6 (Bosgra *et al.* 2004).

Here, the matrix  $H(j\omega)$  characterizes the *initial* MIMO system under investigation, and the block  $\Delta_H(j\omega)$  represents the uncertainties in the system dynamics. In fact, in Figure 2.6, a MIMO system with a feedback loop (note, the feedback is positive!) is depicted. To define

<sup>11</sup> The robust theory embraces both SISO and MIMO systems, but we shall consider only the multidimensional case.

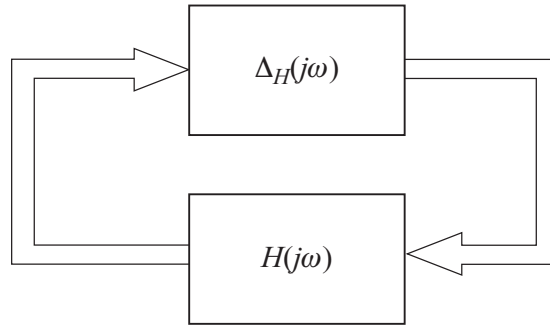


Figure 2.6 Basic perturbation model.

the specific form of  $H(j\omega)$ , we should qualify the *type* (or *form*) of uncertainty, which can be either *additive* or *multiplicative*. In the case of additive uncertainty, the initial open-loop transfer matrix  $W(j\omega)$  is replaced by  $W(j\omega) + \Delta_H(j\omega)$  and, in the second case, by the matrix  $[1 + \Delta_H(j\omega)]W(j\omega)$ .

In the case of the additive form of uncertainty representation, the matrix  $H(j\omega)$  in Figure 2.6 is

$$H(j\omega) = -[I + W(j\omega)]^{-1} = -\Phi_\varepsilon(j\omega), \tag{2.30}$$

i.e. is equal to the taken with minus sign transfer matrix  $\Phi_\varepsilon(j\omega)$  (sensitivity transfer matrix) with respect to the error signal of the initial MIMO system. In the case of multiplicative uncertainty, this matrix has the form

$$H(j\omega) = -[I + W(j\omega)]^{-1}W(j\omega) = -\Phi(j\omega), \tag{2.31}$$

i.e. is equal to the transfer matrix  $\Phi(j\omega)$  (complementary sensitivity matrix) of the initial system with respect to the output signal, also taken with minus sign.

Then, one of the key results of the robust theory based on the *small gain theorem* (Desoer and Vidyasagar 1975) is formulated as follows:

Let  $H(j\omega)$  and  $\Delta_H(j\omega)$  in Figure 2.6 be stable. Then, for stability of the MIMO system with uncertainty  $\Delta_H(j\omega)$ , it is sufficient that for all frequencies  $\omega$ , the following condition holds:

$$\bar{\sigma}(\Delta_H(j\omega)) < \frac{1}{\bar{\sigma}(H(j\omega))} \tag{2.32}$$

or (another sufficient condition)

$$\|\Delta_H(j\omega)\|_\infty < \frac{1}{\|H(j\omega)\|_\infty}. \tag{2.33}$$

If we use our notation, then the sufficient conditions of the MIMO system stability robustness [Equations (2.32) and (2.33)] can be rewritten in the following forms:

$$A_{\text{sup}}^\Delta(\omega) < \frac{1}{A_{\text{sup}}^H(\omega)} \quad \text{and} \quad M^\Delta < \frac{1}{M^H}, \tag{2.34}$$

where the above indices indicate belonging to the corresponding matrices. Thus, having the majorants of the generalized frequency characteristics of the MIMO system with respect to the output or error signals and the corresponding oscillation indices, we can readily check, with the help of Equation (2.34), whether the conditions of stability robustness are satisfied. It is very important and useful that the analysis of the MIMO system robustness can be performed, like the assessment of the oscillation index  $M$ , via the characteristic gain loci  $q_i(j\omega)$  of the open-loop MIMO system.

**Example 2.1** Let us determine the generalized frequency characteristics and the oscillation indices of the general two-axis telescope guidance system of Example 1.2, with transfer functions in Equation (1.66) and angles  $\alpha_1$  and  $\alpha_2$  equal to  $\alpha_1 = 30^\circ$ ,  $\alpha_2 = 20^\circ$  {i.e. for the case of complex conjugate eigenvalues of  $R$  [Equation (1.60)]}. The Nyquist, Bode and Nichols plots (i.e. characteristic gain loci) of the open-loop guidance system are shown in Figure 2.7,

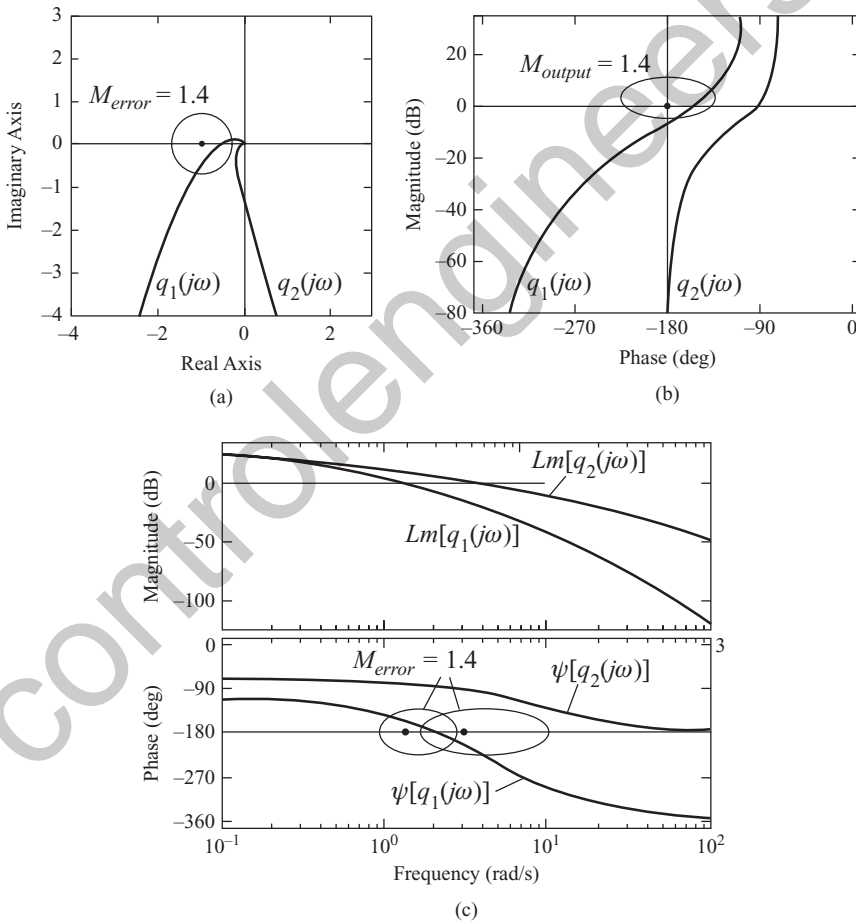


**Figure 2.7** The lines  $M_i = const$  [Equations (2.13) and (2.23)] ( $M$ -circles and  $\mu$ -curves) on the plots of the frequency characteristics of the open-loop guidance system. (a) The Nyquist plots (error signal); (b) the Nichols plots (output signal); (c) the Bode diagrams (error signal).

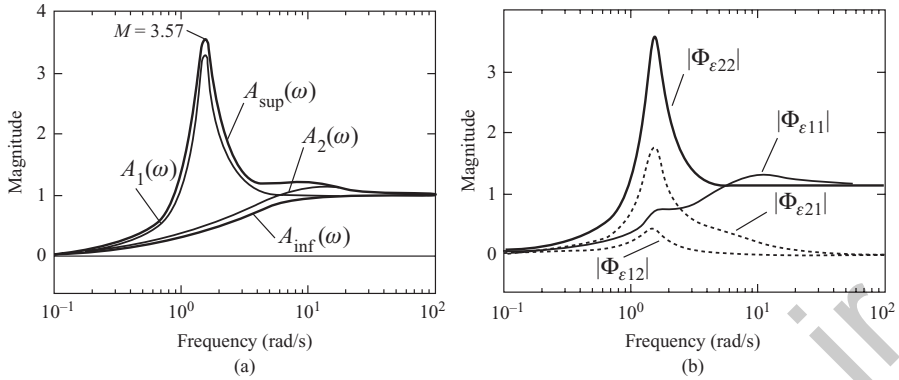


**Figure 2.8** Generalized and usual frequency characteristics of the closed-loop guidance system. (a) Generalized characteristics (error signal); (b) usual characteristics (error signal).

together with the  $M$ -circles and  $\mu$ -curves, for  $M_i = 1.4$  (this value is taken just for illustrative purposes) and for both variants of defining the oscillation indices. Note that on the Bode phase plots, we have *two* closed  $\mu$ -curves corresponding to  $q_1(j\omega)$  and  $q_2(j\omega)$ . The generalized frequency characteristics of the closed-loop system with respect to the error signals are plotted in Figure 2.8(a) and, in Figure 2.8(b), for comparison, the corresponding usual characteristics are shown. The majorants  $A_{sup}(\omega)$  and minorants  $A_{inf}(\omega)$  in Figure 2.8(a) are depicted by thick lines and the generalized frequency characteristics along the canonical basis axes  $A_1(\omega)$  and  $A_2(\omega)$  by thin lines (the index  $\varepsilon$  is not indicated in Figure 2.8, so as not to encumber the plots). The comparison of the generalized and usual characteristics shows that the former adequately represents the frequency responses of the closed-loop system. In particular, the resonant frequencies of both of these characteristics coincide. On the other hand, the resonant peaks of the generalized characteristics are a little larger. This is quite natural, since the generalized characteristics determine the system response (by magnitudes) for arbitrary directions of the sinusoidal input signals, whereas the usual characteristics show the system response when the sinusoidal signals are applied to the inputs of the separate channels. It can also be seen that the generalized frequency characteristics  $A_1(\omega)$  and  $A_2(\omega)$  are quite close to  $A_{sup}(\omega)$  and  $A_{inf}(\omega)$ . The oscillation index  $M$  with respect to the error of the two-axis guidance system equals 3.57, and the resonant peak of  $A_1(\omega)$  (i.e.  $M_1 = M_{i\max}$ ) equals 3.2837. Such closeness is chiefly due to the small degree of non-orthogonality of the canonical basis axes.

**Example 2.2** Let us finally discuss the ‘non-robust’ two-dimensional system of Example 1.3 and clear up the cause of such high sensitivity to small but different perturbations of the separate channel gains. The transfer matrix of the system [Equation (1.67)] has the canonical representation via the similarity transformation with the following *constant* modal matrix  $C$ :

$$C = \begin{pmatrix} 7 & -8 \\ -6 & 7 \end{pmatrix}. \tag{2.35}$$

The columns of that matrix form the axes of the canonical basis. Normalizing these columns and using Equation (1.30), we obtain that the angle included between the canonical basis axes

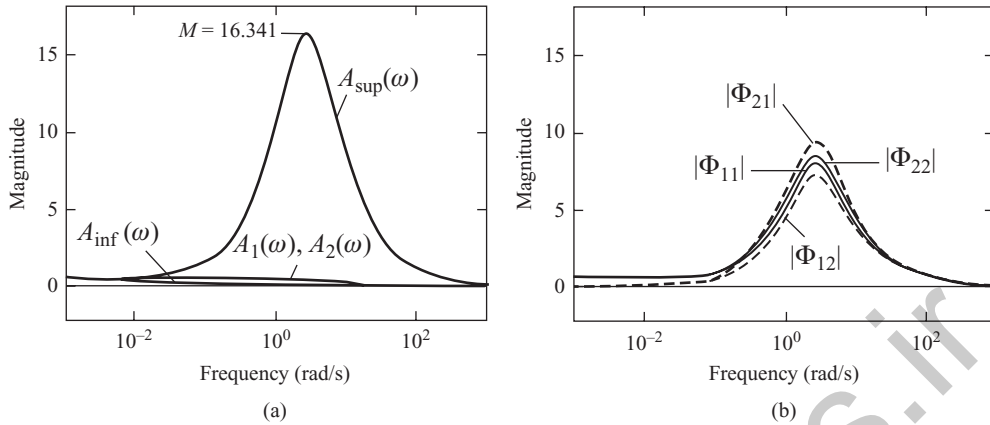


**Figure 2.9** Generalized and usual frequency characteristics of the ideal (non-varied) system of Example 1.3. (a) Generalized frequency characteristics; (b) usual frequency characteristics.

equals  $179.415^\circ$ , i.e. these axes *actually lie on one line*. Correspondingly, the condition number  $\nu[C] = \|C\| \|C^{-1}\|$  [Equation (2.18)] of the matrix  $C$  [Equation (2.35)] equals 196! Taking into account that the oscillation index  $M$  is bounded from above by the product of the largest oscillation index of the characteristic systems (these indices are equal to 0.5) by the number  $\nu[C]$  [Equation (2.20)], it is easy to conclude that the considered system has a high value of  $M$ , and, as a consequence, is non-robust. This is completely confirmed by the generalized frequency characteristics of the closed-loop system with respect to output signals, shown, together with the usual characteristics, in Figure 2.9 [the plots of  $A_1(\omega)$  and  $A_2(\omega)$  in Figure 2.9(a) practically coincide]. It is interesting to note that in the region of resonant frequencies, the influence of cross-connections in the system is very high, and the resonant peaks of the non-diagonal elements of the transfer matrix  $\Phi(j\omega)$  are close to (and even exceed) the corresponding peaks of the direct channels [of the diagonal elements of  $\Phi(j\omega)$ ]. The oscillation index of the system is 16.341, for  $\omega = 2.825$  [if we consider the index  $M$  as a *relative* value of the resonant peak, then it equals 32.682, since the initial value of the majorant  $A_{\text{sup}}(\omega)$  is 0.5]. Based on Equation (2.32) or (2.34), we have that the sufficient conditions of the stability robustness are violated in the case of the gain multiplicative perturbations of order  $1/16.341 \approx 0.0612$ . Recall (see Example 1.3) that under *identical* variations  $\Delta K_1 = \Delta K_2$  of the gains, the system [Equation (1.67)] has infinite gain margins and only the variations of opposite signs, which disrupt the internal geometrical structure of the system, lead to instability. In this sense, the discussed example shows that although the oscillation indices  $M_i$  of the characteristic systems can serve as a *measure of the MIMO system stability margin* in the case of identical perturbations of the gains, when using these indices, it is also necessary to take into account the degree of non-orthogonality of the canonical basis. Note also that information about the system robustness could directly be obtained from the characteristic gain loci of the open-loop system, multiplying the obtained value  $M_{i \text{ max}}$  by the condition number  $\nu[C(j\omega)]$ .

**Example 2.3** This simple example demonstrates that the robustness estimates based on Equations (2.32)–(2.34) should be treated with certain caution, since their formal application,

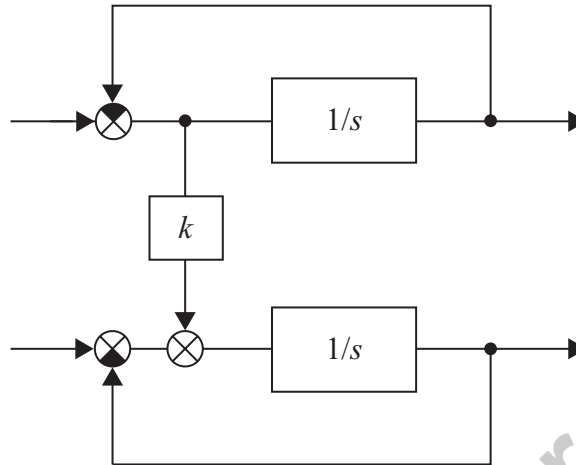


**Figure 2.10** A MIMO system allowing indefinite increase in the coefficient  $k$  without stability loss.

without taking into account real *structural* features of the MIMO system, can bring about misunderstanding or incorrect conclusions about the allowed bounds of the parametric uncertainty. In Figure 2.10, a simple system consisting of two channels with integrators and a *one-sided* static connection with coefficient  $k$  from the first channel to the second is shown. The system is described by the transfer matrix

$$W(s) = \begin{pmatrix} 1/s & 0 \\ 0 & 1/s \end{pmatrix} \begin{pmatrix} 1 & 0 \\ k & 1 \end{pmatrix} = \begin{pmatrix} 1/s & 0 \\ k/s & 1/s \end{pmatrix} \tag{2.36}$$

and belongs to *triangular* MIMO systems, discussed briefly in Remarks 1.5 and 1.14, in which we indicated that the non-diagonal elements of such matrices do not affect the system stability. Indeed, the characteristic equation if the MIMO system in Figure 2.10 has the form

$$\det[I + W(s)] = (s + 1)^2 = 0, \tag{2.37}$$

i.e. it does not depend on  $k$ , and has two multiple roots at the point  $(-1, j0)$ .

Assume now that the *structure* of the system is known exactly, i.e. no new *cross-connections* can appear, and the coefficient  $k$  can take any value within the range from zero to 50 (actually, we have here the *structured* uncertainty). The generalized frequency characteristics of the system for  $k = 0$  are shown in Figure 2.11(a), in which the majorant  $A_{\text{sup}}(\omega)$  and minorant  $A_{\text{inf}}(\omega)$  coincide with each other and coincide with the frequency response characteristics of the closed-loop separate channels, and the same characteristics for  $k = 50$  are given in Figure 2.11(b). The comparison of the plots in these figures can lead to an erroneous conclusion that for  $k = 50$ , the robustness properties of the system are about 25 times worse than those of the system with  $k = 0$  [the resonant peak of the majorant  $A_{\text{sup}}(\omega)$  is approximately equal to  $k/2$  for  $k > 10$ ]. However, we know that the stability of the system does not depend at all on  $k$ . Thus, the discussed elementary example shows that the robustness estimates based on the singular values, if used mechanically, do not always reflect the real state of affairs. Therefore,

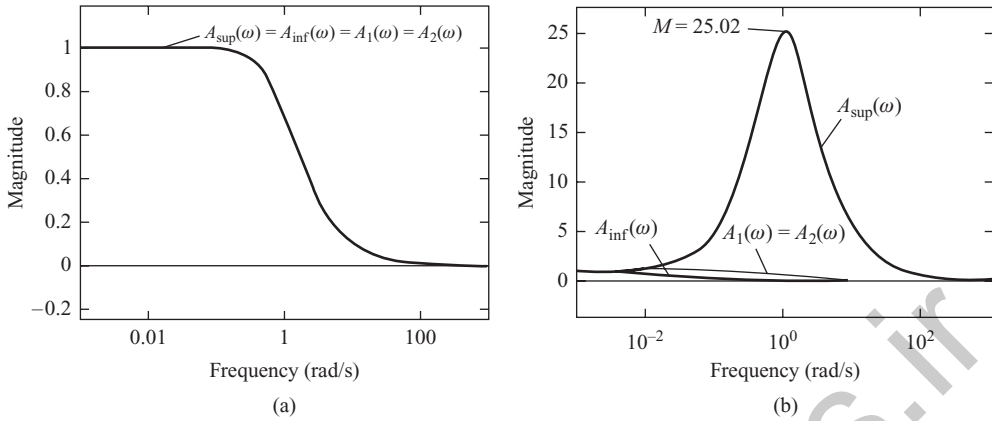


**Figure 2.11** Generalized frequency characteristics of the MIMO system of Figure 2.10 for different values of  $k$ . (a)  $k = 0$ ; (b)  $k = 50$ .

when applying them, one should try to take into account the actual structural properties of the MIMO system under investigation.

## 2.2.2 Frequency characteristics and oscillation index of normal MIMO systems

We already know that the left and right singular bases of an open- and closed-loop normal MIMO system, i.e. a system with orthogonal canonical basis, coincide with each other and coincide with the canonical basis, and the singular values are equal to the magnitudes of the transfer functions of the corresponding characteristic systems (see Section 1.4). This brings about interesting peculiarities of the generalized frequency characteristics and essentially simplifies the determination of the oscillation index. Since the set  $\{c_i(j\omega)\}$  of the eigenvectors of the open-loop transfer matrix  $W(j\omega)$  in this case is orthonormal, the unit sphere  $U_\varphi$  [Equation (2.7)] of the input sinusoidal signals can be defined in the following way:

$$U_\varphi = \left\{ \varphi_o : \varphi_o = \sum_{i=1}^N \alpha_i(\omega) c_i(j\omega), \quad \sum_{i=1}^N |\alpha_i(\omega)|^2 = 1 \right\}. \quad (2.38)$$

Then, using the canonical representation in the dyadic form [Equation (1.118)], we find that the surface  $D_\varepsilon$  [Equation (2.8)], which is mapping of the unit sphere  $U_\varphi$  [Equation (2.38)] by the operator  $\Phi_\varepsilon(j\omega)$  of the normal system, is given by the expression

$$D_\varepsilon = \left\{ \varepsilon_o : \varepsilon_o = \sum_{i=1}^N \left[ \frac{\alpha_i(\omega)}{1 + q_i(j\omega)} \right] c_i(j\omega), \quad \sum_{i=1}^N |\alpha_i(\omega)|^2 = 1 \right\}. \quad (2.39)$$

From the geometrical viewpoint, the surface  $D_\varepsilon$  [Equation (2.39)] is an ellipsoid in  $\mathbb{C}^N$  with the principal axes directed along the canonical basis axes  $c_i(j\omega)$  and the semi-axis  $r_i$  equal to

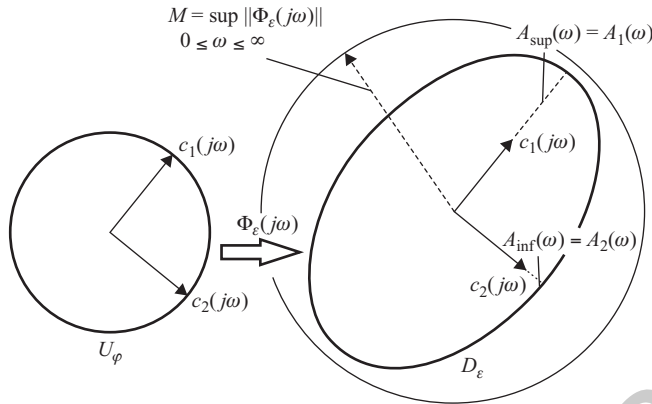


**Figure 2.12** Mapping of the unit sphere  $U_\varphi$  into the ellipsoid  $D_\varepsilon$  by a normal MIMO system.

the magnitudes of the CTF  $\Phi_{\varepsilon i}(j\omega)$  (Figure 2.12):

$$r_i = |\Phi_{\varepsilon i}(j\omega)| = \frac{1}{|1 + q_i(j\omega)|}, \quad i = 1, 2, \dots, N. \quad (2.40)$$

From here, it is evident that for any frequency  $\omega$ , the values of the majorant  $A_{\text{sup}}(\omega)$  and minorant  $A_{\text{inf}}(\omega)$  of the generalized frequency characteristics are equal to the largest and smallest of the magnitudes  $|\Phi_{\varepsilon i}(j\omega)|$ , respectively. On the whole,  $A_{\text{sup}}(\omega)$  and  $A_{\text{inf}}(\omega)$  of the normal MIMO system are determined as the *envelopes from above and from below* of a family of  $N$  generalized frequency characteristics along the canonical basis axes  $A_i^\varepsilon(\omega)$ , i.e.

$$A_{\text{sup}}(\omega) = \|\Phi_\varepsilon(j\omega)\| = \max_i \left( \frac{1}{|1 + q_i(j\omega)|} \right) \quad (2.41)$$

$$A_{\text{inf}}(\omega) = \min_i \left( \frac{1}{|1 + q_i(j\omega)|} \right) \quad (2.42)$$

or, in other words, as the envelopes from above and below of the frequency responses of the closed-loop characteristic systems (Figure 2.13). Based on the above, we come to an important conclusion that the oscillation index  $M$  of a normal MIMO system defined by the resonant peak of the majorant  $A_{\text{sup}}(\omega)$  is equal to the maximum of the oscillation indices  $M_i$  of characteristic

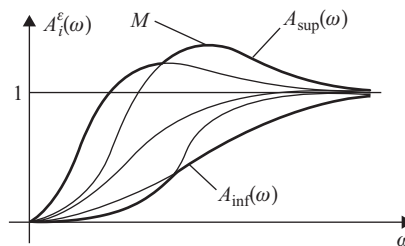


**Figure 2.13** Generalized frequency characteristics of the normal MIMO system.

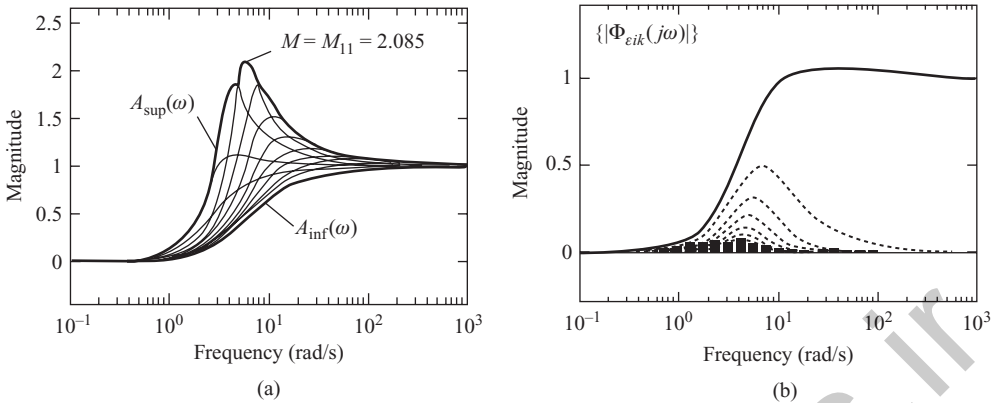


**Figure 2.14** Generalized frequency characteristics of the uniform circulant system of Example 1.8. (a) Generalized characteristics; (b) usual characteristics.

systems,<sup>12</sup> i.e.

$$M = \sup_{0 \leq \omega \leq \infty} \|\Phi_\varepsilon(j\omega)\| = \max_i \left( \sup_{0 \leq \omega \leq \infty} \frac{1}{|1 + q_i(j\omega)|} \right) = M_{i \max}. \quad (2.43)$$

Thus, when investigating normal MIMO systems, the two definitions of the oscillation index introduced in Section 2.2.1 obtain a unique sense and become equivalent. As a consequence, unlike general MIMO systems, in which the directions of the input sinusoidal signals  $\varphi_o$  for which the steady-state errors reach their boundary (by magnitude  $|\varepsilon_o|$ ) values are not connected with the canonical basis, in the discussed case, these directions coincide with certain axes of the canonical basis and, in the normal MIMO system, only one characteristic system reacts.

The obtained equality  $M_{i \max} = M$  [Equation (2.43)] also indicates the crucial role of orthogonality of the canonical basis from the accuracy (and, at the same time, the robustness) viewpoint. Indeed, from that equality and recalling that for general MIMO systems, an inequality  $M_{i \max} \leq M$  holds, it follows that if two MIMO systems have identical CTFs  $q_i(s)$ , where one of the systems is normal and the second is not, then the first one is more accurate and robust. Roughly speaking, with deviation of the canonical basis from orthogonal (all other conditions being equal), the magnitude of the MIMO system sinusoidal error vector generally increases and deteriorates the robustness. However, it should be noted that if the CTFs of two different MIMO systems are the same, then these systems have the same sinusoidal errors along the corresponding axes of the canonical bases, since both MIMO systems have identical generalized frequency characteristics  $A_i^\varepsilon(\omega)$  [Equation (2.10)].

**Example 2.4** The generalized and usual frequency characteristics of the 16-channel uniform circulant system of Example 1.8 with respect to the error signals are shown in Figure 2.14. An interesting conclusion ensues from Figure 2.14(a), namely that in the case of normal MIMO systems, the majorants  $A_{\text{sup}}(\omega)$  and minorants  $A_{\text{inf}}(\omega)$ , being the envelopes from above and

<sup>12</sup> This conclusion also ensues from the statement, well known in the theory of matrices, that the spectral norm of a normal square matrix is equal to the spectral radius, i.e. to the maximum magnitudes of the eigenvalues of the matrix itself (Voevodin and Kuznetsov 1984).

below of continuous generalized frequency characteristics  $A_i^\varepsilon(\omega)$  [or  $A_i(\omega)$ ], are not necessarily, by themselves, continuous functions of the frequency  $\omega$ , and can have a finite number of breakpoints. The ‘worst’ characteristic system, from the point of view of the value of  $M_i$ , is the eleventh system, whose index  $M_{11} = 2.085$  gives the oscillation index  $M$  of the overall uniform circulant system with respect to the error signals.

It is also of certain interest to compare the generalized characteristics in Figure 2.14(a) with the usual frequency characteristics of the closed-loop system of Figure 2.14(b), in which the solid lines correspond to the characteristics of direct channels and the dashed lines to the cross-connections. Here, in each graph, we have 256 characteristics with respect to error, and each curve in Figure 2.14(b) corresponds, due to the system’s being circulant, to 16 identical frequency characteristics.

**Example 2.5** In Example 2.2, we discussed the two-dimensional system of Example 1.3 and discovered that the cause of its being non-robust is a large degree of non-orthogonality of the canonical basis. Let us consider now another non-robust system, which belongs to normal MIMO systems, namely the two-dimensional antisymmetrical system [Equation (1.178)] of Example 1.10, and try to find out whether poor robustness of the system can be predicted via the properties of its characteristic systems. Based on Equation (1.180), it is easy to obtain the following expressions for the closed-loop transfer functions of the characteristic systems, with respect to the error and output signals:

$$\begin{aligned}
 \Phi_{\varepsilon 1}(j\omega) &= \frac{1}{1 + q_1(j\omega)} = \frac{j(\omega - a)}{j\omega + 1}, & \Phi_{\varepsilon 2}(j\omega) &= \frac{1}{1 + q_2(j\omega)} = \frac{j(\omega + a)}{j\omega + 1} \\
 \Phi_1(j\omega) &= \frac{q_1(j\omega)}{1 + q_1(j\omega)} = \frac{1 + ja}{j\omega + 1}, & \Phi_2(j\omega) &= \frac{q_2(j\omega)}{1 + q_2(j\omega)} = \frac{1 - ja}{j\omega + 1}.
 \end{aligned}
 \tag{2.44}$$

The frequency-response characteristics constructed by Equation (2.44) are shown in Figure 2.15. From these curves, it is evident that the values of the oscillation indices with respect to the output and error are practically the same (10.05 и 10), and indicate poor robustness properties of the system, under both additive and multiplicative perturbations of the gains  $K_1$

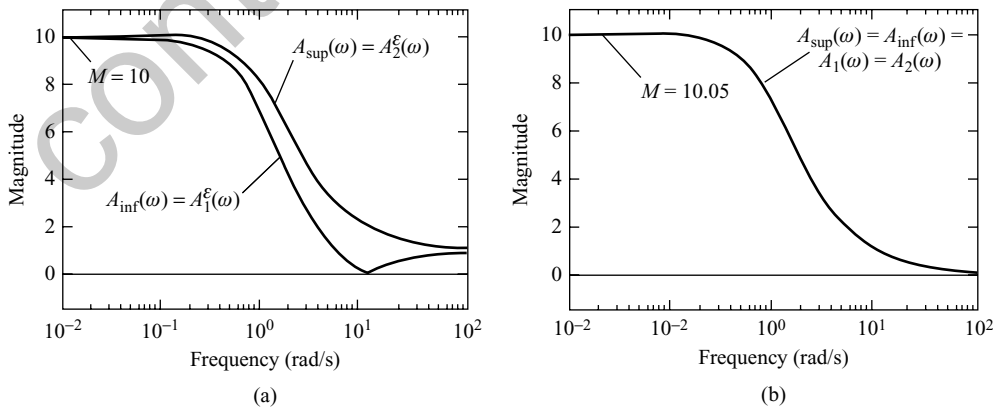


**Figure 2.15** Generalized frequency characteristics of the antisymmetrical system of Example 1.10. (a) With respect to error; (b) with respect to output.

and  $K_2$ . In particular, the application of Equation (2.34) shows that the sufficient conditions of the stability robustness are violated under the multiplicative perturbations of the coefficients  $K_1$  and  $K_2$  by 0.1 [it is well known that the assessments in Equation (2.32) are quite conservative, so one should not be surprised that the loss of stability occurs only in the case of different signs of these perturbations]. Note that the oscillation index of the discussed system is roughly equal to the coefficient  $a$  in Equation (2.44). Therefore, the robustness properties of the system deteriorate as  $a$  increases. Note also that the value of  $M$  could be determined through the characteristic gain loci of the open-loop system in Figure 1.35(b), by plotting tangent circles ( $M$ -circles) to these loci with the help of Equation (2.13) or (2.23). Thus, the discussed example shows that the robustness properties of the system can be assessed by the generalized frequency characteristics of the closed-loop characteristic systems and, which is equivalent, immediately by the characteristic gain loci of the open-loop system.

### 2.2.3 Frequency characteristics and oscillation index of uniform MIMO systems

The construction of the generalized frequency characteristics of uniform systems, including normal uniform systems, can be performed by the above techniques. However, the identity of separate channels enables us to bring the techniques of finding the oscillation index of uniform systems more closely to the standard techniques of the classical control theory. Thus, the oscillation indices  $M_i$  of the characteristic systems can immediately be found via the frequency characteristics  $w(j\omega)$  of the separate channels. To show that, let us rewrite Equation (2.12) for the case of uniform systems in the form

$$M_i = \sup_{0 \leq \omega \leq \infty} |\Phi_{\varepsilon i}(j\omega)| = \sup_{0 \leq \omega \leq \infty} \frac{1}{|1 + \lambda_i w(j\omega)|}, \quad i = 1, 2, \dots, N, \quad (2.45)$$

where  $\lambda_i$  are the eigenvalues of the cross-connections matrix  $R$ . From here, after some simple algebraic transformations, the following equations of constant values  $M_i = const$  on the complex plane of the Nyquist plot of  $w(j\omega)$  can be obtained:

$$[\operatorname{Re}\{w(j\omega)\} + \operatorname{Re}\{1/\lambda_i\}]^2 + [\operatorname{Im}\{w(j\omega)\} + \operatorname{Im}\{1/\lambda_i\}]^2 = 1/(\lambda_i |M_i|)^2 \quad (2.46)$$

$$i = 1, 2, \dots, N$$

These equations describe a family of  $N$  circles with the radii  $1/(\lambda_i |M_i|)$  and the centres located at the critical points  $(-1/\lambda_i)$  (Figure 2.16). The picture presented in Figure 2.16 is actually based on the 'inverse' formulation of the generalized Nyquist criterion given in Section 1.4.2. Having the points  $(-1/\lambda_i)$ , it is easy to find the value of  $M_i$  for any  $i$ , by drawing a tangent circle to the Nyquist plot of  $w(j\omega)$  around the corresponding centre  $(-1/\lambda_i)$  and then determining  $M_{i \max}$  using Equation (2.14). Note that, owing to the independence of the uniform system canonical basis on complex variable  $s$ , the inequality Equation (2.21), characterizing the boundary values of  $M$ , takes on a simpler form:

$$M_{i \max} \leq M \leq \nu(C)M_{i \max}, \quad (2.47)$$

where  $\nu(C)$  is the condition number of the modal matrix  $C$ . This allows, having  $M_{i \max}$ , the upper estimate for the oscillation index  $M$  to be found without difficulty. The values of  $M_i$

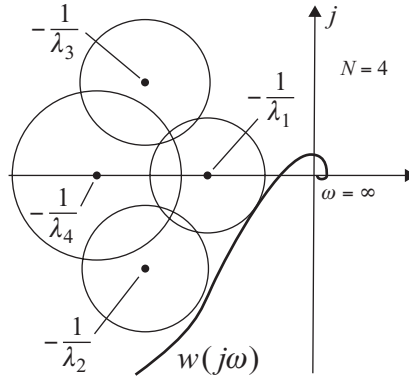


Figure 2.16 Circles  $M_i = \text{const}$  on the complex plane of  $w(j\omega)$ .

[Equation (2.45)] can also be found using the Bode diagrams of the function  $w(j\omega)$ , as well as with the help of the Nichols plots. Thus, mapping of the circles [Equation (2.46)] on the Bode phase plot of the separate channel is performed by the following relationships that can readily be obtained from Figure 2.16:<sup>13</sup>

$$\mu_i = -180^\circ + \arg \lambda_i + \arccos \left( \frac{1 + (|\lambda_i| |w(j\omega)|)^2 - 1/M_i^2}{2|\lambda_i| |w(j\omega)|} \right), \quad i = 1, 2, \dots, N. \quad (2.48)$$

These expressions establish the relationship between the phase margin  $\mu_i$  of the transfer function  $w(j\omega)$  and the magnitude  $|w(j\omega)|$  for the  $i$ th circle and are valid for the magnitudes within the limits

$$\frac{M_i - 1}{|\lambda_i| M_i} \leq |w(j\omega)| \leq \frac{M_i + 1}{|\lambda_i| M_i}. \quad (2.49)$$

Given  $M_i$ , these expressions allow, as in the SISO case (Bessekerski and Popov 2002), the  $\mu$ -curves for uniform systems to be constructed and forbidden regions for the Bode phase plot  $\Psi[w(j\omega)]$  to be determined. Graphically, we shall illustrate this in Example 2.6.

**Example 2.6** Consider the two-axis uniform guidance system, analysed in Examples 1.4 and 1.14. Assume that the transfer function of the separate channels be in the form of Equation (1.103), with the gain decreased by a factor of 10. Assume that the values of angles  $\alpha_1$  and  $\alpha_2$  are  $\alpha_1 = 30^\circ$  and  $\alpha_2 = 20^\circ$ , for which the cross-connections matrix  $R$  [Equation (1.60)] has two complex conjugate eigenvalues:  $\lambda_1 = 0.9029 - j0.4119$  and  $\lambda_2 = 0.9029 + j0.4119$ . The condition number of the modal matrix  $\nu(C)$  is equal to 1.233, which indicates a rather good degree of non-orthogonality of the canonical basis. The frequency characteristics of the system with respect to the output signals are shown in Figure 2.17. In view of the small difference of  $\nu(C)$  from unity, the majorant  $A_{\text{sup}}(\omega)$  and minorant  $A_{\text{inf}}(\omega)$  of the generalized frequency characteristics practically coincide with the frequency responses of the closed-loop

<sup>13</sup> The derivation of these expressions, as well as the expressions for mapping circles [Equation (2.46)] on the plane of the Nichols plots is left to the reader as an exercise. The same concerns also the derivation of the corresponding expressions with respect to the output signals of uniform systems.

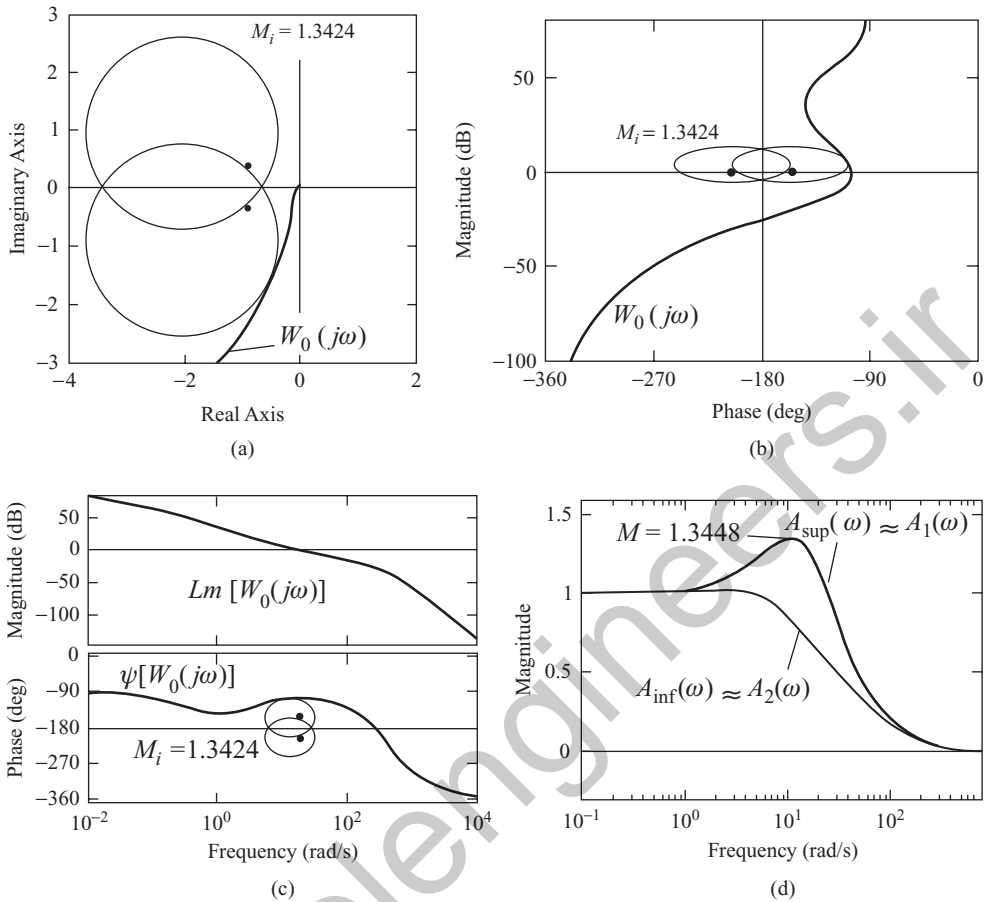


**Figure 2.17** Frequency characteristics of the guidance system with respect to the output signals for  $\alpha_1 = 30^\circ$ ,  $\alpha_2 = 20^\circ$ . (a) Nyquist plot; (b) Nichols plot; (c) Bode diagram; (d) generalized characteristics.

characteristic systems [Figure 2.17(d)]. The value of the oscillation index with respect to the output  $M = 1.3448$  differs from the oscillation index  $M_1 = 1.3424$  of the first characteristic system by the hundredth parts of unity. The Nyquist plot of the system is given in Figure 2.17(a), together with  $M$ -circles for value 1.3424, for which the tangency of the first circle (i.e. for  $i = 1$ ) with the loci of  $W_0(j\omega)$  occurs. The mappings of these circles on the planes of the Bode diagram and Nichols plot are shown in Figure 2.17(b) and (c).

**Example 2.7** In Example 2.4, we constructed the generalized frequency characteristics of the closed-loop 16-channel uniform circulant system, and determined the oscillations indices of that system with respect to output and error, as the values of resonant peaks of the corresponding majorants  $A_{sup}(\omega)$ . Since that system is normal and uniform, the exact value of its oscillation indices can directly be found via the frequency transfer function  $W_0(j\omega)$  of the separate channels. The family of the circles [Equation (2.46)] on the plane of the Nyquist plot of  $W_0(j\omega)$  and their representations on the Nichols plane for  $M_i = 2.0846$  are shown in Figure 2.18.

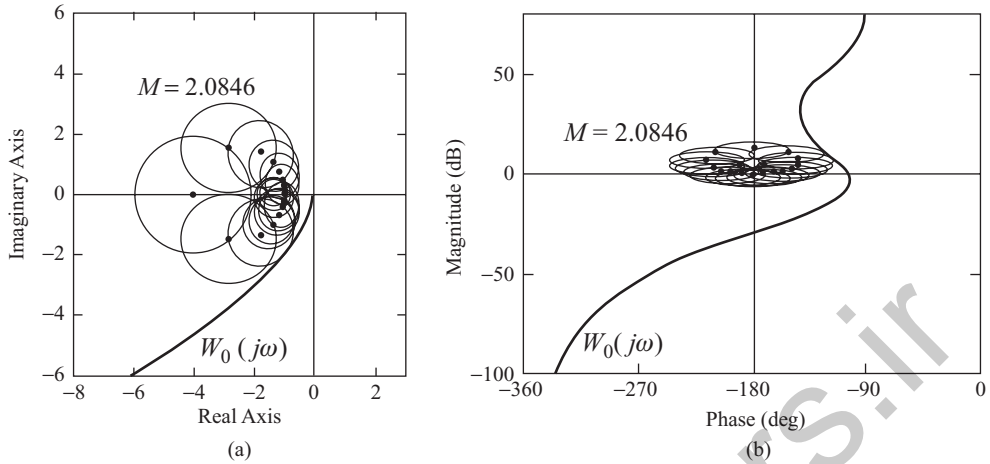


**Figure 2.18** Circles  $M_i = \text{const}$  for the 16-channel uniform system. (a) Nyquist plot; (b) Nichols plot.

Here, the circle tangent to  $W_0(j\omega)$  corresponds to the eleventh characteristic system, with  $\lambda_{11} = 0.3598 - j0.2652$ .

## 2.3 DYNAMICAL ACCURACY OF MIMO SYSTEMS UNDER SLOWLY CHANGING DETERMINISTIC SIGNALS

### 2.3.1 Matrices of error coefficients of general MIMO systems

All reference signals and disturbances acting upon a MIMO system are usually divided into two classes of deterministic and random signals. The first class, in turn, can be subdivided into sinusoidal signals; impulse, step or ramp signals; signals of an arbitrary form but with some restrictions on the derivatives, etc. The methods for analysis of the MIMO systems' accuracy under sinusoidal signals were considered in the previous section. Here, we focus on the issue of determining MIMO systems' steady-state errors in the case of the arbitrary, slowly changing external signals. In this case, the main accuracy characteristics of MIMO systems are *matrices of error coefficients* determined through the closed-loop transfer matrices with respect to the error or output signals.

One of the first works devoted to MIMO systems accuracy analysis in case of the slow signals was the article by Golomb and Usdin (1952). Later on, the results of that article were extended in Meerov (1965), Baranchuk (1968), Morozovski (1970), etc. Below, a general methodical approach to the problem of evaluating the matrices of error coefficients of general MIMO systems is discussed and the relationship between the MIMO system *type* and the types of the separate channels and SISO characteristic systems is established. In the next parts, circulant, anticirculant and uniform systems are considered, as well as the general MIMO systems with rigid cross-connections and different transfer functions of separate channels that are significant in practice.

Let the input signal  $\varphi(t)$  of a stable general MIMO system of Figure 1.1 have a sufficiently smooth form. Then, the *steady-state* error vector  $\varepsilon(t)$  can be determined as follows. Expand the closed-loop transfer matrix with respect to error  $\Phi_\varepsilon(s)$  [Equation (1.4)] into an infinite Taylor

series, in ascending powers of  $s$ :<sup>14</sup>

$$\Phi_\varepsilon(s) = \sum_{m=0}^{\infty} K_m s^m, \quad (2.50)$$

where  $K_m$  ( $m = 0, 1, 2, \dots$ ) are constant numerical matrices. Substituting Equation (2.50) into the expression for  $\varepsilon(s)$  in Equation (1.2) yields the Laplace transform of the error vector represented in the form of an infinite series:

$$\varepsilon(s) = \sum_{m=0}^{\infty} K_m s^m \varphi(s). \quad (2.51)$$

This series converges for small  $s$ , i.e. for sufficiently large values of time  $t$ , which corresponds to steady-state processes in the MIMO system. Applying the inverse Laplace transform to Equation (2.51), we obtain the expression for the steady-state error vector  $\varepsilon(t)$  in the form

$$\varepsilon(t) = \sum_{m=0}^{\infty} \varepsilon_m(t) = \sum_{m=0}^{\infty} K_m \frac{d^m \varphi(t)}{dt^m}. \quad (2.52)$$

This is an expansion of the error vector  $\varepsilon(t)$  into a series in terms of derivatives of the input vector  $\varphi(t)$ . Each term of that series can be interpreted as a vector component  $\varepsilon_m(t)$  of the error  $\varepsilon(t)$  induced by the corresponding derivative of the vector  $\varphi(t)$ . From Equation (2.52), it is evident that the error of the MIMO system can readily be determined if the vector  $\varphi(t)$ , its derivatives  $d^m \varphi(t)/dt^m$  and constant matrices  $K_m$  are known. The  $K_m$  matrices are called, by analogy with the SISO case, the *matrices of error coefficients* of linear MIMO systems. These matrices can be evaluated based on the general rules of the Taylor series expansion, by the formulae:

$$K_m = \frac{1}{m!} \left. \frac{d^m \Phi_\varepsilon(s)}{ds^m} \right|_{s=0}, \quad m = 0, 1, 2, \dots \quad (2.53)$$

The matrices  $K_m$  can also be expressed, taking into account Equation (1.5), via the MIMO system transfer matrix with respect to output  $\Phi(s)$ , in the form

$$K_0 = [I - \Phi(s)]|_{s=0}, \quad K_m = -\frac{1}{m!} \left. \frac{d^m \Phi(s)}{ds^m} \right|_{s=0}, \quad m = 1, 2, \dots \quad (2.54)$$

However, it should be noted that Equations (2.53) and (2.54) are rather inconvenient for practical use. Formulae that are much more convenient can be obtained by using the well known King procedure (Rabinovich *et al.* 1969), according to which the matrices  $K_m$  are computed in sequence, one after another, with the help of the following recurrent relations (Gasparyan 1976):

$$K_0 = \lim_{s \rightarrow 0} \Phi_\varepsilon(s), \quad (2.55)$$

and

$$K_m = \lim_{s \rightarrow 0} \frac{1}{s^m} \left[ \Phi_\varepsilon(s) - \sum_{i=0}^{m-1} K_i s^i \right], \quad m = 1, 2, \dots \quad (2.56)$$

<sup>14</sup> The validity of such a representation ensues from the *final value theorem*, known in the Laplace transform, according to which, if the transform  $\varepsilon(s)$  exists, then the condition  $\lim_{t \rightarrow \infty} \varepsilon(t) = \lim_{s \rightarrow 0} s \varepsilon(s)$  holds (Churchill *et al.* 1974).

Like SISO systems, MIMO systems are distinguished by their *type*. A linear MIMO system is said to be of *type 0* (*type-0 MIMO system*) with respect to  $\varphi(t)$  if the matrix  $K_0$  [Equation (2.55)] differs from the zero matrix, i.e. if the system has non-zero steady-state error under constant inputs  $\varphi(t) = \text{const}$ . If the first  $r$  matrices  $K_0, K_1, \dots, K_{r-1}$  are identically equal to zero matrices, and the matrix  $K_r$  is non-zero, then the MIMO system is said to be of *type r* (*type-r MIMO system*). Such MIMO systems track without error the input signals that can be represented as polynomials  $\varphi(t) = \sum_{i=0}^{\ell} v_i t^i$  ( $v_i = \text{const}$ ) of order  $\ell < r$  and, for  $\ell = r$ , they have *constant* steady-state error.

Let us establish now the relationship between the type of MIMO system and the types of *isolated* separate channels. Note first that if the open-loop transfer matrix  $W(s)$  has  $r$  *absolute* poles at the origin of the complex plane (see Section 1.2.2), i.e. can be expressed in the form<sup>15</sup>

$$W(s) = \frac{1}{s^r} W_1(s), \quad (2.57)$$

then, by utilizing King's formulae [Equations (2.55) and (2.56)], it is easy to show<sup>16</sup> that the first  $r$  matrices of error coefficients vanish. Therefore, the *sufficient* condition for the MIMO system to be of type  $r$  is the presence of  $r$  absolute zero poles of the *open-loop* transfer matrix. However, this condition can be strengthened, if we relax the requirement that the zero poles be absolute. Further, for certainty, we shall always assume that the number of zero poles of the elements of any row in  $W(s)$ , excluding the element on the principal diagonal, is less than the number of zero poles of the diagonal element of that very row. In other words, we shall assume that the number of zero poles of the transfer functions  $w_{km}(s)$  ( $k \neq m$ ), which describe the connections from all other channels to the  $k$ th channel, is less than the number of zero poles of the 'direct' transfer function  $w_{kk}(s)$  of that channel.<sup>17</sup> Represent the return difference matrix of the MIMO system as a product of two matrices:

$$[I + W(s)] = \text{diag} \{1 + w_{kk}(s)\} U(s), \quad (2.58)$$

the left of which is diagonal, and the matrix  $U(s)$  has the entries

$$\begin{cases} u_{km}(s) = 1, & \text{for } k = m \\ u_{km}(s) = \frac{w_{km}(s)}{1 + w_{kk}(s)}, & \text{for } k \neq m \end{cases} \quad (2.59)$$

and is nonsingular for any  $s$ , including  $s = 0$  [under the above assumption about the number of zero poles, the matrix  $U(0)$  is equal to the unit matrix  $I$ ]. Recalling the rule of inversion of the product of matrices (Derusso *et al.* 1965), from Equation (2.58), we obtain the following expression for the transfer matrix  $\Phi_\varepsilon(s)$ :

$$\Phi_\varepsilon(s) = [I + W(s)]^{-1} = U^{-1}(s) \text{diag} \left\{ \frac{1}{1 + w_{kk}(s)} \right\}, \quad (2.60)$$

where  $1/[1 + w_{kk}(s)]$  are the transfer functions with respect to the error of *isolated* separate channels. Let the MIMO system be of *type r* with respect to  $\varphi(t)$ . Then, substituting

<sup>15</sup> For zero poles, we disregard here the assumption of Section 1.2 that the elements  $w_{kr}(s)$  of the transfer matrix  $W(s)$  have no multiple poles.

<sup>16</sup> We leave the proof of that result to the reader, as an exercise.

<sup>17</sup> Practically, in the technical literature, it is difficult to find instances of real MIMO systems that do not satisfy that condition.

Equation (2.60) into the recurrent Equations (2.55) and (2.56), and taking into account that the matrix  $U^{-1}(0)$  under the above assumptions exists and does not vanish, we come to the conclusion that for the conditions  $K_0 = K_1 = \dots = K_{r-1} \equiv \mathbf{0}$ ,  $K_r \neq \mathbf{0}$  to hold, it is necessary and sufficient that the *least* of the separate channel types be equal to  $r$ . Hence, the type of MIMO system with respect to input signal  $\varphi(t)$  is determined by the least type of the channels.

We have not used above any geometrical or structural notions underlying the CTFs method. Consider now the relationship between the accuracy properties of the MIMO system and the analogous properties of the associated characteristic systems. Toward this end, substitute the canonical representations in Equations (1.53) and (1.54) of the transfer matrix  $\Phi_\varepsilon(s)$  into the general formulae for the matrices of error coefficients  $K_m$  [Equation (2.53)]. It can be shown that such a substitution yields the following expressions for  $K_m$ :

$$K_m = \sum_{k=0}^m \sum_{\delta=0}^k \frac{1}{(m-k)!(k-\delta)!\delta!} \left\{ \frac{d^\delta C(s)}{ds^\delta} \text{diag} \left\{ \frac{d^{k-\delta} \Phi_{\varepsilon i}(s)}{ds^{k-\delta}} \right\} \frac{d^{m-k} C^{-1}(s)}{ds^{m-k}} \right\} \Bigg|_{s=0} \quad (2.61)$$

and

$$K_m = \sum_{i=1}^N \sum_{k=0}^m \sum_{\delta=0}^k \frac{1}{(m-k)!(k-\delta)!\delta!} \left\{ \frac{d^\delta c_i(s)}{ds^\delta} > \frac{d^{k-\delta} \Phi_{\varepsilon i}(s)}{ds^{k-\delta}} < \frac{d^{m-k} c_i^+(s)}{ds^{m-k}} \right\} \Bigg|_{s=0} \quad (2.62)$$

$m = 0, 1, 2, \dots$

where  $\Phi_{\varepsilon i}(s)$  are the transfer functions of the closed-loop characteristic systems with respect to the error in Equation (1.55). Either of these expressions, say the first one, can be rewritten in the form that is more convenient for analysis:

$$K_m = \sum_{k=0}^{m-1} \sum_{\delta=1}^k \frac{1}{(m-k)!(k-\delta)!\delta!} \left\{ \frac{d^\delta C(s)}{ds^\delta} \text{diag} \left\{ \frac{d^{k-\delta} \Phi_{\varepsilon i}(s)}{ds^{k-\delta}} \right\} \frac{d^{m-k} C^{-1}(s)}{ds^{m-k}} \right\} \Bigg|_{s=0} + C(s) \text{diag} \left\{ \frac{1}{m!} \frac{d^m \Phi_{\varepsilon i}(s)}{ds^m} \right\} C^{-1}(s) \Bigg|_{s=0}, \quad (2.63)$$

where all derivatives of the transfer functions  $\Phi_{\varepsilon i}(s)$  having the order lesser than  $m$  are collected in the first term of that sum. For the type- $r$  MIMO system, we have  $K_0 = K_1 = \dots = K_{r-1} \equiv \mathbf{0}$  and  $K_r \neq \mathbf{0}$ . From Equation (2.63), it ensues that this is possible only if among the characteristic systems there is at least one of type  $r$ , and all other characteristic systems are of type not less than  $r$ . Consequently, the type of the MIMO system is determined by the *least* type of the characteristic systems, and the first nonvanishing matrix  $K_r$  is given by a simple expression:

$$K_r = C(0) \text{diag}\{k_{ri}\} C^{-1}(0), \quad (2.64)$$

where

$$k_{ri} = \frac{1}{r!} \frac{d^r \Phi_{\varepsilon i}(s)}{ds^r} \Bigg|_{s=0} \quad i = 1, 2, \dots, N \quad (2.65)$$

are the  $r$ th error coefficients of the characteristic systems, some of which (but not all) can be equal to zero. Replacing, for large values of  $t$ , i.e. for  $s \approx 0$ , the modal matrix  $C(s)$  by the

constant matrix  $C(0)$  in Equation (2.63) gives

$$K_m \approx C(0) \text{diag}\{k_{mi}\} C^{-1}(0), m > r, \quad (2.66)$$

where  $k_{mi}$  are the  $m$ th error coefficients of the characteristic systems. Hence, as a first approximation, Equation (2.64) is also valid for the matrices of error coefficients  $K_m$  of higher orders ( $m > r$ ).

The comparison of the conclusions about the relationship of the MIMO system type with the types of separate channels and characteristic systems shows that the minimum type of the separate channels necessarily coincides with the minimum type of the characteristic systems. Note also that if the type of the MIMO system is determined by the *absolute* pole at the origin [Equation (2.57)], then *all* characteristic systems have not the lesser type, as absolute poles are common to all characteristic systems.

In many practical applications, it is expedient to take on, as a generalized measure of the MIMO system accuracy under slowly changing arbitrary signals, an appropriately chosen norm of the steady-state error, i.e. to judge the MIMO system accuracy by a scalar estimate (like it was done in case of sinusoidal signals). One of the most convenient, from the engineering viewpoint, and having simple physical sense is the Euclidian norm (length) [Equation (1.29)] of the error vector:

$$\|\varepsilon(t)\| = \sqrt{\sum_{i=1}^N |\varepsilon_i(t)|^2}, \quad (2.67)$$

Passing in Equation (2.52) to norms yields

$$\|\varepsilon(t)\| \leq \sum_{m=0}^{\infty} \|K_m\| \left\| \frac{d^m \varphi(t)}{dt^m} \right\|, \quad (2.68)$$

where any norm of the matrix  $K_m$  consistent with the chosen norm of the error vector is denoted by  $\|K_m\|$ . It should be emphasized that the most accurate estimate for  $\|\varepsilon(t)\|$  gives the matrix norm of  $K_m$ , which is not only consistent with the norm  $\|\varepsilon(t)\|$ , but also *subordinate* to it (Vulich 1967). For the Euclidian norm of a vector, the subordinate (also called *induced*) norm is the spectral norm equal to the positive value of the square root taken of the eigenvalues of the Hermitian matrix  $K_m K_m^*$  (Porter 1966). If the MIMO system is of type  $r$ , then, for the norm of the first nonvanishing component  $\varepsilon_r(t)$  of  $\varepsilon(t)$ , which corresponds to the  $r$ th derivative of  $\varphi(t)$  (this component usually plays the chief part), it can be written, based on Equations (2.64) and (2.68),

$$\begin{aligned} \|\varepsilon_r(t)\| &\leq \|K_r\| \left\| \frac{d^r \varphi(t)}{dt^r} \right\| = \|C(0) \text{diag}\{k_{ri}\} C^{-1}(0)\| \left\| \frac{d^r \varphi(t)}{dt^r} \right\| \\ &\leq \nu[C(0)] \max_i (|k_{ri}|) \left\| \frac{d^r \varphi(t)}{dt^r} \right\|, \end{aligned} \quad (2.69)$$

where  $\nu[C(0)] = \|C(0)\| \|C^{-1}(0)\|$  is the condition number of the MIMO system modal matrix evaluated for  $s = 0$ . This expression yields the estimate for any norms of the vector  $\varepsilon_r(t)$ . However, the Euclidian norm [Equation (2.67)] should be especially pointed out, since it allows

the essential relationship between the MIMO system error under slowly changing signals and geometrical properties of the canonical basis to be established. Indeed, from Equation (2.69), it follows that the upper boundary of  $\|\varepsilon_r(t)\|$  is directly proportional to the degree of non-orthogonality  $\nu[C(0)]$  of the canonical basis of the steady-state MIMO system. Concerning the higher components  $\varepsilon_m(t) (m > r)$  of  $\varepsilon(t)$ , their magnitudes, as evident from Equation (2.63), also increase with the increase in  $\nu[C(0)]$ , although that dependence is not so obvious here.<sup>18</sup> Thus, the steady-state error of the MIMO system under slowly changing signals substantially depends on the skewness of the canonical basis axes. In this regard, the most accurate are, all other conditions being equal, normal MIMO systems, whose canonical bases are orthogonal, and  $\nu[C(0)] \equiv 1$ .

### 2.3.2 Dynamical accuracy of circulant, anticirculant and uniform MIMO systems

The classes of circulant, anticirculant and uniform systems unite a common feature, namely their canonical bases do not depend on complex variable  $s$  and, thereby, are constant. More specifically, the orthonormal canonical bases of circulant and anticirculant systems coincide with the corresponding bases of the permutation matrix  $U$  [Equation (1.128)], or the anticirculant permutation matrix  $U_-$  [Equation (1.156)], and the canonical bases of uniform systems coincide with the canonical bases of the numerical matrix of cross-connections  $R$ . As a result of the independency of modal matrices  $C$  from  $s$ , from Equations (2.61)–(2.63) and (2.65), we immediately have, for the considered classes of MIMO systems,

$$K_m = C \text{diag}\{k_{mi}\} C^{-1} = \sum_{i=1}^N c_i > k_{mi} < c_i^+, \quad m = 0, 1, 2, \dots, \quad (2.70)$$

where  $k_{mi}$  are the  $m$ th error coefficients of the characteristic systems.

Hence, any matrix of error coefficients  $K_m$  of circulant, anticirculant and uniform systems is connected with the diagonal matrix of the error coefficients  $k_{mi}$  of characteristic systems via a similarity transformation through the modal matrix  $C$ . This, in turn, means that for any  $m$ , the coefficients  $k_{mi}$  ( $i = 1, 2, \dots, N$ ) form the spectrum (the set of all eigenvalues) of the matrix  $K_m$ . The established property of  $K_m$ , as well as the fact that the CTFs  $q_i(s)$  of circulant and anticirculant systems can be written in analytical form for any number of channels  $N$ , and, in the case of uniform systems, they differ from the transfer function of separate channels  $w(s)$  only by the constant multipliers  $\lambda_i$ , considerably simplifies the accuracy analysis under slowly changing signals. It is worth noting that for the discussed systems, the evaluation of the coefficients  $k_{mi}$  can readily be carried out using the well known formulae of the classical control theory, such as King's formulae, although, unlike the common SISO systems, these coefficients can be both real and complex conjugate.

There are two interesting points caused by the orthogonality of canonical bases of circulant and anticirculant systems, or, which is the same, by the fact that their modal matrices  $C$  are unitary. First, the unitarity of  $C$  in Equation (2.70) means that all matrices of error coefficients

<sup>18</sup> For the higher components  $\varepsilon_m(t) (m > r)$ , the linear dependence of  $\|\varepsilon_m(t)\|$  on  $\nu[C(0)]$  takes place as a first approximation [see Equations (2.69) and (2.66)].

$K_m$  are normal. Therefore, their spectral norm is equal to the spectral radius (Marcus and Minc 1992) and coincides with the maximum of magnitudes of the error coefficients of characteristic systems. Second, since the Euclidian norm is invariant under a unitary transformation (Derusso *et al.* 1965), from the evident equality

$$C^{-1} \varepsilon_m(t) = \text{diag}\{k_{mi}\} C^{-1} \frac{d^m \varphi(t)}{dt^m}, \quad (2.71)$$

it follows that for any  $m$ , the magnitudes of the vectors  $\varepsilon_m(t)$  and  $d^m \varphi(t)/dt^m$  evaluated in the natural and canonical bases are equal in pairs to each other.

Among circulant systems, the simple symmetrical MIMO systems, i.e. systems with identical transfer functions of all cross-connections (see Section 1.4), should be especially pointed out. As we know [see Equations (1.138) and (1.139)], such MIMO systems have only two distinct characteristic systems, both with real coefficients; therefore, for any  $m$ , there are only two distinct real coefficients  $k_{m1}$  and  $k_{m2} = \dots = k_{mN}$ . It can readily be shown that the matrices  $K_m$  [Equation (2.70)] in this case are simple symmetrical, and have the form

$$K_m = C \text{diag}\{k_{mi}\} C^* = T \text{diag}\{k_{mi}\} T^{-1}, \quad m = 0, 1, 2, \dots, \quad (2.72)$$

where  $T$  is an orthogonal matrix (i.e.  $T^{-1} = T^T$ ), representing the *real-valued canonical form* of the modal matrix  $C$ .<sup>19</sup>

It should also be noted that Equation (2.70) gives an opportunity to derive a simple formula for the first nonvanishing matrix of error coefficients  $K_r$  for uniform systems. As we know, the CTFs of uniform systems have the form  $\lambda_i w(s)$ . Therefore, their gains differ from the gains  $D$  of the transfer function  $w(s)$  only by the coefficients  $\lambda_i$ , i.e.  $k_{ri} = 1/\lambda_i D$ , and, for the first nonvanishing matrix  $K_r$ ,<sup>20</sup> based on Equation (2.70), we have

$$K_r = C \text{diag} \left\{ \frac{1}{\lambda_i D} \right\} C^{-1} = \frac{1}{D} C \text{diag} \left\{ \frac{1}{\lambda_i} \right\} C^{-1} = \frac{1}{D} R^{-1}, \quad (2.73)$$

i.e. that matrix is equal, up to the scalar multiplier  $1/D$ , to the inverse matrix of cross-connections. The corresponding formulae for all other matrices  $K_m$  ( $m > r$ ) are derived in the next section.

**Example 2.8** Let us use Equation (2.73) for the accuracy analysis of the two-axis uniform indirect guidance system of Example 1.4. Assume that the input signal is described by a linear law, i.e.  $\varphi(t) = vt$ . From the transfer function in Equation (1.103), it can be seen that the system is of type-1 (since it has one ideal integrator in each channel), and therefore it should have constant steady-state error under linear input signals. Taking into account the form of the cross-connection matrix  $R$  [Equation (1.60)], from Equation (2.73), we find the first nonvanishing matrix  $K_1$ :

$$K_1 = \frac{1}{D \cos(\alpha_1 - \alpha_2)} \begin{pmatrix} \cos \alpha_2 & -\sin \alpha_1 \\ \sin \alpha_2 & \cos \alpha_1 \end{pmatrix}. \quad (2.74)$$

<sup>19</sup> See Remark 1.7.

<sup>20</sup> We assume here that the type of the MIMO system exceeds zero.

Then, for the upper boundary of the magnitude  $|\varepsilon|$  of the steady-state *velocity* error vector, we have:

$$|\varepsilon| \leq \|R^{-1}\| \frac{|v|}{D} = \frac{\sqrt{1 + \sin(|\alpha_1 - \alpha_2|)}}{\cos(\alpha_1 - \alpha_2)} |\varepsilon_0|, \quad (2.75)$$

where  $|\varepsilon_0| = |v|/D$  is the magnitude of the error vector of that very system in the case of direct tracking, i.e. for  $\alpha_1 = 0^\circ, \alpha_2 = 0^\circ, R = I$ ,<sup>21</sup> and

$$\|R^{-1}\| = \frac{\sqrt{1 + \sin(|\alpha_1 - \alpha_2|)}}{\cos(\alpha_1 - \alpha_2)} \quad (2.76)$$

is the spectral norm of the matrix  $R^{-1}$ . As is clear from Equation (2.75), for  $\alpha_1 = \alpha_2$ , i.e. in the case of orthogonal sensitivity axes  $OX_1$  and  $OX_2$  of the stellar sensors (see Figure 1.24), the norm  $\|R^{-1}\|$  is equal to unity, and the magnitude  $|\varepsilon|$  of the error vector in the indirect tracking mode is equal to the magnitude  $|\varepsilon_0|$  of the system in the case of direct tracking (i.e. when there are no cross-connections between the channels). On the other hand, if the axes  $OX_1$  and  $OX_2$  are not orthogonal, i.e. for  $\alpha_1 \neq \alpha_2$ , the value of  $|\varepsilon|$  increases, and tends to infinity as  $|\alpha_1 - \alpha_2| \rightarrow 90^\circ$ . It can be argued that the norm  $\|R^{-1}\|$  characterizes the degree of non-orthogonality of the coordinate system  $OX_1X_2$ , composed of the sensitivity axes of the stellar sensors. Consequently, the magnitude of the velocity error vector of the discussed system is directly proportional to the degree of non-orthogonality of the axes  $OX_1$  and  $OX_2$ , and depends only on the absolute value of the *difference* between angles  $\alpha_1$  and  $\alpha_2$ . Recall that the stability of the guidance system, as shown in Examples 1.4 and 1.14, depends on both the values and the signs of the angles  $\alpha_1$  and  $\alpha_2$ .

It is interesting to compare this system, from the accuracy and stability viewpoints, with the examined in Example 1.5 the same guidance system in the case of identical angles  $\alpha_1$  and  $\alpha_2$ , ( $\alpha_1 = \alpha_2 = \alpha$ ), when the coordinate system  $OX_1X_2$  is orthogonal. As was shown there, if the angle  $\alpha$  is equal to the phase margin of the isolated separate channel, then the cross-connected system turns out to be on the stability boundary, and, if that angle further increases, then the system becomes unstable. Consider now the accuracy of that system under the same linear input  $\varphi(t) = vt$ . The matrix  $R$  [Equation (1.109)] in this case is orthogonal. Therefore, for the vector  $\varepsilon$  of the steady-state velocity error, the following can be written, based on Equation (2.73):

$$\varepsilon = R^{-1} \frac{v}{D} = R^T \varepsilon_0 = \begin{pmatrix} \cos \alpha & -\sin \alpha \\ \sin \alpha & \cos \alpha \end{pmatrix} \varepsilon_0, \quad (2.77)$$

where  $\varepsilon_0$ , just as above, denotes the error vector of the system with  $R = I$ . We have already pointed out that the magnitude of a vector is invariant under the orthogonal transformation. As applied to our case, this implies that the magnitude of the vector  $\varepsilon$  in Equation (2.77) is equal to the magnitude of vector  $\varepsilon_0$  for any value of angle  $\alpha$ . In other words, the accuracy of the system (with respect to magnitude  $|\varepsilon|$ ) does not depend on the reciprocal position of the orthogonal coordinate systems  $OX_1X_2$  and  $OY_1Y_2$  in Figure 1.24. This agrees with the above conclusion, but, here, we have circumvented the sign  $\leq$  on the left side of Equation (2.75), which is due to passing from the initial vector in Equation (2.74) to the norms in Equation (2.75).

<sup>21</sup> See Example 1.2.

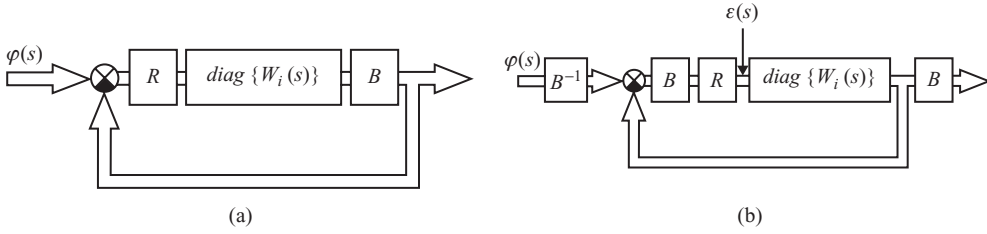


**Figure 2.19** Matrix block diagrams of the MIMO system with rigid cross-connections. (a) Initial block diagram; (b) equivalent block diagram.

### 2.3.3 Accuracy of MIMO systems with rigid cross-connections

In this section, we shall derive analytical expressions for matrices of error coefficients for a significant in practice class of MIMO systems with arbitrary transfer functions of separate channels and rigid cross-connections, on the additional assumption that the type of these systems exceeds zero (Gasparyan and Egiazaryan 1979). The matrix block diagram of such MIMO systems is depicted in Figure 2.19(a), in which  $R = \{r_{ij}\}$  and  $B = \{b_{ij}\}$  are numerical matrices of cross-connections, and  $W_i(s) (i = 1, 2, \dots, N)$  are the transfer functions of separate channels, having the form

$$W_i(s) = \frac{\sum_{k=0}^{m_i} \alpha_{ki} s^k}{\sum_{k=1}^{n_i} \beta_{ki} s^k}, \quad m_i \leq n_i, \quad (2.78)$$

where, depending on the type of the channels, the corresponding coefficients  $\beta_{ki}$  vanish [note that in the denominator of Equation (2.78), the index  $k$  begins from unity, which assumes the presence of at least one ideal integrator in each channel of the MIMO system].

The block diagram in Figure 2.19(a) is typical for many practical systems destined for spatial (two- or three-dimensional) tracking, such as indirect pointing and guidance systems for astronomical telescopes, tracking systems of radio aerials and radars, as well as various other control systems, etc. (Gasparyan 1986). Note also that, assuming in Figure 2.19(a) that  $W_i(s) = W(s)$  and  $B = I$ , we come to the standard block diagram of the uniform system in Figure 1.18, i.e. uniform systems can be regarded as a specific case of the discussed MIMO systems.

Determine, using the King technique, the matrices of error coefficients of the MIMO system of Figure 2.19(a). Towards this end, first, recast the matrix block diagram of that system to the equivalent form in Figure 2.19(b). According to the latter, the closed-loop transfer matrix with respect to error  $\Phi_\varepsilon(s)$ , which relates the vector  $\varepsilon(s)$  with  $\varphi(s)$ , is given by the expression

$$\Phi_\varepsilon(s) = B[I + \text{diag}\{W_i(s)\}RB]^{-1}B^{-1}. \quad (2.79)$$

Represent the matrix  $\Phi_\varepsilon(s)$  [Equation (2.79)] in the following form:

$$\Phi_\varepsilon(s) = BU^{-1}(s)\text{diag} \left\{ \frac{1}{1 + b_{ii}r_{ii}W_i(s)} \right\} B^{-1}, \quad (2.80)$$

where the entries  $u_{ij}(s)$  of the matrix  $U(s)$  are

$$u_{ij}(s) = \begin{cases} \frac{1 + W_i(s) \sum_{k=1}^N r_{ik} b_{ki}}{1 + b_{ii} r_{ii} W_i(s)} & (i = j) \\ \frac{W_i(s) \sum_{k=1}^N r_{ik} b_{kj}}{1 + b_{ii} r_{ii} W_i(s)} & (i \neq j) \end{cases} \quad i, j = 1, 2, \dots, N. \quad (2.81)$$

Note that the limit of the inverse matrix  $U^{-1}(s)$  in Equation (2.80), as  $s \rightarrow 0$ , exists for any  $W_i(s)$  and is equal to

$$U^{-1}(0) = \lim_{s \rightarrow 0} U^{-1}(s) = B^{-1} R^{-1} \text{diag}\{r_{ii} b_{ii}\}. \quad (2.82)$$

The transition to the equivalent scheme of Figure 2.19(b) has been necessary for the reason that in the case of different types of separate channels, the representation of the transfer matrix  $\Phi_\varepsilon(s)$  of the initial MIMO system in Figure 2.19(a) in the form

$$\Phi_\varepsilon(s) = [I + B \text{diag}\{W_i(s)\}R]^{-1} = V^{-1}(s) \text{diag}\left\{\frac{1}{1 + b_{ii} r_{ii} W_i(s)}\right\} \quad (2.83)$$

does not lead in the end to any closed results, since the matrix  $V^{-1}(s)$  in Equation (2.83) tends to infinity as  $s \rightarrow 0$ .

Substituting Equation (2.80) into the recurrent King formulae in Equations (2.55) and (2.56), we obtain

$$K_0 = BU^{-1}(0) \left[ \lim_{s \rightarrow 0} \text{diag}\left\{\frac{1}{1 + b_{ii} r_{ii} W_i(s)}\right\} \right] B^{-1} \equiv \mathbf{0}, \quad (2.84)$$

since the MIMO system is assumed to be of non-zero type, and

$$K_m = \lim_{s \rightarrow 0} \frac{1}{s^m} \left[ BU^{-1}(s) \text{diag}\left\{\frac{1}{1 + b_{ii} r_{ii} W_i(s)}\right\} B^{-1} - \sum_{i=0}^{m-1} K_i s^i \right], \quad m = 1, 2, \dots \quad (2.85)$$

If we assume that the *least* type of the separate channels is equal to some integer number  $r$ , then the first nonvanishing matrix  $K_r$  in Equation (2.85), taking into account Equation (2.72), is equal to

$$K_r = BU^{-1}(0) \text{diag}\left\{\lim_{s \rightarrow 0} \frac{1}{s^r} \frac{1}{1 + b_{ii} r_{ii} W_i(s)}\right\} B^{-1} = R^{-1} \text{diag}\{r_{ii} b_{ii} k_{ri}\} B^{-1}, \quad (2.86)$$

where  $k_{ri}$  ( $i = 1, 2, \dots, N$ ) are the  $r$ th error coefficients of a set of  $N$  SISO systems that are obtained from the MIMO system in Figure 2.19(a) by equating all coefficients of

cross-connections ( $r_{ij} = b_{ij} = 0$  for  $i \neq j$ ) to zero. In can be shown that in the general case, the matrix  $K_{r+n}$  has the form (Gasparyan and Egiazaryan 1979):

$$K_{r+n} = B \left[ B^{-1} R^{-1} \text{diag}\{r_{ii} b_{ii} k_{(r+n)i}\} + \sum_{\delta=1}^n \frac{1}{\delta!} \left. \frac{d^\delta U^{-1}(s)}{ds^\delta} \right|_{s=0} \text{diag}\{r_{ii} b_{ii} k_{(r+n-\delta)i}\} \right] B^{-1} \quad (2.87)$$

$n = 1, 2, \dots,$

where the coefficients  $k_{(r+n)i}$  and  $k_{(r+n-\delta)i}$  are determined in the same manner as  $k_{ri}$  in Equation (2.86), and the derivatives  $U^{-1}(s)$  at  $s = 0$  can be evaluated by the following recurrent formulae:

$$\begin{aligned} \left. \frac{dU^{-1}(s)}{ds} \right|_{s=0} &= B^{-1} R^{-1} \text{diag}\{\beta_{1i}/\alpha_{0i}\} [I - B^{-1} R^{-1} \text{diag}\{r_{ii} b_{ii}\}] \\ \left. \frac{d^\delta U^{-1}(s)}{ds^\delta} \right|_{s=0} &= \delta! B^{-1} R^{-1} \text{diag}\{1/\alpha_{0i}\} \left\{ \text{diag}\{\beta_{\delta i}\} [I - B^{-1} R^{-1} \text{diag}\{r_{ii} b_{ii}\}] \right. \\ &\quad \left. - \sum_{j=1}^{\delta-1} \frac{1}{j!} \left. \frac{d^j U^{-1}(s)}{ds^j} \right|_{s=0} \text{diag}\{\alpha_{(\delta-j)i}\} [I + RB] \right\} \quad \delta = 2, 3, \dots \end{aligned} \quad (2.88)$$

Substituting Equation (2.88) into Equation (2.87), after a number of simple transformations, we get the final expressions for the matrices of error coefficients  $K_m$ :

$$K_m = \left[ R^{-1} \text{diag}\{\beta_{mi}\} - \sum_{j=1}^{m-1} K_j (R^{-1} \text{diag}\{\beta_{(m-j)i}\} + B \text{diag}\{\alpha_{(m-j)i}\}) \right] \text{diag}\{1/\alpha_{0i}\} B^{-1} \quad m = 1, 2, \dots \quad (2.89)$$

Equation (2.89) is valid for any type  $r_i$  ( $r_i \geq 1$ ) of MIMO system separate channels. An essential convenience of these formulae is that they are recurrent and are expressed directly through the matrices of cross-connections  $R$  and  $B$ , and the coefficients  $\alpha_{ki}$  and  $\beta_{ki}$  of the transfer functions  $W_i(s)$ . This creates necessary premises to use them in different optimization procedures for improving the accuracy of linear MIMO control systems.

The analogous formulae for the particular case of uniform systems can easily be found by putting in Equation (2.89)  $W_i(s) = W(s)$  and  $B = I$ , which yields

$$K_m = \frac{1}{\alpha_0} \left[ \beta_m R^{-1} - \sum_{j=1}^{m-1} K_j (\beta_{m-j} R^{-1} + \alpha_{m-j} I) \right], \quad m = 1, 2, \dots \quad (2.90)$$

Finally, assuming that the cross-connections in the MIMO system in Figure 2.19(a) are absent, i.e. assuming  $R = B = I$ , from Equation (2.89), we find that the matrices  $K_m$  have diagonal form  $K_m = \text{diag}\{k_{mi}\}$ , where  $k_{mi}$  are determined by the formulae of the error coefficients for SISO systems well known in the classical control theory (Rabinovich *et al.* 1969):

$$k_{mi} = \frac{1}{\alpha_{0i}} \left[ \beta_{mi} - \sum_{j=1}^{m-1} k_{ji} (\beta_{(m-j)i} + \alpha_{(m-j)i}) \right], \quad i = 1, 2, \dots, n, \quad m = 1, 2, \dots \quad (2.91)$$

## 2.4 STATISTICAL ACCURACY OF LINEAR MIMO SYSTEMS

### 2.4.1 Accuracy of general MIMO systems under stationary stochastic signals

In the literature on modern control, there is a wealth of works devoted to optimal smoothing, estimation and control of multidimensional stochastic processes (Bosgra *et al.* 2004; Anderson and Moore 1971, 1990; Kwakernaak and Sivan 1972; Bryson and Ho 1969; Lifshits *et al.* 1974). At the same time, comparatively little attention is paid to *engineering* techniques of the analysis and design of multivariable control systems subjected to random signals. Here, we mean the techniques which allow for specific structural features of MIMO systems and preserve a close relationship with conventional frequency-domain methods of the classical control theory (James *et al.* 1947; Newton *et al.* 1957; Tsypkin 1977; Bessekerski and Popov 2002). Below, an approach based on using a scalar estimate as a measure of the MIMO system statistical accuracy is presented, namely the *mean square value of the error vector magnitude*, which has an evident physical sense and can readily be found without direct evaluation of the covariance matrix of the MIMO system output (or error) vector.

Consider a linear stable general MIMO system, as in Figure 1.1. Let the input vector  $\varphi(t)$  be a stationary stochastic Gaussian process with zero means,<sup>22</sup> described by a correlation matrix  $R_\varphi(\tau) = E[\varphi(t)\varphi^T(t + \tau)]$ <sup>23</sup> or by a nonnegative-definite Hermitian matrix of spectral densities  $S_\varphi(j\omega)$ , the relationship between which is given by the direct and inverse Fourier transforms (Lifshits *et al.* 1974):

$$S_\varphi(j\omega) = \int_{-\infty}^{+\infty} R_\varphi(\tau)e^{-j\omega\tau} d\tau, \quad R_\varphi(\tau) = \frac{1}{2\pi} \int_{-\infty}^{+\infty} S_\varphi(j\omega)e^{j\omega\tau} d\omega. \quad (2.92)$$

For  $\tau = 0$ , the matrix  $R_\varphi(\tau)$  passes into a symmetrical nonnegative-definite covariance matrix  $P_\varphi = \{P_{\varphi ij}\}$ :

$$P_\varphi = R_\varphi(0) = E[\varphi(t)\varphi^T(t)] = \frac{1}{2\pi} \int_{-\infty}^{+\infty} S_\varphi(j\omega)d\omega. \quad (2.93)$$

Denote the corresponding characteristics of the output vector  $f(t)$  by  $S_f(j\omega)$ ,  $R_f(\tau)$  and  $P_f$ . The spectral densities matrix  $S_f(j\omega)$  of the output vector is connected with  $S_\varphi(j\omega)$  by a well known formula (Lifshits *et al.* 1974):

$$S_f(j\omega) = \Phi(j\omega)S_\varphi(j\omega)\Phi^*(j\omega), \quad (2.94)$$

where  $\Phi(j\omega)$  is the closed-loop MIMO system transfer matrix with respect to the output [see Equation (1.3)]. From Equations (2.93) and (2.94), we obtain the basic expression for the

<sup>22</sup> The signals  $\varphi(t)$  with non-zero means are commented on in Remark 2.5.

<sup>23</sup>  $E[\cdot]$  is the operation of mathematical expectation.

covariance matrix  $P_f$ :

$$P_f = \frac{1}{2\pi} \int_{-\infty}^{+\infty} S_f(j\omega) d\omega = \frac{1}{2\pi} \int_{-\infty}^{+\infty} \Phi(j\omega) S_\varphi(j\omega) \Phi^*(j\omega) d\omega. \quad (2.95)$$

In what follows, we shall assume the vector  $\varphi(t)$  be a vector of random disturbances (noises). Then, the covariance matrix  $P_f$  [Equation (2.95)] provides all usually required, within the correlation theory framework, information about the MIMO system statistical accuracy. However, for systems with a large number of separate channels  $N$  and high orders of the transfer functions  $w_{kr}(s)$  composing the open-loop transfer matrix  $W(s)$ , the procedure of numerical evaluation of  $P_f$  with the help of Equation (2.95) leads to certain computational difficulties. Besides, in many engineering applications, the covariance matrix  $P_f$  by itself is not a very convenient accuracy characteristic for MIMO systems of high dimension. The point is that when using it, an engineer has to keep an eye on  $N$  mean squares  $P_{fii}$  and  $N(N - 1)/2$  cross-correlation moments  $P_{fij} = P_{fji}$  of the output variables. The inconvenience of  $P_f$  as a performance index especially shows when comparing the accuracy of different MIMO systems, or different variants of the same designed system, since the matrix  $P_f$  does not always give a clear and unambiguous answer about the statistical accuracy of the overall MIMO system.

In the preceding sections, when investigating the MIMO system dynamics under harmonic and slowly changing deterministic inputs, we often considered as a measure of steady-state accuracy the Euclidian norm of the error vector, i.e. we judged the accuracy of MIMO systems with the help of one scalar quantity. Proceeding in a similar manner, let us take as a generalized measure of MIMO systems statistical accuracy the *mean square value of the output vector magnitude*:

$$D_f = E[|f(t)|^2]. \quad (2.96)$$

It is easy to note that the mean square value  $D_f$  [Equation (2.96)] is equal to the sum of mean square values  $E[f_i^2(t)]$  of the output vector components and, consequently, to the trace of the covariance matrix  $P_f$ , i.e.

$$D_f = E \left[ \sum_{i=1}^N f_i^2(t) \right] = \sum_{i=1}^N E[f_i^2(t)] = \text{tr}\{P_f\}. \quad (2.97)$$

Then, based on Equation (2.96) and on the left-hand side of Equation (2.95), we have

$$D_f = \text{tr} \left\{ \frac{1}{2\pi} \int_{-\infty}^{+\infty} S_f(j\omega) d\omega \right\} = \frac{1}{2\pi} \int_{-\infty}^{+\infty} \text{tr}\{S_f(j\omega)\} d\omega. \quad (2.98)$$

Let us now express the trace of the matrix  $S_f(j\omega)$  in Equation (2.98) through the characteristics of the MIMO system and input stochastic disturbances. Towards this end, we rewrite the trace  $\text{tr}\{S_f(j\omega)\}$ , taking into account the well known property of a trace of the product of two matrices:  $\text{tr}\{AB\} = \text{tr}\{BA\}$  (Marcus and Minc 1992), in the form

$$\text{tr}\{S_f(j\omega)\} = \text{tr}\{\Phi(j\omega) S_\varphi(j\omega) \Phi^*(j\omega)\} = \text{tr}\{[\Phi^*(j\omega) \Phi(j\omega)] S_\varphi(j\omega)\}, \quad (2.99)$$

where  $\Phi^*(j\omega) \Phi(j\omega) = [\Phi^*(j\omega) \Phi(j\omega)]^*$  is a Hermitian matrix.

For the following operations, we need to prove one inequality for the trace  $tr\{S_f(j\omega)\}$  written in the form of the product of two Hermitian matrices [Equation (2.99)] (Gasparyan 1986). Let  $N \times N$  square matrices  $A = \{a_{ij}\}$  and  $B = \{b_{ij}\}$  be Hermitian. Denote by  $C = \{c_{ij}\}$  their product  $C = AB$ . Then

$$tr\{C\} = tr\{AB\} = \sum_{i=1}^N c_{ii} = \sum_{i=1}^N \sum_{k=1}^N a_{ik}b_{ki}. \quad (2.100)$$

Taking into account that the matrix  $B$  is Hermitian, i.e.  $b_{ki} = \tilde{b}_{ik}$ , where the above wavy line denotes the complex conjugation, from Equation (2.100), we obtain

$$tr\{AB\} = \sum_{i=1}^N \sum_{k=1}^N a_{ik}\tilde{b}_{ik} = \sum_{i=1}^N \langle \bar{a}_i, \bar{b}_i \rangle = \langle \bar{\mathbf{a}}, \bar{\mathbf{b}} \rangle, \quad (2.101)$$

where  $\bar{a}_i$  and  $\bar{b}_i$  are the  $i$ th rows of the matrices  $A$  and  $B$ ,  $\bar{\mathbf{a}}$  and  $\bar{\mathbf{b}}$  are  $(1 \times N^2)$ -dimensional row vectors, composed of  $\bar{a}_i$  and  $\bar{b}_i$  ( $i = 1, 2, \dots, N$ )

$$\bar{\mathbf{a}} = [\bar{a}_1 \ \bar{a}_2 \ \dots \ \bar{a}_N], \quad \bar{\mathbf{b}} = [\bar{b}_1 \ \bar{b}_2 \ \dots \ \bar{b}_N]. \quad (2.102)$$

Using the Cauchy-Schwartz inequality (Porter 1966), from Equation (2.101), we find

$$tr\{AB\} = \langle \bar{\mathbf{a}}, \bar{\mathbf{b}} \rangle \leq |\bar{\mathbf{a}}| |\bar{\mathbf{b}}|, \quad (2.103)$$

where the magnitudes of  $\bar{\mathbf{a}}$  and  $\bar{\mathbf{b}}$  are equal to

$$|\bar{\mathbf{a}}| = \sqrt{\sum_{i=1}^N \sum_{k=1}^N |a_{ik}|^2} = \sqrt{tr\{AA^*\}} = \|A\|_s, \quad |\bar{\mathbf{b}}| = \sqrt{\sum_{i=1}^N \sum_{k=1}^N |b_{ik}|^2} = \sqrt{tr\{BB^*\}} = \|B\|_s \quad (2.104)$$

and the subscript  $s$  denotes the Schmidt norm<sup>24</sup> defined for an arbitrary square matrix  $A = \{a_{ij}\}$  as the square root of the sum of squares of all magnitudes  $|a_{ij}|$  (Bellman 1970). Substituting Equation (2.104) into Equation (2.103), we obtain the required inequality

$$tr\{AB\} \leq \|A\|_s \|B\|_s. \quad (2.105)$$

Notice now that the trace of the matrix  $S_f(j\omega)$  in Equation (2.99) is expressed as the product of two Hermitian matrices  $\Phi^*(j\omega)\Phi(j\omega)$  and  $S_\varphi(j\omega)$ . Then, based on Equation (2.105), from Equation (2.99), we have<sup>25</sup>

$$tr\{S_f(j\omega)\} \leq \|\Phi^*(j\omega)\Phi(j\omega)\|_s \|S_\varphi(j\omega)\|_s \leq \|\Phi(j\omega)\|_s^2 \|S_\varphi(j\omega)\|_s. \quad (2.106)$$

<sup>24</sup> That norm is also called the *Frobenius* norm, *Schatten 2-norm* or *Hilbert-Schmidt* norm.

<sup>25</sup> In Equation (2.106), we have used the following properties of the matrix norm:  $\|AB\| \leq \|A\| \|B\|$ ,  $\|A\| = \|A^T\| = \|A^*\|$ .

If the components of the input disturbances  $\varphi(t)$  are statistically independent and have the same spectral densities  $s_\varphi(\omega)$ , and such situations frequently occur in practice, then the matrix  $S_\varphi(j\omega)$  becomes a scalar matrix  $S_\varphi(j\omega) = s_\varphi(\omega)I$ . In this case, from Equation (2.99) and taking into account that the function  $tr\{\cdot\}$  is linear, we immediately find that

$$tr\{S_f(j\omega)\} = s_\varphi(\omega)tr\{\Phi^*(j\omega)\Phi(j\omega)\} = \|\Phi(j\omega)\|_S^2 s_\varphi(\omega), \quad (2.107)$$

i.e. the inequality in Equation (2.106) becomes a *strict equality*.

Substituting Equation (2.106) into Equation (2.98), we finally obtain the following upper estimate for the mean square value of the magnitude of the MIMO system output vector, in the case of stationary stochastic input disturbances,

$$D_f \leq \frac{1}{2\pi} \int_{-\infty}^{+\infty} \|\Phi(j\omega)\|_S^2 \|S_\varphi(j\omega)\|_S d\omega. \quad (2.108)$$

For  $S_\varphi(j\omega) = s_\varphi(\omega)I$ , this inequality becomes a strict equality, thereby defining the *exact* value of  $D_f$ . Note that, for  $N = 1$ , Equation (2.108) coincides with the well known formula

$$D_f = \frac{1}{2\pi} \int_{-\infty}^{+\infty} |\Phi(j\omega)|^2 s_\varphi(\omega) d\omega \quad (2.109)$$

defining the mean square output of a SISO system subjected to stochastic input signals with the spectral density  $s_\varphi(\omega)$  (James *et al.* 1947; Newton *et al.* 1957; Tsympkin 1977).

In conclusion, we discuss the influence of internal geometrical characteristics of the MIMO system on the steady-state stochastic errors. Toward this end, we can use the canonical representation of the transfer matrix  $\Phi(s)$  via the similarity transformation in Equation (1.49). Replacing the variable  $s$  in Equation (1.49) by  $j\omega$  and passing to the Schmidt norm yields

$$\|\Phi(j\omega)\|_S \leq \nu[C(j\omega)]_S \left\| \text{diag} \left\{ \frac{q_i(j\omega)}{1 + q_i(j\omega)} \right\} \right\|_S, \quad (2.110)$$

where  $\nu[C(j\omega)]_S = \|C(j\omega)\|_S \|C^{-1}(j\omega)\|_S$  is the condition number of the modal matrix  $C(j\omega)$ , evaluated by the Schmidt norm. It should be noted here that the Schmidt norm, being *consistent* with the Euclidian norm of the vector, is not *subordinate* to the latter. Therefore, it has larger values, as compared with the spectral norm. Thus, for orthogonal matrices of order  $N \times N$ , that norm is equal to  $\sqrt{N}$ , whereas the spectral norm is equal to unity. Accordingly, the condition number of an orthogonal basis, being equal to unity under the spectral norm, equals  $N$  in the case of the Schmidt norm. At the same time, in both cases, the condition number tends to infinity if the modal matrix  $C(j\omega)$  becomes degenerate, and, in this sense, that number remains a measure of the canonical basis *non-orthogonality*.

Therefore, from Equations (2.108) and (2.110), we can conclude that the upper boundary of the mean square value  $D_f$  increases, all other conditions being equal, as the non-orthogonality of the canonical basis increases. In this respect, the most accurate, as in the cases of harmonic and slowly changing deterministic signals, are normal MIMO systems, i.e. systems with orthogonal canonical bases.

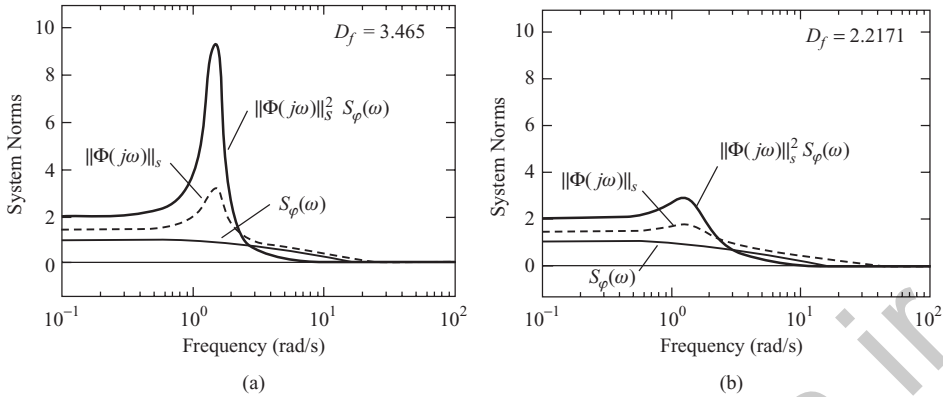


**Figure 2.20** Statistical accuracy analysis of a two-axis guidance system [Equation (1.66)] for different angles  $\alpha_1$  and  $\alpha_2$ . (a)  $\alpha_1 = 30^\circ$ ,  $\alpha_2 = 20^\circ$ ; (b)  $\alpha_1 = 30^\circ$ ,  $\alpha_2 = -20^\circ$ .

**Example 2.9** Let us evaluate the mean square value  $D_f$  of the general two-axis guidance system of Example 1.2 with the transfer functions of separate channels of Equation (1.66), and for two different combinations of angles  $\alpha_1$  and  $\alpha_2$ :  $\alpha_1 = 30^\circ$ ,  $\alpha_2 = 20^\circ$  and  $\alpha_1 = 30^\circ$ ,  $\alpha_2 = -20^\circ$ . Assume that the input signals of the channels are uncorrelated stationary stochastic disturbances, having the same spectral density

$$s_\varphi(\omega) = \frac{1}{1 + 0.04\omega^2} \tag{2.111}$$

The frequency dependencies of the spectral density  $s_\varphi(\omega)$  [Equation (2.11)], the Schmidt norm of the closed-loop transfer matrix  $\Phi(j\omega)$  and the integrand expression in Equation (2.108) are presented in Figure 2.20. The plots for both combinations of angles  $\alpha_1$  and  $\alpha_2$  are shown on the same scale, to make them more visual. The results of numerical computations, with the help of Equation (2.108), of the exact (as the matrix of input spectral densities is scalar) values of the mean squares  $D_f$  are given on the same plots. As we can see, for the second combination of angles  $\alpha_1$  and  $\alpha_2$ , when the eigenvalues of the cross-connections matrix are real, the value  $D_f = 2.2171$  is about 1.6 times as small as the corresponding value  $D_f = 3.465$  for the first combination of  $\alpha_1$  and  $\alpha_2$ .

### 2.4.2 Statistical accuracy of normal MIMO systems

In practice, for normal MIMO systems, as well as for most MIMO systems in general, the situation in which components of the input stochastic vector  $\varphi(t)$  are uncorrelated and have identical spectral densities is quite common. Even if it is not the case, in engineering computations, the real input signals are frequently approximated by statistically independent signals, choosing for them the ‘worst’ spectral density among the available ones. Therefore, we shall always assume that the matrix of input spectral densities  $S_\varphi(j\omega)$  be scalar and equal to  $s_\varphi(\omega)I$ . In such a case, Equation (2.94) transforms into a more simple form:

$$S_f(j\omega) = s_\varphi(\omega)\Phi(j\omega)\Phi^*(j\omega). \tag{2.112}$$

Using the canonical representation of the normal transfer matrix  $\Phi(s)$  via similarity transformation [Equation (1.117)], putting in Equation (1.117)  $s = j\omega$ , and taking into account that the

property  $C^{-1}(j\omega) = C^*(j\omega)$  holds for the unitary modal matrix  $C(j\omega)$ , we obtain (Gasparyan 1986)

$$S_f(j\omega) = C(j\omega) \text{diag} \left\{ \left| \frac{q_i(j\omega)}{1 + q_i(j\omega)} \right|^2 s_\varphi(\omega) \right\} C^*(j\omega), \quad (2.113)$$

from which it follows that the canonical basis of the positive-definite Hermitian matrix  $S_f(j\omega)$  coincides with the canonical basis of the normal system, and the eigenvalues  $s_{f_i}(\omega)$  of the matrix  $S_f(j\omega)$  are

$$s_{f_i}(\omega) = \left| \frac{q_i(j\omega)}{1 + q_i(j\omega)} \right|^2 s_\varphi(\omega), \quad i = 1, 2, \dots, N. \quad (2.114)$$

Then, recalling that the trace of a matrix is equal to the sum of its eigenvalues (Bellman 1970), and based on Equation (2.98), we find the *exact* expression for the mean square value of the output vector magnitude  $|f(t)|$ :

$$D_f = \frac{1}{2\pi} \int_{-\infty}^{+\infty} \text{tr}\{S_f(j\omega)\} d\omega = \frac{1}{2\pi} \sum_{i=1}^N \int_{-\infty}^{+\infty} s_{f_i}(\omega) d\omega = \sum_{i=1}^N D_i, \quad (2.115)$$

where

$$D_i = \frac{1}{2\pi} \int_{-\infty}^{+\infty} \left| \frac{q_i(j\omega)}{1 + q_i(j\omega)} \right|^2 s_\varphi(\omega) d\omega, \quad i = 1, 2, \dots, N \quad (2.116)$$

are the mean square outputs of the SISO characteristic systems. Hence, for normal systems and  $S_\varphi(j\omega) = s_\varphi(\omega)I$ , the mean square value  $D_f$  of the output vector magnitude  $|f(t)|$  is *equal to the sum of the mean square outputs*  $D_i$  of the characteristic systems with stochastic inputs, having the identical spectral density  $s_\varphi(\omega)$ .

A particular interest is the analysis of the statistical accuracy of circulant and anticirculant systems, which also belong to normal systems. As we know, their distinctive feature is the independence of the canonical basis (and the modal matrix  $C$ ) from complex variable  $s$ . Below, we show that for circulant and anticirculant systems, it is possible to obtain not only the mean square value  $D_f$  without any difficulty, but also the canonical representation of the covariance matrix  $P_f$ . Indeed, substituting Equation (2.113) into Equation (2.95) immediately yields

$$P_f = C \text{diag} \left\{ \frac{1}{2\pi} \int_{-\infty}^{+\infty} \left| \frac{q_i(j\omega)}{1 + q_i(j\omega)} \right|^2 s_\varphi(\omega) d\omega \right\} C^* = C \text{diag} \{D_i\} C^*, \quad (2.117)$$

from which we come to the following, final form for  $P_f$ :

$$P_f = T \text{diag}\{D_i\} T^T = T \text{diag}\{D_i\} T^{-1}, \quad (2.118)$$

where  $T$  is the real-valued canonical form of the modal matrix  $C$ .<sup>26</sup>

<sup>26</sup> See Remark 1.7.

Recall that for circulant and anticirculant systems, the CTFs  $q_i(s)$  of characteristic systems can be found analytically for any number of separate channels  $N$ . Note also that in Section 2.4.4, formulae for the evaluation of the mean square outputs  $D_i$  of characteristic systems with *complex-valued* parameters are derived. Therefore, the problem of determining the mean squares  $D_i$  [Equation (2.116)] and, together with them, the canonical representation of the covariance matrix  $P_f$  [Equation (2.118)] proves to be, in principle, no more complicated than in the common SISO case – only the numerical computations become more intensive (allowing for the resources of modern computing aids, the last factor seems to be of little significance).

From Equation (2.118), it also ensues that circulant and anticirculant systems, besides the property common to all normal systems [Equation (2.115)], possess some other specific features. Thus, for instance, since the matrix  $P_f$  [Equation (2.118)] is expressed through  $\text{diag}\{D_i\}$  by means of a similarity transformation, all its eigenvalues are equal to the mean square outputs  $D_i$  of the characteristic systems, and the spectral norm  $\|P_f\|$  is equal to the largest of these mean square outputs. Further, as the matrix of spectral densities  $S_f(j\omega)$  [Equation (2.113)] is circulant (anticirculant),<sup>27</sup> all mean squares of the separate channel outputs  $f_i(t)$  are equal to each other [for  $S_\varphi(j\omega) = s_\varphi(\omega)I$ ], and equal to the *arithmetic average* of  $D_i$ , i.e.

$$E[f_i^2(t)] = P_{fii} = \frac{1}{N} \sum_{k=1}^N D_k = \frac{1}{N} D_f, \quad i = 1, 2, \dots, N. \quad (2.119)$$

This property follows from Equations (2.95), (2.87) and (2.112), taking into account the equality of all diagonal elements of circulant or anticirculant matrices.

In the special and quite significant in practice case of two-dimensional antisymmetrical systems, the CTFs  $q_1(s)$  and  $q_2(s)$  are of the form in Equation (1.166), i.e. are complex conjugate, and the mean square outputs of the characteristic systems are equal to each other:<sup>28</sup>  $D_1 = D_2 = D$ . The real-valued canonical form of the modal matrix has the form  $T = (1/\sqrt{2})I$ , and the covariance matrix  $P_f$  is scalar:  $P_f = DI$ . This implies that for  $S_\varphi(j\omega) = s_\varphi(\omega)I$ , the components of the output vector of two-dimensional antisymmetrical systems are uncorrelated and have the same mean square outputs  $E[f_1^2(t)] = E[f_2^2(t)]$ , equal to the mean square outputs  $D$  of characteristic systems, and the mean square value of the magnitude  $|f(t)|$  is equal to  $2D$ .

### 2.4.3 Statistical accuracy of uniform MIMO systems

The results of two preceding sections remain, of course, valid for uniform systems. At the same time, the identity of separate channels allows the development of a specific technique for evaluating the upper estimate of the mean square value  $D_f$  [Equation (2.108)] for uniform systems with an arbitrary (not normal) matrix of cross-connections  $R$  (Gasparyan 1986). To a certain extent, that technique is closer to the conventional technique for analysing the statistical accuracy of SISO systems (Newton *et al.* 1957; Tsyppkin 1977).

In the case of uniform systems, the same inequality as in Equation (2.110) holds for the Schmidt norm of the transfer matrix  $\Phi(j\omega)$ , where the condition number  $\nu[C(j\omega)]_S$  is constant and does not depend on  $\omega$ , i.e.,  $\nu[C(j\omega)]_S = \nu[C]_S = \text{const}$ , and  $q_i(j\omega) = \lambda_i w(j\omega)$ .

<sup>27</sup> This ensues from the fact that the product of two circulant (anticirculant) matrices also gives a circulant (anticirculant) matrix.

<sup>28</sup> See Section 2.4.4.

Taking this into account, substituting Equation (2.110) into Equation (2.108), and assuming for simplicity that  $S_\varphi(j\omega) = s_\varphi(\omega)I$ , we obtain

$$D_f \leq \frac{\nu^2[C]_S}{2\pi} \int_{-\infty}^{+\infty} \left\| \text{diag} \left\{ \frac{\lambda_i w(j\omega)}{1 + \lambda_i w(j\omega)} \right\} \right\|_S^2 s_\varphi(\omega) d\omega. \quad (2.120)$$

The square of the Schmidt norm of the diagonal matrix in the integrand of Equation (2.120) is equal to

$$\left\| \text{diag} \left\{ \frac{\lambda_i w(j\omega)}{1 + \lambda_i w(j\omega)} \right\} \right\|_S^2 = \sum_{i=1}^N \left| \frac{\lambda_i w(j\omega)}{1 + \lambda_i w(j\omega)} \right|^2. \quad (2.121)$$

Therefore, instead of Equation (2.120), we can write

$$D_f \leq \nu^2[C]_S \sum_{i=1}^N D_i, \quad (2.122)$$

where

$$D_i = \frac{1}{2\pi} \int_{-\infty}^{+\infty} \left| \frac{\lambda_i w(j\omega)}{1 + \lambda_i w(j\omega)} \right|^2 s_\varphi(\omega) d\omega, \quad i = 1, 2, \dots, N \quad (2.123)$$

are the mean square outputs of the characteristic systems whose input stochastic signals are uncorrelated and have the same spectral density  $s_\varphi(\omega)$ .

Thus, the inequality in Equation (2.122) gives an upper estimate for the mean square value  $D_f$  of the uniform system with an arbitrary matrix of cross-connections  $R$ , expressed directly through the mean square outputs of characteristic systems. That estimate is somewhat overstated as compared with the general estimate in Equation (2.111), since, in Equation (2.122), an additional inequality is used [Equation (2.110)].<sup>29</sup> However, it is rather convenient for the practical examination of the uniform system accuracy, since it allows analytical solutions with the help of standard integrals derived in the next section. Besides, the estimate in Equation (2.122) visually reflects the relationship between properties of the matrix  $R$  and statistical accuracy of the uniform system, and, what is very significant, shows that the upper boundary of the mean square value  $D_f$  is directly proportional to the square of the condition number  $\nu[C]_S$ , i.e. that boundary increases as the degree of the canonical basis non-orthogonality increases.<sup>30</sup>

**Remark 2.4** Equation (2.108) for the mean square value  $D_f$  of general MIMO systems is based on the *frequency-domain* concepts, and, in practical computations, it presumes simple operations with the transfer matrix  $\Phi(j\omega)$ , whose order is determined by the number of channels  $N$ . In the cases of uniform and normal systems, the task frequently reduces to a set of one-dimensional tasks. In any case, when using the described techniques, *no practical problems*

<sup>29</sup> For that very reason, we cannot pass in Equation (2.122) to a strict equality for  $S_\varphi(\omega) = s_\varphi(\omega)I$ .

<sup>30</sup> Taking the square root of both sides of the inequality in Equation (2.122), we obtain that the *mean square deviation* of the magnitude  $|f(t)|$  is *directly proportional* to the condition number  $\nu[C]_S$ .

*emerge* connected with the dimension of the MIMO system. In particular, GUI *ControlSysCAD*, which provides the numerical algorithms for the approaches described above, actually enables the user to investigate the statistical accuracy of MIMO systems with any number of channels.

In the application packages of the leading firms, this task is usually solved via the state-space representation of MIMO (and SISO) systems. Thus, for instance, in the package *The Control Systems Toolbox* in MATLAB, there is a special function, *covar*, that evaluates the covariance matrix of the system with stationary stochastic inputs in the form of white noise with given intensity  $W$  (or *intensity matrix*, for  $N > 1$ ). And, although the mathematical model of the system can be given in any available form of *lti*-objects, that model is further transformed to state-space form, i.e. to the form  $dx/dt = Ax + Bu$ , and the output covariance matrix  $P$  is evaluated with the help of the algebraic *Lyapunov equation* (Bryson and Ho 1969):

$$AP + PA^T + BWB^T = \mathbf{0}. \quad (2.124)$$

Here, the dimension of the problem is determined by the dimension of the state vector  $x$ , which is usually much larger than the number  $N$  of separate channels. This can bring about certain computational difficulties, even in investigating MIMO systems of comparatively low order (we mean the number of channels) if the dimension of  $x$  exceeds several tens.

**Remark 2.5** Below, we discuss the assumption about zero means of the input stochastic vector  $\varphi(t)$  (see Section 2.4.1). In Section 2.2, when analysing the dynamical accuracy of MIMO systems under sinusoidal inputs, the signal  $\varphi(t)$  was specified as a periodical time function of frequency  $\omega$ , and, in Section 2.3, we assumed  $\varphi(t)$  to be a slowly changing deterministic function. Evidently, under the nonzero means of the input stochastic signals, the latter can be represented as a sum of two components:  $\varphi(t) = \varphi_1(t) + \varphi_2(t)$ , where  $\varphi_1(t)$  is a deterministic time function (the mathematical expectation of the signal  $\varphi(t)$ ), and  $\varphi_2(t)$  is a stationary stochastic function with  $E[\varphi_2(t)] = 0$ . Then, based on the *superposition principle*, the vector component of the MIMO system error that is caused by the nonzero vector  $\varphi_1(t)$  can be found with the help of the techniques developed in Sections 2.2 and 2.3. As for the stochastic component of the error vector, it can be estimated using the results presented in this section.

Although this issue, by itself, does not present any difficulty, such a free interpretation of the nature and character of the input signal may cause the reader some confusion. This gives us an opportunity to discuss shortly how the *accuracy* of control systems in real engineering applications is analysed. It is also important for that reason that in Section 2.5, we shall present one of the possible approaches to the MIMO systems *design*, where a problem in determining the parameters of the regulator that provide the *specified* system accuracy necessarily arises.

The point is that the *steady-state* dynamical error of any automatic control system (we do not touch here on *transient* responses) is determined in practice by a number of factors. Thus, for example, in Figure 2.21, the block diagram of one channel of a telescope guidance system is shown, in which arrows symbolically indicate some (but not all) possible error sources (Gasparyan 1976; Gasparyan *et al.* 1985). To these sources belong: random noises at the stellar sensors outputs, voltage drops on the electric brushes of the drive motor (if dc motors are used), coulomb friction in the reduction gears, dead bands in the power amplifiers, instrumental errors of the drive and gear, the influence of atmospheric turbulence  $\psi_1(t)$  and wind gusts  $\psi_2(t)$  (for the earth-based telescopes), and many others. It is quite difficult to calculate exactly the joint influence of all these factors, as some of the latter have a nonlinear or random character. Thus,

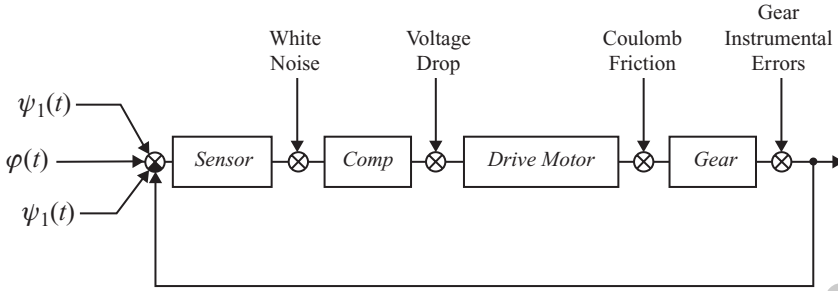


Figure 2.21 Possible error sources of the telescope guidance system.

the instrumental errors of the gear can be represented as a sum of harmonic components:

$$\gamma_{In}(t) = \sum_{k=1}^n B_k \sin(k\Omega(t) + \theta_k), \quad (2.125)$$

where these components are nonlinear functions of the rotation angle  $\Omega(t)$  of the output shaft, and the amplitudes  $B_k$  and phases  $\theta_k$  are random quantities, depending on the accuracy of the manufacturing tooth gears (Gasparyan and Arutyunyan 1981). The input signal of the system  $\varphi(t)$  can be approximated by the function

$$\varphi(t) = v_o + v_1 t + v_2 t^2 + F \sin \omega t, \quad (2.126)$$

where the periodical term  $F \sin \omega t$  reflects, for example, elastic vibrations of solar panels (for the space-borne telescopes), and so on.

Therefore, at the initial stages of the design, it is usually assumed that the influence of all main error sources can be analysed, as a first approximation, independently, based on the linear model of the system, in which such factors as dead bands, frictions, instrumental errors, random noises and so on are regarded as external disturbances. This enables the engineer to estimate the expected accuracy by means of the techniques developed in this chapter or similar techniques of the classical control theory. Having determined, on the basis of such an approach, the required parameters of the regulator, the designer can examine the accuracy of the developed system further with the help of other, more enhanced methods, which provide more adequate and complete calculation of the total error. In particular, it can be done by computer-aided simulation, with the subsequent correction (if needed) of the previously determined regulator parameters.

**Example 2.10** Let us apply Equation (2.122) to the two-dimensional guidance system of Example 2.6, assuming that the separate channels inputs are white noises with unit intensity, i.e.  $s_\varphi(\omega) = I$ . The angles  $\alpha_1$  and  $\alpha_2$  are taken as  $\alpha_1 = 30^\circ$ ,  $\alpha_2 = 20^\circ$ , for which the matrix of cross-connections  $R$  [Equation (1.60)] has two complex conjugate eigenvalues. The calculation in Equation (2.122) gives the following values of the mean square values and the condition number of the modal matrix:  $D_1 = D_2 = 12.998$ ,  $v[C]_S = 2.0443$  and  $D_f \leq 108.6383$ . It is interesting to compare these results with the exact value of  $D_f$  obtained by the technique in Section 2.4.1. The corresponding curves are shown in Figure 2.22, in which the exact (since the matrix of spectral densities of the input noises is scalar) value  $D_f = 26.3931$  is also given. The

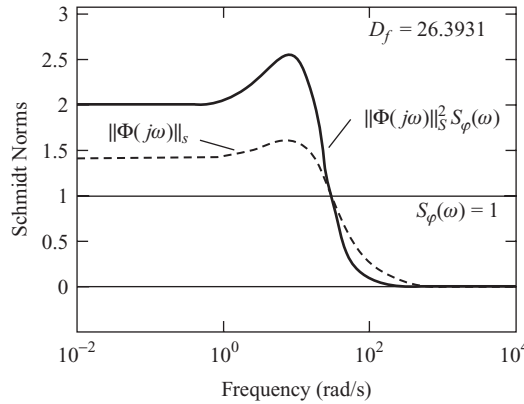


**Figure 2.22** Determination of the exact value of the mean square value  $D_f$ .

comparison of the exact value of  $D_f$  with the above estimate shows that the actual mean square value is about four times smaller than the upper boundary obtained by Equation (2.122). The main reason for such a difference is that, as was mentioned in Section 2.4.1, the Schmidt norm gives overestimated, as compared with the spectral norm, values for the condition number. In our example, the condition number  $\nu[C]_S = 2.0443$  indicates that the canonical basis is rather close to orthogonal (in which case, it would be equal to two), and the sum of mean square outputs of the characteristic systems is 25.9956, i.e. is quite close to the exact value of  $D_f$ . However, the multiplication of that sum by the square  $\nu^2[C]_S = 4.1792$  gives the estimate obtained with the four-fold margin.

This example demonstrates that the estimate in Equation (2.122) is appropriate to use in the initial design stages, when it is necessary to compare the accuracy of the same uniform system with different variants of correction. The final analysis of statistical accuracy is recommended to be carried out based on the general technique described in Section 2.4.1.

### 2.4.4 Formulae for mean square outputs of characteristic systems

Investigating the statistical accuracy of uniform and normal MIMO systems, engineers or researchers frequently have to evaluate integrals of the form<sup>31</sup>

$$J_n = \frac{1}{2\pi j} \int_{-j\infty}^{+j\infty} \frac{M(s) \tilde{M}(-s)}{D(s) \tilde{D}(-s)} ds, \quad n = 1, 2, \dots, \quad (2.127)$$

where

$$M(s) = \sum_{k=0}^{n-1} m_k s^k, \quad D(s) = \sum_{k=0}^n d_k s^k \quad (2.128)$$

<sup>31</sup> The wavy line in Equation (2.127) indicates the complex conjugation of the polynomial coefficients.

are polynomials of degrees  $n - 1$  and  $n$  with *complex-valued* coefficients  $m_k$  and  $d_k$ , and it is assumed that the roots of the polynomial  $D(s)$  are located in the open left half-plane. Mean square outputs of the closed-loop characteristic systems are described, in particular, by the integrals in Equation (2.127). The analytical method of evaluation of  $J_n$  [Equation (2.127)] is an extension of the well known method (Newton *et al.* 1957) exposed further to the case of SISO systems with complex parameters (Gasparyan 1986).

Note, first, that for the purely imaginary  $s$  ( $s = j\omega$ ) in Equation (2.127), we have

$$\tilde{M}(-s) = \sum_{k=0}^{n-1} \tilde{m}_k(-s)^k, \quad \tilde{D}(-s) = \sum_{k=0}^n \tilde{d}_k(-s)^k. \quad (2.129)$$

The integrand in Equation (2.127) can be represented as a sum of two complex conjugate fractions

$$\frac{M(s) \tilde{M}(-s)}{D(s) \tilde{D}(-s)} = \frac{A(s)}{D(s)} + \frac{\tilde{A}(-s)}{\tilde{D}(-s)}, \quad (2.130)$$

where  $A(s) = \sum_{k=0}^{n-1} a_k s^k$  is a polynomial of degree  $n - 1$  with complex coefficients  $a_k$ . The integral  $J_n$  [Equation (2.127)], allowing for Equation (2.130), has the form

$$J_n = \frac{1}{2\pi j} \int_{-j\infty}^{+j\infty} \frac{A(s)}{D(s)} ds + \frac{1}{2\pi j} \int_{-j\infty}^{+j\infty} \frac{\tilde{A}(-s)}{\tilde{D}(-s)} ds = 2\text{Re} \left\{ \frac{1}{2\pi j} \int_{-j\infty}^{+j\infty} \frac{A(s)}{D(s)} ds \right\}, \quad (2.131)$$

i.e. is equal to the doubled real part of the inverse Laplace transform of  $A(s)/D(s)$  evaluated for  $t = 0$ . Since the inverse transform of the time function  $x(t)$ , as  $t \rightarrow 0$ , is equal to half its value, as  $t$  tends to zero from the right (Newton *et al.* 1957), based on *the initial value theorem* (Churchill *et al.* 1974), we obtain

$$J_n = \text{Re} \left\{ \lim_{t \rightarrow 0} L^{-1} \left[ \frac{A(s)}{D(s)} \right] \right\} = \text{Re} \left\{ \lim_{s \rightarrow \infty} \frac{s A(s)}{D(s)} \right\} = \text{Re} \left\{ \frac{a_{n-1}}{d_n} \right\}. \quad (2.132)$$

As follows from Equation (2.132), to evaluate integrals [Equation (2.127)], we need to find the real part of the ratio of the coefficients  $a_{n-1}$  and  $d_n$ , where the coefficient  $d_n$  is known. Below, it will be shown that the necessary condition for the representation in Equation (2.130) is the equality of arguments of the complex numbers  $a_{n-1}$  and  $d_n$ , i.e.

$$\frac{\text{Im}\{a_{n-1}\}}{\text{Re}\{a_{n-1}\}} = \frac{\text{Im}\{d_n\}}{\text{Re}\{d_n\}}. \quad (2.133)$$

In particular, if  $d_n$  is a real number, then  $a_{n-1}$  is also real. Taking into account Equation (2.133), instead of Equation (2.132), we have

$$J_n = \text{Re} \left\{ \frac{a_{n-1}}{d_n} \right\} = \frac{|a_{n-1}|}{|d_n|} = \frac{\text{Re}\{a_{n-1}\}}{\text{Re}\{d_n\}}. \quad (2.134)$$

Rewrite Equation (2.130) in the following form:

$$A(s)\tilde{D}(-s) + \tilde{A}(-s)D(s) = M(s)\tilde{M}(-s). \quad (2.135)$$

The expression  $A(s)\tilde{D}(-s)$  in Equation (2.135) has the form

$$A(s)\tilde{D}(-s) = \left[ \sum_{i=0}^{n-1} a_i s^i \right] \left[ \sum_{k=0}^{n-1} \tilde{d}_k (-s)^k \right] = \sum_{i=0}^{n-1} \sum_{k=0}^n (-1)^k a_i \tilde{d}_k s^{i+k}. \quad (2.136)$$

Combining the terms with the same degrees of  $s$ , we get

$$A(s)\tilde{D}(-s) = \sum_{r=0}^{2n-1} E_r s^r, \quad (2.137)$$

where

$$E_r = \begin{cases} \sum_{i=0}^r (-1)^{r-i} a_i \tilde{d}_{r-i} & (0 \leq r \leq n-1) \\ \sum_{i=r-n}^{n-1} (-1)^{r-i} a_i \tilde{d}_{r-i} & (n \leq r \leq 2n-1) \end{cases}. \quad (2.138)$$

From Equation (2.138), noticing that the second term on the left-hand side of Equation (2.135) is complex conjugate with the first one, and allowing for Equation (2.137), we obtain

$$\tilde{A}(-s)D(s) = \sum_{r=0}^{2n-1} (-1)^r \tilde{E}_r s^r. \quad (2.139)$$

The right-hand part of Equation (2.135) can be expressed as

$$M(s)\tilde{M}(-s) = \left[ \sum_{i=0}^{n-1} m_i s^i \right] \left[ \sum_{k=0}^{n-1} \tilde{m}_k (-s)^k \right] = \sum_{i=0}^{n-1} \sum_{k=0}^{n-1} (-1)^k m_i \tilde{m}_k s^{i+k}, \quad (2.140)$$

from which, combining the terms, we have

$$M(s)\tilde{M}(-s) = \sum_{r=0}^{2n-2} 2C_r s^r, \quad (2.141)$$

where

$$2C_r = \begin{cases} \sum_{k=0}^r (-1)^k m_k \tilde{m}_{r-k} & (0 \leq r \leq n-1) \\ \sum_{k=r-n+1}^{n-1} (-1)^k m_k \tilde{m}_{r-k} & (n \leq r \leq 2n-2) \end{cases}. \quad (2.142)$$

For, *even*  $r$  in Equation (2.142),

$$2C_r = \begin{cases} (-1)^{r/2}|m_{r/2}|^2 + 2\text{Re} \left\{ \sum_{\substack{k=0 \\ k \neq r/2}}^r (-1)^k m_k \tilde{m}_{r-k} \right\}, & (0 \leq r \leq n-1) \\ (-1)^{r/2}|m_{r/2}|^2 + 2\text{Re} \left\{ \sum_{\substack{k=r-n+1 \\ k \neq r/2}}^{n-1} (-1)^k m_k \tilde{m}_{r-k} \right\} & (n \leq r \leq 2n-2) \end{cases}, \quad (2.143)$$

i.e.  $2C_r$  are real numbers.

For *odd*  $r$ ,

$$2C_r = \begin{cases} j2 \text{Im} \left\{ \sum_{k=0}^r (-1)^k m_k \tilde{m}_{r-k} \right\}, & (0 \leq r \leq n-1) \\ j2 \text{Im} \left\{ \sum_{k=r-n+1}^{n-1} (-1)^k m_k \tilde{m}_{r-k} \right\} & (n \leq r \leq 2n-2) \end{cases}, \quad (2.144)$$

i.e. the numbers  $2C_r$  are purely imaginary.

Substituting Equations (2.137), (2.139) and (2.141) into Equation (2.135) yields

$$\sum_{r=0}^{2n-1} \frac{E_r + (-1)^r E_r}{2} s^r = \sum_{r=0}^{2n-2} C_r s^r. \quad (2.145)$$

Equating in Equation (2.145) the coefficients with the same degrees of  $s$ , we obtain, for even  $r$ , the following system of  $n$  algebraic equations:

$$\text{Re}\{E_r\} = C_r, \quad r = 0, 2, \dots, 2n-2, \quad (2.146)$$

where  $C_r$  are found from Equation (2.143).

Analogously, from Equation (2.145), we can get, for odd  $r$ , another system of  $n$  algebraic equations:

$$\text{Im}\{E_r\} = \frac{1}{j} C_r, \quad r = 1, 3, \dots, 2n-1, \quad (2.147)$$

where  $C_r$  are found from Equation (2.144).

Note that the coefficient  $C_{2n-1}$  in Equation (2.147) is identically equal to zero, since the degree of the polynomial  $M(s)$  [Equation (2.128)] cannot exceed  $n-1$ . As a result, the last equation in Equation (2.147),

$$\text{Im}\{E_{2n-1}\} = \text{Im}\{a_{n-1} \tilde{d}_n\} = \text{Im}\{a_{n-1}\} \text{Re}\{d_n\} - \text{Im}\{d_n\} \text{Re}\{a_{n-1}\} = 0 \quad (2.148)$$

gives the necessary condition in Equation (2.133) imposed on the unknown coefficient  $a_{n-1}$ .

Thus, we have obtained a system in Equations (2.146) and (2.147) of  $2n$  linear algebraic equations with  $2n$  unknowns  $\text{Re}\{a_i\}$  and  $\text{Im}\{a_i\}$  ( $i = 0, 1, \dots, n-1$ ). Solving that system and

determining the value of  $\text{Re}\{a_{n-1}\}$ , we shall find the required value of the integral  $J_n$  [Equation (2.127)]. If we denote by  $X = \text{Re}\{X\} + j\text{Im}\{X\}$  an  $n$ -dimensional complex-valued vector with components  $a_0, -a_1, \dots, (-1)^{n-1}a_{n-1}$ , and, by  $c_1$  and  $c_2$ , the  $n$ -dimensional real vectors composed of the coefficients  $C_r$  [Equation (2.143)] for even  $r$  and the coefficients  $(1/j)C_r$  for odd  $r$  [Equation (2.144)], then Equations (2.146) and (2.147) can be written in the equivalent matrix form:

$$\text{Re}\{D_1 X\} = c_1, \quad \text{Im}\{D_2 X\} = -c_2, \quad (2.149)$$

where the matrices  $D_1$  and  $D_2$  depend on the coefficients  $\tilde{d}_i$  complex conjugate to the coefficients  $d_i$  of the polynomial  $D(s)$  [Equation (2.128)].

Analyzing Equation (2.146) for odd  $n$ , we have

$$D_1 = \begin{pmatrix} \tilde{d}_0 & 0 & \cdots & 0 \\ \tilde{d}_2 & \tilde{d}_1 & \cdots & 0 \\ \vdots & \vdots & \cdots & \vdots \\ \tilde{d}_{n-1} & \tilde{d}_{n-2} & \cdots & \tilde{d}_0 \\ 0 & \tilde{d}_n & \cdots & \tilde{d}_2 \\ \vdots & \vdots & \ddots & \vdots \\ 0 & 0 & \cdots & \tilde{d}_{n-1} \end{pmatrix}, \quad D_2 = \begin{pmatrix} \tilde{d}_1 & \tilde{d}_0 & \cdots & 0 \\ \tilde{d}_3 & \tilde{d}_2 & \cdots & 0 \\ \vdots & \vdots & \cdots & \vdots \\ \tilde{d}_{n-2} & \tilde{d}_{n-3} & \cdots & 0 \\ \tilde{d}_n & \tilde{d}_{n-1} & \cdots & \tilde{d}_1 \\ \vdots & \vdots & \ddots & \vdots \\ 0 & 0 & \cdots & \tilde{d}_n \end{pmatrix}. \quad (2.150)$$

For even  $n$ , the matrices  $D_1$  and  $D_2$  have the form

$$D_1 = \begin{pmatrix} \tilde{d}_0 & 0 & \cdots & 0 \\ \tilde{d}_2 & \tilde{d}_1 & \cdots & 0 \\ \vdots & \vdots & \cdots & \vdots \\ \tilde{d}_n & \tilde{d}_{n-1} & \cdots & \tilde{d}_1 \\ 0 & 0 & \cdots & \tilde{d}_3 \\ \vdots & \vdots & \ddots & \vdots \\ 0 & 0 & \cdots & \tilde{d}_{n-1} \end{pmatrix}, \quad D_2 = \begin{pmatrix} \tilde{d}_1 & \tilde{d}_0 & \cdots & 0 \\ \tilde{d}_3 & \tilde{d}_2 & \cdots & 0 \\ \vdots & \vdots & \cdots & \vdots \\ \tilde{d}_{n-1} & \tilde{d}_{n-2} & \cdots & \tilde{d}_2 \\ \tilde{d}_n & \tilde{d}_{n-1} & \cdots & \tilde{d}_1 \\ \vdots & \vdots & \ddots & \vdots \\ 0 & 0 & \cdots & \tilde{d}_n \end{pmatrix}. \quad (2.151)$$

Equation (2.149) can be represented through the real and imaginary parts of the matrices  $D_1$ ,  $D_2$  and vector  $X$  as

$$\text{Re}\{D_1\}\text{Re}\{X\} - \text{Im}\{D_1\}\text{Im}\{X\} = c_1 \quad (2.152)$$

$$\text{Im}\{D_2\}\text{Re}\{X\} + \text{Re}\{D_2\}\text{Im}\{X\} = -c_2. \quad (2.153)$$

Evaluating the vector  $\text{Im}\{X\}$  from Equation (2.153) and substituting it into Equation (2.152) yields, after some simple transformations, the matrix equation

$$N\text{Re}\{X\} = \ell, \quad (2.154)$$

where the matrix  $N$  and vector  $\ell$  are

$$N = \text{Re}\{D_1\} + \text{Im}\{D_1\}[\text{Re}\{D_2\}]^{-1}\text{Im}\{D_2\} \quad (2.155)$$

$$\ell = c_1 - \text{Im}\{D_1\}[\text{Re}\{D_2\}]^{-1}c_2. \quad (2.156)$$

From Equation (2.154), using Cramer's rule (Gantmacher 1964), we find

$$\text{Re}\{a_{n-1}\} = (-1)^{n-1} \frac{\Delta_n}{\Delta}, \quad (2.157)$$

where  $\Delta$  is the determinant of the matrix  $N$  and  $\Delta_n$  is the determinant of the matrix obtained from  $N$  by replacing the last column by the vector  $\ell$  [Equation (2.156)]. This allows the required value of the integral  $J_n$  [Equation (2.127)] to be computed via the expression

$$J_n = \frac{\text{Re}\{a_{n-1}\}}{\text{Re}\{d_n\}} = \frac{(-1)^{n-1} \Delta_n}{\Delta \text{Re}\{d_n\}}. \quad (2.158)$$

If all coefficients of the polynomials  $M(s)$  and  $D(s)$  in Equation (2.128) are real numbers, then Equation (2.158) passes to the well known formula of the classical control theory (Newton *et al.* 1957). Note also that the characteristic systems with complex conjugate coefficients have the same mean square outputs  $D_i$ , which can readily be seen from the form of Equation (2.127).

When analysing statistical accuracy of uniform systems, it is necessary to calculate the mean square outputs  $D_i$  [Equation (2.123)], where  $\lambda_i$  are generally complex numbers. The spectral density  $s_\varphi(\omega)$  in Equation (2.123) can be represented in the form (Lifshits *et al.* 1974)

$$s_\varphi(\omega) = \frac{G_{11}(j\omega)}{V_{11}(j\omega)} \frac{G_{11}(-j\omega)}{V_{11}(-j\omega)}. \quad (2.159)$$

Then, if we represent the transfer function of the uniform system channels as a quotient of polynomials [Equation (1.139)], i.e. in the form  $w(s) = M(s)/D(s)$ , then the integral in Equation (2.123) can be written as follows:

$$D_i = \frac{|\lambda_i|^2}{2\pi} \int_{-\infty}^{+\infty} \frac{H(j\omega)}{F(j\omega)} \frac{H(-j\omega)}{\bar{F}(-j\omega)} d\omega, \quad (2.160)$$

where the polynomials  $H(j\omega) = M(j\omega)G_{11}(j\omega)$  and  $F(j\omega) = [D(j\omega) + \lambda_i M(j\omega)]V_{11}(j\omega)$  have real and complex coefficients, respectively. Consequently, the numerator polynomial in Equation (2.123) always has real coefficients. Therefore, the vector  $c_2$  in Equation (2.149) composed of the coefficients  $C_r$  [Equation (2.144)] is identically equal to zero vector, and the vector  $\ell$  [Equation (2.156)] is equal to  $c_1$ . This considerably simplifies calculations.

**Example 2.11** As an example, below, we give analytical expressions for the integrals  $J_1$  and  $J_2$  in the case of uniform systems subjected to the input white noises with the constant spectral density  $s_\varphi(\omega) = N_\sigma$ . The numerator and denominator polynomials of the transfer function  $w(s) = M(s)/D(s)$  in Equation (2.123) are assumed to be of the form<sup>32</sup>

$$M(s) = \sum_{k=0}^{n-1} m_k s^k, \quad D(s) = \sum_{k=0}^n d_k s^k. \quad (2.161)$$

<sup>32</sup> One should not confuse these designations with those in Equation (2.128).

Using the above expressions in Equations (2.154)–(2.158), we find

$$J_1 = \frac{|\lambda_i|^2 m_0^2 N_o}{2d_1(d_0 + \text{Re}\{\lambda_i\}m_0)} \quad (2.162)$$

and

$$J_2 = \frac{|\lambda_i|^2 N_o \{[(d_0 + \text{Re}\{\lambda_i\}m_0)(d_1 + \text{Re}\{\lambda_i\}m_1) + (\text{Im}\{\lambda_i\})^2 m_0 m_1] m_1^2 + d_2 m_0^2 (d_1 + \text{Re}\{\lambda_i\}m_1)\}}{2d_2 \{ (d_0 + \text{Re}\{\lambda_i\}m_0)(d_1 + \text{Re}\{\lambda_i\}m_1)^2 + (\text{Im}\{\lambda_i\})^2 m_0 [m_1(d_1 + \text{Re}\{\lambda_i\}m_1) - d_2 m_0] \}} \quad (2.163)$$

As is evident from these formulae, the same mean square outputs of the associated characteristic systems correspond to the complex conjugate values of  $\lambda_i$  and  $\lambda_{i+1} = \bar{\lambda}_i$ , since all coefficients in  $J_1$  and  $J_2$  depend on the *squares* of the imaginary parts  $\text{Im}\{\lambda_i\}$ . This confirms the above conclusion about the equality of mean square outputs of the characteristic systems with complex conjugate coefficients. If the eigenvalues  $\lambda_i$  of the cross-connections matrix  $R$  are real, then the expressions for  $J_1$  and  $J_2$  coincide with those well known in the classical control theory (Newton *et al.* 1957).

## 2.5 DESIGN OF LINEAR MIMO SYSTEMS

The notion *design* of an automatic control system is so capacious and many-sided that even a superficial and short description of all the aspects related to it does not seem to be possible within one section or even one chapter. Below, we shall briefly discuss an approach to the MIMO systems design, which actually allows reducing the problem to a *one-dimensional* task, irrespective of the real number of separate channels  $N$ . This allows, to a certain extent, all those ideas and techniques that are widely used in control engineering for the design of usual SISO systems to be applied to multivariable systems. Further, we shall suppose that the reader is familiar, within the classical control theory framework, with the principal design methods of such systems (Evans 1954; Horowitz 1963; Ogata 1970; Kuo 1995; Truxal 1955; Bessekerski and Popov 2002; Bösgra *et al.* 2004, etc.). We also have to come to a clear agreement about the content that we put into the word *design* of MIMO systems.<sup>33</sup> Here, we shall adhere to the most commonly (but not the only) used and plain scheme, in which, under the system design, is presumed the determination of a *matrix regulator (controller)*  $K(s)$ , which is incorporated into the system *in series* with the *given plant* described by a transfer matrix  $W(s)$  (Figure 2.23). The destination of the regulator consists in providing the required performance indices of the *closed-loop* MIMO system.

Before proceeding, we shall give a short review of those design methods of MIMO systems which are close in spirit or immediately adjacent to the described further approach. First of all, in this respect, one should single out the methods which, somewhat conventionally, can be united under the general name (or term) *decentralized control* (Skogestad and Postlethwaite 2005; Hovd and Skogestad 1994, etc.). Usually, the decentralized control presumes introducing into the MIMO system a *diagonal* regulator  $K(s) = \text{diag} \{k_i(s)\}$ , where various procedures and techniques for the design of the *individual* regulators of each channel  $k_i(s)$  ( $i = 1, 2, \dots, N$ )

<sup>33</sup> Sometimes, we shall also use the word *synthesis*, considering it equivalent in this context to the word *design*.

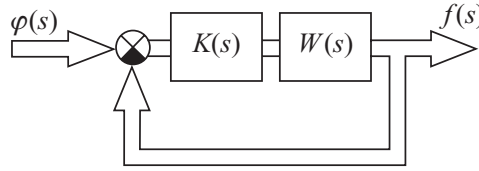


**Figure 2.23** Linear general MIMO system with the matrix regulator  $K(s)$ .

are used. The principle of decentralized control is widely used in many real control systems, particularly in chemical process control, the steel industry and many other applications, where as the diagonal regulators are frequently used PID (*Proportional-Integral-Derivative*) regulators (Ziegler and Nichols 1942; Shinsky 1988; Åström and Hägglund 1995). Ease of practical implementation and tuning, simple and convenient maintenance, etc. are usually attributed as advantages of decentralized control. In the simplest (historically, probably the first) variant, the design of the scalar regulators  $k_i(s)$  is accomplished by the standard techniques of the classical control, and the cross-connections are regarded as external disturbances. Naturally, the efficiency of such an approach substantially depends on the *level* (intensity) of the cross-connections, and, in the case of *weak* couplings, decentralized control can give sufficiently acceptable results. We emphasize once more that in this case, the channels are actually designed as *independent SISO systems*. In the last few decades, many new effective and powerful methods, which are based on the achievements of the modern control theory, particularly on the robust theory, optimal control theory, etc. have been proposed. However, we do not intend to review or analyse all these methods, as it will lead the reader far away from our goal.<sup>34</sup> In any case, the chief issue for us, here, is that the structure of the regulator is assigned *a priori* and has *diagonal* form.

If the cross-connections among the channels are so intensive that the desired performance of the MIMO system cannot be achieved by means of the diagonal regulator, then they resort to a more complicated scheme, which ultimately can also be referred to as a kind of decentralized control. The case in point is a double-step procedure, in which, at the first step, a preliminary matrix regulator  $K_1(s)$  intended for minimization (ideally, full compensation) of the cross-connections<sup>35</sup> is introduced into the MIMO system, and, at the second step, a *diagonal* regulator  $K(s) = \text{diag}\{k_i(s)\}$  is designed that accomplishes the above concept of decentralized control (Figure 2.24). Essentially, in such a scheme, the initial plant  $W(s)$  as if was replaced by a new plant  $W_1(s)$  which would be closer (by the intensities of cross-connections) to the diagonal form.<sup>36</sup> Since the ideal compensation of *dynamical* cross-connections is impossible, in practice, different variants of *partial* compensation are used, in which the following possible cases are usually distinguished (Skogestad and Postlethwaite 2005):

1. *Steady-state (static) decoupling*. The *static* compensator  $K_1(s) = K_1$  in Figure 2.24 is chosen so as to compensate the cross-connections at zero frequency, i.e.  $K_1 = W^{-1}(0)$  (for the plants of *type* one and higher, the integrators are disregarded).

<sup>34</sup> The interested reader is referred, for example, to Hovd and Skogestad (1994).

<sup>35</sup> Such a *compensating* regulator is often called the *decoupling* regulator (Skogestad and Postlethwaite 2005).

<sup>36</sup> As another kind of the compensating regulator, sometimes it is considered a regulator that reduces the resultant transfer matrix  $W_1(s)$  in Figure 2.24 to *triangular* form.

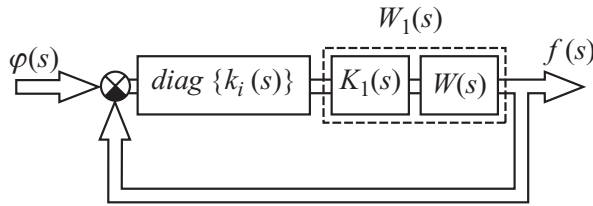


Figure 2.24 MIMO system with the decoupling and diagonal regulators.

2. *Approximate decoupling at a given frequency  $\omega_o$ .* The static compensator is selected so that the transfer matrix  $W_1(s)$  in Figure. 2.24 is at the frequency  $\omega_o$  as close as possible to diagonal form. Usually, towards that end, the complex matrix  $K_1 = W^{-1}(j\omega_o)$  is evaluated, and then it is approximated by a real-valued matrix.
3. *Dynamic decoupling in a given frequency range  $[\omega_1, \omega_2]$ .* In this case, the compensator  $K_1(s)$  is *dynamical*, and is chosen so as to minimize the level of cross-connections over the finite frequency range  $[\omega_1, \omega_2]$ .

The merits of decentralized control have been pointed out earlier. However, if its application demands introducing a compensating regulator in any of the above forms, then, in principle, it makes the system more complicated, since it requires the introduction of *artificial* couplings among the channels. Note that the blocks  $diag\{k_i(s)\}$  and  $K_1(s)$  in Figure 2.24 can be accomplished as a united block  $K(s) = K_1(s)diag\{k_i(s)\}$ , but, in such a case, the possibility of simple tuning of the regulators  $k_i(s)$  in the separate (direct) channels of the MIMO system is lost.

Hence, in both of the discussed variants of the decentralized control, a *diagonal* regulator  $diag\{k_i(s)\}$  is introduced in the MIMO system, whose design is carried out by the classical or other special methods. The complete compensation of cross-connections by means of a decoupling regulator  $K_1(s)$  is practically unrealizable, and, in real MIMO systems, more or less intensive cross-connections will always exist. Note that the well known methods presuming *diagonal-dominance* of the resultant transfer matrix of the open-loop system serve as a theoretical basis for the stability analysis of MIMO systems with *weak* cross-couplings.<sup>37</sup> These methods are based on the various criteria of localization of eigenvalues and probably the most popular in the multivariable control theory are the so-called *Gershgorin's circles* (Marcus and Minc 1992). The methods mentioned allow rigorous investigating, via the transfer functions of the direct channels (diagonal elements of the open-loop transfer matrix  $W(s)$ ), of the stability of the diagonally dominant MIMO systems<sup>38</sup> with the help of a special modification of the Nyquist criterion (Rosenbrock 1969).

Finally, we cannot pass over another undoubted (although having rather psychological context) merit of the very idea of the decentralized control in its 'classical' interpretation.

<sup>37</sup> A square matrix  $A = \{a_{ij}\}$  is called *diagonally dominant* if the conditions  $|a_{ii}| > \sum_{j=1, j \neq i}^N |a_{ij}|$  (row dominance) or  $|a_{ii}| > \sum_{j=1, j \neq i}^N |a_{ji}|$  (column dominance) hold for any row or column.

<sup>38</sup> The eigenvalues localization methods *do not demand* a matrix to be diagonally dominant, but are efficient for such cases because the eigenvalues of the diagonally dominant matrices are located in the complex plane in some 'small' vicinity of the *diagonal* elements.

We mean the physical clearness, naturalness and ‘understandability’ which make that idea so appealing and, sometimes, make it the only substantively possible for the MIMO systems developers in quite different fields of control engineering.

We can attribute the methods exploiting a specially chosen *matrix* (as opposed to *diagonal*) regulator based on the some of the known in mathematics decompositions of numerical matrices, such as the singular value decomposition, similarity transformation, dyadic representation, etc., to the second group of design methods for the MIMO systems that are close in their trend to the approach discussed below. To this group belong, first of all, the methods using *dyadic* transfer function matrices (Owens 1973, 1974), *SVD-controllers* (Hovd and Skogestad 1992, 1994; Hovd *et al.* 1997) and the methods using the MIMO system canonical representations via the CTFs (MacFarlane 1970; MacFarlane and Kouvaritakis 1977; Basilio and Kouvaritakis 1995, 1997; Basilio and Sahate 2000). However, being of great theoretical and practical value, the methods of the second group yield, to a certain extent, in their ‘palpability’ and simplicity to the methods of the decentralized control. Without going into detailed or comparative analysis of the above-listed types of *matrix* regulators, let us dwell briefly on the difficulties arising in the computation and physical implementation of the regulators based on the concepts of the CTFs method (in principle, these difficulties are also inherent in all other types of matrix regulators). The point is that even if we change only *one* CTF  $q_i(s)$  of the plant, i.e. bring it to a certain desirable form  $q_i(s)k_i(s)$ , where  $k_i(s)$  is the ‘correction’ for the  $i$ th characteristic system, then, returning to the natural basis, we get, first, a ‘full’ *matrix* regulator  $K(s)$ , and, secondly, it will generally have *complex* parameters,<sup>39</sup> i.e. will be physically unrealizable. Of course, it can be approximated by a real-valued regulator, but, in this case, in turn, lots of questions arise, particularly how the proximity criterion for the ideal and approximated regulators should be chosen, to what extent such an approximation preserves the features of the desirable correction  $k_i(s)$  for the  $i$ th characteristic system, etc. On the other hand, if we introduce a usual correction  $k_i(s)$  into any *one* direct channel (as in the decentralized control), or create a new *artificial* coupling between any two channels of the MIMO system, then it entirely (and usually in an unpredictable manner) changes the modal decomposition of the initial plant  $W(s)$ , i.e. changes *all* initial CTFs  $q_i(s)$  and the canonical basis axes  $c_i(s)$ . Therefore, the results of the stability analysis of the *initial* plant on the basis of the CTFs prove to be practically useless for the further design of the MIMO system regulator. All this probably explains the situation that the CTFs method is mostly regarded as a sophisticated method, applicable *only for the stability analysis of linear MIMO systems*, and the descriptions of any effective *engineering* procedures for the MIMO systems design based on that method are actually absent in the scientific and technical literature.

In the design of any automatic control system, after (and, sometimes, before) the investigation of dynamical and other characteristics and features of the plant, the *performance specifications* (or *performance indices*) are decided. That task, in fact, is rather complicated and ambiguous. Thus, many requests of the system’s customer may be expressed in terms that have nothing in common with the control theory. Concerning the control theory itself, there is such a wealth and diversity of possible performance indices in the literature that the question of their choice can become crucial or, in any case, one of the centrals for the formation of the final appearance of the designed system. For the developer, that question is especially

<sup>39</sup> As the examples of MIMO systems, in which the SVD regulators have *real* coefficients in the natural basis, can serve anticirculant and circulant systems, for which the unitary modal matrix  $C$  does not depend on the complex variable  $s$ , and permits representation in the *real-valued* canonical form (see Remark 1.7).

important, since the choice of performance indices often uniquely determines the choice of adequate design methods for the whole system. Since our ultimate goal is to extend the principal methods of the *classical* control theory to the multidimensional case, we shall choose as the MIMO systems performance indices those frequency-domain, time-domain and root indices most widely used in practice (Truxal 1955; Horowitz 1963; Bessekerski and Popov 2002). Let us briefly discuss these indices for the SISO systems case. The dynamical accuracy of the system under slowly changing deterministic inputs is usually estimated by means of the *error coefficients* (see Section 2.3), which allow *the gain of the open-loop system* to be selected, given the *system type*.<sup>40</sup> If the input signals are harmonic functions of time (or have both slowly changing and harmonic components), then the amplitudes of the corresponding harmonic errors can be found via the frequency-response characteristics of the *closed-loop* system. Finally, in the case of stochastic inputs, the mean square error is also determined by the *closed-loop* system characteristics, with the help of special formulae (Newton *et al.* 1957; Tsytkin 1977) (see Section 2.4). If the reference signals or disturbances are applied in different points, then, when analyzing the system accuracy and choosing the parameters, one should use the transfer functions relating these signals to the error signal of the system. Of course, in the design, the situations in which the *decrease* in some error components is accompanied by the *increase* in others are not excluded. Therefore, in practice, obtaining the required accuracy is usually connected with finding some trade-off solution.

Besides the steady-state error, system performance is determined by the *time-domain (transient response)* characteristics, which are related to some standard test input signals, first of all, to the unit step signal (Kuo 1995; Bessekerski and Popov 2002). A typical time response of a SISO system with zero initial conditions caused by the unit step input is shown in Figure 2.25(a). The two main characteristics here are:

1. *Overshoot OS*: the peak value of the transient response with respect to the steady-state value, often expressed as a percentage of that value (values of *OS* of about 20–25% are usually regarded as acceptable).
2. *Settling time  $T_S$* : the time required for the response to reach and stay within the specified tolerance band of  $\pm 5\%$  of its final value.<sup>41</sup>

General requirements for the settling time cannot exist, as that quantity may be quite different for different systems (for example, from several milliseconds to tens of minutes), but, intuitively, the aspiration of developers to make it as small as possible is natural. Besides the two time-domain specifications indicated, there are some others (*rise time, peak time, delay time, decay ratio, number of oscillations, excess variation, etc.*), but they are mainly of secondary importance. For SISO systems of high order, there is no rigorous mathematical dependence between the time-domain characteristics and the system parameters; therefore, in the design, either some heuristical relationships are used or the closed-loop system is approximated by a second-order system (Horowitz 1963).

The root and frequency-domain performance indices belong to the *indirect* estimates of the system dynamics, as their relationship with the transient responses bears an indirect character.

<sup>40</sup> This is a somewhat simplified treatment, as it concerns only the first nonvanishing error coefficients  $K_r$ . The following of them allow choosing some other system parameters, such as time constants, etc. (Bessekerski and Popov 2002).

<sup>41</sup> Value  $\pm 5\%$  is conventional; in the literature, one can find other values, beginning from  $\pm 2\%$ .

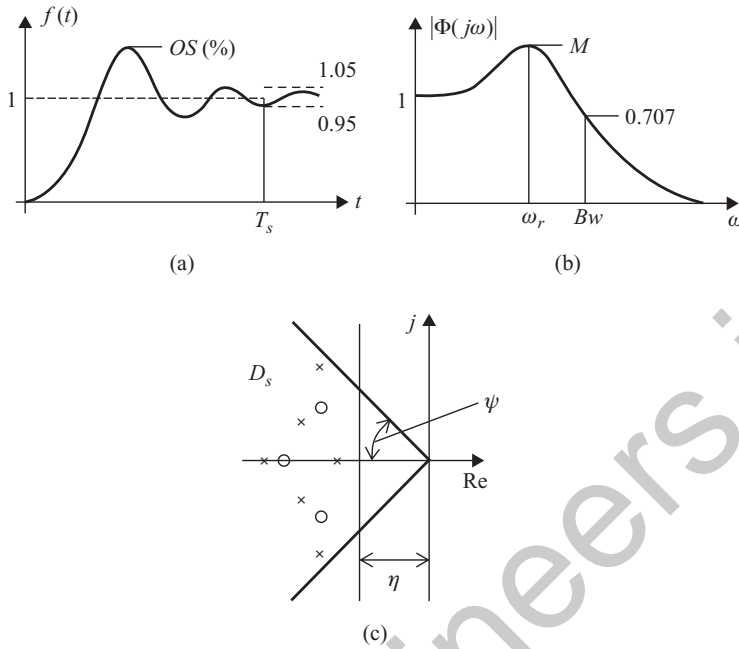


**Figure 2.25** Performance indices for SISO control systems. (a) Time-domain indices; (b) frequency-domain indices; (c) root indices.

On the other hand, the main synthesis methods of the classical control theory are traditionally based on these very indices, and the engineer is usually dealing with these very indices when choosing the system correction. To the frequency-domain performance indices belong: *gain and phase margins*, *resonant peak* of the magnitude of the closed-loop transfer function (*oscillation index  $M$* ) and *bandwidth  $Bw$* , defined as the frequency at which the magnitude of the closed-loop transfer function first crosses level 0.707 from above or below, depending on which of the transfer functions  $\Phi(j\omega)$  or  $\Phi_\varepsilon(j\omega)$  is considered [Figure 2.25(b)].

The root indices are used for the assessment of the character of transient responses, based on the location of *poles* and *zeros* of the closed-loop system [Figure 2.25(c)]. As is well known, the behaviour of any system is usually quite adequately characterized by the two (sometimes, three) so-called *dominant poles*, which are the closest to the imaginary axis (Horowitz 1963). Parameter  $\eta$  in Figure 2.25(c), which is called the *degree of stability*, is equal to the distance from the imaginary axis to the nearest (dominant) pole. Since the real part of the dominant poles corresponds to the components of the transient response that decay most slowly, the settling time can be determined approximately by the degree of stability  $\eta$  (it is considered that  $T_s \leq 3/\eta$ ). Angle  $\psi$  in Figure 2.25(c) defines the sector of the system roots' desirable location. The value  $\mu = \tan \psi$ <sup>42</sup> approximately determines the *overshoot* [ $OS \leq 100 \exp(-\pi/\mu)$ ], and the *decay within a period*  $\xi$  ( $\xi \approx 1 - \exp\{-2\pi/\mu\}$ ) evaluated as  $\xi = 100(C_1 - C_2)/C_1$ , where  $C_1$  and  $C_2$  are the first and second amplitudes of the sinusoidal component  $C \exp\{-\alpha t\} \sin(\beta t + \gamma)$  of the transient response (Makarov and Menski 1977). If both values  $\eta$  and  $\mu$  are specified,

<sup>42</sup> The value  $\cos \psi$  is called the *damping* or *damping ratio* of complex poles.

then they determine the region  $D_S$  in the complex plane, shown in Figure 2.25(c) by bold lines, where the poles of the closed-loop system should be located.

In the literature on classical control, countless recommendations can be found on how one should choose the correction of the system based on the whole variety of performance requirements. Since these requirements are frequently rather incompatible, all of the proposed design procedures are usually reduced to what is called the *trial and error method*, i.e. to the step-by-step approach, taking into account all (or, at least, most of) the significant factors, to the ‘best’ solution.

Most likely, one of the basic contradictions arising in system design is the contradiction between accuracy and stability.<sup>43</sup> As is well known, the most radical and general way to increase the system accuracy consists in *increasing* the system gain. However, an unlimited increase in the system gain inevitably leads, if the *relative order*<sup>44</sup> of the system exceeds two, to instability. On the other hand, the system’s customer is more worried about the accuracy than the stability, since the latter is a necessary condition for the system to work. As for the capacity for work, it is down to the developer’s duty and competence that the system should work properly. Therefore, at the initial stages of the system design, it is appropriate to determine the gains that guarantee system accuracy, and then try to obtain the desired stability margins by means of the corresponding correction. In terms of the *frequency-response characteristics*, this means that the *low-frequency* region of the system characteristics is determined by the accuracy specifications, i.e. as if it was given. Accordingly, the *mid-frequency* (in the neighborhood of the *crossover frequency*) and the *high-frequency* regions are at the developer’s disposal and should be formed based on the stability conditions, not forgetting that these regions, in many respects, determine the system *time-domain* characteristics. If the *root-locus* techniques are used, the design procedure also consists of two stages. First, the gains of the open-loop system are found, based on the required accuracy. Further, the correction which provides the necessary location of the poles (and zeros) of the closed-loop system in the prescribed region is selected [Figure 25(c)]. In the design by either the frequency or the root-locus technique, standard *lead*, *lag*, *lead-lag* controllers or their various combinations, as well as *PID-regulators*, are usually used for the practical implementation of the regulator (controller).

Of course, all this is quite a conventional and rough scheme, but it reflects to a certain extent the sequence of the stages in the design of any real control system.<sup>45</sup> Similar problems take place in the design of MIMO systems, to which we proceed now (Gasparyan 1986). It should be immediately noted that in the following, we shall not impose any restrictions or conditions on the cross-connections in the MIMO system plant, or on the number of channels  $N$ , i.e. the transfer matrix  $W(s)$  in Figure 2.23 can be of any form and order. The idea of the design technique discussed below is quite simple, and is based on the notion of the *scalar regulator*, which implies a regulator of the form  $K(s) = k(s)I$  (Figure 2.26), in which  $k(s)$  is a usual (scalar) transfer function, which we shall call the *absolute* transfer function of the scalar regulator for MIMO systems.<sup>46</sup>

<sup>43</sup> We mean here some general properties, so some contrary instances that disprove such statements can always be found.

<sup>44</sup> i.e. the difference between the orders of the denominator and numerator of the closed-loop system transfer function.

<sup>45</sup> A reverse sequence of the design procedure is also possible, in which the developer first forms the mid-frequency region of the system characteristics, based on the stability conditions and preserving the *initial* gains, and then ‘lifts up’ the low-frequency region to the level needed by introducing a pair of close zero and pole (the so-called *dipole*; see Example 2.12).

<sup>46</sup> The reason for such a name will become clear a little later.

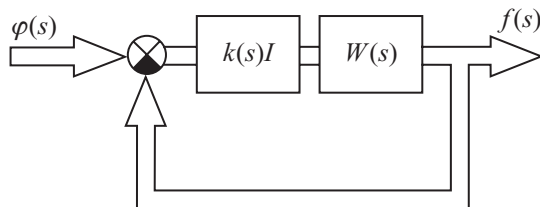


**Figure 2.26** Linear general MIMO system with the scalar regulator  $K(s) = k(s)I$ .

At first sight, it may seem that the scalar regulator is just a simple form of the diagonal regulator  $K(s) = \text{diag} \{k_i(s)\}$  used in the decentralized control, in which all diagonal elements  $k_i(s)$  are assumed to be the same and equal to  $k(s)$ . Formally, it is the case, and from the technical viewpoint, the scalar regulator preserves all the merits inherent in diagonal regulators, such as ease of practical implementation, simple tuning and maintenance, etc. However, the choice of the absolute transfer function  $k(s)$  in the discussed approach is carried out on quite a different conceptual basis, completely resting upon the ideas and mathematical apparatus of the CTFs method. On introducing the scalar regulator  $k(s)I$  in the MIMO system, the transfer matrix  $L(s)$  of the open-loop system (Figure 2.26) is represented in the form

$$L(s) = k(s)W(s), \tag{2.164}$$

i.e. as the product of the scalar transfer function  $k(s)$  and the transfer matrix of the plant  $W(s)$ . Comparing that expression with Equation (1.15), one can state that the zeros and poles of  $k(s)$  are the absolute zeros and poles of the open-loop MIMO system with the transfer matrix  $L(s)$  [Equation (2.164)]<sup>47</sup> and, naturally, the zeros of  $k(s)$  are the absolute zeros of the closed-loop MIMO system. Therefore, these zeros and poles are common to all characteristic systems associated with the MIMO system in Figure 2.26. Moreover, since the multiplication of any square matrix by a scalar brings about the multiplication of all eigenvalues of that matrix by the same scalar, all CTFs  $q_i(s)$  of the plant  $W(s)$  are multiplied by the same transfer function  $k(s)$ . Thereby, the latter becomes the common (or absolute) transfer function of the identical ‘controllers’ introduced into all SISO characteristic systems of the initial MIMO system. Then, for the CTFs  $q_i^L(s)$  of the open-loop MIMO system in Figure 2.26, we can write

$$q_i^L(s) = k(s)q_i(s), \quad i = 1, 2, \dots, N \tag{2.165}$$

and the CTFs of the closed-loop system with respect to the output and error have the form

$$\Phi_i(s) = \frac{k(s)q_i(s)}{1 + k(s)q_i(s)}, \quad \Phi_{ei}(s) = \frac{1}{1 + k(s)q_i(s)}, \quad i = 1, 2, \dots, N. \tag{2.166}$$

Further, since the multiplication of a matrix by a scalar does not change the eigenvectors of that matrix, this means that introducing the scalar regulator into the MIMO system does not change the canonical basis of the plant  $W(s)$ , i.e. does not violate the modal decomposition of the initial system. All of the above is schematically illustrated in Figure 2.27, and the reader can compare this block diagram with that in Figure 1.5.

<sup>47</sup> See Section 1.1.

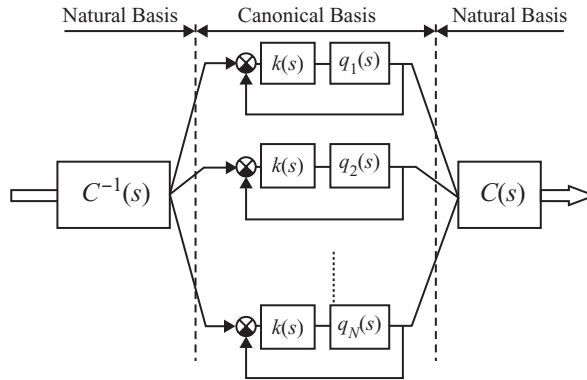


Figure 2.27 General MIMO system with the scalar regulator.

Hence, the scalar regulator  $K(s) = k(s)I$  completely preserves the internal geometrical characteristics of the initial MIMO system, and this, as we shall see later, allows all results of the preliminary investigation of the plant  $W(s)$  via the CTFs method to be used in the choice of the *absolute correction*  $k(s)$ .

Regarding the frequency-domain indices, in the MIMO system design by means of the scalar regulator, it is advisable (and convenient) to use the *oscillation indices*  $M_i$  of the characteristic systems, evaluated through the closed-loop transfer matrix with respect to output [Equation (2.22)] or error [Equation (2.12)]. In some situations, these indices can be supplemented with the *gain and phase margins*, considered in Section 1.2.4. The indicated above damping ratio  $\cos \psi$  and degree of stability  $\eta$  [Figure 2.25(c)] can also be used as the root indices in the MIMO system design, though, in this case, there is no plain relationship between the value  $\mu = \tan \psi$  and the transient responses of the MIMO system.

Now, we have all the prerequisites for proceeding to the procedure of computing the absolute correction  $k(s)$  in Figure 2.26. The first step plays a significant part in that procedure, in which one should select the system which is, based on the chosen performance indices, the *worst* among all characteristic systems of the initial MIMO system (i.e. of the plant). This task does not present any actual difficulty. On using the frequency-domain indices, the worst one is the system with the *largest* oscillation index  $M_i$ . If two or more characteristic systems have such a value of  $M_i$ , then *one* system having the *least* gain and/or phase margins<sup>48</sup> should be selected between (or among) them. In using the root-locus techniques, the worst is the characteristic system with the *least* degree of stability  $\eta$ , or the *largest* damping ratio  $\cos \psi$ . If both parameters  $\eta$  and  $\cos \psi$  are significant, and they are attributed to different characteristic systems, then the developer should select *one* of them, based on some additional factors.<sup>49</sup>

Having selected the worst characteristic system, we need to carry out, using the conventional methods and techniques of the *classical control theory*, the computation of the correction  $k(s)$  for that system in such a manner that the performance indices of the corrected worst system would satisfy the performance indices given for the MIMO system. Then, taking into account that the correction  $k(s)$  in the case of the scalar regulator is *absolute*, i.e. common to *all*

<sup>48</sup> The choice of only one characteristic system is not crucial for the design procedure.

<sup>49</sup> In GUI *ControlSysCAD*, the choice of the worst characteristic system is performed automatically.

characteristic systems (Figure 2.27), we can expect this correction to improve the performance indices of the remaining characteristic systems as well. Thereby, the problem of the MIMO system design, based on the given (frequency or root) performance indices, will be solved. Of course, the statement that the correction computed for the ‘worst’ characteristic system should render a favorable influence on all other characteristic systems is not based on a rigorous mathematical proof and rather bears a heuristical character. However, it is easy to make sure that for the MIMO systems whose characteristic gain loci do not correspond to conditionally stable<sup>50</sup> or some other extraordinary systems, the above statement always holds true (all examples in this book belong to such systems). Even if some characteristic gain loci have complicated form, then computation of the absolute correction  $k(s)$  should be carried out taking into account the necessary number of loci. In any case, it is quite naturally supposed that when designing a MIMO system on the basis of the scalar regulator, the developer must keep an eye on all  $N$  characteristic systems, to exclude unexpected situations.

It is appropriate to point out one significant detail. Like the SISO case, in the design of the MIMO system, a contradiction always arises between accuracy and stability, which predetermines the order of the design stages. In the first stage, with the help of the matrices of error coefficients (see Section 2.3), the required *gains* of the open-loop MIMO system are found. At that, even if these gains are technically accomplished as additional amplifiers, in further computations, it is convenient to attribute them to the plant, i.e. to suppose that the given plant provides the necessary dynamical accuracy of the system. As a result, after passing to the canonical basis and characteristic systems, the low-frequency regions of the corresponding characteristics of the latter proved to be actually determined, and the main concern of the developer will be, as in the SISO case, to provide the necessary stability margins of the MIMO system.

Recall that we have not imposed any restrictions on the *intensity* of the cross-connections in the plant. In practice, situations may occur in which it is impossible to obtain the desired performance of the MIMO system by means of the scalar regulator only. In such cases, one needs, as is customary in decentralized control, to introduce into the MIMO system the preliminary compensator  $K_1(s)$ , whose destination is to decrease the influence of the cross-connections to some acceptable level (Figure 2.28). However, as opposed to the decentralized control, the compensator  $K_1(s)$  here can be of a simpler form, since we do not have the necessary condition of making the transfer matrix  $W_1(s)$  diagonally dominant. Finally, in the MIMO system design, preliminary *balancing* of the channels may prove to be very useful. The essence of balancing consists in bringing all dynamical characteristics of the plant channels to the characteristics of the ‘best’, in a certain sense, channel. With this purpose, one of the channels, say the  $i$ th, with the transfer function  $w_{ii}(s)$  [the  $i$ th diagonal element of the transfer matrix  $W(s)$ ] is chosen as the basic, and corrections with the following transfer functions into all *other* direct channels are introduced:

$$k_{1r}(s) = \frac{w_{ii}(s)}{w_{rr}(s)}, \quad r = 1, 2, \dots, N, \quad r \neq i. \quad (2.167)$$

The transfer matrix of the *balancing* regulator  $K_1(s)$  in Figure 2.28 has diagonal form, with the elements  $k_{1r}(s)$  [Equation (2.167)] on the principal diagonal, where  $k_{1i}(s) = 1$ , and all

<sup>50</sup> i.e. having the ‘beak-shaped’ characteristic gain loci, in which case, the MIMO system becomes unstable *on both increasing and decreasing* of the open-loop gain.

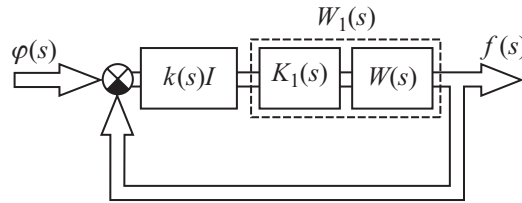


Figure 2.28 MIMO system with the scalar and decoupling regulators.

diagonal elements of the resultant matrix  $W_1(s)$  are equal to  $w_{ii}(s)$ . In practice, evidently, the exact realization of the conditions in Equation (2.167) can be impossible, and balancing will be inaccurate (which is not so essential, though). Note also that the matrix regulator  $K_1(s)$  (Figure 2.28) can be accomplished in the form  $K_1(s) = K_{Com}(s)K_{Bal}(s)$ , where the purpose of  $K_{Com}(s)$  is to compensate the cross-connections, and the matrix  $K_{Bal}(s)$  performs the balancing above, and the regulator  $K_1(s)$  can be realized as a single (united) block.

Thus, summarizing, the overall procedure of the MIMO system design based on the scalar regulator can be represented schematically by the following sequence of steps:

1. Selection of the performance indices for the MIMO system.
2. Investigation, based on the CTFs method, of the corresponding characteristics of the plant (with the necessary gains), and selection of the *worst* characteristic system.
3. Computation of the *absolute* correction  $k(s)$  for the selected characteristic system, with the help of conventional methods of the classical control theory.
4. If necessary, introduction of the decoupling regulator  $K_1(s)$  and repetition of steps 2 and 3.
5. Examination of the performance of the designed MIMO system, including the dynamical accuracy analysis, taking into account all disturbances and other factors, as well as investigation of the transient responses (here, there is no real alternative to the mathematical simulation by means of computer aids).

Different variations of that scheme are possible, consisting, for instance, in the preliminary balancing of the channels, compensation of the cross-connections reasoning from some other factors, etc. All this does not play any particular role, since the *key* step in the design is step 3, in which the choice of the correction for the MIMO system with any number of channels  $N$  and arbitrary cross-connections is carried out quite analogously to the SISO case, based on the customary methods and techniques.

Certain difficulties may occur in step 5, in the analysis of the MIMO system accuracy under the disturbances (both deterministic and stochastic) applied to different points of the system, and in computing the error components owing to such nonlinear factors as dead bands, frictions in the mechanical gears, etc. We discussed this issue in Remark 2.5, and therefore shall not dwell on it here. Note only that for the computation of the error components caused by stochastic or harmonic signals, one should have the corresponding transfer matrices of the *closed-loop corrected* MIMO system, i.e. the system with the correction *having already been computed*. On the other hand, the error components caused by the constant (or slowly varying) instrumental errors and slowly changing external disturbances or reference signals are evaluated with the

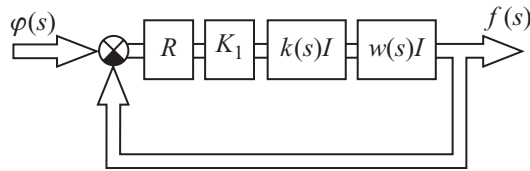


**Figure 2.29** General block diagram of the uniform system with the scalar regulator.

help of the corresponding matrices of error coefficients, and usually demand the knowledge of the *open-loop* MIMO system gains (at least, it is valid for the cases in which the steady-state error of the MIMO system does not have any deterministic components changing in time). As a result, it may turn out that the absolute correction  $k(s)$ , which is actually computed to provide the stability of the MIMO systems, brings to inadmissibly large steady-state errors. In such situations, the developer will have to return to step 2 and, taking into account the gathered information, try to reduce the total error to the given level by changing such parameters as gains, bandwidth, resonant frequencies, intensities of the cross-connections, etc.

Above, we have considered general MIMO systems. In the case of uniform systems, the principal structural features of which are the identity of separate channels and presence of rigid cross-connections, the use of the scalar regulator seems to be the only possibility to preserve belonging to the class of uniform systems. Note that, here, the problem of *decoupling* is solved very easily, since the decoupling regulator  $K_1$  is *static* and can be found from the simple condition  $K_1 = R^{-1}$ , where  $R$  is the matrix of the *natural* cross-connections (Figure 2.29).

Among the other classes of MIMO systems, one should point out circulant and anticirculant systems, for which the concept of the scalar regulator is also quite natural, since it preserves the systems belonging to the initial class. Besides, it is worth noting some interesting opportunities connected with introducing into such systems the matrix regulators of the basic structure (*circulant* or *anticirculant* regulators). Since, in such cases, the CTFs of the plant are *multiplied* by the corresponding CTFs of the matrix regulator (see Section 1.4.4), wide and flexible possibilities for an elaborated design of MIMO systems of these classes are opened up. However, we shall not dwell on that question because of the restricted extent of the book.<sup>51</sup>

**Remark 2.6** As the above discussion has shown, the design of the *practical* MIMO systems is always carried out by the trial-and-error method, and is accompanied by seeking a reasonable trade-off among the different, often quite discrepant, requirements and conditions. Therefore, one should realize that there cannot be any ready recipes or instructions allowing for the total variety of possible disturbances and many other factors affecting the performance of MIMO systems (although this also concerns the SISO systems). In this respect, the *skill, experience and knowledge* of the developer has always played, play now and will play in the future the principle role in the development of control systems in various engineering applications.

In the rest of this section, we shall consider several examples illustrating the design of MIMO systems of different classes on the basis of the scalar regulator.

**Example 2.12** Let the input signal of the two-axis guidance system of Example 1.2 be of linear form  $\varphi(t) = vt$ , where  $|v| = 60$ . The transfer functions of separate channels are given by Equation (1.66), and angles  $\alpha_1$  and  $\alpha_2$  are  $\alpha_1 = 30^\circ$ ,  $\alpha_2 = 20^\circ$ . For these values of angles,

<sup>51</sup> GUI *ControlSysCAD* provides special resources for introducing circulant and anticirculant matrix regulators.

the cross-connections matrix  $R$  has the form

$$R = \begin{pmatrix} 0.866 & 0.5 \\ -0.342 & 0.94 \end{pmatrix}. \tag{2.168}$$

Find a scalar regulator which provides the following requirements:

1. The *magnitude* of the steady-state velocity error vector does not exceed two.
2. The oscillation index  $M$  determined through the majorant of the generalized frequency characteristics with respect to the *output* satisfies the condition  $M \leq 2.2$ .

Based on Equation (2.86), we have for the velocity error vector

$$\varepsilon = K_1 v = R^{-1} \text{diag}\{1/D_i\} v = \begin{pmatrix} 0.3181 & -0.3249 \\ 0.1158 & 0.5628 \end{pmatrix} v, \tag{2.169}$$

where  $D_1 = 3$  and  $D_2 = 1.5625$  are the gains of the transfer functions  $W_1(s)$  and  $W_2(s)$  [Equation (1.66)]. Passing in Equation (2.169) to the magnitudes, we get  $|\varepsilon| \leq \|K_1\| |v|$ , where the spectral norm  $\|K_1\|$  is equal to 0.6535, which leads to the following estimate for the error vector magnitude:  $|\varepsilon| \leq 39.21$ . Consequently, to provide the required system accuracy  $|\varepsilon| \leq 2$ , it is necessary to increase the gains of the separate channels  $D_1$  and  $D_2$  by a factor of about 20, which yields  $D_1 = 60$  and  $D_2 = 31.25$ .

The characteristic gain loci of the open-loop guidance system with the increased gains are shown in Figure 2.30, from which it is evident that the system is unstable, and the ‘worst’ (unstable) of the two characteristic systems is the first, since the second characteristic system is stable under the required gains. Hence, the task of choosing the scalar regulator reduces to the determination of such absolute correction  $k(s)$ , for which the first characteristic system will become stable, and the value of the oscillation index  $M$  with respect to output will

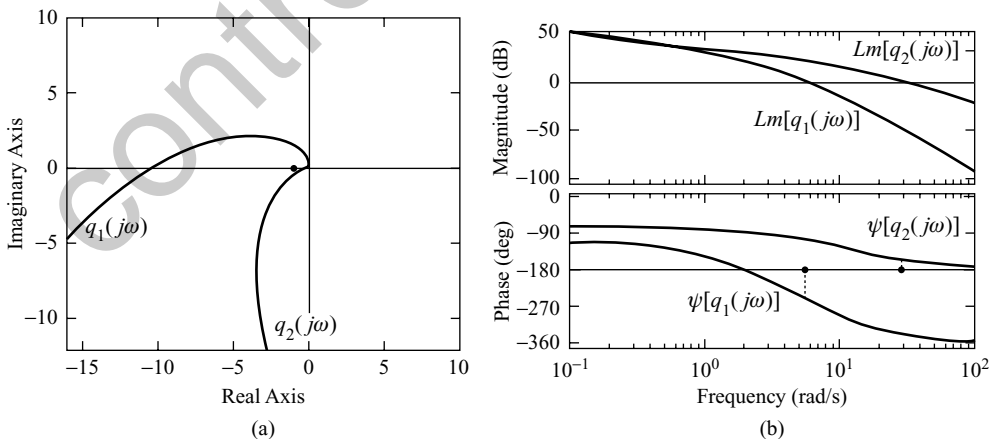


**Figure 2.30** Characteristics of the open-loop guidance system with the increased gains. (a) Nyquist plots; (b) Bode diagrams.

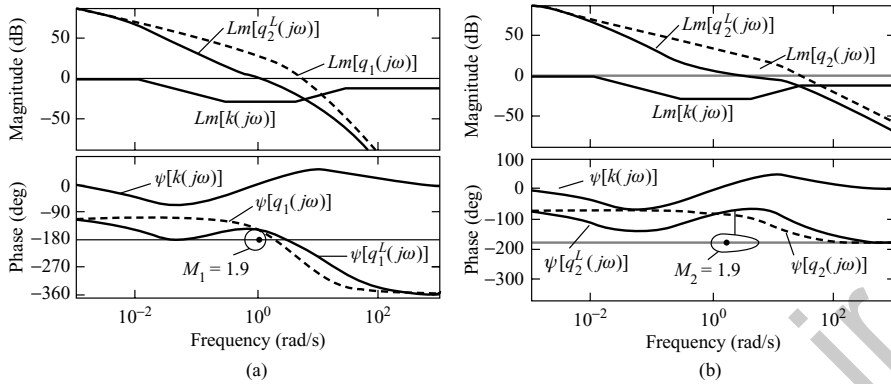


**Figure 2.31** Bode diagrams of the corrected guidance system. (a) First characteristic system; (b) second characteristic system.

not exceed 2.2. Note also that decrease in the gains is not allowed because of the accuracy requirements.

To choose the correction  $k(s)$ , let us follow the standard recommendations, known from the classical control theory (Rabinovich *et al.* 1969; Horowitz 1963). To provide the desired slope  $-20$  dB/decade of the Bode magnitude plot  $Lm[q_1(j\omega)]$  in the vicinity of the crossover frequency whilst preserving the mid-frequency region, introduce into the system a real pole at the point  $-0.01$  and a zero at  $-0.3$ .<sup>52</sup> Also, add a zero at  $-4$  and a pole at  $-30$ , i.e. shift the pole  $-4$  of the transfer function  $W_2(s)$  [Equation (1.66)] to the point  $-30$ . The corresponding transfer function of the absolute correction  $k(s)$  has the form

$$k(s) = \frac{0.25(s + 0.3)(s + 4)}{(s + 0.01)(s + 30)}, \quad (2.170)$$

where the coefficient 0.25 is introduced to provide the unit gain of the correction (2.170) at the zero frequency. The Bode diagrams of the corrected guidance system and the  $\mu$ -curves, for  $M_i = 1.9$  [this value is chosen with some margin, as the condition number of the modal matrix  $C(j\omega)$  changes within the limits from 1.56 to 2.534] are shown in Figure 2.31. Note that in Figure 2.31, the asymptotic Bode magnitude plots (straight-line approximations) of the correction  $k(s)$  are depicted, which are more visual and convenient for design purposes. The majorant  $A_{\text{sup}}(\omega)$  and minorant  $A_{\text{inf}}(\omega)$  of the generalized frequency characteristics with respect to the output signals, as well as the plots  $A_1(\omega)$  and  $A_2(\omega)$  of the closed-loop characteristic systems, are shown in Figure 2.32. The latter shows that the oscillation index  $M$  of the system determined via the resonant peak of the majorant  $A_{\text{sup}}(\omega)$  is equal to 2.1015, i.e. satisfies the specified requirements ( $M \leq 2.2$ ). The transient responses of the guidance system with the chosen scalar regulator are given in Figure 2.33, in which the unit steps are simultaneously applied to the inputs of both channels. If we take the largest overshoot of separate channels as the system overshoot, then, here, it is determined by the second channel ( $OS = OS_2 = 47.89\%$ ). The settling time ( $T_S = 5.024$  sec), on the contrary, is equal to the settling time in the first channel of the system.

<sup>52</sup> Such a combination is often called *dipole* (Truxal 1955).

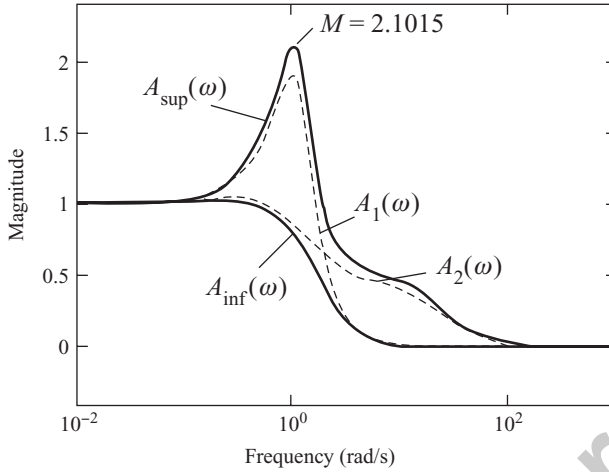


Figure 2.32 Generalized frequency characteristics.

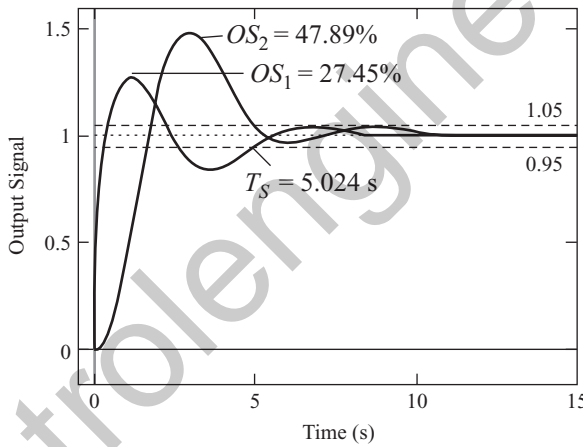
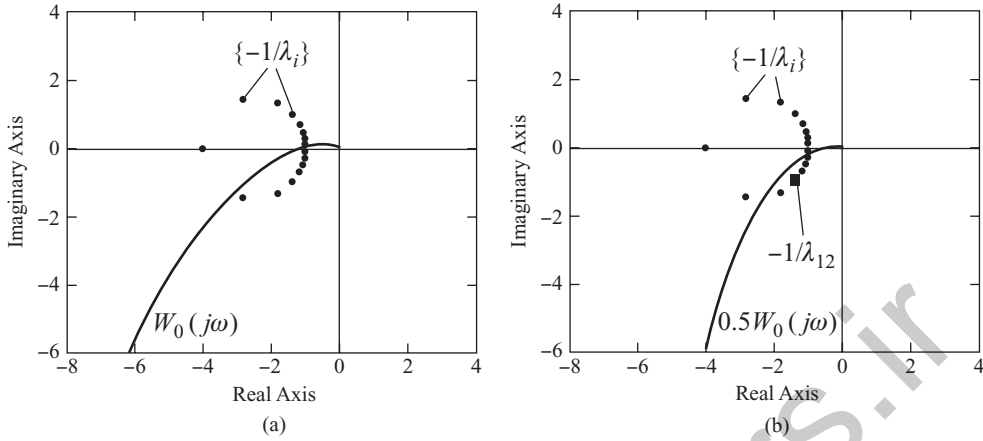


Figure 2.33 Transient responses of the guidance system with the scalar regulator [Equation (2.170)].

**Example 2.13** Below, we consider the design of a uniform system. In addition, the example demonstrates that the design process cannot always be confined to some strict schemes, and demands a flexible and individual approach to each specific case. Assume that we have a 16-channel uniform system with the circulant matrix of rigid cross-connections  $R$  [Equation (1.154)], and the following transfer function of the identical separate channels:

$$W_0(s) = \frac{75000000}{s(s + 25)(s + 400)(s + 500)}. \quad (2.171)$$

Assume also that the input signal of the system is a linear time function  $\varphi(t) = vt$ , where  $|v| = 100$ . Find such an absolute correction, with which the system will have the velocity error  $|\varepsilon| \leq 4$ , and the oscillation index of the system  $M$  with respect to error (i.e. defined by the



**Figure 2.34** Nyquist plots of the circulant uniform system ( $N = 16$ ). (a) Initial system; (b) system with the decreased gain.

sensitivity transfer matrix), will not exceed 2.1. The Nyquist plot of  $W_0(j\omega)$  [Equation (2.171)] is shown in Figure 2.34(a). On the same plot, 16 critical points  $-1/\lambda_i$  there are indicated, where  $\lambda_i$  are the eigenvalues of the matrix  $R$  [Equation (1.154)]. As is evident from Figure 2.34(a), the system is unstable. On the other hand, the spectral norm of the first nonvanishing matrix of error coefficients  $K_1$  [Equation (2.92)] is equal to 0.0167 (and, for the magnitude of the velocity error, we have the estimate:  $|\varepsilon| \leq 1.67$ ), i.e. the system error is more than twice as small as the required value. However, the decrease of the gain in Equation (2.171) by a factor of two does not bring stability to the system, as can be seen from Figure 2.34(b), in which the worst, from the phase margin viewpoint, is the twelfth characteristic system (with  $\lambda_{12} = 0.4815 - j0.3465$ ), whose critical point is labeled in Figure 2.34(b) by a square. Hence, we need to find the dynamical absolute correction which will make the system stable, with  $M \leq 2.1$ . Following the customary procedures of the SISO systems design, it can be shown that the required correction is

$$k(s) = \frac{0.8(s + 3)(s + 25)}{(s + 0.33)(s + 400)} \quad (2.172)$$

and the final (resultant) transfer function of the separate channels of the circulant uniform system has the form

$$L(s) = \frac{600000000(s + 3)}{s(s + 0.33)(s + 400)^2(s + 500)}. \quad (2.173)$$

The spectral norm of the matrix  $K_1$  is equal to 0.0367, and, for the magnitude of the velocity error, we have  $|\varepsilon| \leq 3.67$ , which meets the requirements.

It is interesting to note that in the process of the successive approach to the correction in Equation (2.172), it turns out that the worst, by the oscillation index, has become the eleventh characteristic system, with  $\lambda_{11} = 0.3598 - j0.2652$  (and not the twelfth, as it was for the initial system). This accentuates once more the fact that in choosing the absolute correction via the ‘worst’ characteristic system, the performance indices of all other characteristic

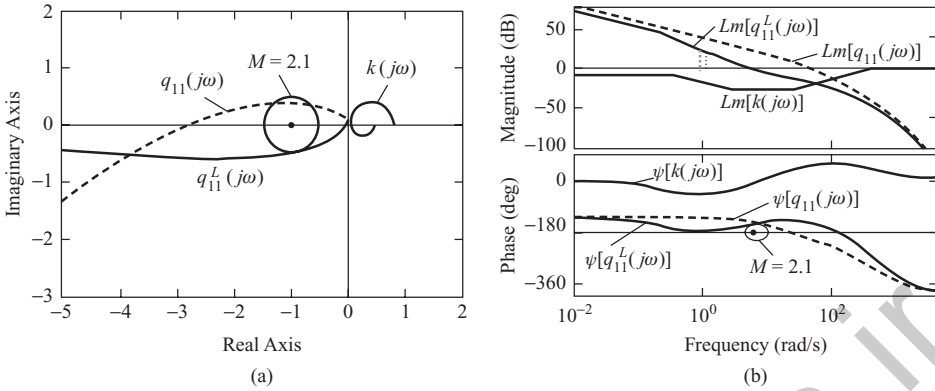


**Figure 2.35** Frequency-domain plots of the 11th characteristic system with the correction in Equation (2.172). (a) Nyquist plots; (b) Bode diagrams.

systems should always be examined, to exclude atypical situations. The Nyquist plots and Bode diagrams of the eleventh characteristic system with the correction in Equation (2.172) are shown in Figure 2.35, in which the  $\mu$ -curve in Figure 2.35(b) is plotted by Equation (2.48), for  $M = 2.1$ .

Recall that, due to the normality of the discussed circulant system, the value of the ‘worst’ oscillation index  $M_{11}$  is equal to the oscillation index  $M$  of the overall system, defined as the resonant peak of the majorant  $A_{\text{sup}}(\omega)$  (Figure 2.36). The exact value of  $M$  is equal to 2.0846, i.e. it agrees with the given value. The transient responses of the system, under the unit steps applied simultaneously to all inputs, are given in Figure 2.37. It is noteworthy, here, that the transient responses of all system channels *are the same*, i.e. in Figure 2.37, there is a superposition of 16 identical time functions. This is a consequence of the structural symmetry of circulant systems. The (same) overshoot of all channels is  $OS = 12.54\%$ . In Figures 1.32, 2.14

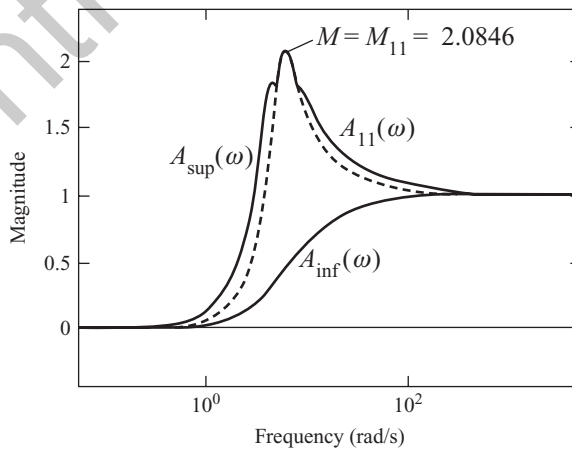


**Figure 2.36** Majorant  $A_{\text{sup}}(\omega)$  and minorant  $A_{\text{inf}}(\omega)$ .

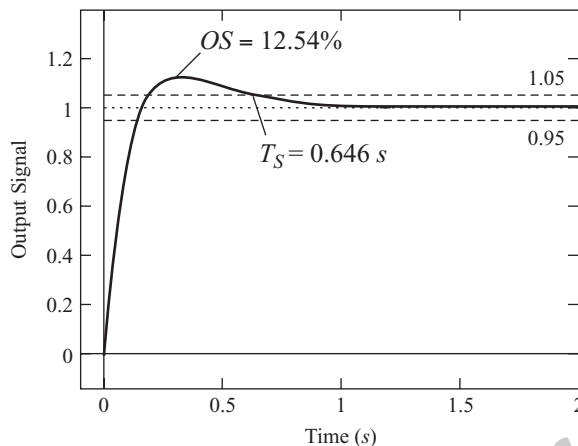


**Figure 2.37** Transient responses.

and 2.18, the reader can observe all other frequency-domain characteristics of the discussed uniform system with the absolute correction in Equation (2.172).

Thus, as is evident from Figure 2.35, the design of the 16-channel system is actually reduced to the computation of the corresponding correction for *one* characteristic system. Further, the plots in Figure 2.35 and the underlying procedures are completely similar to those used in the design of usual SISO systems on the basis of the methods and techniques of the classical control theory.

**Remark 2.7** Figuratively speaking, the scalar regulator is, to a certain extent, a *sufficient* regulator, since it is not excluded that the required performance of the MIMO system could also be achieved by the introduction, say, of a diagonal regulator with *different* diagonal elements. Here, however, a natural question arises as to whether there is any sense in introducing the diagonal *regulator* (with the complicated or not quite definite methods of computation of its elements), if it is *sufficient* to introduce the scalar regulator which guarantees the MIMO system performance. At least, from the standpoint of unification and ease of the technical implementation, the scalar regulator has evident advantages. Of course, if the different channels of the multivariable interconnected plant have substantially different dynamics, then the introduction of the scalar regulator may be difficult or not quite justified. At the same time, in such situations, it is expedient to perform *balancing* of the channels and/or *compensation* of the cross-connections. Somehow or other, and we shall repeat once more this accepted truth, the design of any specific MIMO system should be performed taking into account its individual features and peculiarities.

**Remark 2.8** We already stated in Remark 1.8, and it was confirmed by the above examples, that the described approach *does not impose practically any restrictions on the number of channels and the order of transfer functions of the MIMO system*. Thus, in Example 2.13, the absolute correction for the circulant uniform system with 16 inputs and outputs was determined, which is described in state-space by a system of 80 first-order differential equations. The design in Example 2.13 was brought, without any simplifications or the MIMO system order reduction, to the design of a certain SISO system with generally complex coefficients. Therefore, such tasks as approximation or model order reduction, and they have already become classical in the

modern control theory and to them are devoted whole chapters in textbooks and monographs, not to mention a wealth of articles (Glover 1984; Skogestad and Postlethwaite 2005; Antoulas 1999; Antoulas *et al.* 2001; Benner *et al.* 2005, etc.), on using the discussed approach to the MIMO systems design just lose their urgency and become needless. Another useful feature of that approach, which is worth mentioning, is that the *order of the absolute correction* is chosen by the developer, and that order does not in the least depend on the *order of the plant* in state-space. This also supplements the assertion that, generally, there is no need for any simplification of the MIMO system initial models.

**Remark 2.9** In Remark 2.3, we very briefly discussed some elementary aspects of the robust theory and indicated that, having the majorants of the generalized frequency characteristics of the closed-loop MIMO system and the corresponding oscillation indices  $M$ , one can readily check the system robustness conditions under the additive or multiplicative uncertainties in the plant  $W(s)$ . Also, the robustness analysis can be carried out, like the estimate of the oscillation index  $M$ , through the characteristic gain loci  $q_i(j\omega)$  of the open-loop MIMO system. The latter implies that in the MIMO system design, via the scalar regulator, the corresponding requirements can be imposed on the oscillation index  $M_{i \max}$  of the ‘worst’ characteristic system, based on the condition in Equation (2.20):

$$M \leq \nu[C(j\omega_M)]M_{i \max}, \quad (2.174)$$

where  $\omega_M$  is the resonant frequency of the majorant  $A_{\text{sup}}(\omega)$ . In general, when choosing the scalar regulator, the frequency  $\omega_M$  is *a priori* unknown. However, since the scalar regulator does not change the canonical basis of the plant, *the dependence of the condition number  $\nu[C(j\omega)]$  on the frequency  $\omega$  remains the same*, i.e. coincides with the same dependence for the *plant*. Therefore, at the first design stage, the number  $\nu[C(j\omega_M)]$  in Equation (2.174) can be replaced by  $\nu_{\max} = \max_{\omega}(\nu[C(j\omega)])$ . Then, given the value of the oscillation index  $M$ , which allows for the robustness conditions, one can find the corresponding value for  $M_{i \max}$ :

$$M_{i \max} = \frac{M}{\nu_{\max}}. \quad (2.175)$$

At the next stage, when the actual value of the resonant frequency  $\omega_M$  of the developed MIMO system is found, the required value of  $M_{i \max}$  can be corrected (towards the lesser values).

Note that, for circulant and anticirculant MIMO systems, the number  $\nu[C(j\omega)]$  is always equal to unity and, for uniform systems, it is constant, i.e.  $\nu[C(j\omega)] = \nu[C] = \text{const}$ , which simplifies the computations. On the other hand, as is evident from the examples of this chapter, the upper estimate via the condition number  $\nu[C(j\omega)]$  is usually rather high; this can bring about certain difficulties in choosing the absolute correction.

# Part II

## Nonlinear Multivariable Control Systems

controlengineers.ir

# 3

## Study of one-frequency self-oscillation in nonlinear harmonically linearized MIMO systems

### 3.1 INTRODUCTION

The *harmonic linearization* method, also called the *harmonic balance* or *describing function* method (Atherton 1975; Cook 1994; Gibson 1963; Taylor 1999), is one of the most powerful approximate methods used in the nonlinear control systems design and probably the most widespread in the engineering community. Its principal merit is that it allows, in quite simple mathematical form, the main parameters of the investigated system to be related immediately to those general performance indices, which are specified for the design. The mathematical foundations of the harmonic linearization method were laid out in the works of Krilov and Bogolubov (1934, 1937). Later on, an essential contribution to the development of the method was made by Goldfarb (1947), E. Popov (1962, 1973), Kochenburger (1950), Tustin (1947) and many others.

Let us recall briefly the main ideas of the harmonic linearization method for the simplest case of the investigation of *self-oscillation* (or *limit cycle*) in a nonlinear SISO system with a single nonlinear element (Figure 3.1). Suppose that the input signal is zero, that is  $\varphi(t) = 0$ , and the nonlinear characteristic  $F(x)$  is odd, symmetrical and memoryless. Suppose also that, in the system, we have steady-state symmetrical self-oscillation with some constant frequency  $\Omega$ , and linear part  $W(s)$  is a low pass filter, that is it sufficiently attenuates all higher (beginning from the second) harmonics generated at the *output* of the nonlinearity. That property of the linear part  $W(s)$  is usually called the *low pass filter hypothesis* (Popov 1962) and is written in the following mathematical form:

$$|W(jk\Omega)| \ll |W(j\Omega)| \quad k = 2, 3, \dots \quad (3.1)$$

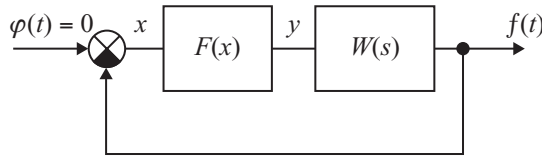


**Figure 3.1** Nonlinear SISO control system.

Then, neglecting to a first approximation the higher harmonics of the signal  $x(t)$  at the *input* to the nonlinear element, that is assuming

$$x(t) = A \sin \Omega t, \quad (3.2)$$

and based on the condition for the harmonic balance for the first (fundamental) harmonic, we come to the following equation for the harmonically linearized closed-loop system in the complex form:

$$\{1 + W(j\Omega)[q^R(A) + jq^I(A)]\} A e^{j\Omega t} = 0, \quad (3.3)$$

The complex coefficient<sup>1</sup>

$$G(A) = q^R(A) + jq^I(A) \quad (3.4)$$

in Equation (3.3), where the superscripts  $R$  and  $I$  indicate the real and imaginary parts, is called the *describing function* (in the Russian technical literature, it is usually termed the *complex gain* of the nonlinear element). The real-valued numbers  $q^R(A)$  and  $q^I(A)$  in Equation (3.4) are determined by the *fundamental* term of the Fourier series of the periodical signal  $y(t)$  at the output of  $F(x)$  and have the form:

$$q^R(A) = \frac{1}{\pi A} \int_0^{2\pi} F(A \sin \psi) \sin \psi d\psi, \quad q^I(A) = \frac{1}{\pi A} \int_0^{2\pi} F(A \sin \psi) \cos \psi d\psi. \quad (3.5)$$

The magnitude  $|G(A)|$  of the complex coefficient  $G(A)$  [Equation (3.4)] is equal to the ratio of amplitudes of the first harmonics of the output and input waveforms of the nonlinear element, and argument  $\arg G(A)$  is equal to the relative phase shift of the output first harmonic. For many common nonlinearities, coefficients  $q^R(A)$  and  $q^I(A)$  can be expressed in analytical form (Atherton 1975; Popov 1973). In the case of single-valued nonlinearities,  $q^I(A)$  in Equation (3.5) is identically equal to zero, which physically means that there is no phase shift between the output and input fundamental harmonics of  $F(x)$ . Finally, for nonlinear elements possessing memory, coefficient  $G(A)$  [Equation (3.4)] depends also on the frequency  $\Omega$ , i.e.  $G(A) = G(A, \Omega)$ .

Thus, supposing that the condition for low pass filter [Equation (3.1)] holds in the nonlinear system of Figure 3.1, and a steady state periodical process with some frequency  $\Omega$  exists, we

<sup>1</sup> Hereinafter, in the worked examples, we shall often use the notation  $N(A)$  for the describing function of common nonlinearities.

have replaced the nonlinear characteristic  $F(x)$  by a linear  $G(A)$ , where the latter depends on the unknown amplitude  $A$  of the oscillation at the *input* to the nonlinearity. It can be said that we have performed the harmonic linearization of the nonlinear element, and that linearization is valid only for the discussed mode of symmetrical self-oscillation. But we know that a linear (linearized) system can exhibit a steady-state oscillation with a constant amplitude only if it is on the *stability boundary*, that is if the characteristic equation of the closed-loop system has a pure imaginary root (or a couple of complex-conjugate imaginary roots) and all other roots are located in the open left half-plane. In other words, the characteristic equation of the closed-loop harmonically linearized system

$$1 + W(j\Omega)G(A) = 0 \tag{3.6}$$

must have at least one pure imaginary root.<sup>2</sup> The fundamental distinction of the harmonically linearized system from a linear system on the stability boundary is that the oscillation amplitude of the linear system depends on the *initial conditions* and can be arbitrary, whereas, in the nonlinear case discussed, the amplitude  $A$  is constant<sup>3</sup> and depends generally on the characteristics of the nonlinearity and the parameters of the linear part. It can be argued that nonlinear properties of the harmonically linearized system exhibit just in the dependence of the gain  $G(A)$  on the oscillation amplitude  $A$  at the input to nonlinearity.

Treating the problem somewhat formally, to evaluate unknown  $A$  and  $\Omega$  in Equation (3.6), one can solve, by any means, the following system of two nonlinear interconnected algebraic equations resulting apparently from Equation (3.6):

$$\operatorname{Re}\{W(j\Omega)G(A)\} = -1, \quad \operatorname{Im}\{W(j\Omega)G(A)\} = 0. \tag{3.7}$$

In the more complicated problems of investigating asymmetrical self-oscillation, accounting for higher harmonics, analyzing ‘slowly varying’ processes in limit cycling systems, etc., the number of nonlinear algebraic equations correspondingly increases, remaining equal to the number of unknowns (Popov 1973). The same refers to the case of single-loop or multiple-loop SISO systems with several nonlinear elements; composing the harmonic balance equations in such systems always brings to as many algebraic equations as there are unknowns in the problem. At first sight, it may seem that extension of the harmonic linearization method to the case of nonlinear multivariable systems must not lead to any principle difficulties. That is true to a certain extent: for any nonlinear MIMO system, a required set of equations can be easily obtained whose solution gives, assuming one-frequency oscillation waveform and sufficient filtering properties of the linear part, all parameters of the steady-state limit cycle in the MIMO system. However, there is a very essential distinction here. The point is that in the SISO case, the discussed method is used not simply for the numerical evaluation of the limit cycle amplitude and frequency, constant biases of the oscillation and so on, but it serves also as an investigation method well suited primarily for the design of nonlinear systems. Let us recall how diverse and flexible the known methods of the investigation of SISO nonlinear systems proposed by different authors (Atherton 1975; Popov 1973) are. The majority of those methods are based not on the direct solution of Equation (3.7), but on the

<sup>2</sup> Only one pure imaginary root is possible in the case of double-valued nonlinearities, when  $G(A)$  [Equation (3.4)] is a complex number.

<sup>3</sup> We assume, here, the simplest case of *unique* solution of Equation (3.6).

fact that if the initial nonlinear system is limit cycling, then the linearized system must be on the stability boundary. Starting from that point and applying the algebraic or frequency-domain *stability criteria* for linear systems to the harmonically linearized system, one can not only calculate the limit cycle parameters, but also outline the ways of eliminating the limit cycle (by means of linear or nonlinear compensators, changing the gains, etc.), or bring it to oscillation with the acceptable amplitude and frequency. The solution to the problem here is put in a handy and visual graphical form (methods of Goldfarb, Teodorchik and others). In addition, which is just as important, all these methods allow not only the conditions for limit cycle occurrence to be revealed, but also its stability analysis to be conducted in a unified manner.

However, even in the SISO case, the ease and clearness of the design graphical techniques are essentially lost if we have to account for nonzero input signals and/or higher harmonics, if there are two or more nonlinearities and so on. Therefore, it is not surprising that in the multidimensional case, when the number of separate channels can be three, four and more, the conventional graphical methods actually prove to be inapplicable. This explains why, in the majority of work devoted to limit cycling MIMO systems (Ogorodnikov 1974, 1975; Nikiforuk and Wintonyk 1968; Patra *et al.* 1995; Patra and Pati 1998; Patra *et al.* 1999, etc.), the discussion is usually restricted to two-dimensional and, rarely, three-dimensional systems and, in these works, there are substantially developed approaches conceptually quite analogous to those used for the analysis of SISO systems with two nonlinearities. In this respect, as an exception, the papers by Gelb (1963) and Lindgren (1964) should be pointed out, in which an interesting 'structural' technique is proposed for the investigation of the limit cycle in two-dimensional symmetrical systems. The papers and monographs by Krassovski (1961), Kazamarov *et al.* (1967), Chorol *et al.* (1976) and some others should also be noted, in which, dynamical processes in nonlinear two- and three-dimensional *simple antisymmetrical* systems are investigated by the *complex coordinates and complex transfer functions* method and in which the harmonic balance equations are reduced to the classical Goldfarb form.

On the whole, the effectiveness of the describing function method in its common graphical interpretation decreases drastically if  $N \geq 3$ . Roughly speaking, that method, being a *design* method in the SISO case, loses that essential quality with the increase in the number of channels, and becomes a method for the numerical solution of the problem. Of course, one can seek the reasonable values of the MIMO system parameters by some enumerative techniques or by the method of successive approximations, but it would demand solving an extremely large number of nonlinear algebraic equations resulting from the harmonic linearization, which makes such approaches rather laborious and not very promising. Besides, since it is impossible to judge about the conditions of existence or absence of a limit cycle proceeding from the general form of the mentioned equations, here, it is not quite clear in what manner one should perform the changes of parameters, and much depends simply on the good luck or engineering experience and intuition of the designer.

The approach based on the application of the CTF method to harmonically linearized MIMO systems discussed in this chapter (Gasparyan 1986) allows these obstacles to be overcome essentially. In the chapter, the necessary conditions for the existence of a limit cycle in nonlinear MIMO systems of an arbitrary dimension are given. On the basis of these conditions, one can virtually extend to multivariable systems all the main results of the classical control theory of nonlinear SISO systems, namely the results concerning the symmetrical and biased one-frequency limit cycle, accounting for higher harmonics, stability analysis of the limit cycle,

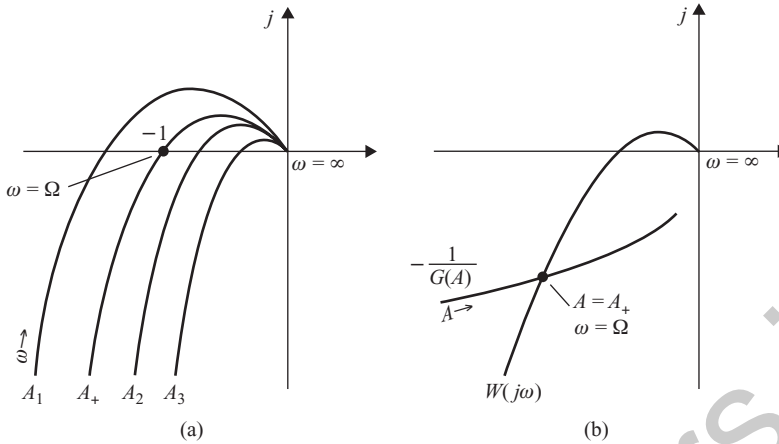


**Figure 3.2** Investigation of the limit cycle in nonlinear SISO systems. (a) A family of the loci  $W(j\omega)G(A)$  for different  $A = A_i$  (the Teodorchik method); (b) the Goldfarb method.

etc. (Popov 1973). A specific feature of the discussed methods is that they look like a direct generalization of the well known classical methods to a high dimensional problem and, for  $N = 1$ , they just coincide with the classical ones. Besides, these methods embrace many of the results now available in the technical literature. First of all, this concerns the above-mentioned methods of investigation of the two-dimensional symmetrical and simple antisymmetrical systems, excluding antisymmetrical systems with the amplitude-phase modulation of signals where the complex coordinates and transfer functions method is more efficient (if not the only one possible) (Kazamarov *et al.* 1967; Chorol *et al.* 1976).

Since, in the following, we shall always emphasize the relationship and succession of the methods of the limit cycle investigation in SISO and MIMO systems, it makes sense to dwell in more detail on the main classical methods and techniques for evaluating the limit cycle parameters in the SISO nonlinear system of Figure 3.1 mentioned earlier. The frequency-domain condition for the harmonically linearized system to be on the stability boundary can be written in two equivalent forms:

$$W(j\Omega)G(A) = -1 \tag{3.8}$$

and

$$W(j\Omega) = -\frac{1}{G(A)}, \tag{3.9}$$

which lead to somewhat different graphical procedures. Let us consider the complex plane of the Nyquist plots first. In accordance with Equation (3.8), for the graphical evaluation of the amplitude  $A$  and frequency  $\Omega$ , we should plot a family of  $G(A_i)W(j\omega)$  loci for different  $A_i = \text{const}$  and for the frequency  $\omega$  changing from zero to infinity [Figure 3.2(a)].<sup>4</sup> In the

<sup>4</sup> In the Russian technical literature, this method is sometimes called the ‘energy’ method of Teodorchik (Naumov 1972). Further, for brevity, we shall refer to it as the Teodorchik method.

case of  $F(x)$ , a single-valued nonlinearity, the coefficients  $G(A_i)$  are real numbers and the family of the loci  $G(A_i)W(j\omega)$  is obtained from the usual locus  $W(j\omega)$  of the linear part by the corresponding changes of the magnitude  $|W(j\omega)|$ . In the case of multiple (usually, double-valued) nonlinearities, besides multiplying each point of  $W(j\omega)$  by  $|G(A_i)|$ , an additional rotation of the whole locus around the origin of the complex plane through the angle  $\arg G(A_i)$  is needed. If, for some  $A_i = A_+$ , the locus of  $G(A_+)W(j\omega)$  passes through the point  $(-1, j0)$ , then that amplitude  $A_+$  is the solution to Equation (3.8) and the limit cycle frequency  $\Omega$  sought is equal to the value of  $\omega$  at the point  $(-1, j0)$  [Figure 3.2(a)]. Note that the described procedure of evaluating the parameters of the predicted limit cycle is the same also in the case of frequency-dependant nonlinearities, when  $G(A) = G(A, \Omega)$ .

Based on Equation (3.9), the locus of the negative reciprocal gain  $-1/G(A)$  (as a function of the amplitude  $A$ ) is drawn on the Nyquist plot of the system linear part  $W(j\omega)$  [Figure 3.2(b)].<sup>5</sup> The limit cycle parameters  $A_+$  and  $\Omega$  are defined here by the intersection point of the loci  $W(j\omega)$  and  $-1/G(A)$ . If the nonlinearity depends also on frequency, then a family of  $-1/G(A, \Omega_i)$  loci is plotted for different  $\Omega_i = const$ . The solution to the problem corresponds here to such an intersection of  $W(j\omega)$  and  $-1/G(A, \Omega_i)$ , for which parameter  $\Omega_i$  of the locus  $-1/G(A, \Omega_i)$  coincides with the frequency  $\omega$  of  $W(j\omega)$  at the intersection point.

If neither of the loci of Figure 3.2(a) traverses the point  $(-1, j0)$  or there are no intersections of the loci of Figure 3.2(b), then this means that there is no limit cycle of the sought sinusoidal form [Equation (3.2)] in the system. At that, it is not excluded that if the linear part does not possess good filtering properties, a limit cycle of more complicated waveform can in fact occur in the system. The graphical evaluation of Equations (3.8) and (3.9) can also be performed by using the logarithmical characteristics (the Bode diagrams) and the Nichols plots. Taking a logarithm of Equations (3.8) and (3.9), we obtain the following conditions for the harmonically linearized system to be on the stability boundary:

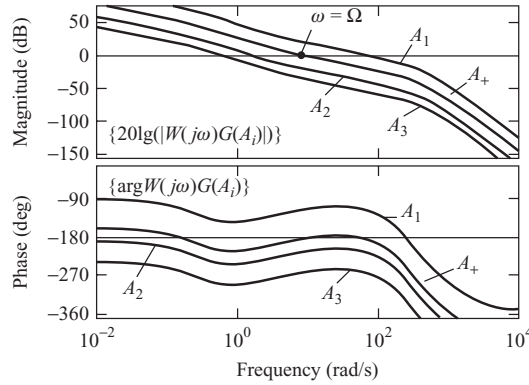
$$20 \lg (|W(j\Omega)G(A)|) = 0, \quad \arg W(j\Omega)G(A) = -180^\circ \quad (3.10)$$

$$20 \lg (|W(j\Omega)|) = -20 \lg (|G(A)|), \quad \arg W(j\Omega) = -180^\circ - \arg G(A). \quad (3.11)$$

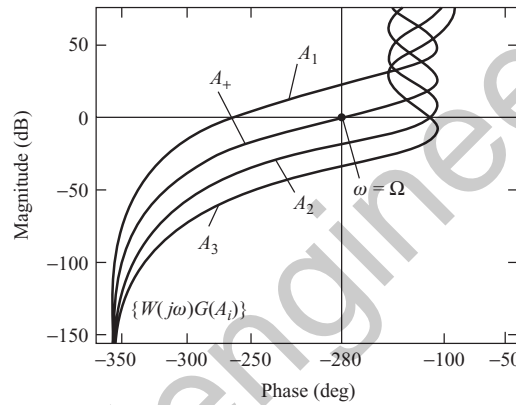
Geometrical constructions on the planes of Bode and Nichols diagrams, corresponding to the conditions in Equation (3.10), are given in Figure 3.3 and do not need any special comments. In Figure 3.4, it is shown how one can solve the problem on the plane of Bode diagrams using Equation (3.11), namely using the logarithmical form of the Goldfarb method. The limit cycle parameters here are determined by the intersection points of the Bode phase diagram of the linear part  $\Psi[W(j\omega)]$  with the so-called *Stability Phase Boundary* (SPB) (Rabinovich 1969), which is the mapping of the locus  $-1/G(A)$  on the Bode phase diagram  $\Psi[W(j\omega)]$ .<sup>6</sup> The construction of the SPB is accomplished with the help of logarithmic characteristics of  $-1/G(A)$ . In Figure 3.4, that procedure is illustrated, for two points, by the solid lines with arrows. The values of  $A_+$  and  $\Omega$  are found by the intersections of the SPB

<sup>5</sup> Seemingly, a similar procedure was first proposed by Goldfarb (1941). Hereinafter, we shall call it the Goldfarb method. It should be noted that the describing function method was actually developed concurrently in different countries by many researchers, so this method, as well as the Teodorchik method, can have other names in the literature on nonlinear control. Nevertheless, we shall retain, for brevity, the above appellations.

<sup>6</sup> Besides plotting the SPB, one can also map the locus of  $-1/G(A)$  on the Bode magnitude plot of the linear part. The resulting curve is called the *Critical Gain Boundary* (CGB) (Vavilov 1970). We suggest that the reader performs the corresponding graphical constructions on his or her own, based on Figure 3.4.



(a)



(b)

**Figure 3.3** Investigation of the limit cycle in SISO systems based on the conditions in Equation (3.10). (a) The plane of Bode diagrams; (b) the Nichols plane.

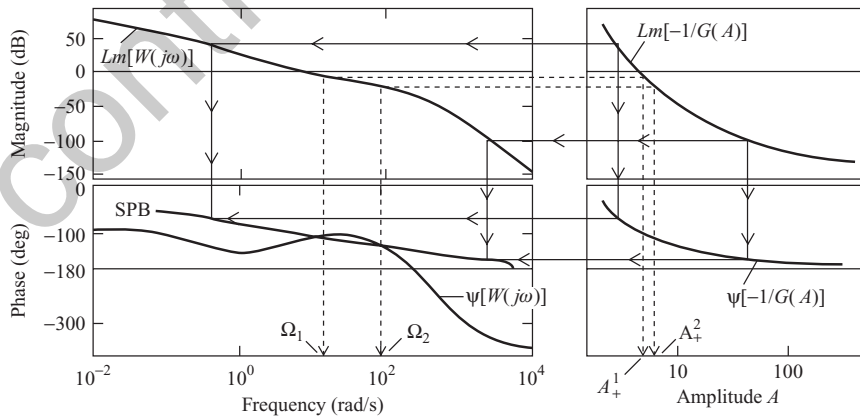


**Figure 3.4** Investigation of the limit cycle in SISO systems on the plane of the Bode phase diagram based on the conditions in Equation (3.11) (the construction of the SPB).

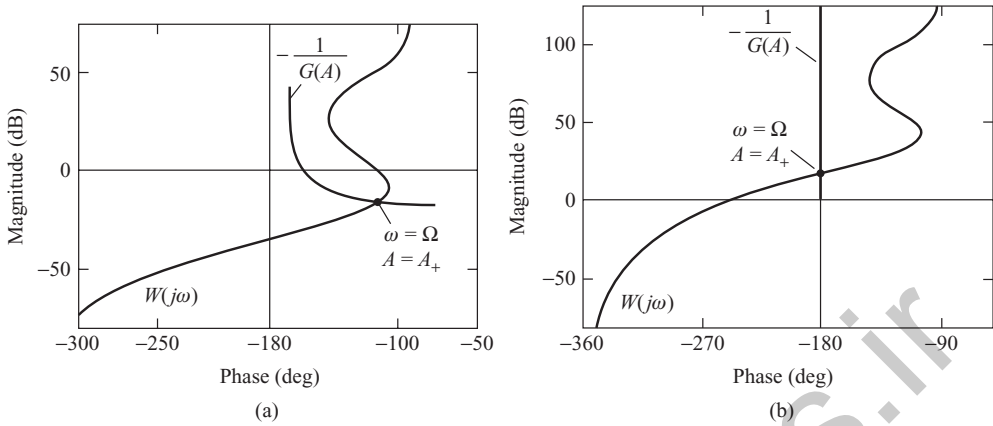


**Figure 3.5** Investigation of the limit cycle in SISO systems on the Nichols plane based on the conditions in Equation (3.11). (a) Double-valued nonlinearity; (b) single-valued nonlinearity.

with  $\Psi[W(j\omega)]$  (the dashed lines in Figure 3.4). Note that in this case, we have two intersections, namely two solutions to the problem, where only one solution corresponds to a *stable* limit cycle.<sup>7</sup>

The geometrical interpretation of the Goldfarb method on the Nichols plane for the cases of single- and double-valued nonlinearities is shown in Figure 3.5.<sup>8</sup> The instance of a single-valued nonlinearity is of certain interest in the SISO case, since, here, there is no phase shift of the fundamental harmonic at the output of the nonlinearity, and the whole locus  $-1/G(A)$  is located on the negative axis of the Nyquist complex plane. Correspondingly, on the Nichols plane, that locus is located along the vertical axis  $-180^\circ$  [Figure 3.5(b)]. It is easy to understand that in the case of single-valued nonlinearities, the limit cycle frequency (if the limit cycle does exist) is determined solely by the system linear part and does not depend at all on the specific form of the nonlinearity. Thus, in Figure 3.5(b), the limit cycle analysis for a system with an ideal saturation nonlinearity is presented, where the describing function  $G(A)$  is real and changes from unity to zero as the amplitude  $A$  changes from zero to infinity (Atherton 1975). It is evident from Figure 3.5(b) that a limit cycle is possible in such a system only if the corresponding linear system (that is the system without saturation) is *unstable*, since, otherwise, there will be no intersection of  $W(j\omega)$  and  $-1/G(A)$ . The limit cycle frequency in that system is equal to the frequency at which the stability gain margin is determined, i.e. where the phase of the open-loop linear system equals  $-180^\circ$ . As we shall see, analogous situations can occur also in nonlinear MIMO systems.

In conclusion, we should note that because of the restriction on the book length, many computational problems of limit cycle evaluation are not discussed. This mainly concerns biased (nonsymmetrical) limit cycles and accounting for higher harmonics. If necessary or desirable, the reader can look more deeply into the solution to these problems on his or her own.

<sup>7</sup> An approximate criterion of limit cycle stability is discussed in Section 3.2.

<sup>8</sup> As another exercise, it is suggested that the reader find out how the SPB and CGB look for single-valued nonlinearity (Figure 3.4 corresponds to the case of a double-valued nonlinear element).

### 3.2 MATHEMATICAL FOUNDATIONS OF THE HARMONIC LINEARIZATION METHOD FOR ONE-FREQUENCY PERIODICAL PROCESSES IN NONLINEAR MIMO SYSTEMS

Let us derive, following the monograph by E. Popov (1973), exact vector equations of a harmonically linearized MIMO system under the assumption of *one-frequency* periodical motions (Gasparyan 1986).<sup>9</sup> The matrix block diagram of a general nonlinear MIMO system is shown in Figure 3.6, where  $\varphi(t)$ ,  $x$ ,  $y$  are  $N$ -dimensional vectors;  $p = d/dt$  is the operator of

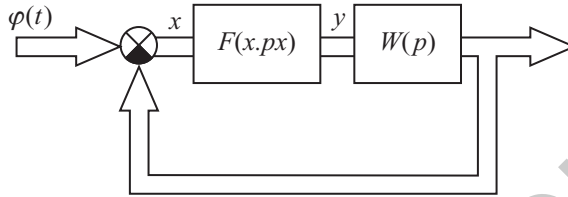


Figure 3.6 Matrix block diagram of a general nonlinear MIMO system.

differentiation;  $W(p) = \{w_{kr}(p)\}$  is an  $N \times N$  transfer matrix of the system linear part in differential form; and  $F(x, px) = \{F_{kr}(x_r, px_r)\}$  is an  $N \times N$  functional matrix of nonlinear elements depending on variables  $x_r$  ( $r = 1, 2, \dots, N$ ) and their derivatives. The elements on the principal diagonals of matrices  $W(p)$  and  $F(x, px)$  characterize linear and nonlinear parts in the direct channels of the MIMO system, and off-diagonal entries describe linear and nonlinear elements in the cross-connections between the channels. The nonlinear MIMO system of Figure 3.6 is described by two vector differential equations in operator form:

$$x + W(p)y = \varphi(t) \quad \text{and} \quad y = F(x, px)\bar{\mathbf{1}}, \quad (3.12)$$

where  $\bar{\mathbf{1}}$  is an  $N$ -dimensional vector with unity components.

Let us assume that the input signals are absent, i.e.  $\varphi(t) \equiv \mathbf{0}$ , and all nonlinearities have odd symmetrical characteristics. Then, investigating the one-frequency periodical motion of the MIMO system, we shall try the solution to the set of nonlinear Equations (3.12) in a waveform close to harmonic

$$x = x_1 + \varepsilon z(t), \quad (3.13)$$

where  $x_1$  is a vector of harmonic oscillations of frequency  $\Omega$  with components

$$x_{1r} = A_r \sin(\Omega t + \gamma_{1r}), \quad r = 1, 2, \dots, N, \quad \gamma_{11} = 0, \quad (3.14)$$

where  $\varepsilon$  is a small parameter and  $z(t)$  a bounded ( $|z(t)| \leq C$ ) but otherwise arbitrary function of time.

The solution for vector  $y$  can be far from sinusoidal and therefore can be written as an expression

$$y = F(x_1, px_1)\bar{\mathbf{1}} + \varepsilon \phi(t), \quad (3.15)$$

<sup>9</sup> This section can be omitted in the first reading.

which is close to the vector nonlinear function of the sinusoidal argument  $x_1$ . To obtain the significant relationship in Equation (3.15), one should substitute Equation (3.13) into the second equation in Equation (3.12) and expand it in the Taylor series in powers of  $\varepsilon$  in the vicinity of the sinusoidal function  $x_1$ . This yields

$$y = F(x_1, px_1)\bar{\mathbf{I}} + \varepsilon \left[ \sum_{r=1}^N \sum_{l=1}^{\infty} \varepsilon^{l-1} \text{diag} \left\{ \frac{\delta^l F_{ir}(\cdot)}{\delta x_r^l} (z_r)^l + \frac{\delta^l F_{ir}(\cdot)}{\delta (px_r)^l} (z_r)^l \right\} \bar{\mathbf{I}} \right], \quad (3.16)$$

where the expression in the square brackets is equal to the sinusoidal function  $\phi(t)$  in Equation (3.15). Assume that entering into Equation (3.16) partial derivatives of nonlinear elements  $F_{ir}(\cdot)$  with respect to  $x_r$  and  $px_r$  are finite, which is satisfied for the majority of nonlinearities occurring in real control systems (E. Popov 1973). Then it can be supposed that the function  $\phi(t)$  with  $\phi_i(t)$  components does not affect noticeably the oscillation waveform of variable  $y$ . Analogously to the SISO case, the small influence of function  $\phi(t)$  can be expected in the presence of discontinuous, for example, relay nonlinearities. Hence, the small by magnitude vector function  $\varepsilon\phi(t)$  in Equation (3.15) symbolizes the negligible influence of higher harmonics of variables  $x_r$  on the waveform of the vector  $y$  oscillation, but not the small size of the higher harmonics generated by nonlinearities  $F_{ir}(\cdot)$  under sinusoidal inputs  $x_{1r}$  [Equation (3.14)].

Resolving the elements of matrix  $F(x_1, px_1)$  in Equation (3.15) in the Fourier series and substituting Equations (3.15) and (3.13) into Equation (3.12), we get

$$\begin{aligned}
 x_1 + W(p) \left[ \sum_{r=1}^N \text{diag}\{F_{ir}^0\} \bar{\mathbf{I}} \right] + W(p) \left[ \sum_{r=1}^N \text{diag}\{C_{ir} \sin(\Omega t + \gamma_{1r}) + B_{ir} \cos(\Omega t + \gamma_{1r})\} \bar{\mathbf{I}} \right] \\
 + W(p) \left[ \sum_{r=1}^N \text{diag} \left\{ \sum_{k=2}^{\infty} F_{irk} \right\} \bar{\mathbf{I}} \right] = -\varepsilon z(t) - \varepsilon W(p)\phi(t), \quad (3.17)
 \end{aligned}$$

where  $F_{ir}^0$  ( $i, r = 1, 2, \dots, N$ ) are the constant (zero frequency) terms of the expansion of nonlinearities  $F_{ir}(x_{1r}, px_{1r})$  in the Fourier series;  $C_{ir}, B_{ir}, \gamma_{ir}$  are the amplitudes and phase shifts of the fundamental harmonics at the outputs of  $F_{ir}(x_{1r}, px_{1r})$ ; and

$$F_{irk} = M_{irk} \sin(k\Omega t + k\gamma_{1r} + \psi_{irk}); \quad i, r = 1, 2, \dots, N; \quad k = 2, 3, \dots \quad (3.18)$$

are the finite higher harmonics, where  $M_{kir} \rightarrow 0$  as  $k \rightarrow \infty$ .

If  $x_1$  is the exact first harmonic of the periodical solution to Equation (3.13) sought, then the functions  $\varepsilon z(t)$  and  $\varepsilon\phi(t)$  can be expanded in the Fourier series:

$$\varepsilon z(t) = \varepsilon \text{diag} \left\{ \sum_{k=2}^{\infty} A_{ki} \sin(k\Omega t + k\gamma_{1i} + \gamma_{ki}) \right\} \bar{\mathbf{I}} \quad (3.19)$$

$$\begin{aligned}
 \varepsilon\phi(t) &= \varepsilon \left[ \sum_{r=1}^N \sum_{l=1}^{\infty} \sum_{k=0}^{\infty} \varepsilon^{l-1} \phi_{rkl} \right] \\
 &= \varepsilon \sum_{r=1}^N \left[ \sum_{l=1}^{\infty} \varepsilon^{l-1} \phi_{r0l} + \sum_{l=1}^{\infty} \varepsilon^{l-1} \sum_{k=1}^{\infty} \text{diag}\{D_{irk} \sin(k\Omega t + k\gamma_{1r} + \theta_{irk})\} \bar{\mathbf{I}} \right], \quad (3.20)
 \end{aligned}$$

where  $\phi_{r0l}$  are constant vectors. Then, from Equation (3.17), we have a set of *exact* vector equalities for the corresponding harmonics:

$$\sum_{r=1}^N \text{diag}\{F_{ir}^0\} \bar{\mathbf{I}} = -\varepsilon \sum_{r=1}^N \sum_{l=1}^{\infty} \varepsilon^{l-1} \phi_{r0l} \quad (3.21)$$

$$x_1 + W(p) \left[ \sum_{r=1}^N \text{diag}\{C_{ir} \sin(\Omega t + \gamma_{1r}) + B_{ir} \cos(\Omega t + \gamma_{1r})\} \bar{\mathbf{I}} \right] =$$

$$-\varepsilon W(p) \left[ \sum_{r=1}^N \sum_{l=1}^{\infty} \varepsilon^{l-1} \sum_{k=1}^{\infty} \text{diag}\{D_{irll} \sin(\Omega t + \gamma_{1r} + \theta_{irll})\} \bar{\mathbf{I}} \right] \quad (3.22)$$

$$W(p) \sum_{r=1}^N \text{diag}\{M_{irk} \sin(k\Omega t + k\gamma_{1r} + \psi_{irk})\} \bar{\mathbf{I}}$$

$$+ \varepsilon \text{diag} \left\{ \sum_{k=2}^{\infty} A_{ki} \sin(k\Omega t + k\gamma_{1i} + \gamma_{ki}) \right\} \bar{\mathbf{I}} =$$

$$-\varepsilon W(p) \left[ \sum_{r=1}^N \sum_{l=1}^{\infty} \varepsilon^{l-1} \phi_{rkl} \right], \quad k = 2, 3, \dots \quad (3.23)$$

From Equation (3.21), the requirement for odd symmetry of  $F_{ir}(x_r, px_r)$  nonlinearities (Popov 1973) ensues:<sup>10</sup>

$$F_{ir}^0(A_r, \Omega) = \int_0^{2\pi} F_{ir}(A_r \sin \psi, A_r \Omega \cos \psi) d\psi = 0. \quad (3.24)$$

Equations (3.22) and (3.23) are the exact equations for the fundamental and higher harmonics, and they contain, on the right-hand side, small (by magnitude) terms of order  $\varepsilon$  and higher. Determining, in Equation (3.22), without these terms, the first approximation  $x_1^*$  for the sought periodical motion, we obtain

$$\left\{ I + W(p) \left[ G_R(A, \Omega) + \frac{p}{\Omega} G_I(A, \Omega) \right] \right\} x_1^* = 0, \quad (3.25)$$

where  $A$  is an  $N$ -dimensional vector with  $A_r$  components, and matrices  $G_R(A, \Omega) = \{q_{ir}^R(A_r, \Omega)\}$  and  $G_I(A, \Omega) = \{q_{ir}^I(A_r, \Omega)\}$  are composed from the common describing functions for nonlinearities  $F_{ir}(x_r, px_r)$  (Popov 1973). If all nonlinearities  $F_{ir}(x_r, px_r)$  are single-valued, then the matrix  $G_I(A, \Omega)$  in Equation (3.25) is identically equal to a zero matrix, and, for nonlinearities of form  $F_{ir}(x_r)$ , i.e. not depending on the derivatives of the variables  $x_r$ , matrices  $G_R(\cdot)$  and  $G_I(\cdot)$  do not depend on the frequency  $\Omega$ .

<sup>10</sup> Recall that the assumption about odd symmetry of nonlinearities has already been made earlier.

Equation (3.23) for the higher harmonics can be rewritten in the form

$$\begin{aligned}
 \varepsilon \text{diag} \left\{ \sum_{k=2}^{\infty} A_{ki} \sin(k\Omega t + k\gamma_{1i} + \gamma_{ki}) \right\} \bar{\mathbf{1}} &= -\varepsilon W(p) \left[ \sum_{r=1}^N \sum_{l=1}^{\infty} \varepsilon^{l-1} \phi_{rkl} \right] \\
 - \sum_{r=1}^N \text{diag} \left\{ \sum_{m=1}^N |w_{im}(jk\Omega)| M_{imk} \sin[k\Omega t + k\gamma_{1r} + \psi_{imk} + \arg w_{im}(jk\Omega)] \right\} \bar{\mathbf{1}}, &k = 2, 3, \dots
 \end{aligned} \tag{3.26}$$

Taking into account that  $M_{imk}$  quantities in [Equation (3.25)] are finite, we obtain the *generalized low pass filter property* of the MIMO system linear part (Figure 3.6) in the following form:

$$|w_{im}(jk\Omega)| \ll |w_{im}(j\Omega)|, \quad i, m = 1, 2, \dots, N; \quad k = 2, 3, \dots \tag{3.27}$$

Physically, the conditions in Equation (3.27) mean that all elements of the system linear part, both in the direct channels and in the cross-connections, must attenuate all higher harmonics, beginning from the second.

Finally, when investigating one-frequency *forced* oscillations in nonlinear MIMO systems, which can occur under external harmonic signals, the latter must be allowed for on the right-hand side of Equations (3.22) and (3.25). That problem is discussed in detail in the next chapter.

### 3.3 ONE-FREQUENCY LIMIT CYCLES IN GENERAL MIMO SYSTEMS

#### 3.3.1 Necessary conditions for the existence and investigation of the limit cycle in harmonically linearized MIMO systems

In this section, we shall derive, based on the concepts of the CTF method, the necessary conditions for the existence of a one-frequency limit cycle in harmonically linearized general MIMO systems (Gasparyan 1986), and shall outline some ways of numerically evaluating the problem.

##### 3.3.1.1 Symmetrical limit cycle

Investigating a symmetrical limit cycle in the MIMO system of Figure 3.6, we shall assume that there are no input signals, all nonlinearities  $F_{kr}(x_r, px_r)$  are odd and symmetrical, and, besides, the generalized low pass filter property of the linear part [Equation (3.26)] holds. Let us suppose that under these conditions, in the MIMO system, there is a steady-state limit cycle of frequency  $\Omega$ . Then, performing the harmonic linearization of nonlinearities, we obtain the following equation for the *approximate* evaluation of amplitudes  $A_i$ , phase shifts  $\gamma_i$  and the frequency  $\Omega$  of the first harmonics of the limit cycle [see Equation (3.25)]:

$$\left\{ I + W(p) \left[ G_R(A, \Omega) + \frac{P}{\Omega} G_I(A, \Omega) \right] \right\} x e^{j\Omega t} = \mathbf{0}, \tag{3.28}$$

where  $x$  designates the vector of *complex amplitudes* with  $x_i = A_i \exp\{j\gamma_i\}$  components (in the following, we shall assume, for convenience, that  $\gamma_i = 0$ ). In the mode of the steady-state limit cycle, the coefficients  $q_{ir}^R(A_r, \Omega)$  and  $q_{ir}^I(A_r, \Omega)$  are constant numbers and, for that mode, substituting  $p = j\Omega$  in Equation (3.28),<sup>11</sup> we have

$$[I + W(j\Omega)G(A, \Omega)]x = \mathbf{0}, \quad (3.29)$$

where

$$G(A, \Omega) = G_R(A, \Omega) + jG_I(A, \Omega) \quad (3.30)$$

is, in the general case of double-valued nonlinearities, a constant complex-valued matrix of the describing functions. We term

$$Q(j\Omega, A) = W(j\Omega)G(A, \Omega) \quad (3.31)$$

the complex transfer matrix of the open-loop harmonically linearized MIMO system. Suppose, for some fixed frequency  $\Omega$  and an amplitudes vector  $A$ , the eigenvalues  $q_i(j\Omega, A)$  of  $Q(j\Omega, A)$  are distinct. In that case, the normalized eigenvectors  $c_i(j\Omega, A)$  of  $Q(j\Omega, A)$  are linearly independent and they form some basis in space  $\mathbb{C}^N$  of the complex vectors  $x$ . Denote by  $\{c_i^+(j\Omega, A)\}$  a set of vectors dual to  $\{c_i(j\Omega, A)\}$ <sup>12</sup> and by  $C(j\Omega, A)$  a modal matrix composed of the eigenvectors  $c_i(j\Omega, A)$ . Then, the matrix  $Q(j\Omega, A)$  [Equation (3.31)] can be represented with the help of a similarity transformation and dyadic designations in the following canonical forms:

$$Q(j\Omega, A) = C(j\Omega, A) \text{diag}\{q_i(j\Omega, A)\} C^{-1}(j\Omega, A) \quad (3.32)$$

and

$$Q(j\Omega, A) = \sum_{i=1}^N c_i(j\Omega, A) q_i(j\Omega, A) c_i^+(j\Omega, A). \quad (3.33)$$

Henceforth, the functions  $q_i(j\Omega, A)$  ( $i = 1, 2, \dots, N$ ) we shall call, analogous to the linear case, the characteristic transfer functions (CTF) or transfer functions of SISO characteristic systems and the basis composed of the vectors  $c_i(j\Omega, A)$  the canonical basis of the open-loop harmonically linearized MIMO system. Nonlinear properties of the harmonically linearized MIMO system exhibit in the dependence of the CTFs  $q_i(j\Omega, A)$  and the canonical basis axes  $c_i(j\Omega, A)$  on the amplitudes vector  $A$  of the limit cycle (Figure 3.7). Recall that in linear general MIMO systems, the CTFs and the canonical basis depend, for  $s = j\omega$ , only on the frequency  $\omega$ . Based upon Equation (3.32), the vector equation [Equation (3.29)] can be represented as

$$C(j\Omega, A) \text{diag}\{1 + q_i(j\Omega, A)\} C^{-1}(j\Omega, A)x = \mathbf{0}, \quad (3.34)$$

<sup>11</sup> Recall that in Equation (3.28),  $p$  designates the operator of differentiation  $p = d/dt$ .

<sup>12</sup> See Section 1.2.3.

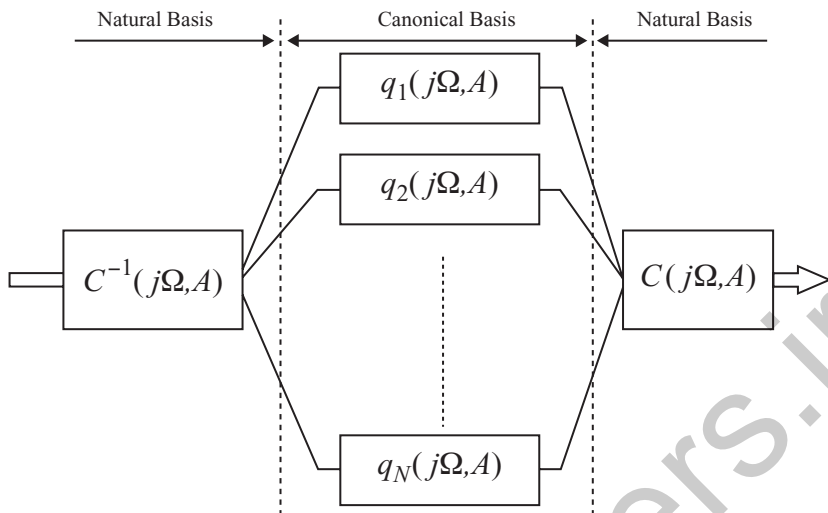


**Figure 3.7** Canonical representation of the open-loop harmonically linearized MIMO system.

from which it immediately follows that the canonical bases of the open- and closed-loop harmonically linearized MIMO systems coincide. The periodical sinusoidal solution  $x$  of Equation (3.29) [or (3.34)] corresponds to the pure imaginary roots of the characteristic equation of the closed-loop MIMO system, having the form

$$\begin{aligned} \det[I + Q(j\Omega, A)] &= \det C(j\Omega, A) \det[\text{diag}\{1 + q_i(j\Omega, A)\}] \det C^{-1}(j\Omega, A) \\ &= \prod_{i=1}^N [1 + q_i(j\Omega, A)] = 0. \end{aligned} \quad (3.35)$$

Evidently, Equation (3.35) splits into  $N$  characteristic equations:

$$1 + q_i(j\Omega, A) = 0, \quad i = 1, 2, \dots, N, \quad (3.36)$$

from which it follows that the root plane of the harmonically linearized MIMO system can be considered as a superposition of  $N$  root planes of SISO characteristic systems. Therefore, the closed-loop harmonically linearized system will have a pure imaginary root if and only if one of the closed-loop characteristic systems has the same root. Further, for the steady-state limit cycle to exist in the MIMO system, it is necessary that all other roots of Equation (3.35) lie in the left half-plane of the complex plane. In terms of the CTFs method, this means that if one of the characteristic systems is on the stability boundary, then all other systems must be *stable* and all dynamical processes in them must decay. This conclusion is very significant, since it leads to important considerations about the intrinsic geometrical features of limit cycling MIMO systems. We can see from the dyadic representation in Equation (3.33) that each characteristic system ‘acts’ in  $\mathbb{C}^N$  along one canonical basis axis. Consequently, if, in the steady-state limit cycle mode, only one (say, the  $r$ th) characteristic system is on the stability boundary and all other characteristic systems are stable, then the complex amplitudes vector  $x$  of the limit cycle must be, to all appearances, directed in  $\mathbb{C}^N$  along the axis  $c_r(j\Omega, A)$  corresponding to

the characteristic system on the stability boundary. Let us show that this extremely important property of limit cycling MIMO systems indeed holds. Toward this end, we rewrite Equation (3.29), using the dyadic representation in Equation (3.33), in the form

$$x = -Q(j\Omega, A)x = - \left[ \sum_{i=1}^N c_i(j\Omega, A) > q_i(j\Omega, A) < c_i^+(j\Omega, A) \right] x. \quad (3.37)$$

From here, it ensues that the vector  $x$  can be a solution to Equation (3.29) only if it is directed along one, for instance the  $r$ th, axis  $c_r(j\Omega, A)$  of the canonical basis of the harmonically linearized MIMO system. Besides, an additional condition must hold true here:

$$q_r(j\Omega, A) = -1, \quad (3.38)$$

which is the well known frequency form of the condition for the  $r$ th characteristic system to be on the stability boundary. Thus, we have established that in the steady-state limit cycle, only *one* of the SISO characteristic systems is ‘excited’ in the MIMO system, and the vector  $x$  of complex amplitudes is directed along the canonical basis axis corresponding to the excited system, i.e.

$$x = \alpha c_r(j\Omega, A), \quad (3.39)$$

where  $\alpha$  is a complex scalar, whose magnitude is equal to the magnitude (Euclidean norm) of the vector  $x$  and is equal, by the definition of a complex vector magnitude, to the magnitude of the real-valued amplitudes vector  $A$ :

$$|\alpha| = |x| = \sqrt{\sum_{i=1}^N |x_i|^2} = \sqrt{\sum_{i=1}^N A_i^2} = |A|. \quad (3.40)$$

Besides this, all other characteristic systems must be stable.

We shall call the condition in Equation (3.39) the *collinearity condition* of the vectors  $x$  and  $c_r(j\Omega, A)$  in the steady-state limit cycle in the MIMO system. Note that for the known vector  $A$  and frequency  $\Omega$ , the phase shifts  $\gamma_i$  of oscillations of the variables  $x_i$  at the inputs to nonlinearities are uniquely determined from vector Equation (3.29). This means that from Equation (3.39), the condition of collinearity of the amplitudes vector  $A$  and the *normalized real-valued vector*  $m_r(\Omega, A)$ , composed of the magnitudes of the vector  $c_r(j\Omega, A)$  components, explicitly follows, i.e.

$$A = |\alpha| m_r(\Omega, A) = |A| m_r(\Omega, A). \quad (3.41)$$

The condition in Equation (3.38) for the  $r$ th characteristic system to be on the stability boundary and the collinearity condition in Equation (3.39) [or (3.41)] are the *necessary conditions* for the existence of a symmetrical limit cycle in the nonlinear harmonically linearized MIMO system. For  $N = 1$ , the collinearity condition loses its meaning, and the condition in Equation (3.38) turns into the condition for a harmonically linearized SISO system to be on the stability boundary, i.e. into the necessary condition for the existence of a limit cycle in

common SISO systems well known from the classical control theory (Atherton 1975; Popov 1973).

Hence, assume that we manage to find such amplitudes  $A_i$  ( $i = 1, 2, \dots, N$ ) and the frequency  $\omega = \Omega$ , for which one of the closed-loop characteristic systems (say, the  $r$ th) is on the stability boundary, and all other characteristic systems are stable and, besides, the amplitudes vector  $A$  is collinear with the vector  $m_r(\Omega, A)$  composed of the magnitudes of components of the  $r$ th canonical basis axis  $c_r(j\Omega, A)$ . Then, these amplitudes  $A_i$  and frequency  $\Omega$  are the solution to the problem of the symmetrical limit cycle in the general nonlinear MIMO system of Figure 3.6. The relative phase shifts  $\gamma_i$  of oscillations of  $x_i$  (with respect to oscillation in the first channel) are equal here, based on Equation (3.39), to the differences in the arguments of the corresponding components and the first component of the  $r$ th canonical basis axis. If we provide, by a proper choice of the argument of the complex scalar multiplier  $\alpha$  in Equation (3.39), equality to zero of the argument of the first component of  $c_r(j\Omega, A)$ , i.e. if we perform ‘phase normalization’ of the vector  $c_r(j\Omega, A)$ , then the phase shifts of oscillations in the remaining channels will simply be equal to arguments of the corresponding components of  $c_r(j\Omega, A)$ .

### 3.3.1.2 Numerical evaluation of the symmetrical limit cycle in general MIMO systems

The problem of numerical evaluation of the limit cycle in nonlinear MIMO systems is rather complicated and cannot be generally solved without modern computer aids. As we discovered earlier, in the limit cycling MIMO system, only one of the characteristic systems is excited, where the obtained conditions necessary for limit cycle existence [Equation (3.38), (3.39) or (3.41)] do not give *a priori* any information about a specific characteristic system which can occur on the stability boundary. Therefore, when performing the numerical evaluation, it is necessary, with the purpose of finding all possible periodical solutions, to investigate each of  $N$  characteristic systems, one after another, by the conditions in Equation (3.38), (3.39) or (3.41), i.e. ‘to check up for limit cycle’ each of  $N$  canonical basis axes of the harmonically linearized MIMO system. There are two principal approaches to the solution of that problem. The first of them consists of determining a set of all vectors  $A$  and frequencies  $\Omega$  for which the  $r$ th characteristic system is on the stability boundary [i.e. the condition in Equation (3.38) is satisfied], and subsequent verification of the collinearity condition in Equation (3.41). Such an approach can prove efficient for the two-dimensional nonlinear uniform systems, which frequently occur in different technical applications and whose CTFs can be simply determined in analytical form. As for the general case, to study the limit cycle, it is more expedient to use the second approach, which is based on the necessary collinearity condition in Equation (3.41). Schematically, the essence of the approach consists in the following. Let us assign some constant values to the magnitude  $|\alpha| = |A|$  and the frequency  $\Omega$  in Equation (3.41). Then, we come, for some chosen index  $r$ , to the following nonlinear equation with respect to the amplitudes vector  $A$ :

$$A = |A|m_r(\Omega, A), \quad |A| = const, \Omega = const. \quad (3.42)$$

The distinctive feature of this equation is that for  $N > 3$ , its right-hand part cannot always be expressed in analytical form, and is to be found with the help of iterative procedures for evaluating eigenvalues and eigenvectors of complex-valued square matrices (Voevodin and

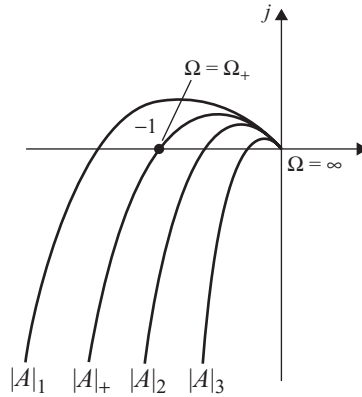


**Figure 3.8** Investigation of limit cycle along the  $r$ th canonical basis axis [a family of loci  $q_r(j\Omega, A)$  for different  $|A| = \text{const}$  as  $\Omega$  changes from 0 to  $\infty$ ].

Kuznetsov 1984). The solution to Equation (3.42) (if it does exist) gives the amplitudes vector  $A$  satisfying (for the chosen  $|A| = \text{const}$  and  $\Omega = \text{const}$ ) the collinearity condition in Equation (3.41), as well as the corresponding value of the CTF  $q_r(j\Omega, A)$ .<sup>13</sup> Changing, for  $|A| = \text{const}$ , the frequency  $\Omega$  with some step  $\Delta\Omega$  and solving each time Equation (3.42), we shall find a parametrical set  $\{A(\Omega)\}$  of vectors  $A$ , satisfying the necessary collinearity condition in Equation (3.41), and a set  $\{q_r(j\Omega, A)\}$  of the CTFs of the  $r$ th characteristic system. This enables us to plot in the complex plane the locus  $q_r(j\Omega, A)$ , whose distinctive feature is that at any of its points (for any frequency  $\Omega$ ), the condition in Equation (3.41) is satisfied and there is a ‘collinear’ vector  $A$ . Varying the value of the magnitude  $|A|$ , we get a parametrical family of the  $r$ th characteristic system loci for different  $|A| = \text{const}$  as the frequency  $\Omega$  changes over the appropriate range (Figure 3.8). If, for some value  $|A| = |A|_+$ , the locus  $q_r(j\Omega, A)$  passes in the complex plane through the point  $(-1, j0)$ , then both necessary conditions in Equations (3.38) and (3.41) for limit cycle existence are satisfied, and the parameter  $\Omega = \Omega_+$  at the locus  $q_r(j\Omega, A)$  at the point  $(-1, j0)$  determines both the frequency  $\Omega_+$  and the vector  $A_+ = A(\Omega_+)$  of amplitudes  $A_i$ .<sup>14</sup> If Equation (3.42) has no solution for any values of  $|A|$  and  $\Omega$ , or none of the loci of the family  $\{q_r(j\Omega, A)\}$  traverses the point  $(-1, j0)$ , then the limit cycle with the excitation of the  $r$ th characteristic system is impossible in the MIMO system. Note that for  $N = 1$ , the discussed approach to the investigation of the limit cycle coincides with the ‘energy’ method of Teodorchik known in the classical nonlinear control theory [see Figure 3.2(a)].

As indicated earlier, for the limit cycle in the MIMO system to exist, it is also required, besides the satisfaction of the conditions in Equations (3.38), (3.39) and (3.41) for some  $r$ , that all other characteristic systems be stable. The test for stability of these systems can be carried out by any method of the stability analysis of linear MIMO systems, but the most appropriate and simple way is based on the frequency-domain approach, consisting in the following. The vector  $A_+$  and frequency  $\Omega_+$  found at the first stage are substituted in the matrix  $G(A, \Omega)$

<sup>13</sup> The eigenvalues of the matrix  $Q(j\Omega, A)$  are evaluated at each step of the numerical solution of Equation (3.42) when evaluating the set of eigenvectors  $c_i(j\Omega, A)$  and separating the  $r$ th vector  $c_r(j\Omega, A)$ .

<sup>14</sup> Hereinafter, we shall preserve designations  $A_+$  and  $\Omega_+$  for indicating the limit cycle parameters in the MIMO system.

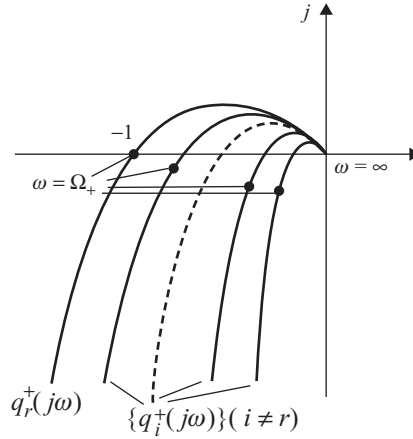


**Figure 3.9** Stability investigation of not excited characteristic systems.

[Equation (3.39)], which results in a constant numerical matrix  $G^+$ . Afterwards,  $N$  loci of the CTFs  $q_i^+(j\omega)$  of the matrix

$$Q_+(j\omega) = W(j\omega)G^+ \quad (3.43)$$

are plotted in the complex plane as  $\omega$  changes from zero to infinity (Figure 3.9). Matrix  $Q_+(j\omega)$  [Equation (3.43)] represents the complex transfer matrix of the open-loop MIMO system harmonically linearized in the vicinity of the investigated periodical mode with the excitation of the  $r$ th characteristic system. For  $\omega = \Omega_+$ , the set of points at the family of loci  $q_i^+(j\omega)$  ( $i = 1, 2, \dots, N$ ) coincides with the set of eigenvalues of the matrix  $Q(j\Omega_+, A_+)$  [see Equation (3.31)]. In particular, the  $r$ th characteristic gain loci  $q_r^+(j\omega)$  passes through the point  $(-1, j0)$  for  $\omega = \Omega_+$ . Even if one of other loci  $q_i^+(j\omega)$  ( $i \neq r$ ) of  $Q_+(j\omega)$  encompasses the point  $(-1, j0)$ , then the determined earlier vector  $A$  and frequency  $\Omega$  cannot correspond to the actual limit cycle, since the characteristic Equation (3.35) will have not only a pure imaginary root (or two pure imaginary roots), but also some roots in the right half-plane. Finally, note that the investigation of the conditions for the  $r$ th characteristic system being on the stability boundary and the stability analysis of other characteristic systems can be accomplished, similarly to a common SISO case (see Section 3.1), at the planes of the Bode and Nichols diagrams.

**Example 3.1** Consider the two-axis indirect guidance system of the telescope described in Example 1.1. Let there be nonlinear elements  $F_1(x_1)$  and  $F_2(x_2)$  in the separate channels of the system [Figure 3.10(a)]. In particular, the stellar sensors in the practical guidance systems usually have static characteristics with saturation [Figure 10(b)]. Assume that the angles  $\alpha_1$  and  $\alpha_2$  are  $\alpha_1 = 30^\circ$  and  $\alpha_2 = 20^\circ$ , and the transfer functions  $W_1(s)$  and  $W_2(s)$  of the linear parts of the channels are

$$W_1(s) = \frac{5000}{s(s+10)(s+20)}, \quad W_2(s) = \frac{10000}{s(s+15)(s+25)}. \quad (3.44)$$

As is evident from the characteristic gain loci of the linear part shown in Figure 3.11, the linear guidance system with the transfer function  $W_1(s)$  and  $W_2(s)$  [Equation (3.44)] is unstable.

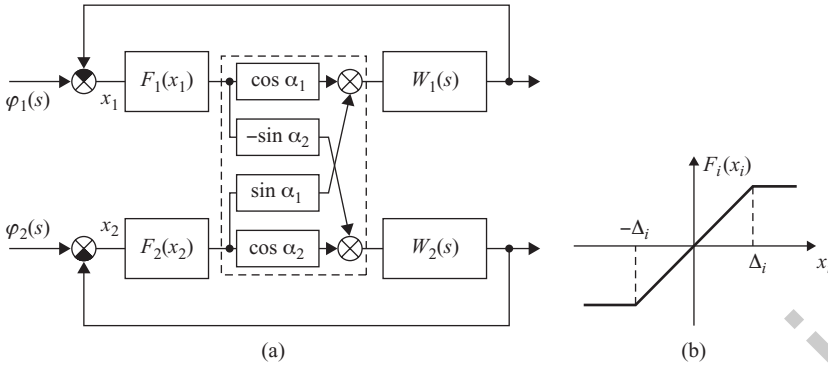


**Figure 3.10** Nonlinear guidance system of the telescope. (a) Block diagram of the system; (b) characteristic with saturation.

The nonlinearities in the separate channels we suppose to be identical and having an ideal saturation characteristic with unity gains and linear zone  $\Delta_1 = \Delta_2 = 4$  [Figure 3.10(b)]. Investigate the dynamics of that system assuming zero input signals, i.e.  $\varphi_1(t) = \varphi_2(t) = 0$ . The describing functions of the nonlinearities are defined by the known formulae (Popov 1973):

$$\begin{aligned}
 N_i(A_i) &= 1 \quad \text{for } 0 \leq A_i \leq \Delta_i \\
 N_i(A_i) &= \frac{2}{\pi} \left[ \sin^{-1} \left( \frac{\Delta_i}{A_i} \right) + \frac{\Delta_i}{A_i} \sqrt{1 - \left( \frac{\Delta_i}{A_i} \right)^2} \right] \quad \text{for } A_i > \Delta_i. \quad (3.45)
 \end{aligned}$$

In Figure 3.12(a) and (b), the families of the characteristic gain loci  $q_1(j\Omega, A)$  and  $q_2(j\Omega, A)$  of the open-loop harmonically linearized system constructed for different  $|A| = \text{const}$  as the frequency  $\Omega$  changes from zero to infinity are depicted, for vectors  $A$  satisfying the necessary condition of collinearity in Equation (3.41).

As can be seen from Figure 3.12, the loci of the second characteristic system for ‘collinear’ vectors  $A$  do not pass through the critical point  $(-1, j0)$  for any values of  $|A|$ , and the locus

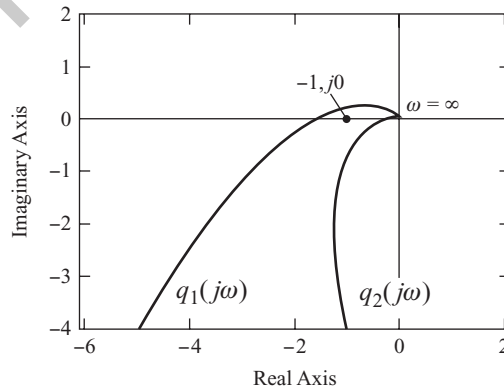


**Figure 3.11** Characteristic gain loci of the linear part.

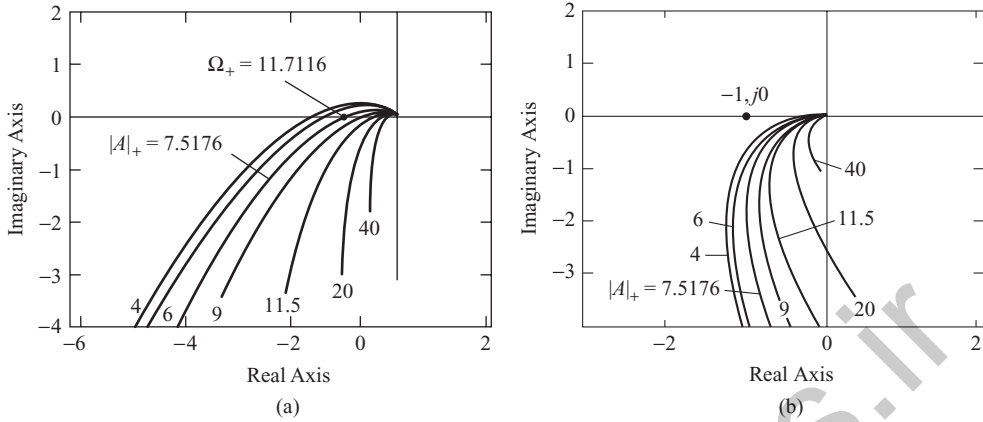


**Figure 3.12** Characteristic gain loci of the open-loop harmonically linearized system (the numbers indicate the values of  $|A|$ ). (a) First characteristic system [a family of loci  $\{q_1(j\Omega, A)\}$ ]; (b) second characteristic system [a family of loci  $\{q_2(j\Omega, A)\}$ ].

$q_1(j\Omega, A)$  traverses that point for  $|A| = |A|_+ = 7.5176$  and  $\Omega = \Omega_+ = 11.7116$ . This means that both the necessary conditions in Equations (3.38) and (3.41) for limit cycle existence in the first characteristic system are satisfied for the indicated values of  $|A|$  and  $\Omega$ . The calculated values of the self-oscillation amplitudes in the separate channels are  $A_1 = 6.7047$  and  $A_2 = 3.4$ , and the relative phase shift of oscillation in the second channel is equal to the difference in arguments of the second and first components of  $c_1(j\Omega_+, A_+)$  and is equal to  $\gamma_2 = -35.457^\circ$ . The characteristic gain loci  $q_1^+(j\omega)$  and  $q_2^+(j\omega)$  of the matrix  $Q_+(j\omega)$  [Equation (3.43)] are shown in Figure 3.13, from which it follows that the second characteristic system is stable in the vicinity of the discovered periodical mode with the excitation of the first characteristic system. Thus, for  $\Omega = 11.7116$ ,  $A_1 = 6.7047$  and  $A_2 = 3.4$ , all necessary conditions for existence of the limit cycle in the system of Figure 3.10 are satisfied.

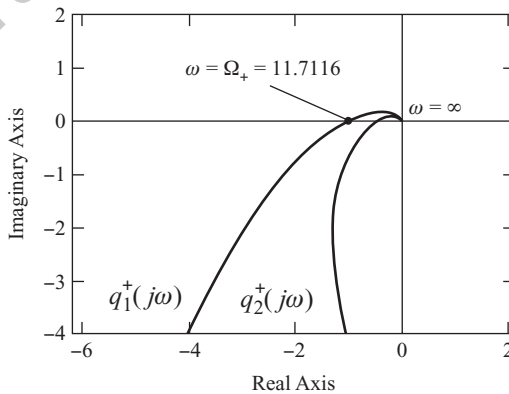


**Figure 3.13** Characteristic gain loci of matrix  $Q_+(j\omega)$ .

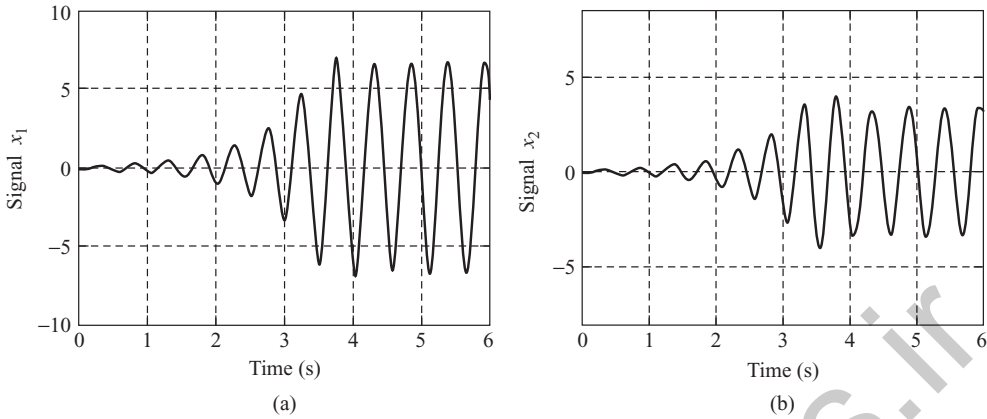


**Figure 3.14** The results of the system modelling with the help of Simulink. (a) First channel; (b) second channel.

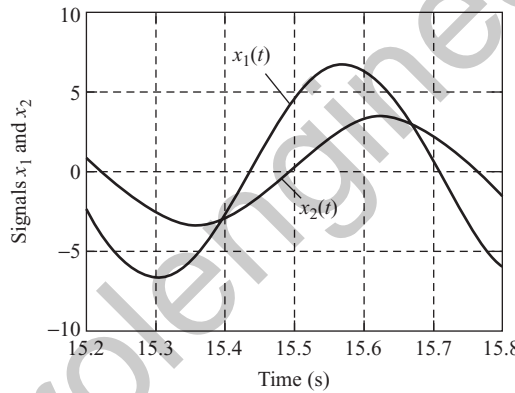


**Figure 3.15** Steady-state motion.

The results of the dynamical modelling of the system with the help of Simulink<sup>®15</sup> are shown in Figure 3.14. The graphs of the steady-state limit cycle are presented in Figure 3.15 and give the following values:  $A_1 = 6.702$ ,  $A_2 = 3.3551$  and  $\Omega = 11.6791$ . The numerical computation errors with respect to those obtained by modelling are less than 0.3% for the frequency, and 0.04 and 1.34% for amplitudes  $A_1$  and  $A_2$ , respectively. The high accuracy of the application of the *approximate* harmonic balance method is explained by the fact that the linear part of the system is quite a good low pass filter. The frequency dependencies of the magnitudes  $|W_1(j\omega)|$  and  $|W_2(j\omega)|$  of the transfer functions in Equation (3.44) are shown in Figure 3.16, in which the bold dots indicate the points corresponding to the frequencies of the fundamental and the third harmonics (since the saturation belongs to odd symmetrical nonlinearities, the output signals of nonlinear elements contain only odd harmonics). The

<sup>15</sup> Simulink<sup>®</sup> is a registered trademark of The MathWorks, Inc. Dynamical modelling of nonlinear systems in all worked examples of this chapter was performed with the help of the Simulink software.

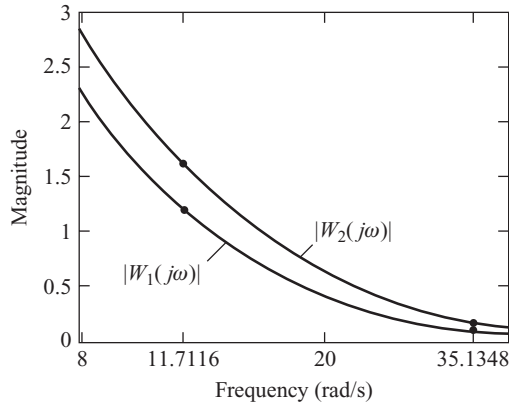


**Figure 3.16** Magnitude versus frequency characteristics of the linear part.

numerical values of magnitudes of the transfer functions  $W_1(j\omega)$  and  $W_2(j\omega)$  for the fundamental and third harmonics are:  $|W_1(j11.7116)| = 1.1961$ ,  $|W_2(j11.7116)| = 1.6252$  and  $|W_1(j35.1348)| = 0.0964$ ,  $|W_2(j35.1348)| = 0.1728$ . The third harmonic in the first channel is attenuated more than 10 times, and in the second channel about six times (note that the computational error of 1.34% of the oscillation amplitude in the second channel given above considerably exceeds the corresponding value of 0.04% for the first channel).

### 3.3.2 Stability of the limit cycle in MIMO systems

Having investigated each of  $N$  canonical basis axes of the harmonically linearized MIMO system, with the help of the technique discussed in the previous section, and thereby having determined all possible periodical solutions of Equations (3.38) and (3.39), one should further perform the analysis of their stability, to single out the solutions that can correspond to the real limit cycles. A rigorous classical way of limit cycle stability analysis, based on composing the so-called *variational equations*, leads to the rather complicated task of the stability analysis of the equilibrium point of linear differential equations with periodical coefficients (Popov 1973). Therefore, for engineering computations, it is more expedient to use, as in the SISO case, approximate frequency-domain stability criteria similar to common stability criteria of classical nonlinear control (Atherton 1975). As is known (see Section 3.3.1), in the steady-state limit cycle, the characteristic equation of the closed-loop harmonically linearized MIMO system must have at least one pure imaginary root (or a couple of complex-conjugate pure imaginary roots), under the additional condition for all other roots to be in the open left half-plane of the complex plane. Then, for the limit cycle to be stable, small positive increments  $\Delta A_i > 0$  of any amplitudes  $A_i$  and their combinations must cause the pure imaginary roots to move to the left half-plane and the negative increments  $\Delta A_i < 0$  to the right half-plane. In the previous section, it was shown that the complex plane of roots of the characteristic equation of the linearized MIMO system can be considered as a superposition of  $N$  root planes of SISO characteristic systems, in which the pure imaginary roots correspond to the characteristic system excited in the limit cycle. The last fact also becomes apparent in the passing of the locus  $q_r^+(j\omega)$  of the matrix  $Q_+(j\omega)$  [Equation (3.43)] through the critical point  $(-1, j0)$ ,

where  $r$  is the index of the excited system (Figure 3.9). This allows us to reduce the stability analysis of the limit cycle in the MIMO system to the stability analysis of the characteristic systems and to formulate the following *approximate* criterion:

*If, for any positive increments  $\Delta A_i > 0$  of any amplitudes  $A_i$  and their combinations, the characteristic gain locus  $q_r^+(j\omega)$  of the matrix  $Q_+(j\omega)$  [Equation (3.42)] corresponding to the excited characteristic system does not encompass and, for negative increments  $\Delta A_i < 0$ , does encompass the point  $(-1, j0)$ , then the limit cycle under investigation is stable.*

Note that all other loci  $q_i^+(j\omega)$  ( $i \neq r$ ) must not encompass here the point  $(-1, j0)$  or traverse it. Besides, if the matrix of the describing functions  $G(A, \Omega)$  [Equation (3.30)] depends on the frequency  $\Omega$ , then the above criterion must be satisfied for small deviations  $\pm\Delta\Omega$  in the limit cycle frequency. It should be emphasized once more that the above criterion is approximate and therefore one needs to exercise certain caution in using it. It is possible to judge to a first approximation about the limit cycle stability by the behaviour of the pure imaginary roots of the characteristic equation of the MIMO system under small variations in the *magnitude* of the amplitude vector  $A$ . Indeed, in the case of the stable limit cycle, the increase in the magnitude  $|A|$  must bring about moving the pure imaginary roots into the left half-plane, and the decrease in  $|A|$  moving them into the right half-plane. For the assessment of limit cycle stability, here, the parametrical family of the loci  $\{q_r(j\Omega, A)\}$  of transfer matrix  $Q(j\Omega, A)$  [Equation (3.31)], constructed for different values  $|A| = \text{const}$  (Figure 3.8), can be used. Thus, if, due to the increase in the magnitude  $|A|$ , the gain locus  $q_r(j\Omega, A)$  of the  $r$ th characteristic system encompasses the point  $(-1, j0)$  and, due to the decrease, does not encompass that point, then the investigated limit cycle is unstable. Let us dwell on that question in more detail. Geometrically, any perturbation of the amplitudes vector  $A$  is accompanied, due to nonlinear properties of the harmonically linearized MIMO system, by the perturbations of the axes of its canonical basis. In this respect, there are possible such perturbations of  $A$ , or, more correctly, of the vector of complex amplitudes  $x$ , for which the collinearity condition in Equation (3.39) is not violated, i.e. the perturbed vector  $x$  is directed along the same axis of the perturbed canonical basis of the MIMO system. For such situations, the inspection of the family of  $q_r(j\Omega, A)$  loci for different  $|A| = \text{const}$  gives an unambiguous answer about the stability or instability of the limit cycle. As for arbitrary perturbations of the amplitudes vector  $A$ , for the limit cycle to be stable, the above-formulated criterion must be satisfied.

Thus, when analysing the limit cycle stability, one should first assess the location of the family of the loci  $q_r(j\Omega, A)$  with respect to the critical point  $(-1, j0)$ . If it turns out that the investigated periodical solution is unstable under the ‘collinear’ perturbations, it cannot correspond to the practical limit cycle in the MIMO system. Otherwise, it is necessary, strictly speaking, to check up the satisfaction of the above general criterion. Of course, the situations in which the ‘collinear’ perturbations of the vector  $A$  indicate stability of the limit cycle but the general criterion does not hold are exceptional. Such situations are possible, for the most part, if there is no sufficient ground for the application of the describing function method. The issue here is not even in the influence of higher harmonics, but rather in the assumption of one-frequency oscillation. Therefore, in practical computation, it is usually enough to consider the family of  $q_r(j\Omega, A)$  loci for different  $|A| = \text{const}$  (Figure 3.8). Besides, for the practical assessment of the stability of the predicted limit cycle under ‘collinear’ perturbations, one can base on the characteristic gain loci  $q_i^+(j\omega)$  of the matrix  $Q_+(j\omega)$  [Equation (3.43)], without solving the nonlinear equation of the collinearity in Equation (3.41). For that purpose, the vectors  $(1 \pm \Delta)A_+$  are substituted in the matrix  $G(A, \Omega)$  [Equation (3.30)], where  $\Delta$  is a small *scalar*

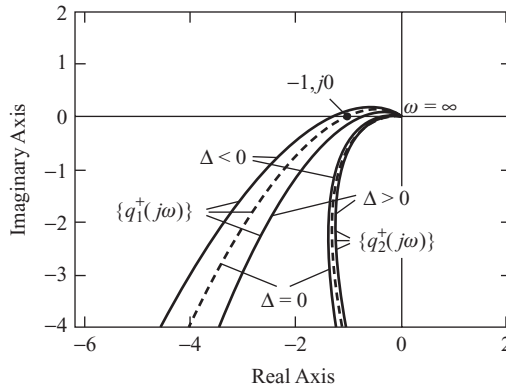


**Figure 3.17** Investigation of limit cycle stability.

increment, and then the characteristic gain loci  $q_i^+(j\omega)$  of the obtained matrices  $Q_+(j\omega)$  [Equation (3.43)] are plotted. In principle, taking into account that the stability criterion is approximate, as well as the geometrical nature of the limit cycle (excitation of only one characteristic system), such an analysis gives quite adequate results, being, at the same time, much less computationally intensive.

**Example 3.2** Investigate the stability of the limit cycle in the two-axis guidance systems of the previous example. The characteristic gain loci of the matrix  $Q_+(j\omega)$  in the Nyquist plane, plotted for positive and negative increments of the *magnitude* of vector  $A_+$ , i.e. for  $A = (1 + \Delta)A_+$  and  $A = (1 - \Delta)A_+$ , where  $\Delta = 0.2$ , are shown in Figure 3.17. The dotted lines in these graphs correspond to the initial (nonperturbed) limit cycle and coincide with the loci in Figure 3.13. As can be seen from Figure 3.17, under the positive increments of magnitude  $|A_+|$ , the  $q_1^+(j\omega)$  loci of the first characteristic systems excited in the limit cycle do not encompass the point  $(-1, j0)$  in the Nyquist plane. Under the negative increments of  $|A_+|$ , the picture bears an opposite character. As for the family of loci  $q_2^+(j\omega)$  of the second characteristic systems for  $\Delta = -0.2, 0, +0.2$ , they all correspond to stable systems. Hence, the approximate criterion of the limit cycle stability is satisfied and the discovered limit cycle with the excitation of the first characteristic system is stable. Of course, an analogous conclusion could also be drawn on the basis of the parametrical families of loci  $\{q_1(j\Omega, A)\}$  and  $\{q_2(j\Omega, A)\}$  of Figure 3.12, which were used for the investigation of the limit cycle with the help of necessary conditions in Equations (3.38)–(3.41).

Before proceeding to the discussion of nonlinear MIMO systems of different structural classes, we shall make some general remarks which are very important for proper comprehension of the material given in the present and next chapters.

**Remark 3.1** In Remark 1.5, we have already put a question as to what one should understand by the term *multivariable control system*. We concluded there that special attention should be paid to the *structure* of cross-connections in the MIMO system, since, very often, the initial system may be split, from the viewpoint of the stability analysis, into a number of subsystems of a lower order. Moreover, in some cases, the stability analysis of a linear MIMO system can be reduced to the analysis of its separate channels by conventional methods of the classical control theory (for example, for *triangular* systems). In the nonlinear case, the issue of the

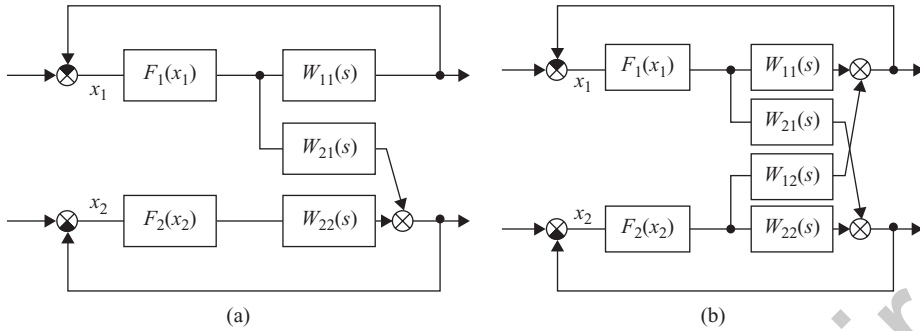


**Figure 3.18** Nonlinear two-dimensional systems. (a) System with one-directional cross-connections (triangular system); (b) system with a ‘full’ set of cross-connections.

MIMO system structure is more significant and demands very careful consideration. Thus, sometimes, the assumption of the *one-frequency* limit cycle in the MIMO system may be disputable. Furthermore, for some structures of MIMO systems, even the question of applying only the methods of limit cycle investigation can be doubtful and those methods must be supplemented by the methods of *forced* oscillation analysis.

To explain the essence of the matter more clearly, let us turn to a simple case of the two-dimensional nonlinear systems depicted in quite a general form in Figure 3.18, in which  $W_{ij}(s)$  ( $i, j = 1, 2$ ) are the elements of the system linear part and  $F_i(x_i)$  the nonlinear elements.

Consider, first, the triangular system in Figure 3.18(a), which is a system with one-directional connections from the first channel to the second. In the linear aspect (after excluding the nonlinearities), the stability of that system is determined only by the stability of separate channels, as pointed out in Remark 1.5, and does not depend on the transfer function  $W_{21}(s)$  (if we assume the latter to be stable). The possible dynamical processes in the *nonlinear* system of Figure 3.18(a) may have a much more diverse nature. Thus, if both nonlinear channels are stable, then the cross-connection  $W_{21}(s)$  cannot affect the stability of the overall system. The picture here is quite analogous to the linear variant. If the first channel is stable and a limit cycle exists in the second one, then that limit cycle does not have any action on the stability and dynamical processes of the first channel. If a limit cycle of some frequency  $\Omega_1$  exists in the first channel and the second channel is stable, then the latter goes to a forced oscillation mode of the same frequency and the whole system will oscillate with the frequency  $\Omega_1$  determined by the limit cycle in the first channel. Finally, if both isolated channels have limit cycles with different frequencies  $\Omega_1$  and  $\Omega_2$ , then two distinct situations are possible in the *second* channel. Thus, here, there may be a complex oscillatory motion which is the result of the superposition of the forced component of the frequency  $\Omega_1$  on the natural oscillations of the frequency  $\Omega_2$ . Note that unlike the linear systems, in this case, we do not have a simple superposition of two independent oscillations, but a complex motion with interrelated amplitudes and phase shifts. Also, the possibility of *capturing* (also called *entrainment* or *forced synchronization*) in the system is not excluded when the periodical signal from the first channel completely suppresses the existing limit cycle in the second channel and makes it oscillate with the frequency  $\Omega_1$ .

Note, however, that in most cases, the limit cycling modes are undesirable and the designers aim at the elimination of such modes. In this regard, it is easy to understand that there will be no limit cycle in the system of Figure 3.18(a) if there are no limit cycles in the isolated separate channels, and this can be achieved by exploiting usual methods of the classical control.

If the structure of cross-connections is ‘full’ [Figure 3.18(b)], then the system must be treated as a *single whole*, though, and in this case, the characteristics of the direct channels may significantly affect the system dynamics. The practice shows that if the separate channels of such a system are stable, or the frequencies of their limit cycles are close enough, and the cross-connected system is limit cycling, then a *one-frequency* limit cycle usually occurs whose parameters are determined by both characteristics of the direct channels and the cross-connections. Moreover, like the SISO case (Paltov 1975), beyond the region of parametrical stability of nonlinear MIMO systems, very often there is a region of self-oscillations which are mainly one-frequency. This feature has quite a sound justification. We know that the dynamics of linear systems is usually determined by a pair of *dominant* complex-conjugate roots that are the closest to the imaginary axis. As the gains of the channels increase, the dominant roots tend (if the difference between the number of all poles and zeros of the system exceeds two) to the right half-plane. It is very difficult to attain a situation here when more than one pair of pure imaginary roots appear at the imaginary axis for some critical values of the gains of the linear (linearized) system.<sup>16</sup> Of course, a two-frequency limit cycle may exist in the system of Figure 3.18(b). For instance, this can occur in the case of limit cycling separate channels, where the frequencies differ greatly, or if the cross-connections are ‘weak’. However, it is easy to eliminate limit cycles in the channels of such systems (and, consequently, in the cross-connected system) by common methods.

All that has been stated can immediately be extended to the case of nonlinear MIMO systems of higher dimensionality ( $N > 2$ ). In such systems, one should first inspect the structure of the cross-connections. The *scalar*, *diagonal* and *triangular* systems are of no special interest in this regard, since their investigation is reduced to the investigation of separate channels. If the transfer matrix of the harmonically linearized MIMO system has *block-scalar*, *block-diagonal* or *block-triangular* form, then each of the *diagonal* blocks of such a system, taken independently, characterizes some *interconnected* MIMO system of a lower order. The block-scalar and block-diagonal systems here are just a collection of separate interconnected subsystems that should be investigated independently. Each diagonal block of *subdiagonal* or *superdiagonal* block-triangular MIMO systems is connected with the next or previous blocks by one-directional cross-connections and does not affect their dynamics at all. Therefore, here also, one should investigate, first of all, the isolated diagonal blocks in which the one-frequency limit cycles are possible.

Thus, the situations in which nonlinear MIMO systems (or some of their subsystems) have just *one-frequency* limit cycles are typical and quite, if not the most, widespread in practice. Therefore, the methods discussed in Chapter 3, which actually represent an extension to the multivariable case of the well known classical methods, are very significant for the investigation of nonlinear MIMO system dynamics.

**Remark 3.2** In principle, for the numerical evaluation of parameters of the one-frequency limit cycle in MIMO systems, one can solve a set of  $N$  nonlinear complex-valued equations [Equation (3.29)] with respect to  $N$  unknown amplitudes  $A_1, A_2, \dots, A_N$ , frequency  $\Omega$  and  $(N - 1)$  relative phase shifts  $\gamma_2, \gamma_3, \dots, \gamma_N$ , where the phase of oscillation in the first channel is taken to be zero. However, such a direct evaluation of the algebraic equations of the system does not give any useful information on how and in what direction one should change the

<sup>16</sup> The presence of more than one pair of pure imaginary roots is necessary for more than one frequency to exist in the steady-state oscillation of the linear system on the stability boundary.

parameters of the MIMO system to eliminate the limit cycle or to reduce it, if necessary, to oscillations with the specified amplitudes and frequency. Generally, if a task of simply determining the parameters of limit cycle is posed, then it seems more expedient to model the dynamics of the nonlinear MIMO systems (for example, by Simulink). This allows the engineer or researcher not only to reveal the presence of the limit cycle, but also to obtain its exact waveform, as well as the curves of the transient processes.

The approach on the basis of the necessary conditions for limit cycle existence provides, in addition to a clear geometrical picture of the steady-state periodical processes in the MIMO system, a powerful leverage for developing engineering methods for the *design* of nonlinear MIMO systems. As we shall see in the next chapter, the designer has an opportunity, based on the results of the limit cycle analysis, to choose purposefully and reasonably the correction of the nonlinear system, preserving at the same time complete succession and connection with the design methods for linear MIMO systems.

### 3.4 LIMIT CYCLES IN UNIFORM MIMO SYSTEMS

The fact that the transfer functions of separate channels of uniform MIMO systems are the same and the cross-connections are rigid must evidently have an effect on the procedures of the investigation of that significant class of multivariable control systems. Indeed, we showed in the first chapters that the CTFs of linear uniform systems differ from the transfer function  $w(s)$  of identical channels only by the ‘gains’  $\lambda_i$  equal to eigenvalues of the numerical matrix of cross-connections  $R$ . Accordingly, the methods for stability and performance analysis of linear uniform systems may be brought quite close to the classical methods for SISO systems, as compared with the methods of investigation of general MIMO systems. It seems that the uniformity of separate channels must play an important role in the examination of nonlinear uniform MIMO systems. As the reader will discover, this assumption is completely valid. We shall see that the CTFs of the harmonically linearized uniform systems also differ from the transfer function  $w(s)$  only by the numerical coefficients  $\lambda_i(A)$ , which depend here on the amplitudes vector of limit cycle  $A$ , and which are the eigenvalues of a numerical matrix equal to the product of the cross-connections matrix  $R$  and a matrix of describing functions of nonlinearities. This allows us to reduce the conditions for the existence of a limit cycle in nonlinear uniform systems to the Goldfarb form, and thereby to simplify considerably the solution of the problem.

#### 3.4.1 Necessary conditions for the existence and investigation of limit cycles in uniform MIMO systems

Below, we shall extend the results of the previous section to the case of nonlinear uniform systems, the generalized block diagram of which is shown in Figure 3.19, where  $w(s)$  is the transfer function of identical separate channels,  $R$  the numerical matrix of rigid cross-connections and  $F(x) = \{F_{kr}(x_r)\}$  a functional matrix of the nonlinearities, where, for simplicity, it is assumed that they do not depend on the derivatives of the input variables  $x_r$ . Note that the representation of cross-couplings in the uniform system in the form of series connection of two matrices, where the elements of the first one are described by nonlinear dependencies  $F_{kr}(x_r)$  and the

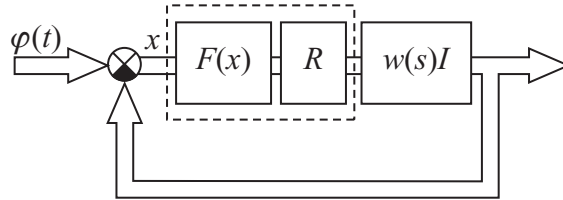


Figure 3.19 Matrix block diagram of the nonlinear uniform MIMO system.

second matrix is numerical, is rather conventional and not necessary. As will be clear later, the methods of investigation of periodical processes in nonlinear uniform systems are applicable without any alterations and if either of the indicated matrices is diagonal, if they are interchanged, when the cross-connections are described by a single matrix, some elements of which are specified as constant numbers and the others by nonlinear dependencies, etc. The analysis of one-frequency limit cycles in nonlinear uniform systems is totally based on the vector equations of harmonically linearized MIMO systems derived in Section 3.2, where one should replace the matrix  $F(x, px)$  by  $RF(x)$ , and the matrix of linear part  $W(s)$  by a scalar matrix  $w(s)I$ . An especially simple form here has the condition for the linear part to be a low pass filter:

$$|w(jk\Omega)| \ll |w(j\Omega)|, \quad k = 2, 3, \dots \tag{3.46}$$

in accordance with which, for the applicability of the harmonic balance method, it is required that the transfer function of the separate channels  $w(s)$  be a low pass filter.

Consider the uniform system of Figure 3.19, supposing that there are no input signals [ $\varphi(t) \equiv \mathbf{0}$ ], all nonlinearities  $F_{kr}(x_r)$  are odd-symmetrical and the transfer function  $w(s)$  satisfies the filter condition in Equation (3.46). If these assumptions hold and there is a limit cycle in the uniform system, then one can perform the harmonic linearization of nonlinearities and write down the following equation:

$$[I + w(j\Omega)RG(A)]x = \mathbf{0} \tag{3.47}$$

for an approximate evaluation of the amplitudes  $A_i$ , phases  $\gamma_i$  and the frequency  $\Omega$  of the fundamental harmonic of the periodical process. In Equation (3.47),  $x$  is the vector of complex amplitudes of the first harmonic or, more correctly, its first approximation, and  $G(A)$  the square matrix of the describing functions of nonlinearities. Let us term the significant for the further constructions matrix

$$N(A) = RG(A) \tag{3.48}$$

the *concomitant* matrix of cross-connections of the harmonically linearized uniform system in the steady-state limit cycle mode. If we exclude the nonlinear elements from the uniform system of Figure 3.19, then the concomitant matrix  $N(A)$  transforms into the numerical matrix of cross-connections  $R$ . As for the nonlinear uniform systems,  $N(A)$  depends here on the amplitudes vector  $A$  and, in the general case of double-valued nonlinearities, has *complex-valued* elements.

The transfer matrix

$$Q(j\Omega, A) = w(j\Omega)N(A) \quad (3.49)$$

of the open-loop harmonically linearized uniform system coincides up to the scalar multiplier  $w(j\Omega)$  with the concomitant matrix  $N(A)$ , which predetermines some essential geometrical features of the periodical processes. Suppose that in the steady-state limit cycle, the eigenvalues  $\lambda_i(A)$  of  $N(A)$  are *distinct*, i.e. the set  $\{c_i(A)\}$  of normalized eigenvectors of that matrix forms the basis of space  $\mathbb{C}^N$ . Then, denoting by  $\{c_i^+(A)\}$  the set of vectors, *dual* to  $c_i(A)$  ( $i = 1, 2, \dots, N$ ), and by  $C(A)$  the modal matrix composed of the vectors  $c_i(A)$ , Equation (3.34) can be represented in two canonical forms:

$$C(A)\text{diag}\{1 + \lambda_i(A)w(j\Omega)\}C^{-1}(A)x = \mathbf{0} \quad (3.50)$$

and

$$x = - \left[ \sum_{i=1}^N c_i(A) > \lambda_i(A)w(j\Omega) < c_i^+(A) \right] x \quad (3.51)$$

and the characteristic equation of the uniform system, in turn, in the form

$$\det[I + Q(j\Omega, A)] = \prod_{i=1}^N [1 + \lambda_i(A)w(j\Omega)] = 0. \quad (3.52)$$

Functions  $\lambda_i(A)w(j\Omega)$  in Equations (3.50)–(3.52) are called the CTFs or the transfer functions of the SISO characteristic systems, and the basis composed of the vectors  $c_i(A)$  – the canonical basis of the harmonically linearized uniform system. As can be seen from Equations (3.50) and (3.51), the CTFs  $\lambda_i(A)w(j\Omega)$  coincide up to the ‘gains’  $\lambda_i(A)$  [up to eigenvalues of the concomitant matrix  $N(A)$ ] with the transfer function  $w(j\Omega)$  of identical separate channels, and the canonical basis of the limit cycling uniform system coincides with the canonical basis of  $N(A)$  and does not depend at all on  $w(s)$ . Besides, if, in the case of linear uniform systems, the coefficients  $\lambda_i$  and vectors  $c_i$  are constant and completely determined by the matrix of cross-connections  $R$ , here, they depend in a nonlinear manner on the amplitudes vector  $A$ . It is evident from Equations (3.50)–(3.52) that only one of the characteristic systems ‘excites’ in the limit cycling uniform system, and the vector of the complex amplitudes  $x$  is directed along the corresponding eigenvector of the concomitant matrix  $N(A)$ , i.e. along the corresponding canonical basis axis. Thus, if we manage to find such a vector  $A$  and frequency  $\Omega$ , for which one of the characteristic systems is on the stability boundary, all other characteristic systems are stable, and the vector  $A$  is directed along the vector  $m_r(A)$  composed of the magnitudes of components of the axis  $c_r(A)$  associated with the excited characteristic system, then these  $A$  and  $\Omega$  satisfy the necessary conditions for the existence of the limit cycle in the uniform system. Mathematically, this can be written in the following form:

$$\lambda_r(A)w(j\Omega) = -1 \quad (3.53)$$

$$A = |A|m_r(A). \quad (3.54)$$

Here, the phase shifts of oscillations in the separate channels with respect to the first channel are equal to the differences of arguments of the corresponding components and the first component of  $c_r(A)$ .

### 3.4.1.1 Numerical evaluation of the limit cycle in uniform systems

In essence, the task of determining of  $A$  and  $\Omega$  by Equations (3.53) and (3.54) can be solved by the same methods as in the investigation of the limit cycle in nonlinear general MIMO systems. However, taking into account a relatively simple form of the conditions in Equations (3.53) and (3.54), those methods can be modified to a certain extent and maximally approached to the conventional Goldfarb method. To this end, rewrite the condition for the  $r$ th characteristic system to be on the stability boundary [Equation (3.53)] in the form

$$w(j\Omega) = -\frac{1}{\lambda_r(A)}. \tag{3.55}$$

Changing the value of the magnitude  $|A|$  in Equation (3.54) with some step  $\Delta|A|$  from zero to infinity, and solving Equation (3.54) for the corresponding  $|A| = const$  each time, we shall find a parametrical (with parameter  $|A|$ ) set of vectors  $A$ , satisfying the necessary collinearity condition in Equation (3.41), as well as the set  $\{\lambda_r(A)\}$  of the ‘gains’ of the  $r$ th characteristic system. We emphasize once more that we operate here with the concomitant matrix of cross-connections  $N(A)$  [Equation (3.48)]. Let us draw now on the Nyquist plot of  $w(j\Omega)$  the parametrical (with  $|A|$  a parameter) locus  $-1/\lambda_r(A)$ , corresponding to the right part of Equation (3.55) as  $|A|$  changes from zero to infinity (Figure 3.20). The locus  $-1/\lambda_r(A)$  is plotted, naturally, for those values of the parameter  $|A|$  for which there is the solution to Equation (3.54). If, for some  $|A| = |A|_+$ , there is an intersection of  $-1/\lambda_r(A)$  with  $w(j\Omega)$ , then this means that both the necessary conditions in Equations (3.53) and (3.54) for limit cycle existence hold and we have only to check the stability of all other characteristic systems. To this end, all other eigenvalues  $\lambda_i^+(A_+)(i \neq r)$  of the concomitant matrix  $N(A_+)$  are evaluated and the critical points  $-1/\lambda_i^+(A_+)(i = 1, 2, \dots, N, i \neq r)$  are marked in the complex plane (Figure 3.20). Evidently, for other characteristic systems to be stable in the vicinity of the revealed

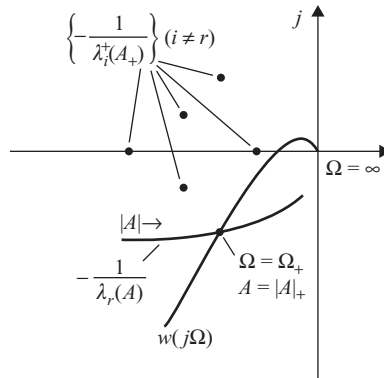
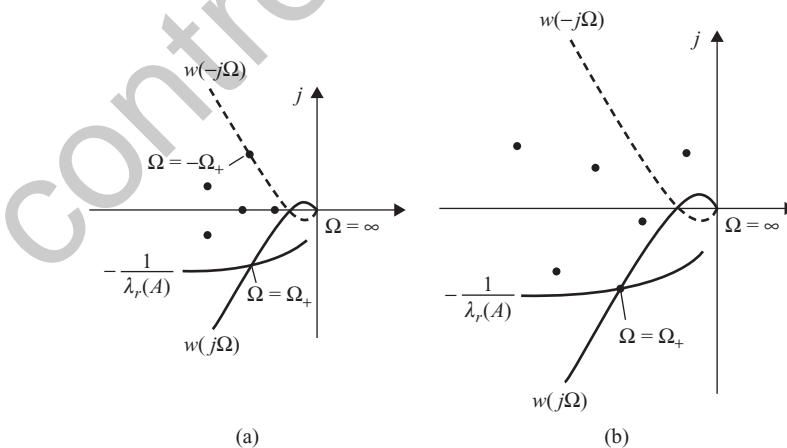


Figure 3.20 Investigation of the symmetrical limit cycle in uniform systems.

periodical mode with the excitation of the  $r$ th characteristic system, it is necessary that these points not be encompassed by the locus  $w(j\Omega)$  for positive frequencies  $\Omega > 0$ . If the critical points are not encompassed, then the solution determined by the intersection of  $w(j\Omega)$  and  $-1/\lambda_r(A)$  can correspond to the actual limit cycle in the uniform system; the frequency  $\Omega_+$  of oscillation is equal to the parameter  $\Omega$  at the locus  $w(j\Omega)$  at the intersection point, and the vector  $A_+$  is found by the value of  $|A| = |A|_+$  at the locus  $-1/\lambda_r(A)$ . No intersections of loci  $-1/\lambda_r(A)$  and  $w(j\Omega)$  indicate that a limit cycle with the excitation of the  $r$ th characteristic system is impossible. The same is true if there is an intersection but at least one of the critical points  $-1/\lambda_i^+(A_+)$  ( $i \neq r$ ) is encompassed by the locus  $w(j\Omega)$ . The latter means that the corresponding characteristic system is unstable for the vector  $A_+$  and, therefore, besides the pure imaginary roots of Equation (3.52), there are some roots in the right half-plane. Repeating the procedure described for all characteristic systems, we can find the set of all solutions satisfying the necessary conditions for the existence of the one-frequency limit cycle in the nonlinear uniform system.

When evaluating the critical points  $-1/\lambda_i^+(A_+)$ , there are two possible situations, depending on the types of nonlinearities  $F_{kr}(x_r)$ . Thus, if all nonlinearities of the system are single-valued, then, for any vectors  $A$ , all elements of the concomitant matrix  $N(A_+)$  [Equation (3.48)] are real numbers. The eigenvalues  $\lambda_i^+(A_+)$  of  $N(A_+)$  in such a case can be either real or complex-conjugate. The same concerns the eigenvectors of  $N(A_+)$ . Therefore, all critical points  $-1/\lambda_i^+(A_+)$  are located either on the real axis or, in pairs, symmetrically with respect to that axis, and a ‘complex-conjugate’ critical point at the negative ( $\Omega < 0$ ) branch of  $w(j\Omega)$  for  $\Omega = -\Omega_+$  corresponds to any intersection point of loci  $-1/\lambda_r(A)$  and  $w(j\Omega)$  for some frequency  $\Omega = \Omega_+$  [Figure 3.21(a)]. For the double-valued nonlinearities, the describing functions are complex-valued numbers and the concomitant matrix  $N(A)$  becomes complex-valued, i.e. its eigenvalues and eigenvectors cease to be complex-conjugate. This means that the distribution of the critical points  $-1/\lambda_i^+(A_+)$  ( $i \neq r$ ) loses the property of being symmetrical with respect to the real axis [Figure 3.21(b)]. Here, however, it is necessary to note a significant detail. The describing functions  $q_{ir}^R(\cdot) + jq_{ir}^I(\cdot)$  in the matrix  $G(A)$  in Equation (3.48) are



**Figure 3.21** Distribution of the critical points (the latter are shown by the bold dots). (a) Single-valued nonlinearity; (b) double-valued nonlinearity.

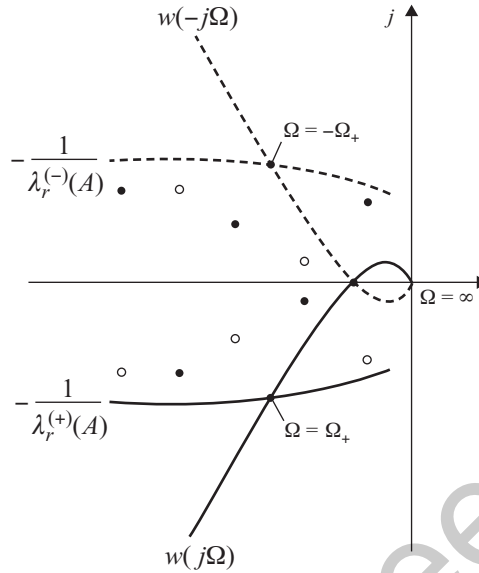


**Figure 3.22** Stability analysis in the case of double-valued nonlinearities.

obtained by the substitution of  $p = +j\Omega$  (see Section 3.3.1), i.e. they correspond to the positive frequencies  $\Omega > 0$ . For negative frequencies  $\Omega < 0$ , the describing functions have the form  $q_{ir}^R(\cdot) - jq_{ir}^I(\cdot)$ . Hence, in the case of double-valued nonlinearities, the matrix  $N(A)$  [Equation (3.48)] for  $\Omega < 0$  turns out to be complex-conjugate to  $N(A)$  for  $\Omega > 0$ . This results in eigenvalues and eigenvectors of  $N(A)$  for positive and negative frequencies being complex-conjugate to each other. To each critical point  $-1/\lambda_i^+(A_+)$  for  $\Omega > 0$  corresponds a complex-conjugate point  $-1/\lambda_i^-(A_+)$  for  $\Omega < 0$ , and to the whole locus  $-1/\lambda_r^+(A)$  for  $\Omega > 0$  corresponds a complex-conjugate locus  $-1/\lambda_r^-(A)$  for  $\Omega < 0$ . The latter cuts the negative branch of the locus  $w(j\Omega)$  at the frequency  $\Omega = -\Omega_+$  if there is the intersection of  $-1/\lambda_r^+(A)$  with the positive branch of  $w(j\Omega)$  at  $\Omega = \Omega_+$  (see Figure 3.22, in which the critical points for positive frequencies  $\Omega > 0$  are denoted by  $\bullet$  and for negative frequencies  $\Omega < 0$  by  $\circ$ ). In fact, we can state that the number of critical points in the frequency region of  $-\infty < \Omega < +\infty$  for uniform systems with double-valued nonlinearities is twice as large as the number of critical points for uniform systems with single-valued nonlinearities. The indicated symmetry with respect to the real axis of all loci and critical points for positive and negative frequencies allows one to plot the locus  $w(j\Omega)$  only for the positive frequencies. However, if there are any double-valued nonlinearities, then the critical points should be evaluated and plotted, to provide the proper stability analysis of the remaining characteristic systems, for both  $\Omega > 0$  and  $\Omega < 0$ . One can also plot the locus  $w(j\Omega)$  for all frequencies  $-\infty < \Omega < +\infty$  and mark the critical points  $-1/\lambda_i^+(A_+)$  only for  $\Omega > 0$ . In the case of single-valued nonlinearities, it is enough to consider only positive frequencies, since the critical points here do not depend on the sign of  $\Omega$  [Figure 3.21(a)].

As in the investigation of linear uniform systems, a considerable simplification of the solution can be achieved by using the Bode and Nichols diagrams. Finding the logarithm of both sides of Equation (3.55) yields that the  $r$ th characteristic system will be on the stability

boundary if the following conditions are simultaneously satisfied:

$$20 \lg (|W(j\Omega)|) = 20 \lg \left( \frac{1}{|\lambda_r(A)|} \right) = -20 \lg (|\lambda_r(A)|) \quad (3.56)$$

and

$$\arg W(j\Omega) = \arg \left( -\frac{1}{\lambda_r(A)} \right) = -180^\circ - \arg \lambda_r(A). \quad (3.57)$$

The comparison of Equations (3.56) and (3.57) with Equation (3.13) for SISO nonlinear systems clearly shows that the graphical procedure of solution here is quite analogous to the classical SISO case and is essentially illustrated in Figures 3.4 and 3.5. In these graphs, the scalar describing functions  $G(A)$  should be replaced by the  $r$ th eigenvalue  $\lambda_r(A)$  of the concomitant matrix of cross-connections  $N(A)$ , and the scalar parameter (amplitude)  $A$  by the magnitude  $|A|$  of the amplitudes vector of the limit cycle. Note that in the practical computations, if the order of the uniform system is not very high (usually, if  $N \leq 3$ ), all loci  $-1/\lambda_i(A)$  ( $i = 1, 2, \dots, N$ ) can be simultaneously plotted on the corresponding Bode, Nyquist or Nichols diagrams of the linear part  $w(j\Omega)$ .

### 3.4.2 Analysis of the stability of limit cycles in uniform systems

For the limit cycle in the uniform system to be stable, it is necessary to a first approximation that the positive increments  $\Delta A_i > 0$  of any amplitudes  $A_i$  and their combinations result in moving the pure imaginary roots of the excited characteristic system to the left half-plane, and the negative increments to the right half-plane of the complex plane. Also, the same must hold for positive and negative increments of the magnitude  $|A|$ . Therefore, the approximate criterion of limit cycle stability introduced in Section 3.3.2 can be reformulated for the discussed case of uniform systems as:

*If, for any positive increments  $\Delta A_i > 0$  of any amplitudes  $A_i$  and their combinations, the critical point  $-1/\lambda_r^+(A)$  corresponding to the excited characteristic system<sup>17</sup> is not encompassed by the locus  $w(j\Omega)$  and, for negative increments  $\Delta A_i < 0$ , is encompassed, then the limit cycle under investigation is stable.*

For the stability of the limit cycle, it is also necessary that under the increase in the magnitude  $|A|$ , i.e. under the ‘collinear’ perturbations of the amplitudes vector  $A$ , the corresponding point at  $-1/\lambda_r(A)$  be outside the locus  $w(j\Omega)$  and under the decrease in  $|A|$  inside it. Thus, first of all, for the stability of a limit cycle in the uniform system, the direction of the numbering of the magnitude  $|A|$  along the locus  $-1/\lambda_r(A)$  at the intersection point must be from the *inside* of  $w(j\Omega)$ .<sup>18</sup> If this condition is satisfied, then, strictly speaking, the above general criterion should be applied. However, if, for the larger values of  $|A|$ , the corresponding point at the  $-1/\lambda_r(A)$  locus is encompassed by  $w(j\Omega)$ , then the limit cycle under investigation cannot be stable and no additional checking is needed. Note that all other (not excited in the limit cycle)

<sup>17</sup> Recall that on substitution in the concomitant matrix  $N(A)$  [Equation (3.48)] of the vector  $A = A_+$  corresponding to the point of intersection of  $w(j\Omega)$  and  $-1/\lambda_r(A)$ , the point  $-1/\lambda_r^+(A_+)$  coincides with that intersection point.

<sup>18</sup> In this respect, the intersection of  $w(j\Omega)$  and  $-1/\lambda_r(A)$  in Figure 3.20 corresponds to an *unstable* limit cycle, taking into account the direction of the increase in  $|A|$ , shown by the arrow.

characteristic systems should remain stable under both positive and negative increments of amplitudes  $A_i$  and magnitude  $|A|$ . This requires that the critical points  $-1/\lambda_i^+(A_+)$  ( $i \neq r$ ) be not encompassed by  $w(j\Omega)$  under the indicated increments. In practice, of course, usually, it is enough to check the ‘collinear’ perturbations of the amplitudes vector  $A$ . The point is that the situations in which the direction of the numbering of  $|A|$  at the intersection of  $w(j\Omega)$  and  $-1/\lambda_r(A)$  indicates a stable limit cycle but the general criterion does not satisfy are quite exotic and, rather, mean that, as was noted in Section 3.3.2, there are no valid grounds to apply the harmonic balance method.

**Example 3.3** Consider the two-axis nonlinear guidance system of Example 3.1 (Figure 3.10) with saturations in the separate channels assuming that the transfer functions  $W_1(s)$  and  $W_2(s)$  are the same and are given by Equation (2.171). The systems then become uniform, since the cross-connections are rigid, and can be investigated by the above methods. The characteristic gain loci of the linear part  $q_i(j\omega) = \lambda_i w(j\omega)$  ( $i = 1, 2$ ) are shown in Figure 3.23 on the Nichols plane in both the direct and inverse forms (see Section 1.3), from which it is evident that in the linear variant (without nonlinear elements), the system is unstable. It should be noted that only the second characteristic system is unstable, to which, in Figure 3.23(a), corresponds the *left* locus  $q_2(j\omega)$  and, in Figure 3.23(b), the *right* critical point  $-1/\lambda_2$ . The results of the limit cycle investigation on the basis of the general technique discussed in Section 3.3, i.e. on the basis of the general condition in Equation (3.38), are given in Figure 3.24 (the numbers in Figure 3.24 indicate the values of  $|A|$ ). The left-most loci in Figure 3.24 coincide with the corresponding loci of the linear part in Figure 3.23(a), as the describing functions [Equation (3.45)] for  $|A| = 0.001$  are equal to unity. As can be seen from Figure 3.24(b), for  $|A| = |A|_+ = 14.0984$  (the  $A_+$  vector has, here, the  $A_1 = 11.5516$  and  $A_2 = 8.0824$  components, and the evaluated phase shift in the second channel is  $\gamma_2 = -62.7914^\circ$ ) and  $\Omega = \Omega_+ = 39.959$ , the necessary conditions for limit cycle existence [Equations (3.38) and (3.41)] are satisfied in the second characteristic system. The corresponding constructions on the Nichols plane, based on Equations (3.56) and (3.57), are given in Figure 3.25 (some values of  $|A|$  are not indicated in this figure so as not to encumber the graphs).

It is interesting to note that the  $-1/\lambda_{1,2}(A)$  loci in this case are complex-valued, although the saturation nonlinearities by themselves are single-valued and have real describing functions

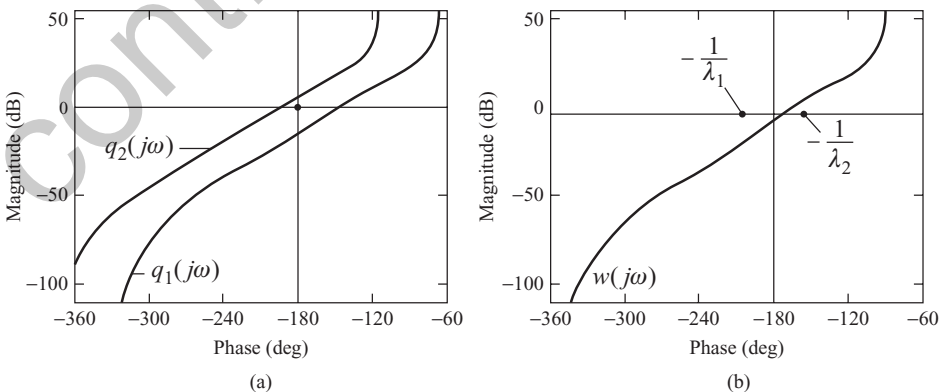


**Figure 3.23** Stability analysis of the linear system on the Nichols plane. (a) ‘Direct’ form; (b) ‘inverse’ form.

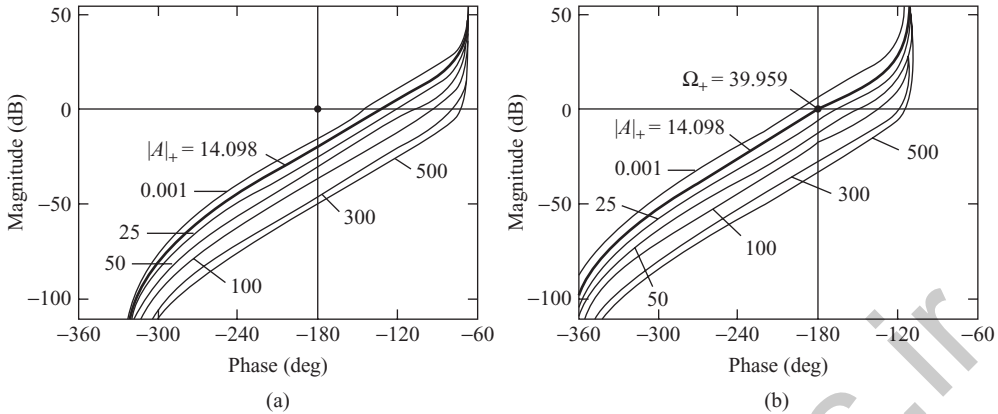


**Figure 3.24** Investigation of the limit cycle in the guidance system by the general technique. (a) First characteristic system [family of the  $q_1(j\Omega, A)$  loci]; (b) second characteristic system [family of the  $q_2(j\Omega, A)$  loci].

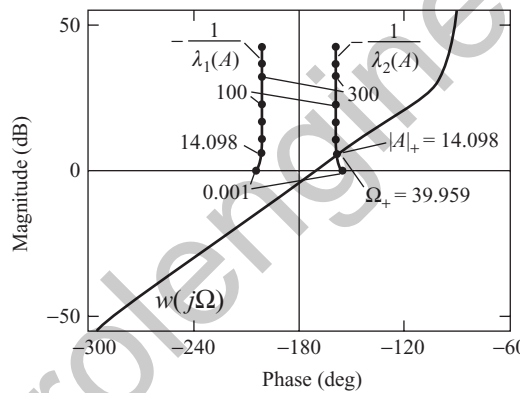


**Figure 3.25** Investigation of the limit cycle in the system on the Nichols plane based on the condition in Equation (3.55).

[Equation (3.45)].<sup>19</sup> Here, we have encountered a specific property of uniform systems, for which the form of the  $-1/\lambda_{1,2}(A)$  loci is determined not only by nonlinearities, but also by eigenvalues of the cross-connections matrix  $R$  (in the discussed case, these eigenvalues are complex-conjugate). The stability analysis of the first characteristic system for the discovered limit cycle with the excitation of the second canonical basis axis is shown in Figure 3.26.

As expected, the first characteristic system is stable for the evaluated  $A_+$  and  $\Omega_+$ , i.e. all the necessary conditions for the existence of the limit cycle with excitation of the second characteristic system hold. The characteristic gain loci of matrix  $Q_+(j\omega)$  [Equation (3.53)], evaluated for positive and negative perturbations of the magnitude of  $A_+$  [for  $A = (1 \pm \Delta)A_+$ , where  $\Delta = 0.2$ ], are shown in Figure 3.27(a), in which the dotted lines correspond to the initial

<sup>19</sup> Recall that in the SISO case, the  $-1/G(A)$  locus for a single-valued nonlinearity always belongs to the real axis.

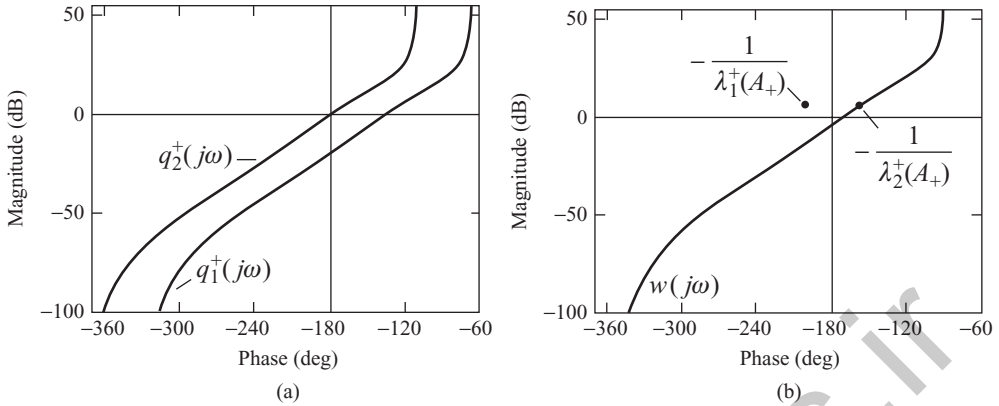


**Figure 3.26** Stability analysis for the first characteristic system. (a) ‘Direct’ form; (b) ‘inverse’ form.

vector  $A_+$ . The stability analysis of the limit cycle, based on the changes in the eigenvalues of the concomitant matrix  $N(A_+)$ , under the variations in the magnitude of  $A_+$  given above, is shown in Figure 3.27(b). It ensues from Figure 3.27 that, for  $\Delta > 0$ , the excited second characteristic system becomes stable (i.e. the oscillation decays) and, for  $\Delta < 0$ , unstable (which leads to the increase in the magnitude of  $A$ ). In other words, Figure 3.27 verifies that the approximate criterion of stability of the limit cycle holds true. The results of modelling of the system dynamics are given in Figure 3.28, in which the *input* signals of nonlinearities in separate channels are denoted by  $x_1(t)$  and  $x_2(t)$ . The modelling gives the following values for the limit cycle parameters:  $A_1 = 11.7169$ ,  $A_2 = 7.9578$  and  $\Omega_+ = 39.5518$ . The computation errors of all parameters with respect to the results of modelling do not exceed 1.6%. Such a high accuracy of computation is explained by the fact that the frequency of the limit cycle is rather high and the linear parts of the channels have good filtering properties. The dependence of the magnitude  $|w(j\omega)|$  on the frequency  $\omega$  is depicted in Figure 3.29. It can be seen from that graph that at the limit cycle frequency, the magnitude  $|w(j\omega)|$  equals 1.9749 and, at the frequency

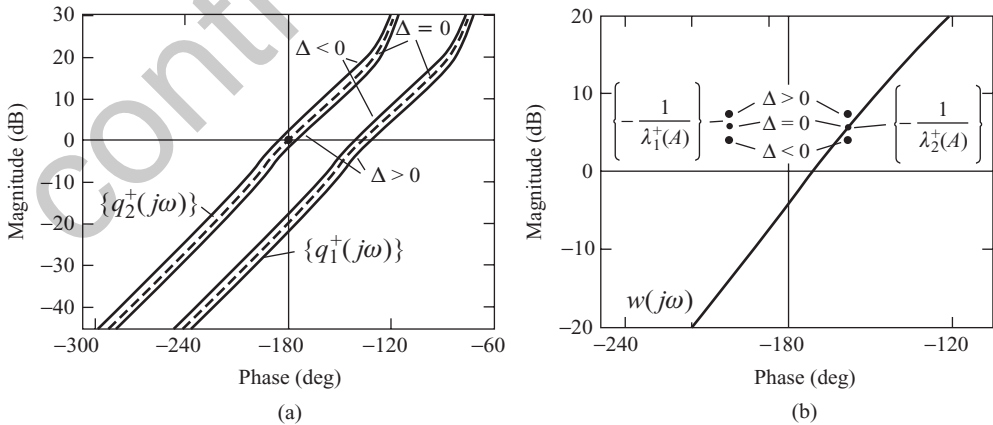


**Figure 3.27** Stability analysis of the limit cycle under small variations in the magnitude of  $A_+$  ( $\Delta = \pm 0.2$ ). (a) ‘Direct’ form; (b) ‘inverse’ form.

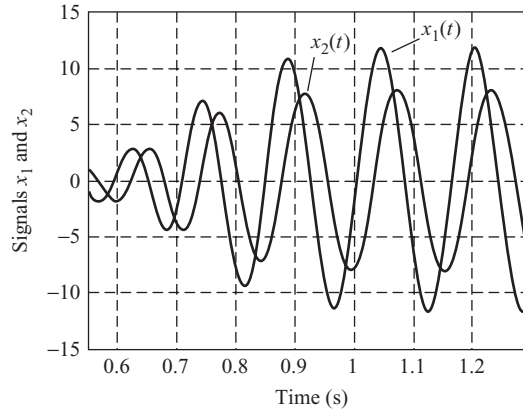


**Figure 3.28** System modelling with the help of Simulink.

of the third harmonic, the value of  $|w(j\omega)|$  equals 0.238, i.e. the ratio of these magnitudes is approximately 8.3. Therefore, the higher harmonics of the limit cycle do not particularly affect the waveform of the input signals to nonlinearities in the steady-state oscillation (this is also evident from the time dependences in Figure 3.28), and the evaluated parameters of the limit cycle are quite close to those obtained by modelling.

**Example 3.4** Consider the system in Example 3.3 with another type of nonlinearities, namely those with saturation and dead zones [Figure 3.30(a)], assuming unity gain and the following values of the linear and dead zones:  $\Delta = 4$  and  $d = 0.6$ . The investigation of the limit cycle in that system is shown in Figure 3.31, from which it can be seen that the  $-1/\lambda_1(A)$  locus does not cut the locus  $w(j\Omega)$  and there are two intersections of  $-1/\lambda_2(A)$  and  $w(j\Omega)$  for  $|A|_+^1 = 1.8944$ ,  $\Omega_+^1 = 36.9221$  and  $|A|_+^2 = 11.9387$ ,  $\Omega_+^2 = 39.5026$ . Thus, we have obtained two different solutions satisfying the necessary conditions in Equations (3.41) and (3.55), in which both solutions belong to the same (second) axis of the canonical basis. In addition, the graphs in Figure 3.32 show that the first characteristic system is stable for both periodical modes.

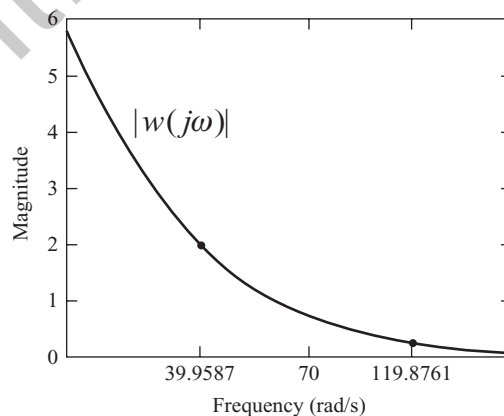


**Figure 3.29** Magnitude characteristic of the linear part.

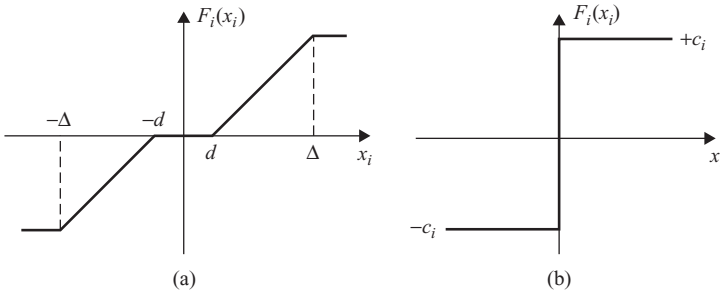


Figure 3.30 Characteristics of nonlinear elements. (a) Saturation and dead zone; (b) ideal relay.

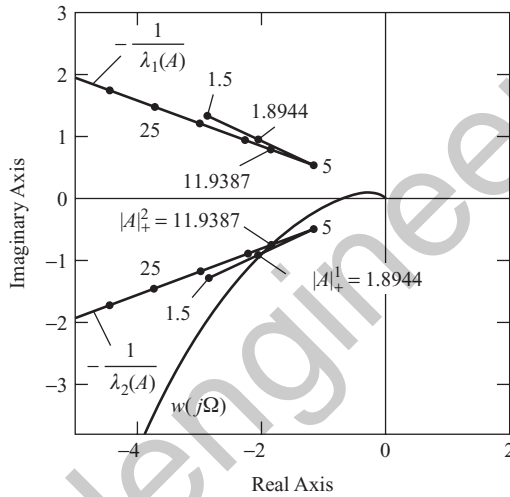


Figure 3.31 Investigation of the limit cycle for the case of nonlinearities with saturation and dead zone.

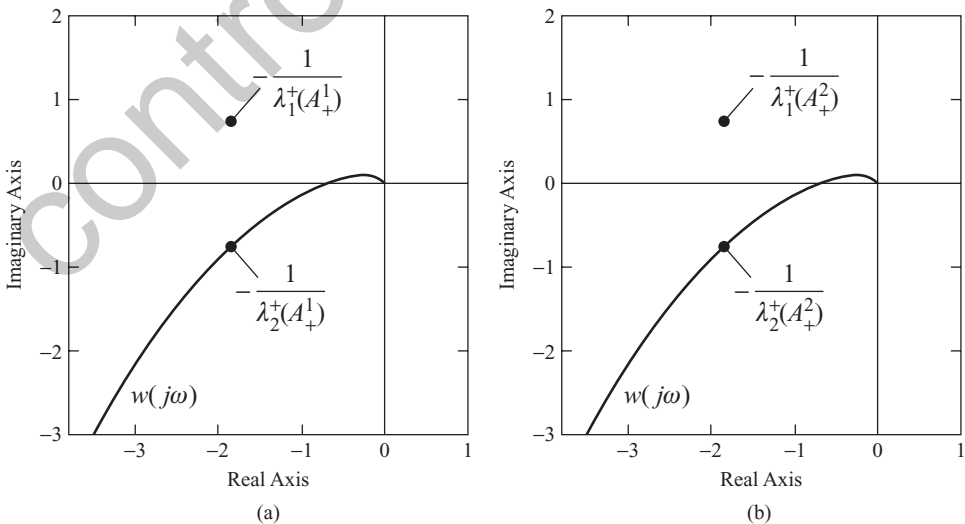


Figure 3.32 Stability analysis of the first characteristic system. (a)  $|A|_+^1 = 1.8944$ ; (b)  $|A|_+^2 = 11.9387$ .

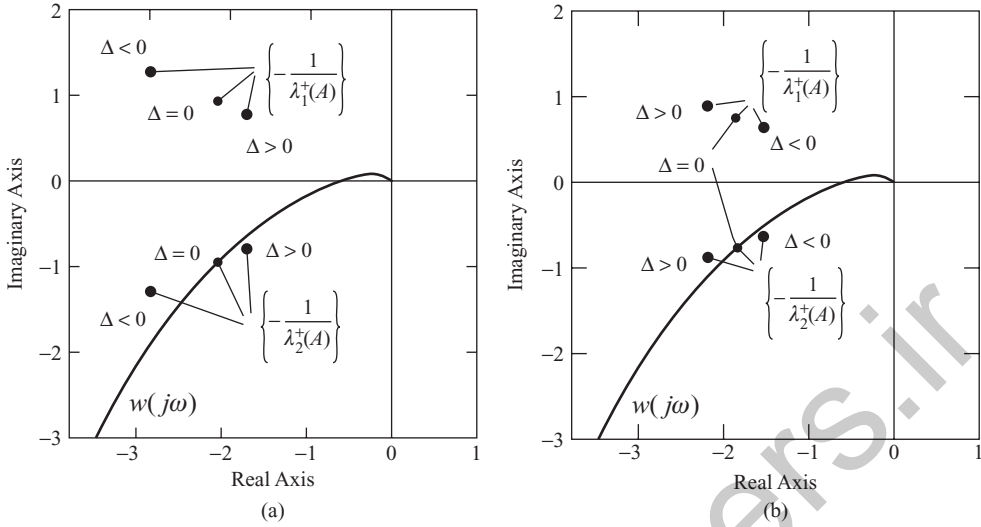


Figure 3.33 Investigation of the stability of the limit cycle. (a)  $|A|_+^1 = 1.8944$ ; (b)  $|A|_+^2 = 11.9387$ .

To select from the two obtained solutions the one that corresponds to the real limit cycle, it is necessary to perform the stability analysis of these solutions under small variations in the magnitude  $|A|_+$ . That analysis is shown in Figure 3.33, from which it is clear that the first solution (for  $|A|_+^1 = 1.8944$ ) is unstable, and only the limit cycle with the magnitude  $|A|_+ = 11.9387$  (to which the amplitudes  $A_1 = 9.7351$  and  $A_2 = 6.9109$  correspond) and the frequency  $\Omega_+ = 39.5026$  is possible in the system.

The modelling of the system (Figure 3.34) gives the following parameters of the limit cycle:  $A_1 = 9.7525$ ,  $A_2 = 6.7226$  and  $\Omega_+ = 39.4124$ . The evaluation errors here do not exceed 2.8%. The steady-state oscillations at the inputs and outputs of nonlinearities are shown on a small time scale in Figure 3.34(c) and (d). It is interesting to note that the waveform of the output oscillations  $y_1(t)$  and  $y_2(t)$  is rather far from sinusoidal. However, the input oscillations  $x_1(t)$  and  $x_2(t)$  to the nonlinearities practically do not differ from harmonic. This is due to the good filtering properties of the linear part (see Figure 3.29).

**Example 3.5** Consider, now, the same system of Example 3.3, in the separate channels of which ideal relays are introduced [Figure 3.30(b)]. The describing functions for the latter have a simple form:

$$N(A_i) = \frac{4c}{\pi A_i}. \tag{3.58}$$

Investigate the steady-state dynamical processes in that system, assuming the value of  $c$  in Equation (3.58) to be unity. The corresponding plots are represented in Figure 3.35, which shows that, in this case, the  $w(j\Omega)$  locus cuts both  $-1/\lambda_1(A)$  (for  $|A|_+ = 0.38292$ ,  $\Omega_+ = 127.925$ ) and  $-1/\lambda_2(A)$  (for  $|A|_+ = 3.5141$ ,  $\Omega_+ = 40.7694$ ). Here, we meet a specific feature of nonlinear MIMO systems, which is also inherent in SISO systems. In all previous examples, in which there was a linear zone and saturation, for the limit cycle in the system to occur, it was necessary that the corresponding linear system be *unstable*. Also, if only one of the ‘linear’ characteristic systems was unstable, then the limit cycle was caused by the excitation

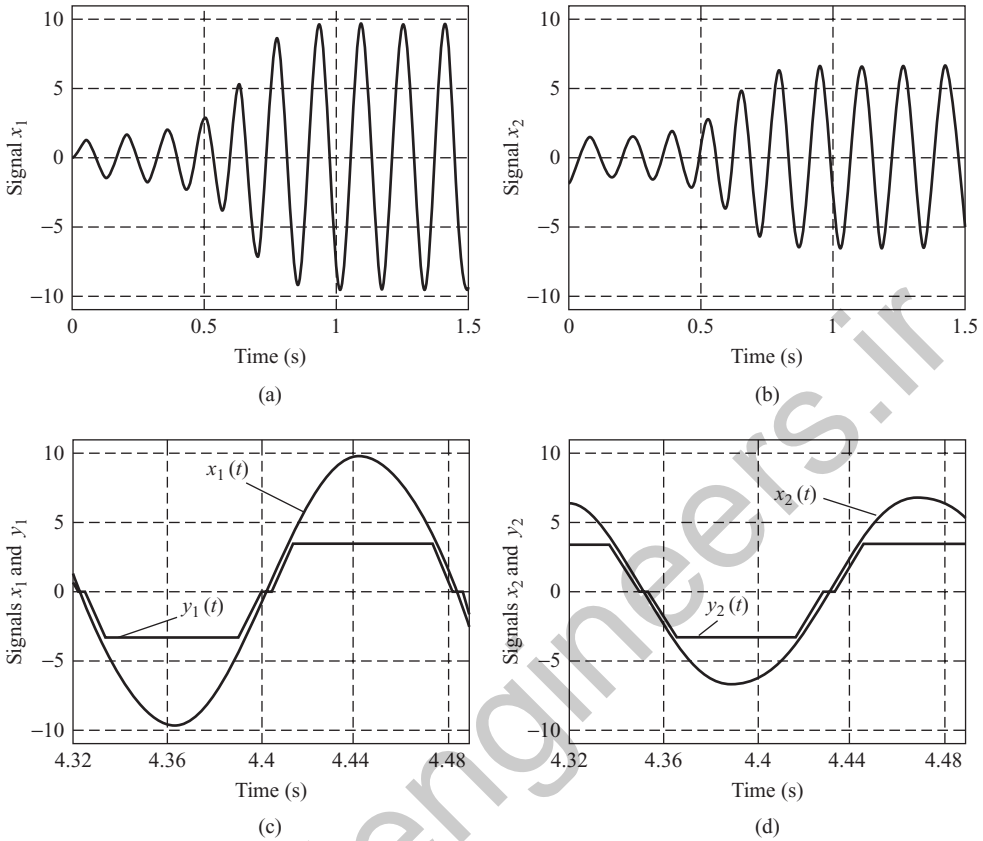


**Figure 3.34** Modelling of the system with saturations and dead zones. (a) First channel; (b) second channel; (c) first channel; (d) second channel.

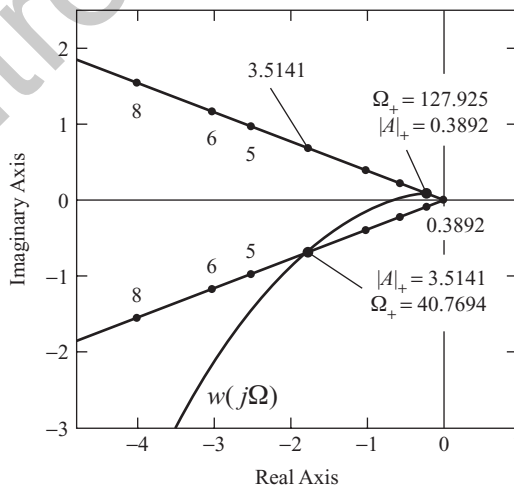


**Figure 3.35** Investigation of the limit cycle in the system with ideal relays.

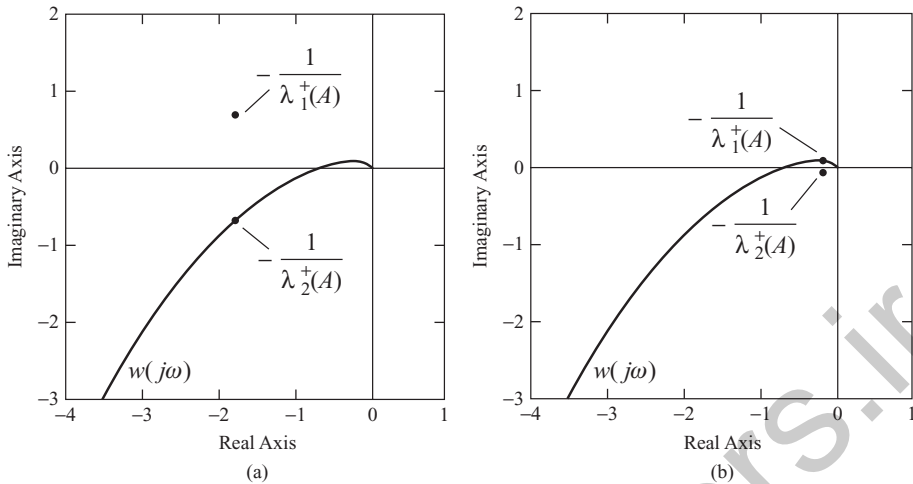


**Figure 3.36** Stability analysis of the unexcited characteristic systems. (a)  $|A|_+ = 3.5141$ ; (b)  $|A|_+ = 0.3829$ .

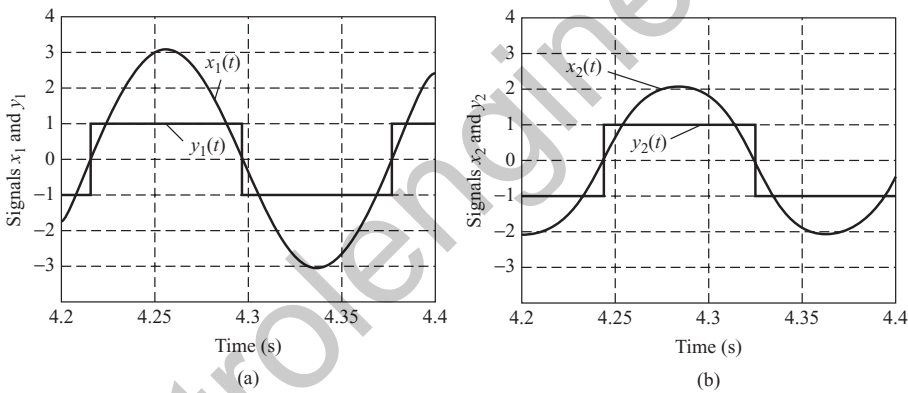


**Figure 3.37** Modelling of the system with ideal relays. (a) First channel; (b) second channel.

of that very characteristic system. Quite another picture is observed on introducing the relay elements into the system. Inspection of Figure 3.35 shows that we have intersections of  $w(j\Omega)$  with both  $-1/\lambda_{1,2}(A)$  loci, which emerge for  $|A| = 0$  from the origin of the complex plane, and the occurrence of the limit cycle here does not depend on the stability or instability of the system without nonlinear elements.<sup>20</sup> The stability analysis of unexcited characteristic systems is given in Figure 3.36, which shows that only the solution of  $|A|_+ = 3.5141$  (with  $A_1 = 2.9008$ ,  $A_2 = 1.99836$ ,  $\gamma_2 = -59.4443^\circ$ ) and  $\Omega_+ = 40.7694$  can correspond to the limit cycle. Modelling of the system (Figure 3.37) produces the following parameters of the limit

<sup>20</sup> The matter concerns the system with the transfer function  $w(s)$  given by Equation (2.171). If the difference between the numbers of poles and zeros of  $w(s)$  is equal to unity and the *type* (number of pure integrators) of the system does not exceed one, then one of the possible limit cycle frequencies is equal to infinity, and the  $|A|$  magnitude is equal to zero. If the indicated difference is zero, then it is possible that there will be no intersections of the loci in Figure 3.35. In that case, however, we cannot argue the validity of using the harmonic linearization method.

cycle:  $A_1 = 3.0725$ ,  $A_2 = 2.0886$  and  $\Omega_+ = 39.0512$ . The computational errors here are less than 5.6%, although the output waveforms  $y_1(t)$  and  $y_2(t)$  of nonlinearities are ideal square pulses.

### 3.5 LIMIT CYCLES IN CIRCULANT AND ANTICIRCULANT MIMO SYSTEMS

We have frequently seen in the first part of this book that normal linear MIMO systems possess some very remarkable features and properties, due to the orthogonality of their canonical basis. A question naturally arises as to whether a similar picture is also observed on introducing nonlinear elements into normal MIMO systems. Unfortunately, in the general case of normal linear parts, the answer to this question is negative; the normality of the transfer matrix  $W(s)$  still does not guarantee specific qualitative and, above all, dynamic characteristics of nonlinear MIMO systems. However, there are classes of normal MIMO systems preserving many significant features of the linear case in the nonlinear case. Moreover, these systems also have other exceptional properties, drastically distinguishing them from all other classes of nonlinear MIMO systems. This concerns the nonlinear circulant and anticirculant systems in which the limit cycle of equal amplitudes in separate channels is intrinsic. We now proceed to the investigation of these systems.

#### 3.5.1 Necessary conditions for the existence and investigation of limit cycles in circulant and anticirculant systems

Let the transfer matrix of the linear part  $W(s)$  of the MIMO system in Figure 3.6 be circulant, i.e. it can be represented as polynomial [Equation (1.127)]:

$$W(s) = w_0(s)I + \sum_{i=1}^{N-1} w_i(s)U^i, \tag{3.59}$$

where  $w_0(s)$ ,  $w_i(s)$  ( $i = 1, 2, \dots, N - 1$ ) are the elements of the first row of  $W(s)$ , and  $U$  is the orthogonal *permutation matrix* [Equation (1.128)]. Further, let the  $F(x) = \{F_{kr}(x_r)\}$  matrix, where, for simplicity, all nonlinearities are assumed memoryless, be also circulant by the *structure* of introducing the nonlinear elements into the system, i.e. it has the form

$$F(x) = \begin{pmatrix} F_0(x_1) & F_1(x_2) & F_2(x_3) & \dots & F_{N-1}(x_N) \\ F_{N-1}(x_1) & F_0(x_2) & F_1(x_3) & \dots & F_{N-2}(x_N) \\ F_{N-2}(x_1) & F_{N-1}(x_2) & F_0(x_3) & \dots & F_{N-3}(x_N) \\ \dots & \dots & \dots & \dots & \dots \\ F_1(x_1) & F_2(x_2) & F_3(x_3) & \dots & F_0(x_N) \end{pmatrix}. \tag{3.60}$$

Then, instead of Equation (3.60), we can formally write

$$F(x) = F_0(\cdot)I + \sum_{i=1}^{N-1} F_i(\cdot)U^i. \tag{3.61}$$

The formality of the representation of  $F(x)$  as polynomial [Equation (3.61)] lies in the fact that the matrix  $F(x)$  of nonlinearities is a *functional* matrix, the  $i$ th column of which depends in a nonlinear manner on the  $i$ th component  $x_i$  of the vector  $x$ . Note, now, that on each diagonal of  $W(s)$  and  $F(x)$ , the same linear and nonlinear elements are situated and, besides, the diagonals located at the same distance from the lower-left corner and from the principal diagonal consist of identical elements. This means that circulant systems have different ‘cyclical’ groups of cross-connections between identical channels, with the same (linear and nonlinear) transfer operators. That internal structural symmetry of nonlinear circulant systems predetermines the possibility of periodical processes with equal amplitudes in all channels. Therefore, in the following, we shall concentrate mainly on the investigation of such dynamical modes. We shall proceed from an assumption that in the circulant system, there is a symmetrical, one-frequency limit cycle with equal amplitudes  $A_i = A$  in the channels.<sup>21</sup> Then, based on the necessary conditions for the existence of a limit cycle in nonlinear MIMO systems, we shall check whether that assumption leads to contradiction.

Thus, suppose that, in the circulant system, there is a limit cycle with equal amplitudes  $A_i = A$  and frequency  $\Omega$ , and the generalized low pass filter property of the linear part holds. That property, here, has the form

$$|w_i(jk\Omega)| \ll |w_i(j\Omega)|, \quad i = 0, 1, 2, \dots, N - 1; \quad k = 2, 3, \dots \quad (3.62)$$

Under such conditions, all nonlinear characteristics  $F_i(\cdot)$  ( $i = 0, 1, \dots, N - 1$ ), which are assumed odd-symmetrical, can be replaced by their describing functions. Owing to the assumption about the equality of the oscillations amplitudes  $A_i = A$ , the structurally ‘circulant’ matrix  $F(x)$  reduces to a really circulant numerical matrix (which is complex-valued in the case of double-valued nonlinearities), depending only on a single scalar amplitude  $A$ :

$$G(A) = G_0(A)I + \sum_{i=1}^{N-1} G_i(A)U^i, \quad (3.63)$$

where the describing functions for the  $F_i(\cdot)$  are denoted by  $G_i(A)$  ( $i = 0, 1, \dots, N - 1$ ). Since the product of two circulant matrices is a circulant matrix, the transfer matrix  $Q(j\Omega, A)$  of the open-loop harmonically linearized circulant system is also circulant and can be represented in the form

$$Q(j\Omega, A) = W(j\Omega)G(A) = Q_0(j\Omega, A)I + \sum_{i=1}^{N-1} Q_i(j\Omega, A)U^i, \quad (3.64)$$

where the elements  $Q_0(j\Omega, A)$  and  $Q_i(j\Omega, A)$  ( $i = 1, 2, \dots, N - 1$ ) of the first row of  $Q(j\Omega, A)$  can be found by the common rules of multiplication of the two circulant matrices  $W(s)$  [Equation (3.59)] and  $G(A)$  [Equation (3.63)] (Voevodin and Kuznetsov 1984).

As was shown in Section 3.3, in the steady-state limit cycle in the MIMO system, the vector of complex amplitudes  $x$  must be directed along the canonical basis axis associated with the excited characteristic system. Consequently, the geometrical properties of the limit cycle are

<sup>21</sup> So as not to enter redundant notations, by  $A$ , we shall mean the *scalar* amplitude of oscillation in separate channels of the circulant system, and not the amplitudes *vector*, as it was before.

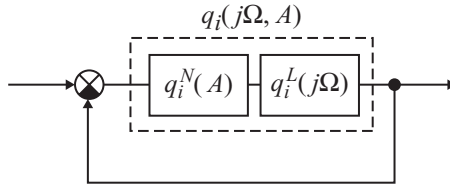


**Figure 3.38** Block diagram of the closed-loop characteristic systems of the harmonically linearized circulant system ( $i = 1, 2, \dots, N$ ).

completely determined by the structure of eigenvalues and eigenvectors of the transfer matrix of the harmonically linearized system. From this point of view, the fact that the transfer matrix  $Q(j\Omega, A)$  [Equation (3.64)] is circulant brings about principal peculiarities in using the CTFs method and, as will be seen further, considerably simplifies the investigation of the limit cycle. First of all, note that the CTFs  $q_i(j\Omega, A)$  of the circulant matrix  $Q(j\Omega, A)$  can be represented, regardless the number  $N$  of separate channels, as polynomials:<sup>22</sup>

$$q_i(j\Omega, A) = Q_0(j\Omega, A) + \sum_{k=1}^{N-1} Q_k(j\Omega, A) \exp \left\{ j \frac{2\pi(i-1)}{N} k \right\}, \quad i = 1, 2, \dots, N. \quad (3.65)$$

Moreover, the CTFs  $q_i(j\Omega, A)$  [Equation (3.65)] are equal, based on the eigenvalue properties of the product of circulant matrices, to the product of the corresponding CTFs  $q_i^L(j\Omega)$  and  $q_i^N(A)$  of the ‘linear’ and ‘nonlinear’ matrices  $W(j\Omega)$  and  $G(A)$ , i.e.<sup>23</sup>

$$q_i(j\Omega, A) = q_i^L(j\Omega) q_i^N(A), \quad i = 1, 2, \dots, N, \quad (3.66)$$

where

$$q_i^L(j\Omega) = w_0(j\Omega) + \sum_{k=1}^{N-1} w_k(j\Omega) \exp \left\{ j \frac{2\pi(i-1)}{N} k \right\} \quad (3.67)$$

and

$$q_i^N(A) = G_0(A) + \sum_{k=1}^{N-1} G_k(A) \exp \left\{ j \frac{2\pi(i-1)}{N} k \right\}. \quad (3.68)$$

Hence, the block diagrams of the closed-loop characteristic systems for the circulant system have the form shown in Figure 3.38.

The indicated properties of the CTFs of the harmonically linearized circulant systems are quite essential in practice, but they rather relate to the computational aspects of the problem. Much more significant for the theory of nonlinear circulant systems are some other properties of circulant matrices, connected with the structure of their canonical basis. We know that the canonical basis of any circulant matrix coincides, regardless of the specific form of the matrix

<sup>22</sup> See Equation (1.133) in Section 1.4.2.

<sup>23</sup> We hope that the reader will not mix up the  $N$  superscript in  $q_i^N(A)$ , which points out belonging to the *nonlinear* part, with the number of channels  $N$  of the circulant system.

elements, with the canonical basis of the permutation matrix  $U$  [Equation (1.128)], composed of the normalized eigenvectors  $c_i$  of the latter. These vectors constitute the orthonormal basis of space  $\mathbb{C}^N$  coinciding with its dual, and have the form of Equation (1.132). Substituting in Equation (1.132) instead of eigenvalues  $\beta_i$  of  $U$  their expressions in Equation (1.131), yields

$$c_i = \frac{1}{\sqrt{N}} \left[ 1 \exp \left\{ j \frac{2\pi(i-1)}{N} \right\} \exp \left\{ j 2 \frac{2\pi(i-1)}{N} \right\} \dots \exp \left\{ j(N-1) \frac{2\pi(i-1)}{N} \right\} \right]^T$$

$$i = 1, 2, \dots, N. \tag{3.69}$$

The mentioned property of the canonical basis of circulant matrices and the form of eigenvectors  $c_i$  [Equation (3.69)] play an extremely important role. Indeed, so far, we have just assumed equality of the amplitudes  $A_i = A$  of the limit cycle in the circulant system, without any strict grounds. But the second necessary condition for the existence of the limit cycle in nonlinear MIMO systems, namely the collinearity condition [Equation (3.41)], demands that the amplitudes vector of oscillations be directed along the real vector composed of the magnitudes of components of the ‘excited’ canonical basis axis. As can be seen from Equation (3.69), all eigenvectors of the permutation matrix  $U$  and, as a consequence, of the transfer matrix  $Q(j\Omega, A)$  [Equation (3.64)] have identical magnitudes of the components equal to  $1/\sqrt{N}$ . From here, it ensues that for  $A_i = A$ , the condition in Equation (3.39) holds *a fortiori*, i.e. the limit cycle with equal amplitudes is really possible in circulant systems.

Hence, under equal amplitudes of the one-frequency limit cycle in circulant systems, the collinearity condition *necessarily holds* and the problem is reduced to the determination of such *single* amplitude  $A$  and frequency  $\Omega$ , for which one of the characteristic systems is on the stability boundary and all other systems are stable. Note that the collinearity condition in circulant systems holds (for  $A_i = A$ ) regardless of the specific form of elements of the linear part and nonlinearities. It can also be stated that the limit cycle with equal amplitudes in separate channels is inherent to circulant systems. Obviously, the first two necessary conditions for limit cycle existence in circulant systems are reduced here to a *single* condition for the  $r$ th characteristic system to be on the stability boundary:

$$q_r(j\Omega, A) = Q_0(j\Omega, A) + \sum_{k=1}^{N-1} Q_k(j\Omega, A) \exp \left\{ j \frac{2\pi(r-1)}{N} k \right\} = -1. \tag{3.70}$$

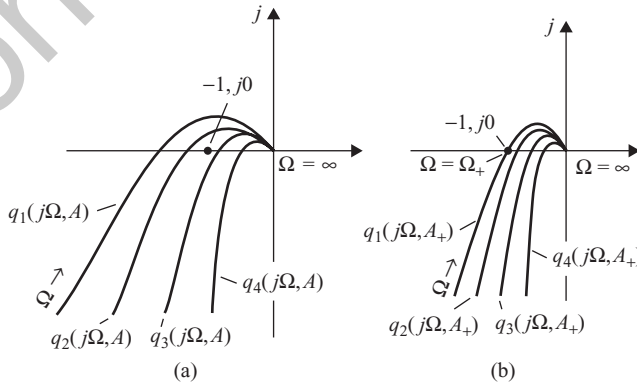


Figure 3.39 Investigation of the limit cycle in the circulant system by the Teodorchik method ( $N = 4$ ).

For the numerical evaluation of  $A$  and  $\Omega$  by that condition, two simple and evident methods can be suggested that actually are the direct analogues of the Teodorchik and Goldfarb methods well known from the classical control theory. The first of them consists in the following. The family of  $N$  loci  $q_i(j\Omega, A)$  ( $i = 1, 2, \dots, N$ ) is plotted in the complex plane for a fixed value of amplitude  $A = const$ , as  $\Omega$  changes from zero to infinity [Figure 3.39(a)]. Varying the value of  $A$ , we can plot for each  $A = const$  its own parametrical family  $\{q_i(j\Omega, A)\}$  of the loci of *all* characteristic systems. If we manage now to find such a value  $A = A_+$  for which any one of the loci, say the  $r$ th, passes through the point  $(-1, j0)$  and all other loci do not encompass that point, then the given amplitude  $A_+$  satisfies the necessary condition in Equation (3.70) for the existence of the limit cycle and all other ‘unexcited’ characteristic systems are stable. The  $\Omega_+$  frequency of the limit cycle is determined here by the  $q_r(j\Omega, A)$  locus at the point  $(-1, j0)$  [Figure 3.39(b)]. Note that in Figure 3.39, we have a family of  $N$  (in this case,  $N = 4$ ) characteristic gain loci  $q_i(j\Omega, A)$  for only *one* value  $A = const$ , whereas, in Figure 3.2(a), a family of loci of an open-loop SISO system for *different*  $A = A_i = const$  is constructed. The phase shifts of oscillations in different channels of the circulant system are equal to the arguments of the corresponding components (as the argument of the first component of all  $c_i$  vectors is equal to zero) of the canonical basis axis associated with the excited characteristic system. As can be seen from Equation (3.69), in circulant systems, there are possible only ‘plane’, cophased limit cycles, occurring under the excitation of the first characteristic system (for  $r = 1$ ), or ‘hyperspherical’, characterized by equal phase shifts

$$\Delta\gamma = \frac{2\pi(r-1)}{N}, 2 \leq r \leq N \quad (3.71)$$

in separate channels. Besides, if, for even  $N$ , the characteristic system with index  $r = (N/2) + 1$  is excited, then  $\Delta\gamma = \pi$  and oscillation in each of the next channels is in the antiphase to the oscillation in the previous channel.

For the limit cycle in the circulant system to be stable, it is necessary that the gain locus of the excited characteristic system does not encompass under the increase in the amplitude  $A$  and does encompass under the decrease in  $A$  the critical point  $(-1, j0)$ . In essence, this condition is the condition of *equal* variations of amplitudes, for which the transfer matrix  $Q(j\Omega, A)$  remains circulant and the collinearity of  $x$  and  $c_r$  is not violated. If this rule does not hold, then the limit cycle is unstable and, if the rule holds, then it is necessary, strictly speaking, to check whether the introduced in Section 3.3.2 general criterion of the limit cycle stability under arbitrary variations  $\Delta A_i$  of any amplitudes and their combinations holds. It should be emphasized that in the case of arbitrary variations  $\Delta A_i$ , the describing functions matrix of the nonlinear part of the circulant system ceases to be circulant and, for the stability analysis of the limit cycle, we need to construct the characteristic gain loci  $q_i^+(j\omega)$  of the transfer matrix  $Q_+(j\omega)$  [Equation (3.43)]. In practice, however, it is usually enough to check only the case of ‘collinear’ perturbations of  $x$ , i.e. to check only equal variations in the amplitudes in the separate channels.

The second approach to the problem of limit cycle investigation in circulant systems is based on the representation of the condition in Equation (3.70), taking into account Equation (3.66), in the Goldfarb form

$$q_r^L(j\Omega) = -\frac{1}{q_r^N(A)}. \quad (3.72)$$

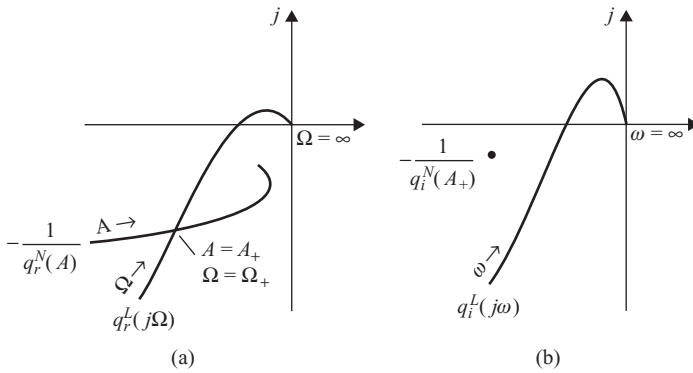


**Figure 3.40** Investigation of the limit cycle in the circulant system by the Goldfarb method. (a) Checking the condition in Equation (3.72); (b) stability analysis of other characteristic systems ( $i \neq r$ ).

Apparently, for the graphical determination of  $A$  and  $\Omega$  satisfying the condition of excitation of the  $r$ th characteristic system in the form of Equation (3.72), one should plot in the complex plane the gain loci  $q_r^L(j\Omega)$  of the linear part as  $\Omega$  changes from zero to infinity as well as the negative reciprocal locus  $-1/q_r^N(A)$  as the amplitude  $A$  changes in an appropriate range [Figure 3.40(a)]. If there is an intersection of these loci, the condition in Equation (3.72) holds and  $A_+$  and  $\Omega_+$  are determined by the loci numbering at the intersection point. The stability analysis of any other characteristic system is carried out as follows. The gain locus  $q_i^L(j\omega)$  of the  $i$ th ( $i \neq r$ ) characteristic system is plotted in the complex plane, and the critical point  $-1/q_i^N(A_+)$  for the previously determined amplitude  $A_+$  is marked in the same plane [Figure 3.40(b)]. If the critical point is not encompassed by the locus  $q_i^L(j\omega)$ , then the  $i$ th characteristic system is stable. Repeating similar constructions for all  $i$  ( $i = 1, 2, \dots, N; i \neq r$ ), one can analyze the stability of all other characteristic systems. As in the case of nonlinear general MIMO systems, analysis by the above scheme should be carried out for all  $r$  ( $r = 1, 2, \dots, N$ ), i.e. for all canonical basis axes. For the stability of the revealed limit cycle with excitation of the  $r$ th characteristic system, it is necessary that the amplitude  $A$  numbering along the locus  $-1/q_r^N(A)$  at the intersection point be directed *outside* of  $q_r^L(j\Omega)$ . Thus, for the increase in  $A$  indicated by the arrow in Figure 3.40(a), the limit cycle corresponding to the intersection point is unstable. In practical computations, such checking is usually sufficient for reliable judgment about the stability of the limit cycle, as pointed out before.

The advantage of the first method (the analogue of the Teodorchik method) is that on using it, the condition for the excitation of the  $r$ th characteristic system and conditions of stability of other characteristic systems are checked jointly, by simultaneously plotting *all* loci  $q_i(j\Omega, A)$ .<sup>24</sup> As for the analogue of the Goldfarb method, it allows simpler determination of the conditions for excitation of each characteristic system, at least for memoryless nonlinearities. The advantage of the second approach is expressed especially clearly in investigating a particular, but quite significant and widespread in technical application, case of circulant systems with diagonal matrix of nonlinearities:

$$F(x) = \text{diag}\{F_0(x_i)\}. \quad (3.73)$$

<sup>24</sup> Another merit of that method is that the presence of *dynamical* nonlinearities, when the CTFs  $q_i^N(A)$  of the nonlinear part in Equation (3.68) also depend on the frequency  $\Omega$ , does not affect the evaluation procedure.

In such systems, the  $G(A)$  matrix [Equation (3.63)] becomes scalar, i.e.  $G(A) = G_0(A)I$ , and the transfer matrix  $Q(j\Omega, A)$  of the open-loop circulant system is equal to the transfer matrix of the linear part  $W(j\Omega)$ , up to the scalar multiplier  $G_0(A)$ :

$$Q(j\Omega, A) = G_0(A)W(j\Omega). \tag{3.74}$$

Therefore, the CTFs of the  $Q(j\Omega, A)$  matrix coincide, up to the same  $G_0(A)$  multiplier, with the CTFs of the linear part, i.e.

$$q_i(j\Omega, A) = G_0(A)q_i^L(j\Omega), \quad i = 1, 2, \dots, N, \tag{3.75}$$

where  $q_i^L(j\Omega)$  are given by Equation (3.67). Here, the condition for the  $r$ th characteristic system to be on the stability boundary is more convenient to represent in the Goldfarb form

$$q_r^L(j\Omega) = -\frac{1}{G_0(A)} \tag{3.76}$$

and the solution to the problem is much simpler. Indeed, for the evaluation of the limit cycle in this case, one needs to plot in the complex plane the family of *all* characteristic gain loci  $q_i^L(j\Omega)$  of the linear part  $W(j\Omega)$  and the *common* negative reciprocal locus of the describing function  $G_0(A)$  (Figure 3.41). If there are no intersections of  $q_i^L(j\Omega)$  with  $-1/G_0(A)$ , then a limit cycle with equal amplitudes is impossible. If there are such intersections with some loci, then the limit cycle is determined by that intersection point of  $-1/G_0(A)$  with one of the loci  $q_i^L(j\Omega)$ , which is not encompassed by other loci. In Figure 3.41, it is the point marked by number 4, which corresponds to a stable cophased (since  $r = 1$ ) limit cycle.

It can be readily shown, and we leave it to the reader as an exercise, that all the above results and conclusions remain valid for the case of nonlinear anticirculant systems, i.e. MIMO systems with anticirculant matrices  $W(j\Omega)$  and  $G(A)$ .

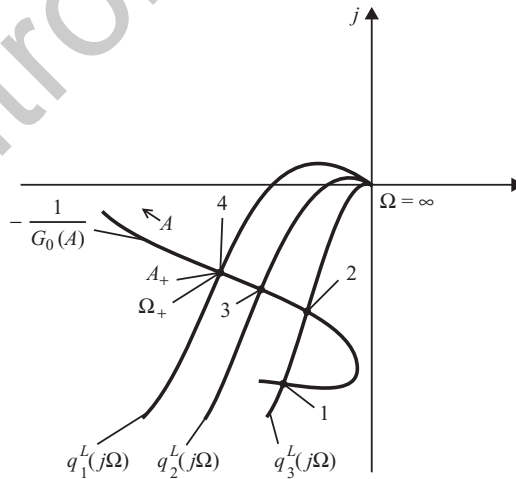


**Figure 3.41** Investigation of the limit cycle in the circulant system with the diagonal matrix of nonlinearities ( $N = 3$ ).

### 3.5.1.1 Simple symmetrical MIMO systems

In nonlinear simple symmetrical MIMO systems,<sup>25</sup> which belong to circulant systems, the transfer functions of all cross-connections in the linear part are the same and, also, all nonlinearities connecting separate channels are identical, i.e.

$$w_k(s) = w_1(s), \quad F_k(\cdot) = F_1(\cdot), \quad k = 2, \dots, N - 1. \quad (3.77)$$

In the limit cycle of equal amplitudes in the simple symmetrical system, the matrix  $G(A)$  of describing functions is also simple symmetrical. Consequently, the transfer matrix  $Q(j\Omega, A)$  [Equation (3.64)] of the open-loop system proves to be simple symmetrical. As a result, we have, as in the linear case, only *two* distinct characteristic systems:

$$q_1(j\Omega, A) = Q_0(j\Omega, A) + (N - 1)Q_1(j\Omega, A) \quad (3.78)$$

and

$$q_2(j\Omega, A) = q_3(j\Omega, A) = \dots = q_N(j\Omega, A) = Q_0(j\Omega, A) - Q_1(j\Omega, A), \quad (3.79)$$

where  $Q_0(j\Omega, A)$  and  $Q_1(j\Omega, A)$  are the elements of the first row of  $Q(j\Omega, A)$ , and the CTFs  $q_1(j\Omega, A)$  and  $q_i(j\Omega, A)$  ( $i = 2, 3, \dots, N$ ) are called the transfer functions of *average* and *relative* motions.

We know that only one characteristic system is excited in the limit cycle in any nonlinear MIMO system. Hence, in the limit cycling simple symmetrical system, either the characteristic system of the average motion [Equation (3.78)], with no motion in all other characteristic systems (systems of relative motions), or one of the characteristic systems [Equation (3.79)], where the average motion should be equal to zero, can become excited. The structure of the canonical basis of the simple symmetrical system justifies that statement. Indeed, the transfer function  $q_1(j\Omega, A)$  of the average motion corresponds to the *real* eigenvalue  $\beta_1 = 1$  of the permutation matrix  $U$  [Equation (1.128)], with which the eigenvector  $c_1$  is associated with real and equal components. Therefore, if the characteristic system of the average motion [Equation (3.78)] is excited in the limit cycle, the oscillations in the channels are cophased, i.e.  $x_i = A \exp\{j\Omega t\}$ , and the average value  $\bar{x}$  of the  $x_i$  variables

$$\bar{x} = \frac{1}{N} \sum_{k=1}^N x_k \equiv A \exp\{j\Omega t\} \quad (3.80)$$

coincides identically at an arbitrary time  $t$  with the value of any variable  $x_i$ . As for the difference between any two coordinates  $x_i$  and  $x_j$  ( $i \neq j$ ), it is identically equal to zero, i.e. there is no relative motion of the  $x_i$  signals in the system. Under the excitation of any of the characteristic systems of relative motions [Equation (3.79)], the oscillations bear a ‘hyperspherical’ character with equal relative phase shifts in the separate channels. The average motion of the variables  $x_i$

$$\bar{x} = \frac{1}{N} \sum_{k=1}^N x_k \equiv \frac{1}{N} A \exp\{j\Omega t\} \left[ 1 + \sum_{k=1}^{N-1} \exp\left\{j \frac{2\pi(r-1)}{N} k\right\} \right] \quad (3.81)$$

<sup>25</sup> See Section 1.4.2.

in this case is identically equal to zero, since the expression in the square brackets in Equation (3.81) is equal to zero for all  $r$ , where  $r \geq 2$  is the index of the excited characteristic system. Finally, note that since the conditions for all characteristic systems of relative motions [Equation (3.79)] to be on the stability boundary are identical, in the simple symmetrical system, depending on the initial conditions, any of them can excite. The limit cycle here will have the same amplitudes but different relative phase shifts, depending on the index  $r$  of the excited characteristic system.

### 3.5.1.2 Antisymmetrical circulant and anticirculant systems

When investigating the limit cycle in nonlinear antisymmetrical circulant and anticirculant systems, it is necessary to distinguish between two cases, depending on the number of channels. For odd  $N$ , the analysis of antisymmetrical MIMO systems requires involving the apparatus of circulant matrices and, for even  $N$ , of anticirculant matrices. A nonlinear circulant system of odd order  $N$  is called antisymmetrical if the elements of the first rows of the  $W(s)$  and  $G(A)$  matrices satisfy the conditions

$$w_k(s) = -w_{N-k}(s), \quad G_k(A) = -G_{N-k}(A), \quad k = 1, 2, \dots, N - 1. \quad (3.82)$$

The transfer function  $Q(j\Omega, A)$  of the open-loop antisymmetrical circulant system is antisymmetrical:

$$Q(j\Omega, A) = Q_0(j\Omega, A)I + \left\{ \sum_{k=1}^{(N-1)/2} Q_k(j\Omega, A)[U^k - (U^k)^{-1}] \right\}, \quad (3.83)$$

where  $Q_0(j\Omega, A)$  and  $Q_k(j\Omega, A) = -Q_{N-k}(j\Omega, A)$  can be found by common rules of the product of circulant matrices and the curly braces encompass a skew-symmetrical matrix. The condition for existence of the limit cycle with equal amplitudes in the antisymmetrical circulant system, i.e. the condition for the  $r$ th characteristic system to be on the stability boundary, have the form<sup>26</sup>

$$Q_0(j\Omega, A) = -1 \quad (3.84)$$

for  $r = 1$  and

$$Q_0(j\Omega, A) + j 2 \sum_{k=1}^{(N-1)/2} Q_k(j\Omega, A) \sin\left(\frac{2\pi(r-1)}{N} k\right) = -1 \quad (3.85)$$

for  $2 \leq r \leq N$ . Note that the condition in Equation (3.84) coincides with the condition for the isolated separate channel of the system to be on the stability boundary. Hence, if the channels of the antisymmetrical circulant system are limit cycling, with some amplitude  $A$ , and all characteristic systems for  $2 \leq r \leq N$  are stable for that  $A$ , then the limit cycle in the MIMO system is cophased, and the amplitudes and frequency of the limit cycle coincide with the amplitude and frequency of the limit cycle in the isolated separate channels. One might

<sup>26</sup> For brevity, we consider only the analogue of the Teodorchik method.

say that for  $r = 1$ , the presence of antisymmetrical cross-connections in the circulant system does not affect the parameters of limit cycle and these parameters are determined only by the separate channels. In the case of excitation of any other characteristic system, the oscillations are ‘hyperspherical’ and depend on both the direct channels and the cross-connections.

If the number of channels  $N$  is even, then the investigation of nonlinear antisymmetrical MIMO systems is based on the concept of an anticirculant matrix. A nonlinear anticirculant system of *even* order  $N$  is called antisymmetrical if elements of the first rows of the anticirculant matrices  $W(s)$  and  $G(A)$  satisfy the conditions

$$w_k(s) = w_{N-k}(s), \quad G_k(A) = G_{N-k}(A), \quad k = 1, 2, \dots, N - 1. \quad (3.86)$$

Then, the antisymmetrical transfer matrix  $Q(j\Omega, A)$  of the open-loop anticirculant system can be represented in the form

$$Q(j\Omega, A) = Q_0(j\Omega, A)I + \left\{ Q_{N/2}(j\Omega, A)U_-^{N/2} + \sum_{k=1}^{(N/2)-1} Q_k(j\Omega, A)[U_-^k - (U_-^k)^{-1}] \right\}, \quad (3.87)$$

where  $Q_0(j\Omega, A)$  and  $Q_k(j\Omega, A) = Q_{N-k}(j\Omega, A)$  are calculated via  $W(j\Omega)$  and  $G(A)$  by the standard rules, the curly braces include a skew-symmetrical matrix, and  $U_-$  is the *anticirculant permutation matrix* [Equation (1.156)]. The condition for the existence of the limit cycle here has the form

$$Q_0(j\Omega, A) + j(-1)^{r+1}Q_{N/2}(j\Omega, A) + 2j \sum_{k=1}^{(N/2)-1} Q_k(j\Omega, A) \sin \left\{ \frac{[2(r-1)+1]\pi k}{N} \right\} = -1. \quad (3.88)$$

**Example 3.6** Investigate the three-dimensional circulant system in Figure 3.42, assuming no input signals  $[\varphi(t) \equiv \mathbf{0}]$ . Assume also that the output signals of the ideal relays in the direct channels are equal to  $\pm 1$ , and the saturation nonlinearities in the cross-connections have unit gains ( $k = 1$ ) and a linear zone of  $[-1, +1]$ . The transfer matrix of the linear part of the system has the form

$$W(s) = \begin{pmatrix} w_0(s) & w_1(s) & -w_2(s) \\ -w_2(s) & w_0(s) & w_1(s) \\ w_1(s) & -w_2(s) & w_0(s) \end{pmatrix}, \quad (3.89)$$

where the transfer functions of the first row are

$$w_0(s) = \frac{10000}{s(s+5)(s+10)}, \quad w_1(s) = \frac{2400(s+3)}{s(s+2)(s+4)(s+15)}, \quad w_2(s) = \frac{800}{s(s+1)(s+20)}. \quad (3.90)$$

The matrix  $G(A)$  of the describing functions for the system of Figure 3.42 is taken as

$$G(A) = \begin{pmatrix} G_R(A) & 0.3G_S(A) & -0.4G_S(A) \\ -0.4G_S(A) & G_R(A) & 0.3G_S(A) \\ 0.3G_S(A) & -0.4G_S(A) & G_R(A) \end{pmatrix}, \quad (3.91)$$

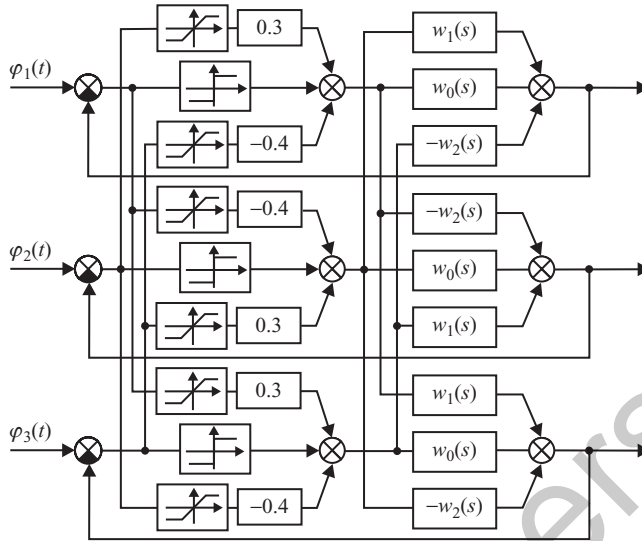


Figure 3.42 Three-dimensional nonlinear circulant system.

where the describing functions  $G_R(A)$  for the relays have the form in Equation (3.58) and, for saturation elements  $G_S(A)$ , the form in Equation (3.45), where  $\Delta = 1$ . The characteristic gain loci of the linear part are shown in Figure 3.43, from which it ensues that on excluding from the system the nonlinearities, it becomes unstable. It should be noted that, here, all three associated characteristic systems are unstable.

The results of investigation of the limit cycle by different methods are given in Figure 3.44. The use of the Teodorichik method [Figure 3.44(a)–(c)] shows that all three characteristic systems satisfy, for different  $A$  and  $\Omega$ , the necessary conditions for being on the stability boundary. The numerical values for the solutions along each canonical basis axis

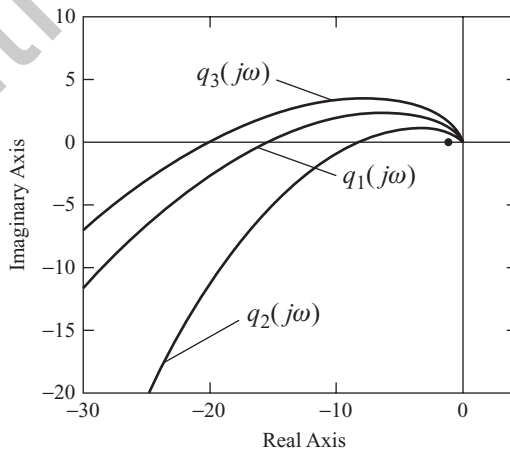
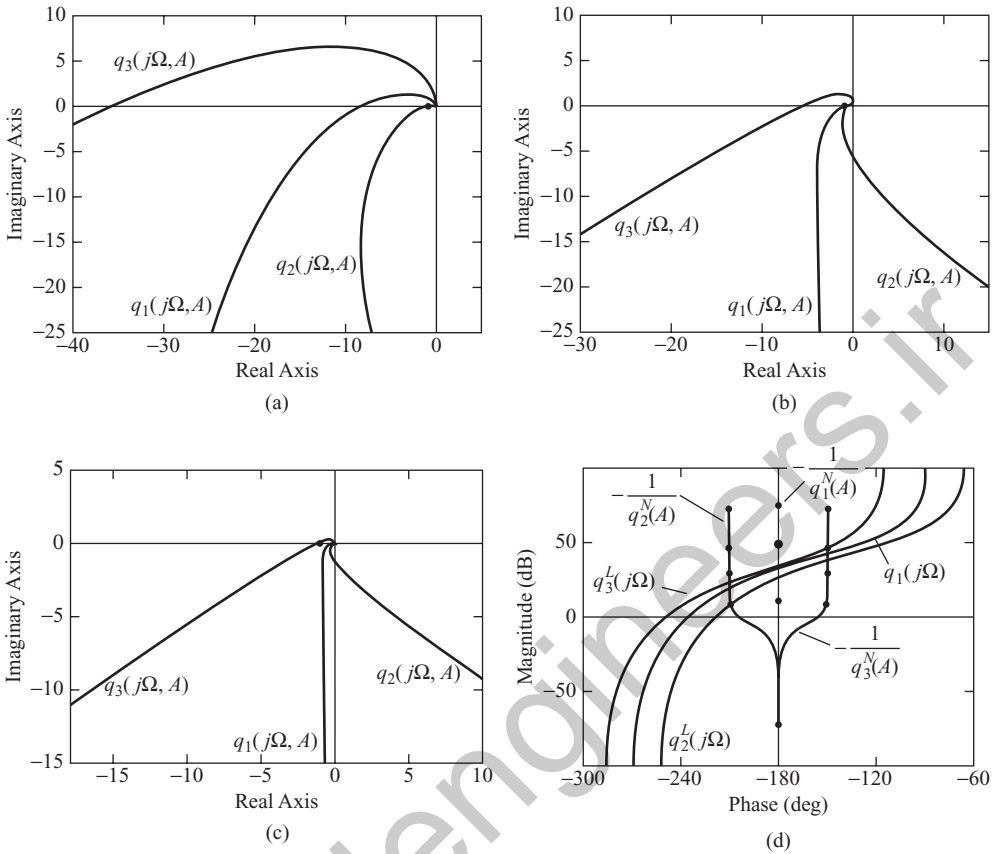
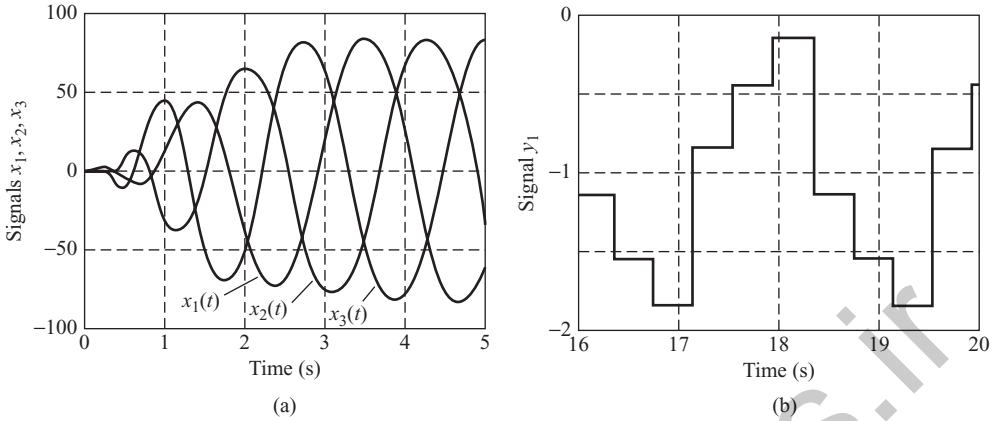


Figure 3.43 Gain loci of the linear part of the system in Figure 3.42.



**Figure 3.44** Investigation of the limit cycle in the circulant system of Figure 3.42. (a)  $A_2 = 2.3063$ ,  $\Omega_2 = 17.2606$ ; (b)  $A_1 = 17.3857$ ,  $\Omega_1 = 7.067$ ; (c)  $A_+ = 85.4158$ ,  $\Omega_+ = 2.6846$ ; (d) Nichols plane.

are:  $A_1 = 17.3857$ ,  $\Omega_1 = 7.067$ ;  $A_2 = 2.3063$ ,  $\Omega_2 = 17.2606$ ;  $A_3 = 85.4158$ ,  $\Omega_3 = 2.6846$ . However, based on the third condition for the existence of a limit cycle, namely the condition for stability of not excited characteristic systems, we arrive at a conclusion that only the oscillation along the third axis ( $r = 3$ ) can correspond to the actual limit cycle, i.e.  $A_+ = A_3 = 85.4158$ ,  $\Omega_+ = \Omega_3 = 2.6846$  [Figure 3.44(c)]. This oscillation is ‘spherical’ with relative phase shift of  $120^\circ$  with respect to the oscillation in the previous channel. Constructions in the Nichols plane, based on the analogue of the Goldfarb method [Equation (3.72)], are shown in Figure 3.44(d). Here, all characteristic gain loci of the linear and nonlinear parts of the system are shown jointly, where only the intersections of the loci with the same indices should be taken into consideration. Note that since all nonlinearities in the system of Figure 3.42 are single-valued and have real-valued describing functions, the locus  $-1/q_1^N(A)$  of the first characteristic system is also real. The bold dots in Figure 3.44(d) at the loci  $-1/q_i^N(A)$  indicate the value  $A_+ = 85.4158$  corresponding to the limit cycle along the third canonical basis axis, and the other dots at these loci correspond to the solutions along two other axes. The results of dynamical modelling of the three-dimensional system are shown in Figure 3.45. The



**Figure 3.45** Dynamical modelling of the system. (a) Signals at the inputs to nonlinearities; (b) waveform at the output of the nonlinearity in the first channel.

modelling gives the following values:  $A = 83.8287$ ,  $\Omega = 2.6449$ , i.e. the computational errors are less than 2%. It is interesting to note that the actual waveform of the signals at the outputs of nonlinearities is quite far from harmonical. This can be seen in Figure 3.45(b), in which the exact waveform of the oscillation in the first channel is given (the oscillations in the two other channels have the same waveform but are shifted by  $\pm 120^\circ$ ). However, owing to good filtering properties of the linear part, the oscillations at the *inputs* to the nonlinear elements are quite close to harmonical [Figure 3.45(a)], which provides high accuracy in the numerical evaluation.

**Example 3.7** As an example of the circulant systems with diagonal matrix of nonlinearities, consider the three-dimensional system depicted in Figure 3.46, in which the identical nonlinearities in the separate channels represent two-position relays with hysteresis having unit output levels and unit hysteresis zones. Each channel of the linear part is connected to the previous one by a link with the transfer function  $-w_2(s)$ , and the last channel is connected to the first one. Hence, we have here a really circulant (‘circular’) connection of the channels, where the transfer matrix of the linear part has the form

$$W(s) = \begin{pmatrix} w_0(s) & 0 & -w_2(s) \\ -w_2(s) & w_0(s) & 0 \\ 0 & -w_2(s) & w_0(s) \end{pmatrix}. \quad (3.92)$$

The transfer functions  $w_0(s)$  and  $w_2(s)$  in Equation (3.92) are taken as

$$w_0(s) = \frac{2000}{s(s+5)(s+10)}, \quad w_2(s) = \frac{640}{s(s+1)(s+20)} \quad (3.93)$$

The describing function of the two-position relay with hysteresis is (Popov 1973):

$$G_R(A) = \frac{4c}{\pi A} \sqrt{1 - \frac{\Delta^2}{A^2}} - j \frac{4c\Delta}{\pi A^2}, \quad (3.94)$$

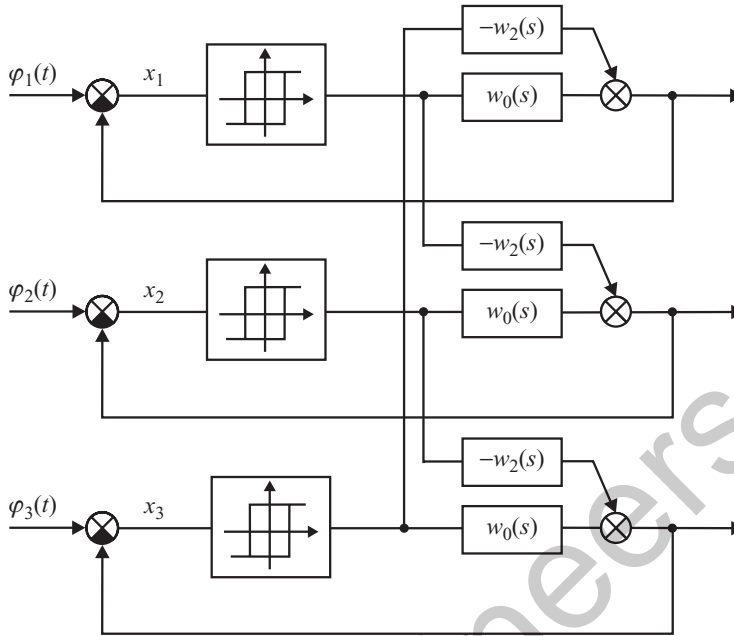


**Figure 3.46** Circulant system with the diagonal matrix of nonlinearities.

where the output level and the hysteresis zone of the relay are denoted by  $c$  and  $\Delta$  (in our case,  $c = 1$  and  $\Delta = 1$ ). Figure 3.47 illustrates the investigation of the limit cycle in the system on the basis of the Goldfarb method, i.e. by Equation (3.76).

As can be seen from these graphs, the periodical solution exists along all three axes of the canonical basis (for  $A_1 = 3.8221$ ,  $\Omega_1 = 5.839$ ;  $A_2 = 4.642$ ,  $\Omega_2 = 6.5124$ ;  $A_3 = 7.4181$ ,  $\Omega_3 = 4.7548$ ), but only the solution along the third axis, i.e. for  $A_+ = 7.4181$ ,  $\Omega_+ = 4.7548$  corresponds to the real limit cycle, for which the other characteristic systems are stable. Besides, that solution is stable, since, with the increase in  $A$ , the corresponding points at  $-1/G_R(A)$  move out of the locus  $q_3^L(j\Omega)$ . Figure 3.48 depicts the results of the system modelling which reveal some interesting features of the circulant systems behaviour; under the zero initial conditions [Figure 3.48(a)], the steady-state limit cycle has the following parameters:  $A = 4.7546$ ,  $\Omega = 6.4371$ , which, with an accuracy of up to 2.4%, corresponds to the solution along the second, and not the third, canonical basis axis. However, under the nonzero initial conditions [Figure 3.48(b)], the amplitude and the frequency of the limit cycle are  $A = 7.5876$ ,  $\Omega = 4.6628$ , which, up to the same accuracy ( $\approx 2.3\%$ ), corresponds to the determined stable solution along the third axis. Thus, in the presence of more than one periodical solution along different canonical basis axes of circulant and anticirculant systems, one can attain, by the proper choice of the initial conditions, the limit cycle along different directions of complex space  $\mathbb{C}^N$ . The practice shows that this feature is inherent only in the classes of MIMO systems discussed, for which the amplitudes of the limit cycle in different channels are the same, and the vectors of the complex amplitudes of oscillations along the canonical basis axes are mutually orthogonal. If the initial perturbations have an arbitrary direction, then the dynamical processes converge to the solution satisfying all the necessary conditions for limit cycle existence in MIMO systems.

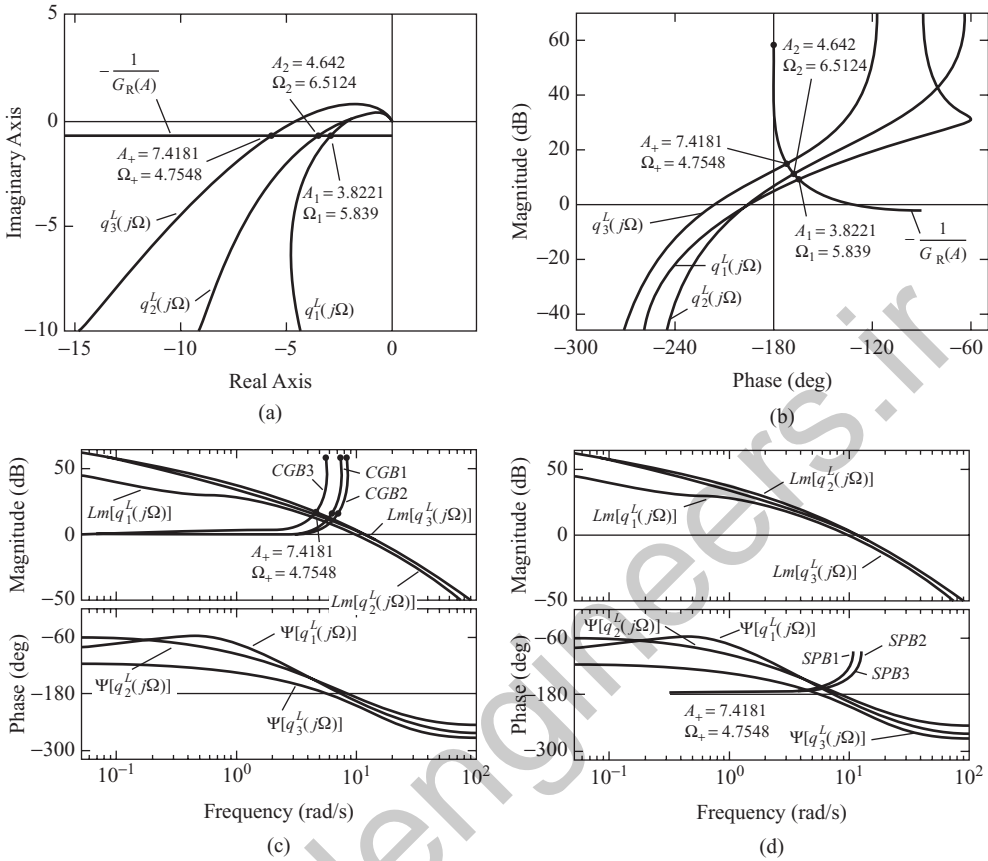


**Figure 3.47** Investigation of the limit cycle in the system of Figure 3.46. (a) Nyquist plane; (b) Nichols plane; (c) Bode diagrams and the *Critical Gain Boundaries* (CGBs); (d) Bode diagrams and the *Stability Phase Boundaries* (SPBs).

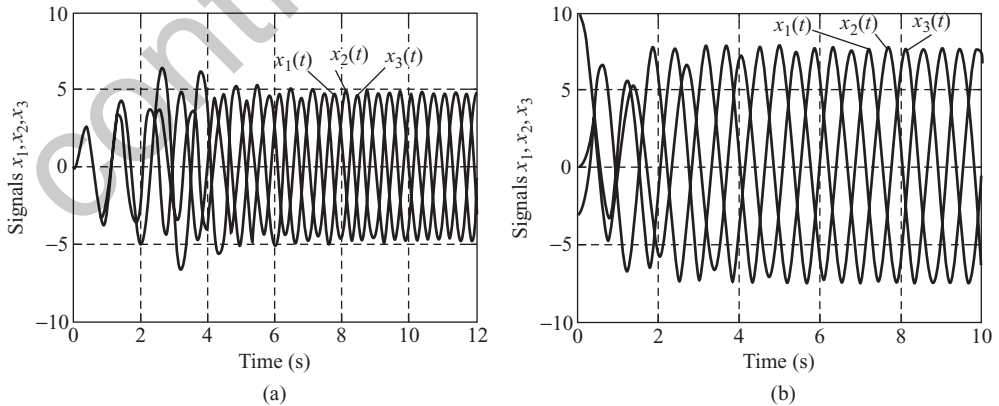


**Figure 3.48** Modelling of the circulant system in Figure 3.46. (a) Zero initial conditions; (b) nonzero initial conditions.

### 3.5.2 Limit cycles in uniform circulant and anticirculant systems

In discussing limit cycles with equal amplitudes in *uniform* circulant and anticirculant systems, we shall, for brevity, only consider circulant uniform systems, taking into account the complete similarity in methods for investigating circulant and anticirculant systems.

The main distinction of nonlinear uniform circulant systems from the general class of nonlinear uniform MIMO systems lies in that the matrix of rigid cross-connections  $R$  is circulant and the functional matrix of nonlinearities  $F(x)$  is 'structurally-circulant' (Figure 3.19). Let all nonlinearities in the uniform circulant system have odd-symmetrical characteristics and the input signals are not applied. Then, in the system, as in any other nonlinear circulant system, limit cycles with equal amplitudes in separate channels are possible. If, in addition, the low pass filter property for the linear part [Equation (3.46)] holds, then replacing all nonlinear characteristics by their describing functions, we come to a conclusion that the concomitant matrix of cross-connections  $N(A)$  [Equation (3.48)] is circulant and can be represented as a polynomial in the permutation matrix  $U$ :

$$N(A) = RG(A) = N_0(A)I + \sum_{i=1}^{N-1} N_i(A)U^i, \quad (3.95)$$

where  $N(A)$  depends on the amplitude  $A$ , and the elements  $N_i(A)$  ( $i = 0, 1, \dots, N - 1$ ) of the first row of  $N(A)$  can be determined by the general rules of the product of two circulant matrices  $R$  and  $G(A)$ . Since the transfer matrix  $Q(j\Omega, A)$  of the open-loop uniform circulant system coincides up to  $w(j\Omega)$  with the concomitant matrix  $N(A)$ , the CTFs  $q_i(j\Omega, A)$  have the common for uniform MIMO systems form

$$q_i(j\Omega, A) = \lambda_i(A)w(j\Omega), \quad i = 1, 2, \dots, N, \quad (3.96)$$

where  $\lambda_i(A)$  are the eigenvalues of  $N(A)$ . Therefore, the condition for the excitation of the  $r$ th characteristic system can be written in the conventional Goldfarb form:<sup>27</sup>

$$w(j\Omega) = -\frac{1}{\lambda_r(A)}, \quad (3.97)$$

but, unlike Equation (3.55), it depends not on the amplitudes vector of oscillations, but on only *one* amplitude  $A$ . Hence, the condition for the existence of the symmetrical limit cycle with equal amplitudes in uniform circulant systems does not differ at all from the condition for the existence of the limit cycle in nonlinear SISO systems. Also taking into account that the 'gains'  $\lambda_i(A)$  can be represented in analytical form for any number  $N$  of separate channels, one might say that the problem here is as complicated as in the usual SISO case. The graphical investigation of the limit cycle in the uniform circulant system by the condition in Equation (3.97) can be carried out as follows. The gain locus  $w(j\Omega)$  of the linear part is plotted in the complex plane. Then, the  $N$  loci  $-1/\lambda_i(A)$  are plotted in the same plane, as the scalar parameter  $A$  changes in appropriate limits (Figure 3.49). If  $w(j\Omega)$  does not intersect any of the loci  $-1/\lambda_i(A)$ , then the limit cycle is impossible. If there are intersections of  $w(j\Omega)$  with some loci from the family

<sup>27</sup> The use of the Teodorichik method has, in this case, no distinction from the general case of nonlinear circulant and anticirculant systems.

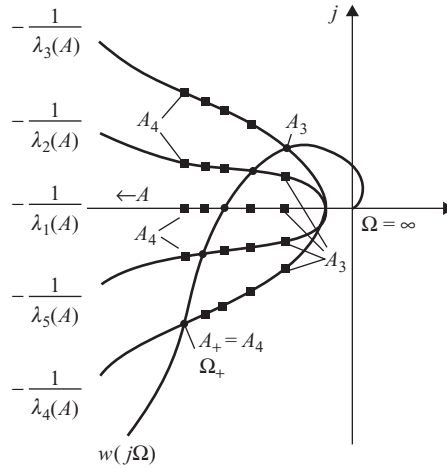
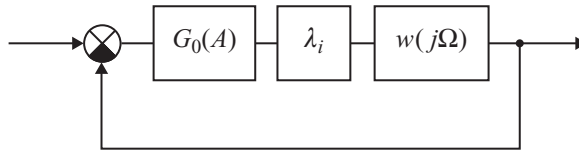


Figure 3.49 Investigation of the limit cycle in a uniform circulant system ( $N = 5$ ).

$\{-1/\lambda_i(A)\}$ , then it is necessary to find such a value of  $A$  for which one of the characteristic systems is on the stability boundary and all other systems are stable. To this end, each locus  $-1/\lambda_i(A)$  having an intersection with  $w(j\Omega)$  is subsequently checked by the following rule. One of the mentioned loci, say the  $r$ th, is selected and the value of the parameter  $A = A_r$  at the point of intersection with  $w(j\Omega)$  is determined. That value  $A_r$  is marked at all other loci  $-1/\lambda_i(A)$  ( $i \neq r$ ), which gives the critical points for  $w(j\Omega)$ . Now, it is clear that for the other characteristic systems to be stable under the determined  $A_r$ , it is necessary that the critical points be not encompassed by the locus  $w(j\Omega)$ . If this is the case, then the limit cycle with excitation of the  $r$ th characteristic system is possible, where the amplitude  $A_+$  of oscillations is equal to  $A_r$  and the frequency  $\Omega_+$  is determined by  $w(j\Omega)$  at the point of intersection with  $-1/\lambda_r(A)$ . Having similarly analyzed all intersection points, one can single out all possible periodical processes with equal amplitudes in the nonlinear uniform circulant system. In Figure 3.49, in which all critical points are shown but, for simplicity, only two amplitudes  $A_3$  and  $A_4$  ( $A_4 > A_3$ ) are labelled, the solution corresponds to the intersection with  $A_+ = A_4$ . The limit cycle here is possible only along the fourth axis of the canonical basis. For the stability of the limit cycle, it is necessary, first of all, that, on the increase in  $A$  ('collinear' perturbations of the vector  $x$ ), the corresponding point at the locus  $-1/\lambda_r(A)$  will move out of the locus  $w(j\Omega)$  and, on the decrease in  $A$ , it will move inside of the locus  $w(j\Omega)$ . In practice, it is usually enough to carry out such an analysis, but, if there are any doubts, it is advisable to check whether the general criterion of limit cycle stability under arbitrary variations of the amplitudes holds. Naturally, the investigation of limit cycles in uniform circulant systems can be performed in the Nichols and Bode planes, having taken in advance the logarithms of both parts in Equation (3.97). We have discussed such a procedure several times before and therefore we shall not dwell on that question here.

In conclusion, let us consider an important case of uniform circulant systems with the diagonal matrix of nonlinearities. In such systems, the concomitant matrix  $N(A)$  is equal to the circulant numerical matrix of cross-connections  $R$ , up to the scalar describing function  $G_0(A)$  of nonlinearities. The block diagrams of the characteristic systems here take a particularly simple form, depicted in Figure 3.50, in which  $\lambda_i$  are the eigenvalues of  $R$ . Based on Figure 3.50, the



**Figure 3.50** Block diagrams of the characteristic systems for the uniform circulant system with the diagonal matrix of nonlinearities ( $i = 1, 2, \dots, N$ ).

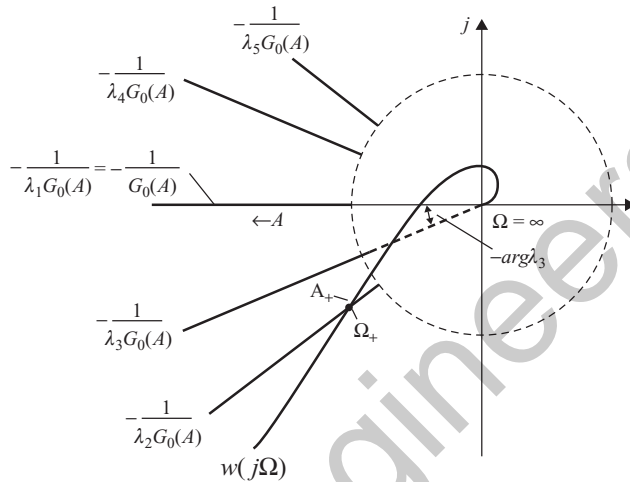


**Figure 3.51** Investigation of the limit cycle in a uniform circulant system with the diagonal matrix of cross-connections ( $N = 5$ ).

condition for the  $r$ th characteristic system to be on the stability boundary can be written in two equivalent forms:<sup>28</sup>

$$w(j\Omega) = -\frac{1}{\lambda_r G_0(A)} \quad (3.98)$$

or

$$\lambda_r w(j\Omega) = -\frac{1}{G_0(A)}. \quad (3.99)$$

Based on the first (*inverse*) form, to analyze the limit cycle in the system, we have to plot in the complex plane of  $w(j\Omega)$  a family of  $N$  loci corresponding to the right part in Equation (3.98) for all  $r = 1, 2, \dots, N$ . These loci can be obtained from the common graph  $-1/G_0(A)$  by changing its scale by a factor of  $1/|\lambda_r|$  and rotating it through an angle  $-\arg \lambda_r$  about the origin. The determination of the limit cycle parameters is carried out by the above scheme. The procedure is qualitatively illustrated for the case of a five-channel system with single-valued nonlinearities in Figure 3.51, in which all  $\lambda_i$  have unity magnitudes, i.e.  $|\lambda_i| = 1$ . The limit cycle in that system is stable and is directed along the second axis of the canonical basis. If the

<sup>28</sup> In the following, we shall conventionally call the first of these forms [Equation (3.98)] *inverse* and the second [Equation (3.99)] *direct*.

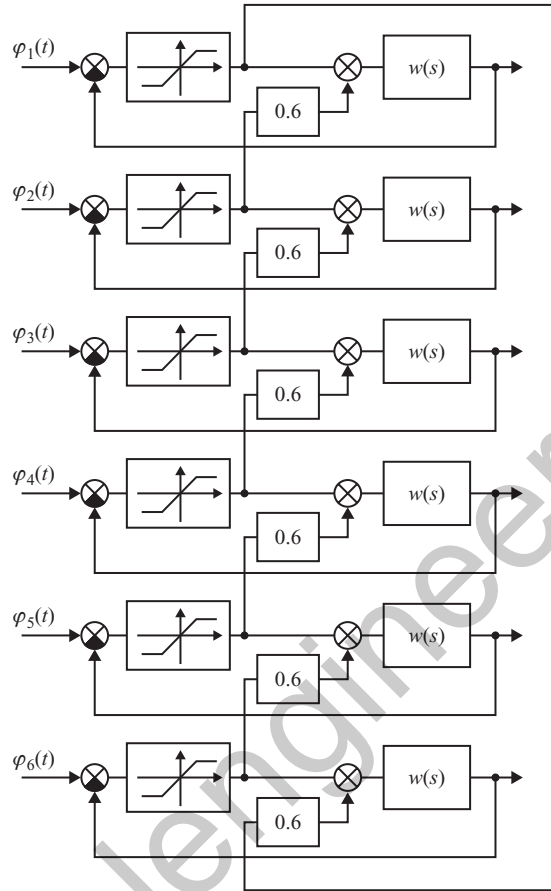


**Figure 3.52** Six-channel uniform circulant system with the diagonal matrix of nonlinearities.

second (*direct*) form [Equation (3.99)] is used, then a family of  $N$  loci  $\lambda_r w(j\Omega)$  is drawn in the complex plane and the location of these loci with respect to a single common characteristic  $-1/G_0(A)$  is analyzed. These constructions are illustrated in Figure 3.41. The simplification here, as compared with the more general case of circulant systems with a diagonal matrix of nonlinearities discussed in Section 3.5.1, lies in that the loci  $q_r^L(j\Omega) = \lambda_r w(j\Omega)$  of the linear part are obtained from the locus  $w(j\Omega)$  of the separate channels by changing the magnitudes  $w(j\Omega)$  by a factor of  $|\lambda_r|$  and subsequently rotating  $|\lambda_r|w(j\Omega)$  about the origin through the angle  $\arg \lambda_r$ . The intersection point of any  $\lambda_r w(j\Omega)$  with  $-1/G_0(A)$ , which is not encompassed by the characteristic gain loci of the linear part of other characteristic systems, will correspond to the real limit cycle in the uniform system (in Figure 3.41, it is the point labeled by 4).

**Example 3.8** Consider the six-channel uniform system in Figure 3.52 with saturation nonlinearities in separate channels, assuming that the linear zones are equal to  $[-4, +4]$ . The transfer function of identical separate channels of the system is taken in the form

$$w(s) = \frac{3750000000}{s(s + 25)(s + 400)(s + 500)}. \quad (3.100)$$

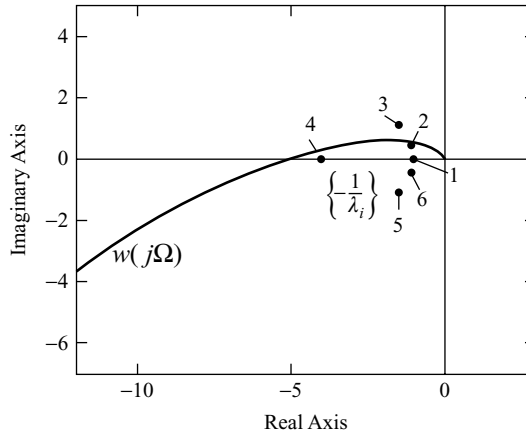


**Figure 3.53** Characteristic gain loci of the linear uniform system.

The cross-connections matrix  $R$  of the system is represented via the permutation matrix  $U$  as  $R = I + 0.6U$ . The characteristic gain loci of the linear part and the critical points  $-1/\lambda_i$  (where the numbers indicate the number of characteristic systems) are given in Figure 3.53. It is evident that the linear (i.e. without nonlinearities) uniform system is unstable, where five of its six characteristic systems are unstable.

The only stable characteristic system is the third one, with  $\lambda_3 = 0.7 + j0.5196$ , and the ‘worst’ from the stability margins viewpoint is the fifth system, with the complex conjugate (with respect to the third) ‘gain’  $\lambda_5 = 0.7 - j0.5196$ . As we shall see, the limit cycle in the uniform system is due to the excitation of that very fifth characteristic system. Such a situation, in which the ‘worst’ characteristic system excites in the limit cycle, is usually inherent in MIMO systems with nonlinearities whose describing functions decrease as the amplitude of oscillation increases. In our case, with the saturation nonlinearities, this is true, which follows from Equation (3.45). The investigation on the Nichols plane of the discussed uniform system, using both Equations (3.98) and (3.99), is represented in Figure 3.54. The

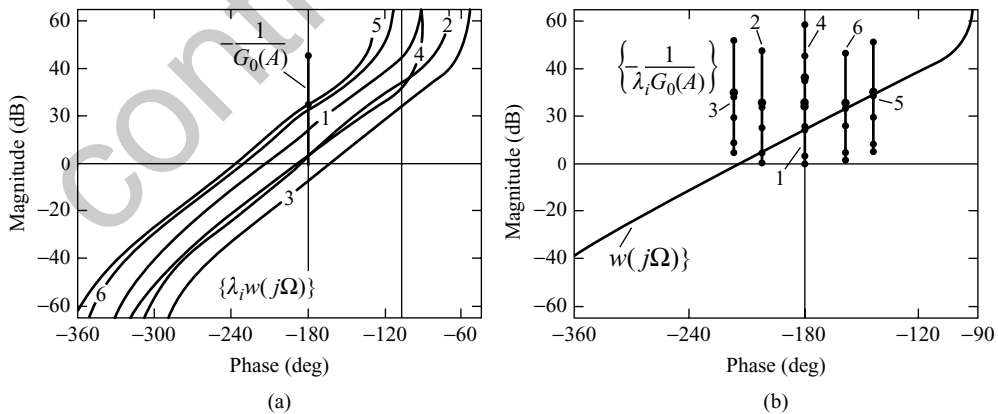


**Figure 3.54** Investigation of the limit cycle in the uniform circulant system on the Nichols plane. (a) ‘Direct’ form; (b) ‘inverse’ form.

computations show that there are five possible periodical solutions (corresponding to unstable characteristic systems) with the following parameters, in which the indices indicate the number of the characteristic systems:

$$\begin{aligned}
 A_1 &= 25.8431, & \Omega_1 &= 73.5213; & A_2 &= 6.6437, & \Omega_2 &= 130.295; \\
 A_4 &= 5.9611, & \Omega_4 &= 73.5213 & A_5 &= 86.1217, & \Omega_5 &= 26.4253; \\
 A_6 &= 70.212, & \Omega_1 &= 39.908
 \end{aligned}$$

Note that the frequencies of the periodical solutions along the first and fourth axes of the canonical basis, to which the real eigenvalues of the circulant matrix  $R$  correspond, coincide with each other and coincide with the frequency at which the  $w(j\Omega)$  locus cuts the real axis. So as not to encumber the graphs, the numerical values of the solution parameters are not shown in Figure 3.54 and the Arabic numerals indicate the characteristic systems. Also, the big dots belong to the stable solution along the fifth axis of the canonical basis and the remaining dots show solutions along other axes. The  $A$  amplitudes numbering (as  $A$  increases) in Figure 3.54 is directed upward. Note also that in Figure 3.54(b), the negative reciprocal loci of the nonlinear part coincide for the first and the fourth characteristic systems. To determine the periodical solutions that can correspond to the real limit cycle in the uniform system, it is necessary to check for each  $r$ th solution the stability of all other ( $i \neq r$ ) characteristic systems. Such an analysis for the solutions directed along the fourth ( $A_4 = 5.9611$ ) and the fifth ( $A_5 = 86.1217$ ) axes of the canonical basis is given in Figure 3.55 (pay attention to the scales of these graphs).

As is evident from these graphs, the solution along the fifth canonical basis axis (for  $A_+ = A_5 = 86.1217, \Omega_+ = \Omega_5 = 26.4253$ ) satisfies the necessary condition for the existence of a limit cycle in the uniform circulant system. The modelling of the discussed system gives the following values for the limit cycle parameters:  $A = 81.5102, \Omega = 26.1191$ . The dynamical processes in the first and fourth channels of the system are represented in Figure 3.56. The computational error for the amplitude here is about 6% and, for the frequency, it is 1.17%. The larger computed value for the amplitude  $A_+ = 86.1217$ , as compared with the one obtained

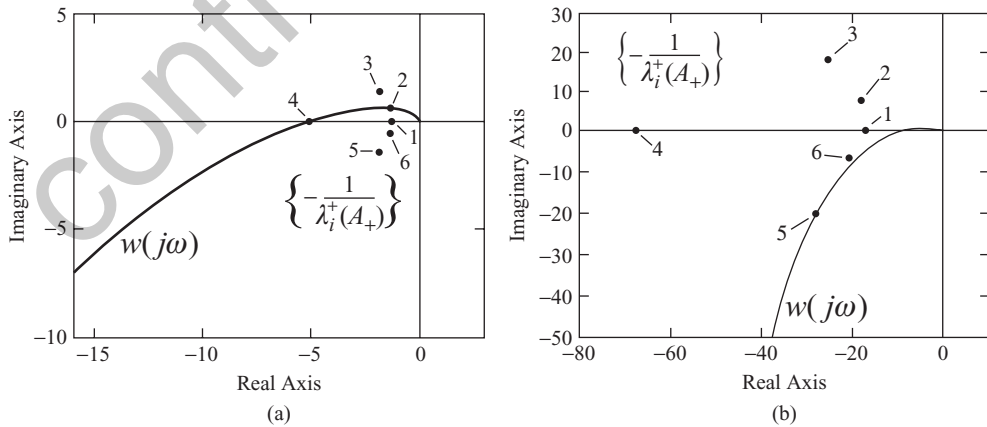


**Figure 3.55** Stability analysis of ‘unexcited’ characteristic systems (the dots represent the critical points). (a) Solution  $A_4 = 5.9611, \Omega_4 = 73.5213$ ; (b) Solution  $A_5 = 86.1217, \Omega_5 = 26.4253$ .

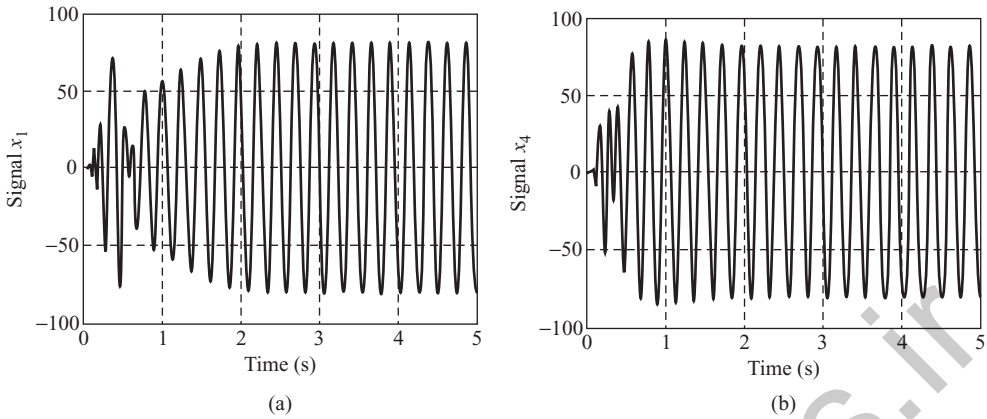


**Figure 3.56** Dynamical modelling of the nonlinear uniform circulant system in Figure 3.52. (a) First channel; (b) fourth channel.

by the modelling, could be explained to a certain extent by the fact that the output signals of the saturation nonlinearities, produced from the input waveforms by truncation at levels  $\pm 4$ , are quite close to the square waveforms. The third harmonic of such pulses is relatively large and its amplitude in the Fourier series expansion is subtracted from the amplitude of the fundamental harmonic, i.e. it decreases the peak amplitude of the real waveform. Therefore, the computation based on the harmonic balance method (which takes into account only the fundamental harmonic) yields here a value for the limit cycle amplitude that is slightly overestimated but quite acceptable for engineering purposes.

# 4

## Forced oscillation and generalized frequency response characteristics of nonlinear MIMO systems

### 4.1 INTRODUCTION

The problem of the investigation of forced oscillations in nonlinear systems is very complicated and interesting, owing to the diversity of forms of possible dynamical responses. Thus, if we apply one-frequency sinusoidal signals to the inputs of a limit cycling system, the latter may exhibit a complex motion, which is not strictly periodical and, in many respects, is like the beating mode in a linear oscillatory system driven by a sinusoidal signal. Under some conditions, the phenomenon of *capturing* (also called *entrainment* or *forced synchronization*) can occur in the system, when the external signal enforces its own frequency on the system, suppressing completely the existing limit cycle. Besides, in limit cycling nonlinear systems, the possibility of synchronization at the frequency of one of the subharmonics or higher harmonics is not excluded (Popov 1973; Tsytkin 1974).

Note that so far, in the classical control theory, only the problem of the investigation of one-frequency forced oscillation under the above-mentioned capturing condition has adequately been solved or brought in any way to real engineering applications. At that, if exact methods exist for systems with relay nonlinearities (Thaler and Pastel 1962; Tsytkin 1974), in the case of general nonlinear characteristics, the numerical analysis of systems is mainly based on the describing function method. Consider briefly the primary ways of solving that task for SISO systems (Popov 1973). Let the input signal of the system in Figure 3.1, in which the nonlinearity  $F(x)$  is supposed to be odd-symmetrical, be of the periodical form

$$\varphi(t) = B \sin \Omega t \quad (4.1)$$

and the low pass filter property [Equation (3.1)] holds at the frequency  $\Omega$  of the input signal. Then, if the system steady-state response is also periodical with the same frequency  $\Omega$ , one can perform the harmonic linearization of the nonlinearity  $F(x)$  and, assuming that  $x$  is

of the form

$$x = A \sin(\Omega t + \psi), \quad (4.2)$$

write the following complex equation of the closed-loop system:

$$A \exp\{j\psi\} = \frac{1}{1 + W(j\Omega)G(A)} B, \quad (4.3)$$

where the unknowns are the amplitude  $A$  and the phase shift  $\psi$  of oscillation at the *input* to  $F(x)$ , and the frequency  $\Omega$ , unlike the task of investigation of the limit cycle, is given by the input signal  $\varphi(t)$  [Equation (4.1)]. From Equation (4.3), two nonlinear algebraic equations in the unknowns  $A$  and  $\psi$  immediately follow:

$$A = \frac{1}{|1 + W(j\Omega)G(A)|} B \quad (4.4)$$

and

$$\psi = \arg \left\{ \frac{1}{1 + W(j\Omega)G(A)} \right\}. \quad (4.5)$$

Note that the *only* actual unknown in the problem is the amplitude  $A$ , since, having determined it from Equation (4.4), one can readily calculate  $\psi$  using Equation (4.5). In this regard, the investigation of the forced oscillation is simpler than that of the limit cycle, where two values –  $A$  and  $\Omega$  – are unknown. Note also that we do not fix whether the system of Figure 3.1 is stable or exhibits a limit cycle of some frequency  $\Omega_+$  before applying the input signal [Equation (4.1)]. The only condition is that after applying the input sinusoidal signal of frequency  $\Omega$ , the system must have the sinusoidal forced motion of the same frequency. For a *stable* nonlinear system, this corresponds to a common mode of forced oscillation. If the system is limit cycling, the above condition assumes *forced synchronization*, i.e. Equation (4.4) allows a solution to be found only for that mode. If Equation (4.4) has no solution in the case of a limit cycling system, then this means that in the system, there is a complex motion that cannot be investigated by the describing function method (Popov 1973).

The direct solution of Equation (4.4) presents no difficulties but, in practice, graphical techniques closely connected to the conventional methods for the investigation of limit cycles in nonlinear control systems, such as the Teodorchik and Goldfarb methods, are usually resorted to. Besides, as we shall see later, these methods provide a basis for the development of corresponding methods for nonlinear systems *design*.

Suppose that we have carried out the investigation of a limit cycle in the system by the Teodorchik method, i.e. we have the family of the  $W(j\omega)G(A)$  loci for different  $A = const$ , as the frequency  $\omega$  changes from zero to infinity [see Figure 3.2(a)]. Rewrite Equation (4.4) in the form

$$|1 + W(j\Omega)G(A)| = \frac{B}{A}. \quad (4.6)$$

From here, raising both sides to the second power, it is easy to obtain

$$[\operatorname{Re}\{W(j\Omega)G(A)\} + 1]^2 + [\operatorname{Im}\{W(j\Omega)G(A)\}]^2 = \left(\frac{B}{A}\right)^2, \quad (4.7)$$

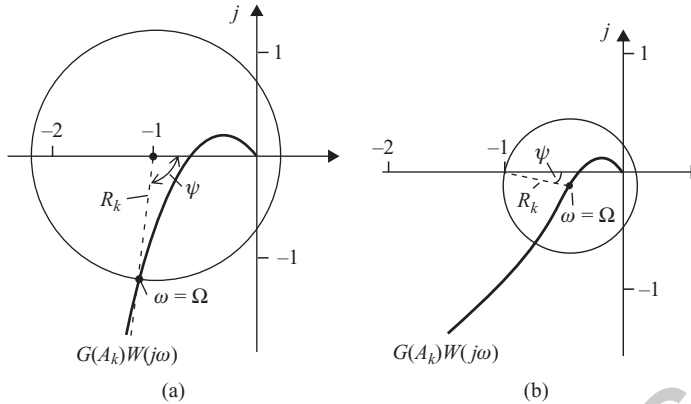


**Figure 4.1** Graphical interpretation of the solution to Equation (4.7) (two different systems). (a) First variant; (b) second variant.

which represents in the complex plane of the family  $\{W(j\omega)G(A)\}$  an equation of a circle with its centre at the point  $(-1, j0)$  and radius  $R = B/A$ . It becomes clear now that the sought amplitude  $A$  is equal to the parameter  $A_k$  of that locus of the family  $\{W(j\omega)G(A)\}$ , for which the circle with its centre at  $(-1, j0)$  and radius  $R_k = B/A_k$  cuts  $W(j\omega)G(A_k)$  at a point at which  $\omega = \Omega$  [Figure 4.1(a)]. One can also give another, equivalent interpretation to the solution, namely if  $A_k$  is the solution to the problem, then the circle with its centre at the point  $\omega = \Omega$  at  $W(j\omega)G(A_k)$  must pass through the point  $(-1, j0)$  [Figure 4.1(b)].

Suppose, now, that the investigation of the limit cycle was performed by the Goldfarb method [Figure 3.2(b)]. Dividing both parts of Equation (4.6) by  $G(A)$ , after a number of simple manipulations, yields, instead of Equation (4.7),

$$\left[ \operatorname{Re}\{W(j\Omega)\} + \operatorname{Re}\left\{\frac{1}{G(A)}\right\} \right]^2 + \left[ \operatorname{Im}\{W(j\Omega)\} + \operatorname{Im}\left\{\frac{1}{G(A)}\right\} \right]^2 = \left[ \frac{B}{AG(A)} \right]^2, \quad (4.8)$$

which gives an equation of a circle with its centre at the point  $-1/G(A)$  and radius  $R = B/AG(A)$  on the plane of  $W(j\omega)$ . Evidently, the solution to the problem is that value  $A_k$  for which the circle with its centre at  $-1/G(A_k)$  and radius  $R_k = B/A_k G(A_k)$  cuts  $W(j\omega)$  at the point at which  $\omega = \Omega$  (Figure 4.2).

In fact, one can say that for the case of limit cycling systems, the graphs in Figure 4.1 and 4.2 give the geometrical interpretation of the occurrence of forced synchronization at frequency  $\Omega$  of the sinusoidal input. Besides the discussed techniques, there is another graphical technique proposed by E. Popov (1973), which, in some cases, proves to be more convenient, especially for determining the so-called *threshold value* of the input amplitude, i.e. the minimal value of the amplitude  $B$  in Equation (4.1), for which the synchronization in the limit cycling system occurs. The essence of the technique consists in the following. Equation (4.3) is rewritten in the form

$$[1 + W(j\Omega)G(A)]A = B \exp\{-j\psi\}. \quad (4.9)$$

Based on Equation (4.9), an auxiliary locus

$$Z(A) = [1 + W(j\Omega)G(A)]A \quad (4.10)$$

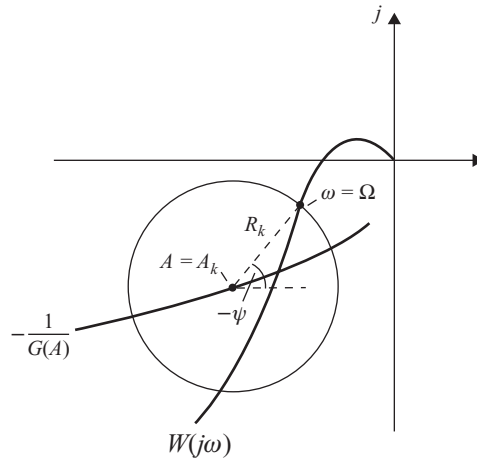


**Figure 4.2** Graphical interpretation of the solution to Equation (4.8).

corresponding to the left part of Equation (4.9) is plotted in the complex plane for the given value  $\Omega = const$  of the input frequency, as the unknown amplitude  $A$  changes from zero to infinity. The right part of Equation (4.9) is depicted in the form of a circle of radius  $B$  with its centre at the origin. The intersection of that circle with the locus  $Z(A)$  gives the solution to the problem: the phase shift  $\psi$  is determined here by the arc of the circle at the intersection point and the  $A$  amplitude of the forced oscillation by the  $Z(A)$  locus [Figure 4.3(a)]. The graphs in Figure 4.3(a) correspond to a *stable* nonlinear system. In stable systems, the locus  $Z(A)$  [Equation (4.10)] for  $A = 0$  usually starts at the origin. Therefore, the nonlinear system exhibits forced oscillation at any input frequencies under arbitrary small amplitudes  $B$ . For the case of *limit cycling* systems, the picture is somewhat different. In Figure 4.3(b), the  $Z(A)$  loci are plotted for two input frequencies, where these frequencies are indicated explicitly as the parameters of the  $Z(A)$  loci. If the  $\Omega$  frequency of the input signal is not equal to the limit

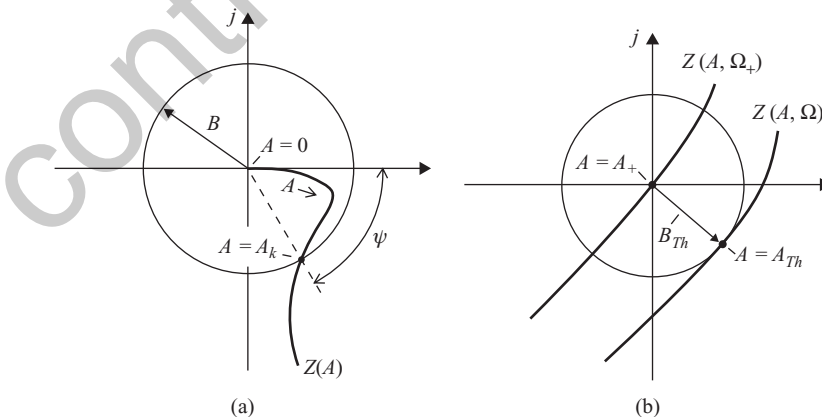


**Figure 4.3** Investigation of the forced oscillation by the Popov method. (a) Stable system; (b) limit cycling system.

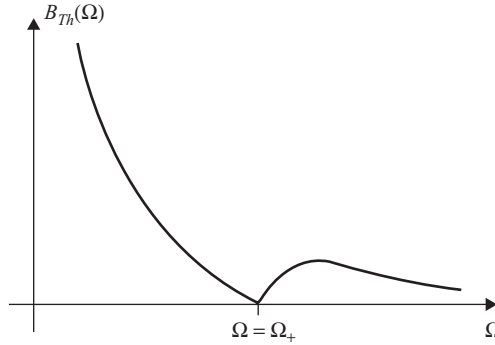


**Figure 4.4** Frequency dependence of the input threshold amplitude in limit cycling systems.

cycle frequency  $\Omega_+$ , then the locus  $Z(A, \Omega)$  passes at some distance from the origin and, for small  $B$  amplitudes, the corresponding circles  $B = \text{const}$  and the  $Z(A)$  locus do not intersect. This means that there is no capturing in the system and the forced response bears a complex oscillatory character. The increase in the  $B$  amplitude results in that for some *threshold* value  $B = B_{Th}$ , the circle of the  $B_{Th}$  radius becomes tangent to  $Z(A)$ , as shown in Figure 4.3(b). Correspondingly, the synchronization takes place and the system goes into the mode of one-frequency forced oscillation at the input frequency  $\Omega$ . If the latter is equal to the frequency  $\Omega_+$  of the limit cycle, then, for  $A = A_+$ , the locus  $Z(A, \Omega_+)$  passes through the origin. This follows from Equation (4.10), since, in limit cycling systems, we have  $W(j\Omega_+)G(A_+) = -1$ . Therefore, for  $\Omega = \Omega_+$ , the  $B_{Th}$  threshold value is equal to zero. This is physically evident, as the limit cycling system already oscillates at that frequency without applying any input signal. The possibility of simple determination of the threshold values  $B_{Th}$  is one of the advantages of the approach proposed by E. Popov. Typical dependence of the threshold value  $B_{Th}$  on the frequency  $\Omega$  in the limit cycling systems is shown in Figure 4.4. The character of that curve is clear from the above. The capturing in the system occurs only for  $B > B_{Th}$ , i.e. the region of the forced synchronization lies above the threshold curve in Figure 4.4. In practice, the threshold curve is usually situated slightly higher, except the point at the limit cycling frequency  $\Omega_+$ , since only the fundamental harmonic is taken into account in computations on the basis of the describing function method.

The problem of the investigation of forced oscillation implicitly abuts the problem of determining the frequency response characteristics of *stable* nonlinear systems. The relative value of the resonant peak of these characteristics can serve as a measure of the remoteness of the closed-loop nonlinear system from the stability boundary, analogously to the *oscillation index* of linear systems. The principle distinction of the frequency characteristics of a nonlinear system from the corresponding characteristics of linear systems is that in the nonlinear case, these characteristics depend on not only the frequency  $\Omega$  of the input signal, but also on the *magnitude* of the amplitude  $B$ . This matter is very important and should be considered in more detail. Denote by  $\Phi_x(j\Omega, A)$  the transfer function of the closed-loop harmonically linearized system with respect to the input  $x$  to the nonlinearity. Then, based on Equation (4.4), we have

$$|\Phi_x(j\Omega, A)| = \frac{A}{B} = \frac{1}{|1 + W(j\Omega)G(A)|}. \quad (4.11)$$

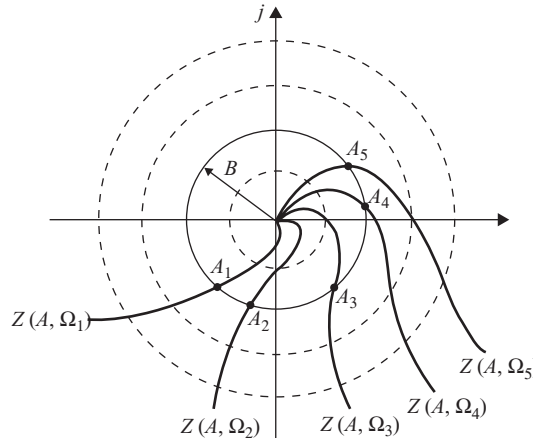


**Figure 4.5** Computation of the frequency characteristics of stable nonlinear systems with the help of E.P. Popov’s method.

Actually, the  $\Phi_x(j\Omega, A)$  depends, for  $B = const$  and  $\Omega = const$ , on the *unknown* amplitude  $A$  and, to define the latter, it is necessary to solve nonlinear algebraic Equation (4.4). That solution gives one point at the frequency characteristic  $|\Phi_x(j\Omega, A)|$ . Changing  $\Omega$  from zero to infinity and solving Equation (4.4) each time, we obtain the whole frequency characteristic for the given  $B = const$ . For different  $B$ , we have *different* frequency responses, owing to the nonlinear properties of the system. Figure 4.5 illustrates how this can be solved with the help of E. Popov’s method.

In Figure 4.5, the concentric circles correspond to different  $B$  and a family of the  $Z(A) = Z(A, \Omega)$  loci for different  $\Omega = const$  under the changes of  $A$  is plotted. The possible forms of the family of the frequency characteristics  $|\Phi_x(j\Omega, A)|$  determined by the described procedure are qualitatively represented in Figure 4.6(a).

The amplitude  $C$  of the fundamental harmonic of the output signal  $f(t)$  of the system in Figure 3.1 is related to  $A$  by an evident relationship  $C = |W(j\Omega)G(A)|A$ . Therefore, denoting the closed-loop transfer function with respect to the output signal by  $\Phi(j\Omega, A)$ , for the

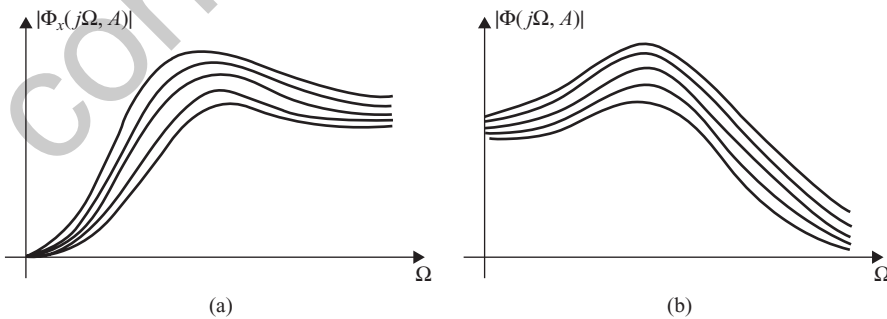


**Figure 4.6** Frequency characteristics of the harmonically linearized system for different input amplitudes  $B = const$ . (a) With respect to the input signal of the nonlinearity; (b) with respect to the output signal of the system.

corresponding characteristic  $|\Phi(j\Omega, A)|$ , we have

$$|\Phi(j\Omega, A)| = \frac{C}{B} = \left| \frac{W(j\Omega)G(A)}{1 + W(j\Omega)G(A)} \right|, \quad (4.12)$$

where the  $A$  amplitude is determined by solving the same Equation (4.4). A possible sketch of  $|\Phi(j\Omega, A)|$  for different  $B = const$  is shown in Figure 4.6(b). As can be seen from Figure 4.6, the relative value of the resonant peak of the frequency characteristics, as well as the resonant frequency, depend on the amplitude  $B$ . This is due to the nonlinear properties of the system. Of course, the computation of the resonant peak for nonlinear systems by finding their frequency responses under various input amplitudes  $B$  is an extremely cumbersome and, in many respects, senseless task. Therefore, in practical computations, instead of solving nonlinear Equation (4.4), which yields the unknown amplitude  $A$  for the given  $B$  and  $\Omega$ , quite another procedure is turned to (Paltov 1975). Note that the frequency characteristics  $|\Phi_x(j\Omega, A)|$  [Equation (4.11)] and  $|\Phi(j\Omega, A)|$  [Equation (4.12)] are in fact, for the given  $\Omega$ , functions of the unknown amplitude  $A$ , which can take only positive values. Therefore, one can find the boundary curves encompassing from above all frequency characteristics in Figure 4.6, not by solving Equation (4.4) for various  $B$ , but by *maximizing*  $|\Phi_x(j\Omega, A)|$  and  $|\Phi(j\Omega, A)|$  with respect to the amplitude  $A$  at every frequency  $\Omega$ , i.e. by finding the curves

$$\Phi_{\max}^x(\Omega) = \max_{A \geq 0} |\Phi_x(j\Omega, A)|, \quad \Phi_{\max}^f(\Omega) = \max_{A \geq 0} |\Phi(j\Omega, A)|. \quad (4.13)$$

Evidently, the  $\Phi_{\max}^x(\Omega)$  and  $\Phi_{\max}^f(\Omega)$  curves bound from above, owing to the way in which they are determined, all the frequency characteristics in Figure 4.6. The resonant peaks of these curves

$$M_x = \sup_{0 < \Omega < \infty} [\max_{A \geq 0} |\Phi_x(j\Omega, A)|], \quad M_f = \sup_{0 < \Omega < \infty} [\max_{A \geq 0} |\Phi(j\Omega, A)|], \quad (4.14)$$

termed, respectively, the *oscillation indices* of the nonlinear system with respect to signals at the input to the nonlinearity and the system output, can serve as a measure of the remoteness from the ‘limit cycling’ stability boundary. Indeed, if, for some  $A$  and  $\Omega$ , the harmonic balance condition  $W(j\Omega)G(A) = -1$  holds, then the denominators of  $|\Phi_x(j\Omega, A)|$  [Equation (4.11)] and  $|\Phi(j\Omega, A)|$  [Equation (4.12)] vanish at frequency  $\Omega$  and values of  $\Phi_{\max}^x(\Omega)$  and  $\Phi_{\max}^f(\Omega)$  [Equation (4.13)] tend to infinity. On the other hand, the larger the *minimal* value of the magnitude  $|W(j\Omega)G(A) + 1|$  for various  $A$  and  $\Omega$ , the smaller the resonant peaks of the curves [Equation (4.13)]. The methods for determining the oscillation index of nonlinear SISO systems by the frequency response characteristics of the open-loop system proposed by Paltov (1975) are based on these observations. For brevity, we shall consider only the case of determining  $M_x$  in Equation (4.14), since the technique for determining the oscillation index  $M_f$  with respect to the system output differs only in some minor details. Find, first, the geometrical locus of points corresponding to some constant value  $M = const$  of the magnitude  $|\Phi_x(j\Omega, A)|$  on the complex plane of the family  $\{W(j\Omega)G(A)\}$  for different  $A = const$ . Equating  $|\Phi_x(j\Omega, A)|$  in Equation (4.11) to that value of  $M$ , after simple manipulations, we obtain an equation analogous to Equation (4.7):

$$[\text{Re}\{W(j\Omega)G(A)\} + 1]^2 + [\text{Im}\{W(j\Omega)G(A)\}]^2 = \frac{1}{M^2}. \quad (4.15)$$

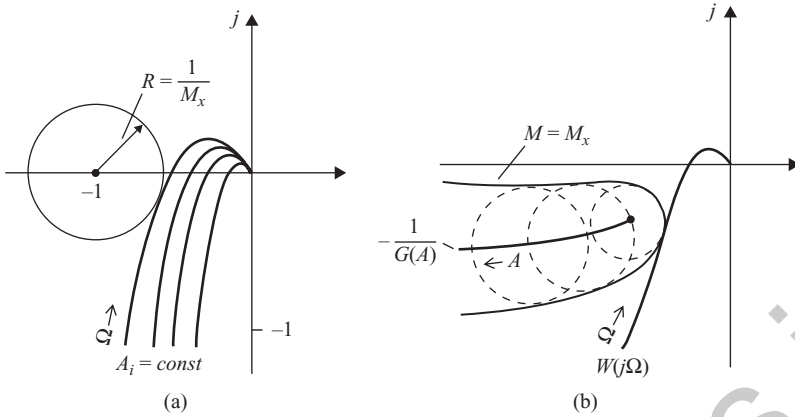


**Figure 4.7** Evaluation of the oscillation index for nonlinear systems. (a) Family of the  $W(j\Omega)G(A)$  loci for different  $A = A_i$ ; (b) the Goldfarb method.

Equation (4.15) defines in the complex plane a circle with its centre at the point  $(-1, j0)$  and radius  $R = 1/M$ . As  $M \rightarrow \infty$ , that circle degenerates into the point  $(-1, j0)$  and spreads out over the whole complex plane as  $M_i \rightarrow 0$ . It is clear that the maximum value of  $M_x$  in Equation (4.14) is reciprocal to the radius of that ‘smallest’ circle which is tangent to the envelope of the family  $\{W(j\Omega)G(A)\}$  used for determining the limit cycle parameters by the Teodorchik method [Figure 4.7(a)]. Let us now rewrite Equation (4.11) in the form

$$|\Phi_x(j\Omega, A)| = \frac{1/G(A)}{|1/G(A) + W(j\Omega)|}. \quad (4.16)$$

Equating Equation (4.16) to a constant  $M$  and performing some simple manipulations yield

$$\left[ \text{Re}\{W(j\Omega)\} + \text{Re}\left\{\frac{1}{G(A)}\right\} \right]^2 + \left[ \text{Im}\{W(j\Omega)\} + \text{Im}\left\{\frac{1}{G(A)}\right\} \right]^2 = \frac{1}{[MG(A)]^2}. \quad (4.17)$$

For given  $M = \text{const}$  and  $A = \text{const}$ , Equation (4.17) determines, in the complex plane of the locus  $W(j\Omega)$  of the linear part, a circle with its centre at  $-1/G(A)$  and radius  $R = 1/MG(A)$  [these circles, for different values of  $A$ , are shown in Figure 4.7(b) by dashed lines]. The envelope of all these circles for various  $A$  and the given  $M = \text{const}$  determine the forbidden region for  $W(j\Omega)$ . As  $M \rightarrow \infty$ , the envelope of all circles reduces to the locus  $-1/G(A)$  used for the limit cycle investigation by the Goldfarb method and, as  $M \rightarrow 0$ , it spreads out over the whole complex plane. Evidently, the oscillation index  $M_x$  of the system is equal to that value of  $M$  for which the forbidden region is tangent to  $W(j\Omega)$  [Figure 4.7(b)]. Both the discussed graphical techniques for evaluating  $M_x$  are equivalent in the SISO case and serve as a basis for the corresponding design methods for nonlinear systems, i.e. for finding system correction based on the specified value of the oscillation index. Note that all graphical procedures for determining the parameters of forced oscillation and of the oscillation index, based on the representations in the forms of the Teodorchik and Goldfarb methods, can be easily transferred into the Bode and Nichols planes. We shall not dwell especially on that question here, since the reader will see how it looks in the many worked examples below.

Thus, we have given a brief review of some methods of investigation of forced oscillation and performance of nonlinear SISO systems, based on the describing function method. The present chapter is devoted to the extension of most of these methods to the case of general nonlinear MIMO systems, as well as uniform, circulant and anticirculant systems. Like the methods of the preceding chapter, the distinctive feature of the discussed further methods is that they look like a direct generalization to the multivariable case of the above methods of classical control and, for  $N = 1$ , coincide with them (Gasparyan 1986).

## 4.2 NONLINEAR GENERAL MIMO SYSTEMS

### 4.2.1 One-frequency forced oscillation and capturing in general MIMO systems

Let, in the nonlinear MIMO system of Figure 3.6, after applying the input sinusoidal signal  $\varphi(t)$  with components

$$\varphi_i(t) = B_i \sin(\Omega t + \psi_i), \quad i = 1, 2, \dots, N, \quad (4.18)$$

we have the forced oscillation with the same frequency  $\Omega$ . Then, assuming that the generalized low pass filter property of the linear part [Equation (3.27)] holds and performing the harmonic linearization of the nonlinearities, we obtain the following approximate equation of the MIMO system dynamics:

$$x = \Phi_x(j\Omega, A)\varphi, \quad (4.19)$$

where

$$\Phi_x(j\Omega, A) = [I + W(j\Omega)G(\Omega, A)]^{-1} \quad (4.20)$$

is the frequency transfer matrix of the harmonically linearized system with respect to  $x(t)$ , and  $\varphi$  and  $x$  are the complex amplitudes vectors of the input in Equation (4.18) and the fundamental harmonics<sup>1</sup> of the variables  $x_i(t)$ , respectively, with components  $\varphi_i = B_i \exp\{j\psi_i\}$  and  $x_i = A_i \exp\{j\gamma_i\}$ . The unknowns in the problem are the amplitudes  $A_i$  and the phase shifts  $\gamma_i$ , and the frequency  $\Omega$  is given by the input signal in Equation (4.18). If we make use of the canonical representations in Equations (3.32) and (3.33), Equation (4.19) can be rewritten in two equivalent forms:

$$x = C(j\Omega, A) \text{diag} \left\{ \frac{1}{1 + q_i(j\Omega, A)} \right\} C^{-1}(j\Omega, A)\varphi \quad (4.21)$$

and

$$x = \sum_{i=1}^N c_i(j\Omega, A) \left[ \frac{\langle c_i^+(j\Omega, A), \varphi \rangle}{1 + q_i(j\Omega, A)} \right], \quad (4.22)$$

<sup>1</sup> So as not to encumber the discussion, we shall not introduce new designations for the complex amplitudes vectors of the fundamental harmonics of  $\varphi(t)$  and  $x(t)$ .

from which it immediately ensues that in the case of synchronization in the nonlinear MIMO system at some frequency  $\Omega$ , synchronization at that frequency in all  $N$  characteristic systems occurs. The dyadic form of the representation in Equation (4.22) gives a simple geometrical picture of one-frequency forced oscillation in the nonlinear MIMO system. As can be seen from Equation (4.22), the complex amplitudes vector  $x$  is represented as a linear combination of the nonlinear MIMO system ‘responses’ along the canonical basis axes. Taking up successively scalar products of both sides of Equation (4.22) with  $c_i^+(j\Omega, A)$  and allowing for properties of the dual basis yield the set of complex equations

$$\langle c_i^+(j\Omega, A), x \rangle = \frac{1}{1 + q_i(j\Omega, A)} \langle c_i^+(j\Omega, A), \varphi \rangle, \quad i = 1, 2, \dots, N. \quad (4.23)$$

From here, we conclude that the projection of  $x$  on the  $i$ th canonical basis axis of the MIMO system in steady-state forced oscillation is equal to the corresponding projection of the input vector  $\varphi$  onto the same axis multiplied by the complex closed-loop transfer function of the  $i$ th characteristic system. In other words, the projection of the input complex amplitudes vector onto the  $i$ th canonical basis axis experiences ‘stretching’ or ‘shrinking’, determined by the  $i$ th characteristic system.

By their form, Equations (4.21) and (4.22) are quite analogous to the equations of a linear MIMO system driven by one-frequency sinusoidal input signals. However, owing to the nonlinear properties of the harmonically linearized MIMO system, its canonical basis and the set of CTFs depend here on the unknown amplitudes vector  $A$ , or, ultimately, on the input vector  $\varphi$ . Note also that only the amplitudes vector  $A$  is actually unknown here, since, having that vector, the phase shifts  $\gamma_i$  can readily be evaluated via the following formulae, ensuing from Equation (4.22):

$$\gamma_i = \arg \left\{ \sum_{k=1}^N c_{ik}(j\Omega, A) \left[ \frac{\langle c_k^+(j\Omega, A), \varphi \rangle}{1 + q_k(j\Omega, A)} \right] \right\}, \quad i = 1, 2, \dots, N, \quad (4.24)$$

where  $c_{ik}(j\Omega, A)$  denote the  $k$ th components of  $c_i(j\Omega, A)$ .

Passing to magnitudes in Equation (4.23), we obtain the required set of  $N$  nonlinear algebraic equations with respect to the amplitudes vector  $A$ :

$$\left| \langle c_i^+(j\Omega, A), x \rangle \right| - \frac{|\langle c_i^+(j\Omega, A), \varphi \rangle|}{|1 + q_i(j\Omega, A)|} = 0, \quad i = 1, 2, \dots, N. \quad (4.25)$$

This set can be solved by the well known numerical methods, and a simple and visual geometrical interpretation can be imparted to the solution. To this end, let us rewrite Equation (4.25) in the form

$$|1 + q_i(j\Omega, A)| = \frac{|\langle c_i^+(j\Omega, A), \varphi \rangle|}{|\langle c_i^+(j\Omega, A), x \rangle|}, \quad i = 1, 2, \dots, N. \quad (4.26)$$

Suppose that there is some amplitudes vector  $A$ . Substituting it into the transfer matrix of the open-loop system  $Q(j\omega, A)$ , one can plot the set of  $N$  characteristic gain loci  $q_i(j\omega, A)$  as the frequency  $\omega$  changes from zero to infinity. Marking the points  $\omega = \Omega$  corresponding to the

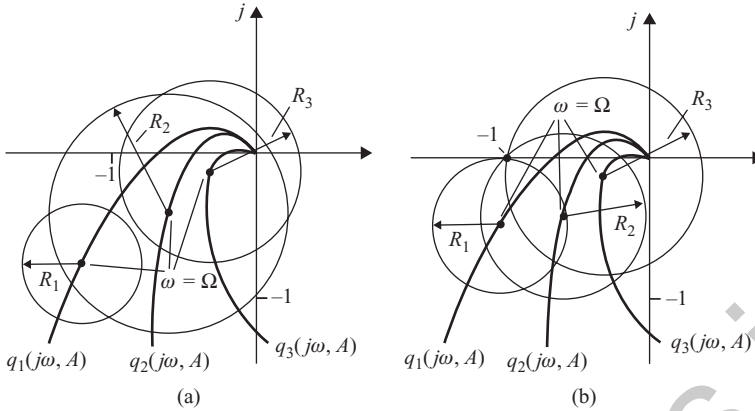


**Figure 4.8** Geometrical interpretation of the forced synchronization phenomenon in the nonlinear MIMO system ( $N = 3$ ). (a) No synchronization; (b) there is synchronization.

input frequency at each of the loci  $q_i(j\omega, A)$  and taking these points as the centres, we can draw the circles of radii

$$R_i = \frac{|\langle c_i^+(j\Omega, A), \varphi \rangle|}{|\langle c_i^+(j\Omega, A), x \rangle|} \quad (4.27)$$

equal for each  $i$  to the quotient of the magnitudes of the projections of  $\varphi$  and  $x$  onto the  $i$ th canonical basis axis. Then, taking into account Equation (4.26), we have that  $A$  is the solution to the problem only if all these circles pass through the point  $(-1, j0)$ . This is illustrated in Figure 4.8 for  $N = 3$ . In fact, the picture in Figure 4.8 represents a superposition of  $N$  pictures, giving a geometrical interpretation of the forced synchronization phenomenon in SISO characteristic systems. Thus, the geometrical structure of the solution to the problem of investigating one-frequency forced oscillation in the nonlinear MIMO system is closely connected to the internal characteristics of the harmonically linearized system and, in particular, to the canonical basis and the set of characteristic systems. It is important to note that from the geometrical viewpoint, here, there is a principle difference from the problem of investigating the limit cycle, since only one characteristic system is excited in the limit cycling MIMO system, and the vector  $x$  is always directed along the corresponding canonical basis axis (the necessary collinearity condition). As for the discussed problem, all characteristic systems are generally excited (captured) in the case of an arbitrary vector  $\varphi$ , and the vector  $x$  is expressed as a weighted sum of the MIMO system ‘responses’ along  $N$  canonical basis axes.<sup>2</sup>

If, when solving Equation (4.25), it turns out that there is no satisfying vector  $A$ , then this means that under the given input signal, no synchronization occurs in the nonlinear MIMO system and its motion bears a more complicated character. Usually, such situations are encountered in limit cycling MIMO systems. For such systems, one can find, using Equation

<sup>2</sup> The situations are possible when the vector  $\varphi$  excites not all, but some of the SISO characteristic systems. For example, if  $\varphi$  belongs to some  $k$ -dimensional ( $k < N$ ) subspace in  $\mathbb{C}^N$ , only  $k$  characteristic systems will participate in the MIMO system response and in the geometrical interpretation of the synchronization phenomenon. In particular, in Sections 4.2.2 and 4.2.3, the conditions are discussed under which in the nonlinear MIMO system responds only one characteristic system.

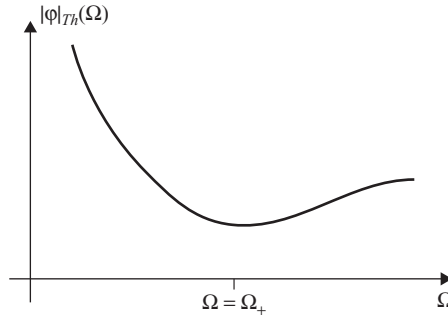


**Figure 4.9** Typical frequency dependence of the threshold value  $|\varphi|_{Th}$  for the limit cycling MIMO system.

(4.25), the threshold value  $|\varphi|_{Th}$  of the magnitude of the input vector  $\varphi$  directed along the given unit vector  $\ell$  ( $\varphi = |\varphi|\ell$ ) in  $\mathbb{C}^N$  for which the synchronization takes place. That threshold value  $|\varphi|_{Th}$  is equal to the minimal value of  $|\varphi|$  for which Equation (4.25) is solvable. Changing the input frequency  $\Omega$ , one can find the frequency dependence of the threshold value  $|\varphi|_{Th}$  of the magnitude of  $\varphi$  directed along  $\ell$ . A typical threshold curve  $|\varphi|_{Th}(\Omega)$  for the case of an arbitrary direction  $\ell$  in  $\mathbb{C}^N$  is shown in Figure 4.9. Above that curve are the values of  $|\varphi|$  bringing about synchronization in the limit cycling MIMO system and, for the values of  $|\varphi|$  lying below the  $|\varphi|_{Th}(\Omega)$  curve, the forced response has a complicated character. At the limit cycle frequency  $\Omega = \Omega_+$ , the threshold curve usually has a minimum or is equal to zero. A possible character of threshold dependence is discussed in more detail in Section 4.4, but we emphasize here that *different* threshold dependencies  $|\varphi|_{Th}(\Omega)$  correspond to *different* directions  $\ell$ .

**Remark 4.1** In practice, one frequently needs only to evaluate the complex amplitudes vector  $x$  of the steady-state forced response, without going deeper into the geometrical structure of the solution. In such a case, without resorting to a rather laborious (for large  $N$ ) procedure for determining the CTFs  $q_i(j\Omega, A)$ , as well as the modal matrix  $C(j\Omega, A)$ , one can evaluate the following system of  $N$  equations in the unknown vector  $A$ :

$$A_i = \left| \sum_{r=1}^N \Phi_{xir}(j\Omega, A) B_r \exp\{j\psi_r\} \right|, \quad i = 1, 2, \dots, N, \quad (4.28)$$

where  $\Phi_{xir}(j\Omega, A)$  are the elements of the transfer matrix  $\Phi_x(j\Omega, A)$  [Equation (4.20)]. That system ensues from vector Equation (4.19) on rewriting the latter in the form of  $N$  scalar equations and passing to the magnitudes. Having solved Equation (4.28), one can readily evaluate the phase shifts of oscillations by the formulae

$$\gamma_i = \arg \left\{ \sum_{r=1}^N \Phi_{xir}(j\Omega, A) B_r \exp\{j\psi_r\} \right\}, \quad i = 1, 2, \dots, N. \quad (4.29)$$

**Example 4.1** Consider the nonlinear two-axis guidance system of Example 3.1, reducing the gains of the transfer functions [Equation (3.44)] by a factor of 5. The characteristic gain

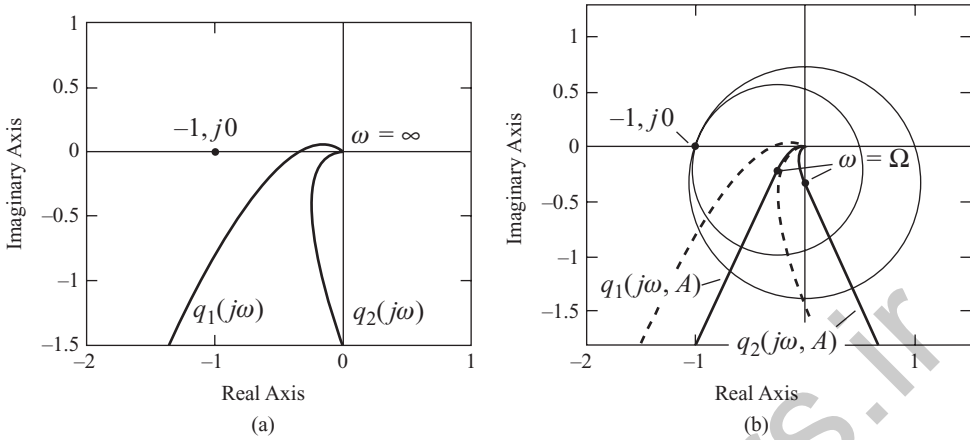


**Figure 4.10** Analysis of forced oscillation in the stable nonlinear system. (a) Characteristic gain loci of the linear part; (b) characteristic gain loci of the harmonically linearized system.

loci of the system linear part are shown in Figure 4.10(a), from which it is evident that the corresponding linear system is stable. As shown below, in Example 4.4, the system preserves stability and with the saturation nonlinearities, i.e. there is no limit cycle in the nonlinear system. Apply now, to the system inputs, oscillations with  $\Omega = 3.5$ , whose complex amplitudes vector has the components  $\varphi_1 = 15$  and  $\varphi_2 = 20 \exp\{-30^\circ\}$ , i.e. the oscillations are of the form

$$\varphi_1(t) = 15 \sin 3.5t, \quad \varphi_2(t) = 20 \sin(3.5t - 30^\circ). \quad (4.30)$$

Evaluation of the forced oscillation parameters in the system gives the following results for the vector  $x$ :  $x_1 = 19.7142 \exp\{j24.255^\circ\}$  and  $x_2 = 23.006 \exp\{-j18.045^\circ\}$ . The characteristic gain loci of the open-loop nonlinear system harmonically linearized in the vicinity of the evaluated forced oscillation are shown in Figure 4.10(b), in which the circles of the radii in Equation (4.27) and centres at the points with frequency  $\omega = \Omega$  are also depicted. For comparison, the dashed lines in Figure 4.10(b) represent the characteristic gain loci of the linear part. Both plotted circles pass through the point  $(-1, j0)$ , i.e. the geometrical conditions for the existence of one-frequency forced oscillation hold. The results of modelling the nonlinear system with the help of Simulink<sup>®3</sup> are shown in Figure 4.11. They give the following values for the amplitudes of oscillations at the inputs to nonlinearities:  $A_1 = 19.429$  and  $A_2 = 22.38$  (the computational error for the first amplitude is about 1.47% and 2.8% for the second).

**Example 4.2** Let us turn to the initial limit cycling system of Example 3.1, i.e. to the system with the transfer functions in Equation (3.44). The investigation of that system under the one-frequency input signals in Equation (4.30) revealed that Equation (4.25) has no solution, which indicates that there is no capturing in the limit cycling system under the given inputs.

<sup>3</sup> Simulink<sup>®</sup> is a registered trademark of The MathWorks, Inc. Dynamical modelling of nonlinear systems in all worked examples of this chapter was performed with the help of Simulink software.

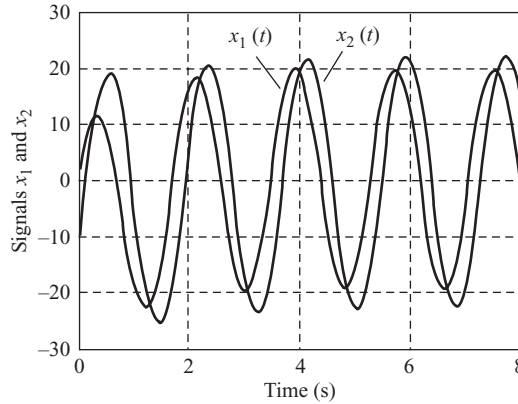


**Figure 4.11** Modelling forced oscillation in the system.

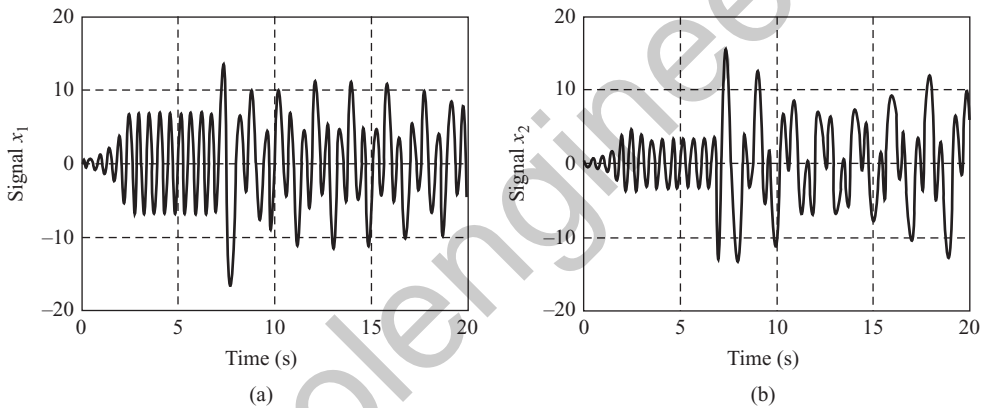


**Figure 4.12** Modelling of the limit cycling system under the input signals in Equation (4.30). (a) First channel; (b) second channel.

This is confirmed by the results of modelling shown in Figure 4.12. The graphs in Figure 4.12 represent the dynamical processes in the system which, first, was in the limit cycling mode and, from time  $t = 7$  sec., the given signals [Equation (4.30)] were applied to the inputs. As can be seen from Figure 4.12, the forced motion in the system indeed bears a complicated character. The frequency dependence of the threshold value of the magnitude  $|\varphi|$  in the direction defined by oscillations [Equation (4.40)] (the components of the unit vector  $\ell$  here are  $\ell_1 = 0.6$  and  $\ell_2 = 0.8 \exp\{-j30^\circ\}$ ) is shown in Figure 4.13. At the limit cycle frequency  $\Omega_+ = 11.7116$ , the threshold value  $|\varphi|_{Th}$  is equal to zero, since the system itself is oscillating with that frequency without applying any inputs, and we do not impose any conditions on the direction of the vector  $x$ . In the following, we shall discuss the problems that are more complicated and where provision of the given direction of  $x$  is also required. In such cases, the threshold value of  $|\varphi|$  at the frequency of the limit cycle can be greater than zero. Let us now increase the magnitude of the vector of the input sinusoidal signals [Equation (4.30)] by a factor of 6, preserving the

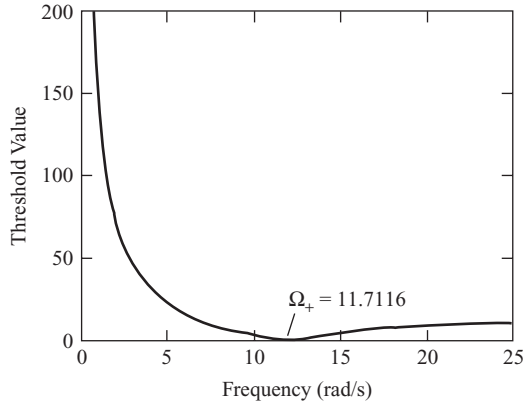


**Figure 4.13** The frequency dependence  $|\varphi|_{Th}(\Omega)$  for the limit cycling system.

direction of the complex amplitudes vector  $\varphi$ , i.e. assuming

$$\varphi_1(t) = 90 \sin 3.5t, \quad \varphi_2(t) = 120 \sin(3.5t - 30^\circ). \quad (4.31)$$

The corresponding value  $|\varphi| = 150$ , here, exceeds the threshold value  $|\varphi|_{Th} = 40.842$  at the frequency  $\Omega = 3.5$  by more than three times. The results of the numerical evaluation show that forced synchronization in the system really occurs under the input signals [Equation (4.31)], i.e. the limit cycle in the two-axis system is entirely suppressed and the system goes to the mode of forced oscillation at the input frequency  $\Omega = 3.5$ . The graphical solution to the task is shown in Figure 4.14, and the components of the vector  $x$  are  $x_1 = 114.496 \exp\{j20.466^\circ\}$  and  $x_2 = 135.124 \exp\{-j20.086^\circ\}$ .

The numerical computation is verified by the dynamical modelling of the system. As can be seen from Figure 4.15, on applying the sinusoidal signals [Equation (4.31)] to the inputs of the limit cycling system (also at  $t = 7$  sec.), the system goes to the mode of forced oscillation at the external frequency  $\Omega = 3.5$ , where the amplitudes of the steady-state oscillations in Figure 4.15 are  $A_1 = 113.8896$  and  $A_2 = 131.7875$  (the computational errors for the amplitudes are 0.53 and 2.53%, respectively).

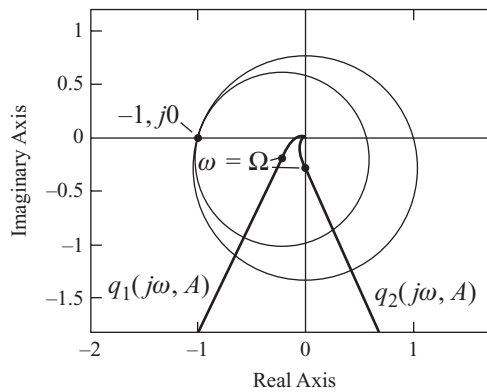


**Figure 4.14** Synchronization in the limit cycling system.

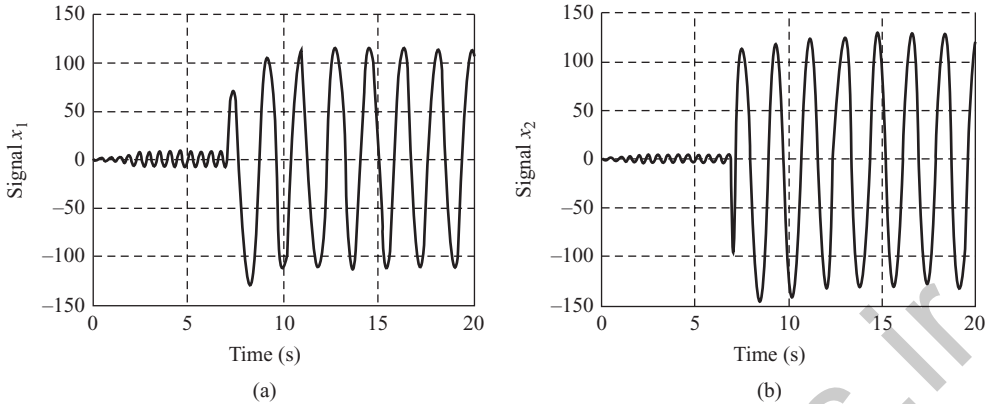


**Figure 4.15** Modelling of the limit cycling system under the input signals in Equation (4.31). (a) First channel; (b) second channel.

### 4.2.2 Generalized frequency response characteristics and oscillation index of stable nonlinear MIMO systems

In this section, the notions of the generalized frequency response characteristics (FRC) and of the oscillation index for linear MIMO systems introduced in Chapter 2 are extended to the nonlinear case (Gasparyan 1986). The methods discussed below apply to the performance analysis of *stable* nonlinear systems with strongly expressed oscillatory transient processes converging to an equilibrium state. The nonlinear properties of the harmonically linearized MIMO systems bring certain difficulties in constructing generalized frequency characteristics in different directions of space  $\mathbb{C}^N$  of the input harmonic signals. Recall that in linear MIMO systems, to each direction of the complex amplitudes vector  $\varphi^4$  corresponds *one*, strictly determined direction of the output or error vectors of the system and, for any direction in  $\mathbb{C}^N$ , there is a *single* generalized FRC. In the case of nonlinear MIMO systems, the notion of generalized FRCs is not so simple. The point is that the closed-loop transfer matrix  $\Phi_x(j\Omega, A)$  with respect to the vector  $x^5$  of the harmonically linearized MIMO system depends nonlinearly on the amplitudes vector  $A$  of oscillations at the inputs to nonlinearities. Therefore, for any fixed direction  $\ell$  ( $|\ell| = 1$ ) in  $\mathbb{C}^N$ , one can determine, using the techniques of the previous section, an infinite set of generalized FRCs, depending on the *magnitude* of the input vector  $\varphi$ . In other words, owing to the nonlinear properties of the MIMO system, the generalized FRCs in the given direction depend also on the ‘length’ of the input vector  $\varphi$ . Now, it is evident that for nonlinear MIMO systems, the definition of the majorant of the generalized FRCs as a real function equal at each  $\Omega$  to the *least upper bound* of the magnitude of  $x$  on the unit sphere  $U_\varphi = \{\varphi : |\varphi| = 1\}$  in  $\mathbb{C}^N$  is unacceptable, since to each sphere of an arbitrary radius  $r$  in  $\mathbb{C}^N$  corresponds its own value of the ratio of the magnitudes of  $x$  and  $\varphi$  (where  $|\varphi| = r$ ). Hence, to define the majorant of generalized FRCs, one should consider the spheres of every possible radius, which leads to the following

<sup>4</sup> In Chapter 2, the complex amplitudes vector of the input harmonic signals was denoted by  $\varphi_0$ .

<sup>5</sup> For brevity, we shall concentrate mainly on the case of determining the generalized FRCs with respect to  $x$ .

definition:

The majorant of the generalized FRCs is called a real-valued function  $A_{sup}(\Omega)$ , equal at each frequency  $\Omega$  of the input harmonic signals to the least upper bound of the ratio of the magnitudes of the vectors  $x$  and  $\varphi$  over the whole space  $\mathbb{C}^N$ .

Mathematically, this can be written as

$$A_{sup}(\Omega) = \sup_{|\varphi| \neq 0} \frac{|x|}{|\varphi|} = \sup_{|\varphi| \neq 0} \frac{|A|}{|\varphi|} = \sup_{|\varphi| \neq 0} \frac{|\Phi_x(j\Omega, A)\varphi|}{|\varphi|}. \quad (4.32)$$

It is easy to see that in the linear case, when the operator  $\Phi_x(\cdot)$  does not depend on  $A$ , the right-hand side in Equation (4.32) is equal to the norm  $\|\Phi_x(\cdot)\|$  induced by the Euclidian norm (magnitude) of  $\varphi$ . In the case of a nonlinear MIMO system, the situation is much more complicated, since, to evaluate the function  $A_{sup}(\Omega)$  using Equation (4.32), it is necessary to solve the set of nonlinear equations [Equation (4.19)] of the closed-loop MIMO system for all possible complex vectors  $\varphi$ , which is practically an unrealizable and senseless task, even in the case of SISO systems. However, the value of  $A_{sup}(\Omega)$  for  $\Omega = const$ , or at least its upper estimate, can be determined without solving nonlinear Equation (4.19), (4.25) or (4.28). The approach to this problem is suggested largely by an analogous idea exploited in the practice of SISO systems (see Section 4.1). Let us take some amplitudes vector  $A$ . Then, the describing functions of nonlinearities become known numbers and the expression on the right-hand side of Equation (4.32) is equal, by definition, to the norm of the operator  $\Phi_x(j\Omega, A)$ . Evidently, for any specific  $A$ , the norm  $\|\Phi_x(j\Omega, A)\|$  takes quite a definite value. Assume now that the operator  $\Phi_x(j\Omega, A)$  is defined over the whole space  $\mathbb{C}^N$ . Then, taking into account the single-valued correspondence between  $x$  and  $A$ , one can argue that at any  $\Omega$ , the value of  $A_{sup}(\Omega)$  cannot exceed the upper boundary of the norm  $\|\Phi_x(j\Omega, A)\|$  defined on the first (positive) quadrant of the real  $N$ -dimensional space  $E^N$ , i.e.

$$A_{sup}(\Omega) \leq \sup_{A_i > 0} \|\Phi_x(j\Omega, A)\|. \quad (4.33)$$

Thus, to evaluate the upper estimate for the majorant of the generalized FRCs of the nonlinear MIMO system, there is no need to find the solutions of nonlinear Equation (4.19) for all vectors  $\varphi$ . Instead, it is sufficient to determine the norm of the transfer matrix  $\Phi_x(j\Omega, A)$  and to maximize it with respect to the vector  $A$ , which is a much simpler task. Hence, changing the frequency  $\Omega$  and repeating each time the procedure of maximization of  $\|\Phi_x(j\Omega, A)\|$  with respect to  $A$ , we will obtain a curve bounding from above all generalized FRCs of the nonlinear MIMO system for different directions  $\ell$  in  $\mathbb{C}^N$  and different magnitudes  $|\varphi|$  (Figure 4.16). Keeping in mind the above remarks, we shall, for simplicity, call that curve the majorant of the generalized FRCs. Let us now introduce the following definition:

The oscillation index  $M$  of the nonlinear MIMO system is called the resonant peak value of the majorant of the generalized FRCs, i.e.

$$M = \sup_{0 \leq \Omega \leq \infty} A_{sup}(\Omega). \quad (4.34)$$

We shall see further that the value  $M$  [Equation (4.34)] can indeed serve as a measure of the stability margin for the nonlinear MIMO system, since, as the system approaches the stability boundary (usually, it is the ‘limit cycling’ stability boundary),  $M$  tends to infinity. It is not out

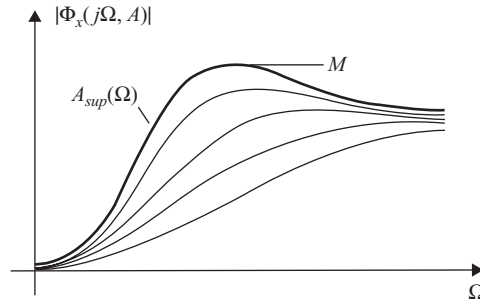


**Figure 4.16** Majorant of the generalized FRCs of the nonlinear MIMO system.

of place to note that the oscillation index  $M$ , resulting from the way in which it is evaluated, is also a measure of the accuracy of the nonlinear MIMO system under harmonic input signals. Evidently, on excluding the nonlinear elements from the MIMO system of Figure 3.6, the value  $M$  [Equation (4.34)] becomes equal to the oscillation index of the linear MIMO system of Figure 1.1. Also, for  $N = 1$ , the above definition in fact coincides with the definition of the oscillation index attributed to Fedorov *et al.* (1972).

**Remark 4.2** In principle, acting as in the linear case (see Section 2.2.1), one could introduce the notion of the *minorant*  $A_{\text{inf}}(\Omega)$  as a real-valued function bounding from below all generalized FRCs of the nonlinear MIMO system for different directions  $\ell$  in  $\mathbb{C}^N$  and magnitudes  $|\varphi|$ . However, unlike the case of linear MIMO systems, in which the minorant  $A_{\text{inf}}(\omega)$  [Equation (2.5)] is a quite definite function characterizing the lower boundary of the error norm under harmonic external signals, the situation for nonlinear MIMO systems is somewhat different. The point is that the describing functions of many nonlinearities tend to zero on an unbounded increase in the input amplitude. Among such nonlinearities are, for example, the saturation, saturation with dead zone, relays, etc. (Atherton 1975). For MIMO systems with the indicated types of nonlinearities, the minorant of the generalized FRCs with respect to the output vector, which is obtained by *minimizing*  $\|\Phi(j\Omega, A)\|$  with respect to  $A$  over the whole first quadrant of space  $E^N$ , in many cases, is zero at all frequencies, i.e. just coincides with the abscissa axis. Similarly, the minorant of the generalized FRCs with respect to the vector  $x$  is constant and equal to unity. That fact substantially decreases, if not excludes entirely, the practical value of the notion of the minorant of the generalized FRCs for nonlinear MIMO systems.

Let us proceed now to the discussion of a special, but very important for the analysis and design of nonlinear MIMO systems, set of the FRCs along  $N$  canonical basis axes. These characteristics radically differ, by their internal connection with the geometrical structure of the harmonically linearized MIMO system, from the generalized FRCs for different but *fixed* directions in  $\mathbb{C}^N$  discussed above. First of all, that distinction is that under an arbitrary direction of the vector  $\varphi$ , all  $N$  characteristic systems take part in the MIMO system response. However, if we manage to find a vector  $\varphi$  directed along any one of the canonical basis axes, then only one characteristic system reacts, and the MIMO system response will be directed in space  $\mathbb{C}^N$  along that very axis. Another distinction is that for the excitation of the same characteristic system by the vectors  $\varphi$  of various magnitudes, those vectors should generally have different directions in  $\mathbb{C}^N$ , whereas the generalized FRCs are defined above for a *single*, fixed direction.

Determine the conditions under which only one, say the  $i$ th, characteristic system participates in the nonlinear MIMO system response. Since the input vector  $\varphi$  here must be directed along the  $i$ th canonical basis axis, it can be represented in the form

$$\varphi = |\varphi|c_i(j\Omega, A). \tag{4.35}$$

Then, making use of dyadic notation [Equation (4.22)] and taking into account the properties of the dual basis, we obtain

$$x = \frac{1}{1 + q_i(j\Omega, A)} |\varphi| c_i(j\Omega, A) \tag{4.36}$$

As follows from Equation (4.36), in the forced oscillation with the excitation of the  $i$ th characteristic system, the vector  $x$  must be directed along the same axis as the input vector  $\varphi$ , and its magnitude is equal to

$$|x| = |A| = \frac{|\varphi|}{|1 + q_i(j\Omega, A)|}. \tag{4.37}$$

The arguments of the components of  $c_i(j\Omega, A)$  (assuming the argument of the first component to be zero) determine here the relative phase shifts of oscillations of the variables  $x_k$  and  $\varphi_k$  in the different channels with respect to the first channel. Further, the oscillation of each  $x_k$  is shifted with respect to the input oscillation  $\varphi_k$  in that very channel by the same quantity:

$$\Delta\gamma = \arg \left\{ \frac{1}{1 + q_i(j\Omega, A)} \right\}. \tag{4.38}$$

Also, from the condition for collinearity of  $x$  and  $c_i(j\Omega, A)$  pointed out, the condition for collinearity of the amplitudes vector  $A$  and the real-valued vector  $m_i(\Omega, A)$  already well known from the limit cycle analysis ensues, where  $m_i(\Omega, A)$  is composed of the magnitudes of components of  $c_i(j\Omega, A)$ , i.e.

$$A = |A| m_i(\Omega, A). \tag{4.39}$$

Thus, in order that only the  $i$ th characteristic system be excited at the fixed frequency  $\Omega$ , it is necessary that the conditions in Equations (4.35), (4.37) and (4.39) hold. The procedure for the numerical evaluation of the problem consists in the following. First, as in the limit cycle analysis, a parametric set of the vectors  $A$  must be found, satisfying (for  $\Omega = const$ , and as the magnitude  $|A|$  changes) the collinearity condition in Equation (4.39). Simultaneously, for each  $|A|$  for which the solution to Equation (4.39) exists, the eigenvalue  $q_i(j\Omega, A)$  of the transfer matrix  $Q(j\Omega, A)$  [Equation (3.30)] must be evaluated and plotted in the complex plane, i.e. the locus  $q_i(j\Omega, A)$  is plotted for all  $A$  from Equation (4.39) [Figure 4.17(a)]. Further, taking each point of that locus as a centre, a circle of radius

$$R = \frac{|\varphi|}{|A|} \tag{4.40}$$

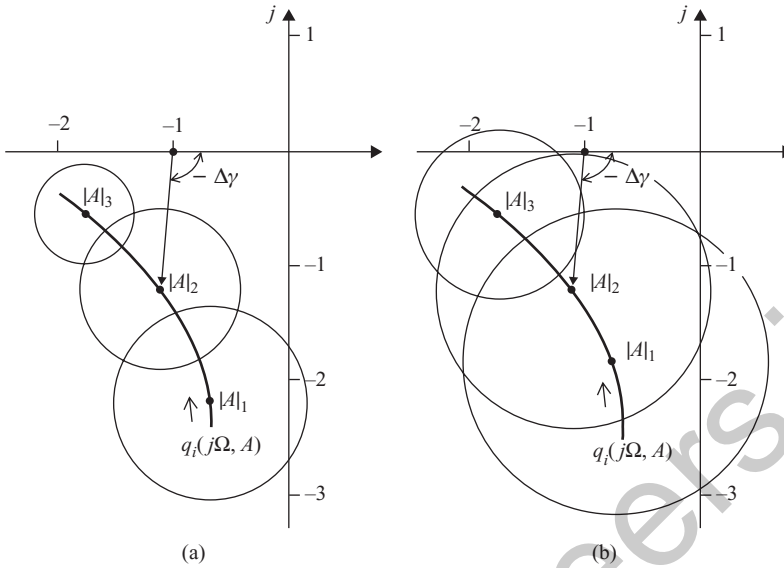


**Figure 4.17** Evaluation of the FRCs along the canonical basis axes of the nonlinear MIMO system.

is drawn, where  $|A|$  is the parameter at  $q_i(j\Omega, A)$  for the taken point. Then, according to the condition in Equation (4.37), which can be rewritten in the form

$$|1 + q_i(j\Omega, A)| = \frac{|\varphi|}{|A|} \quad (4.41)$$

the solution to the problem is that value of  $|A|$  for which the corresponding circle passes through the point  $(-1, j0)$  [Figure 4.17(b)]. The obtained value  $|A|$  determines uniquely the vector  $A$ , the phase shift  $\Delta\gamma$  [Equation (4.38)], as well as the vectors  $\varphi$  and  $c_i(j\Omega, A)$  [Equation (4.35)], and the quotient  $|A|/|\varphi|$  yields one point at the FRC along the  $i$ th canonical basis axis. Carrying out the described computations for different  $\Omega = const$ , we shall find the entire FRC of the nonlinear MIMO system along the  $i$ th canonical basis axis for the given  $|\varphi| = const$ . Changing the magnitude  $|\varphi|$ , we can determine a set of the FRCs along  $c_i(j\Omega, A)$ . Recall that only one FRC corresponds to each canonical basis axis in the linear case and, altogether, there are  $N$  such characteristics. As for a nonlinear MIMO system, here, an infinite set of FRCs corresponds to each canonical basis axis, depending on the magnitude  $|\varphi|$ . Note that if the FRC for some specific  $|\varphi| = const$  is constructed, then the evaluation of the FRC for other values of  $|\varphi|$  does not present any difficulties, since the loci  $q_i(j\Omega, A)$  do not depend on the value of  $|\varphi|$ , and an increase or decrease in the latter results only in a proportional increase or decrease in the circles' radii  $R$  [Equation (4.40)].

There is also another graphical technique for evaluating the vector  $A$  by Equations (4.35), (4.37) and (4.39), which can be viewed as an extension of the well known method by E. Popov (1973). Write, based on Equations (4.36)–(4.38), the expression

$$|A| \exp\{j\Delta\gamma\} = \frac{1}{1 + q_i(j\Omega, A)} |\varphi| \quad (4.42)$$

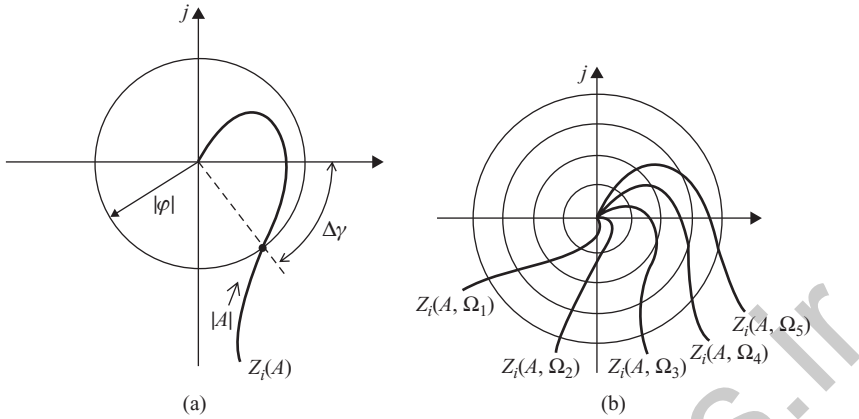


**Figure 4.18** Construction of the FRCs along the canonical basis axes by E.P. Popov's method.

and represent it in the form

$$Z_i(A) = |\varphi| \exp\{-j \Delta\gamma\}, \tag{4.43}$$

where

$$Z_i(A) = |A| [1 + q_i(j\Omega, A)] \tag{4.44}$$

For all vectors  $A$  satisfying the collinearity condition in Equation (4.39) for  $\Omega = const$ , draw the locus  $Z_i(A)$  with the parameter  $|A|$  in the complex plane and the circle of radius  $|\varphi|$  with its centre at the origin [Figure 4.18(a)]. The intersection of the locus  $Z_i(A)$  with that circle provides the solution to the problem of investigating the forced oscillation along the  $i$ th canonical basis axis for the given  $\Omega$  and  $|\varphi|$ . Having drawn the family of the loci  $Z_i(A)$  for different  $\Omega$  and the series of concentric circles of different radii  $|\varphi|$  [Figure 4.18(b)], one can find, quite analogously to the SISO case, the family of FRCs along  $c_i(j\Omega, A)$ . Concluding the presentation of questions concerning the evaluation of FRCs along the canonical basis axes of the harmonically linearized MIMO system, we emphasize the evident fact that all these FRCs are bounded from above by the majorant of the generalized FRCs  $A_{sup}(\Omega)$  [Equation (4.32)].

The discussed FRCs along the canonical basis axes are interesting and important, not so much by themselves, but because of their close connection with the stability margins of nonlinear MIMO systems. In nonlinear MIMO systems, as in SISO systems, beyond the area of stability of the equilibrium point, in many cases, there is the area of limit cycles and we know that only one characteristic system is excited in the limit cycle, and the vector of the complex amplitudes  $x$  is directed along the corresponding canonical basis axis. Roughly speaking, this means that the nonlinear MIMO system can 'pass' from the stability area to the area of limit cycle only along one of the canonical basis axes. Consequently, the farther the characteristic systems are from the boundary of the limit cycle area, the larger the stability margins and the better the transient responses that the nonlinear MIMO system will have.

The oscillation index  $M_i$ , defined as the maximum relative value of the resonant peak of the FRC along the  $i$ th canonical basis axis for all vectors  $\varphi$  under which only the given characteristic system is excited, can serve as a frequency-domain measure of the stability margin of that  $i$ th

characteristic system. Mathematically, this can be written in the following form:

$$M_i = \sup_{0 \leq \Omega \leq \infty} \frac{|A|}{|\varphi|} = \sup_{0 \leq \Omega \leq \infty} \frac{1}{|1 + q_i(j\Omega, A)|} \quad (4.45)$$

for all  $A$ , satisfying the collinearity condition in Equation (4.39). To determine graphically the oscillation index  $M_i$ , map Equation (4.45) in the complex plane of the characteristic gain loci  $q_i(j\Omega, A)$ . Raising the left and right parts in Equation (4.45) to the second power, after simple manipulations, yields

$$[\operatorname{Re}\{q_i(j\Omega, A)\} + 1]^2 + [\operatorname{Im}\{q_i(j\Omega, A)\}]^2 = \frac{1}{M_i^2}. \quad (4.46)$$

Geometrically, it is an equation of the circle with its centre at point  $(-1, j0)$  and radius  $R_i = 1/M_i$ , i.e. in the plane of  $\{q_i(j\Omega, A)\}$ , a family of concentric circles with centres at  $(-1, j0)$  corresponds to the constant values of  $M_i$ . From here, we conclude that the oscillation index of  $i$ th characteristic systems is reciprocal to the radius of that circle which is tangent to the envelope of the family of  $q_i(j\Omega, A)$  loci, used for the investigation of limit cycles (Figure 4.19). As the envelope of the family  $\{q_i(j\Omega, A)\}$  approaches the point  $(-1, j0)$ , the radius of the ‘tangent’ circle decreases. Correspondingly, the value of  $M_i$  increases, tending in the limit to infinity.

Since all FRCs along the canonical basis axes are bounded from above by the majorant  $A_{\text{sup}}(\Omega)$  [Equation (4.32)], then, in the case of tending of any  $M_i$  to infinity, the same happens with the oscillation index  $M$  defined as the magnitude of the resonant peak of  $A_{\text{sup}}(\Omega)$ . This verifies the above statement that the value of  $M$  [Equation (4.34)] is a measure of the stability margin of the nonlinear MIMO system. It is also clear that for  $N = 1$ , both introduced definitions of the oscillation index – by the resonant peak of the majorant  $A_{\text{sup}}(\Omega)$  [Equation (4.34)] and by the FRCs of the characteristic systems [Equation (4.45)] – just coincide.

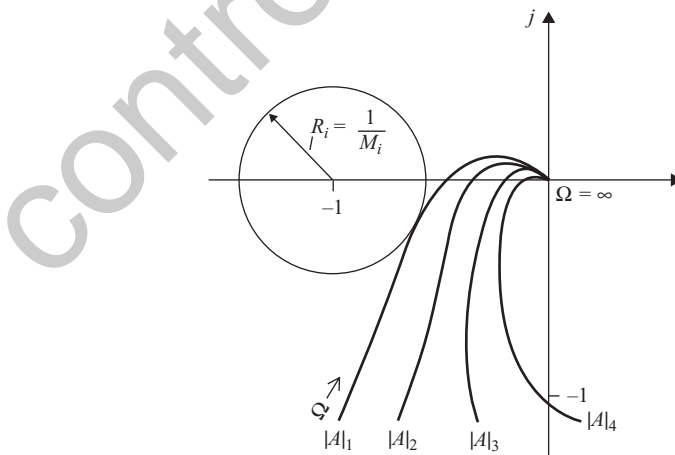


**Figure 4.19** Evaluation of the oscillation index  $M_i$  of the  $i$ th characteristic system in the complex plane of the family  $\{q_i(j\Omega, A)\}$ .

Let us make some general remarks concerning the applicability of the introduced performance indices. Perhaps the largest of the oscillation indices  $M_i$  of characteristic systems is the determinative measure of the stability margin for the nonlinear MIMO system. In turn, the value of  $M$  [Equation (4.34)] bounds from above the maximum  $M_{i \max}$  of the indices  $M_i$  and, owing to that, also plays a role of the frequency-domain test for stability margin and performance of the oscillatory transient responses. Therefore, in practical computations, one can use both  $M_{i \max}$  and  $M$  values, depending on the specific situation. In particular, if the investigation of the limit cycle has been performed and the family of the  $q_i(j\Omega, A)$  loci has been drawn for all  $i$ , then, of course, it is simpler to find the value of  $M_{i \max}$ . If it is known in advance that there is no limit cycle in the MIMO system, then maybe it would be more worthwhile to calculate the value of  $M$ , remembering that it characterizes, as in the linear case, the accuracy of the system under harmonic input signals.

**Remark 4.3** Above, we defined the oscillation index with respect to the vector  $x$  of the input variables of nonlinearities (Figure 3.6). As a matter of fact, this corresponds to the definition of the oscillation index of the linear MIMO system with respect to the *error* vector (see Section 2.2.1). Analogously to the linear case, the oscillation index of the nonlinear MIMO system can also be defined with respect to the system output, i.e. with the help of the transfer matrix

$$\Phi(j\Omega, A) = [I + W(j\Omega)G(\Omega, A)]^{-1}W(j\Omega)G(\Omega, A). \quad (4.47)$$

We shall not dwell on that question in detail, since all previous reasonings remain valid for this variant. The same concerns the definition of the oscillation indices  $M_i$  of the characteristic systems with respect to the output of the MIMO system. As in the linear case, Equation (2.23) represents a circle  $M_i = \text{const}$  in the plane of the  $q_i(j\Omega, A)$  loci constructed for the ‘collinear’ vectors  $A$ . Correspondingly, Equations (2.15) and (2.25) can be used for mapping the circles  $M_i = \text{const}$  on the Bode diagrams of the characteristic systems. Note, finally, that the introduced notions of the oscillation index defined by the resonant peak of the majorant of the generalized FRCs actually correspond to the definition of the  $\|H\|_\infty$  norm (see Remark 2.2) for the harmonically linearized MIMO system. The connection of these notions with the common robustness issues is briefly discussed in Remark 2.3.

**Example 4.3** The majorants of the generalized FRCs for the stable nonlinear system of Example 4.1 are shown in Figure 4.20. For comparison, the majorants of the corresponding linear system [these majorants are denoted by  $A_{\text{sup}}^{\text{Lin}}(\Omega)$ ] are given by the dotted lines. As can be seen from Figure 4.20, the resonant peaks of majorants of linear and nonlinear systems here coincide. Therefore, these systems have the same oscillation indices  $M$  and resonant frequencies: with respect to the vector  $x$ , the oscillation index is  $M = 2.2421$  at the frequency  $\Omega = 6.007$  and, with respect to the output vector, these values are  $M = 1.8124$  and  $\Omega = 4.9745$ .

**Example 4.4** Determine the oscillation indices of the characteristic systems  $M_i$  [Equation (4.45)] for the two-axis guidance system from the previous example. In Figure 4.21, the families of the characteristic gain loci  $q_1(j\Omega, A)$  and  $q_2(j\Omega, A)$  of the open-loop system in the Nyquist plane are depicted, plotted for different  $|A| = \text{const}$ , for the vectors  $A$  satisfying the necessary collinearity condition in Equation (4.39) (the values of  $|A|$  are indicated by the numbers). The circles with their centres at  $(-1, j0)$ , tangent to the envelopes of the families

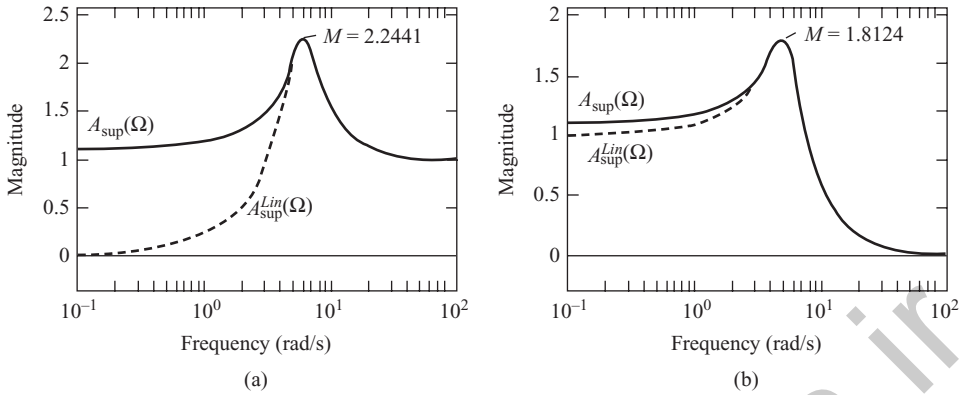


**Figure 4.20** Majorants of the generalized FRCs for the nonlinear guidance system of Example 4.1. (a) With respect to the  $x$  vector; (b) with respect to the output vector.

of the  $q_1(j\Omega, A)$  and  $q_2(j\Omega, A)$  loci, give the following values for oscillation indices of the characteristic systems:  $M_1 = 2.2081$  and  $M_2 = 1.24$ . Note that the indicated envelopes of the  $\{q_1(j\Omega, A)\}$  and  $\{q_2(j\Omega, A)\}$  families coincide with the left-most loci (for  $|A| = 4$ ) and coincide with the characteristic gain loci of the linear part shown in Figure 4.10(a). Therefore, the oscillation indices of the characteristic systems  $M_i$  for the harmonically linearized system with respect to  $x$  are equal to the oscillation indices of the linear system with respect to the error vector. Naturally, the maximum oscillation index  $M_1 = 2.2081$  of the characteristic systems is smaller than the oscillation index  $M = 2.2421$  evaluated by the resonant peak of the majorant  $A_{sup}(\Omega)$  in Figure 4.20. In conclusion, note that the highlighted property of the discussed guidance system with saturations in separate channels, in accordance with which the oscillation indices of the linear and nonlinear systems coincide, cannot be accepted as a general rule. As the reader will see later, the oscillation indices of nonlinear MIMO systems usually exceed those of linear systems.

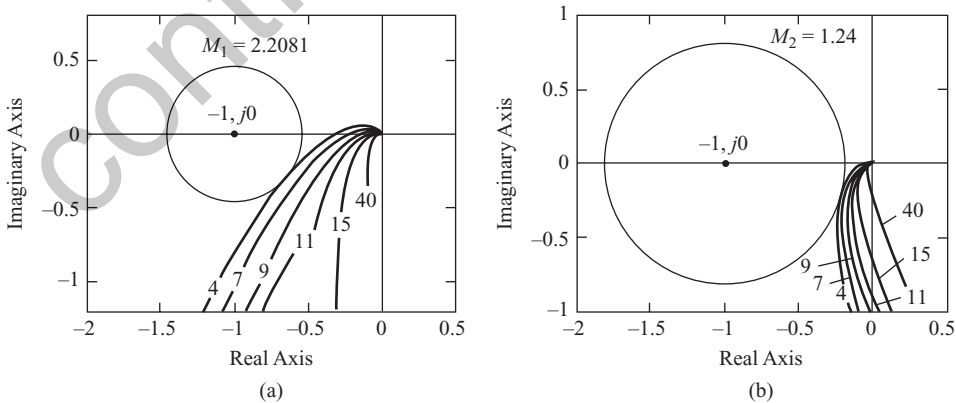


**Figure 4.21** Determining the oscillation indices of the characteristic systems with respect to the vector  $x$ . (a) First characteristic system; (b) second characteristic system.

### 4.2.3 Generalized frequency response characteristics of limit cycling MIMO systems

In the previous section, we discussed the evaluation of the generalized FRCs of *stable* nonlinear MIMO systems. In such systems, the threshold values of the magnitude of  $\varphi$  are usually equal to zero for any directions in space  $\mathbb{C}^N$ . Here, under the threshold value, we mean (see Section 4.2) that minimal value of the magnitude  $|\varphi| = |\varphi|_{Th}$  for which, in the MIMO system, a forced oscillation at the frequency of the input harmonic signals occurs.<sup>6</sup> In Section 4.2.1, we ascertained that in the case of limit cycling MIMO systems, to each direction  $\ell$  in  $\mathbb{C}^N$  corresponds its own threshold dependence  $|\varphi|_{Th}(\Omega)$ , determining those boundary values of  $|\varphi|_{Th}$  below which synchronization does not occur and oscillation in the MIMO system bears a complicated character. It was also pointed out in Section 4.2.1 that for an arbitrary direction of  $\varphi$ , all characteristic systems can take part (be captured) in the response of either stable or limit cycling MIMO systems. Below, we shall concentrate on the peculiarities of the evaluation of frequency dependence  $|\varphi|_{Th}(\Omega)$  along the canonical basis axes of *limit cycling* MIMO systems. The essential feature of such MIMO systems is the *nonequivalence* of their canonical basis axes, since, in the absence of input signals, the complex amplitudes vector of limit cycle  $x$  is always directed along an axis associated with the excited characteristic system. Therefore, the character of the  $|\varphi|_{Th}(\Omega)$  curve along the canonical basis axis ‘excited’ in the limit cycle considerably differs from the character of the corresponding curve along any other axis. Physically, this distinction is determined by the fact that if the input vector  $\varphi$  and the ‘limit cycling’ axis  $c_i(j\Omega, A)$  are collinear, and the condition for synchronization holds, then the forced oscillation in the MIMO system occurs along the same axis  $c_i(j\Omega, A)$  and, also, the same characteristic system remains excited. Evidently, the threshold dependence  $|\varphi|_{Th}(\Omega)$  in this case must have the same character as the common frequency dependence of the threshold input amplitude in the limit cycling SISO system (Figure 4.4). Thus, at an input frequency coinciding with the limit cycle frequency  $\Omega_+$ , the threshold value  $|\varphi|_{Th}$  must become zero. However, if the vector  $\varphi$  is directed along any other canonical basis axis, for the MIMO system to really go into forced oscillation along that axis, it is necessary, aside from satisfaction of the synchronization condition, that the oscillation along the ‘limit cycling’ axis  $c_i(j\Omega, A)$  be suppressed, i.e. the characteristic system excited in the limit cycle must become stable. This feature is inherent only in nonlinear MIMO systems and has no analogues in the classical control theory.

It is convenient to carry out the evaluation of  $|\varphi|_{Th}$  for fixed  $\Omega$  in limit cycling MIMO systems with the help of a technique which can be regarded as an extension to the multivariable case of E. Popov’s technique (Figure 4.18) (Gasparyan 1986), described in Section 4.2.2. In accordance with that technique, a parametrical locus  $Z_i(A)$  [Equation (4.44)] is plotted in the complex plane for  $\Omega = const$ , as the  $|A|$  parameter changes, for all vectors  $A$  satisfying the collinearity condition in Equation (4.39). Further, the stability of characteristic systems is analyzed for each point at the locus  $Z_i(A)$ . That procedure is quite similar to the procedure of stability analysis of characteristic systems not excited in the limit cycle described in Section 3.3.2. To this end, the ‘collinear’ vector  $A$  corresponding to the taken point and the input frequency  $\Omega$  are substituted in the describing functions matrix  $G(A, \Omega)$  [Equation (3.29)], which reduces

<sup>6</sup> In the *stable* MIMO systems with the dead zone nonlinearities, the threshold values of  $|\varphi|_{Th}$  are, naturally, larger than zero.

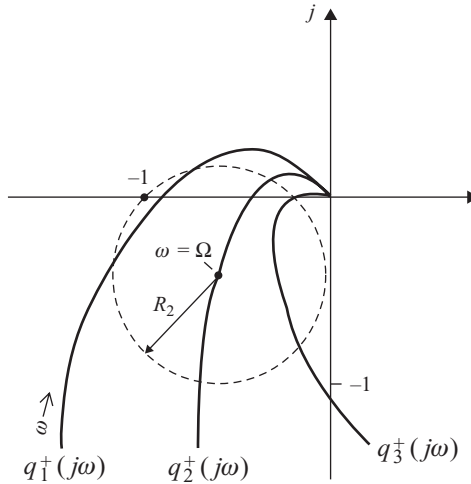


**Figure 4.22** Checking the stability of the characteristic systems in forced oscillation along the canonical basis axes of the limit cycling MIMO system ( $N = 3$ ).

to a certain constant numerical matrix  $G^+$ . After that, the characteristic gain loci  $q_k^+(j\omega)$  ( $k = 1, 2, \dots, N$ ) of the matrix

$$Q_+(j\omega) = W(j\omega)G^+ \quad (4.48)$$

are plotted as the frequency  $\omega$  changes from zero to infinity, and their location with respect to the point  $(-1, j0)$  is analyzed. The matrix  $Q_+(j\omega)$  represents the complex open-loop transfer matrix of the MIMO system, harmonically linearized in the vicinity of the investigated forced oscillation along the  $i$ th canonical basis axis. The characteristic gain loci of  $Q_+(j\omega)$  [Equation (4.59)] are qualitatively shown for  $N = 3$  in Figure 4.22 for the case in which the forced oscillation occurs along the second canonical basis axis, and the limit cycling axis is the first one. In the same plot, the circle of radius  $R_2$  [Equation (4.27)] is shown by the dotted line, with its centre at the point  $\omega = \Omega$  at the locus  $q_2^+(j\omega)$ . That circle, apparently, must pass through the point  $(-1, j0)$ . Note that the loci of Figure 4.22 differ from the analogous loci of Figure 3.9 used for the stability analysis of characteristic systems not excited in the limit cycle. As can be seen from Figure 3.9, the locus  $q_r^+(j\omega)$  of the ‘limit cycling’ characteristic system passes through the point  $(-1, j0)$  for  $\omega = \Omega_+$ , where  $\Omega_+$  is the limit cycle frequency, since the  $r$ th characteristic system is on the stability boundary. On the other hand, *all* loci  $q_k^+(j\omega)$  of the matrix  $Q_+(j\omega)$  [Equation (4.48)], including the  $r$ th one (in Figure 4.22, it is the first), must correspond to stable characteristic systems. To check the stability of the linearized system with the transfer matrix  $Q_+(j\omega)$ , one can use, of course, any other stability criteria for linear MIMO systems. In particular, one of the simplest ways in practice consists in determining the roots of the characteristic equation

$$\det[I + Q_+(s)] = 0 \quad (4.49)$$

with the help of numerous application programs (available in MATLAB, for example).

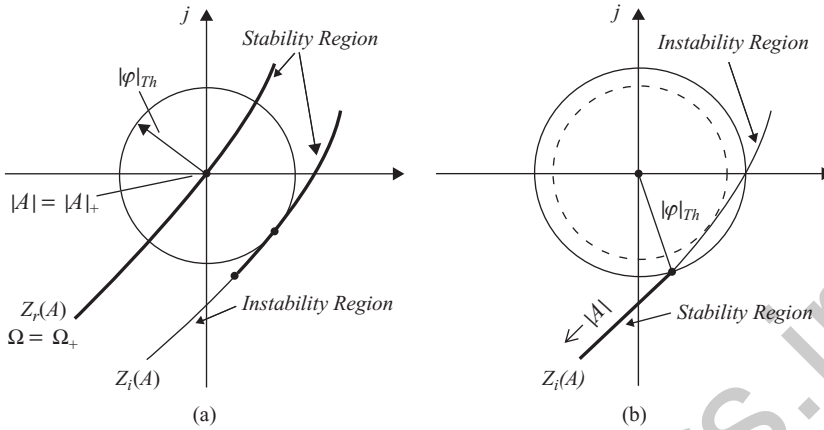


**Figure 4.23** Evaluation of the threshold values  $|\varphi|_{Th}$  along the canonical basis axes of limit cycling MIMO systems.

Carrying out similar operations for all points, one can easily single out at the locus  $Z_i(A)$  the *stability regions* or, in other words, the set of those values of  $|A|$  for which all characteristic systems are stable. In Figure 4.23, illustrating the above statements, thick lines show the stability regions for characteristic systems. The forced oscillation along the  $i$ th canonical basis axis is really only possible for the values of  $|A|$  belonging to the indicated regions.

In the SISO case, the threshold value of the amplitude of input sinusoidal signals is equal to the radius of the smallest circle with its centre at the origin, tangent to  $Z(A)$  [Equation (4.10)] (see Figure 4.3). It is clear from what has been stated that the threshold value of the magnitude  $|\varphi| = |\varphi|_{Th}$  in the direction of the  $i$ th canonical basis axis will be equal to the radius of the tangent circle only if the tangent point belongs to the stability region of the characteristic systems [Figure 4.23(a)]. If that condition does not hold, then one should increase the radius of the circle until the intersection point with  $Z_i(A)$  reaches the boundary between the stability and instability regions [Figure 4.23(b)]. The radius determined in such a manner gives the desired value for  $|\varphi|_{Th}$ . Changing the  $\Omega$  frequency, one can readily obtain the whole  $|\varphi|_{Th}(\Omega)$  curve along the  $i$ th canonical basis axis of the limit cycling MIMO system.

Above, we pointed out the non-equivalence of the canonical basis axes for limit cycling MIMO systems. That non-equivalence exhibits and in the evaluation of the threshold dependence  $|\varphi|_{Th}(\Omega)$  along the ‘limit cycling’ (assume, the  $r$ th) axis. Thus, for example, the threshold values  $|\varphi|_{Th}$  at the frequencies differing from the limit cycle frequency  $\Omega_+$  are usually equal to the radius of the smallest circle tangent to the  $Z_r(A)$  locus. Besides, if the input frequency  $\Omega$  is equal to  $\Omega_+$  and the  $|A|$  magnitude is equal to the magnitude  $|A|_+$  of the amplitudes vector of the limit cycle, then the locus  $Z_r(A)$  [Equation (4.44)] passes through the origin of the complex plane [Figure 4.23(a)], since, here, the equality  $q_r(j\Omega, A) = -1$  holds. Consequently, the threshold value  $|\varphi|_{Th}$  along the ‘limit cycling’ axis of the canonical basis is always zero at the limit cycle frequency  $\Omega_+$ . The stability of all other characteristic systems is checked here during the analysis of the limit cycle. As for the threshold values  $|\varphi|_{Th}$  at the frequency  $\Omega_+$  along the other ( $i \neq r$ ) axes, these values are always larger than zero, since, in this case, the limit cycle along the  $r$ th axis must be suppressed (Figure 4.24). Note that the loci  $Z_i(A)$  for  $i \neq r$  may also pass through the origin for some  $|A|$  and  $\Omega$ , or originate from that point

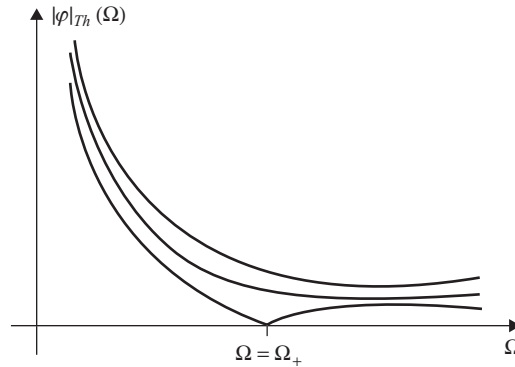


**Figure 4.24** Threshold dependencies  $|\varphi|_{Th}(\Omega)$  along the canonical basis axes of limit cycling MIMO systems ( $N = 3$ ).

for  $|A| = 0$ . However, the origin of the complex plane in such cases always belongs to the instability regions of the characteristic systems.

**Example 4.5** Consider the nonlinear two-axis guidance system of Example 3.1. In the absence of external signals, that system is limit cycling with frequency  $\Omega_+ = 11.7116$  and amplitudes  $A_1 = 6.7047$  and  $A_2 = 3.4$  ( $|A|_+ = 7.5176$ ). The  $Z_1(A)$  and  $Z_2(A)$  loci for two different frequencies  $\Omega = 4$  and  $\Omega = 11.7116$ , where the second frequency coincides with  $\Omega_+$ , are shown in Figure 4.25. For  $\Omega = 4$  [Figure 4.25(a)], the threshold value  $|\varphi|_{Th}^1 = 26.8704$  along the first ‘limit cycling’ axis is equal to the radius of the circle tangent to  $Z_1(A)$ , as the tangent point belongs to the stability region of the characteristic systems (that region is represented by the thick line). The value of  $|A|$  at the tangent point is 20.4417, and the components of  $x$  and  $\varphi$  are:  $x_1 = 20.2903 \exp\{-j275.2833^\circ\}$ ,  $x_2 = 2.4837 \exp\{-j278.776^\circ\}$ ,  $\varphi_1 = 26.6713$  and  $\varphi_2 = 3.2647 \exp\{-j3.4928^\circ\}$ . The threshold value  $|\varphi|_{Th}^2 = 42.3312$  along

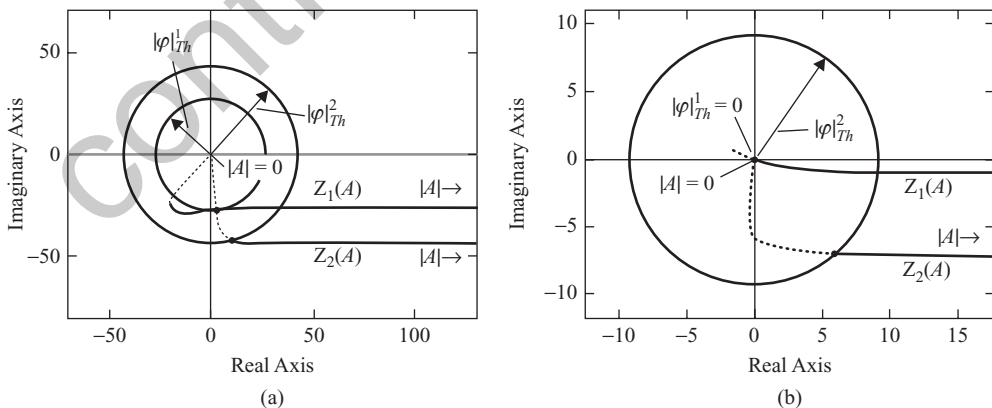


**Figure 4.25** Evaluation of the threshold values  $|\varphi|_{Th}$  along the canonical basis axes of the limit cycling system of Example 3.1. (a)  $\Omega = 4$ ; (b)  $\Omega = \Omega_+ = 11.7116$ .

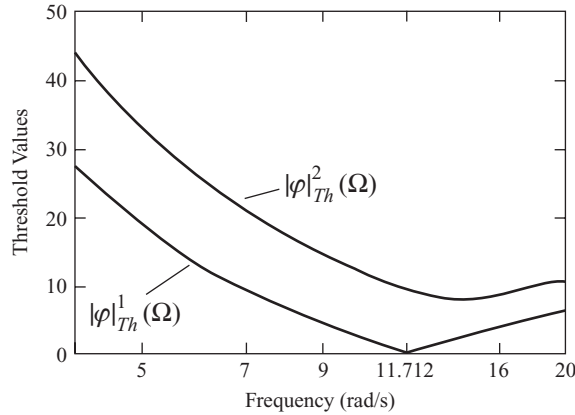


**Figure 4.26** The threshold dependencies  $|\varphi|_{Th}^1(\Omega)$  and  $|\varphi|_{Th}^2(\Omega)$  along the canonical basis axes.

the second axis is equal to the distance from the origin to the boundary between the stability and instability regions<sup>7</sup> at  $Z_2(A)$ . That point yields the following parameters for the forced oscillation and the complex amplitudes vector of the corresponding input signals:  $x_1 = 7.5889 \exp\{-j281.4341^\circ\}$ ,  $x_2 = 8.159 \exp\{-j194.7563^\circ\}$ ,  $|A| = 11.1427$ ,  $\varphi_1 = 28.83$  and  $\varphi_2 = 30.9961 \exp\{+j86.6777^\circ\}$ . Note that for  $|A| = 0$ , both  $Z_1(A)$  and  $Z_2(A)$  loci in Figure 4.25(a) start from the origin. For  $\Omega = 11.7116$  [Figure 4.25(b)], the character of the  $Z_2(A)$  locus is the same as for  $\Omega = 4$ , although the threshold value  $|\varphi|_{Th}^2 = 9.1496$  considerably decreases. The parameters of the forced oscillation  $x$  and the input ‘collinear’ vector  $\varphi$  along the second axis here are  $x_1 = 6.7038 \exp\{-j309.905^\circ\}$ ,  $x_2 = 11.1891 \exp\{-j206.7534^\circ\}$ ,  $|A| = 13.0437$ ,  $\varphi_1 = 4.7024$  and  $\varphi_2 = 7.8487 \exp\{+j103.1521^\circ\}$ . As for the locus  $Z_1(A)$ , it also starts, for  $|A| = 0$ , from the origin towards the fourth quadrant of the complex plane; then (for  $|A| = |A|_+ = 7.5176$ ), it returns to the origin [since, for that value of  $|A|$ , we have  $q_1(j\Omega_+, A_+) = -1$ ] and, after that, it continues in the second quadrant. Here, the point  $(0, j0)$  at the locus  $Z_1(A)$  is the boundary point of the stability and instability regions of the characteristic systems. Naturally, the threshold value  $|\varphi|_{Th}^1$  in this case is equal to zero. The threshold dependencies  $|\varphi|_{Th}^1(\Omega)$  and  $|\varphi|_{Th}^2(\Omega)$  along the canonical basis axes for the frequency interval of  $[2, 20]$  are shown in Figure 4.26. The larger values of  $|\varphi|_{Th}^2$  are due to the fact that it is necessary to suppress the limit cycle oscillation along the first canonical basis axis. As for the  $|\varphi|_{Th}^1(\Omega)$  dependency, it has the same form as that for the case of limit cycling SISO systems. The computed data are verified by the results of the system modelling given in Figure 4.27. In Figure 4.27, the transient responses in the limit cycling system under the input harmonic signals along the second canonical basis axis are shown, with the frequency equal to the limit cycle frequency  $\Omega = \Omega_+ = 11.7116$  and the computed before threshold value  $|\varphi|_{Th}^2 = 9.1496$  [see Figure 4.25(b)]. Recall (see Example 3.1) that in the absence of input signals, the amplitudes of the limit cycle in the channels are  $A_1 = 6.7047$  and  $A_2 = 3.4$ , and the relative phase shift of the oscillation in the second channel is  $\gamma_2 = -35.457^\circ$ . On applying (at  $t = 2.0$  sec.) the input signals with the above values of the components  $\varphi_1 = 4.7024$  and  $\varphi_2 = 7.8487 \exp\{+j103.1521^\circ\}$ , synchronization occurs and the system begins to oscillate

<sup>7</sup> The instability regions are shown in Figure 4.25 by the dotted lines.

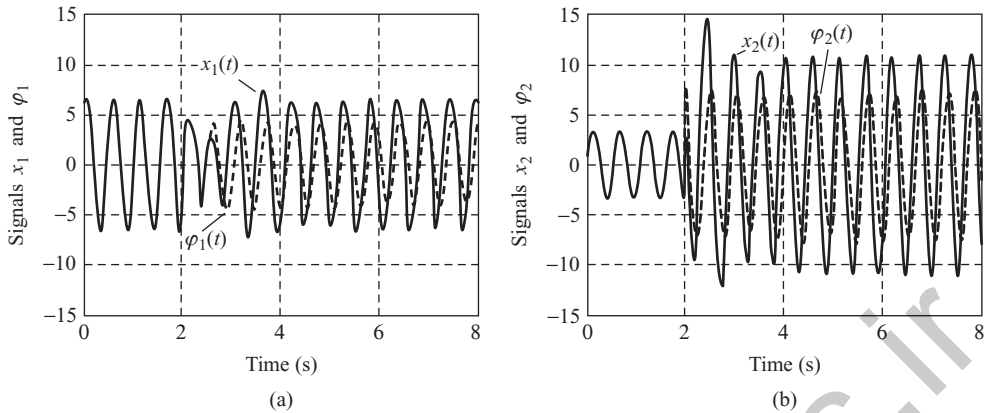


**Figure 4.27** Forced oscillations along the second canonical basis axis for  $\Omega = 11.7116$  and  $|\varphi|_{Th}^2(\Omega) = 9.1496$ . (a) First channel; (b) second channel.

along the second canonical basis axis. The amplitudes of the forced oscillation obtained by the modelling are  $A_1 = 6.7386$  and  $A_2 = 11.1477$ , which differ from the computed values  $A_1 = 6.7038$  and  $A_2 = 11.1891$  by less than 0.6%. It is interesting to note that the limit cycle amplitudes and those of the discussed forced oscillation in the first channel are practically the same. However, applying the input harmonic signals along the second axis results in the increase in the oscillation amplitude in the second channel and quite another phase shifts in both channels.

### 4.3 NONLINEAR UNIFORM MIMO SYSTEMS

Obviously, all the results of the previous section concerning the investigation of one-frequency forced oscillation under the synchronization condition, the evaluation of the generalized FRCs and of the oscillation index of stable nonlinear MIMO systems, the computation of the threshold values for the magnitude of the input harmonic vector, etc. are completely valid for the case of nonlinear uniform systems. Therefore, below, we shall focus on those aspects of the problem that are due to the structural features of the class of MIMO systems discussed and allow us to bring the procedures and techniques for the investigation of forced oscillation in uniform systems very close to the corresponding procedures and techniques for SISO systems.

#### 4.3.1 One-frequency forced oscillation and capturing in uniform systems

Consider the one-frequency forced oscillation in the nonlinear uniform system of Figure 3.19 under the harmonic input signals of the form in Equation (4.18). Let all nonlinearities of the system have odd-symmetrical characteristics, and the transfer function  $w(s)$  of identical separate channels possesses the low pass filter property [Equation (3.46)]. Then, if the synchronization condition in the uniform system holds, in the general case, synchronization in all  $N$  SISO

characteristic systems occurs and we can write down

$$x = \sum_{i=1}^N c_i(A) \left[ \frac{\langle c_i^+(A), \varphi \rangle}{1 + \lambda_i(A)w(j\Omega)} \right], \quad (4.50)$$

where the designations are the same as in Section 3.4. Multiplying successively Equation (4.50) by the dual vectors  $c_i^+(A)$  and taking the magnitudes, we obtain the following set of  $N$  nonlinear algebraic equations with respect to the unknown amplitudes vector  $A$ :

$$|\langle c_i^+(A), x \rangle| - \frac{|\langle c_i^+(A), \varphi \rangle|}{|1 + \lambda_i(A)w(j\Omega)|} = 0, \quad i = 1, 2, \dots, N. \quad (4.51)$$

To give a geometrical interpretation of the solution to the problem, rewrite these equations, after some simple manipulations, in the form

$$\begin{aligned} & \left[ \operatorname{Re}\{W(j\Omega)\} + \operatorname{Re} \left\{ \frac{1}{\lambda_i(A)} \right\} \right]^2 + \left[ \operatorname{Im}\{W(j\Omega)\} + \operatorname{Im} \left\{ \frac{1}{\lambda_i(A)} \right\} \right]^2 \\ & = \left[ \frac{|\langle c_i^+(A), \varphi \rangle|}{|\lambda_i(A)| |\langle c_i^+(A), x \rangle|} \right]^2 \quad i = 1, 2, \dots, N \end{aligned} \quad (4.52)$$

Each of Equations (4.52) defines in the complex plane of the locus  $w(j\omega)$  a circle with its centre at the point  $-1/\lambda_i(A)$  and radius

$$R_i = \frac{|\langle c_i^+(A), \varphi \rangle|}{|\lambda_i(A)| |\langle c_i^+(A), x \rangle|} \quad (4.53)$$

Consequently, the amplitudes vector  $A$  will be the solution to the problem of forced oscillation in the nonlinear uniform system for an arbitrary direction of  $\varphi$  only if  $N$  circles with their centres at the points  $-1/\lambda_i(A)$  and radii  $R_i$  [Equation (4.53)] traverse the locus  $w(j\omega)$  at the point marked by the frequency  $\omega = \Omega$  of the input harmonic signal (Figure 4.28).<sup>8</sup> In fact, Figure 4.28 gives the geometrical picture of the synchronization phenomenon in the nonlinear uniform system and represents the superposition of  $N$  (in this case,  $N = 3$ ) pictures characterizing synchronization in common SISO systems (see Figure 4.2).

**Example 4.6** Let us analyze the forced oscillation in the uniform nonlinear system of Example 3.3, in which it was shown that in the absence of input signals, the system is limit cycling with the frequency  $\Omega_+ = 39.959$ , amplitudes  $A_1 = 11.5516$  and  $A_2 = 8.0824$ , and the relative phase shift of the oscillation in the second channel  $\gamma_2 = -62.7914^\circ$ . Apply the harmonic oscillation with the frequency  $\Omega = 50$  and the vector  $\varphi$  with components  $\varphi_1 = 30$  and  $\varphi_2 = 20 \exp\{-30^\circ\}$  to the inputs of the discussed system. The computations show that for the given input signals, the synchronization in the system takes place and the vector  $x$  has the following components:  $x_1 = 38.866 \exp\{+j0.73^\circ\}$  and  $x_2 = 24.495 \exp\{-j30.36^\circ\}$  (note that the oscillations in the separate channels are actually cophased with the corresponding input oscillations). The corresponding graphs in the Nyquist and Nichols planes are given in

<sup>8</sup> See also footnote 2 in Section 4.2.1.

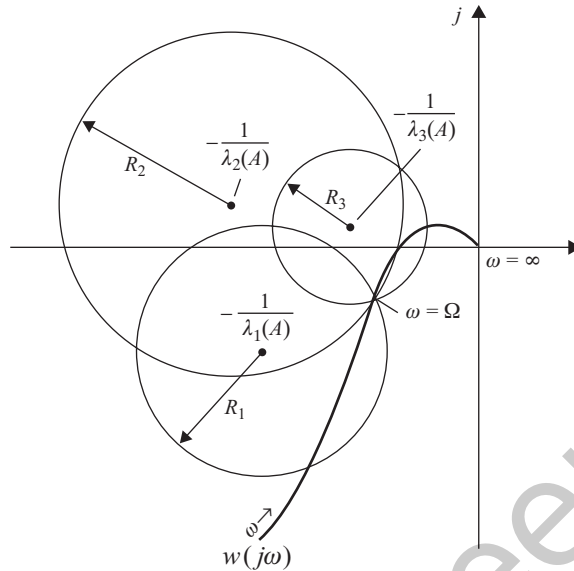


**Figure 4.28** Geometrical interpretation of synchronization in the uniform system ( $N = 3$ , double-valued nonlinearities).

Figure 4.29. The computed data are completely justified by the system modelling. The transient responses in the separate channels, together with the input signals (shown by the dotted lines), are given in Figure 4.30, in which the input harmonic signals are applied to the system inputs after the settling of the limit cycle mode (at  $t = 1.0$  sec.). It can be seen from Figure 4.30 that the oscillations in the channels are indeed cophased with the input oscillations. The amplitudes of the forced oscillations at the inputs to the nonlinearities, determined by the curves in Figure 4.30, are  $A_1 = 38.513$  and  $A_2 = 23.865$  (the computational error is less than 3%).

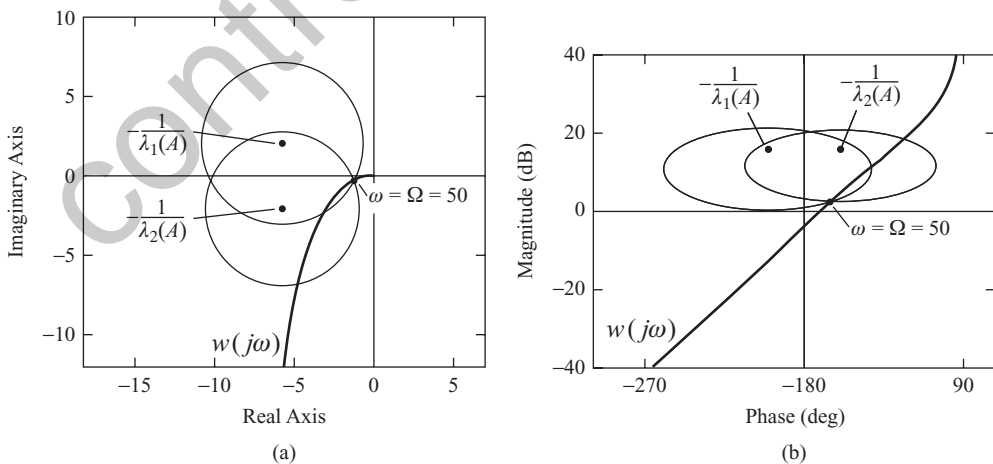


**Figure 4.29** Synchronization in the limit cycling uniform system. (a) Nyquist plane; (b) Nichols plane.

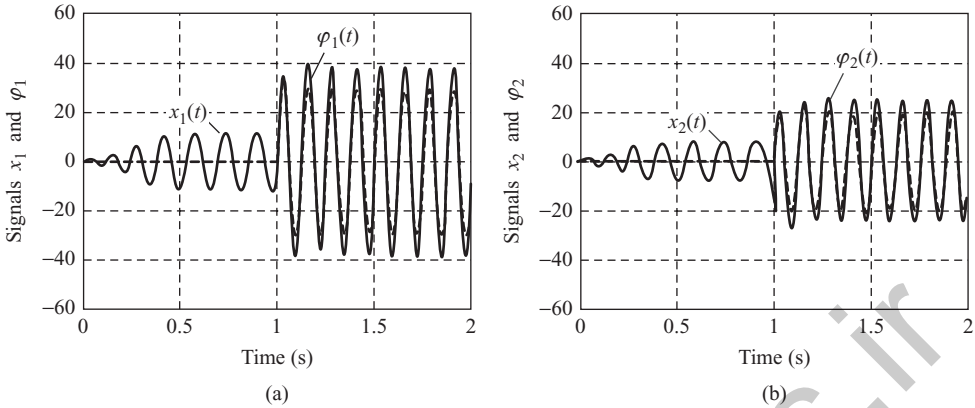


**Figure 4.30** Modelling of forced oscillation in the uniform system. (a) First channel; (b) second channel.

### 4.3.2 Generalized frequency response characteristics of stable nonlinear uniform systems

The computation of the oscillation index  $M$  of stable nonlinear uniform systems by the resonant peak of the majorant  $A_{\text{sup}}(\Omega)$  of the generalized FRCs does not differ at all from the case of general MIMO systems (see Section 4.2.2). Therefore, we shall only discuss some aspects of the evaluation of the oscillation indices  $M_i$  of characteristic systems, allowing for the structural features of uniform systems.

The necessary conditions for excitation of the  $i$ th characteristic system of the uniform system under the sinusoidal input signal  $\varphi(t)$  [Equation (4.18)] with the given frequency  $\Omega$  and magnitude  $|\varphi|$  have the form

$$A = |A| m_i(A), \quad (4.54)$$

$$\varphi = |\varphi| c_i(A) \text{ and} \quad (4.55)$$

$$|A| = \frac{|\varphi|}{|1 + \lambda_i(A)w(j\Omega)|}, \quad (4.56)$$

where the designations are the same as in Section 3.4. Transform Equation (4.56) into the form

$$\left[ \text{Re}\{w(j\Omega)\} + \text{Re} \left\{ \frac{1}{\lambda_i(A)} \right\} \right]^2 + \left[ \text{Im}\{w(j\Omega)\} + \text{Im} \left\{ \frac{1}{\lambda_i(A)} \right\} \right]^2 = \left[ \frac{|\varphi|}{|\lambda_i(A)| |A|} \right]^2. \quad (4.57)$$

This defines the equation of the circle with its centre at  $-1/\lambda_i(A)$  and radius

$$R_i = \frac{|\varphi|}{|\lambda_i(A)| |A|}. \quad (4.58)$$

To evaluate the amplitudes vector of the forced oscillation along the  $i$ th canonical basis axis using Equations (4.54)–(4.58), one should find the set of the vectors  $A$  satisfying the collinearity condition in Equation (4.54) as the magnitude  $|A|$  changes in the appropriate range (usually from zero to infinity). Then, as in the investigation of the limit cycle, the parametrical locus

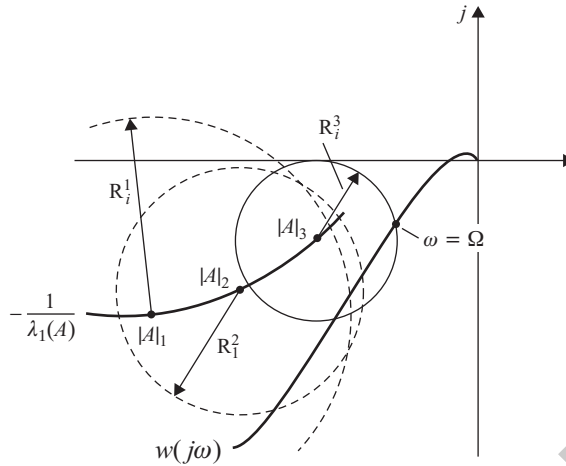


**Figure 4.31** Evaluation of the parameters of forced oscillation along the  $i$ th canonical basis axis of the uniform system.

$-1/\lambda_i(A)$  must be plotted in the complex plane of  $w(j\omega)$ . Further, in accordance with Equation (4.57), for each point at the locus  $-1/\lambda_i(A)$ , taken as a centre, the circle of radius  $R_i$  [Equation (4.58)] is drawn, where the value of  $|A|$  equals the parameter of the taken point (Figure 4.31). The circle which traverses  $w(j\omega)$  at the given frequency  $\omega = \Omega$  yields the sought vector  $A$ . Thereby, the corresponding point at the FRC along the  $i$ th canonical basis axis of the uniform system is determined. The intersections of the plotted circles with different points at the locus  $w(j\omega)$  determine, for the given  $|\varphi| = \text{const}$ , the whole FRC along  $c_i(A)$ . For different values of  $|\varphi|$ , we obtain different FRCs. As in the case of general MIMO systems, it is expedient to assess the stability margin of the  $i$ th characteristic system, or, in other words, the stability margin of the nonlinear uniform system in the direction of the  $i$ th canonical basis axis, using the oscillation index  $M_i$ :<sup>9</sup>

$$M_i = \sup_{0 \leq \Omega \leq \infty} \frac{1}{|1 + \lambda_i(A)w(j\Omega)|}, \quad (4.59)$$

where all those vectors  $A$  that satisfy the collinearity condition in Equation (4.54) should be taken into consideration. For the graphical evaluation of  $M_i$ , one can use the general technique discussed in Section 4.2.2. However, in the performance analysis of uniform systems, it is more convenient to exploit another way, especially if the limit cycle analysis by the Goldfarb method was first carried out and the loci  $-1/\lambda_i(A)$  for all  $A$  satisfying the condition in Equation (4.54) were plotted. From Equation (4.59), it is easy to obtain the following equation for the locus of the constant values of  $M_i$  in the complex plane of  $w(j\Omega)$ :

$$\left[ \text{Re}\{w(j\Omega)\} + \text{Re}\left\{\frac{1}{\lambda_i(A)}\right\} \right]^2 + \left[ \text{Im}\{w(j\Omega)\} + \text{Im}\left\{\frac{1}{\lambda_i(A)}\right\} \right]^2 = \frac{1}{[|\lambda_i(A)|M_i]^2}. \quad (4.60)$$

<sup>9</sup> Further, to emphasize that we are dealing with forced oscillation, we shall write  $w(j\Omega)$  instead of  $w(j\omega)$ .

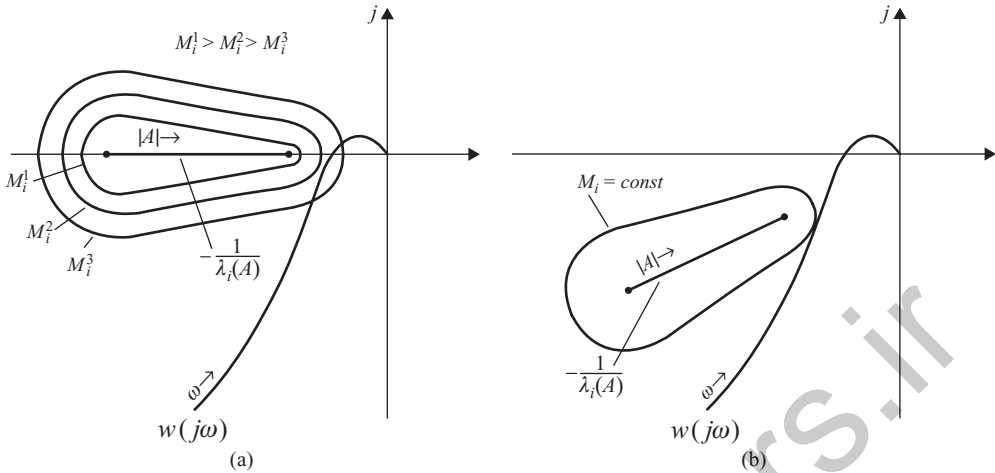
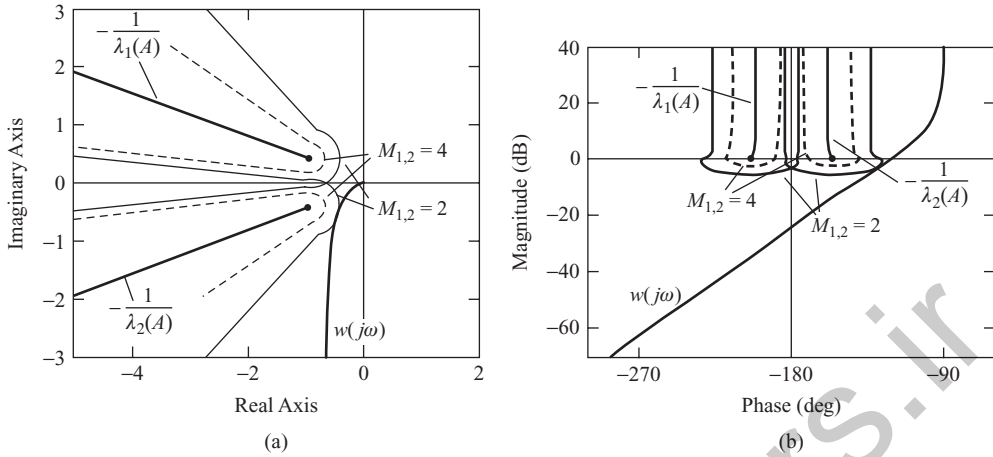


Figure 4.32 Evaluation of the oscillation index  $M_i$  of nonlinear uniform systems.

This equation defines the circle with its centre at the point  $-1/\lambda_i(A)$  and radius  $1/|\lambda_i(A)|M_i$ . If we draw the circles for all ‘collinear’  $A$ , then their envelope forms a forbidden region for  $w(j\Omega)$  (Figure 4.32). As  $M \rightarrow \infty$ , the forbidden region reduces to the locus  $-1/\lambda_i(A)$  and, as  $M_i \rightarrow 0$ , it spreads out over the whole complex plane. The oscillation index of the  $i$ th characteristic system is equal to the parameter  $M_i$  of that forbidden region which is tangent to  $w(j\Omega)$  [Figure 4.32(b)]. Having successively evaluated the oscillation indices of all characteristic systems and choosing the maximum of them  $M_{i\max} = \max(M_i)$ , we obtain the estimate of the stability margin and the performance of the oscillatory transient responses for the nonlinear uniform system.

It is interesting to compare the lines of constant values of  $M_i$  for linear and nonlinear uniform systems. In the linear uniform system, the forbidden regions in the complex plane of  $w(j\Omega)$  corresponding to different constant values of  $M_i$  represent concentric circles of radii  $1/|\lambda_i| M_i$ , with their centre at the critical point  $-1/\lambda_i$ , where  $\lambda_i$  is the  $i$ th eigenvalue of the numerical matrix of cross-connections  $R$  (see Section 2.2.3). In the nonlinear harmonically linearized uniform system, the critical points  $-1/\lambda_i$  stretch, owing to the nonlinear properties of the system, into the loci  $-1/\lambda_i(A)$ , where  $\lambda_i(A)$  is the  $i$ th eigenvalue of the concomitant matrix of cross-connections  $N(A)$  [Equation (3.48)] computed for all  $A$  vectors satisfying the collinearity condition in Equation (4.54). The forbidden regions  $M_i = \text{const}$  here are deformed correspondingly, and somewhat similar regions, with respect to the locus  $-1/\lambda_i(A)$ , correspond to different values of  $M_i$ . As we see, there is a deep resemblance to the features of forbidden regions for nonlinear SISO systems (Paltov 1975).

**Example 4.7** As an illustrative example, consider the two-dimensional uniform system of Example 3.3 with saturations in the separate channels. Decreasing the gains of the transfer function  $w(s)$  [Equation (2.171)] by a factor of 10 yields a system stable in the linear variant (this can easily be seen from Figure 3.23), and not limit cycling in the presence of saturations. The locus  $w(j\omega)$  of the linear part of the system, the loci  $-1/\lambda_{1,2}(A)$  and the forbidden regions  $M_{1,2} = \text{const}$  for two different values 2 and 4 of the oscillation indices are shown in Figure 4.33, in which the dotted lines correspond to the value of 4.



**Figure 4.33** Forbidden regions  $M_i = \text{const}$  for the two-dimensional uniform system. (a) Nyquist plane; (b) Nichols plane.

### 4.3.3 Generalized frequency response characteristics of limit cycling uniform systems

Below, we shall briefly consider the questions of evaluating the threshold frequency dependence  $|\varphi|_{Th}(\Omega)$  along the canonical basis axes of limit cycling uniform systems. Here, of course, one can use the general technique described in Section 4.2.2. At the same time, based on Equations (4.56) and (4.57), the threshold value  $|\varphi|_{Th}$  for every fixed frequency  $\Omega$  can be readily determined by the loci  $w(j\omega)$  and  $-1/\lambda_i(A)$ . To this end, the regions of stability and instability of all characteristic systems should be found at each  $i$ th parametrical locus  $-1/\lambda_i(A)$  with the help of the following simple procedure. For each value of  $|A|$  at the locus  $-1/\lambda_i(A)$ , the corresponding ‘collinear’ vector  $A$  is substituted into the concomitant matrix of cross-connections  $N(A)$  [Equation (3.48)], which reduces to a constant numerical matrix  $N^+$ . After that,  $N$  critical points  $-1/\lambda_k^+$  ( $k = 1, 2, \dots, N$ ), where  $\lambda_k^+$  are the eigenvalues of  $N^+$ , are plotted in the complex plane of  $w(j\omega)$ .<sup>10</sup> Then, the selected value of  $|A|$  belongs to the stability region if none of these critical points is encompassed by the locus  $w(j\omega)$ . Otherwise, the  $|A|$  parameter belongs to the instability region. Repeating similar operations for all  $|A|$ , we shall obtain the desired partition of the locus  $-1/\lambda_i(A)$  into the stability and instability regions (in Figure 4.34, the instability regions are shown by dotted lines). According to Equation (4.58), the threshold value  $|\varphi|_{Th}$  here is equal to

$$|\varphi|_{Th} = R_{\min} |\lambda_i(A)| |A|, \quad (4.61)$$

where  $R_{\min}$  is the minimal distance from the point  $\omega = \Omega$  at  $w(j\omega)$  to the stability region. In the simplest case, the value of  $R_{\min}$  is equal to the radius of the circle with its centre at the point  $\omega = \Omega$  at  $w(j\omega)$  tangent to  $-1/\lambda_i(A)$  [Figure 4.34(a)]. A similar situation occurs mostly

<sup>10</sup> One of the critical points  $-1/\lambda_k^+$ , namely the  $i$ th, always coincides with the chosen point  $|A|$  at the  $-1/\lambda_i(A)$  locus.

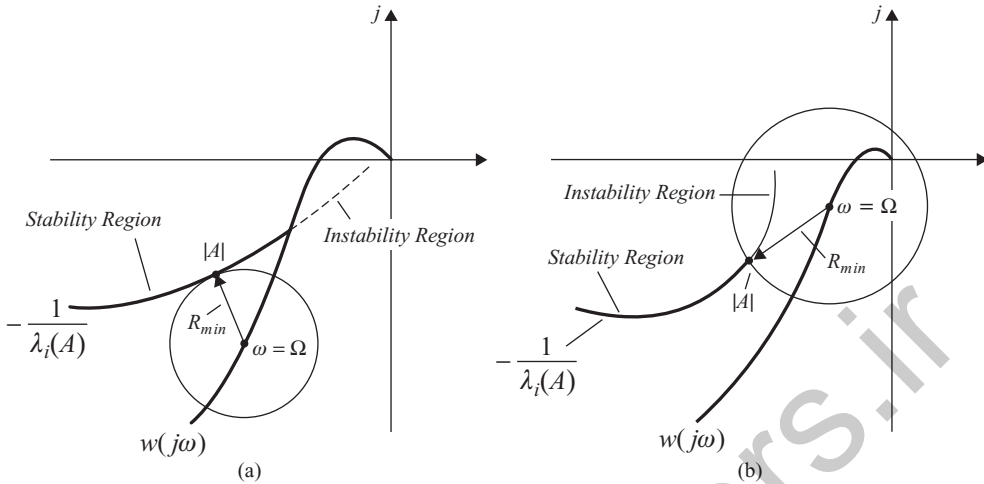


**Figure 4.34** Determination of the threshold value  $|\varphi|_{Th}$  along the canonical basis axes of the limit cycling uniform system. (a) ‘Limit cycling’ axis; (b) other axes.

in the investigation of forced oscillation along the ‘limit cycling’ axis. In forced oscillation along the other axes, the value of  $R_{min}$  is usually equal to the distance from the point  $w(j\Omega)$  to the point dividing the stability and instability regions at  $-1/\lambda_i(A)$  [Figure 4.34(b)]. It is clear that the  $A$  vector in Equation (4.61) corresponds to either the boundary of the stability region [Figure 4.34(b)] or the tangent point of the circle with its centre at  $w(j\Omega)$  with that region [Figure 4.34(a)]. Changing the frequency  $\Omega$ , one can readily determine the threshold dependence  $|\varphi|_{Th}(\Omega)$  in the direction of any canonical basis axis of the limit cycling uniform system using the described technique.

**Example 4.8** Determine the threshold values of the magnitude  $|\varphi|$  along the canonical basis axes of the limit cycling system of Examples 3.3 and 4.6, if the frequency of the input harmonic signals is  $\Omega = 20$ . The necessary constructions in the Nyquist and Nichols planes are given in Figure 4.35. For the second (‘limit cycling’) characteristic systems, the threshold value  $|\varphi|_{Th}^{(2)} = 18.468$  is determined by the circle with its centre at  $w(j20)$  and radius  $R_{min}^2 = 2.483$ , tangent to  $-1/\lambda_2(A)$  at the point  $|A| = 41.2463$ . The following components of  $\varphi$  and  $x$  correspond to that input vector:  $\varphi_1 = 15.2439$ ,  $\varphi_2 = 10.4254 \exp\{-59.459^\circ\}$ ,  $x_1 = 34.0457 \exp\{-j276.838^\circ\}$  and  $x_2 = 23.284 \exp\{-j336.2964^\circ\}$ . The threshold value  $|\varphi|_{Th}^{(1)} = 38.7486$  along the first canonical basis axis is determined by the circle with its centre at the same point  $w(j20)$  and radius  $R_{min}^1 = 5.3774$ , traversing the boundary of the stability and instability regions at  $-1/\lambda_1(A)$ . The value  $|A| = 14.251$  corresponds to that boundary. The components of  $\varphi$  and  $x$  here are  $\varphi_1 = 31.7667$ ,  $\varphi_2 = 22.1884 \exp\{+62.5464^\circ\}$ ,  $x_1 = 11.6832 \exp\{-j267.811^\circ\}$  and  $x_2 = 8.1605 \exp\{-j205.2646^\circ\}$ . Note that the threshold value  $|\varphi|_{Th}$  along the first axis is more than twice as large as the threshold value along the second axis. Physically, this is because to force the system to oscillate along the first axis, it is necessary to suppress the limit cycle oscillation along the second axis, as well as to make the second characteristic system stable. In Figures 4.36 and 4.37, the results of the system modelling, on applying the input harmonic signals along the second canonical basis axis, for two different values of  $|\varphi|$ , where the first value  $|\varphi| = 19.3914$  exceeds the evaluated

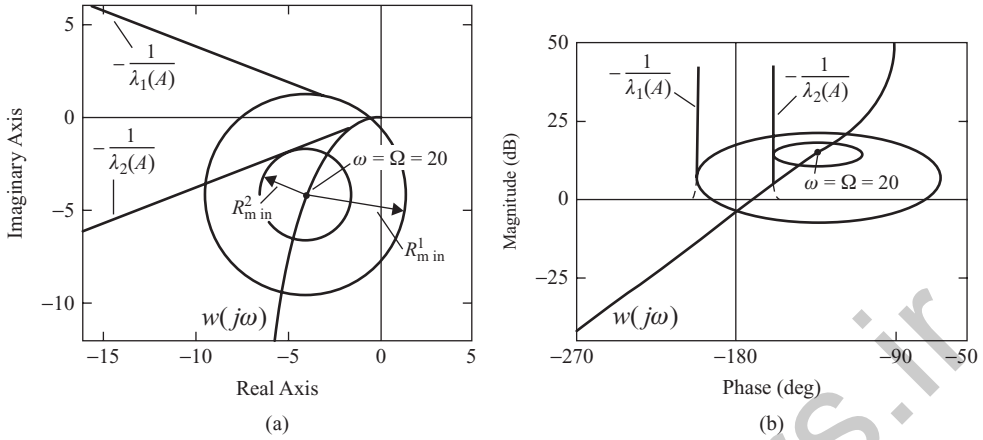


**Figure 4.35** Evaluation of the threshold values of  $|\varphi|_{Th}$  along the canonical basis axes of the two-axis uniform system of Example 4.6 for  $\Omega = 20$ . (a) Nyquist plane; (b) Nichols plane.

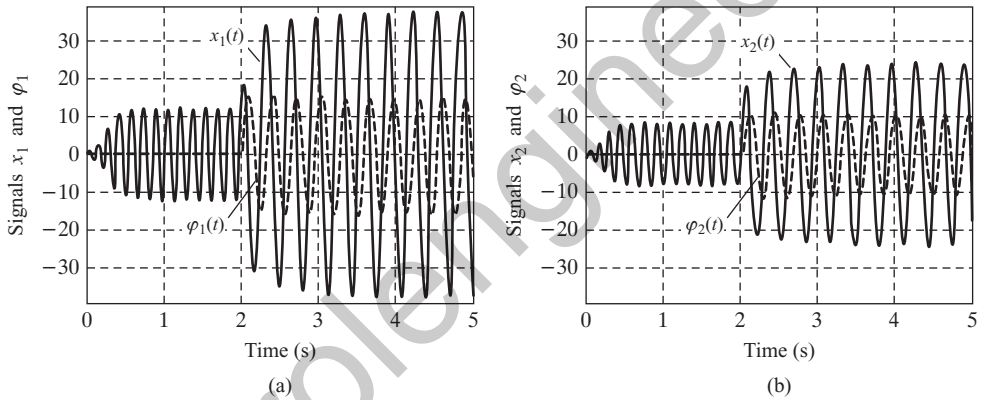


**Figure 4.36** Modelling of the system for  $|\varphi| = 1.05|\varphi|_{Th}^{(2)}$ . (a) First channel; (b) second channel.

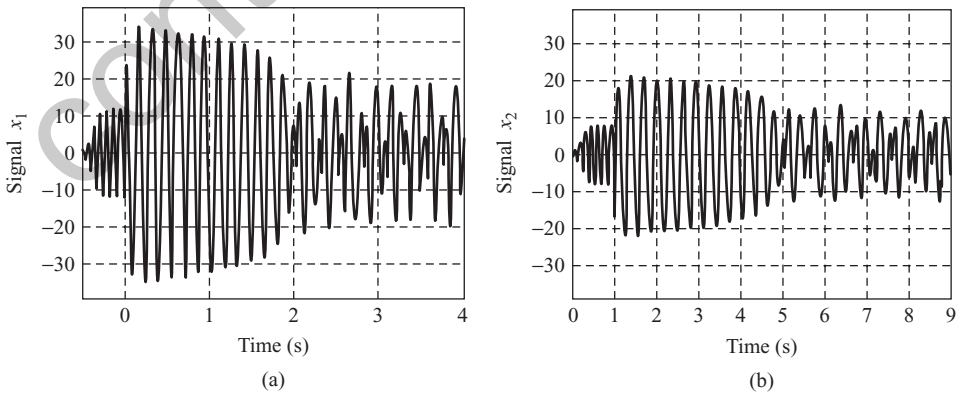


**Figure 4.37** Modelling of the system for  $|\varphi| = 0.99|\varphi|_{Th}^{(2)}$ . (a) First channel; (b) second channel.

threshold value  $|\varphi|_{Th}^{(2)} = 18.468$  by  $5\%^{11}$  and the second value  $|\varphi| = 18.2833$  is smaller than the evaluated one by  $1\%$ , are shown. As can be seen from Figure 4.36, in the limit cycling uniform system, synchronization occurs under the first of the above input signals, in which the amplitudes values of the forced oscillation are  $A_1 = 36.7333$  (the computational error of the evaluated value is about  $7\%$ ) and  $A_2 = 23.3206$  (the computational error is less than  $0.2\%$ ). As for the case in which  $|\varphi|$  is less than the evaluated threshold value only by  $1\%$  (Figure 4.37), the synchronization in the limit cycling system does not occur and the motion in the separate channels bears a complicated character. Note that in the system modelling, the input harmonic signals were applied at the point of time  $t = 2.0$  sec. (in Figure 4.36) and  $t = 1.0$  sec. (in Figure 4.37).

#### **4.4 FORCED OSCILLATIONS AND FREQUENCY RESPONSE CHARACTERISTICS ALONG THE CANONICAL BASIS AXES OF NONLINEAR CIRCULANT AND ANTICIRCULANT SYSTEMS**

The problem of investigating forced oscillation in nonlinear circulant and anticirculant systems under arbitrary input harmonic signals  $\varphi(t)$  (when all characteristic systems are excited), as well as the closely connected problem of evaluating the generalized FRCs in various directions of complex space  $\mathbb{C}^N$ , can be solved by the general techniques described in Section 4.2. Below, we shall consider the forced oscillation of equal amplitudes  $A_i = A$  directed along the canonical basis axes of *stable* circulant and anticirculant MIMO systems, and the related questions of evaluating the oscillation indices of SISO characteristic systems.<sup>12</sup> In any circulant or anticirculant system of order  $N$ ,  $N$  different forced oscillations with equal amplitudes may exist, which are accompanied by the excitation of only one characteristic system. These forced oscillations correspond to  $N$  mutually orthogonal directions along the canonical basis axes of the permutation matrix  $U$  [Equation (1.128)] (for circulant systems) or anticirculant permutation matrix  $U_-$  [Equation (1.156)] (for anticirculant systems). One can easily arrive at that conclusion following the reasoning used in Section 3.5, in which we studied the limit cycle in circulant and anticirculant systems. Indeed, if we assume that the amplitudes of the forced oscillations in all channels are equal to each other, then the circulant or anticirculant (by their structure) functional matrices of nonlinearities  $F(x)$  reduce after harmonic linearization to the circulant or anticirculant numerical matrices  $G(A)$ , depending on *one* unknown amplitude  $A$ . The open- and closed-loop transfer matrices of circulant and anticirculant systems here also become circulant or anticirculant, and their canonical bases coincide with the canonical bases (composed of the normalized eigenvectors  $c_i$ ) of matrices  $U$  or  $U_-$ . The specific property of eigenvectors of  $U$  and  $U_-$  is the equality of the magnitudes of all their components. This verifies the fact that forced oscillation with equal amplitudes is the only possible dynamic mode in circulant and anticirculant systems if the input harmonic signal excites only one characteristic system.

<sup>11</sup> Since the describing function method is approximate, the value of  $|\varphi|$  is taken in the system modelling with the indicated margin.

<sup>12</sup> The problem of evaluating the threshold value of  $|\varphi|$  in *limit cycling* circulant and anticirculant systems is left for the reader as an exercise (see also Example 4.9).

From the necessary condition in Equation (4.35) for collinearity of  $x$ ,  $\varphi$  and the axis  $c_i$  of the excited characteristic system, it follows that, first, the amplitudes of the input signals in the separate channels must be equal ( $B_i = B$ ) and, second, both input and forced oscillations must be ‘hyperspherical’, ‘plane’ or ‘antiphase’ (see Section 3.5). Hence, if the input vector of the complex amplitudes  $\varphi$  is directed along one of the eigenvectors of  $U$  ( $U_-$ ), then only one characteristic system responds, and forced oscillation with equal amplitudes occurs in the circulant (anticirculant) MIMO system.<sup>13</sup> Note that the directions of  $c_i$  in  $\mathbb{C}^N$  are strictly fixed and do not depend on either the frequency  $\Omega$  or the amplitudes  $B_i = B$  of the input signals, or the particular form of nonlinearities or elements of the linear part of circulant systems. This fundamentally sets apart the discussed systems from the case of nonlinear general MIMO systems.

As follows from the above-stated, in the investigation of forced oscillation in stable circulant systems with excitation of one characteristic system, and in the evaluation of FRCs along the canonical basis axes, the necessary collinearity condition for the vectors  $A$  and  $m_i$ <sup>14</sup> holds *a fortiori* if we assume that the oscillation amplitudes in separate channels are equal. This essentially simplifies the problem, since, for the given frequency  $\Omega$  and amplitude  $B$  of the external sinusoidal signals, the only unknown is a scalar value  $A$ , which can be determined from the equation

$$A = \frac{B}{|1 + q_i(j\Omega, A)|}. \quad (4.62)$$

Having determined  $A$  from Equation (4.62), it is easy to find the phase shift  $\Delta\gamma$  of the oscillations of  $x_k$  with respect to the input oscillations  $\varphi_k$  ( $k = 1, 2, \dots, N$ ) in the same channels:

$$\Delta\gamma = \arg \left\{ \frac{1}{1 + q_i(j\Omega, A)} \right\}, \quad (4.63)$$

where, unlike in Equation (4.38), the CTF  $q_i(j\Omega, A)$  depends on *one* amplitude  $A$ , and not on the amplitudes vector. Taking into account that the expressions for the CTFs can be written in analytical form for any  $N$ , we conclude that the problem under discussion proves as simple as in the common SISO case. Moreover, the well developed techniques for the investigation of forced oscillation in nonlinear SISO systems are completely applicable for determining the unknown amplitude  $A$  by Equation (4.62) and for finding the FRCs along  $c_i$ . Thus, for example, the graphical solution to the problem by E. Popov’s method does not differ at all from that which is well known in the classical control theory (Popov 1973) and is actually illustrated in Figure 4.3.

Consider, now, the problem of determining the oscillation index

$$M_i = \sup_{0 \leq \Omega \leq \infty} \frac{1}{|1 + q_i(j\Omega, A)|} \quad (4.64)$$

of the characteristic systems, the largest of which is, as in the case of general MIMO systems, a measure of the stability margin for nonlinear circulant systems. Evidently, the mapping of Equation (4.64) into the complex plane of  $q_i(j\Omega, A)$  is given by the same Equation (4.46)

<sup>13</sup> For the sake of brevity, below we shall speak only about the circulant systems, remembering that the features of anticirculant systems are actually exactly the same.

<sup>14</sup> Real-valued vectors  $m_i$  are composed of the magnitudes of components of  $c_i$ .

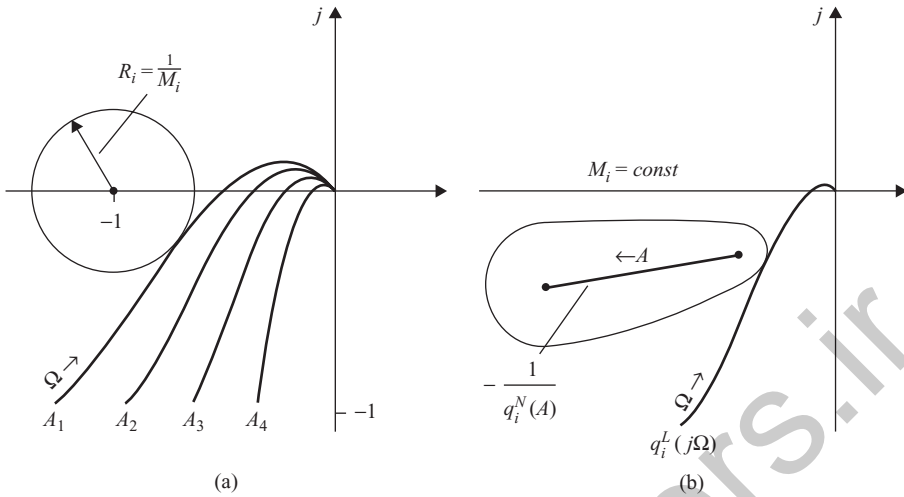


**Figure 4.38** Determining the oscillation index  $M_i$  for nonlinear circulant systems. (a) Nyquist plane of the family  $\{q_i(j\Omega, A)\}$ ; (b) Nyquist plane of the  $i$ th locus  $q_i^L(j\Omega)$ .

defining the circle with its centre at the point  $(-1, j0)$  and radius  $R_i = 1/M_i$ . Correspondingly, the oscillation index of the circulant system along the  $i$ th canonical basis axis is reciprocal to the radius of the circle tangent to the envelope of the family of the loci  $q_i(j\Omega, A)$  for different  $A = const$ . Graphically, that procedure is shown in Figure 4.38(a), and also is quite analogous to the common SISO case in Figure 4.7(a). To determine  $M_i$  [Equation (4.64)], one can proceed and otherwise, taking into account that the  $i$ th CTF  $q_i(j\Omega, A)$  of circulant systems is equal to the product of the corresponding CTFs  $q_i^L(j\Omega)$  and  $q_i^N(A)$  of the matrices  $W(j\Omega)$  and  $G(A)$  [see Equations (3.66)–(3.68) and Figure 3.38]. Rewrite, substituting  $q_i(j\Omega, A) = q_i^L(j\Omega)q_i^N(A)$ , Equation (4.64) in the form

$$M_i = \sup_{0 \leq \Omega \leq \infty} \frac{1/q_i^N(A)}{|1/q_i^N(A) + q_i^L(j\Omega)|}, \quad (4.65)$$

which gives the following equation of lines  $M_i = const$  in the complex plane of the  $i$ th characteristic gain locus  $q_i^L(j\Omega)$  of the linear part:

$$\left[ \operatorname{Re}\{q_i^L(j\Omega)\} + \operatorname{Re}\left\{\frac{1}{q_i^N(A)}\right\} \right]^2 + \left[ \operatorname{Im}\{q_i^L(j\Omega)\} + \operatorname{Im}\left\{\frac{1}{q_i^N(A)}\right\} \right]^2 = \frac{1}{[|q_i^N(A)| M_i]^2}. \quad (4.66)$$

For the fixed amplitude  $A$ , this is an equation of a circle with its centre at  $-1/q_i^N(A)$  and radius  $R_i = 1/|q_i^N(A)|M_i$ . Having drawn these circles for all points at the locus  $-1/q_i^N(A)$  and drawing the envelope, we obtain the forbidden region for the  $i$ th characteristic gain loci  $q_i^L(j\Omega)$ . For different  $M_i = const$ , we have different forbidden regions. The oscillation index of the  $i$ th characteristic system is equal here to that value of  $M_i$  for which the forbidden region is tangent to  $q_i^L(j\Omega)$  [Figure 4.38(b)]. In the case of a diagonal matrix of nonlinearities  $F(x) = \operatorname{diag}\{F_0(x_i)\}$ , the  $q_i^N(A)$  function in Equations (4.65) and (4.66) should be replaced

by the *common* describing function  $G_0(A)$ . It is important to emphasize that forbidden regions in such a case are the same for all  $q_i^L(j\Omega)$  ( $i = 1, 2, \dots, N$ ) and coincide with the forbidden regions used for performance analysis in nonlinear SISO systems (Paltov 1975; Gasparyan 1986).

Finally, in the case of nonlinear *uniform* circulant systems, the procedure for determining  $M_i$  is essentially described in Section 4.3.2, where it should be noted that all  $\lambda_i(A)$  depend on a single amplitude  $A$  and can be written in analytical form for any  $N$ , and the collinearity condition in Equation (4.54) holds *a fortiori*.

**Example 4.9** In Example 3.8, a limit cycling six-dimensional uniform circulant system with saturations in the separate channels (Figure 3.52) was considered and it was demonstrated that the limit cycle is due to the excitation of the fifth characteristic system. Let us determine such a gain of the separate channels for which the nonlinear system becomes stable and the largest of the oscillation indices  $M_i$  is equal to 1.85. The computations show that to solve the posed task, it is necessary to decrease the gain in the numerator of the transfer function  $w(s)$  [Equation (3.100)] by a factor of 100, i.e. assume it to be equal to 37 500 000. The worst, from the stability margin viewpoint, here remains the same, fifth characteristic system. The results of computation by different techniques are shown in Figure 4.39. The solution to the task, based on the Teodorchik method, is given in Figure 4.39(a), in which the family of the characteristic gain loci  $q_5(j\Omega, A) = \lambda_5 G_0(A)w(j\Omega)$  of *only the fifth* characteristic system for different constant values of  $A$  is shown (the values of amplitude are indicated by the Arabic numerals). The left-most locus of that family (for  $A = 0 \div 4$ ) coincides with the corresponding locus of the linear part, since, for these values of  $A$ , the describing function  $G_0(A)$  is equal to unity. As is evident from Figure 4.39(a), for  $M_5 = 1.85$ , the circle with its centre at the point  $(-1, j0)$  and radius  $1/M_5$  [see Equation (4.36) and Figure 4.19] is tangent to the envelope of the family of the characteristic gain loci  $q_5(j\Omega, A)$ , which yields the largest of the oscillation indices  $M_i$ . Figure 4.39(b) illustrates the approach based on Equation (4.66), in which, owing to the diagonal form of the matrix  $F(x)$ , the function  $q_i^N(A)$  must be replaced by  $G_0(A)$ , and the characteristic gain loci of the linear part  $q_i^L(j\Omega)$  have the form  $\lambda_i w(j\Omega)$ . In this graph, the Arabic numerals indicate the numbers of the characteristic systems. As we see,

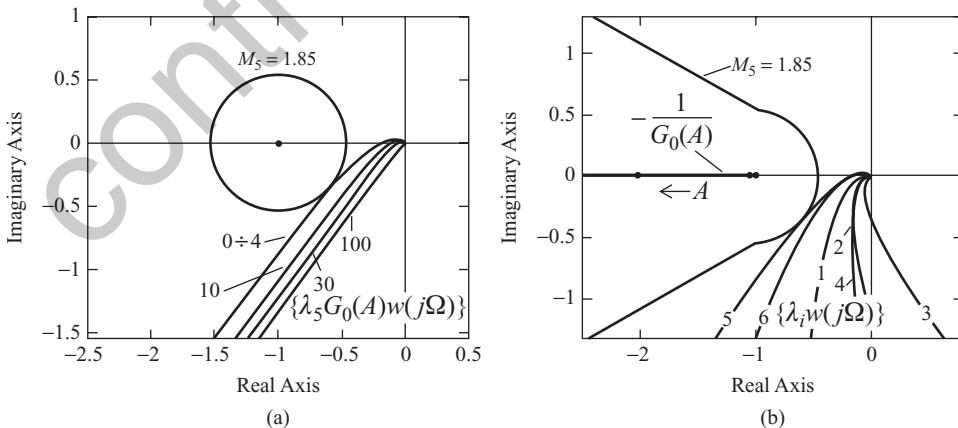


**Figure 4.39** Evaluation of the largest oscillation index  $M_{i \max}$ . (a) General approach (the fifth characteristic system); (b) application of Equation (4.66).

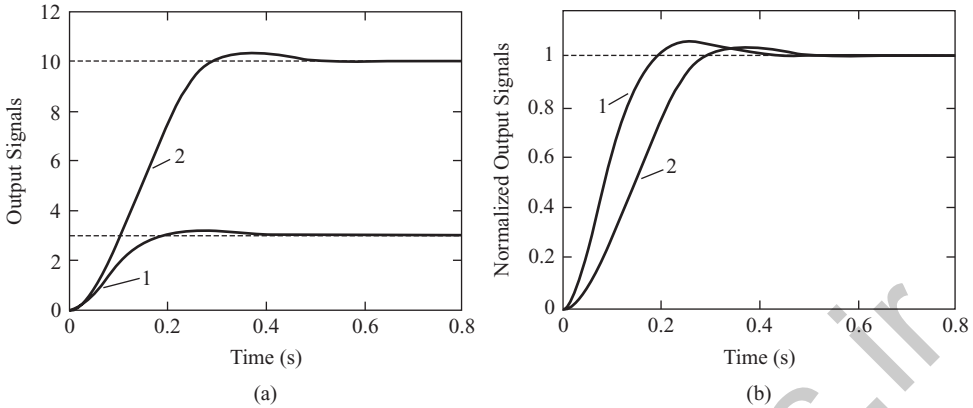


**Figure 4.40** Transient responses of the system under different step signals. (a) Initial signals; (b) normalized signals.

the forbidden region  $M_5 = 1.85$  is tangent here to the fifth characteristic gain locus of the linear part. Thus, the decrease in the channels gains by a factor of 100 not only results in the stability of the circulant system, but also provides the desired value  $M_{i \max} = 1.85$  for the largest of the oscillation indices of the characteristic systems. The output transient responses of the system channels caused by applying to all inputs the step signals of two levels  $-\varphi_i = 3$  and  $\varphi_i = 10$  – are shown in Figure 4.40(a). For  $\varphi_i = 3$ , the transient responses of the system lie entirely within the linear zones of the saturation nonlinearities (recall that the intervals of the linear zones are taken as  $[-4, +4]$ ). The modelling gives the following values for the settling time (estimated by  $\pm 2\%$  deviations from the output final value) and the overshoot:  $T_S = 0.3491$  sec and  $\sigma = 5.3644\%$ . For  $\varphi_i = 10$ , when the motions enter the saturation regions, the corresponding values are:  $T_S = 0.4193$  sec. and  $\sigma = 3.1563\%$ , i.e. the influence of the saturations appears as an increase in the transient response duration and some decrease in the overshoot. To represent this more clearly, the same output responses normalized with respect to the levels of the input step signals are shown in Figure 4.40(b).

## 4.5 DESIGN OF NONLINEAR MIMO SYSTEMS

In Section 2.5, we discussed one of the possible approaches to the *linear* MIMO systems design. That approach was based on the introduction in the linear MIMO system of the *scalar compensator*, i.e. of the diagonal regulator of the form  $K(s) = k(s)I$  (Figure 2.26), where  $I$  is the unit matrix and  $k(s)$  a scalar transfer function called *absolute*. As shown in Section 2.5, the scalar compensator does not affect the canonical basis of the initial plant and the absolute transfer function  $k(s)$  becomes the mutual compensator for *all* characteristic systems. This allows us to choose from the set of  $N$  characteristic systems the ‘worst’ one, from the standpoint of the given performance specifications, and, in fact, to reduce the design of the linear MIMO system of an arbitrary dimension to the design of one characteristic system with the help of the well known classical techniques. If necessary or desirable, one can also introduce a *decoupling* compensator into the MIMO system or accomplish *balancing* of the channels (see Section 2.5).

The presence of nonlinear elements may essentially change the dynamical characteristics of MIMO systems. In particular, the nonlinear MIMO system may exhibit a stable or unstable limit cycle, it may have several equilibrium points, etc. All this necessitates involving adequate techniques in the nonlinear MIMO systems design which would allow the engineer to grasp and take into account those specific features of the system that cannot be predicted by a linear model. In engineering practice, as was stated before, one of the most popular and efficient methods for the investigation of nonlinear systems is the describing function method, extended in the last two chapters to the problems of the investigation of limit cycles and forced oscillation, as well as to the performance analysis of oscillatory transient responses in nonlinear MIMO systems. Below, we shall show that the concept of the scalar compensator in combination with the describing function method proves efficient for nonlinear MIMO systems design, and also allows the correction of the MIMO system of an arbitrary dimension  $N$  to be chosen on the basis of the customary techniques of the classical control theory.

Thus, suppose that we have the nonlinear MIMO system of Figure 3.6, in which, for simplicity, all nonlinearities are assumed memoryless, i.e.  $F(x, px) = F(x)$ . Assume also that the transfer matrix of the linear part  $W(s)$  characterizes the initial plant, including the dynamics of the measuring units and, possibly, the decoupling and balancing matrix compensators. Since the MIMO system is nonlinear, at the first stage, it is usually checked whether the presence of nonlinearities causes a limit cycle. This can be carried out with the help of the techniques discussed in Chapter 3. Hence, having investigated the possible limit cycle in the initial harmonically linearized system, we have the corresponding constructions in the Nyquist, Nichols or Bode planes of the characteristic gain loci, where, naturally, these constructions depend on the structural class of the MIMO system (see Sections 3.3–3.5). In the following, we shall admit that what is required is to design a *stable* MIMO system, i.e. we shall not consider the cases in which the limit cycle is desirable [such cases occur sometimes in practice, such as in the development of scanning systems, vibration regulators, etc. (Popov 1973; Gasparyan 1986)]. As pointed out in Section 2.5, the main design methods for linear systems are conventionally based on the frequency-domain and root performance indices. Among these indices, the frequency-domain indices can be immediately and most naturally extended to the nonlinear case.<sup>15</sup> First of all, this concerns the oscillation index, which can be considered as an indirect measure of the stability margin for stable MIMO systems.<sup>16</sup> Therefore, we shall specify the requirements for the stability margins of the nonlinear MIMO system with the help of the largest oscillation index  $M_{i \max}$  of the characteristic systems.

Introduce into the designed nonlinear MIMO system the scalar compensator  $k(s)I$  (Figure 4.41). The open-loop complex transfer function of the harmonically linearized system has, here, the form

$$Q(j\Omega, A) = k(j\Omega)W(j\Omega)G(A), \quad (4.67)$$

where  $G(A)$  is the matrix of the describing functions. An inspection of Equation (4.67) allows us to make a number of evident but, at the same time, quite significant conclusions. Since, on

<sup>15</sup> In the classical literature on nonlinear control, design techniques by the root locus method are also discussed (Thaler and Pastel 1962), but these techniques apply mainly to SISO systems with single-valued nonlinearities and have not gained wide dissemination in control engineering.

<sup>16</sup> The question of providing the dynamical accuracy of MIMO systems was briefly discussed in Remark 2.5 in Section 2.4.

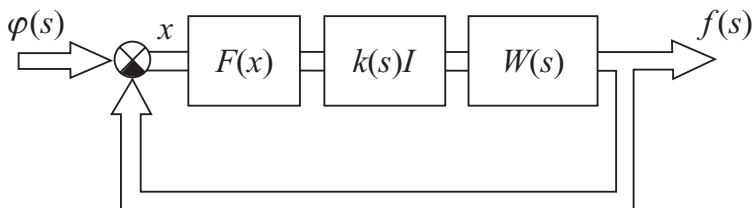


Figure 4.41 Nonlinear MIMO system with the scalar compensator.

multiplying the square matrix by a scalar, all eigenvalues of that matrix are multiplied by the same scalar, all CTFs  $q_i(j\Omega, A)$  of the initial system  $W(j\Omega)G(A)$  are multiplied by the transfer function  $k(j\Omega)$ , i.e. the latter becomes, as in the linear case, an *absolute* transfer function of the ‘correction’ introduced into *all* characteristic systems of the initial MIMO system. For the CTFs  $q_i^O(j\Omega, A)$  of the open-loop MIMO system with the scalar compensator, we can write down

$$q_i^O(j\Omega, A) = k(j\Omega)q_i(j\Omega, A), \quad i = 1, 2, \dots, N. \tag{4.68}$$

Further, since the multiplication of a matrix by a scalar does not affect the eigenvectors of that matrix, this implies that introducing the scalar compensator into the nonlinear MIMO system *does not change the canonical basis* of the initial harmonically linearized MIMO system, i.e. does not affect the modal decomposition of the initial system. Schematically, the above statements are illustrated in Figure 4.42, in which it should be noted that the modal matrix  $C(j\Omega, A)$  does not depend on the choice of  $k(j\Omega)$  and coincides with the modal matrix of the initial system.

The above conclusions are indeed very important. In particular, the last of them implies that the introduction of the scalar compensator does not violate one of the necessary conditions for the existence of a limit cycle in the MIMO system, namely the collinearity condition in Equation

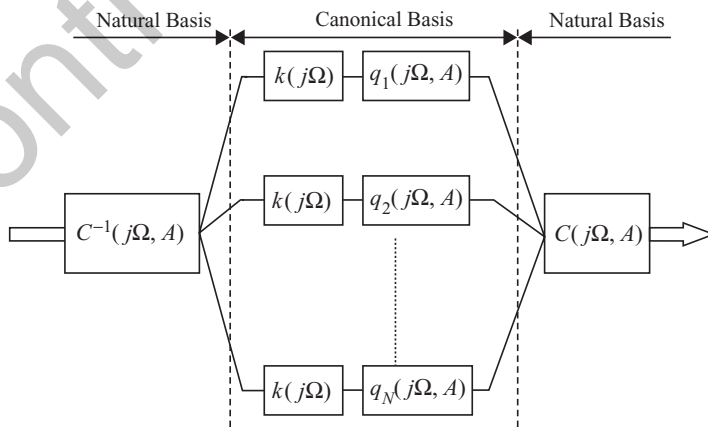
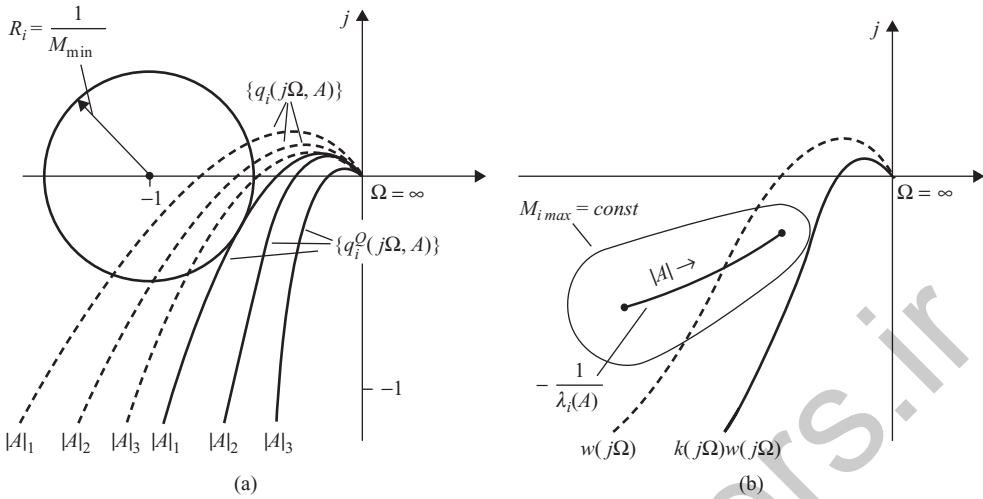


Figure 4.42 Canonical representation of the open-loop harmonically linearized MIMO system with the scalar compensator.



**Figure 4.43** Selection of the absolute correction of the nonlinear system based on the given value of  $M_{i \max}$ . (a) General MIMO system; (b) uniform system.

(3.39) [or (3.41)]. Consequently, if the investigation of the initial system has already been done, and we have the corresponding numerical results and graphical constructions in the planes of the characteristic gain loci  $q_i(j\Omega, A)$ , then all these results and constructions can be used for choosing the absolute transfer function  $k(s)$  based on the desired value of the oscillation index  $M_{i \max}$ . To this end, one should simply draw in the planes of the characteristic gain loci of the initial system the forbidden regions for the given  $M_{i \max}$ , and then choose a correction  $k(j\Omega)$  such that all corrected loci  $q_i^Q(j\Omega, A)$  do not enter into the corresponding forbidden regions.<sup>17</sup> If the initial MIMO system is limit cycling, in practice, it is usually enough to choose the correction  $k(j\Omega)$  for the ‘limit cycling’ characteristic system. As for the case of the stable initial MIMO system, it is enough to choose  $k(j\Omega)$  for the characteristic system with the largest value of  $M_i$  (for the ‘worst’ characteristic system). In both cases, we deal with a one-dimensional task, and the recommendations for the appropriate selection of the absolute correction  $k(j\Omega)$  may be found in many textbooks on classical control. For the cases of general and uniform NIMO systems, this is illustrated in Figure 4.43, in which the dotted lines show the characteristic gain loci for the initial system and the solid lines for the corrected one. The graphical constructions for circulant and anticirculant systems look quite analogous: one need only replace in Figure 4.43 the magnitude  $|A|$  of the amplitudes vector by the scalar amplitude  $A$ . Obviously, the selection of  $k(j\Omega)$  may also be carried out using the Bode and Nichols diagrams. We shall not dwell on that question, as this does not present any difficulty for a trained reader.

**Example 4.10** Consider the two-axis limit cycling guidance system with saturations in the separate channels of Example 3.1. In Example 4.4, it was shown that on decreasing the gains in the channels by a factor of 5, the system becomes stable and the largest oscillation index  $M_1 = 2.2081$  belongs to the first characteristic system. Suppose that we want to suppress the limit cycle and provide the value of 1.8 for the largest of the oscillation indices  $M_i$  without decreasing

<sup>17</sup> In fact, in Examples 4.4 and 4.9, we have already solved a similar task for general and circulant uniform MIMO systems, by the corresponding selection of gains of transfer functions of separate channels.

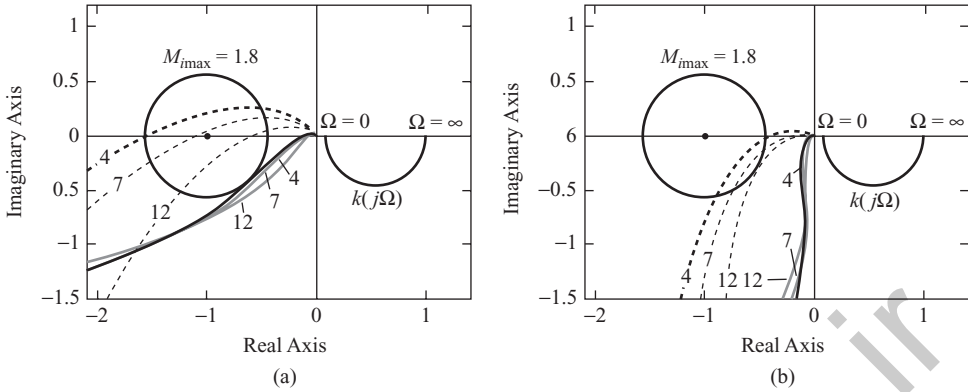


**Figure 4.44** Forbidden regions  $M_{i\max} = 1.8$  in the Nyquist plane. (a) First characteristic system; (b) second characteristic system.

the gains of the initial system, i.e. by introducing the corresponding absolute correction.<sup>18</sup> It can be shown that the transfer function

$$k(s) = \frac{0.0833(s + 0.6)}{s + 0.05} \quad (4.69)$$

can serve as such a correction, where the coefficient  $0.0833 = 0.05/0.6$  is introduced to provide the unit total gain of  $k(s)$ . The corresponding constructions in the Nyquist plane are shown in Figure 4.44, in which the dotted lines are the characteristic gain loci of the initial system and the solid lines present the gain loci of the system with the absolute correction in Equation (4.69). The numbers 4, 7 and 12 in Figure 4.44 indicate the values of the magnitude  $|A|$  for the ‘collinear’ amplitudes vectors  $A$ . The forbidden region represents a circle with its centre at  $(-1, j0)$  and radius  $R = 1/M_{i\max} = 0.5556$ . As can be seen from Figure 4.44, the nonlinear system is stable with the selected absolute correction [Equation (4.69)], and the gain loci  $q_1^Q(j\Omega, A)$  of the first characteristic system (which was ‘limit cycling’ in the initial system) are tangent to the forbidden region  $M_{i\max} = 1.8$ ; the oscillation index of the second characteristic system here is even smaller ( $M_2 = 1.112$ ). It is interesting to note that in this case, the oscillation index  $M_{i\max}$  of the harmonically linearized nonlinear system and the corresponding resonant frequency coincide with the largest oscillation index and the resonant frequency of the linear system, i.e. the same system but without the saturation nonlinearities. This is evident from Figure 4.44, in which, for  $|A| = 4$ , both describing functions are equal to unity [see Equation (3.45)], and the locus  $q_1^Q(j\Omega, A)$ , which is tangent to the forbidden region  $M_{i\max} = 1.8$ , coincides with the corresponding locus  $q_1(j\Omega)$  of the linear system. The results of modelling the discussed nonlinear system for two levels of the input step signals  $\varphi_i$  ( $\varphi_i = 3$  and  $\varphi_i = 10$ ) are given in Figure 4.45(a). The same transient responses normalized with respect to the levels of the input signals are given Figure 4.45(b), in which the dotted lines refer to the input signals  $\varphi_i = 10$ . For  $\varphi_i = 3$ , the motion of  $x_1(t)$  and  $x_2(t)$  takes

<sup>18</sup> Recall that the decrease in the channel gain brings about the deterioration of the system dynamical accuracy with respect to the input deterministic signals. To provide the required value  $M_{i\max} = 1.8$ , the gains should be decreased not by a factor of 5, but of 7.4.

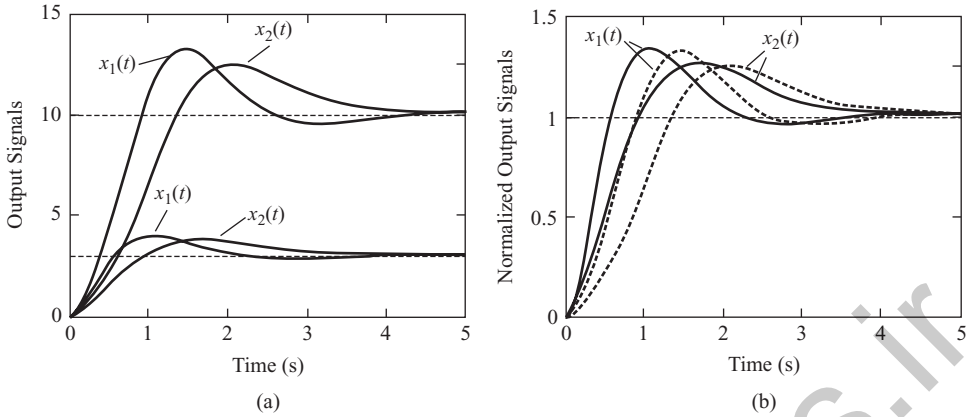


**Figure 4.45** Modelling of the system under the input step signals  $\varphi_i = 3$  and  $\varphi_i = 10$ . (a) Initial signals; (b) normalized signals.

place within the linear zone of nonlinearities. The overshoot in the first channel is 34.03% and, in the second, it is 26.84%. For  $\varphi_i = 10$ , these quantities are 32.36 and 25.353%, respectively. The settling times  $T_S$ , calculated by the level of 2% from the steady-state output response, are equal to 4.2057 and 4.4651 sec., respectively. Hence, as we have already seen in Example 4.9, the influence of saturation appears as an increase in the transient response duration and some decrease in the overshoot.

# 5

## Absolute stability of nonlinear MIMO systems

### 5.1 INTRODUCTION

The problem of nonlinear systems stability has always attracted the attention of researchers and engineers. Rigorous analytical methods for investigating the stability of nonlinear systems are those based on the works of prominent Russian scientist A. Lyapunov (1892, 1907). In his works, Lyapunov considered in general form the stability of the solution of nonlinear differential equations, and gave precise notions of stability, asymptotical stability, etc. Lyapunov's theorems of stability at a first approximation, actually reducing the issue of the stability analysis of a nonlinear system to the analysis of a linear (linearized) system, constitute the basis of linear control theory. The second (or direct) Lyapunov method, which allows finding *sufficient* conditions for motion stability, has had a huge impact on the development of nonlinear control theory. At the same time, the necessity for representing nonlinear systems in state-space, as Lyapunov's second method presumes, has restricted to a certain extent its application in practice. In many respects, it is because the basis of the classical control theory is formed by the frequency-domain methods. This led to the interest of technicians in the search for *frequency* stability criteria of nonlinear systems motion, which finally resulted in a great breakthrough in that field.

The beginning of impetuous development of the frequency-oriented direction in the theory of absolute stability were the seminal works of Romanian scientist V. Popov, dated in the late 1950s (Popov 1959, 1960, 1961). In the following years, a large number of papers devoted to the problem of absolute stability were published (Aizerman and Gantmacher 1964; Hsu and Meyer 1968; Narendra and Taylor 1973; Voronov 1979, etc). Among them, the works of Yakubovich, who proved the so-called 'frequency theorem', should be especially noted. That theorem generalized many of the available results and brought about new efficient criteria, as well the expansion of classes of nonlinearities for which the conditions of absolute stability can be found (Yakubovich 1962, 1964, 1967, 1973). Later, V. Popov, Yakubovich, Jury and Li (1965), Moore and Anderson (1967, 1968) and many others extended the main absolute stability criteria of nonlinear SISO systems to the multidimensional case. However, in spite of the elegance and mathematical completeness of 'multivariable' criteria of absolute stability,

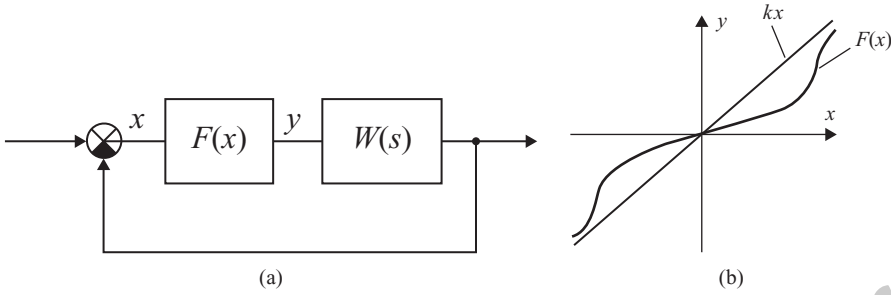


**Figure 5.1** Nonlinear SISO system. (a) Block diagram; (b) sector nonlinearity.

their use in engineering practice presents some difficulties. It can be explained especially clearly by the example of Popov's most common classical criterion, on the basis of which, in the SISO case, many other criteria are derived rather simply, such as circle and parabolic criteria, the criterion of absolute stability of forced motions, etc. (Hsu and Meyer 1968; Nelepin 1975). Consider the nonlinear SISO system in Figure 5.1(a), where  $W(s)$  is the transfer function of the *stable* linear part and  $F(s)$  is a single-valued memoryless (static) nonlinearity whose output versus input characteristic belongs to a sector  $[0, k]$  [Figure 5.1(b)], i.e. it satisfies the condition<sup>1</sup>

$$0 \leq \frac{F(x)}{x} \leq k. \quad (5.1)$$

The determination of *sufficient* conditions for the absolute stability of such systems by Popov's criterion is reduced to finding a numerical value of a real parameter  $\tau$  in the range  $-\infty < \tau < \infty$ , for which the following inequality holds:

$$\operatorname{Re}\{(1 + j\omega\tau)W(j\omega)\} + \frac{1}{k} > 0 \quad (5.2)$$

for all positive frequencies  $\omega \geq 0$  (Popov 1961). If such a value of  $\tau$  *does exist*, then it guarantees the absolute stability of the *equilibrium point*  $x \equiv \mathbf{0}$  for the system in Figure 5.1(a), i.e. the asymptotical stability *in the large* for *all* nonlinearities satisfying the condition in Equation (5.1) and belonging to the indicated class of single-valued static nonlinearities. However, there are no regular techniques for determining the 'needed' value of the parameter  $\tau$  based on analytical form of the inequality in Equation (5.2). In particular, all analytical methods of investigating absolute stability are usually reduced to finding the conditions for nonnegativity, or absence of real positive roots, of an algebraic equation ensuing from Popov's inequality [Equation (5.2)] (Aisagaliev 1969; Konovalov and Zacharov 1978). In utilizing the mentioned methods, it is recommended that the choice of the numerical value for  $\tau$  be performed by successive iterations or just by the trial-and-error method (Siljak 1969; Naumov 1972). At the same time, a very simple and visual graphical solution to the problem can be obtained in the complex plane, via the *modified frequency characteristic*  $W^M(j\omega)$  of the linear part of the system having the form:

$$W^M(j\omega) = \operatorname{Re}\{W(j\omega)\} + j\omega\operatorname{Im}\{W(j\omega)\}. \quad (5.3)$$

<sup>1</sup> For simplicity, we shall call such nonlinearities the *sector* nonlinearities.

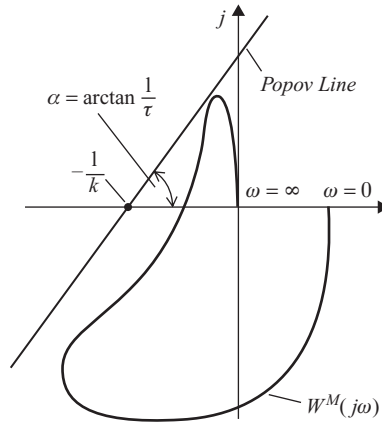


**Figure 5.2** Absolute stability analysis of the SISO system.

As is known, the inequality in Equation (5.2) will hold if it is possible to draw in the complex plane such a straight line (the *Popov line*) passing through the point  $(-1/k, j0)$  that the plot of the modified linear part  $W^M(j\omega)$  is situated entirely to the right of that line (Figure 5.2). The indicated features of the application of Popov's criterion are much more salient in the analysis of nonlinear MIMO systems, for which, in the formulation of the absolute stability criterion, there appears a diagonal matrix  $\text{diag}\{\tau_i\}$  of  $N$  parameters  $\tau_i$  (Jury and Li 1965; Nelepin 1975).<sup>2</sup> The difficulties owing to the increase in the dimension are redoubled here by the fact that, for  $N > 2$ , there is generally no possibility of imparting a simple geometrical interpretation to conditions of absolute stability, which makes Popov's criterion so efficient in the SISO case. It should be noted that for some specific types of nonlinear MIMO systems, such as two-dimensional symmetric, diagonally dominant (i.e. with weak cross-connections) MIMO systems, Lindgren and Pinkos (1966), Ozay (1973), Shankar and Atherton (1977), etc. obtained significant results, but they all have a somewhat restricted character and are not applicable to general MIMO systems. Based on most publications, the practical examination of MIMO systems absolute stability consists in the analysis, using the algebraic methods, of positive definiteness of a Hermitian matrix depending on  $N$  unknown parameters  $\tau_i$ , whose selection is carried out by successive iterations (Pyatnicki 1968; Aisagaliev 1970; Nelepin 1975; Orurk *et al.* 1978). In this respect, the trick of replacing the diagonal matrix  $\text{diag}\{\tau_i\}$  by a scalar  $\tau I$  (i.e. equating  $\tau_i = \tau$  for all  $i$ ) proposed in Petrov (1970) and Mutter (1981) does not lead to any tangible simplifications. The point is that, though reducing the number of varied parameters to one, it gives no answer about the relationship of the sought value for  $\tau$  with the transfer matrix of the linear part  $W(s)$  and the numerical characteristics of the sectors confining the nonlinearities. Recall that this problem is actually not also solved, regarding the analytical choice of  $\tau$  from the inequality Equation (5.2), in the SISO case.

Below, in Section 5.2, we shall discuss how the analysis of the absolute stability of the MIMO system can be performed via Popov's method, based on the characteristic gain loci of the linear part  $W(s)$ . In fact, in Section 5.2, the choice of  $\tau$  in the scalar matrix  $\tau I$  is accomplished by the same geometrical constructions in the complex plane as in the classical SISO case. Note

<sup>2</sup> In a more general formulation, not considered further, the conditions of absolute stability depend on two diagonal matrices of selected (unknown) parameters.

that the presented criteria narrow to a certain extent the area of MIMO systems absolute stability, i.e. they belong to the so-called ‘very sufficient’ criteria. However, it is compensated for by the fact that the problem is readily solved for any number of channels  $N$ , and the results are expressed in a convenient and familiar form. Note also that if, in the case of general MIMO systems, the geometrical procedures discussed below play a somewhat auxiliary role and serve only for the ‘optimal’ choice of the parameter  $\tau$ , for normal MIMO systems, they obtain a self-dependent meaning and allow the problem to be completely solved without any additional examinations of the positive definiteness of the above-mentioned Hermitian matrix. In the following sections, we shall formulate the multidimensional analogues of the circle and parabolic criteria of absolute stability of the equilibrium point as well as of the forced motions of nonlinear MIMO systems.

## 5.2 ABSOLUTE STABILITY OF GENERAL AND UNIFORM MIMO SYSTEMS

### 5.2.1 Multidimensional Popov’s criterion

Consider the  $N$ -dimensional nonlinear MIMO system with zero inputs in Figure 5.3(a), in which  $\text{diag}\{F_i(x_i)\}$  is a *diagonal* matrix of nonlinearities, and  $W(s)$  is the transfer matrix of the linear part. We shall also include here, without especially mentioning them in most cases, uniform systems with an arbitrary matrix of cross-connections  $R$ . In these cases, we shall assume that  $W(s) = w(s)R$ , where  $w(s)$  is the transfer function of identical separate channels.

The nonlinear elements  $F_i(x_i)$  are assumed static, possibly with hysteresis, and/or nonstationary, with the characteristics lying in the sectors  $[0, k_i]$  [Figure 5.3(b)]:

$$0 \leq \frac{F_i(x_i)}{x_i} \leq k_i, \quad i = 1, 2, \dots, N. \quad (5.4)$$

The transfer matrix  $W(s)$  is assumed *stable* or, under some restrictions on the form of the characteristic gain loci  $q_i(j\omega)$ , which will be discussed further, of *type one*, i.e. the MIMO system of Figure 5.3(a) can be either *type-0* or *type-1*. In the latter case, we shall also suppose that the left limits in Equation (5.4) are equal to arbitrary small positive numbers  $\varepsilon_i > 0$ , and the *marginal* closed-loop MIMO system obtained from the system in Figure 5.3(a) by

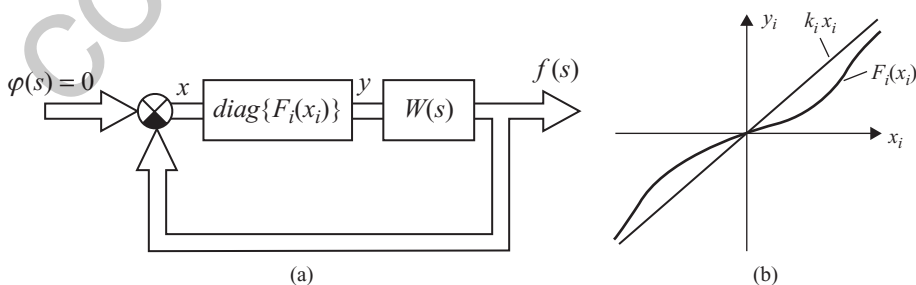


**Figure 5.3** MIMO system with the diagonal matrix of nonlinearities. (a) Matrix block diagram; (b) nonlinearity in the  $i$ th channel.

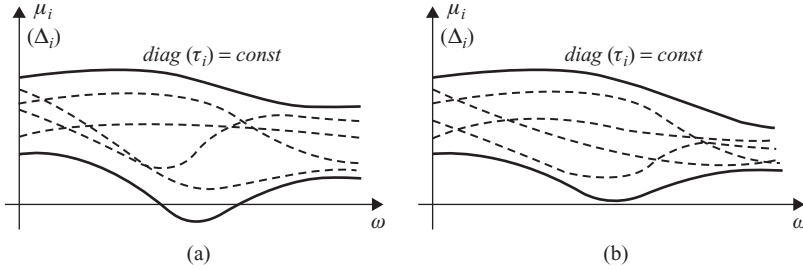


**Figure 5.4** Examination of the sufficient conditions  $\text{Re}P(j\omega) > 0$ . (a) Conditions are not satisfied; (b) conditions are satisfied.

replacing the nonlinear functional block  $\text{diag}\{F_i(x_i)\}$  by the numerical diagonal matrix  $\text{diag}\{\varepsilon_i\}$  is asymptotically stable (Nelepin 1975).<sup>3</sup> In the following, we shall not divide these two cases, as they lead to the same formulations and results. The equilibrium point  $x \equiv \mathbf{0}$  of the nonlinear MIMO system is said to be *absolutely stable* if it is asymptotically stable *in the large* for any nonlinearities  $F_i(x_i)$  satisfying the *sector restrictions* in Equation (5.4). For absolute stability of the MIMO system under the formulated assumptions it is *sufficient* that there exist a diagonal matrix  $\text{diag}\{\tau_i\}$  with real  $\tau_i$  such that for all  $\omega \geq 0$  the Hermitian matrix

$$\text{Re}P(j\omega) = \frac{1}{2}[P(j\omega) + P^*(j\omega)] \tag{5.5}$$

be positive definite (for brevity we shall write  $\text{Re}P(j\omega) > 0$ ), where  $P(j\omega)$  has the form

$$P(j\omega) = [I + j\omega \text{diag}\{\tau_i\}]W(j\omega) + \text{diag}\left\{\frac{1}{k_i}\right\}. \tag{5.6}$$

The stated criterion represents the generalization of Popov’s conventional criterion to the multidimensional case. Different proofs of that criterion are given in Jury and Li (1965) and Nelepin (1975). It is well known that for the positive definiteness of any Hermitian matrix, it is necessary and sufficient that all its eigenvalues or, according to Sylvester’s criterion, all the leading principal minors (Voevodin and Kuznetsov 1984) be positive. From this, it follows that for checking the sufficient condition  $\text{Re}P(j\omega) > 0$  under any particular matrix  $\text{diag}\{\tau_i\}$ , the dependences on frequency  $\omega$  of the eigenvalues  $\mu_i$  or the principal leading minors  $\Delta_i$  of the matrix  $\text{Re}P(j\omega)$  [Equation (5.5)] should be determined [Figure 5.4(a)]. If we manage to find such a matrix  $\text{diag}\{\tau_i\}$  for which all  $\mu_i(\omega)$  or  $\Delta_i(\omega)$  are positive for  $\omega \geq 0$ , then the nonlinear MIMO system under consideration is absolutely stable [Figure 5.4(b)]. Of course, besides the described ‘direct’ evaluation of the condition  $\text{Re}P(j\omega) > 0$ , we can also apply special algebraic methods establishing conditions for the positive definiteness (nonnegativity) of  $N$  polynomials  $\Delta_i(\omega)$  (Siljak 1969, 1970; Orurk *et al.* 1978; Mutter 1981).

Let us proceed now to the derivation of inequalities expressing the sufficient conditions of absolute stability for the MIMO system in Figure 5.3 via the CTFs of the linear part  $W(s)$  (Gasparyan 1986; Gasparyan and Alexanyan 2004). To this end, first of all, replace the diagonal matrix  $\text{diag}\{\tau_i\}$  in Equation (5.6) by the scalar  $\tau I$ , where  $\tau$  is a real parameter. If all

<sup>3</sup> Further, we shall call this condition the *marginal stability*.

nonlinearities  $F_i(x_i)$  are of the same type, which is the most common in the practical applications case, then the usual restrictions are imposed on the possible limits for  $\tau$  (Tsyppkin 1977; Voronov 1979). Thus, if all  $F_i(x_i)$  are single-valued and stationary, then  $\tau$  can accept any finite value ( $-\infty < \tau < \infty$ ); for nonlinearities with passive (negative) hysteresis, the value of  $\tau$  cannot be negative ( $0 \leq \tau < \infty$ ); for nonstationary nonlinearities,  $\tau$  should be equal to zero, etc. If nonlinearities  $F_i(x_i)$  in separate channels are of different types, then the possible values for  $\tau$  belong to an interval, *common* to all nonlinearities. For example, if some nonlinear elements have single-valued stationary characteristics and the rest of them have passive hysteresis, then  $0 \leq \tau < \infty$ ; if there are nonlinear elements in the system with both passive and active hysteresis, or at least one of them is nonstationary, then  $\tau$  should be equated to zero, etc.

Further, replace Equation (5.4) by the evident inequalities

$$0 \leq \frac{F_i(x_i)}{x_i} \leq k_{\max}, \quad i = 1, 2, \dots, N, \quad (5.7)$$

where  $k_{\max} = \max(k_i)$ . Geometrically, this corresponds to introducing a *common* sector  $[0, k_{\max}]$ , which confines all characteristics  $F_i(x_i)$  (Figure 5.5), and, mathematically, to replacing in Equation (5.6) the diagonal matrix  $\text{diag}\{1/k_i\}$  by the scalar matrix  $(1/k_{\max})I$ . For MIMO systems with the same types of nonlinearities in the separate channels, such an operation is quite natural, since all  $k_i$  in those systems are usually the same. Moreover, in practice, MIMO systems with *identical* nonlinearities in the channels frequently occur, for which conditions in Equation (5.7) are satisfied automatically.

Then, using the canonical representation of the transfer matrix  $W(j\omega)$  [Equation (1.27)]

$$W(j\omega) = C(j\omega)\text{diag}\{q_i(j\omega)\}C^{-1}(j\omega), \quad (5.8)$$

the matrix  $P(j\omega)$  [Equation (5.6)] can be represented, taking into account all of the above, in the form

$$P(j\omega) = C(j\omega)\text{diag}\left\{1 + j\omega\tau q_i(j\omega) + \frac{1}{k_{\max}}\right\}C^{-1}(j\omega). \quad (5.9)$$

Thus, under the stated assumptions, the matrix  $P(j\omega)$  is brought to diagonal form with the help of the similarity transformation through the modal matrix  $C(j\omega)$  of the matrix  $W(j\omega)$ ,

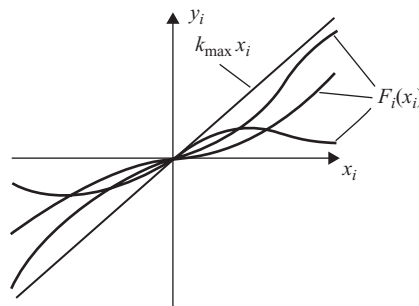


**Figure 5.5** Common sector for nonlinearities.

or, in other words, is brought to diagonal form in the canonical basis of the linear part. The complex-valued eigenvalues  $\gamma_i(j\omega)$  of the matrix  $P(j\omega)$  [Equation (5.9)] are evidently equal to

$$\gamma_i(j\omega) = (1 + j\omega\tau)q_i(j\omega) + \frac{1}{k_{\max}}, \quad i = 1, 2, \dots, N. \quad (5.10)$$

Thus, we have expressed the eigenvalues of the matrix  $P(j\omega)$  [Equation (5.6)] through the CTFs  $q_i(j\omega)$  of the linear part and the parameters  $\tau$  and  $k_{\max}$ . However, the sufficient condition for absolute stability is determined by the eigenvalues of the Hermitian matrix  $\mathbf{Re}P(j\omega)$  [Equation (5.5)], and not by the eigenvalues of  $P(j\omega)$ . Therefore, we have to link together eigenvalues of these two matrices. To this end, we shall use Hirsch's theorem (Bellman 1970; Marcus and Minc 1992), well known in the theory of matrices. According to that theorem, the largest  $\mu_{\max}(\omega)$  and the smallest  $\mu_{\min}(\omega)$  of the eigenvalues  $\mu_i(\omega)$  of a Hermitian matrix represented in the form of Equation (5.5), where the matrix  $P(j\omega)$  is of general type, bound strictly from above and from below the set of  $N$  real-valued numbers  $\text{Re}\{\gamma_i(j\omega)\}$  composed of the real parts of the eigenvalues  $\gamma_i(j\omega)$  of  $P(j\omega)$ :

$$\mu_{\min}(\omega) < \text{Re}\{\gamma_i(j\omega)\} < \mu_{\max}(\omega), \quad i = 1, 2, \dots, N. \quad (5.11)$$

As applied to our case, this means that the plots of  $\text{Re}\{\gamma_i(j\omega)\}$  versus  $\omega$  lie entirely within the region bounded from above and below by the corresponding envelopes of the plots  $\mu_i(\omega)$  (the bold lines in Figure 5.4). As was pointed out above, for the matrix  $\mathbf{Re}P(j\omega)$  to be positive definite, i.e. for the sufficient condition of absolute stability to hold, all eigenvalues  $\mu_i(\omega)$  of the matrix  $\mathbf{Re}P(j\omega)$  must be positive for  $\omega \geq 0$ . It is clear that the necessary condition for that is the positivity of the *least* eigenvalue  $\mu_{\min}(\omega)$ . But, based on Equation (5.11), the value of  $\mu_{\min}(\omega)$  is bounded from above by the numbers  $\text{Re}\{\gamma_i(j\omega)\}$ . Therefore, if some of the numbers  $\text{Re}\{\gamma_i(j\omega)\}$  vanish or are negative at any frequency  $\omega$ , then, from Equation (5.11), it ensues that the same will take place at that very frequency and for  $\mu_{\min}(\omega)$ . Hence, the *necessary* conditions for the positivity of  $\mu_{\min}(\omega)$  for  $\omega \geq 0$  are reduced to the condition for the positivity of real parts of the eigenvalues  $\gamma_i(j\omega)$  [Equation (5.10)], i.e. to the form

$$\text{Re}\{(1 + j\omega\tau)q_i(j\omega)\} + \frac{1}{k_{\max}} \geq \mu_{\min}(\omega) > 0, \quad i = 1, 2, \dots, N. \quad (5.12)$$

This implies that the fact that the condition  $\mathbf{Re}P(j\omega) > 0$  does not hold can be readily established via Equation (5.12), which permits simple and visual geometrical interpretation analogous to that used for the stability analysis of nonlinear SISO systems (Popov 1961). Let us call the complex-valued functions

$$q_i^M(j\omega) = \text{Re}\{q_i^M(j\omega)\} + j\text{Im}\{q_i^M(j\omega)\} = \text{Re}\{q_i(j\omega)\} + j\omega\text{Im}\{q_i(j\omega)\} \quad (5.13)$$

the *modified CTFs* of the linear part. Then, the equation

$$\text{Re}\{(1 + j\omega\tau)q_i(j\omega)\} + \frac{1}{k_{\max}} = \text{Re}\{q_i^M(j\omega)\} - \tau\text{Im}\{q_i^M(j\omega)\} + \frac{1}{k_{\max}} = 0 \quad (5.14)$$

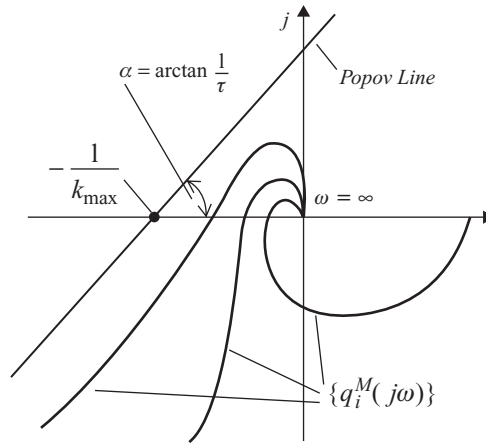


**Figure 5.6** Determination of the necessary conditions for the matrix  $\text{Re}P(j\omega)$  to be positive definite.

defines in the complex plane of the family  $\{q_i^M(j\omega)\}$  a straight line (the *Popov line*) passing through the point  $(-1/k_{\max}, j0)$  and having the slope  $1/\tau$  (Figure 5.6). This enables us to formulate the following criterion:

*In the case of MIMO systems with general linear part, for the matrix  $\text{Re}P(j\omega)$  (5.4) to be positive definite for all  $\omega \geq 0$ , assuming the scalar matrices  $\text{diag}\{1/k_i\} = (1/k_{\max})I$  and  $\text{diag}\{\tau_i\} = \tau I$ , it is necessary (but not sufficient) that all modified characteristic gain loci of the linear part  $q_i^M(j\omega)$  lie to the right of the Popov line.*

Roughly speaking, for the absolute stability of the equilibrium point of the MIMO system with general linear part  $W(s)$ , it is necessary that all  $N$  characteristic systems with the transfer functions of the linear part  $q_i(j\omega)$ , nonlinearities in which are confined by the same sector  $[0, k_{\max}]$  as the nonlinearities  $F_i(x_i)$  in the investigated MIMO system, be absolutely stable. Even if only one of the loci  $q_i^M(j\omega)$  crosses the Popov line [Equation (5.14)], then the sufficient condition for absolute stability does not hold under the stated assumptions. On the other hand, from Equation (5.12), it is clear that the satisfaction of the above geometrical criterion does not yet guarantee absolute stability. Therefore, the procedure of absolute stability analysis is as follows. The Popov line is drawn in the complex plane through the point  $(-1/k_{\max}, j0)$ , at an angle providing the largest distance from the family of modified gain loci  $q_i^M(j\omega)$ . This gives us the ‘best’ value of the sought parameter  $\tau$ . Then, the graphically determined value of  $\tau$  is substituted into the matrix  $P(j\omega)$  [Equation (5.6)], and the positive definiteness of the matrix  $\text{Re}P(j\omega)$  is examined by standard methods. Note that this can readily be performed with the help of the available application packages, such as MATLAB<sup>®</sup>.<sup>4</sup> The examination of the  $q_i^M(j\omega)$  plots also allows one to determine the ‘dangerous’ frequencies, i.e. the frequencies  $\omega$  for which these plots are close to the Popov line, and to check first the condition  $\text{Re}P(j\omega) > 0$  for these frequencies. Intuitively, it is clear that the larger the distance between the Popov line and the modified characteristic gain loci  $q_i^M(j\omega)$ , the higher the probability for the

<sup>4</sup> MATLAB<sup>®</sup> is a registered trademark of The MathWorks, Inc.

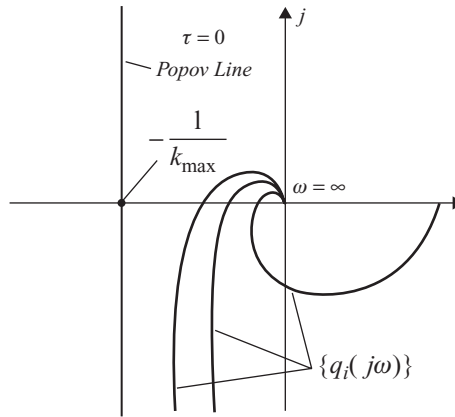


Figure 5.7 Absolute stability analysis for  $\tau = 0$ .

condition  $\text{Re}P(j\omega) > 0$  to hold. Hence, one can purposefully change the form of  $q_i^M(j\omega)$ , in particular, by decreasing the gains, introducing the scalar regulator or any other correction, etc.

It should be noted that in the case of *type-1* MIMO systems, it is possible to use the Popov criterion only if, besides the marginal stability, the *ordinary* characteristic gain loci of the linear part  $q_i(j\omega)$  approach infinity, as  $\omega \rightarrow 0$ , along the negative imaginary axis. If this condition does not hold, then the modified gain loci  $q_i^M(j\omega)$  will tend, as  $\omega \rightarrow 0$ , to  $-\infty$  along a straight line which is parallel to the real axis, and a ‘nonintersecting’ Popov line cannot be obtained for any values of  $\tau$  or  $k_{\max}$ .<sup>5</sup> In the case of *type-1* MIMO systems with rigid cross-connections, including uniform systems, the stated condition corresponds to the absence of complex conjugate eigenvalues of the cross-connections matrix  $R$ . This is the very restriction on the form of the ordinary characteristic gain loci of  $W(j\omega)$  that we pointed out at the beginning of this section. Thus, the described procedure enables the engineer to determine easily an ‘optimal’ value, in a certain sense, of the parameter  $\tau$ , which considerably simplifies the analysis of absolute stability of the MIMO system equilibrium point. For the MIMO system that contains the nonlinear elements with both active and passive hysteresis and/or nonstationary nonlinearities, the parameter  $\tau$  must be zero and, instead of Equation (5.12), we have

$$\text{Re}\{q_i(j\omega)\} + \frac{1}{k_{\max}} \geq \mu_{\min}(\omega) > 0, \quad i = 1, 2, \dots, N. \quad (5.15)$$

The inequalities in Equation (5.15) hold if the *ordinary* characteristic gain loci  $q_i(j\omega)$  of the linear part are situated to the right of the *vertical* line passing through the point  $(-1/k_{\max}, j0)$  (Figure 5.7). Of course, here, there is no problem of determining  $\tau$ , as the only possible value  $\tau = 0$  is predetermined by the types of nonlinearities. However, in this case, the conditions in Equation (5.15) are also necessary and allow, for example, for a given  $W(j\omega)$ , the limiting (maximum) value of  $k_{\max}$  for which the sufficient condition of absolute stability  $\text{Re}P(j\omega) > 0$  does not hold to be readily determined.

<sup>5</sup> See Example 5.1.

### 5.2.2 Application of the Bode diagrams and Nichols plots

Below, we describe the geometrical analogues of multidimensional Popov’s criterion in the above form on the Bode diagrams of the *ordinary* characteristics of the MIMO system linear part, as well as on the plane of the *modified* Nichols plots (Gasparyan 1986). The need for such representations arises due to the wide application of Bode diagrams and Nichols plots in engineering practice. Consider, first, the geometrical interpretation of the inequalities in Equation (5.12) in the complex plane of the ordinary characteristic gain loci  $q_i(j\omega)$ , for  $\tau \neq 0$ . That interpretation is not very significant by itself, but proves to be quite useful for the representation of the Popov line [Equation (5.14)] on the Bode diagrams of the ordinary frequency characteristics of the MIMO system linear part. To this end, rewrite Equation (5.14), taking into account Equation (5.13), in the form

$$\operatorname{Re}\{q_i(j\omega)\} - \omega\tau \operatorname{Im}\{q_i(j\omega)\} + \frac{1}{k_{\max}} = 0, \quad (5.16)$$

i.e. express it through the ordinary characteristic gain loci  $q_i(j\omega)$ . Equation (5.16) describes in the complex plane of the family  $\{q_i(j\omega)\}$  a straight line (for simplicity, we shall also call it the Popov line) which passes through the point  $(-1/k_{\max}, j0)$  and has a slope  $1/\omega\tau$ , depending on the product  $\omega\tau$  (Hsu and Meyer 1968). For different  $\omega = \omega_n$ , the slope of the line in Equation (5.16) will be different (Figure 5.8). Choose, assuming the parameter  $\tau$  to be given, any frequency  $\omega_n$  and mark it at all the loci  $q_i(j\omega)$ . Then, the necessary conditions in Equation (5.12) will hold at the *frequency*  $\omega_n$  if all points at  $q_i(j\omega)$  labelled by  $\omega_n$  are situated to the right of the corresponding Popov line [Equation (5.16)]. This means that we do not put here a requirement that all  $q_i(j\omega)$  wholly lie to the right of the line [Equation (5.16)], and the matter concerns only a set of  $N$  fixed points  $q_i(j\omega_n)$  ( $i = 1, 2, \dots, N$ ). Changing  $\omega = \omega_n$ , one can check the conditions in Equation (5.12) for any other frequencies. Evidently, the described procedure is quite cumbersome, and it complicates the choice of  $\tau$ . Therefore, in practice, they

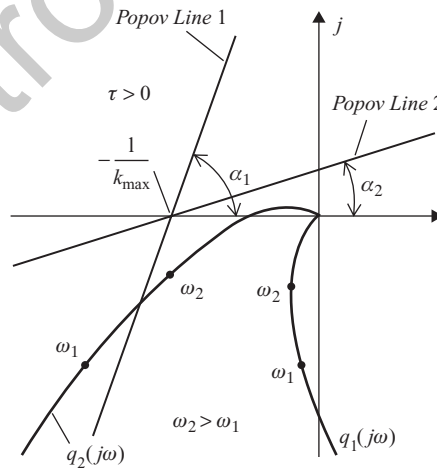


**Figure 5.8** Representation of the Popov line on the plane of the *ordinary* characteristic gain loci of the MIMO system linear part.

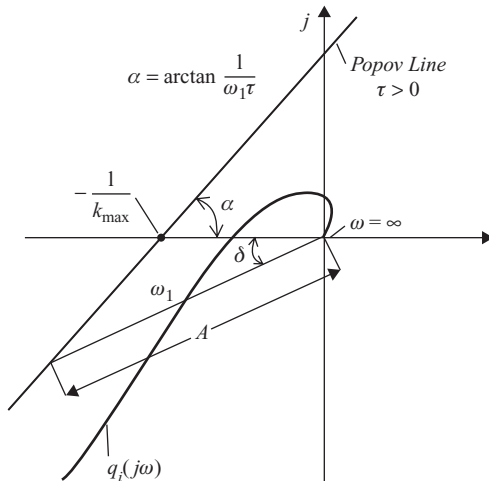


Figure 5.9 Representation of the Popov line on the Bode diagrams.

usually go to the complex plane of the modified loci  $q_i^M(j\omega)$ , where the slope of the Popov line does not depend on the frequency  $\omega$  and is, for  $\tau = const$ , constant. At the same time, the above interpretation permits us to represent easily the Popov line on the Bode diagrams of the CTFs  $q_i(j\omega)$ . Consider Figure 5.9, in which the Popov line [Equation (5.16)] for  $\tau > 0$  and some frequency  $\omega = \omega_1$  is shown. On the same plot, the  $i$ th characteristic gain locus  $q_i(j\omega)$  with the marked point  $\omega = \omega_1$  is qualitatively depicted.

Draw a straight line from the origin of the complex plane through the point  $q_i(j\omega_1)$  until the intersection with the Popov line, and denote by  $A$  the length of the obtained segment. Denote by  $\delta$  the angle that this segment makes with the negative real axis, assuming this angle positive in the anticlockwise direction. From Figure 5.9, it is easy to find

$$A = \frac{\sin(\tan^{-1}(1/\omega_1\tau))}{k_{max} \sin(\tan^{-1}(1/\omega_1\tau) - \delta)}. \tag{5.17}$$

This quantity represents the value of the magnitude  $|q_i(j\omega_1)|$  for a given  $\delta$ , for which the point  $q_i(j\omega_1)$  turns out to be at the Popov line, and such a possibility exists for the values of  $\delta$  that satisfy the inequality

$$-[180^\circ - \tan^{-1}(1/\omega_1\tau)] \leq \delta \leq \tan^{-1}(1/\omega_1\tau). \tag{5.18}$$

Hence, if we have the Bode diagrams of the CTF  $q_i(j\omega)$  of the  $i$ th characteristic system, then, determining at each frequency  $\omega$  the value of  $\delta$ , then calculating the value of  $A$  using Equation (5.17) and marking on the Bode magnitude plot the value  $Lm[A] = 20 \lg A$ , we shall obtain a curve line (the *Popov line*), which is the mapping of the usual Popov line (Figure 5.10). The similar lines can readily be constructed on the Bode magnitude plots of all remaining characteristic systems. If, for the given  $\tau > 0$ , none of the plots  $Lm[q_i(j\omega)]$  ( $i = 1, 2, \dots, N$ ) intersects with its Popov line, then the necessary conditions in Equation (5.12) for the positive definiteness of  $ReP(j\omega)$  hold. It is easy to show that for  $\tau < 0$ , mapping of the Popov line is performed by the same expression [Equation (5.17)], on replacing  $\tau$  by  $-\tau$  and  $-\delta$  by  $+\delta$  in

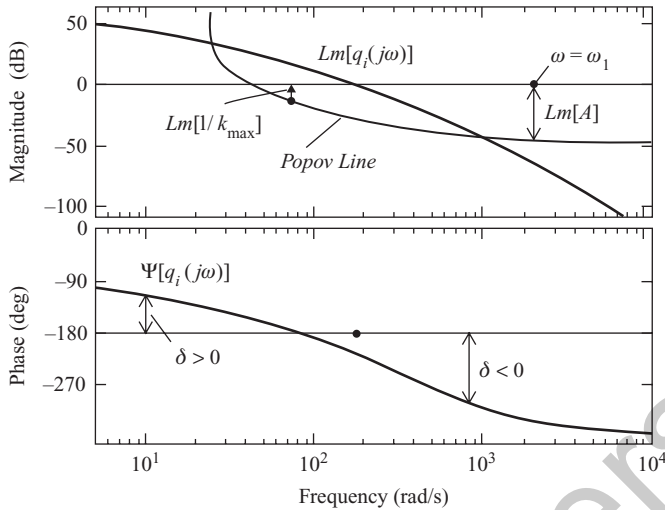


**Figure 5.10** Mapping of the Popov line on the Bode magnitude plot (the frequency  $\omega = \omega_1$  is shown conventionally and does not correspond to Figure 5.9).

it, and preserving the above rule of determining the sign of  $\delta$ . Instead of Equation (5.18), we then have

$$\tan^{-1}(1/\omega_1\tau) \leq \delta \leq [180^\circ - \tan^{-1}(1/\omega_1\tau)]. \quad (5.19)$$

For  $\tau = 0$ , when the slope of the Popov line [Equation (5.16)] is equal to  $90^\circ$  and does not depend on the frequency  $\omega$ , from Equation (5.17), we obtain a simpler formula  $A = 1/k_{\max} \cos \delta$ , known in the classical control theory (Vavilov 1970).

It is clear that the choice of the value of  $\tau$  on the basis of the Bode diagrams is not so evident, since different Popov lines correspond to different values of  $\tau = const$  [they all pass through the point  $(Lm[1/k_{\max}], \delta = 0)$ ], having rather complicated forms, but the advantage of such an approach is that the ordinary, but not the modified, characteristics  $q_i(j\omega)$  are analysed. Note that a distinctive feature of the described technique is that we have, for every  $\tau = const$ , only one Popov line, whereas the methods proposed in Hsu and Meyer (1968), Vavilov (1970), Naumov (1972) and Couros and Goodwin (1973) presume the construction on the Bode diagrams of a parametric family of the lines depending on the product  $\omega\tau$ .

In conclusion, let us consider briefly the question of mapping the Popov line in the plane of modified Nichols plots, i.e. the Nichols plots of the modified CTFs  $q_i^M(j\omega)$ . It is easy to understand that if we replace in Equations (5.17)–(5.19) the product  $\omega_1\tau$  by  $\tau$  and write

$$A = \frac{\sin(\tan^{-1}(1/\tau))}{k_{\max} \sin(\tan^{-1}(1/\tau) - \delta)}, \quad (5.20)$$

where  $-[180^\circ - \tan^{-1}(1/\tau)] \leq \delta \leq \tan^{-1}(1/\tau)$  for  $\tau > 0$  and

$$A = \frac{\sin(\tan^{-1}(1/\tau))}{k_{\max} \sin(\tan^{-1}(1/\tau) + \delta)}, \quad (5.21)$$

where  $\tan^{-1}(1/\tau) \leq \delta \leq [180^\circ - \tan^{-1}(1/\tau)]$  for  $\tau < 0$ , and also replace in Figure 5.9 the ordinary locus  $q_i(j\omega)$  by the modified  $q_i^M(j\omega)$ , then the obtained expressions give the dependence of the magnitude versus the corresponding phase for any point at the Popov line drawn in the complex plane of  $q_i^M(j\omega)$ . This allows the Popov line on the Nichols plots of the modified characteristic loci  $q_i^M(j\omega)$  to be mapped without any difficulty. To illustrate that statement, in Figure 5.11(a), Popov lines for three different values of  $\tau$  ( $\tau = +1, 0, -1$ ) and  $k_{\max} = 1$ , in the complex plane of the modified CTFs  $q_i^M(j\omega)$ , are shown. The corresponding lines on the Nichols plots are represented in Figure 5.11(b). It is interesting to note that, in the Nichols plane, to the same by the absolute value positive and negative parameters  $\tau$  correspond the Popov lines, which are the mirror images of each other with respect to the vertical axis. Also, all Popov lines in Figure 5.11(b) pass through the origin, since  $k_{\max} = 1$  ( $20 \lg k_{\max} = 0$ ).

### 5.2.3 Degree of stability of nonlinear MIMO systems

All of the results of the present section can readily be extended if we follow the standard schemes of the proof (Nelepin 1975; Tsytkin 1977) to the problem of determining the *degree of stability* of nonlinear MIMO systems. Similarly to the SISO case, the nonlinear MIMO system is said to be absolutely stable of degree  $\eta$  if

$$\lim_{t \rightarrow \infty} x_f(t) \exp\{\eta t\} = 0, \tag{5.22}$$

where  $x_f(t)$  is the vector of free motions at the inputs to the MIMO system nonlinearities. This condition implies that the components of the vector  $x_f(t)$  [or its magnitude  $|x_f(t)|$ ] decrease (decreases), tending to the equilibrium point  $x \equiv \mathbf{0}$ , faster than the decaying exponent  $\exp\{-\eta t\}$ .

Let us introduce the notion of the *shifted* (or *expanded*) transfer matrix of the linear part  $W(j\omega - \eta)$  as well as the *shifted* ordinary  $q_i(j\omega - \eta)$  and modified  $q_i^M(j\omega - \eta)$  characteristic gain loci. Then, if the above frequency criteria hold with respect to the shifted characteristics, then it guarantees that the degree of stability of the nonlinear MIMO system is not less than  $\eta$ .

**Example 5.1** As a simple example illustrating the particular features of absolute stability investigation with the help of multidimensional Popov's criterion, consider the two-axis guidance system of Example 1.1, assuming that the transfer functions of separate channels are the same and equal to

$$W(s) = \frac{0.5}{s(s + 0.5)}. \tag{5.23}$$

The angles  $\alpha_1$  and  $\alpha_2$  are given, as in Example 2.6, by two different combinations:  $\alpha_1 = 30^\circ$ ,  $\alpha_2 = 20^\circ$  and  $\alpha_1 = 30^\circ$ ,  $\alpha_2 = -20^\circ$ . For the first combination of  $\alpha_1$  and  $\alpha_2$ , the eigenvalues of the cross-connections matrix  $R$  [Equation (1.60)] are complex conjugate:  $\lambda_{1,2} = 0.9029 \pm j0.4119$ , and, for the second, they are real:  $\lambda_1 = 0.4877$ ,  $\lambda_2 = 1.380$ . Nonlinearities in separate channels are assumed to be single-valued and belonging to the sector  $[0, 0.5]$ . The modified characteristic gain loci of the linear part for the first combination of  $\alpha_1$  and  $\alpha_2$ , as well as the frequency dependences of eigenvalues of the Hermitian matrix  $\mathbf{Re}P(j\omega)$  (5.4), for  $k_{\max} = 0.5$  and  $\tau = 1$ , are shown in Figure 5.12. As can be seen from Figure 5.12(a), as  $\omega \rightarrow 0$ , the loci

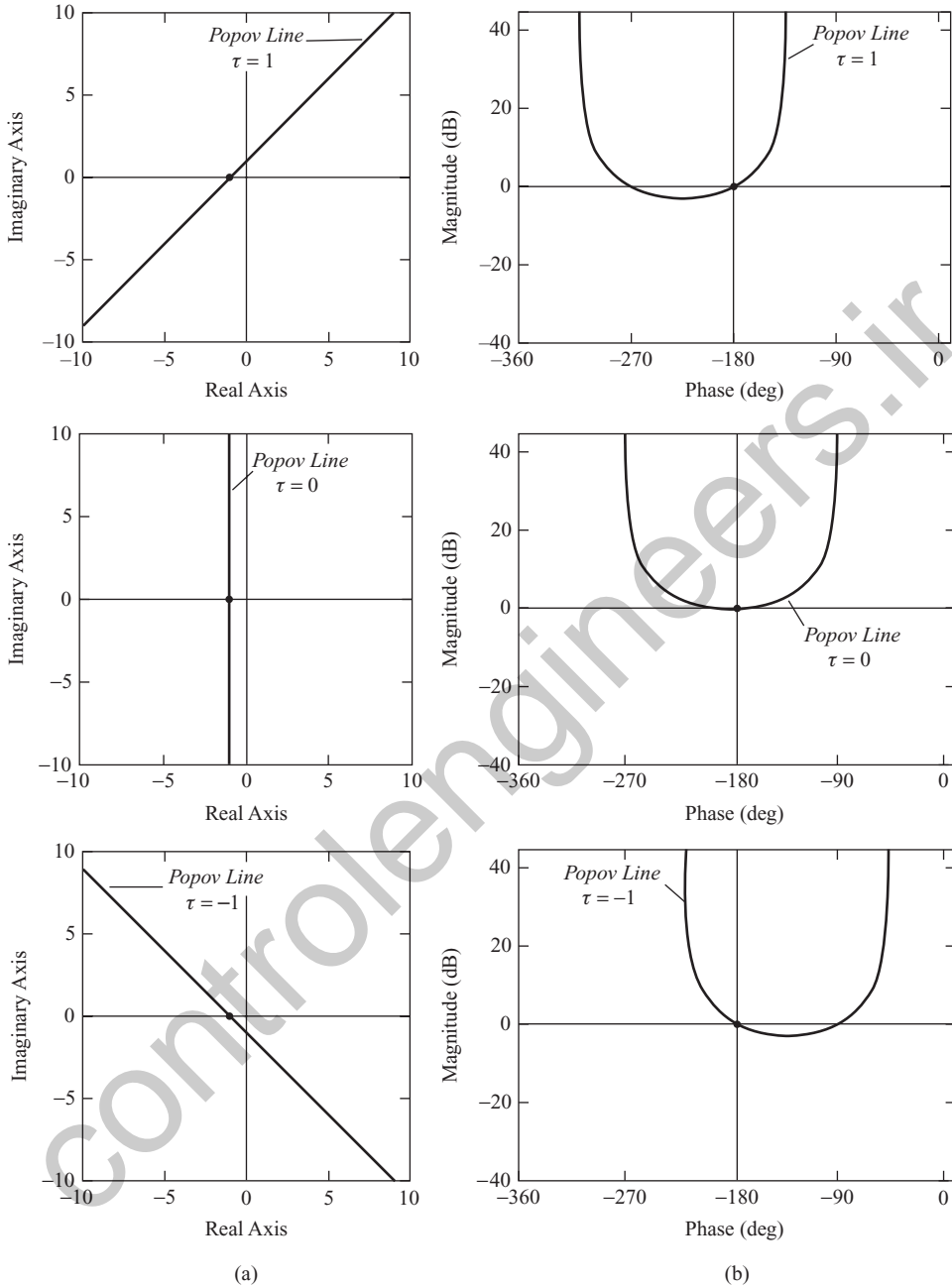


**Figure 5.11** Mapping of the Popov line on the plane of the Nichols plots for different values of the parameter  $\tau$  ( $k_{\max} = 1$ ). (a) Nyquist plane; (b) Nichols plane.

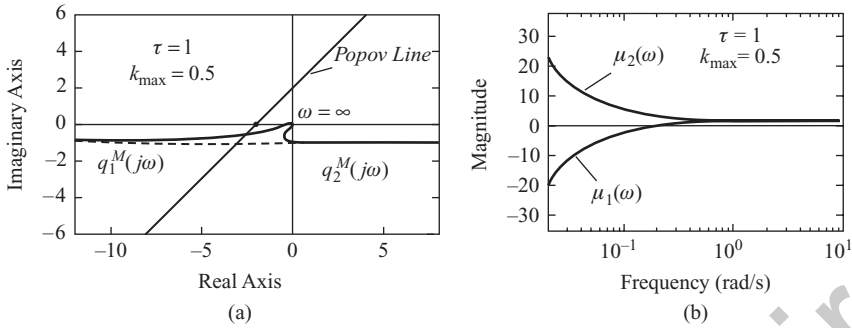


**Figure 5.12** Absolute stability analysis for  $\alpha_1 = 30^\circ$ ,  $\alpha_2 = 20^\circ$ . (a) Modified gain loci and the Popov line; (b) eigenvalues of the matrix  $\mathbf{Re}P(j\omega)$ .

$q_1^M(j\omega)$  and  $q_2^M(j\omega)$  tend respectively to  $-\infty$  and  $+\infty$  along the horizontal (dashed) line located in the lower half-plane at the unit distance from the real axis. Apparently, the Popov line will intersect the plot of  $q_1^M(j\omega)$  for any final values of  $k_{\max}$  and  $\tau$ , i.e. in this case (for the complex eigenvalues of the matrix  $R$ ), in principle, Popov's criterion cannot give an answer about the absolute stability.

The corresponding constructions in the planes of the Bode diagrams and Nichols plots are given in Figure 5.13. Note that on the Bode magnitude plots, we have only one representation of the Popov line corresponding to the first characteristic system, since, for the second system, the phase characteristic  $\Psi[q_2(j\omega)]$  does not satisfy, for  $\tau = 1$ , the inequality in Equation (5.18). The Nyquist plots of the modified characteristic gain loci  $q_1^M(j\omega)$  and  $q_2^M(j\omega)$  of the same system for the second combination of  $\alpha_1$  and  $\alpha_2$ , i.e. for the case of real eigenvalues of  $R$ , are shown in Figure 5.14(a) and (b), and the Nichols plots are given in Figure 5.14(c) [the plots of  $q_1^M(j\omega)$  and  $q_2^M(j\omega)$  here practically coincide]. The start points (for  $\omega = 0$ ) of both loci  $q_1^M(j\omega)$  and  $q_2^M(j\omega)$  in this case are finite and, therefore, there is no problem in finding 'nonintersecting' Popov lines (any Popov line with  $\tau > 0.5$  does not intersect the modified gain loci of the linear part). However, the eigenvalues of the Hermitian matrix  $\mathbf{Re}P(j\omega)$  [Equation (5.5)] prove to be

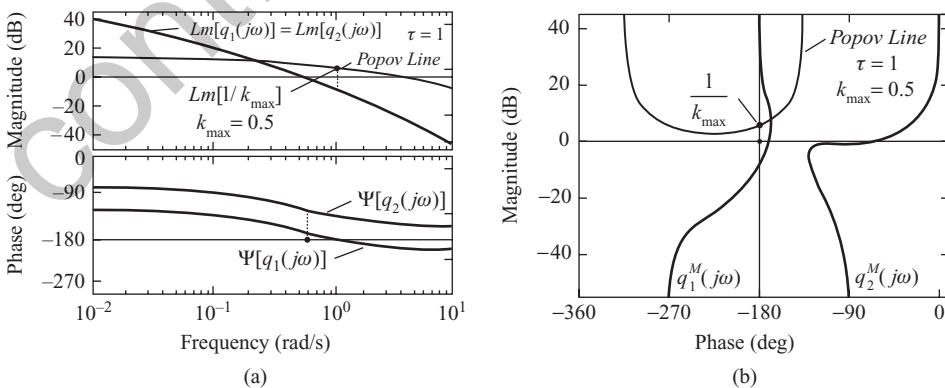


**Figure 5.13** Absolute stability analysis for  $\alpha_1 = 30^\circ$ ,  $\alpha_2 = 20^\circ$ . (a) Bode diagrams of the ordinary gain loci  $q_i(j\omega)$ ; (b) Nichols plots of the modified gain loci  $q_i^M(j\omega)$ .

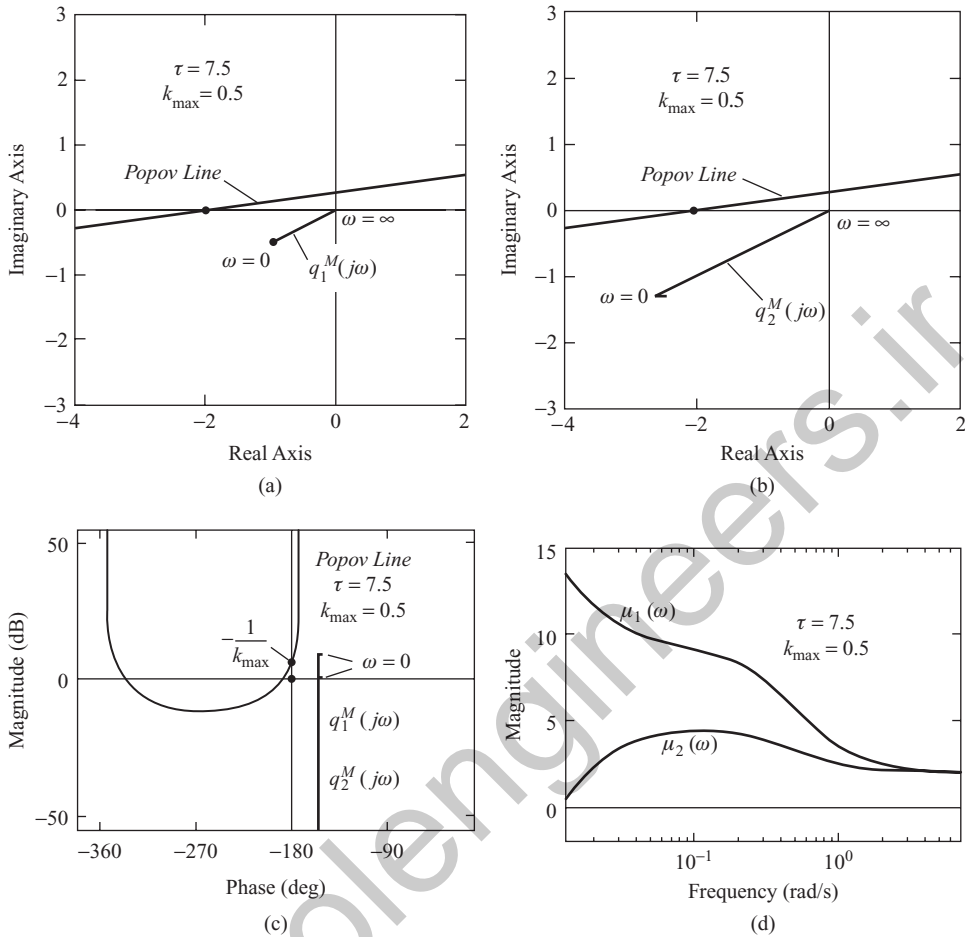


**Figure 5.14** Absolute stability analysis for  $\alpha_1 = 30^\circ$ ,  $\alpha_2 = -20^\circ$ . (a) First characteristic system; (b) second characteristic system; (c) Nichols plots; (d) eigenvalues of the matrix  $\mathbf{Re}P(j\omega)$ .

positive for all  $\omega \geq 0$  only for  $\tau > 6.95$ . The Popov lines in Figure 5.14(a)–(c) are drawn for  $\tau = 7.5$ , and the corresponding eigenvalues  $\mu_1(\omega)$  and  $\mu_2(\omega)$  of  $\mathbf{Re}P(j\omega)$  are shown in Figure 5.14(d). Thus, in the case of real eigenvalues of the cross-connections matrix  $R$ , the application of multidimensional Popov’s criterion has allowed us to establish the absolute stability of the equilibrium point for the discussed uniform guidance system.

### 5.3 ABSOLUTE STABILITY OF NORMAL MIMO SYSTEMS

In Section 5.2, we discussed the absolute stability of nonlinear MIMO systems with general linear part. We have shown that for such systems, the *necessary* conditions for the Hermitian matrix  $\mathbf{Re}P(j\omega)$  [Equation (5.5)] to be positive definite consist in the satisfaction of classical Popov’s criterion as applied to each of  $N$  characteristic systems with nonlinearities in the sector

$[0, k_{\max}]$ , to which *all* nonlinearities  $F_i(x_i)$  of the MIMO system belong. Therefore, having chosen the ‘needed’ slope of the Popov line in the complex plane of the modified characteristic loci  $q_i^M(j\omega)$  for the general MIMO system, i.e. having determined the unknown parameter  $\tau$  in the matrix  $P(j\omega)$  [Equation (5.9)], we must also check the satisfaction of the condition  $\mathbf{Re}P(j\omega) > 0$  for all  $\omega \geq 0$  by the common methods.

Let us proceed now to the study of absolute stability for the important class of MIMO systems with *normal* transfer matrices of the linear part  $W(s)$ , i.e. with matrices  $W(s)$  that commute with their conjugate  $W^*(s)$  and have orthonormal canonical bases. Recall that systems with circulant and anticirculant, symmetrical and antisymmetrical, unitary and some other types of  $W(s)$  belong to normal systems, i.e. a great deal of the real multivariable systems described in the technical literature. Owing to the normality of the matrix  $W(j\omega)$ , the modal matrix  $C(j\omega)$  in Equations (5.8) and (5.9) is *unitary* [ $C^{-1}(j\omega) = C^*(j\omega)$ ]. Then, substituting the canonical representation of the normal matrix  $W(j\omega)$  into Equation (5.9) shows that the matrix  $P(j\omega)$  also belongs to normal:

$$P(j\omega) = C(j\omega) \text{diag} \{ \gamma_i(j\omega) \} C^*(j\omega), \quad (5.24)$$

where the eigenvalues  $\gamma_i(j\omega)$  of  $P(j\omega)$  are given by Equation (5.10).

In Hirsch’s theorem (Bellman 1970; Marcus and Minc 1992), on which the results of the preceding section were based, it is stated that if a *Hermitian* matrix  $\mathbf{Re}P(j\omega)$  is represented in the form of Equation (5.5), where  $P(j\omega)$  is *normal*, then the following inequalities take place:

$$\mu_{\min}(\omega) \leq \mathbf{Re}\{ \gamma_i(j\omega) \} \leq \mu_{\max}(\omega), \quad i = 1, 2, \dots, N, \quad (5.25)$$

where  $\mu_{\max}(\omega)$  and  $\mu_{\min}(\omega)$  are the largest and the smallest eigenvalues of  $\mathbf{Re}P(j\omega)$ . These inequalities mean that the envelopes from above and below of the frequency dependences  $\mathbf{Re}\{ \gamma_i(j\omega) \}$  coincide with the corresponding envelopes of the eigenvalues  $\mu_i(\omega)$  of  $\mathbf{Re}P(j\omega)$  (Figure 5.4). It can also be said that at any frequency  $\omega \geq 0$ , two such complex-valued eigenvalues of  $P(j\omega)$  always exist that the real parts of them are *equal* to the largest and the smallest eigenvalues of the Hermitian matrix  $\mathbf{Re}P(j\omega)$ . Moreover, substituting the canonical representation in Equation (5.24) of  $P(j\omega)$  into Equation (5.5), we obtain

$$\begin{aligned} \mathbf{Re}P(j\omega) &= \frac{1}{2} [ C(j\omega) \text{diag} \{ \gamma_i(j\omega) \} C^*(j\omega) + (C^*(j\omega))^* \text{diag} \{ \bar{\gamma}_i(j\omega) \} C^*(j\omega) ] \\ &= C(j\omega) \text{diag} \{ \mathbf{Re}\{ \gamma_i(j\omega) \} \} C^*(j\omega), \end{aligned} \quad (5.26)$$

from which it is evident that the matrix  $\mathbf{Re}P(j\omega)$  is brought to diagonal form in the same canonical basis as the matrices  $W(j\omega)$  and  $P(j\omega)$ , and its eigenvalues  $\mu_i(\omega)$  ( $i = 1, 2, \dots, N$ ) are identically equal to the real parts of the corresponding eigenvalues  $\gamma_i(j\omega)$  of  $P(j\omega)$ . Hence, the *necessary and sufficient* conditions for the matrix  $\mathbf{Re}P(j\omega)$  to be positive definite, which consists in the positivity of all its eigenvalues  $\mu_i(\omega)$  for  $\omega \geq 0$ , in the case of normal MIMO systems, accept, taking into account Equations (5.24) and (5.26), the form

$$\mathbf{Re}\{ (1 + j\omega\tau) q_i(j\omega) \} + \frac{1}{k_{\max}} > 0 \quad i = 1, 2, \dots, N \quad (5.27)$$

and are directly expressed through the characteristic gain loci  $q_i(j\omega)$  of the linear part (Gasparyan 1986). From here, we come to an extremely important conclusion that for absolute

stability of the equilibrium point of the MIMO system with normal  $W(s)$ , it is *sufficient* that there exist such a real scalar  $\tau$ , for which the inequalities in Equation (5.27) hold for all  $\omega \geq 0$ . In other words, for absolute stability of the MIMO system with a normal linear part, it is sufficient that the usual Popov's criterion holds for all SISO characteristic systems with the transfer functions  $q_i(j\omega)$  and with the nonlinearities satisfying the same sector restriction  $[0, k_{\max}]$  as the nonlinearities of the MIMO system. Recall once more that in the case of general MIMO systems, the satisfaction of the conditions in Equation (5.27) is necessary but does not guarantee the absolute stability of the equilibrium point. Thus, the investigation of the absolute stability of normal systems proves to be considerably simpler than that for general MIMO systems; it can be performed completely via the ordinary or modified characteristic gain loci of the linear part. In the discussed case, the multidimensional Popov's criterion preserves the same form, including the geometrical form, as the conventional Popov's criterion in the classical control theory.<sup>6</sup> Note especially how easy that task can be solved for circulant and anticirculant systems, including simple symmetrical systems, as well as uniform systems with normal cross-connections matrices, since, in all these cases, the CTFs  $q_i(j\omega)$  in Equation (5.27) are expressed in analytical form for any number  $N$  of the system channels.

### 5.3.1 Generalized Aizerman's hypothesis

For normal systems, not only the sufficient, but also the necessary conditions for absolute stability of the equilibrium point can sometimes be established (Gasparyan 1986). In such cases, the generalized 'multidimensional' Aizerman's hypothesis must hold, formulated as follows. Assume that the MIMO system in Figure 5.3 has a stable normal linear part  $W(s)$ . Replace the nonlinear diagonal block  $\text{diag}\{F_i(x_i)\}$  by a *linear* one described by a scalar matrix  $kI$ . Then, the open-loop transfer matrix of the linearized MIMO system is  $kW(s)$ , and the closed-loop system will be stable for those values of  $k$  for which none of the characteristic gain loci  $q_i(j\omega)$  ( $i = 1, 2, \dots, N$ ) of the initial linear part encloses the critical point  $(-1/k, j0)$  in the complex plane [Figure 5.15(a)]. Evidently, the same statement is also valid for the modified loci  $q_i^M(j\omega)$ <sup>7</sup> [Figure 5.15(b)]. It is clear that the left-most of the intersection points of  $q_i(j\omega)$  or  $q_i^M(j\omega)$  with the negative real axis gives the marginal value  $k = k_{\max}$  for which the linearized normal MIMO system is on the stability boundary. That marginal value  $k_{\max}$  determines the *Hurwitz angle (sector)*  $[0, k_{\max}]$  for the linearized MIMO system, i.e. the admissible gains  $k$  in the separate channels, from the point of view of stability in the linear approximation. Now, let us draw the Popov line in the plane of the family  $\{q_i^M(j\omega)\}$  in such a manner that it is tangent to the utmost characteristic gain locus at the point of its intersection with the real negative axis (that point has the coordinates  $-1/k_{\max}, j0$ ) [Figure 5.15(b)]. Then, if all of the modified loci are located to the right of the Popov line, then this yields the *necessary and sufficient* conditions for absolute stability of the normal MIMO system whose nonlinearities belong to the Hurwitz sector  $[0, k_{\max}]$ . Indeed, in the described case, coincidence of the *Hurwitz sector* with the *Popov sector* is provided, since, for  $k > k_{\max}$ , the linearized MIMO system becomes unstable and, for the nonlinear characteristics belonging to the sector  $[0, k_{\max}]$ , the sufficient condition

<sup>6</sup> Further, we shall see that this conclusion is also valid for the off-axis and parabolic criteria of absolute stability, and for the circle criteria, including the circle criteria of absolute stability of *forced* motions of normal MIMO systems.

<sup>7</sup> Recall that the intersection points of the characteristic gain loci  $q_i(j\omega)$  and  $q_i^M(j\omega)$  with the negative real axis coincide.

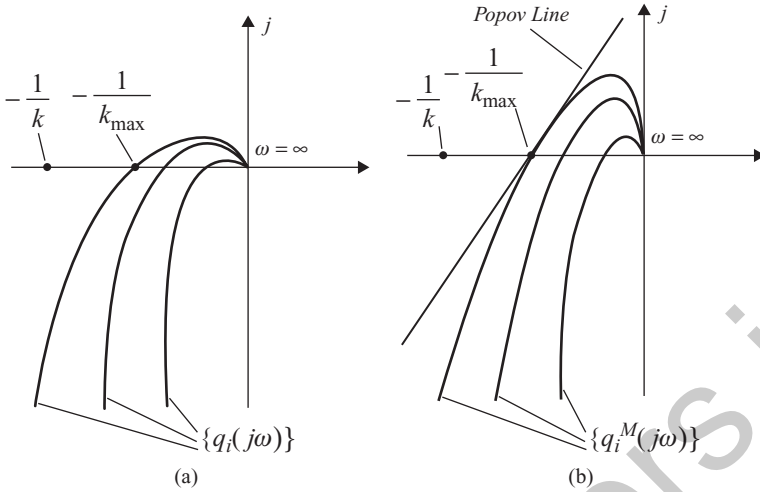


**Figure 5.15** Determination of the necessary and sufficient conditions for absolute stability of normal MIMO systems. (a) Ordinary characteristic gain loci; (b) modified characteristic gain loci.

for absolute stability holds. Therein lies the generalization of the well known Aizerman's hypothesis (Aizerman 1949; Voronov 1979) to the multidimensional case.

If it is impossible to draw the *marginal tangent* to the family  $\{q_i^M(j\omega)\}$ , i.e. the tangent to the utmost modified characteristic gain locus at the point of its intersection with the real axis, where all  $q_i^M(j\omega)$  are located to the right of that tangent, then the admissible Popov angle is smaller than the Hurwitz angle. Correspondingly, the conditions for absolute stability are only sufficient (Figure 5.16).

In essence, the investigation of the absolute stability of normal systems that satisfy the generalized Aizerman's hypothesis is reduced to the investigation of the linearized MIMO

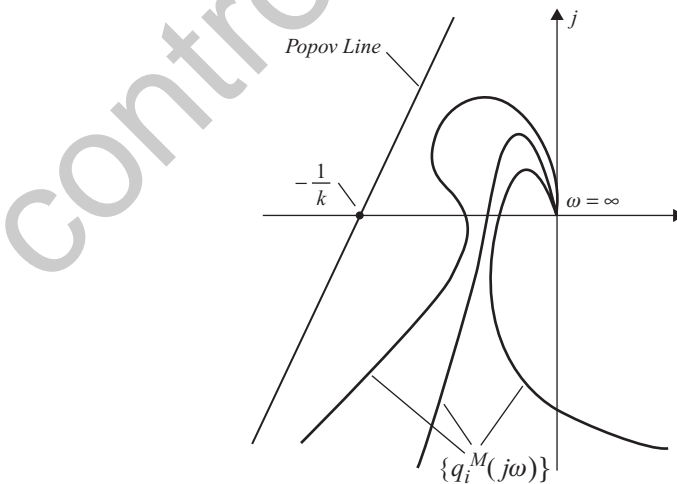


**Figure 5.16** The case in which it is impossible to draw the marginal Popov line.

system and is performed by linear methods. It should be emphasized that the above conclusions have become possible due to the normality of the MIMO system linear part, since, for general MIMO systems, the geometrical constructions in the plane of the modified characteristic gain loci  $q_i^M(j\omega)$  give only necessary but not sufficient conditions for the matrix  $\mathbf{Re}P(j\omega)$  [Equation (5.5)] to be positive definite.

**Example 5.2** Let us consider the application of Aizerman’s hypothesis in simple examples of two-dimensional normal uniform systems, i.e. the systems with identical transfer functions of the channels and rigid cross-connections described by normal matrices. The transfer function of the system channels is of *type zero* and has the form

$$w(s) = \frac{20}{(s + 0.5)(s + 0.7)(s + 2)} \tag{5.28}$$

and the matrix of cross-connections is given in two forms:

$$R_{Sym} = \begin{pmatrix} 1 & 0.6 \\ 0.6 & 1 \end{pmatrix}, \quad R_{Asym} = \begin{pmatrix} 1 & 0.6 \\ -0.6 & 1 \end{pmatrix}, \tag{5.29}$$

where the symmetrical matrix  $R_{Sym}$  has real eigenvalues  $\lambda_1 = 1.6, \lambda_2 = 0.4$ , and the eigenvalues of the antisymmetrical matrix  $R_{Asym}$  are complex conjugate:  $\lambda_1 = 1 + j0.6, \lambda_2 = 1 - j0.6$ .

The ordinary and modified (represented by the dashed and solid lines, respectively) characteristic gain loci of the system with the symmetrical matrix  $R_{Sym}$  in Equation (5.29) are shown in Figure 5.17(a). The enlarged modified loci of the same system, with the marginal Popov line at the point  $(-3.95, j0)$ , are given in Figure 5.17(b). Hence, for the discussed uniform system with symmetrical cross-connections, the necessary and sufficient conditions of absolute stability hold in the sector  $[0, 0.2534]$ . Similar plots for the uniform system with the antisymmetrical matrix of cross-connections  $R_{Asym}$  are given in Figure 5.18, from which it is evident that in the case of complex conjugate eigenvalues of  $R_{Asym}$ , the necessary and sufficient conditions for absolute stability also hold, but the ‘admissible’ sector  $[0, 0.1439]$  here is about twice as narrow.

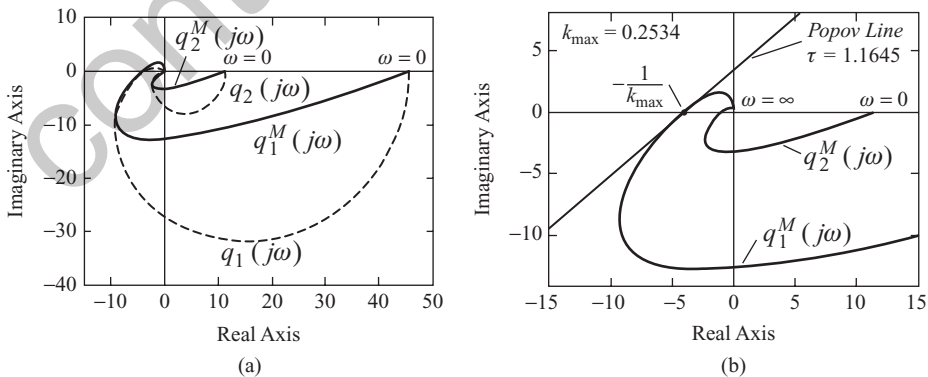


**Figure 5.17** Investigation of the absolute stability of the symmetrical uniform system. (a) Characteristic gain loci of the linear part; (b) modified loci with the marginal Popov line.

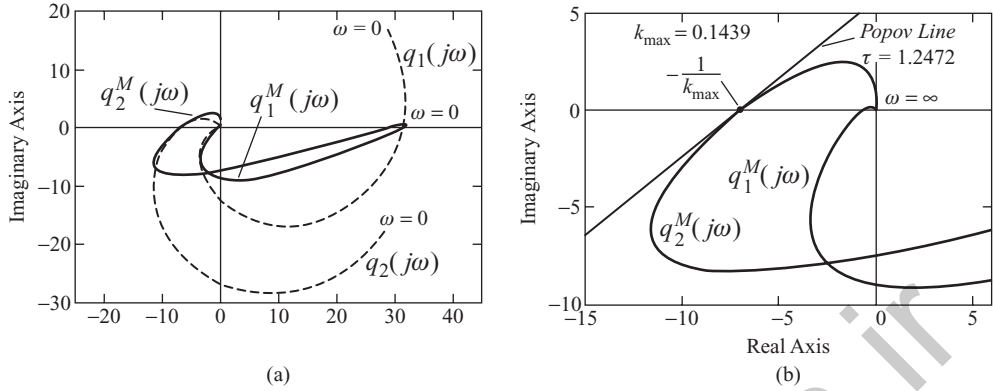


**Figure 5.18** Investigation of the absolute stability of the antisymmetrical uniform system. (a) Characteristic gain loci of the linear part; (b) modified loci with the marginal Popov line.

## 5.4 OFF-AXIS CIRCLE AND PARABOLIC CRITERIA OF THE ABSOLUTE STABILITY OF MIMO SYSTEMS

In this section, we shall focus on the asymptotic behaviour of nonlinear MIMO systems of a broader class, namely MIMO systems with unstable and ‘conditionally stable’ linear part  $W(s)$ . Further, under conditionally stable, we shall assume the transfer matrices  $W(j\omega)$ , some (or all) characteristic gain loci  $q_i(j\omega)$  of which have a ‘beak-shaped’ form (Figure 5.19). If we replace in such MIMO systems the nonlinear block  $\text{diag}\{F_i(x_i)\}$  by a linear  $\alpha I$ , where  $\alpha$  is a scalar with unit nominal value, then the CTFs  $q_i(j\omega)$  of the linear part are multiplied by the same scalar  $\alpha$ . As a result, both an increase and a decrease in  $\alpha$  lead to instability of the closed-loop linear MIMO system. To embrace these situations in the analysis of absolute stability, we should replace the conditions of belonging the characteristics  $F_i(x_i)$  to sectors

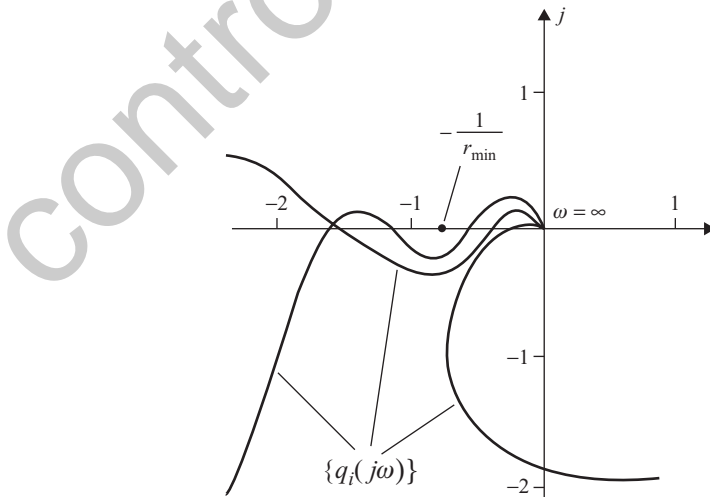


**Figure 5.19** MIMO system with the conditionally stable linear part.

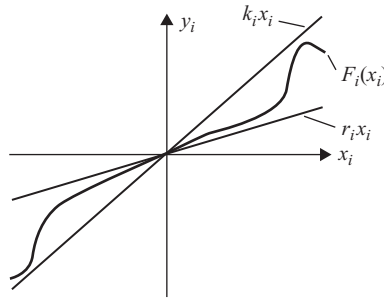


Figure 5.20 Sectoral restrictions of the nonlinear MIMO system.

$[0, k_i]$ , as they were in Section 5.2, by the conditions of belonging to sectors  $[r_i, k_i]$ , where  $r_i$  are some positive finite numbers<sup>8</sup> (Figure 5.20), i.e. we should introduce, instead of the inequalities in Equation (5.4), the following:

$$r_i \leq \frac{F_i(x_i)}{x_i} \leq k_i, \quad i = 1, 2, \dots, N. \quad (5.30)$$

The need for such restrictions is due to the fact that the linearized closed-loop MIMO system with unstable or conditionally stable linear part, which is obtained from the nonlinear system by replacing the nonlinear elements  $F_i(x_i)$  with the linear  $r_i x_i$ , will be unstable for sufficiently small  $r_i$ . The latter excludes the possibility of the initial MIMO system's being absolutely stable. Let us define, as in Section 5.2, a sector  $[r_{\min}, k_{\max}]$  confining *all* characteristics  $F_i(x_i)$ :

$$r_{\min} \leq \frac{F_i(x_i)}{x_i} \leq k_{\max}, \quad i = 1, 2, \dots, N, \quad (5.31)$$

where the numbers  $r_{\min}$  and  $k_{\max}$  are determined from the evident conditions  $r_{\min} = \min(r_i)$  and  $k_{\max} = \max(k_i)$ .

### 5.4.1 Off-axis circle criterion

Assume that the transfer matrix  $W(s)$  with negative feedback introduced around it via the scalar matrix  $r_{\min} I$  is stable, i.e. the characteristic gain loci  $q_i(j\omega)$  either do not encircle the point  $(-1/r_{\min}, j0)$ , in the case of conditionally stable  $W(s)$  (Figure 5.19) or the total sum of anticlockwise encirclements of that point is equal to  $\ell/2$ , where  $\ell$  is the number of unstable poles of  $W(s)$ . Then, we can use the equivalent transformation of the MIMO system block diagram represented in Figure 5.21 (Gasparyan 1986). The transfer matrix of the transformed linear part  $W_T(s)$  indicated in Figure 5.21 by the dashed line is stable under the above assumption, and is described by the expression

$$W_T(s) = [I + r_{\min} W(s)]^{-1} W(s). \quad (5.32)$$

<sup>8</sup> The cases of negative  $r_i$  and  $k_i$ , discussed in Nelepin (1975), are not so significant in engineering practice and, therefore, are omitted. Besides, the results presented further can be readily extended to these cases.

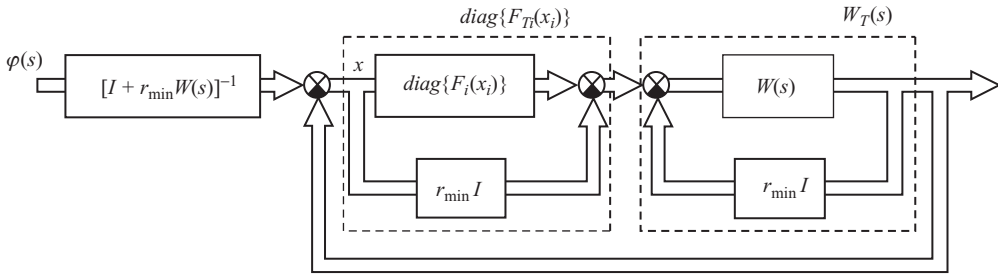


Figure 5.21 Transformed matrix block diagram of the MIMO system.

The characteristics of the transformed nonlinear elements  $F_{Ti}(x_i)$  are

$$F_{Ti}(x_i) = F_i(x_i) - r_{\min}x_i \tag{5.33}$$

and satisfy the following inequalities:

$$0 \leq \frac{F_{Ti}(x_i)}{x_i} \leq k_{\max} - r_{\min}, \quad i = 1, 2, \dots, N \tag{5.34}$$

i.e. lie in the sector  $[0, k_{\max} - r_{\min}]$ .

Hence, all the conditions of applicability of Popov’s criterion in the form discussed in Section 5.2 hold with respect to the transformed MIMO system in Figure 5.21. The transfer matrix  $W_T(s)$  [Equation (5.32)] has the canonical representation

$$W_T(j\omega) = C(j\omega) \text{diag}\{q_{Ti}(j\omega)\}C^{-1}(j\omega), \tag{5.35}$$

where

$$q_{Ti}(j\omega) = \frac{q_i(j\omega)}{1 + r_{\min}q_i(j\omega)}, \quad i = 1, 2, \dots, N \tag{5.36}$$

are the *stable* CTFs of the *transformed* linear part, and  $q_i(j\omega)$  and  $C(j\omega)$  are the CTFs and the modal matrix of the *initial* linear part, respectively. Then, the matrix  $P(j\omega)$  [Equation (5.9)] can be represented, allowing for Equation (5.36), in the form

$$P(j\omega) = C(j\omega) \text{diag} \left\{ (1 + j\omega\tau) \frac{q_i(j\omega)}{1 + r_{\min}q_i(j\omega)} + \frac{1}{k_{\max} - r_{\min}} \right\} C^{-1}(j\omega) \tag{5.37}$$

The necessary conditions [Equation (5.12)] for positive definiteness of  $\mathbf{Re}P(j\omega)$  [Equation (5.5)] accept the following form:

$$\mathbf{Re} \left\{ (1 + j\omega\tau) \frac{q_i(j\omega)}{1 + r_{\min}q_i(j\omega)} \right\} + \frac{1}{k_{\max} - r_{\min}} > 0, \quad i = 1, 2, \dots, N. \tag{5.38}$$

According to Equation (5.38), for the condition  $\mathbf{Re}P(j\omega) > 0$  to hold, it is necessary that there exist such a real number  $\tau$  that, for  $\omega \geq 0$ , all modified loci  $q_{Ti}^M(j\omega)$  of the transformed linear part  $W_T(j\omega)$  lie in the complex plane to the right of the Popov line passing through the point

$(-1/[k_{\max} - r_{\min}], j0)$  at the angle  $\tan^{-1}(1/\tau)$  to the real axis. The admissible range of values for the parameter  $\tau$  depends, as always, on the types of nonlinear elements.

The inequalities in Equation (5.38) are not so convenient for practical use, since they are expressed through the characteristic gain loci of the transformed rather than the initial linear part. Therefore, let us discuss another approach which allows the absolute stability analysis to be conducted directly through the characteristic gain loci  $q_i(j\omega)$  of the initial linear part, and which results in the generalization to the multidimensional case of the off-axis circle criterion (Hsu and Meyer 1968). Having determined the real parts in Equation (5.38), we can obtain, instead of Equation (5.38), after some simple algebraic transformations,

$$\left[ \operatorname{Re}\{q_i(j\omega)\} + \frac{k_{\max} + r_{\min}}{2k_{\max}r_{\min}} \right]^2 + \left[ \operatorname{Im}\{q_i(j\omega)\} + \omega\tau \frac{k_{\max} - r_{\min}}{2k_{\max}r_{\min}} \right]^2 > R^2(\omega), \quad i = 1, 2, \dots, N \quad (5.39)$$

where

$$R(\omega) = \frac{\sqrt{1 + \omega^2\tau^2}}{2} \left( \frac{1}{r_{\min}} - \frac{1}{k_{\max}} \right). \quad (5.40)$$

However, replacing the sign  $>$  by the sign of equality in Equation (5.39), we come to an equation of the circle in the complex plane of  $\{q_i(j\omega)\}$ , having its centre at the point  $U(\omega)$  with the coordinates

$$\operatorname{Re}\{U(\omega)\} = -\frac{1}{2} \left( \frac{1}{r_{\min}} + \frac{1}{k_{\max}} \right), \quad \operatorname{Im}\{U(\omega)\} = \frac{\omega\tau}{2} \left( \frac{1}{r_{\min}} - \frac{1}{k_{\max}} \right) \quad (5.41)$$

and radius  $R(\omega)$  (5.40).<sup>9</sup> Both the centre  $U(\omega)$  and the radius  $R(\omega)$  of the circle are functions of the frequency  $\omega$ , and, regardless of its value, all circles intersect the real axis at the points  $-1/r_{\min}$  and  $-1/k_{\max}$  (Figure 5.22). The angular coefficients of the tangents to the circles at these points are equal to  $-1/\omega\tau$  and  $1/\omega\tau$ , i.e. the tangent at the point  $-1/k_{\max}$  coincides with the Popov line [Equation (5.16)]. Now, we can give the following geometrical interpretation of the conditions in Equation (5.38) in the complex plane of  $\{q_i(j\omega)\}$ . For the Hermitian matrix  $\operatorname{Re}P(j\omega)$  [Equation (5.5)] to be positive definite at some frequency  $\omega_n$  and a given value  $\tau = \text{const}$ , it is necessary (but generally not sufficient) that the set of  $N$  points at the loci  $q_i(j\omega)$  marked by the frequency  $\omega_n$  be located outside the corresponding circle [Equation (5.39)] having its centre at  $U(\omega_n)$  and radius  $R(\omega_n)$  (see Figure 5.22). In other words, for the above condition to hold, it is necessary that the common off-axis criterion (Hsu and Meyer 1968) hold for each of  $N$  SISO characteristic systems. If it takes place for all  $\omega \geq 0$ , then the necessary conditions in Equation (5.38) hold, and one has only to check the condition  $\operatorname{Re}P(j\omega) > 0$  with the help of customary methods, in particular, by calculating the frequency dependencies of eigenvalues of  $\operatorname{Re}P(j\omega)$ . The choice of the appropriate value of the parameter  $\tau$  in this case is accomplished, as in the SISO case, by successive iterations.

Evidently, if the transfer matrix of the linear part  $W(s)$  is normal, i.e. it commutes with its conjugate matrix  $W^*(s)$ , then, as shown in Section 5.3, the obtained necessary geometrical criterion is also *sufficient*, and there is no need for any additional verification of the condition  $\operatorname{Re}P(j\omega) > 0$ .

<sup>9</sup> For brevity, we shall call Equation (5.39) the equation of the off-axis circle.

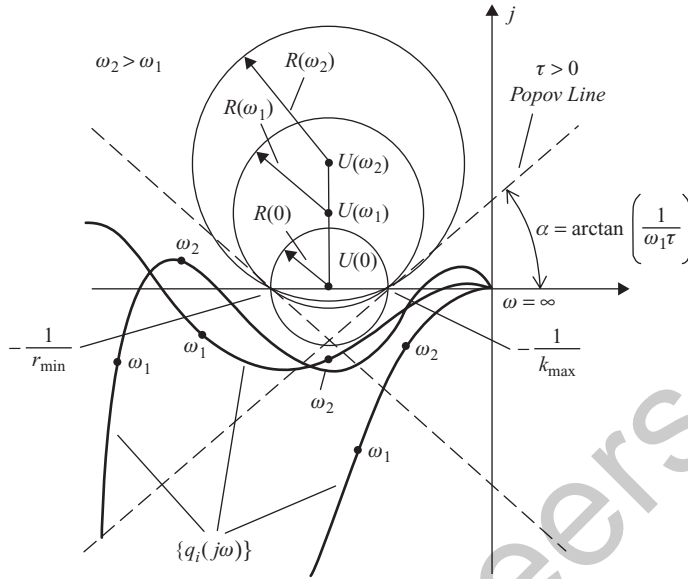


Figure 5.22 Off-axis circles for different frequencies  $\omega$ .

It should be noted that the choice of  $\tau$  in the complex plane of  $\{q_i(j\omega)\}$  is not as trivial as in the plane of the modified loci  $q_{Ti}^M(j\omega)$ , where the slope of the Popov line does not depend on the frequency  $\omega$ . On the other hand, judging from the form of  $q_{Ti}^M(j\omega)$ , it is not always easy to decide how we should change the actual transfer matrix  $W(j\omega)$  based on the conditions for absolute stability. In this respect, the discussed constructions and analysis in the plane of the initial characteristic gain loci  $q_i(j\omega)$  possess a certain advantage.

**Example 5.3** Let us examine, using the off-axis circle criterion, the absolute stability of the three-dimensional uniform system with the nonlinearities in the sector  $[0.3, 1]$ , and the following transfer function of separate channels:

$$w(s) = \frac{600000000(s+3)}{s(s+0.33)(s+400)^2(s+500)}. \quad (5.42)$$

The matrix of cross-connections  $R$  in the linear part is given as

$$R = \begin{pmatrix} 0.9 & 0.3 & -0.01 \\ -0.05 & 0.866 & 0.5 \\ 0.02 & -0.5 & 0.866 \end{pmatrix}. \quad (5.43)$$

This matrix has one real and two complex conjugate eigenvalues:

$$\lambda_1 = 0.9084, \quad \lambda_2 = 0.8618 + j0.5153, \quad \lambda_3 = 0.8618 - j0.5153. \quad (5.44)$$

The characteristic gain loci  $q_i(j\omega) = \lambda_i w(j\omega)$  of the initial linear part are shown in Figure 5.23(a) and (b), in which off-axis circles [Equation (5.39)] for  $\tau = 0.3$  and two different

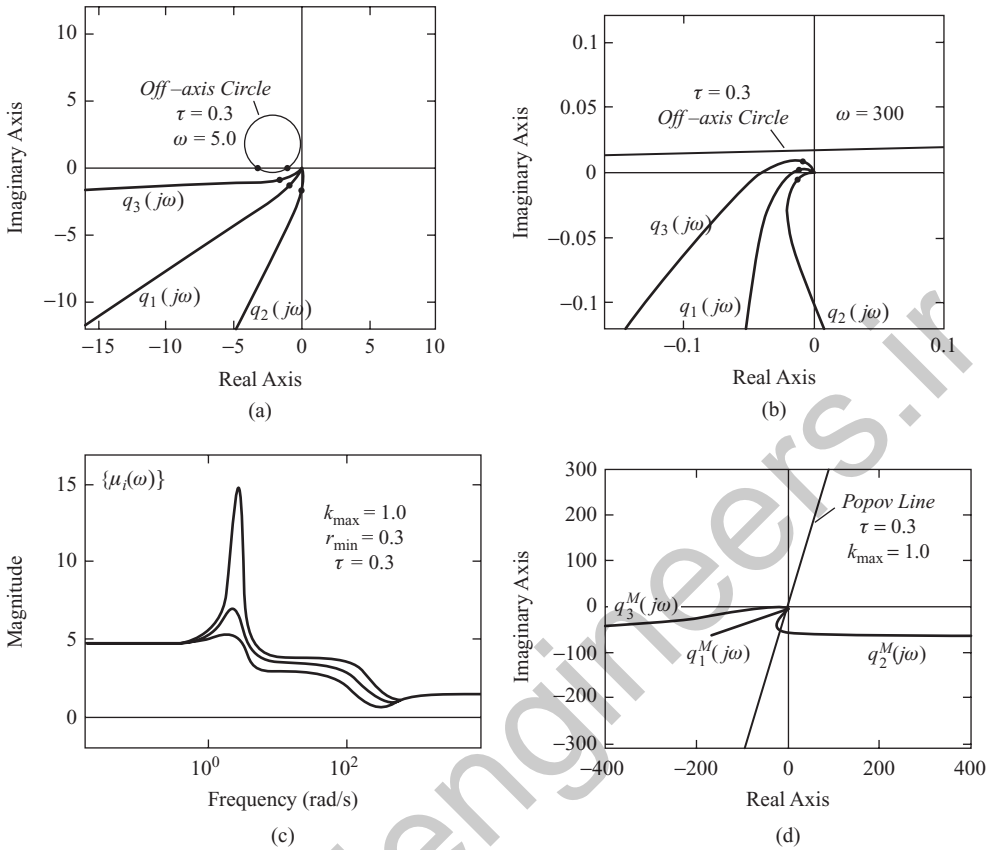


**Figure 5.23** Absolute stability analysis for  $\tau = 0.3$ . (a) Off-axis circle for  $\omega = 5.0$ ; (b) off-axis circle for  $\omega = 300.0$ ; (c) eigenvalues of the matrix  $\text{Re}P(j\omega)$ ; (d) application of Popov's criterion.

values of the frequency  $\omega$  ( $\omega = 5.0, 300.0$ ) are also plotted. The frequency dependencies of the eigenvalues  $\mu_i(\omega)$  of  $\text{Re}P(j\omega)$  [Equation (5.5)] [Figure 5.23(c)] confirm that the sufficient conditions of absolute stability hold under the chosen value  $\tau = 0.3$ .

Hence, in the discussed example, we have demonstrated the application of the generalized off-axis criterion, and have shown that absolute stability can be established by choosing an appropriate value of  $\tau$ . Note that since the eigenvalues in Equation (5.44) are complex-valued, the conventional Popov's criterion is not applicable to the discussed uniform system, which is visually illustrated in Figure 5.23(d). As is clear from Figure 5.23(d), the modified gain loci  $q_3^M(j\omega)$  of the third characteristic system tends to minus infinity in parallel with the real axis. Therefore, a 'nonintersecting' Popov line cannot be drawn for any values of  $\tau$  or  $k_{\max}$ .

## 5.4.2 Logarithmic form of the off-axis criterion of absolute stability

In Section 5.2, we described the technique of mapping the Popov line on the Bode diagrams of the ordinary characteristic gain loci  $q_i(j\omega)$ , which enhances the application potentialities of Popov's criterion. The advantages of passing to the Bode diagrams become apparent largely in

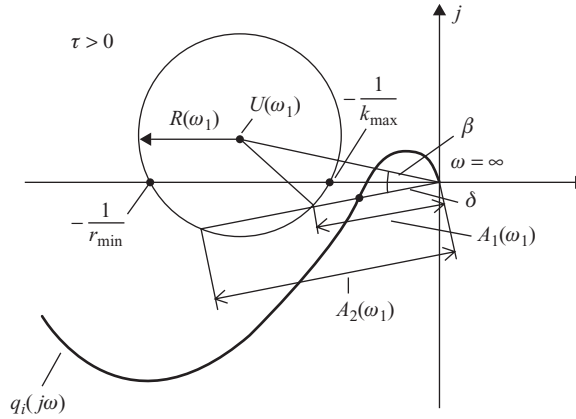


Figure 5.24 Mapping of the off-axis circle on the plane of Bode diagrams.

using the off-axis circle criterion. The point is that in this case, it is possible to find for the Bode magnitude plot  $Lm[q_i(j\omega)]$  of each characteristic system a forbidden region which depends only on the parameter  $\tau$  and, in a certain sense, is a mapping of the envelope of off-axis circles [Equation (5.39)] for all  $\omega \geq 0$  (Gasparyan 1986). Consider Figure 5.24, in which the off-axis circle [Equation (5.39)] for some frequency  $\omega = \omega_1$  and the  $i$ th gain locus  $q_i(j\omega)$ , with the given frequency marked by a bold dot, are shown. Draw a straight line from the origin of the complex plane through the point  $q_i(j\omega_1)$ , and denote by  $\delta$  the angle that that line makes with the real negative axis. The angle  $\delta$  is assumed positive in the anticlockwise direction. Denote by  $A_1(\omega_1)$  the length of the segment on the plotted line from the origin until the first intersection with the circle (smaller segment) and, by  $A_2(\omega_1)$ , until the second intersection (larger segment). It can readily be shown that the values  $A_1(\omega_1)$  and  $A_2(\omega_1)$  are determined by the following relationship:

$$A_{1,2}(\omega_1) = |U(\omega_1)| \cos(\delta - \beta) \pm \sqrt{[|U(\omega_1)| \cos(\delta - \beta)]^2 - \frac{1}{k_{\max} r_{\min}}}, \quad (5.45)$$

where

$$\beta = -\tan^{-1} \left( \omega_1 \tau \frac{k_{\max} - r_{\min}}{k_{\max} + r_{\min}} \right) \quad (5.46)$$

is the angle that the segment connecting the origin with the centre of the circle makes with the negative real axis, and

$$|U(\omega_1)| = \frac{1}{2k_{\max} r_{\min}} \sqrt{(1 + \omega_1^2 \tau^2) \left( k_{\max}^2 + r_{\min}^2 + 2k_{\max} r_{\min} \frac{1 - \omega_1^2 \tau^2}{1 + \omega_1^2 \tau^2} \right)} \quad (5.47)$$

is the length of that segment [the plus sign in Equation (5.45) corresponds to the larger segment  $A_2(\omega_1)$ ].

Intersections of the line passing through the point  $q_i(j\omega_1)$  with the circle having its centre at  $U(\omega_1)$  and radius  $R(\omega_1)$  are possible only for the angles  $\delta$  belonging to the range

$$\begin{aligned}
 & -\tan^{-1} \left\{ \frac{(k_{\max} - r_{\min}) \left( \frac{1}{2} \sqrt{\frac{1 + \omega_1^2 \tau^2}{k_{\max} r_{\min}}} + \frac{\omega_1 \tau}{k_{\max} + r_{\min}} \right)}{1 - \frac{\omega_1 \tau (k_{\max} - r_{\min})}{2(k_{\max} + r_{\min})} \sqrt{\frac{1 + \omega_1^2 \tau^2}{k_{\max} r_{\min}}}} \right\} \leq \delta \\
 & \leq \tan^{-1} \left\{ \frac{(k_{\max} - r_{\min}) \left( \frac{1}{2} \sqrt{\frac{1 + \omega_1^2 \tau^2}{k_{\max} r_{\min}}} - \frac{\omega_1 \tau}{k_{\max} + r_{\min}} \right)}{1 + \frac{\omega_1 \tau (k_{\max} - r_{\min})}{2(k_{\max} + r_{\min})} \sqrt{\frac{1 + \omega_1^2 \tau^2}{k_{\max} r_{\min}}}} \right\}. \quad (5.48)
 \end{aligned}$$

For  $\delta = 0$ , from Equation (5.45) and allowing for Equations (5.46) and (5.47), we find

$$A_1(\omega_1) = \frac{1}{k_{\max}}, \quad A_2(\omega_1) = \frac{1}{r_{\min}}, \quad (5.49)$$

i.e. the values of  $A_1(\omega_1)$  and  $A_2(\omega_1)$  do not depend on either the frequency  $\omega$  or the parameter  $\tau$ , and are completely determined by the sector  $[r_{\min}, k_{\max}]$  confining the nonlinear characteristics  $F_i(x_i)$ . Finally, for  $\delta = \beta$ , from Equation (5.45), we obtain the maximum and minimum possible values for  $A_{1,2}(\omega_1)$  equal to

$$A_{1,2}(\omega_1) = \frac{\sqrt{1 + \omega_1^2 \tau^2}}{2k_{\max} r_{\min}} \left[ \sqrt{k_{\max}^2 + r_{\min}^2 + 2k_{\max} r_{\min} \frac{1 - \omega_1^2 \tau^2}{1 + \omega_1^2 \tau^2}} \mp (k_{\max} - r_{\min}) \right]. \quad (5.50)$$

The values  $Lm[A_1(\omega_1)] = 20 \lg A_1(\omega_1)$  and  $Lm[A_2(\omega_1)] = 20 \lg A_2(\omega_1)$  are *critical* for the Bode magnitude plot  $Lm[q_i(j\omega_1)]$  of the  $i$ th characteristic system, since, for

$$Lm[A_1(\omega_1)] \leq Lm[q_i(j\omega_1)] \leq Lm[A_2(\omega_1)], \quad (5.51)$$

the point  $q_i(j\omega_1)$  necessarily lies in the complex plane inside the corresponding off-axis circle [Equation (5.39)]. Plotting these critical values for different  $\omega$  on the Bode magnitude plots, we obtain a forbidden area for  $Lm[q_i(j\omega_1)]$  (Figure 5.25). If the plot of  $Lm[q_i(j\omega)]$  does not enter into that forbidden area for any frequency  $\omega$ , then, in the complex plane, none of the points of the characteristic gain locus  $q_i(j\omega)$  can be inside the corresponding off-axis circle with its centre at  $U(\omega)$  [Equation (5.41)] and radius  $R(\omega)$  [Equation (5.40)]. In this regard, the forbidden area on the Bode magnitude plots is like the representation of the envelope (for each individual  $i$ ) of all off-axis circles (for all  $\omega \geq 0$ ) in the complex plane of  $q_i(j\omega)$ . If the above is valid for all  $i$ , then the necessary condition for positive definiteness of the matrix  $\mathbf{Re}P(j\omega)$  [Equation (5.5)] holds. Note that the forbidden regions on the Bode magnitude plots pass, for all  $i$  and regardless of the value of  $\tau$ , through the points  $(\delta = 0, -Lm[k_{\max}])$  and  $(\delta = 0, -Lm[r_{\min}])$ . It is also worth mentioning that a comparatively simple procedure for

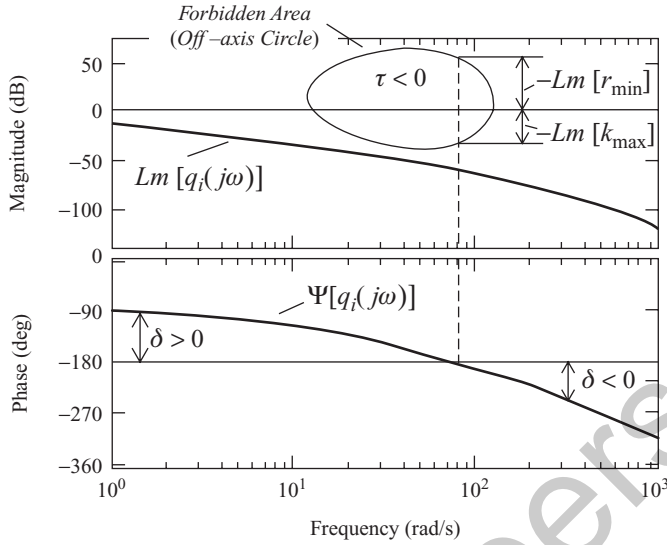


**Figure 5.25** Mapping of the envelope of the off-axis circles on the Bode magnitude plot of the  $i$ th characteristic system.

finding the forbidden area in the logarithmical plane is because, in that plane, for  $\omega = \omega_1$ , only two points of the off-axis circle [Equation (5.39)] lying at the intersections with the straight line passing through the point  $q_i(j\omega_1)$  are mapped, but not the whole circle (Figure 5.24).

**Example 5.4** Let us examine once again, using the logarithmic form of the off-axis circle criterion, the three-dimensional uniform system of Example 5.3. The required constructions on the Bode diagrams of  $q_i(j\omega)$ , for  $\tau = 0.3$ , are given in Figure 5.26, in which the plots of all characteristic systems are represented jointly. Here, the Bode magnitude plots  $Lm[q_i(j\omega)]$  for all characteristic systems actually merge, since the magnitudes of eigenvalues [Equation (5.44)] ( $|\lambda_1| = 0.9084$ ,  $|\lambda_2| = |\lambda_3| = 1.0041$ ) are very close to unity. Naturally, these results

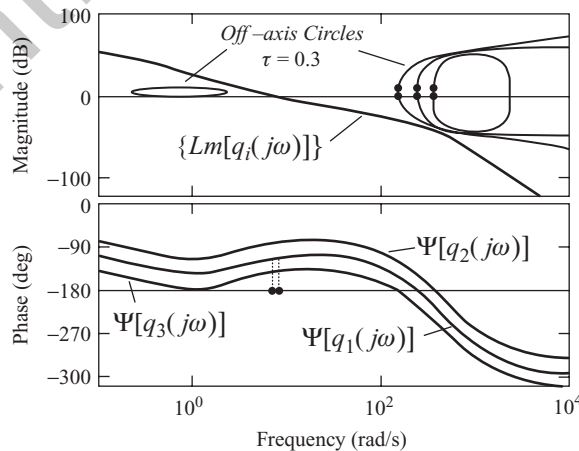


**Figure 5.26** Logarithmic form of the off-axis circle criterion.

completely agree with those obtained in Example 5.3. It is interesting to note that mappings of off-axis circles on the Bode plane may have a rather complicated form. Thus, these mappings may close at infinite frequencies, or, for each  $i$  (for each characteristic system), several closed or nonclosed curves may exist, etc.

### 5.4.3 Parabolic criterion of absolute stability

In the rest of this section, we shall discuss generalization to the multidimensional case of the so-called *parabolic* criterion (Hsu and Meyer 1968; Tsytkin 1977), which is also applicable to MIMO systems with unstable or conditionally stable linear parts (Gasparyan 1986).

Substituting Equation (5.40) into Equation (5.39), after some simple transformations, yields

$$\left[ \operatorname{Re}\{q_i(j\omega)\} + \frac{1}{2} \left( \frac{1}{r_{\min}} + \frac{1}{k_{\max}} \right) \right]^2 - \omega\tau \left( \frac{1}{r_{\min}} - \frac{1}{k_{\max}} \right) \operatorname{Im}\{q_i(j\omega)\} + [\operatorname{Im}\{q_i(j\omega)\}]^2 - \frac{1}{4} \left( \frac{1}{r_{\min}} - \frac{1}{k_{\max}} \right)^2 > 0, \quad i = 1, 2, \dots, N. \quad (5.52)$$

Apparently, these inequalities will certainly hold if

$$\left[ \operatorname{Re}\{q_i(j\omega)\} + \frac{1}{2} \left( \frac{1}{r_{\min}} + \frac{1}{k_{\max}} \right) \right]^2 - \omega\tau \left( \frac{1}{r_{\min}} - \frac{1}{k_{\max}} \right) \operatorname{Im}\{q_i(j\omega)\} - \frac{1}{4} \left( \frac{1}{r_{\min}} - \frac{1}{k_{\max}} \right)^2 > 0, \quad i = 1, 2, \dots, N, \quad (5.53)$$

since the left parts in Equation (5.53) are smaller than those in Equation (5.52) by the positive quantities  $[\operatorname{Im}\{q_i(j\omega)\}]^2$ , i.e. the conditions in Equation (5.53) are sufficient for the satisfaction of the necessary conditions in Equation (5.52). But, if we replace Equation (5.53) by an equality (by changing sign  $>$  to  $=$ ), then these equations will define a *parabola* passing through the points  $-1/r_{\min}$  and  $-1/k_{\max}$  in the complex plane of modified characteristic gain loci  $q_i^M(j\omega)$  of the *initial* linear part. The tangents to the parabola at these points have slopes  $-1/\tau$  and  $+1/\tau$ , i.e. the right-hand tangent coincides with the standard Popov line (Figure 5.27). From here, it ensues that the conditions in Equation (5.53), and, consequently, Equation (5.38), will be satisfied if the family of the modified gain loci  $q_i^M(j\omega)$  is situated outside the parabola in Equation (5.53).<sup>10</sup> The parabolic criterion is simpler than the off-axis circle criterion in practical applications, since the parabola in Equation (5.53) does not depend on the frequency  $\omega$  and is entirely determined by the numbers  $r_{\min}$ ,  $k_{\max}$  and  $\tau$ . At the same time, it narrows to a certain extent the area of absolute stability, and allows the investigation of only MIMO systems whose stable linear part is of a *type* not exceeding 2 or, in the case of unstable  $W(s)$ , if the number of unstable poles of any open-loop characteristic system does not exceed one. If the indicated restrictions on the linear part do not hold, then the parabolic criterion is not applicable, since the modified loci  $q_i^M(j\omega)$  will necessarily traverse the parabola in Equation (5.53), even when the off-axis circle criterion is satisfied. On tending  $r_{\min}$  to zero, the off-axis circle [Equation (5.39)] and parabola [Equation (5.53)] degenerate into the Popov line, and the transfer matrix of the transformed linear part  $W_T(s)$  [Equation (5.32)] coincides in the

<sup>10</sup> Similar to the case of the off-axis circle, we shall, for brevity, call Equation (5.53) the parabola equation.

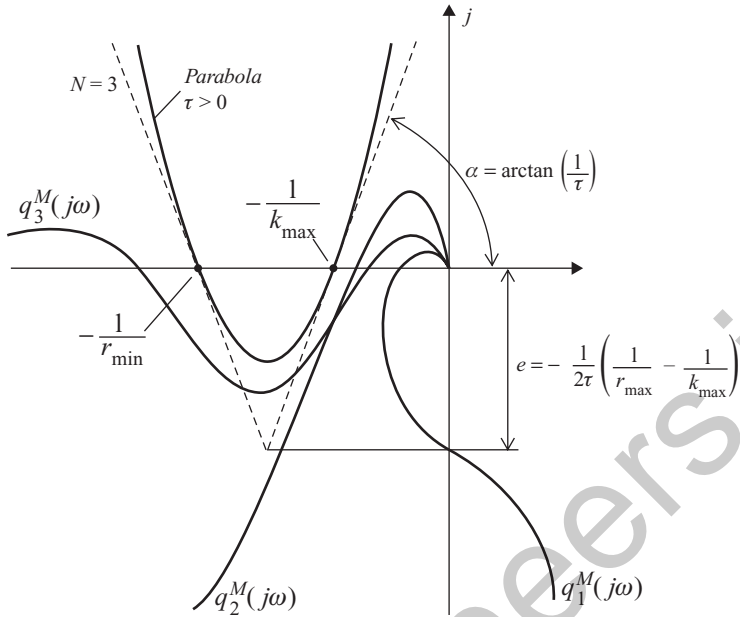


Figure 5.27 Parabolic criterion of absolute stability.

limit with the initial matrix  $W(s)$ . As a result, both the off-axis circle and the parabolic criteria of absolute stability of the equilibrium point reduce to the usual multidimensional Popov’s criterion.

Mapping of the parabola in Equation (5.53) in the plane of the modified Nichols plots can easily be performed by separating the real and imaginary parts in Equation (5.53) and passing from the orthogonal coordinate system to the polar system in the complex plane. Parabolas [Equation (5.53)] in the complex plane of the modified gain loci of the linear part for the sector restrictions  $[0.1, 1.0]$  and different values of the parameter  $\tau$  are shown in Figure 5.28, as well as those in the plane of the corresponding modified Nichols plots. The dotted lines in Figure 5.28(a) represent the tangents to the parabolas at the points of their intersections with the real axis.

In conclusion, note that the off-axis circle and parabolic criteria can also be used for determining the *degree of stability*  $\eta$  of absolutely stable nonlinear MIMO systems with unstable or conditionally stable linear parts. To this end, one should just replace the characteristics  $W(j\omega)$  or  $W_T(j\omega)$  by the shifted (expanded) characteristics  $W(j\omega - \eta)$  or  $W_T(j\omega - \eta)$ .

### 5.5 MULTIDIMENSIONAL CIRCLE CRITERIA OF ABSOLUTE STABILITY

A separate discussion on the circle criterion, which directly ensues from the off-axis circle criterion for  $\tau = 0$ , is needed, for a number of reasons. First, it embraces MIMO systems with conditionally stable and unstable linear parts, and with nonlinear elements of the most general form, including nonstationary elements (Nelepin 1975). Second, it can be readily extended to

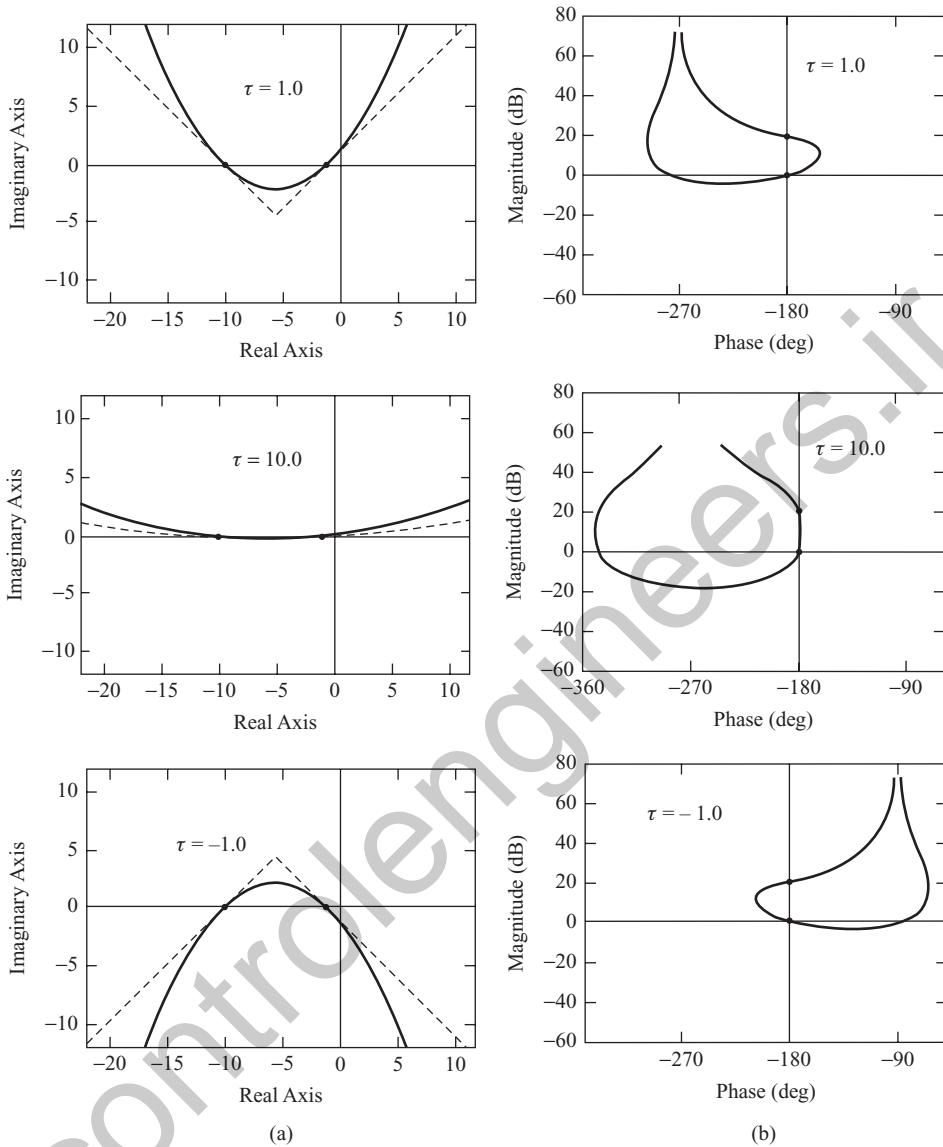


Figure 5.28 Parabolae [Equation (5.53)] for the sector of nonlinearities  $[0.1, 1.0]$ .

the absolute stability analysis of forced motions caused by bounded external signals. Further, by graphical interpretation, the circle criterion may be viewed as a generalization to the nonlinear case of the conventional Nyquist criterion, where the critical point  $(-1, j0)$  is replaced by some *critical (forbidden) circle*. Finally, and no less importantly, its analytical or graphical check-up does not present any difficulty, since the conditions for positive definiteness of the matrix  $\mathbf{Re}P(j\omega)$  [Equation (5.5)] do not depend here on the parameter  $\tau$ .

### 5.5.1 General and normal MIMO systems

Let the linear part of the MIMO system be conditionally stable or unstable (naturally, it can also be stable or on the stability boundary), and all nonlinear characteristics satisfy the sector restrictions

$$r_{\min} \leq \frac{F_i(x_i, t)}{x_i} \leq k_{\max}, \quad i = 1, 2, \dots, N, \quad (5.54)$$

where the dependency of  $F_i(x_i, t)$  on time  $t$  is explicitly emphasized, and let the linear part  $W(s)$  enclosed by the negative feedback via the scalar matrix  $r_{\min}I$  be stable. Then, according to Section 5.4, the matrix  $P(j\omega)$  [Equations (5.6) and (5.37)] can be represented, taking into account that  $\tau = 0$ , as

$$P(j\omega) = C(j\omega) \text{diag} \left\{ \frac{q_i(j\omega)}{1 + r_{\min}q_i(j\omega)} + \frac{1}{k_{\max} - r_{\min}} \right\} C^{-1}(j\omega). \quad (5.55)$$

The conditions for positive definiteness of the Hermitian matrix  $\mathbf{Re}P(j\omega)$  [Equation (5.5)] take the simple form

$$\mathbf{Re} \left\{ \frac{q_i(j\omega)}{1 + r_{\min}q_i(j\omega)} \right\} + \frac{1}{k_{\max} - r_{\min}} > 0, \quad i = 1, 2, \dots, N. \quad (5.56)$$

These conditions can be easily transformed into the form

$$\mathbf{Re} \{ [1 + k_{\max}q_i(j\omega)][1 + r_{\min}\tilde{q}_i(j\omega)] \} > 0, \quad i = 1, 2, \dots, N, \quad (5.57)$$

where the wavy line  $\sim$  from above denotes, as before, complex conjugation. Replacing sign  $>$  by the sign of equality in Equation (5.57), performing some simple transformations and separating the real parts, we obtain the equations

$$\left[ \mathbf{Re}\{q_i(j\omega)\} + \frac{1}{2} \left( \frac{1}{r_{\min}} + \frac{1}{k_{\max}} \right) \right]^2 + [\mathbf{Im}\{q_i(j\omega)\}]^2 = \frac{1}{4} \left( \frac{1}{r_{\min}} - \frac{1}{k_{\max}} \right)^2, \quad i = 1, 2, \dots, N. \quad (5.58)$$

In the complex plane of the characteristic gain loci  $q_i(j\omega)$  of the initial linear part, these equations describe a circle located symmetrically with respect to the real axis and crossing the latter at the points  $-1/r_{\min}$  and  $-1/k_{\max}$  (Figure 5.29). The necessary conditions in Equation (5.57) will be satisfied if all loci  $q_i(j\omega)$  are outside of the circle in Equation (5.58) and do not cross it. If the linear part  $W(s)$  is stable or conditionally stable, then none of  $q_i(j\omega)$  must enclose the circle in Equation (5.58). For unstable  $W(s)$ , the loci  $q_i(j\omega)$  must enclose that circle a total of  $\ell/2$  times in the anticlockwise direction, where  $\ell$  is the number of unstable poles of  $W(s)$ . Note that, here, we speak about the *total* number of encirclements of the forbidden circle [Equation (5.58)] by *all* characteristic gain loci  $q_i(j\omega)$ .

It is easy to see that the above formulation of the necessary conditions for absolute stability, or, more strictly, of the necessary conditions for positive definiteness of the Hermitian matrix  $\mathbf{Re}P(j\omega)$  [Equation (5.5)], coincides with the common formulation of the Nyquist criterion,

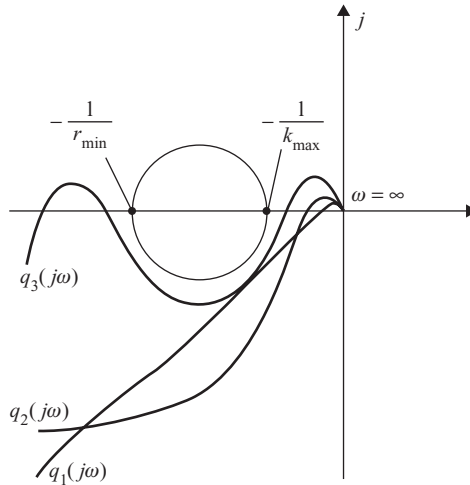


**Figure 5.29** Circle [Equation (5.58)] on the complex plane of ordinary characteristic gain loci  $q_i(j\omega)$  of the linear part ( $N = 3$ ).

in which the ‘critical’ circle [Equation (5.58)] plays the role of the critical point  $(-1, j0)$ . When  $r_{\min} \rightarrow 0$ , the circle in Equation (5.58) degenerates into a vertical line passing through the point  $(-1/k_{\max}, j0)$ , and the circle criterion transforms into Popov’s criterion.

Hence, for the condition  $\text{Re}P(j\omega) > 0$  to hold, it is, roughly speaking, necessary that the conventional circle criterion be satisfied for all loci  $q_i(j\omega)$ . And vice versa, if the circle criterion does not hold for any of the characteristic systems, then this immediately results in nonfulfillment of the condition  $\text{Re}P(j\omega) > 0$ . It is also evident that if the transfer matrix  $W(s)$  is normal, then the considered geometrical picture gives not only the necessary, but also the *sufficient* conditions for the positive definiteness of  $\text{Re}P(j\omega)$ , i.e. it guarantees absolute stability of the equilibrium point of the MIMO system.

The circle in Equation (5.58) can be transformed on the Bode diagrams of  $q_i(j\omega)$ , with the help of the following relationships ensuing from Equations (5.45)–(5.47) for  $\tau = 0$ :

$$A_{1,2}(\omega_1) = \frac{1}{2} \left( \frac{1}{r_{\min}} + \frac{1}{k_{\max}} \right) \cos \delta \pm \sqrt{\left[ \frac{1}{2} \left( \frac{1}{r_{\min}} + \frac{1}{k_{\max}} \right) \cos \delta \right]^2 - \frac{1}{k_{\max} r_{\min}}}, \quad (5.59)$$

where the angle  $\delta$  is counted from the level of  $-180^\circ$ , and changes in the range

$$-\arcsin \left( \frac{k_{\max} - r_{\min}}{k_{\max} + r_{\min}} \right) \leq \delta \leq \arcsin \left( \frac{k_{\max} - r_{\min}}{k_{\max} + r_{\min}} \right). \quad (5.60)$$

Unlike the off-axis circle in Equation (5.39), the circle in Equation (5.58) does not depend on the frequency  $\omega$  and therefore is entirely mapped on the Bode magnitude plot  $Lm[q_i(j\omega)]$  (Figure 5.30) (for each  $i$ , we have its own forbidden circle).

**Example 5.5** Let us consider a two-dimensional general system with different transfer functions of the separate channels, the first of which has a pole in the right half-plane at  $s = +2.0$ ,

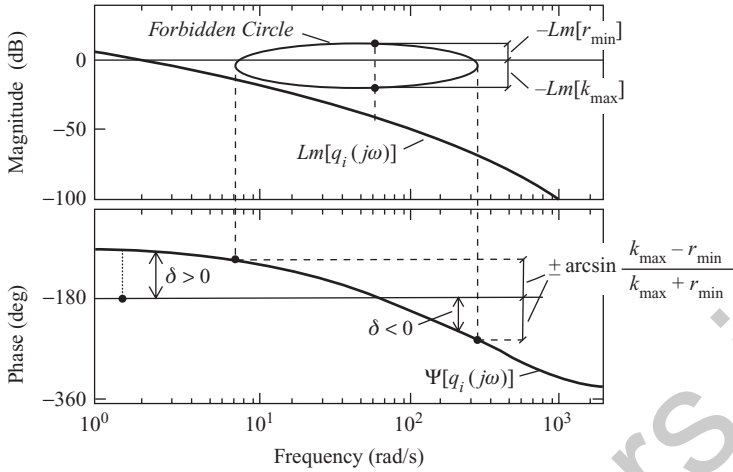


Figure 5.30 Mapping of circle [Equation (5.58)] on the Bode magnitude plot of  $q_i(j\omega)$ .

i.e. is unstable:

$$W_1(s) = \frac{800}{(s-2)(s+10)(s+20)}, \quad W_2(s) = \frac{2500(s+12)}{(s+8)(s+25)(s+50)} \quad (5.61)$$

and the following matrix of rigid cross-connections:

$$R = \begin{pmatrix} 0.9 & 0.2 \\ 0.35 & 0.85 \end{pmatrix}. \quad (5.62)$$

Assume, first, that the nonlinear characteristics lie in the sector  $[0.35, 2.0]$ . Figure 5.31(a) represents the results of analysis in the complex plane of the initial CTFs  $q_i(j\omega)$ , where the

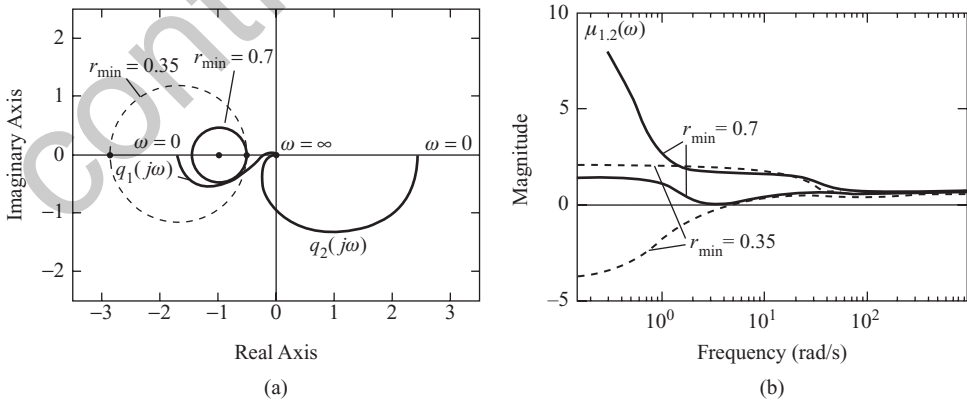
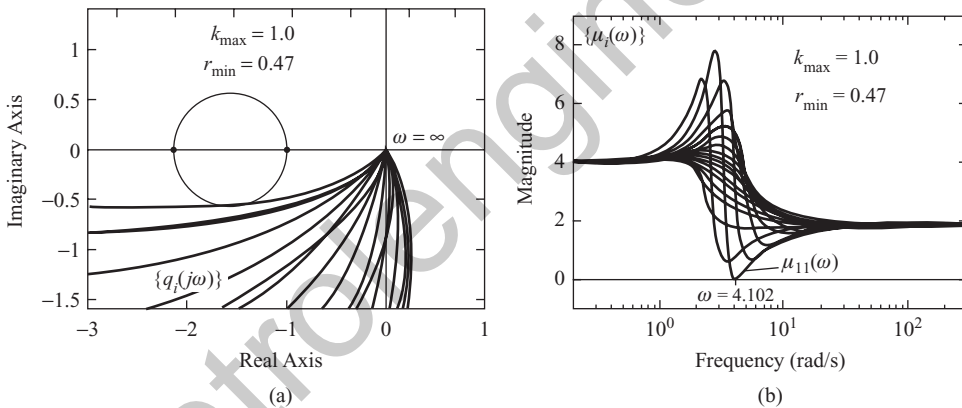


Figure 5.31 Application of the circle criterion to the general two-dimensional system with the unstable linear part. (a) Nyquist plots; (b) eigenvalues of the matrix  $\mathbf{Re}P(j\omega)$ .

dashed lines correspond to the circle in Equation (5.58) for the sector  $[0.35, 2.0]$ . From these graphs, it is evident that the geometrical conditions for absolute stability do not hold. Let us now increase the lower bound of the sector restrictions by a factor of 2, i.e. assume  $r_{\min} = 0.7$ , leaving the value of  $k_{\max}$  unchanged. The corresponding circles are shown in Figure 5.31(a) by the solid lines. The frequency dependencies of the eigenvalues  $\mu_{1,2}(\omega)$  of  $\mathbf{Re}P(j\omega)$  [Equation (5.5)] are given in Figure 5.31(b). These graphs show that the sufficient conditions for absolute stability of the equilibrium point hold for the sector  $[0.7, 2.0]$ .

**Example 5.6** Assume that we have introduced in the separate channels of the 16-channel circulant system of Example 1.8 identical nonlinear elements with a unit upper bound of sector restrictions, i.e. with  $k_{\max} = 1$ . Let us find a minimal possible value for  $r_{\min}$  for which the absolute stability of the equilibrium point is guaranteed. Since the discussed circulant system belongs to normal systems, its absolute stability can be directly established by the characteristic gain loci of the linear part  $q_i(j\omega) = \lambda_i w(j\omega)$  ( $i = 1, 2, \dots, 16$ ). Evidently, the sought value of  $r_{\min}$  will correspond to that ‘largest’ (for the constant value  $k_{\max} = 1$ ) circle that is *tangent* to the envelope of the family  $\{q_i(j\omega)\}$ . The necessary constructions are shown in Figure 5.32(a), and give the sought value  $r_{\min} = 0.47$ . The frequency dependencies of the eigenvalues of  $\mathbf{Re}P(j\omega)$  are given in Figure 5.32(b), which confirms satisfaction of the condition  $\mathbf{Re}P(j\omega) > 0$  for all  $\omega \geq 0$ .



**Figure 5.32** Examination of the absolute stability of the 16-channel circulant system. (a) Circle tangent to the family  $\{q_i(j\omega)\}$ ; (b) eigenvalues of the matrix  $\mathbf{Re}P(j\omega)$ .

### 5.5.2 Inverse form of the circle criterion for uniform systems

It is worth especially discussing the application of the circle criterion to nonlinear uniform systems (see Section 1.4). Of course, the investigation of such systems can be conducted with the help of the general techniques described above. However, the structural features of uniform systems allow passing, analogously to the inverse form of the stability analysis of linear uniform systems (see Section 1.3.2), from the complex plane of  $N$  characteristic gain loci  $q_i(j\omega) = \lambda_i w(j\omega)$ , where  $\lambda_i$  are the eigenvalues of the cross-connections matrix  $R$ , to the complex plane of a single Nyquist plot of  $w(j\omega)$ . Indeed, based on Equation (5.57), for the

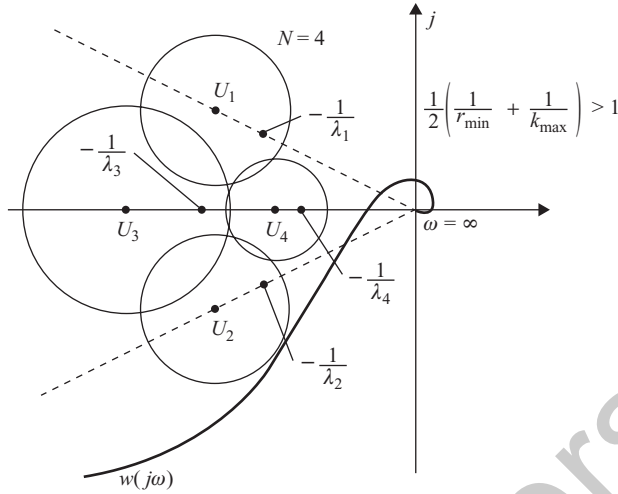


Figure 5.33 Circles [Equation (5.64)] on the plane of the Nyquist plot of  $w(j\omega)$ .

case of uniform systems, we have

$$\begin{aligned} & \mathbf{Re} \left\{ [1 + k_{\max} \lambda_i w(j\omega)][1 + r_{\min} \tilde{\lambda}_i \tilde{w}(j\omega)] \right\} \\ &= \mathbf{Re} \left\{ |\lambda_i|^2 \left[ \frac{1}{\lambda_i} + k_{\max} w(j\omega) \right] \left[ \frac{1}{\tilde{\lambda}_i} + r_{\min} \tilde{w}(j\omega) \right] \right\} > 0, \quad i = 1, 2, \dots, N. \end{aligned} \quad (5.63)$$

From here, replacing sign  $>$  by the sign of equality and discarding the real multiplier  $|\lambda_i|^2$ , after separating the real part and simple transformations, we find

$$\begin{aligned} & \left[ \mathbf{Re}\{w(j\omega)\} + \frac{1}{2} \left( \frac{1}{r_{\min}} + \frac{1}{k_{\max}} \right) \frac{\mathbf{Re}\{\lambda_i\}}{|\lambda_i|^2} \right]^2 + \left[ \mathbf{Im}\{w(j\omega)\} - \frac{1}{2} \left( \frac{1}{r_{\min}} + \frac{1}{k_{\max}} \right) \frac{\mathbf{Im}\{\lambda_i\}}{|\lambda_i|^2} \right]^2 \\ &= \left[ \frac{1}{2|\lambda_i|^2} \left( \frac{1}{r_{\min}} - \frac{1}{k_{\max}} \right) \right]^2, \quad i = 1, 2, \dots, N. \end{aligned} \quad (5.64)$$

Equations (5.64) define in the complex plane of  $w(j\omega)$  a family of  $N$  circles with centres at the points  $U_i$ , where

$$\mathbf{Re}\{U_i\} = -\frac{1}{2} \left( \frac{1}{r_{\min}} + \frac{1}{k_{\max}} \right) \frac{\mathbf{Re}\{\lambda_i\}}{|\lambda_i|^2}, \quad \mathbf{Im}\{U_i\} = \frac{1}{2} \left( \frac{1}{r_{\min}} + \frac{1}{k_{\max}} \right) \frac{\mathbf{Im}\{\lambda_i\}}{|\lambda_i|^2}, \quad (5.65)$$

and radii

$$R_{O_i} = \frac{1}{2|\lambda_i|^2} \left( \frac{1}{r_{\min}} - \frac{1}{k_{\max}} \right). \quad (5.66)$$

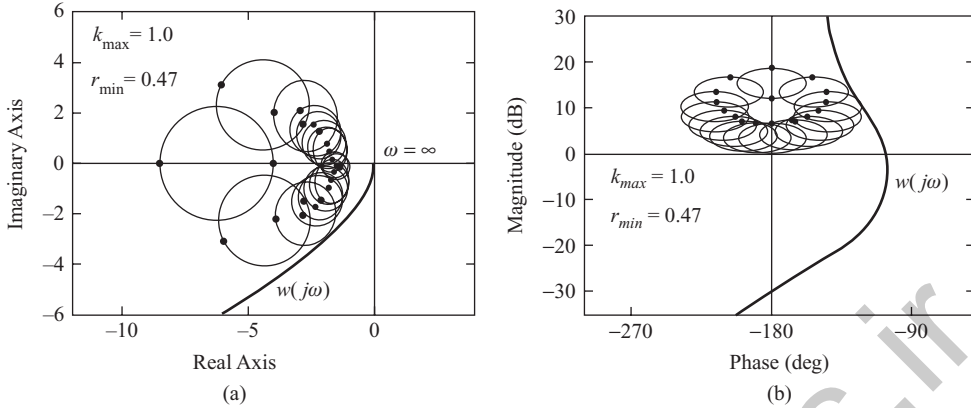


**Figure 5.34** Absolute stability analysis of the 16-channel circulant uniform system. (a) Nyquist plot; (b) Nichols plot.

The circle centres  $U_i$  [Equation (5.65)] are located at the straight lines drawn from the origin of the complex plane through the critical points  $-1/\lambda_i$ , at distances from the origin equal to

$$|U_i| = \frac{1}{2|\lambda_i|} \left( \frac{1}{r_{\min}} + \frac{1}{k_{\max}} \right), \quad (5.67)$$

where the corresponding distances to the intersection points of the circles with the drawn lines are equal to  $1/|\lambda_i|r_{\min}$  and  $1/|\lambda_i|k_{\max}$ . Since all complex-valued eigenvalues  $\lambda_i$  of  $R$  are complex conjugate in pairs, this is also valid for the complex centres  $U_i$  [Equation (5.65)]. Therefore, in the plane of the Nyquist plot of  $w(j\omega)$ , the circles in Equations (5.64) are located in pairs, symmetrically with respect to the real axis. For the real-valued  $\lambda_i$ , the centres  $U_i$  lie just at that axis (Figure 5.33).

In the case of stable or conditionally stable transfer function  $w(s)$ , the necessary conditions in Equations (5.63) for  $\text{Re}P(j\omega) > 0$  hold if the Nyquist plot of  $w(j\omega)$  does not encircle any of the circles in Equations (5.64) and does not cross them. For unstable  $w(s)$ , the plot of  $w(j\omega)$  must enclose the *whole* family of circles in Equations (5.64) in the anticlockwise direction  $\ell/2$  times, where  $\ell$  is the number of unstable poles of  $w(s)$ . The circles in Equations (5.64) can be mapped on the Bode diagrams and Nichols plots. We leave derivation of the corresponding expressions, similar to Equations (5.59) and (5.60), as an exercise for the reader.

**Example 5.7** Let us apply the inverse form of the circle criterion to the 16-channel circulant uniform system of Example 5.6. The circles in Equations (5.64) on the Nyquist and Nichols plots of the transfer function  $w(j\omega)$  are shown in Figure 5.34 and agree, naturally, with the results of Example 5.6.

## 5.6 MULTIDIMENSIONAL CIRCLE CRITERIA OF THE ABSOLUTE STABILITY OF FORCED MOTIONS

Let us now proceed to a more general problem of the absolute stability of *forced motions* in nonlinear MIMO systems, caused by the bounded ( $|\varphi(t)| < M_0$ ) external signals  $\varphi(t)$ . In a

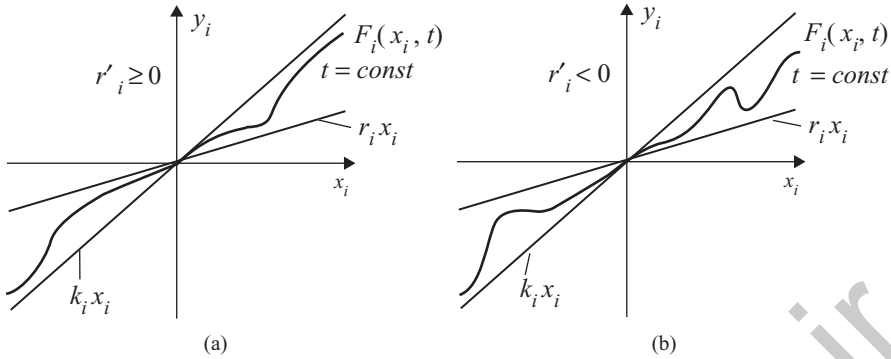


**Figure 5.35** Nonlinear characteristics with different slopes. (a) Non-negative slopes; (b) negative slopes.

certain sense, investigation of the absolute stability of the equilibrium point is a specific case of that problem, since it corresponds to zero external signals  $\varphi(t) = 0$ . Further, we shall consider the single-valued nonstationary nonlinearities  $F_i(x_i, t)$ , whose characteristics obey, for some  $r_i > 0$  and  $k_i > r_i$ , the sector restrictions in Equation (5.30). Besides, we shall assume the characteristics  $F_i(x_i, t)$  differentiable with respect to  $x_i$  and, for any  $t$ , satisfying the conditions

$$r'_i \leq \frac{\delta F_i(x_i, t)}{\delta x_i} \leq k'_i, \quad i = 1, 2, \dots, N. \quad (5.68)$$

Evidently, for each  $i$ , the values  $r_i, k_i, r'_i$  and  $k'_i$  are connected by the relationships

$$r'_i \leq r_i < k_i \leq k'_i, \quad (5.69)$$

where, for nonnegative  $r_i \geq 0$ , the values of  $r'_i$  can be both nonnegative, for nondecreasing characteristics  $F_i(x_i, t)$  [Figure 5.35(a)], and negative, for the characteristics  $F_i(x_i, t)$  having negative slopes over some intervals of  $x_i$  (for  $t = \text{const}$ ) [Figure 5.35(b)]. In the following, we shall distinguish these two cases, since they give somewhat different results.

In Hsu and Meyer (1968), Naumov (1972), Nelepin (1975), Tsytkin (1977), etc., it is shown that the analysis of the absolute stability of forced motions under the above assumptions is reduced to the stability analysis of the equilibrium point for the MIMO system with the same linear part  $W(s)$ , but with the transformed nonstationary (even if all initial nonlinear elements are stationary) nonlinearities

$$\Psi_i(\Delta x_i, t) = F_i[x_i(t) + \Delta x_i(t), t] - F_i[x_i(t), t], \quad i = 1, 2, \dots, N, \quad (5.70)$$

where  $\Psi_i(0, t) \equiv 0$  and  $\Delta x_i(t)$  are the components of the vector of free motions caused, for instance, by perturbations of initial conditions or by any bounded or vanishing external signals. Based on Equation (5.68), for the transformed characteristics  $\Psi_i(\Delta x_i, t)$ , we have

$$r'_i \leq \frac{\Psi_i(\Delta x_i, t)}{\Delta x_i} \leq k'_i, \quad i = 1, 2, \dots, N. \quad (5.71)$$

For the study of the absolute stability of the equilibrium point  $\Delta x = 0$  of the nonlinear MIMO system with the transformed nonstationary nonlinearities  $\Psi_i(\Delta x_i, t)$ , we can apply the circle

criterion in the form presented in the preceding section. To this end, let us introduce a common sector  $[r'_{\min}, k'_{\max}]$  embracing all transformed characteristics  $\Psi_i(\Delta x_i, t)$ , i.e. let us replace the inequalities in Equation (5.71) by the following:

$$r'_{\min} \leq \frac{\Psi_i(\Delta x_i, t)}{\Delta x_i} \leq k'_{\max}, \quad i = 1, 2, \dots, N. \quad (5.72)$$

The values  $r'_{\min} = \min(r'_i)$  and  $k'_{\max} = \max(k'_i)$  are connected with the analogous values  $r_{\min}$  and  $k_{\max}$ , which determine the sector confining the initial characteristics  $F_i(x_i, t)$  by the inequalities

$$r'_{\min} \leq r_{\min} < k_{\max} \leq k'_{\max}. \quad (5.73)$$

Consider, first, the case of nondecreasing characteristics  $F_i(x_i, t)$ , i.e. the case  $r'_{\min} \geq 0$ . Let the transfer matrix  $W(s)$  with negative feedback around it via the scalar matrix  $r'_{\min} I$  be stable. Then, based on the above, for absolute stability of the equilibrium point of the MIMO system with the transformed nonlinearities  $\Psi_i(\Delta x_i, t)$ , i.e. for absolute stability of forced motions in the *initial* MIMO system, it is sufficient that, for  $\omega \geq 0$ , the Hermitian matrix  $\mathbf{Re}P(j\omega)$  [Equation (5.5)] be positive definite, where  $P(j\omega)$  is given on replacing  $r_{\min}$  by  $r'_{\min}$  and  $k_{\max}$  by  $k'_{\max}$  in Equation (5.55). The necessary conditions for positive definiteness of  $\mathbf{Re}P(j\omega)$  take, in accordance with Equation (5.57), the form

$$\mathbf{Re} \{ [1 + k'_{\max} q_i(j\omega)] [1 + r'_{\min} \tilde{q}_i(j\omega)] \} > 0, \quad i = 1, 2, \dots, N. \quad (5.74)$$

Passing in Equation (5.74) to equality, we obtain the equation of a circle, the centre of which is on the real axis and which traverses the latter at the points  $-1/r'_{\min}$  and  $-1/k'_{\max}$  (Figure 5.36). As is evident from Equation (5.73) and Figure 5.36, this circle encloses the circle in

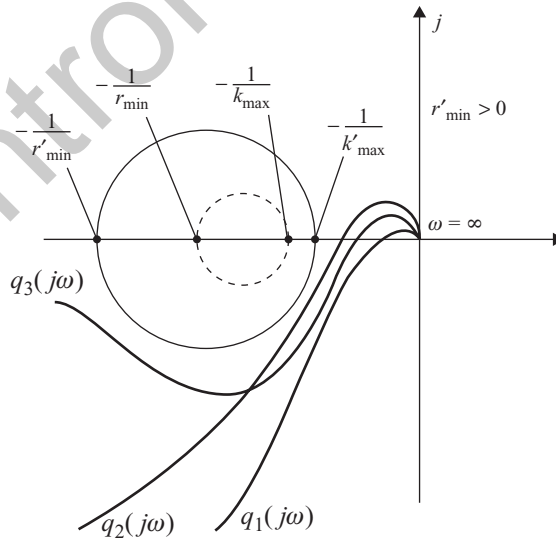
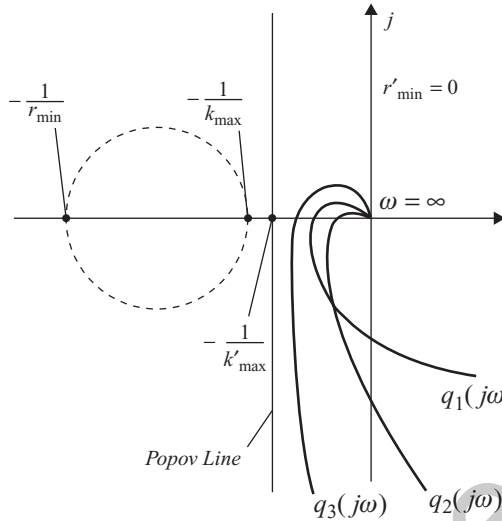


Figure 5.36 Investigation of the absolute stability of forced motions in the MIMO system ( $N = 3$ ).



**Figure 5.37** Analysis of the absolute stability of forced motions in the presence of horizontal parts in the nonlinear characteristics  $F_i(x_i, t)$  ( $N = 3$ ).

Equation (5.58), which is used in the analysis of the absolute stability of the equilibrium point. With respect to the larger circle, all those conditions which were previously put on the characteristic gain loci of the linear part  $q_i(j\omega)$  should hold regarding the location, number of encirclements, etc. This clearly shows that the conditions for absolute stability of forced motions impose more stringent requirements on the linear part  $W(s)$  than the conditions of absolute stability of the equilibrium point.

For  $r'_{\min} = 0$ , i.e. in the case of horizontal parts in the characteristics  $F_i(x_i, t)$ , the necessary conditions in Equation (5.15) have a simpler form:

$$\operatorname{Re}\{q_i(j\omega)\} + \frac{1}{k'_{\max}} > 0, \quad i = 1, 2, \dots, N, \quad (5.75)$$

which geometrically corresponds to the location of the family  $\{q_i(j\omega)\}$  to the right of the vertical line (actually, the common Popov line) passing through the point  $-1/k'_{\max} \cdot j0$  (Figure 5.37). Here, obviously, the cases of conditionally stable or unstable linear part  $W(s)$  are excluded.

Assume, now, that the characteristics  $F_i(x_i, t)$  can have negative slopes, i.e.  $r'_{\min} < 0$ . The formulation of the circle criterion does not change in this case. However, for the condition  $\operatorname{Re}P(j\omega) > 0$  to hold, it is necessary that all characteristic gain loci  $q_i(j\omega)$  be *inside* the circle with its centre on the real axis and crossing the latter at the points  $-1/k'_{\max} < 0$  and  $-1/r'_{\min} > 0$  (Figure 5.38). Evidently, it is only possible for the *stable*  $W(s)$ , i.e. for  $r'_{\min} < 0$ ; the case of the MIMO system linear part's being on the stability boundary is also excluded.

Since the conditions of absolute stability of forced motions embrace, as a specific case, the corresponding conditions for the equilibrium point, the nonlinear MIMO systems for which all possible forced motions caused by the bounded external signals are absolutely stable are sometimes simply called the *absolutely stable MIMO systems*.

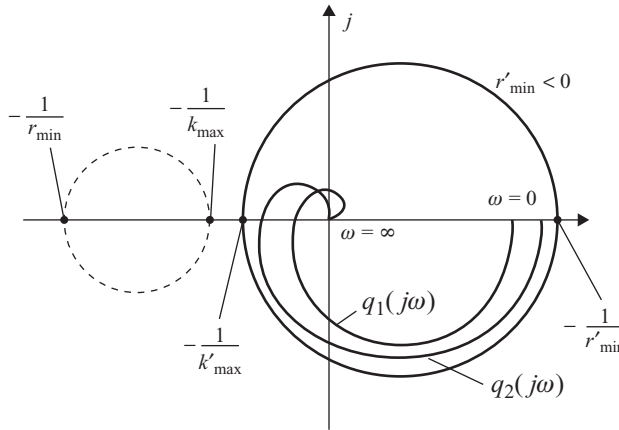


**Figure 5.38** Circle criterion of absolute stability of forced motions for  $r'_{\min} < 0$  ( $N = 2$ ).

It is easy to see that the necessary geometrical criteria of positive definiteness of  $\mathbf{Re}P(j\omega)$  [Equation (5.5)] stated above become *sufficient* if the transfer matrix of the linear part  $W(s)$  is *normal*.

**Example 5.8** Examine the stability of forced motions in the two-dimensional feedback system with the unstable linear part of Example 5.5, assuming that the nonlinear elements in the separate channels are identical and have the characteristics depicted in Figure 5.39(a), where  $k_{\max} = k'_{\max} = 0.5$ ,  $r_{\min} = 0.125$  and  $r'_{\min} = -0.15$ , i.e. have characteristics with negative slopes. The results of computations are represented in Figure 5.40(a), in which the circle in Equation (5.74) is plotted by the solid line and the circle which is used for the analysis of the absolute stability of the equilibrium point is not shown, since it is located outside the circle in Equation (5.74) and is of no interest here. The frequency dependencies of the eigenvalues of  $\mathbf{Re}P(j\omega)$  are shown by solid lines in Figure 5.40(b). These dependencies indicate that the sufficient conditions of absolute stability of forced motions for the MIMO system with the nonlinearities in Figure 5.40(a) hold.

It is interesting to note that the geometrical conditions for absolute stability also hold for the nonlinearities  $F_i(x_i)$  having a negative slope of their characteristics that is twice as large

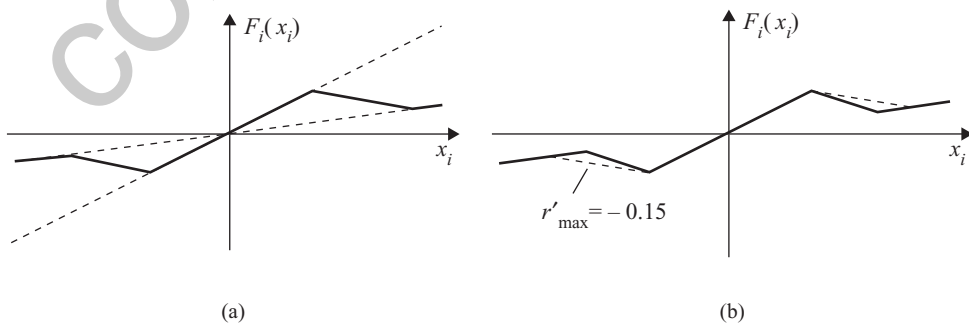


**Figure 5.39** Characteristics of nonlinearities  $F_i(x_i)$ . (a)  $r'_{\min} = -0.15$ ; (b)  $r'_{\min} = -0.3$ .

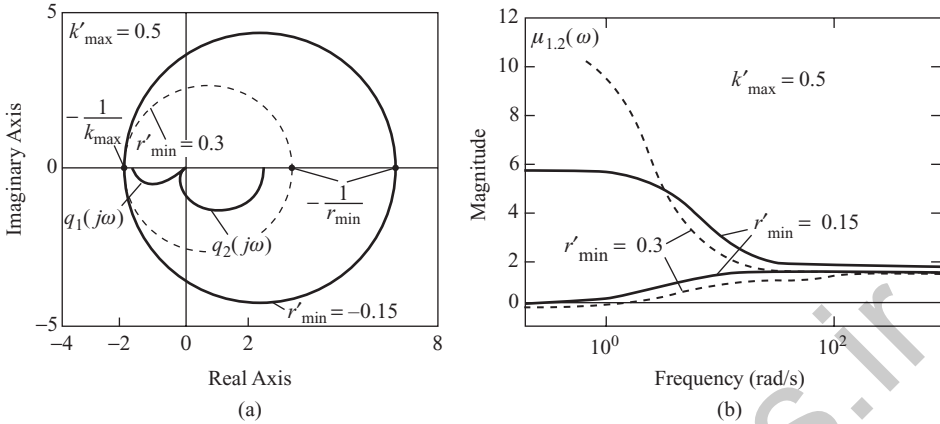


**Figure 5.40** Analysis of absolute stability of forced motions in the MIMO system with an unstable linear part. (a) Nyquist plots; (b) eigenvalues of the matrix  $\mathbf{Re}P(j\omega)$ .

[Figure 5.40(b)], i.e. for  $r'_{\min} = -0.3$  [the corresponding circle in Figure 5.40(a) is shown by the dashed line]. However, as shown in Figure 5.40(b), for  $r'_{\min} = -0.3$ , one of the eigenvalues of  $\mathbf{Re}P(j\omega)$  is negative in the low-frequency region, i.e. the condition  $\mathbf{Re}P(j\omega) > 0$  does not hold. On the other hand, we should not forget that the condition  $\mathbf{Re}P(j\omega) > 0$  is *sufficient*, and its violation does not yet mean that the forced motions in the considered two-dimensional system are unstable.

# Bibliography

- Aisagaliev, S. A. (1969). 'On defining the area of absolute stability of forced motion in nonlinear systems' (in Russian), *Izv. AN SSSR, Technicheskaya kibernetika*, 5.
- Aisagaliev, S. A. (1970). 'On defining the area of absolute stability of control systems with several nonlinear elements' (in Russian), *Automation and Remote Control*, 12.
- Aizerman, M. A. (1949). 'On a problem concerning stability "in the large" of dynamical systems' (in Russian), *Usp. Mat. Nauk*, 4(4), pp. 187–8.
- Aizerman, M. A. and Gantmacher, F. R. (1964). *Absolute Stability of Regulator Systems*, Holden-Day, San Francisco, CA.
- Anderson, B. D. O. and Moore, J. B. (1971). *Linear Optimal Control*, Prentice-Hall, Englewood Cliffs, NJ.
- Anderson, B. D. O. and Moore, J. B. (1990). *Optimal Control: Linear Quadratic Methods*, Prentice Hall, Englewood Cliffs, NJ.
- Antoulas, A. C. (1999). 'Approximation of linear dynamical systems', *Wiley Encyclopedia of Electrical and Electronics Engineering*, 11, pp. 403–22.
- Antoulas, A., Sorensen, D. and Gugercin, S. (2001). 'A survey of model reduction methods for large-scale systems', *Contemp. Math.*, 280, pp. 193–219.
- Åström, K. J. and Hägglund, T. (1995). *PID Controllers: Theory, Design, and Tuning*, Instrument Society of America, Research Triangle Park, NC.
- Atherton, D. P. (1975). *Nonlinear Control Engineering*, Van Nostrand Reinhold Co., London and New York.
- Baranchuk, E. I. (1968). *Cross-Connected and Multiple-Loop Control Systems* (in Russian), Energia, Leningrad.
- Barski, A. G. (1966). 'About two-channel control systems with cross-connections' (in Russian), *Automation and Remote Control*, 6.
- Basilio, J. C. and Kouvaritakis, B. (1995). 'The use of rational eigenvector approximations in commutative controllers', *Int. J. Contr.*, 61, pp. 333–56.
- Basilio, J. C. and Kouvaritakis, B. (1997). 'Design of causal reversed-frame-normalizing controllers using bicausal expansions', *Int. J. Contr.*, 66, pp. 1–14.
- Basilio, J. C. and Sahate, J. A. (2000). 'A normalizing precompensator for the design of effective and reliable commutative controllers', *Int. J. Contr.*, 73, pp. 1280–97.
- Benner P., Mehrmann, V. and Sorensen, D., eds (2005). 'Dimension reduction of large-scale systems', volume 45 of *Lecture Notes in Computational Science and Engineering*, Springer-Verlag, Berlin/Heidelberg.
- Bellman, R. (1970). *Introduction to Matrix Analysis*, McGraw-Hill, New York.

- Bendrikov, G. A. and Ogorodnikova, V. I. (1967). 'On theory of two-channel systems with symmetric cross-connections' (in Russian), *Vestnik MFU*, seria III, 5.
- Bendrikov, G. A. and Ogorodnikova, V. I. (1968). 'Investigation of the three-channel automatic control system with antisymmetrical cross-connections by the root locus method' (in Russian), *Automation and Remote Control*, 9.
- Bendrikov, G. A. and Teodorchik, K. F. (1964). *The Root Trajectories of Linear Automatic Systems* (in Russian), Nauka, Moscow.
- Bessekerski, V. A. and Popov, E. P. (2002). *Theory of Automatic Control Systems* (in Russian), Nauka, Moscow.
- Bliss, G. A. (1966). *Algebraic Functions*, Dover, New York.
- Bode, H. W. (1945). *Network Analysis and Feedback Amplifier Design*, D. Van Nostrand Co., New York.
- Bosgra, O. H., Kwakernaak, H. and Meinsma, G. (2004). 'Design methods for control systems', notes for a course of the Dutch Institute of Systems and Control, Winter term, DISC.
- Bryson, E. and Cho, Y. (1969). *Applied Optimal Control*, Ginn, Waltham, MA.
- Butterworth, S. (1930). 'On the theory of filter amplifiers', *Wireless Engineer*, 7, pp. 536–41.
- Chorol, D. M., Barski, A. G. and Orlova, M. S. (1976). *Dynamical Systems with One-Channel Measuring Devices* (in Russian), Mashinostroenie, Moscow.
- Churchill, R. V., Brown, J. W. and Verhey, R. F. (1974). *Complex Variables and Applications*, McGraw-Hill, New York.
- Cook, P. A. (1994). *Nonlinear Dynamical Systems*, Prentice Hall, Englewood Cliffs, NJ.
- Couros, C. and Goodwin, R. W. (1973). 'Determining the stability of the nonlinear systems', *Instrum. and Contr. Syst.*, 46(6).
- Danford, N. and Schwartz, J. T. (1962). *Linear Operators* (in Russian), Izdat. Inostran. Lit., Moscow.
- Davis, P. J. (1979). *Circulant Matrices*, John Wiley & Sons, Inc., New York.
- Derusso, P. M., Roy, R. J. and Close, C. M. (1965). *State Variables for Engineers*, John Wiley & Sons, Inc., New York.
- Desoer, C. A. and Vidyasagar, M. (1975). *Feedback Systems: Input–Output Properties*, Academic Press, New York.
- Desoer, C. A. and Wang, Y. T. (1980). 'On the generalized Nyquist stability criterion', *IEEE Trans. on Autom. Control*, V Ac-25, N 2, Apr, pp. 187–96.
- Doyle, J. C. (1984). *Lecture Notes on Advances in Multivariable Control*, ONR/Honeywell Workshop, Minneapolis, October.
- Doyle, J. C. and Stein, G. (1981). 'Multivariable feedback design: Concepts for a classical/modern synthesis', *IEEE Trans. on Autom. Control*, AC-26(1), 4–16 February.
- Doyle, J. C., Francis, B. and Tannenbaum, A. (1992). *Feedback Control Theory*, Macmillan Publishing Company, New York.
- Evans, W. R. (1948). 'Graphical analysis of control systems', *Trans. Amer. Institute of Electrical Engineers*, 67, pp. 547–51.
- Evans, W. R. (1950). 'Control system synthesis by root locus method', *Trans. Amer. Institute of Electrical Engineers*, 69, pp. 66–9.
- Evans, W. R. (1954). *Control System Dynamics*, McGraw-Hill Book Co., New York, NY.
- Fedorov, S. M. (1959). 'Application of the oscillation index to the design of tracking systems' (in Russian), *Izv. AN SSSR, OTN, Energetika I Avtomatika*, 2.
- Fedorov, S. M., Luchko, S. V. and Belyakov, V. L. (1972). 'On performance estimate of nonlinear stabilizing systems' (in Russian), *Izv. vuzov SSSR, Priborostroenie*, 7.
- Fortescue, P. W. (1976). 'The generalized root locus method (for similar systems with antisymmetric coupling)', *Int. J. Contr.*, 4(4).
- Francis, B. (1987). 'A course in  $H_\infty$  control theory', *Lecture Notes in Control and Information Sciences*, Springer-Verlag, Berlin.
- Franklin, G. F., Powell, J. D. and Emami-Naeini, A. (1991). *A. Feedback Control of Dynamic Systems*. Addison-Wesley Publ. Co., Reading, MA, Second Edition.

- Gantmacher, F. R. (1964). *The Theory of Matrices*, Chelsea Publishing Company, New York, NY, Reprinted.
- Gasparyan, O. N. (1976). Ph.D. Thesis (in Russian), Moscow Aviation Institute, Moscow.
- Gasparyan, O. N. (1981). 'Characteristic transfer functions method in multivariable control' (in Russian), *Proc. RA Control Conference*, Yerevan, Armenia.
- Gasparyan, O. N. (1985). 'Investigation of absolute stability of nonlinear multivariable systems by the characteristic transfer function method' (in Russian), *Izv. AN ASSR*, Yerevan, Armenia, 37(2).
- Gasparyan, O. N. (1986). Doctoral thesis (in Russian), Moscow Aviation Institute, Moscow.
- Gasparyan, O. N. and Aleksanyan, G. A. (2004). 'On absolute stability investigation of nonlinear uniform multidimensional control systems by means of circle criteria' (in Russian), *Modelling, Optimization, Control*, Yerevan, Armenia, 1(7).
- Gasparyan, O. N. and Arutyunyan, S. (1981). 'Influence of the mechanical gear instrumental errors on the accuracy of multivariable systems under periodical inputs' (in Russian), *Proc. RA Control Conference*, Yerevan, Armenia.
- Gasparyan, O. N. and Egiazaryan, G. G. (1979). 'On dynamical accuracy of multivariable tracking systems dynamics' (in Russian), *Izv. AN ASSR*, Yerevan, 1.
- Gasparyan, O. N. and Vardanyan, N. H. (2007). 'On behaviour of root loci of uniform multivariable feedback control systems' (in Russian), *Modelling, Optimization, Control*, Yerevan, Armenia, 1(8).
- Gasparyan, O. N., Abgaryan, S. V., Vardanyan, N. H. and Mkhitarian, E. A. (2006). 'On construction of root loci of multivariable control systems' (in Russian), *Modelling, Optimization, Control*, Yerevan, Armenia, 2(7).
- Gasparyan, O. N., Zackaryan, A. Z. and Egiazaryan, G. G. (1985). 'Dynamics analysis of precise stabilization system for "Astron" telescope' (in Russian), *Byurakan Observatory Reprts*, AS ASSR, Yerevan, Armenia, LVI.
- Gelb, A. (1963). 'Limit cycles in symmetric multiple nonlinearity systems', *IRE Trans. Autom. Control*, AC-8(2), April, pp. 177–8.
- Gelfand, I. M. (1966). *Lectures on Linear Algebra* (in Russian), Nauka, Moscow.
- Geng, J. Z. and Haynes, L. S. (1994). 'Six degree-of-freedom active vibration control using the Stewart platform', *IEEE Transactions on Control Systems Technology*, 2(1), pp. 45–53.
- Gerasimov, A. N. (1962). 'On choice of parameters in two-channel tracking systems with antisymmetrical cross-connections' (in Russian), *Izv. AN SSSR, OTN Energetika I avtomatika*, 2.
- Gibson, J. E. (1963). *Nonlinear Automatic Control*, McGraw-Hill Book Co., New York, NY.
- Glaria, J., Rojas, R. and Salgado, M. (1994). 'Logarithmic root loci for continuous time loops', *IEEE Contr. Syst. Mag.*, 14(April), pp. 47–52.
- Glover, K. (1984). 'All optimal Hankel-norm approximations of linear multivariable systems and their  $L_\infty$  norms', *Int. J. Contr.*, 39, pp. 1115–93.
- Goldfarb, L. C. (1941). 'About nonlinearity of regulatory systems' (in Russian), *Bulleten VEI*, 3.
- Goldfarb, L. C. (1947). 'On some nonlinearities in control systems' (in Russian), *Automation and Remote Control*, 8(5), pp. 349–83.
- Goldstein, H. (1959). *Classical Mechanics*, Addison-Wesley, Massachusetts.
- Golomb, M. and Usdin, E. (1952). 'A theory of multidimensional servosystem', *J. Franklin Inst.*, 1.
- Havre, K. and Skogestad, S. (1998). 'Effect of RHP zeros and poles on performance in multivariable systems', *Journal of Process Control*, 8, pp. 155–64.
- Horowitz, I. M. (1963). *Synthesis of Feedback Systems*, Academic Press, London.
- Hovd, M. and Skogestad, S. (1992). 'Robust control of systems consisting of symmetrically interconnected subsystems', *Proc. American Control Conference*, Chicago, pp. 3021–5.
- Hovd, M. and Skogestad, S. (1994a). 'Control of symmetrically interconnected plants', *Automatica*, 30(6), pp. 957–73.
- Hovd, M. and Skogestad, S. (1994b). 'Sequential design of decentralized controllers', *Automatica*, 30(10), pp. 1601–7.

- Hovd, M., Braatz, R. D. and Skogestad, S. (1997). 'SVD controllers for H<sub>2</sub>-H<sub>∞</sub>- and  $\mu$ -optimal control', *Automatica*, 33(3), pp. 433–9.
- Hsu, J. C. and Meyer, A. U. (1968). *Modern Control Principles and Applications*, McGraw-Hill, New York.
- Hung, Y. S. and MacFarlane, A. G. J. (1981). 'On the relationships between the unbounded asymptote behaviour of multivariable root loci, impulse response and infinite zeros', *Int. J. Contr.*, 34(1), pp. 31–69, July.
- James, H. M., Nichols, N. B. and Phillips, R. S. (1947). *Theory of Servomechanisms*, McGraw-Hill, New York.
- Joshi, A. A. and Kim, W.-J. (2004). 'System identification and multivariable control design for a satellite ultraquiet isolation technology experiment (SUITE)', *European Journal of Control*, 10(2), pp. 174–86, September.
- Joshi, A. A. and Kim, W.-J. (2005). 'Modeling and multivariable control design methodology for hexapod-based satellite vibration isolation', *ASME Journal of Dynamic Systems, Measurement and Control*, 127(4), pp. 700–4, December.
- Jury, E. and Li, B. (1965). 'Absolute stability of systems with many nonlinearities' (in Russian), *Automation and Remote Control*, 6.
- Kailath, T. (1980). *Linear Systems*, Prentice-Hall, Inc., New Jersey.
- Kazamarov, A. A., Palatnik, A. M. and Rodnyanski, L. O. (1967). *Dynamics of Two-Dimensional Automatic Systems* (in Russian), Nauka, Moscow.
- Kononov, A. S. and Zacharov, V. M. (1978). 'On absolute stability analysis of nonlinear automatic systems on the base of V.M.Popov's criterion' (in Russian), *Izv. vuzov SSSR, Priborostroe-nie*, 3.
- Kouvaritakis, B. (1978). 'The optimal root loci of linear multivariable systems', *Int. J. Contr.*, 28, pp. 33–62, July.
- Kouvaritakis, B. and Edmunds, J. M. (1979). 'Multivariable root loci: A unified approach to finite and infinite zeros', *Int. J. Contr.*, 29(3), pp. 393–428, March.
- Kouvaritakis, B. and Shaked, U. (1976). 'Asymptotic behavior of root-loci of multivariable systems', *Int. J. Contr.*, 23, pp. 297–340.
- Krall, A. M. (1970). 'The root-locus method: A survey', *SIAM Review*, 12, pp. 64–72.
- Krassovski, A. A. (1957). 'On two-channel automatic systems with antisymmetrical connections' (in Russian), *Automation and Remote Control*, 2.
- Krassovski, A. A. (1961). 'On theory of two-channel tracking systems with relay in alternating-current circuit' (in Russian), *Automation and Remote Control*, 2.
- Krilov, N. M. and Bogolyubov, N. N. (1934). *New Methods in Nonlinear Mechanics* (in Russian), Gostechizdat.
- Krilov, N. M. and Bogolyubov, N. N. (1937). *Introduction to Nonlinear Mechanics* (in Russian), AN USSR, Kiev.
- Kochenburger, R. J. (1950). 'A frequency response method for analyzing and synthesizing contactor servomechanisms', *Tram. AIEE*, Part 11, 69, pp. 270–84.
- Kuo, B. J. (1995). *Automatic Control Systems*, 7th edn, Prentice Hall, EC, NJ.
- Kuzovkov, N. T. (1959). 'Control systems synthesis by logarithmical root locus and generalized frequency-response characteristics' (in Russian), *Izv. AN SSSR, OTN, Energetika I Avtomatika*, 5.
- Kwakernaak, H. (1976). 'Asymptotic root loci of optimal linear regulators', *IEEE Trans. Aut. Control*, 21(3), pp. 378–82.
- Kwakernaak, H. and Sivan, R. (1972). *Linear Optimal Control Systems*, Wiley Interscience, New York.
- Lifshits, N. A., Vinogradov, V. N. and Golubev, G. A. (1974). *Correlation Theory of Multidimensional Processes Optimal Control* (in Russian), Sovetskoe Radio, Moscow.
- Lindgren, A. G. (1964). 'Limit cycles in symmetric multivariable systems', *IEEE Trans. on Autom. Control*, AC-9, January.
- Lindgren, A. G. and Pinkov, R. F. (1966). 'Stability of symmetric nonlinear multivariable systems', *J. of Franklin Inst.*, 282(2).

- Lyapunov, A. M. (1892). *General Problem of Motion*, Gostechizdat, Moscow, 1950 (1st edn – Kharkov, 1982).
- Lyapunov, A. M. (1907). 'Problem general de la stabilite du mouvement', *Ann. Fac. Sci. Univ. Toulouse*, 9, pp. 203–474.
- MacFarlane, A. G. J. (1970). 'Commutative controller: A new technique for the design of multivariable control systems', *Electronic Letters*, 6, pp. 121–3.
- MacFarlane, A. G. J. (1975). 'Relationships between recent developments in linear control theory and classical design techniques', *Measurement and Control*, 8, pp. 179–87, 219–23, 278–84, 319–23, 371–5, May–Sept.
- MacFarlane, A. G. J. and Belletrutti, J. J. (1970). 'The characteristic locus design method', *Automatica*, 9(5), pp. 575–88.
- MacFarlane, A. G. J. and Kouvaritakis, B. (1977). 'A design technique for linear multivariable feedback systems', *Int. J. Contr.*, 25, pp. 837–74.
- MacFarlane, A. G. J., Kouvaritakis, B. and Edmunds, J. M. (1977). 'Complex variable methods for multivariable feedback systems analysis and design', *Alternatives for Linear Multivariable Control*, National Engineering Consortium, Chicago, IL, pp. 189–228.
- MacFarlane, A. G. J. and Postlethwaite, I. (1977). 'Characteristic frequency functions and characteristic gain functions', *Int. J. Contr.*, 26, pp. 265–78.
- Maciejowski, J. M. (1989). *Multivariable Feedback Design*, Addison-Wesley, Wokingham.
- Makarov, I. M. and Menski, B. M. (1977). *Linear Automatic Systems*, Mashinostroenie, Moscow.
- Marcus, M. and Minc, H. (1992). *A Survey of Matrix Theory and Matrix Inequalities*, Dover Pubns.
- Meerov, M. V. (1965). *Multivariable Control Systems* (in Russian), Nauka, Moscow.
- Moore, J. B. and Anderson, B. D. O. (1967). 'Applications of the multivariable Popov criterion', *Int. J. Contr.*, 5(4), pp. 345–53.
- Moore, J. B. and Anderson, B. D. O. (1968). 'A generalization of the Popov criterion', *Journal of the Franklin Institute*, 285(6), June.
- Morari, M. and Zafriou, E. (1989). *Robust Process Control*, Prentice-Hall, Englewood Cliffs.
- Morozovski, V. T. (1970). *Multivariable Control Systems* (in Russian), Energia, Moscow.
- Mutter, V. M. (1981). *Analog-Digital Control Systems* (in Russian), Mashinostroenie Leningrad.
- Narendra, K. S. and Taylor, J. (1973). *Frequency Domain Methods for Absolute Stability*, Academic, New York.
- Naumov, B. N. (1972). *Theory of Nonlinear Control Systems: Frequency-Domain Methods* (in Russian), Nauka, Moscow.
- Nelepin, R. F., ed. (1975). *Methods of Investigation of Nonlinear Control Systems* (in Russian), Nauka, Moscow.
- Newton, G. C., Gould, L. A. and Kaiser, J. F. (1957). *Analytical Design of Linear Feedback Control*, John Wiley & Sons, Inc.
- Nikiforuk, P. L. and Wintonyk, B. L. (1968). 'Frequency response analysis of two-dimensional nonlinear symmetrical and non-symmetrical control systems', *Int. J. Control.*, 7(1).
- Ogata, K. (1970). *Modern Control Engineering*, Prentice Hall, Englewood Cliffs, NJ.
- Ogorodnikov, G. V. (1974). 'About analysis of natural periodic motions of two-dimensional nonlinear systems' (in Russian), *Izv. Vuzov SSSR, Priborostroenie*, 6.
- Ogorodnikov, G. V. (1975). 'On investigation of symmetrical periodic modes in nonlinear two-dimensional systems' (in Russian), *Izv. Vuzov SSSR, Priborostroenie*, 2.
- Orurk, I. A., Osipov, L. A. and Konovalov, A. S. (1978). 'On absolute stability investigation of systems with several nonlinearities' (in Russian), *Izv. vuzov SSSR, Priborostroenie*, 2.
- Owens, D. H. (1973). 'Dyadic approximation method for multivariable control systems analysis with a nuclear application', *Proceedings IEE*, 120(7), pp. 801–9.
- Owens, D. H. (1974). 'Dyadic expansion for the analysis of linear multivariable systems', *Proceedings IEE*, 121(7), pp. 713–16.
- Owens, D. H. (1976). 'Root-loci concepts for kth-order-type multivariable structures', *Proceedings IEE*, 123(9), pp. 933–40.

- Ozay, H. (1973). 'On the Popov criterion', *Int. J. Contr.*, 6.
- Packard, A. and Doyle, J. C. (1993). 'The complex structured singular value', *Automatica*, 29(1), pp. 71–109.
- Paltov, I. P. (1975). *Performance of Processes and Design of Compensating Devices in Nonlinear Control Systems* (in Russian), Nauka, Moscow.
- Patra, K. C. and Pati, B. B. (1998). 'An investigation of forced oscillation for signal stabilisation of two-dimensional nonlinear system', *Journal of Systems and Control Letters*, Netherlands, 35, p. 229.
- Patra, K. C., Pati, B. B. and Kacprzyk, J. (1995). 'Prediction of limit cycles in nonlinear multivariable systems', *Archives of Control Science* (Poland), 4(3–4), p. 281.
- Patra, K. C., Pati, B. B. and Lozowicki, A. (1999). 'Structural formulation and self-oscillation prediction in multidimensional nonlinear closed-loop autonomous systems', *Int. J. Appl. Math. and Comp. Sci.*, 9(2), pp. 327–46.
- Pernechele, C., Bortoletto, F. and Reif, K. (1998). 'Hexapod control for an active secondary mirror: General concept and test results', *Appl. Opt.*, 37(28), pp. 6816–21.
- Petrov, N. P. (1970). 'A method of construction of absolute stability area for a system with several nonlinearities' (in Russian), *Automation and Remote Control*, 10.
- Popov, V. M. (1961). 'Absolute stability of nonlinear systems of automatic control' (in Russian), *Automation and Remote Control*, 22, pp. 857–75.
- Popov, E. P. (1973). *Applied Theory of Control Processes in Nonlinear Systems* (in Russian), Nauka, Moscow.
- Popov, V. M. (1959). 'Criterii suficiente de stabilitate simptotica in mare pentru sistemele automate on mai multe organe de executie', *Studei si Cercetari de Energetica, Acad. RPR*, 9(1).
- Popov, V. M. (1960). 'Nonrelaux criterium de stabilitate pour les systemes automatiques non lineairies', *Revue D'electron, et energ*, V(1).
- Popov, E. P. (1962). *The Dynamics of Automatic Control Systems*, Addison-Wesley Publishing Company, Reading, MA.
- Porter, W. A. (1966). *Modern Foundations of Systems Engineering*, The Macmillan Company, New York.
- Postlethwaite, I. and MacFarlane, A. G. J. (1979). 'A complex variable approach to the analysis of linear multivariable feedback systems', Vol. 12 of *Lecture Notes in Control and Information Sciences*, Springer-Verlag, Berlin.
- Pyatnicki, E. S. (1968). 'New research on control systems absolute stability survey' (in Russian), *Automation and Remote Control*, 6.
- Rabinovich, L. V. et al. (1969). *Design of Tracking Systems* (in Russian), Mashinostroenie, Moscow.
- Rimski, G. V. (1969). 'Generalized root loci of control systems' (in Russian), *Izv. AN BSSR, seria fiz.-tekh. nauk*, 2.
- Rosenbrock, H. H. (1974). 'Correction on "The zeros of a system"', *Int. J. Contr.*, 20, pp. 525–7.
- Rosenbrock, H. H. (1969). 'Design of multivariable control systems using the inverse Nyquist array', *Proc. ZEEE*, 1 IQ(11), November.
- Rosenbrock, H. H. (1970). *State-Space and Multivariable Theory*, Nelson, London.
- Rosenbrock, H. H. (1973). 'The zeros of a system', *Int. J. Contr.*, 18, pp. 297–9.
- Safonov, M. G. (1980). *Stability and Robustness of Multivariable Feedback System*, 2nd edn, The MIT Press, Cambridge.
- Safonov, M. G. (1981). 'Stability margins of diagonally perturbed multivariable feedback systems', *Proc. IEEE Conf. on Decision and Control*, San Diego, CA, 16–18 December.
- Sain, M. K. and Schrader, C. B. (1990). 'The role of zeros in the performance of multi-input, multi-output feedback systems', *IEEE Transactions on Education*, 33, pp. 244–57.
- Shaked, U. (1976). 'The angles of departure and approach of the root-loci in linear multivariable systems', *Int. J. Contr.*, 23(3), pp. 445–7.
- Shaked, U. and Kouvaritakis, B. (1977). 'The zeros of linear optimal control systems and their role in high feedback gain stability design', *IEEE Trans. Automat. Contr.*, AC-22(4), pp. 597–9, August.
- Shankar, S. and Atherton, D. (1977). 'Graphical stability analysis of nonlinear multivariable control systems', *Int. J. Contr.*, 3.

- Shinsky, F. G. (1988). *Process Control Systems*, 3rd edn, McGraw Hill, New York.
- Siljak, D. D. (1969). *Nonlinear Systems: The Parameter Analysis and Design*, John Wiley & Sons, Inc., New York.
- Siljak, D. D. (1970). 'Nonnegative polynomials: A criterion', *Proceedings of the IEEE*, 9.
- Skogestad, S. and Postlethwaite, I. (1995, 2005). *Multivariable Feedback Control: Analysis and Design*, John Wiley & Sons, Ltd, Chichester, Sussex, UK (2nd edn, 2005).
- Sobolev, O. S. (1973). *Uniform Connected Control Systems* (in Russian), Energia, Moscow.
- Stevens, P. K. (1981). 'Generalization of the Nyquist stability criterion', *IEEE Transactions on Automatic Control*, Ac-26(3), June, pp. 664–9.
- Strang, G. (1976). *Linear Algebra and its Applications*, Academic Press, New York.
- Taylor, J. H. (1999). 'Describing functions', an article in the *Electrical Engineering Encyclopedia*, John Wiley & Sons, Inc., New York.
- Thaler, G. J. and Pastel, M. P. (1962). *Analysis and Design of Nonlinear Feedback Control Systems*, McGraw-Hill Book Company, New York.
- Tichonov, Y. L. (1969). 'On performance investigation of two-dimensional systems' (in Russian), *Izv. vuzov SSSR, Priborostroenie*, 10.
- Truxal, J. G. (1955). *Automatic Feedback Control System Synthesis*, McGraw-Hill Book Co., New York.
- Tsytkin, J. Z. (1977). *Control Systems Theory Fundamentals* (in Russian), Nauka, Moscow.
- Tsytkin, J. Z. (1974). *Relay Automatic Systems* (in Russian), Nauka, Moscow.
- Tustin, A. (1947). 'The effects of backlash and of speed-dependent friction on the stability of closed-cycle control systems', *J. IEE*, London, Part 11, 94(May), pp. 143–51.
- Uderman, E. G. (1963). *Root Locus Method in Control Theory* (in Russian), Gostekhizdat.
- Vardulakis, A. I. G. (1991). *Linear Multivariable Control: Algebraic Analysis and Synthesis Methods*, John Wiley & Sons, Ltd, Chichester, Sussex, UK.
- Vavilov, A. A. (1970). *Frequency-Domain Methods for Nonlinear Systems Design* (in Russian), Energia, Leningrad.
- Voevodin, V. I. and Kuznetsov, J. A. *Matrices and Calculations* (in Russian), Nauka, Moscow.
- Voronov, A. A. (1979). *Stability, Controllability, Observability* (in Russian), Nauka, Moscow.
- Vulich, B. Z. (1967). *Introduction to Functional Analysis* (in Russian), Nauka, Moscow.
- Wonham, W. M. (1979). *Linear Multivariable Control: A Geometric Approach*, Springer-Verlag, New York.
- Yagle, A. E. (1981). MS Thesis, Dept of Elec. Engin. and Comput. Science, MIT, Cambridge, MA.
- Yakubovich, V. A. (1962). 'Solution to some matrix inequalities occurring in nonlinear control theory' (in Russian), *DAN SSSR*, 143(6).
- Yakubovich, V. A. (1964). 'Solution to some matrix inequalities occurring in nonlinear control theory' (in Russian), *DAN SSSR*, 156(2).
- Yakubovich, V. A. (1967). 'Frequency conditions for the absolute stability of control systems with several nonlinear and linear non-stationary blocks' (in Russian), *Automation and Remote Control*, 28, pp. 857–80.
- Yakubovich, V. A. (1973). 'Minimization of quadratic functionals under the quadratic constraints and the necessity of a frequency condition in the quadratic criterion for absolute stability of nonlinear control systems' (in Russian), *Soviet Mathematics Doklady*, 14, pp. 593–7.
- Ziegler, J. G. and Nichols, N. B. (1942). 'Optimum settings for automatic controllers', *Transactions of the ASME*, 64, pp. 759–68.

# Index

- Absolute correction, 159–169, 281, 282.  
     *See also* Absolute transfer function;  
     Scalar regulator
- Absolute pole
  - circulant and anticirculant system, 64
  - open-loop MIMO system, 6, 8, 10, 84, 158
  - uniform system, 41, 90
- Absolute stability
  - equilibrium point, 285
  - forced motions, 323
  - necessary and sufficient conditions, 301
  - sufficient condition
    - SISO case, 285
    - MIMO case, 288
- Absolute transfer function, 157, 158, 278–281.  
     *See also* Scalar regulator
- Absolute zero
  - general MIMO system, 6–10, 16, 84, 158
  - uniform system, 41, 90
- Absolutely stable MIMO system, 324
- Adjoint matrix, 9
- Algebraic functions, 35, 49, 65, 75–78  
     discriminant of, 78
- Algebraic multiplicity of a pole, 6, 8, 35
- Angle between two vectors, 12
- Angles of asymptotes of multivariable root loci
  - circulant system, 95
  - general MIMO system, 79
  - uniform systems, 91
- Angles of departure and arrival of multivariable root loci, 81
- Anticirculant
  - MIMO system, 62
  - antisymmetrical, 64
  - simple antisymmetrical, 64
  - matrix, 62
  - permutation matrix, 62
  - proper orthogonality, 62
- Anticirculant regulator, 162
- Antisymmetrical
  - cross-connections, 39, 66
  - matrix, 53, 64
  - system, two-dimensional, 64
- Aizerman's hypothesis, generalized, 301
- Asymptotical stability, 284, 285
- Average motion, 57, 58, 221. *See also* Transfer function of the average motion
- Axially-symmetrical body, 65
- Balancing of channels, 161, 278
- Bandwidth, 156
- Basic perturbation model, 111
- Basis
  - canonical, 11
  - dual, 12
  - reciprocal, 12
  - input singular, 32, 34. *See also* Singular basis
  - left singular, 32, 34. *See also* Singular basis
  - orthogonal, 33
  - output singular, 32, 34. *See also* Singular basis
  - right singular, 32, 34. *See also* Singular basis
- Block-scalar, block-diagonal, block-triangular MIMO systems, 37
- Branch points (of an algebraic function), 24, 35, 49, 65, 75, 79

- Breakaway points of multivariable root loci, 81, 82, 96, 98
- Butterworth configuration, 75, 79, 80, 91, 95
- Canonical basis, 11  
 anticirculant system, 63  
 circulant system, 56  
 general MIMO system, 11  
 normal MIMO system, 51  
 uniform system, 42
- Canonical basis of a closed-loop MIMO system, 17
- Canonical basis of a harmonically linearized  
 circulant and anticirculant system, 217  
 general MIMO system, 185  
 uniform MIMO system, 201
- Capturing, 197, 236, 248, 265. *See also*  
 Entrainment; Forced synchronization
- Cauchy-Schwartz inequality, 137
- Characteristic gain loci, 24
- Characteristic polynomial  
 closed-loop MIMO system, 10, 20  
 open-loop MIMO system, 7
- Characteristic system  
 anticirculant system, 63  
 circulant system, 56  
 general MIMO system, 11  
 uniform system, 42
- Characteristic vectors, 11  
 normalized, 11
- Characteristic values, 11
- Characteristic transfer function (CTF)  
 closed-loop linear MIMO system, 17  
 feedback connection of two circulant elements, 72  
 harmonically linearized  
 circulant and anticirculant system, 216  
 general MIMO system, 185  
 uniform MIMO system, 201  
 open-loop linear MIMO system, 11  
 series connection of circulant elements, 71  
 parallel connection of circulant elements, 72
- Circle criterion of absolute stability, 315–317  
 inverse form ( for uniform systems), 320  
 forced motion, 323
- Circulant system, 54  
 antisymmetrical, 58  
 symmetrical, 56  
 uniform, 56
- Circulant regulator, 162
- Closed-loop transfer function of a SISO system  
 with respect to output signals, 8
- Closed-loop transfer function of a SISO system  
 with respect to error signals, 8
- Collinearity condition  
 for finding frequency response characteristic  
 along canonical basis axes, 246, 254, 268, 275, 280  
 of existence of limit cycle  
 circulant and anticirculant system, 217  
 general MIMO system, 187  
 uniform MIMO system, 201, 202
- Collinear vectors, 12
- Condition number, 108
- Conditionally stable  
 SISO system, 25  
 MIMO system, 160, 304–324
- Conditions of a MIMO system normality, 51
- Complementary sensitivity function matrix, 4, 17, 19
- Commutative matrices, 50, 70
- Complex amplitude, 102
- Complex coordinates and transfer functions  
 method, 59, 64, 65, 176
- Complex gain of a nonlinear element, *see*  
 Describing function.
- Complex transfer function, 66. *See also* Complex  
 coordinates and transfer functions  
 method
- Concomitant matrix of cross-connections, 200
- Conjugation of a matrix, 32
- Constant-M circle, 106
- Correlation matrix, 135
- Covariance matrix, 135
- Cramer's rule, 150
- Critical (forbidden) circle, 315
- Critical Gain Boundary, 178
- Critical point, 44, 293, 204, 219, 230, 270
- Critical time delay, 26
- Cross-connections, 4  
 dynamical, 53, 65  
 rigid, 41, 124
- Cross-correlation moments, 136
- Crossover frequency, 25, 157
- Damping ratio (damping), 156, 159
- Dead zone nonlinearity, 210, 253, 260
- Decoupling compensator, *see* Decoupling  
 regulator
- Decay ratio, 155
- Decentralized control, 151

- Decoupling regulator, 152, 153, 161, 162
- Degenerate branches of multivariable root loci, 84
- Degree of non-orthogonality, 108. *See also* Degree of skewness
- Degree of skewness, 108. *See also* Degree of non-orthogonality
- Degree of stability
- linear MIMO system, 156, 159
  - nonlinear MIMO system, 296, 314
- Delay margin, 26
- Delay time, 155
- Denominator polynomial, 5
- Describing function, 174
- Describing function method, 173–180
- Diagonal-dominant matrix, 153
- Diagonal matrix, 11
- Diagonal MIMO system, 36
- Diagonal regulator, 151, 152
- Dipole, 157, 164
- Direction of the input vector, 102
- Discriminant, 35, 78–81. *See also* Algebraic function.
- Dominant poles, 156
- Dual basis, 12. *See also* Reciprocal basis
- Dyad
- of rank one, 13
  - of rank  $N$ , 13
- Dyadic designations, 13
- Dyadic transfer function matrix, 154
- Dynamical compensator, 153
- Ellipsoid in  $C^N$ , 104, 117
- Entrainment, 197, 236. *See also* Capturing; Forced synchronization
- Error coefficients of characteristic systems, 127
- Error vector, 4
- Equilibrium point (state), 194, 256, 285, 291, 296, 322
- Euclidean norm (length) of a vector, 11
- Euler's dynamical equations, 65
- Excess variation, 155
- Expanded transfer matrix, 296, 314
- Fictitious pole, 89
- Fictitious zero, 89
- Final value theorem, 125
- Forbidden region
- linear MIMO system, 107, 110, 122
  - nonlinear SISO system, 243
  - nonlinear MIMO system
    - circulant and anticirculant system, 276
    - general MIMO system, 281
    - uniform system, 270
- for Bode magnitude plot (in absolute stability analysis), 310
- Forced motion, 321
- Forced synchronization, 197, 236, 246. *See also* Capturing; Entrainment
- Fourier transform, 135
- Frequency transfer matrix, 102
- Gain margin
- MIMO system, 26
  - SISO system, 25
- Gain matrix of a MIMO system, 38
- Gaussian process, 135
- General MIMO system, 4
- Generalized frequency characteristics (linear case), 101
- in the direction  $\ell$ , 102
  - along  $N$  axes of the MIMO system canonical basis, 104
  - of normal systems, 118, 119
- Generalized frequency characteristics along
- canonical basis axes (nonlinear case)
  - circulant and anticirculant system, 274
  - general MIMO system, 251, 260
  - uniform systems 268
- Geometric multiplicity of a pole, 6, 8. *See also* Rank of a pole
- Gershgorin's circles, 153
- Goldfarb method, *see* Method of Goldfarb
- Guidance system (worked examples), 21, 28, 45, 85, 92, 113, 122, 130, 139, 143, 162, 190, 196, 206, 247, 258, 263, 281, 296
- Gyrostabilized platform, 73
- Hardy space, 111
- Harmonic balance method, 173. *See also* Describing function method
- Harmonic linearization method, 173. *See also* Describing function method
- Hermitian matrix, 32
- Hexapod, 59
- Hirsch's theorem, 290, 300
- Hurwitz angle (sector), 301
- Hysteresis, 226, 287, 289, 292
- Identity operator, 13
- Imaginary unit, 66
- Improper orthogonality, 55
- Initial value theorem, 146

- Inner product, 11. *See also* Scalar product  
 Input singular basis, *see* Singular basis  
 Input vector, 4  
 Instability regions (in forced oscillations along canonical basis axes)  
     general MIMO system, 262  
     uniform system, 271  
  
 Jordan basis, block, canonical form, 35, 36  
  
 King procedure, 125, 132  
 Kronecker, symbol of, 12  
  
 Lag controller, 157  
 Lead controller, 157  
 Lead–lag controller, 157  
 Left singular basis, 32, 34. *See also* Singular basis  
 Limit cycle, 157–281  
     with equal amplitudes, 274  
 Local zero of rank  $k$ , 6, 16  
 Localization of eigenvalues, 153  
 Low pass filter (low pass filter hypothesis)  
     circulant and anticirculant system, 200  
     general MIMO system, 184  
     SISO system, 173  
     uniform system, 200  
 Lyapunov equation, 143  
 Lyapunov’s second method, 284  
  
 M-circle, 106  
 Marginal closed-loop MIMO system, 287  
 Marginal stability, 288, 292  
 Marginal tangent, 302  
 MATLAB, 25, 40, 76, 143, 261, 291  
 Matrices of error coefficients, 124–134, 160  
 Matrix  
     adjoint, 9  
     anticirculant, 62  
     anticirculant permutation, 62  
     antisymmetrical, 53  
     circulant matrix, 54  
     conjugation of, 32  
     concomitant, 200  
     correlation, 135  
     covariance, 135  
     diagonal-dominant, 153  
     diagonal, 11  
     Hermitian, 32  
     modal, 11  
     orthogonal, 42, 130  
     permutation, 54  
     residue, 6  
     scalar, 26, 138, 200, 286, 289, 305  
     skew-symmetrical, 53, 64, 222, 223  
     of spectral densities, 135  
     spectral representation, 13  
     of simple structure, 13  
     Toeplitz, 54  
     unit, 10  
     unitary, 32  
     unimodular, 37  
 Matrix controller, 151  
 Matrix polynomial, 56  
 Matrix regulator, 151, 154  
 Majorant of the generalized frequency response characteristics  
     linear MIMO system, 102–105, 109  
     nonlinear MIMO system, 251–258  
 Mean square value of the output vector  
     magnitude, 136  
 Mean square outputs of characteristic systems, 140, 142  
 Method of Goldfarb, 178, 202, 218–220, 229, 237, 243, 269  
 Method of successive approximations, 176  
 Method of Teodorchik, 176–178, 218, 237, 243  
 MIMO system  
     anticirculant, 62  
         antisymmetrical, 64  
         simple antisymmetrical, 64  
     block-diagonal, block-scalar, block-triangular, 37  
     circulant, 54  
         antisymmetrical, 58  
         symmetrical, 56  
         uniform, 56  
     diagonal, 11, 36  
     general type, 4  
     normal, 51  
         uniform, 53  
     scalar, 36  
     square, 3  
     simple symmetrical, 57  
     triangular, 36, 196–198  
     uniform, 41, 50  
 Minorant of the generalized frequency characteristic  
     linear MIMO system, 103, 104  
     nonlinear MIMO system, 253  
 Modal matrix  
     anticirculant system, 63

- circulant system, 56
- general MIMO system, 11
- uniform system, 41
- Model reduction, 40
- Modified characteristic transfer functions of the linear part, 291
- Modified frequency characteristic of the linear part (SISO case), 285
- Modified Nichols plots, 293, 295, 314
- Monic polynomial, 77, 83
- $\mu$ -curves, 107
  
- Necessary conditions for the existence of limit cycle
  - circulant and anticirculant system, 217
  - general MIMO system, 187
  - SISO system, 175
  - uniform system, 201
- Nonlinearity
  - double-valued, 175, 180, 185, 200–204, 215, 267
  - single-valued, 173–180, 203–207, 231, 285
- Norm of a matrix
  - Frobenius, 137
  - Schmidt, 137–145
  - spectral, 33
  - subordinate (induced), 128, 138
- Normal MIMO system, 51
  - canonical representations, 51
  - singular value decomposition, 52
- Normal rank of  $W(s)$ , 7, 37
- Normal uniform systems, 53
- Normality condition of a uniform system, 53
- Number of branches of root loci
  - circulant system, 94
  - general MIMO system, 77
  - uniform system, 90
- Numerator polynomial, 5
- Nyquist criterion, 24
  - generalized, 24
  - direct formulation (for uniform systems), 44
  - inverse formulation (for uniform systems), 44
  - logarithmical form, 44
  
- Off-axis circle
  - criterion, 307
  - logarithmic form, 312
  - equation of, 307
- Orthogonal matrix, 42, 130
- Orthogonal vectors, 12
  
- Orthogonal transformation, 131
- Oscillation index
  - linear control systems
    - $i$ th characteristic system, 106
    - MIMO system, 104
    - normal MIMO system, 119
    - SISO system, 101
  - nonlinear control systems
    - characteristic system
      - circulant and anticirculant system, 275–279
      - general MIMO system, 256–258
      - uniform system, 269
    - MIMO system, 252
    - SISO system, 242
- Output singular basis, *see* Left singular basis; Singular basis
- Output vector, 4
- Overshoot, 155
  
- Paltov's method for determining the oscillation index of nonlinear systems, 242
- Parabolic criterion of absolute stability, 313
- Partial fraction expansion, 6
- Peak time, 155
- Performance indices, 154. *See also* Performance specifications
- Performance specifications, 154. *See also* Performance indices
- Permutation matrix, 54
  - improper orthogonality, 55
- Phase margin
  - linear MIMO, 26
  - linear SISO system, 25
- PID (Proportional-Integral-Derivative) regulator, 152, 157
- Pivot(s) of root loci, 75
  - circulant and anticirculant system, 95, 96
  - general MIMO system, 79
  - uniform system, 91
- Pole
  - absolute, 41, 84
  - fictitious, 89
  - of an open-loop MIMO system, 5–7
  - of an open-loop SISO system, 5
  - of rank  $k$ , 6
- Poles polynomial of an open-loop MIMO system, 7
- Popov line, 286, 291
  - on Bode diagrams, 294, 295
  - on Nichols plots, 295–297

- Popov sector, 301  
 Popov's criterion of absolute stability, 285  
 Popov's method (forced oscillation analysis), 238, 255, 260, 275  
 Preliminary compensator, 160  
 Proper orthogonality, 62
- Rank of a pole, 6  
 Real-valued canonical form, 39, 130, 140, 154  
 Reference signal, 5  
 Relative coordinates, 58. *See also* Transfer functions of the relative motion  
 Relative motion, 57. *See also* Transfer functions of the relative motion  
 Relative order of a system, 157  
 Relay nonlinearity  
     ideal, 210, 223  
     with hysteresis, 226  
 Residue matrix at a MIMO system pole, 6  
 Reciprocal basis, *see* Dual basis  
 Resonant peak  
     of a closed-loop SISO system, 101, 156  
     of a MIMO system majorant, 102  
 Return difference matrix, *see* Return difference  
 Return difference  
     MIMO system, 9, 20, 126  
     SISO system, 9  
 RHP-zeros, 99  
 Riemann surface, 20, 35, 49, 75–84  
     one-sheeted, 50, 90, 93  
 Right singular basis, 32, 34. *See also* Singular basis  
 Rise time, 155  
 Robust theory, 111  
 Robustness of MIMO systems, 111–121, 169, 258  
 Root locus method, 74
- Saturation nonlinearity, 180, 190, 206, 211, 223, 232, 248, 253, 278  
     describing function of, 191  
 Scalar compensator, 278–280. *See also* Scalar regulator  
 Scalar matrix, 26, 138, 200, 286, 289, 305  
 Scalar MIMO system, 36  
 Scalar product, 11. *See also* Inner product.  
 Scalar regulator, 157  
 Sector nonlinearities, 285. *See also* Sector restrictions  
 Sector restrictions, 288, 316, 322. *See also* Sector nonlinearities
- Self-oscillation, *see* Limit cycle  
 Sensitivity function matrix, 14, 17  
 Sensitivity transfer function, 108  
 Separate channel, 4  
 Settling time, 155  
 Shift of the root loci starting points, 89  
 Shifted characteristic transfer functions, 296  
 Shifted transfer matrix, *see* Expanded transfer matrix  
 Silvester's criterion, 288  
 Silvester's low of degeneracy, 9  
 Similarity transformation, 11  
 Simple antisymmetrical circulant system, 58  
 Simple structure (of a matrix), 13  
 Simple symmetrical MIMO system, 57, 64, 95, 130, 221  
 Singular basis  
     input (left), 32, 34  
     output (right), 32, 34  
 Singular points of a transfer function, 80, 83, 92  
 Singular value, 32  
 Singular value decomposition  
     general MIMO system, 31–35  
     normal MIMO system, 52  
     uniform system, 41  
 Skewness of axes, 15, 108, 129  
 Skew-symmetrical matrix, 53, 58, 64, 222, 223  
 Small gain theorem, 112  
 Smith-McMillan canonical form, 5, 8, 37  
 Spectral decomposition of a transfer matrix, 14  
 Spectral densities, matrix of, 135  
 Spectral norm of a matrix, 33  
 Spectral radius, 119, 130  
 Spectral representation of a transfer matrix, 10, 14  
 Spectrum of a matrix, 129  
 Square MIMO system, 3  
 Stability Phase Boundary, 178  
 Stability regions (in forced oscillations along canonical basis axes)  
     general MIMO system, 262  
     uniform system, 272  
 State vector, 143  
 Static compensator, 152  
 Stationary Gaussian process, 135  
 Steady-state dynamical error, 143  
 Steady-state (static) decoupling, 152  
 Superposition principle, 5, 143  
 SVD-controllers, 154  
 Symmetrical circulant MIMO system, 56

- Telescope, astronomic, 21
- Teodorchik method, *see* Method of Teodorchik.
- Threshold value
- of the input amplitude (SISO case), 238, 240
  - of the input vector magnitude for an arbitrary direction  $\ell$  in  $C^N$ , 247, 260, 262
  - in the direction of the  $i$ th canonical basis axis
    - general MIMO system, 260, 262
    - uniform system, 271, 272
- Time delay, 26, 27, 40
- Toeplitz matrix, 54
- Trace
- of a covariance matrix, 136
  - of a matrix, 35
- Transfer function of the average motion, 57.  
*See also* Simple symmetrical system
- Transfer functions of the relative motion, 57.  
*See also* Simple symmetrical system
- Transfer function matrix of an open-loop MIMO system, 4
- Transfer function matrices of a closed-loop MIMO system, 4
- with respect to error signals, 4
  - with respect to output signals, 4
- Transformed linear part, 305, 306, 313
- Transformed nonstationary nonlinearity, 322
- Transient response characteristics, 155
- Trial and error method, 157
- Triangular MIMO system, 36, 196–198
- Two-dimensional antisymmetrical system, 64, 141
- Two-dimensional uniform antisymmetrical system, 101
- Type
- of a MIMO system, 38, 109, 124–134
  - of a SISO system, 4
- Uncertain parameter, 111
- Uncertainty
- additive, 112, 169
  - multiplicative, 112, 169
  - structured, 111, 116
  - unstructured, 111
- Uniform circulant MIMO system, 56
- Uniform MIMO system, 41, 50
- Unit matrix, 4
- Unit sphere in  $C^N$ , 102–105, 117, 118, 251
- Unit step signal, 155
- Unit vector, 10
- Unitary matrix, 32
- Unitary transformation, 130
- Unimodular matrix, 37
- Variational equations, 194
- Vector of complex amplitudes, 102
- Velocity error vector, 131, 163–166
- Viete's theorem, 83, 84
- Weak couplings (weak cross-couplings), 153
- White noise, 143, 144, 150
- Zero
- absolute, 6, 41, 84
  - fictitious, 89
  - local of rank  $k$ , 6, 16
  - of a SISO system, 5
- Zeros polynomial of an open-loop MIMO system, 7